

**GUIDELINES FOR PAVING ADJACENT CONCRETE LANES SEPERATELY**

by

**Kerri Alyssa Gatti**

Bachelor of Science in Civil Engineering,

University of Pittsburgh, 2008

Submitted to the Graduate Faculty of  
Swanson School of Engineering in partial fulfillment  
of the requirements for the degree of  
Master of Science

University of Pittsburgh

2010

UNIVERSITY OF PITTSBURGH  
SWANSON SCHOOL OF ENGINEERING

This thesis was presented

by

Kerri Alyssa Gatti

It was defended on

November 19, 2010

and approved by

John Brigham Ph.D., Assistant Professor,  
Department of Civil and Environmental Engineering

Jeen-Shang Lin, Ph D., Associate Professor,  
Department of Civil and Environmental Engineering

Julie M. Vandebossche, Ph.D., Assistant Professor,  
Department of Civil and Environmental Engineering  
Thesis Advisor

Copyright © by Kerri Alyssa Gatti

2010

## **GUIDELINES FOR PAVING ADJACENT CONCRETE LANES SEPERATELY**

Kerri Alyssa Gatti, M.S.

University of Pittsburgh, 2010

Often times concrete pavements are constructed by first paving the mainline followed by the shoulder some time later. It is important to factor differences in structure, material properties, and climatic conditions between the mainline and shoulder into the design; otherwise, premature cracking can develop. Cracking can occur in the newly paved lane, the existing lane, or both. The primary objective of this research was to develop guidelines to protect against premature cracking from paving adjacent lanes separately.

A review of several case studies revealed that longitudinal shear cracking and transverse cracking in the shoulder are the main distresses associated with delayed shoulder construction. Longitudinal shear cracking occurs due to dissimilar transverse joint openings in the mainline and shoulder. In warm weather, shoulder joints close first causing shear stresses to develop in the mainline. Transverse cracking in the shoulder is caused by thermal incompatibility between the mainline and the shoulder and small shoulder widths (less than 5 ft).

The following study uses finite element analysis to analyze the causes of longitudinal shear cracking and transverse cracking in the shoulder. A parametric study was developed for each distress so that guidelines could be established and future occurrences of the distresses can be prevented.

Thermal incompatibility between the mainline and the shoulder was the primary factor that caused premature cracking for both distresses. Every effort should be made to prevent the difference of the zero-stress temperatures of the mainline and shoulder from going beyond 25°F.

## TABLE OF CONTENTS

<b>PREFACE</b> .....	<b>XLII</b>
<b>1.0 INTRODUCTION</b> .....	<b>1</b>
<b>1.1 BACKGROUND</b> .....	<b>1</b>
<b>1.2 OBJECTIVE</b> .....	<b>2</b>
<b>1.3 RESEARCH APPROACH</b> .....	<b>2</b>
<b>2.0 LITERATURE REVIEW</b> .....	<b>4</b>
<b>2.1 DOCUMENTED DISTRESSES</b> .....	<b>4</b>
<b>2.1.1 Longitudinal Shear Cracking</b> .....	<b>4</b>
<b>2.1.2 Transverse Cracking</b> .....	<b>11</b>
<b>2.2 FACTORS THAT INFLUENCE DISTRESS DUE TO DELAYED LANE CONSTRUCTION</b> .....	<b>13</b>
<b>2.2.1 Structure</b> .....	<b>13</b>
<b>2.2.1.1 Geometry</b> .....	<b>14</b>
<b>2.2.1.2 Shoulder Type</b> .....	<b>15</b>
<b>2.2.1.3 Tie Bar Layout</b> .....	<b>15</b>
<b>2.2.1.4 Base Type</b> .....	<b>16</b>
<b>2.2.2 Materials</b> .....	<b>17</b>
<b>2.2.2.1 Portland Cement Concrete</b> .....	<b>17</b>
<b>2.2.3 Construction</b> .....	<b>18</b>

2.2.3.1	<b>Built in Construction Gradient.....</b>	<b>18</b>
2.2.3.2	<b>Zero-Stress Temperature .....</b>	<b>19</b>
2.2.3.3	<b>Construction Sequence .....</b>	<b>19</b>
2.2.3.4	<b>Mortar Intrusion.....</b>	<b>20</b>
<b>3.0</b>	<b>PARAMETRIC STUDIES .....</b>	<b>21</b>
<b>3.1</b>	<b>INTRODUCTION .....</b>	<b>21</b>
<b>3.2</b>	<b>PARAMETRIC STUDIES.....</b>	<b>22</b>
3.2.1	<b>Longitudinal Shear Cracking.....</b>	<b>22</b>
3.2.2	<b>Shoulder Transverse Cracking.....</b>	<b>24</b>
<b>3.3</b>	<b>LONGITUDINAL SHEAR CRACKING MODEL .....</b>	<b>26</b>
3.3.1	<b>Overview.....</b>	<b>26</b>
3.3.2	<b>Parts and Material Properties .....</b>	<b>27</b>
3.3.2.1	<b>Inside 2-ft Shoulder Section .....</b>	<b>29</b>
3.3.2.2	<b>Outside 10-ft Shoulder Section .....</b>	<b>29</b>
3.3.2.3	<b>Mainline Section.....</b>	<b>29</b>
3.3.2.4	<b>Steel Section .....</b>	<b>29</b>
3.3.3	<b>Contact Interactions .....</b>	<b>29</b>
3.3.3.1	<b>Elastic Foundation .....</b>	<b>29</b>
3.3.3.2	<b>Surface-to-Surface Contact.....</b>	<b>30</b>
3.3.4	<b>Loading.....</b>	<b>32</b>
3.3.4.1	<b>Gravity Load .....</b>	<b>33</b>
3.3.4.2	<b>Temperature Load .....</b>	<b>33</b>
3.3.4.3	<b>Surface Traction.....</b>	<b>34</b>

3.3.5	Boundary Conditions .....	36
3.3.6	Mesh .....	38
3.4	<b>SHOULDER TRANSVERSE CRACKING MODEL.....</b>	<b>38</b>
3.4.1	Overview.....	38
3.4.2	Parts and Material Properties .....	39
3.4.2.1	Shoulder Section.....	41
3.4.2.2	Mainline Section .....	41
3.4.2.3	Steel Section .....	41
3.4.3	Contact Interactions .....	41
3.4.4	Loading.....	42
3.4.4.1	Gravity Load .....	42
3.4.4.2	Temperature Load .....	42
3.4.4.3	Surface Traction.....	42
3.4.5	Boundary Conditions .....	43
3.4.6	Mesh.....	43
3.5	<b>VALIDATION .....</b>	<b>44</b>
4.0	<b>PARAMETRIC STUDY RESULTS .....</b>	<b>47</b>
4.1	<b>LONGITUDINAL SHEAR CRACKING MODEL .....</b>	<b>48</b>
4.1.1	Construction Sequence.....	50
4.1.2	Coefficient of Thermal Expansion .....	54
4.1.3	Depth of Mortar Intrusion.....	56
4.1.4	Gradients .....	60
4.1.5	Overall Conclusions.....	66

<b>4.2</b>	<b>SHOULDER TRANSVERSE CRACKING MODEL.....</b>	<b>67</b>
4.2.1	Construction Sequence.....	67
4.2.2	Coefficient of Thermal Expansion .....	71
4.2.3	Shoulder Width.....	71
4.2.4	Stiffness.....	76
4.2.5	Gradients .....	77
4.2.6	Overall Conclusions.....	78
<b>5.0</b>	<b>CONCLUSIONS AND RECOMMENDATIONS.....</b>	<b>80</b>
<b>5.1</b>	<b>CONCLUSIONS .....</b>	<b>80</b>
5.1.1	General .....	80
5.1.2	Longitudinal Shear Cracking.....	81
5.1.3	Shoulder Transverse Cracking.....	82
<b>5.2</b>	<b>RECOMMENDATIONS .....</b>	<b>83</b>
<b>APPENDIX A</b>	<b>.....</b>	<b>84</b>
<b>APPENDIX B</b>	<b>.....</b>	<b>196</b>
<b>APPENDIX C</b>	<b>.....</b>	<b>297</b>
<b>APPENDIX D</b>	<b>.....</b>	<b>323</b>
<b>BIBLIOGRAPHY</b>	<b>.....</b>	<b>336</b>

## LIST OF TABLES

Table 2.1. Summary of compressive strengths and elastic moduli for each core. ....	13
Table 3.1. Combination of construction sequences critical to longitudinal shear cracking. ....	23
Table 3.2. Varied parameters not related to construction sequence for longitudinal shear cracking.....	24
Table 3.3. Combination of construction sequences critical to shoulder transverse cracking. ....	25
Table 3.4. Varied parameters not related to construction sequence for shoulder transverse cracking.....	25
Table 3.5. Material properties for longitudinal shear cracking model.....	28
Table 3.6. Material properties for shoulder transverse cracking model. ....	41
Table 4.1. Review of field observations for longitudinal shear cracking model. ....	53
Table 4.2. Guidelines for choosing appropriate construction sequence in Pennsylvania for longitudinal shear cracking. ....	54
Table 4.3. Typical coefficient of thermal expansion ranges for common aggregates and concrete (ARA Inc., ERES Consultants Division, 2004).....	55
Table 4.4. Summary of construction sequences simulated using gradients.....	60
Table 4.5. Guidelines for determining crack potential based on construction sequence and CTE. ....	70
Table 4.6. Temperature distributions for gradients used in shoulder transverse cracking model.	77

## LIST OF FIGURES

Figure 2.1. Typical crack pattern documented by the ACPA (copied from ACPA R&T Update).	5
Figure 2.2. Schematic of factors leading to cracking (copied from ACPA R&T Update).	6
Figure 2.3. Interstate 81, Franklin County pavement layout.	7
Figure 2.4. Typical longitudinal cracking pattern on Interstate 64 West Virginia.	10
Figure 2.5. Typical crack found in 2-ft shoulder at US 22 Clyde.	12
Figure 3.1. Overall view of longitudinal shear cracking model.	27
Figure 3.2. Overall view of parts that make up longitudinal shear cracking model.	28
Figure 3.3. Model of slab resting on Winkler foundation.	30
Figure 3.4. Definition of anchor point and local tangent plane for small sliding (ABAQUS/CAE, 2007).	31
Figure 3.5. Surface traction applied to bottom of slab to represent base.	35
Figure 3.6. Longitudinal shear cracking boundary conditions with no mortar intrusion.	37
Figure 3.7. Longitudinal shear cracking boundary conditions with mortar intrusion.	37
Figure 3.8. Overall view of shoulder transverse cracking model.	39
Figure 3.9. Overall view of parts that make up shoulder transverse cracking model.	40
Figure 3.10. Shoulder transverse cracking boundary conditions.	43
Figure 3.11. Predicted vs. measured strains for the top of the slab.	45
Figure 3.12. Predicted vs. measured strains for the middle of the slab.	46
Figure 3.13. Predicted vs. measured strains for the bottom of the slab.	46

Figure 4.1. Comparison of shear stresses and tensile stresses for longitudinal shear cracking model.....	50
Figure 4.2. Summary of construction sequence results for longitudinal shear cracking. ....	52
Figure 4.3. $T_D$ versus stress with no mortar intrusion in longitudinal shear cracking model. ....	53
Figure 4.4. Comparison of 3.5-in mortar intrusion and 7-in mortar intrusion for the longitudinal shear cracking model. ....	57
Figure 4.5. Close-up of lane-shoulder longitudinal joint where the mainline extends beyond the shoulder in longitudinal shear cracking model. ....	58
Figure 4.6. Close-up of lane-shoulder longitudinal joint with the shoulder removed for the longitudinal shear cracking model. ....	59
Figure 4.7. Overall view of lane-shoulder longitudinal joint with the shoulder removed for the longitudinal shear cracking model. ....	59
Figure 4.8. Summary of effect of positive and negative gradients in comparison to uniform temperature for longitudinal shear cracking model. ....	61
Figure 4.9. Observed error when using positive and negative gradients in ABAQUS. ....	62
Figure 4.10. Effect of positive and negative gradient throughout the depth of the mainline for $T_M=100^\circ\text{F}$ , $T_S=90^\circ\text{F}$ and $T_C=110^\circ\text{F}$ for longitudinal shear cracking model. ....	63
Figure 4.11. Effect of positive and negative gradient throughout the depth of the mainline for $T_M=80^\circ\text{F}$ , $T_S=70^\circ\text{F}$ and $T_C=90^\circ\text{F}$ for longitudinal shear cracking model. ....	63
Figure 4.12. Effect of positive and negative gradient throughout the depth of the mainline for $T_M=80^\circ\text{F}$ , $T_S=70^\circ\text{F}$ and $T_C=100^\circ\text{F}$ for longitudinal shear cracking model. ....	64
Figure 4.13. Effect of positive and negative gradient throughout the depth of the mainline for $T_M=90^\circ\text{F}$ , $T_S=80^\circ\text{F}$ and $T_C=100^\circ\text{F}$ for longitudinal shear cracking model. ....	64
Figure 4.14. Effect of positive and negative gradient throughout the depth of the mainline for $T_M=100^\circ\text{F}$ , $T_S=80^\circ\text{F}$ and $T_C=110^\circ\text{F}$ for longitudinal shear cracking model. ....	65
Figure 4.15. Effect of positive and negative gradient throughout the depth of the mainline for $T_M=90^\circ\text{F}$ , $T_S=70^\circ\text{F}$ and $T_C=100^\circ\text{F}$ for longitudinal shear cracking model. ....	65
Figure 4.16. Effect of positive and negative gradient throughout the depth of the mainline for $T_M=100^\circ\text{F}$ , $T_S=70^\circ\text{F}$ and $T_C=110^\circ\text{F}$ for longitudinal shear cracking model. ....	66
Figure 4.17. Critical value of $T_C$ for different CTE values with a trigger value of 450 psi. ....	69

Figure 4.18. Influence of shoulder width when $T_D=-20^\circ\text{F}$ and $T_A=30^\circ\text{F}$ for the shoulder transverse cracking model.....	72
Figure 4.19. Influence of shoulder width when $T_D=-10^\circ\text{F}$ and $T_A=60^\circ\text{F}$ for the shoulder transverse cracking model.....	73
Figure 4.20. Influence of shoulder width when $T_D=-30^\circ\text{F}$ and $T_A=50^\circ\text{F}$ for the shoulder transverse cracking model.....	74
Figure 4.21. Illustration of tensile stress concentration surrounding tie bars in shoulder transverse cracking model.....	75
Figure 4.22. Influence of concrete stiffness on the shoulder transverse cracking model. ....	76
Figure 4.23. Effect of gradients when $T_S = 110^\circ\text{F}$ in the shoulder transverse cracking model... ..	78
Figure A1. Longitudinal shear cracking model in which $T_M=100^\circ\text{F}$ , $T_S=70^\circ\text{F}$ , and $T_C=100^\circ\text{F}$ for a mortar intrusion of 0 in and a CTE of $4 \times 10^{-6}/^\circ\text{F}$ .....	84
Figure A2. Longitudinal shear cracking model in which $T_M=100^\circ\text{F}$ , $T_S=70^\circ\text{F}$ , and $T_C=110^\circ\text{F}$ for a mortar intrusion of 0 in and a CTE of $4 \times 10^{-6}/^\circ\text{F}$ .....	85
Figure A3. Longitudinal shear cracking model in which $T_M=100^\circ\text{F}$ , $T_S=70^\circ\text{F}$ , and $T_C=120^\circ\text{F}$ for a mortar intrusion of 0 in and a CTE of $4 \times 10^{-6}/^\circ\text{F}$ .....	85
Figure A4. Longitudinal shear cracking model in which $T_M=100^\circ\text{F}$ , $T_S=80^\circ\text{F}$ , and $T_C=100^\circ\text{F}$ for a mortar intrusion of 0 in and a CTE of $4 \times 10^{-6}/^\circ\text{F}$ .....	86
Figure A5. Longitudinal shear cracking model in which $T_M=100^\circ\text{F}$ , $T_S=80^\circ\text{F}$ , and $T_C=110^\circ\text{F}$ for a mortar intrusion of 0 in and a CTE of $4 \times 10^{-6}/^\circ\text{F}$ .....	86
Figure A6. Longitudinal shear cracking model in which $T_M=100^\circ\text{F}$ , $T_S=80^\circ\text{F}$ , and $T_C=120^\circ\text{F}$ for a mortar intrusion of 0 in and a CTE of $4 \times 10^{-6}/^\circ\text{F}$ .....	87
Figure A7. Longitudinal shear cracking model in which $T_M=100^\circ\text{F}$ , $T_S=90^\circ\text{F}$ , and $T_C=100^\circ\text{F}$ for a mortar intrusion of 0 in and a CTE of $4 \times 10^{-6}/^\circ\text{F}$ .....	87
Figure A8. Longitudinal shear cracking model in which $T_M=100^\circ\text{F}$ , $T_S=90^\circ\text{F}$ , and $T_C=110^\circ\text{F}$ for a mortar intrusion of 0 in and a CTE of $4 \times 10^{-6}/^\circ\text{F}$ .....	88
Figure A9. Longitudinal shear cracking model in which $T_M=110^\circ\text{F}$ , $T_S=100^\circ\text{F}$ , and $T_C=110^\circ\text{F}$ for a mortar intrusion of 0 in and a CTE of $4 \times 10^{-6}/^\circ\text{F}$ .....	88
Figure A10. Longitudinal shear cracking model in which $T_M=110^\circ\text{F}$ , $T_S=100^\circ\text{F}$ , and $T_C=120^\circ\text{F}$ for a mortar intrusion of 0 in and a CTE of $4 \times 10^{-6}/^\circ\text{F}$ . ....	89

Figure A11. Longitudinal shear cracking model in which $T_M=110^\circ\text{F}$ , $T_S=70^\circ\text{F}$ , and $T_C=110^\circ\text{F}$ for a mortar intrusion of 0 in and a CTE of $4 \times 10^{-6}/^\circ\text{F}$ .....	89
Figure A12. Longitudinal shear cracking model in which $T_M=110^\circ\text{F}$ , $T_S=70^\circ\text{F}$ , and $T_C=120^\circ\text{F}$ for a mortar intrusion of 0 in and a CTE of $4 \times 10^{-6}/^\circ\text{F}$ .....	90
Figure A13. Longitudinal shear cracking model in which $T_M=110^\circ\text{F}$ , $T_S=80^\circ\text{F}$ , and $T_C=110^\circ\text{F}$ for a mortar intrusion of 0 in and a CTE of $4 \times 10^{-6}/^\circ\text{F}$ .....	90
Figure A14. Longitudinal shear cracking model in which $T_M=110^\circ\text{F}$ , $T_S=80^\circ\text{F}$ , and $T_C=120^\circ\text{F}$ for a mortar intrusion of 0 in and a CTE of $4 \times 10^{-6}/^\circ\text{F}$ .....	91
Figure A15. Longitudinal shear cracking model in which $T_M=110^\circ\text{F}$ , $T_S=90^\circ\text{F}$ , and $T_C=110^\circ\text{F}$ for a mortar intrusion of 0 in and a CTE of $4 \times 10^{-6}/^\circ\text{F}$ .....	91
Figure A16. Longitudinal shear cracking model in which $T_M=110^\circ\text{F}$ , $T_S=90^\circ\text{F}$ , and $T_C=120^\circ\text{F}$ for a mortar intrusion of 0 in and a CTE of $4 \times 10^{-6}/^\circ\text{F}$ .....	92
Figure A17. Longitudinal shear cracking model in which $T_M=120^\circ\text{F}$ , $T_S=100^\circ\text{F}$ , and $T_C=120^\circ\text{F}$ for a mortar intrusion of 0 in and a CTE of $4 \times 10^{-6}/^\circ\text{F}$ .....	92
Figure A18. Longitudinal shear cracking model in which $T_M=120^\circ\text{F}$ , $T_S=110^\circ\text{F}$ , and $T_C=120^\circ\text{F}$ for a mortar intrusion of 0 in and a CTE of $4 \times 10^{-6}/^\circ\text{F}$ .....	93
Figure A19. Longitudinal shear cracking model in which $T_M=120^\circ\text{F}$ , $T_S=70^\circ\text{F}$ , and $T_C=120^\circ\text{F}$ for a mortar intrusion of 0 in and a CTE of $4 \times 10^{-6}/^\circ\text{F}$ .....	93
Figure A20. Longitudinal shear cracking model in which $T_M=120^\circ\text{F}$ , $T_S=80^\circ\text{F}$ , and $T_C=120^\circ\text{F}$ for a mortar intrusion of 0 in and a CTE of $4 \times 10^{-6}/^\circ\text{F}$ .....	94
Figure A21. Longitudinal shear cracking model in which $T_M=120^\circ\text{F}$ , $T_S=90^\circ\text{F}$ , and $T_C=120^\circ\text{F}$ for a mortar intrusion of 0 in and a CTE of $4 \times 10^{-6}/^\circ\text{F}$ .....	94
Figure A22. Longitudinal shear cracking model in which $T_M=80^\circ\text{F}$ , $T_S=70^\circ\text{F}$ , and $T_C=100^\circ\text{F}$ for a mortar intrusion of 0 in and a CTE of $4 \times 10^{-6}/^\circ\text{F}$ .....	95
Figure A23. Longitudinal shear cracking model in which $T_M=80^\circ\text{F}$ , $T_S=70^\circ\text{F}$ , and $T_C=110^\circ\text{F}$ for a mortar intrusion of 0 in and a CTE of $4 \times 10^{-6}/^\circ\text{F}$ .....	95
Figure A24. Longitudinal shear cracking model in which $T_M=80^\circ\text{F}$ , $T_S=70^\circ\text{F}$ , and $T_C=120^\circ\text{F}$ for a mortar intrusion of 0 in and a CTE of $4 \times 10^{-6}/^\circ\text{F}$ .....	96
Figure A25. Longitudinal shear cracking model in which $T_M=80^\circ\text{F}$ , $T_S=70^\circ\text{F}$ , and $T_C=80^\circ\text{F}$ for a mortar intrusion of 0 in and a CTE of $4 \times 10^{-6}/^\circ\text{F}$ .....	96

Figure A26. Longitudinal shear cracking model in which $T_M=80^\circ\text{F}$ , $T_S=70^\circ\text{F}$ , and $T_C=90^\circ\text{F}$ for a mortar intrusion of 0 in and a CTE of $4 \times 10^{-6}/^\circ\text{F}$ .....	97
Figure A27. Longitudinal shear cracking model in which $T_M=90^\circ\text{F}$ , $T_S=70^\circ\text{F}$ , and $T_C=100^\circ\text{F}$ for a mortar intrusion of 0 in and a CTE of $4 \times 10^{-6}/^\circ\text{F}$ .....	97
Figure A28. Longitudinal shear cracking model in which $T_M=90^\circ\text{F}$ , $T_S=70^\circ\text{F}$ , and $T_C=110^\circ\text{F}$ for a mortar intrusion of 0 in and a CTE of $4 \times 10^{-6}/^\circ\text{F}$ .....	98
Figure A29. Longitudinal shear cracking model in which $T_M=90^\circ\text{F}$ , $T_S=70^\circ\text{F}$ , and $T_C=120^\circ\text{F}$ for a mortar intrusion of 0 in and a CTE of $4 \times 10^{-6}/^\circ\text{F}$ .....	98
Figure A30. Longitudinal shear cracking model in which $T_M=90^\circ\text{F}$ , $T_S=70^\circ\text{F}$ , and $T_C=90^\circ\text{F}$ for a mortar intrusion of 0 in and a CTE of $4 \times 10^{-6}/^\circ\text{F}$ .....	99
Figure A31. Longitudinal shear cracking model in which $T_M=90^\circ\text{F}$ , $T_S=80^\circ\text{F}$ , and $T_C=100^\circ\text{F}$ for a mortar intrusion of 0 in and a CTE of $4 \times 10^{-6}/^\circ\text{F}$ .....	99
Figure A32. Longitudinal shear cracking model in which $T_M=90^\circ\text{F}$ , $T_S=80^\circ\text{F}$ , and $T_C=110^\circ\text{F}$ for a mortar intrusion of 0 in and a CTE of $4 \times 10^{-6}/^\circ\text{F}$ .....	100
Figure A33. Longitudinal shear cracking model in which $T_M=90^\circ\text{F}$ , $T_S=80^\circ\text{F}$ , and $T_C=120^\circ\text{F}$ for a mortar intrusion of 0 in and a CTE of $4 \times 10^{-6}/^\circ\text{F}$ .....	100
Figure A34. Longitudinal shear cracking model in which $T_M=90^\circ\text{F}$ , $T_S=80^\circ\text{F}$ , and $T_C=90^\circ\text{F}$ for a mortar intrusion of 0 in and a CTE of $4 \times 10^{-6}/^\circ\text{F}$ .....	101
Figure A35. Longitudinal shear cracking model in which $T_M=100^\circ\text{F}$ , $T_S=70^\circ\text{F}$ , and $T_C=100^\circ\text{F}$ for a mortar intrusion of 0 in and a CTE of $6.5 \times 10^{-6}/^\circ\text{F}$ .....	101
Figure A36. Longitudinal shear cracking model in which $T_M=100^\circ\text{F}$ , $T_S=70^\circ\text{F}$ , and $T_C=110^\circ\text{F}$ for a mortar intrusion of 0 in and a CTE of $6.5 \times 10^{-6}/^\circ\text{F}$ .....	102
Figure A37. Longitudinal shear cracking model in which $T_M=100^\circ\text{F}$ , $T_S=70^\circ\text{F}$ , and $T_C=120^\circ\text{F}$ for a mortar intrusion of 0 in and a CTE of $6.5 \times 10^{-6}/^\circ\text{F}$ .....	102
Figure A38. Longitudinal shear cracking model in which $T_M=100^\circ\text{F}$ , $T_S=80^\circ\text{F}$ , and $T_C=100^\circ\text{F}$ for a mortar intrusion of 0 in and a CTE of $6.5 \times 10^{-6}/^\circ\text{F}$ .....	103
Figure A39. Longitudinal shear cracking model in which $T_M=100^\circ\text{F}$ , $T_S=80^\circ\text{F}$ , and $T_C=110^\circ\text{F}$ for a mortar intrusion of 0 in and a CTE of $6.5 \times 10^{-6}/^\circ\text{F}$ .....	103
Figure A40. Longitudinal shear cracking model in which $T_M=100^\circ\text{F}$ , $T_S=80^\circ\text{F}$ , and $T_C=120^\circ\text{F}$ for a mortar intrusion of 0 in and a CTE of $6.5 \times 10^{-6}/^\circ\text{F}$ .....	104

Figure A41. Longitudinal shear cracking model in which $T_M=100^\circ\text{F}$ , $T_S=90^\circ\text{F}$ , and $T_C=100^\circ\text{F}$ for a mortar intrusion of 0 in and a CTE of $6.5 \times 10^{-6}/^\circ\text{F}$ .....	104
Figure A42. Longitudinal shear cracking model in which $T_M=100^\circ\text{F}$ , $T_S=90^\circ\text{F}$ , and $T_C=110^\circ\text{F}$ for a mortar intrusion of 0 in and a CTE of $6.5 \times 10^{-6}/^\circ\text{F}$ .....	105
Figure A43. Longitudinal shear cracking model in which $T_M=100^\circ\text{F}$ , $T_S=90^\circ\text{F}$ , and $T_C=120^\circ\text{F}$ for a mortar intrusion of 0 in and a CTE of $6.5 \times 10^{-6}/^\circ\text{F}$ .....	105
Figure A44. Longitudinal shear cracking model in which $T_M=110^\circ\text{F}$ , $T_S=100^\circ\text{F}$ , and $T_C=110^\circ\text{F}$ for a mortar intrusion of 0 in and a CTE of $6.5 \times 10^{-6}/^\circ\text{F}$ .....	106
Figure A45. Longitudinal shear cracking model in which $T_M=110^\circ\text{F}$ , $T_S=100^\circ\text{F}$ , and $T_C=120^\circ\text{F}$ for a mortar intrusion of 0 in and a CTE of $6.5 \times 10^{-6}/^\circ\text{F}$ .....	106
Figure A46. Longitudinal shear cracking model in which $T_M=110^\circ\text{F}$ , $T_S=70^\circ\text{F}$ , and $T_C=110^\circ\text{F}$ for a mortar intrusion of 0 in and a CTE of $6.5 \times 10^{-6}/^\circ\text{F}$ .....	107
Figure A47. Longitudinal shear cracking model in which $T_M=110^\circ\text{F}$ , $T_S=70^\circ\text{F}$ , and $T_C=120^\circ\text{F}$ for a mortar intrusion of 0 in and a CTE of $6.5 \times 10^{-6}/^\circ\text{F}$ .....	107
Figure A48. Longitudinal shear cracking model in which $T_M=110^\circ\text{F}$ , $T_S=80^\circ\text{F}$ , and $T_C=110^\circ\text{F}$ for a mortar intrusion of 0 in and a CTE of $6.5 \times 10^{-6}/^\circ\text{F}$ .....	108
Figure A49. Longitudinal shear cracking model in which $T_M=110^\circ\text{F}$ , $T_S=80^\circ\text{F}$ , and $T_C=120^\circ\text{F}$ for a mortar intrusion of 0 in and a CTE of $6.5 \times 10^{-6}/^\circ\text{F}$ .....	108
Figure A50. Longitudinal shear cracking model in which $T_M=110^\circ\text{F}$ , $T_S=90^\circ\text{F}$ , and $T_C=110^\circ\text{F}$ for a mortar intrusion of 0 in and a CTE of $6.5 \times 10^{-6}/^\circ\text{F}$ .....	109
Figure A51. Longitudinal shear cracking model in which $T_M=110^\circ\text{F}$ , $T_S=90^\circ\text{F}$ , and $T_C=120^\circ\text{F}$ for a mortar intrusion of 0 in and a CTE of $6.5 \times 10^{-6}/^\circ\text{F}$ .....	109
Figure A52. Longitudinal shear cracking model in which $T_M=120^\circ\text{F}$ , $T_S=100^\circ\text{F}$ , and $T_C=120^\circ\text{F}$ for a mortar intrusion of 0 in and a CTE of $6.5 \times 10^{-6}/^\circ\text{F}$ .....	110
Figure A53. Longitudinal shear cracking model in which $T_M=120^\circ\text{F}$ , $T_S=110^\circ\text{F}$ , and $T_C=120^\circ\text{F}$ for a mortar intrusion of 0 in and a CTE of $6.5 \times 10^{-6}/^\circ\text{F}$ .....	110
Figure A54. Longitudinal shear cracking model in which $T_M=120^\circ\text{F}$ , $T_S=70^\circ\text{F}$ , and $T_C=120^\circ\text{F}$ for a mortar intrusion of 0 in and a CTE of $6.5 \times 10^{-6}/^\circ\text{F}$ .....	111
Figure A55. Longitudinal shear cracking model in which $T_M=120^\circ\text{F}$ , $T_S=80^\circ\text{F}$ , and $T_C=120^\circ\text{F}$ for a mortar intrusion of 0 in and a CTE of $6.5 \times 10^{-6}/^\circ\text{F}$ .....	111

Figure A56. Longitudinal shear cracking model in which $T_M=120^\circ\text{F}$ , $T_S=90^\circ\text{F}$ , and $T_C=120^\circ\text{F}$ for a mortar intrusion of 0 in and a CTE of $6.5 \times 10^{-6}/^\circ\text{F}$ .....	112
Figure A57. Longitudinal shear cracking model in which $T_M=80^\circ\text{F}$ , $T_S=70^\circ\text{F}$ , and $T_C=100^\circ\text{F}$ for a mortar intrusion of 0 in and a CTE of $6.5 \times 10^{-6}/^\circ\text{F}$ .....	112
Figure A58. Longitudinal shear cracking model in which $T_M=80^\circ\text{F}$ , $T_S=70^\circ\text{F}$ , and $T_C=110^\circ\text{F}$ for a mortar intrusion of 0 in and a CTE of $6.5 \times 10^{-6}/^\circ\text{F}$ .....	113
Figure A59. Longitudinal shear cracking model in which $T_M=80^\circ\text{F}$ , $T_S=70^\circ\text{F}$ , and $T_C=120^\circ\text{F}$ for a mortar intrusion of 0 in and a CTE of $6.5 \times 10^{-6}/^\circ\text{F}$ .....	113
Figure A60. Longitudinal shear cracking model in which $T_M=80^\circ\text{F}$ , $T_S=70^\circ\text{F}$ , and $T_C=80^\circ\text{F}$ for a mortar intrusion of 0 in and a CTE of $6.5 \times 10^{-6}/^\circ\text{F}$ .....	114
Figure A61. Longitudinal shear cracking model in which $T_M=80^\circ\text{F}$ , $T_S=70^\circ\text{F}$ , and $T_C=90^\circ\text{F}$ for a mortar intrusion of 0 in and a CTE of $6.5 \times 10^{-6}/^\circ\text{F}$ .....	114
Figure A62. Longitudinal shear cracking model in which $T_M=90^\circ\text{F}$ , $T_S=70^\circ\text{F}$ , and $T_C=100^\circ\text{F}$ for a mortar intrusion of 0 in and a CTE of $6.5 \times 10^{-6}/^\circ\text{F}$ .....	115
Figure A63. Longitudinal shear cracking model in which $T_M=90^\circ\text{F}$ , $T_S=70^\circ\text{F}$ , and $T_C=110^\circ\text{F}$ for a mortar intrusion of 0 in and a CTE of $6.5 \times 10^{-6}/^\circ\text{F}$ .....	115
Figure A64. Longitudinal shear cracking model in which $T_M=90^\circ\text{F}$ , $T_S=70^\circ\text{F}$ , and $T_C=120^\circ\text{F}$ for a mortar intrusion of 0 in and a CTE of $6.5 \times 10^{-6}/^\circ\text{F}$ .....	116
Figure A65. Longitudinal shear cracking model in which $T_M=90^\circ\text{F}$ , $T_S=70^\circ\text{F}$ , and $T_C=90^\circ\text{F}$ for a mortar intrusion of 0 in and a CTE of $6.5 \times 10^{-6}/^\circ\text{F}$ .....	116
Figure A66. Longitudinal shear cracking model in which $T_M=90^\circ\text{F}$ , $T_S=80^\circ\text{F}$ , and $T_C=100^\circ\text{F}$ for a mortar intrusion of 0 in and a CTE of $6.5 \times 10^{-6}/^\circ\text{F}$ .....	117
Figure A67. Longitudinal shear cracking model in which $T_M=90^\circ\text{F}$ , $T_S=80^\circ\text{F}$ , and $T_C=110^\circ\text{F}$ for a mortar intrusion of 0 in and a CTE of $6.5 \times 10^{-6}/^\circ\text{F}$ .....	117
Figure A68. Longitudinal shear cracking model in which $T_M=90^\circ\text{F}$ , $T_S=80^\circ\text{F}$ , and $T_C=90^\circ\text{F}$ for a mortar intrusion of 0 in and a CTE of $6.5 \times 10^{-6}/^\circ\text{F}$ .....	118
Figure A69. Longitudinal shear cracking model in which $T_M=100^\circ\text{F}$ , $T_S=70^\circ\text{F}$ , and $T_C=100^\circ\text{F}$ for a mortar intrusion of 3.5 in and a CTE of $4 \times 10^{-6}/^\circ\text{F}$ .....	118
Figure A70. Longitudinal shear cracking model in which $T_M=100^\circ\text{F}$ , $T_S=70^\circ\text{F}$ , and $T_C=100^\circ\text{F}$ for a mortar intrusion of 3.5 in and a CTE of $4 \times 10^{-6}/^\circ\text{F}$ .....	119

Figure A71. Longitudinal shear cracking model in which $T_M=100^\circ\text{F}$ , $T_S=70^\circ\text{F}$ , and $T_C=120^\circ\text{F}$ for a mortar intrusion of 3.5 in and a CTE of $4 \times 10^{-6}/^\circ\text{F}$ .....	119
Figure A72. Longitudinal shear cracking model in which $T_M=100^\circ\text{F}$ , $T_S=80^\circ\text{F}$ , and $T_C=100^\circ\text{F}$ for a mortar intrusion of 3.5 in and a CTE of $4 \times 10^{-6}/^\circ\text{F}$ .....	120
Figure A73. Longitudinal shear cracking model in which $T_M=100^\circ\text{F}$ , $T_S=80^\circ\text{F}$ , and $T_C=120^\circ\text{F}$ for a mortar intrusion of 3.5 in and a CTE of $4 \times 10^{-6}/^\circ\text{F}$ .....	120
Figure A74. Longitudinal shear cracking model in which $T_M=100^\circ\text{F}$ , $T_S=80^\circ\text{F}$ , and $T_C=120^\circ\text{F}$ for a mortar intrusion of 3.5 in and a CTE of $4 \times 10^{-6}/^\circ\text{F}$ .....	121
Figure A75. Longitudinal shear cracking model in which $T_M=100^\circ\text{F}$ , $T_S=90^\circ\text{F}$ , and $T_C=100^\circ\text{F}$ for a mortar intrusion of 3.5 in and a CTE of $4 \times 10^{-6}/^\circ\text{F}$ .....	121
Figure A76. Longitudinal shear cracking model in which $T_M=100^\circ\text{F}$ , $T_S=90^\circ\text{F}$ , and $T_C=110^\circ\text{F}$ for a mortar intrusion of 3.5 in and a CTE of $4 \times 10^{-6}/^\circ\text{F}$ .....	122
Figure A77. Longitudinal shear cracking model in which $T_M=100^\circ\text{F}$ , $T_S=90^\circ\text{F}$ , and $T_C=120^\circ\text{F}$ for a mortar intrusion of 3.5 in and a CTE of $4 \times 10^{-6}/^\circ\text{F}$ .....	122
Figure A78. Longitudinal shear cracking model in which $T_M=110^\circ\text{F}$ , $T_S=100^\circ\text{F}$ , and $T_C=110^\circ\text{F}$ for a mortar intrusion of 3.5 in and a CTE of $4 \times 10^{-6}/^\circ\text{F}$ .....	123
Figure A79. Longitudinal shear cracking model in which $T_M=110^\circ\text{F}$ , $T_S=100^\circ\text{F}$ , and $T_C=120^\circ\text{F}$ for a mortar intrusion of 3.5 in and a CTE of $4 \times 10^{-6}/^\circ\text{F}$ .....	123
Figure A80. Longitudinal shear cracking model in which $T_M=110^\circ\text{F}$ , $T_S=70^\circ\text{F}$ , and $T_C=110^\circ\text{F}$ for a mortar intrusion of 3.5 in and a CTE of $4 \times 10^{-6}/^\circ\text{F}$ .....	124
Figure A81. Longitudinal shear cracking model in which $T_M=110^\circ\text{F}$ , $T_S=70^\circ\text{F}$ , and $T_C=120^\circ\text{F}$ for a mortar intrusion of 3.5 in and a CTE of $4 \times 10^{-6}/^\circ\text{F}$ .....	124
Figure A82. Longitudinal shear cracking model in which $T_M=110^\circ\text{F}$ , $T_S=80^\circ\text{F}$ , and $T_C=110^\circ\text{F}$ for a mortar intrusion of 3.5 in and a CTE of $4 \times 10^{-6}/^\circ\text{F}$ .....	125
Figure A83. Longitudinal shear cracking model in which $T_M=110^\circ\text{F}$ , $T_S=80^\circ\text{F}$ , and $T_C=120^\circ\text{F}$ for a mortar intrusion of 3.5 in and a CTE of $4 \times 10^{-6}/^\circ\text{F}$ .....	125
Figure A84. Longitudinal shear cracking model in which $T_M=110^\circ\text{F}$ , $T_S=90^\circ\text{F}$ , and $T_C=110^\circ\text{F}$ for a mortar intrusion of 3.5 in and a CTE of $4 \times 10^{-6}/^\circ\text{F}$ .....	126
Figure A85. Longitudinal shear cracking model in which $T_M=110^\circ\text{F}$ , $T_S=90^\circ\text{F}$ , and $T_C=120^\circ\text{F}$ for a mortar intrusion of 3.5 in and a CTE of $4 \times 10^{-6}/^\circ\text{F}$ .....	126

Figure A86. Longitudinal shear cracking model in which $T_M=120^\circ\text{F}$ , $T_S=100^\circ\text{F}$ , and $T_C=120^\circ\text{F}$ for a mortar intrusion of 3.5 in and a CTE of $4 \times 10^{-6}/^\circ\text{F}$ .	127
Figure A87. Longitudinal shear cracking model in which $T_M=120^\circ\text{F}$ , $T_S=110^\circ\text{F}$ , and $T_C=120^\circ\text{F}$ for a mortar intrusion of 3.5 in and a CTE of $4 \times 10^{-6}/^\circ\text{F}$ .	127
Figure A88. Longitudinal shear cracking model in which $T_M=120^\circ\text{F}$ , $T_S=70^\circ\text{F}$ , and $T_C=120^\circ\text{F}$ for a mortar intrusion of 3.5 in and a CTE of $4 \times 10^{-6}/^\circ\text{F}$ .	128
Figure A89. Longitudinal shear cracking model in which $T_M=120^\circ\text{F}$ , $T_S=80^\circ\text{F}$ , and $T_C=120^\circ\text{F}$ for a mortar intrusion of 3.5 in and a CTE of $4 \times 10^{-6}/^\circ\text{F}$ .	128
Figure A90. Longitudinal shear cracking model in which $T_M=120^\circ\text{F}$ , $T_S=90^\circ\text{F}$ , and $T_C=120^\circ\text{F}$ for a mortar intrusion of 3.5 in and a CTE of $4 \times 10^{-6}/^\circ\text{F}$ .	129
Figure A91. Longitudinal shear cracking model in which $T_M=80^\circ\text{F}$ , $T_S=70^\circ\text{F}$ , and $T_C=100^\circ\text{F}$ for a mortar intrusion of 3.5 in and a CTE of $4 \times 10^{-6}/^\circ\text{F}$ .	129
Figure A92. Longitudinal shear cracking model in which $T_M=80^\circ\text{F}$ , $T_S=70^\circ\text{F}$ , and $T_C=110^\circ\text{F}$ for a mortar intrusion of 3.5 in and a CTE of $4 \times 10^{-6}/^\circ\text{F}$ .	130
Figure A93. Longitudinal shear cracking model in which $T_M=80^\circ\text{F}$ , $T_S=70^\circ\text{F}$ , and $T_C=120^\circ\text{F}$ for a mortar intrusion of 3.5 in and a CTE of $4 \times 10^{-6}/^\circ\text{F}$ .	130
Figure A94. Longitudinal shear cracking model in which $T_M=80^\circ\text{F}$ , $T_S=70^\circ\text{F}$ , and $T_C=80^\circ\text{F}$ for a mortar intrusion of 3.5 in and a CTE of $4 \times 10^{-6}/^\circ\text{F}$ .	131
Figure A95. Longitudinal shear cracking model in which $T_M=80^\circ\text{F}$ , $T_S=70^\circ\text{F}$ , and $T_C=90^\circ\text{F}$ for a mortar intrusion of 3.5 in and a CTE of $4 \times 10^{-6}/^\circ\text{F}$ .	131
Figure A96. Longitudinal shear cracking model in which $T_M=90^\circ\text{F}$ , $T_S=70^\circ\text{F}$ , and $T_C=100^\circ\text{F}$ for a mortar intrusion of 3.5 in and a CTE of $4 \times 10^{-6}/^\circ\text{F}$ .	132
Figure A97. Longitudinal shear cracking model in which $T_M=90^\circ\text{F}$ , $T_S=70^\circ\text{F}$ , and $T_C=110^\circ\text{F}$ for a mortar intrusion of 3.5 in and a CTE of $4 \times 10^{-6}/^\circ\text{F}$ .	132
Figure A98. Longitudinal shear cracking model in which $T_M=90^\circ\text{F}$ , $T_S=70^\circ\text{F}$ , and $T_C=120^\circ\text{F}$ for a mortar intrusion of 3.5 in and a CTE of $4 \times 10^{-6}/^\circ\text{F}$ .	133
Figure A99. Longitudinal shear cracking model in which $T_M=90^\circ\text{F}$ , $T_S=70^\circ\text{F}$ , and $T_C=90^\circ\text{F}$ for a mortar intrusion of 3.5 in and a CTE of $4 \times 10^{-6}/^\circ\text{F}$ .	133
Figure A100. Longitudinal shear cracking model in which $T_M=90^\circ\text{F}$ , $T_S=80^\circ\text{F}$ , and $T_C=100^\circ\text{F}$ for a mortar intrusion of 3.5 in and a CTE of $4 \times 10^{-6}/^\circ\text{F}$ .	134

Figure A101. Longitudinal shear cracking model in which  $T_M=90^\circ\text{F}$ ,  $T_S=80^\circ\text{F}$ , and  $T_C=110^\circ\text{F}$  for a mortar intrusion of 3.5 in and a CTE of  $4 \times 10^{-6}/^\circ\text{F}$ . ..... 134

Figure A102. Longitudinal shear cracking model in which  $T_M=90^\circ\text{F}$ ,  $T_S=80^\circ\text{F}$ , and  $T_C=120^\circ\text{F}$  for a mortar intrusion of 3.5 in and a CTE of  $4 \times 10^{-6}/^\circ\text{F}$ . ..... 135

Figure A103. Longitudinal shear cracking model in which  $T_M=90^\circ\text{F}$ ,  $T_S=80^\circ\text{F}$ , and  $T_C=90^\circ\text{F}$  for a mortar intrusion of 3.5 in and a CTE of  $4 \times 10^{-6}/^\circ\text{F}$ . ..... 135

Figure A104. Longitudinal shear cracking model in which  $T_M=100^\circ\text{F}$ ,  $T_S=70^\circ\text{F}$ , and  $T_C=100^\circ\text{F}$  for a mortar intrusion of 3.5 in and a CTE of  $6.5 \times 10^{-6}/^\circ\text{F}$ . ..... 136

Figure A105. Longitudinal shear cracking model in which  $T_M=100^\circ\text{F}$ ,  $T_S=70^\circ\text{F}$ , and  $T_C=110^\circ\text{F}$  for a mortar intrusion of 3.5 in and a CTE of  $6.5 \times 10^{-6}/^\circ\text{F}$ . ..... 136

Figure A106. Longitudinal shear cracking model in which  $T_M=100^\circ\text{F}$ ,  $T_S=70^\circ\text{F}$ , and  $T_C=120^\circ\text{F}$  for a mortar intrusion of 3.5 in and a CTE of  $6.5 \times 10^{-6}/^\circ\text{F}$ . ..... 137

Figure A107. Longitudinal shear cracking model in which  $T_M=100^\circ\text{F}$ ,  $T_S=80^\circ\text{F}$ , and  $T_C=100^\circ\text{F}$  for a mortar intrusion of 3.5 in and a CTE of  $6.5 \times 10^{-6}/^\circ\text{F}$ . ..... 137

Figure A108. Longitudinal shear cracking model in which  $T_M=100^\circ\text{F}$ ,  $T_S=80^\circ\text{F}$ , and  $T_C=110^\circ\text{F}$  for a mortar intrusion of 3.5 in and a CTE of  $6.5 \times 10^{-6}/^\circ\text{F}$ . ..... 138

Figure A109. Longitudinal shear cracking model in which  $T_M=100^\circ\text{F}$ ,  $T_S=80^\circ\text{F}$ , and  $T_C=120^\circ\text{F}$  for a mortar intrusion of 3.5 in and a CTE of  $6.5 \times 10^{-6}/^\circ\text{F}$ . ..... 138

Figure A110. Longitudinal shear cracking model in which  $T_M=100^\circ\text{F}$ ,  $T_S=90^\circ\text{F}$ , and  $T_C=100^\circ\text{F}$  for a mortar intrusion of 3.5 in and a CTE of  $6.5 \times 10^{-6}/^\circ\text{F}$ . ..... 139

Figure A111. Longitudinal shear cracking model in which  $T_M=100^\circ\text{F}$ ,  $T_S=90^\circ\text{F}$ , and  $T_C=110^\circ\text{F}$  for a mortar intrusion of 3.5 in and a CTE of  $6.5 \times 10^{-6}/^\circ\text{F}$ . ..... 139

Figure A112. Longitudinal shear cracking model in which  $T_M=100^\circ\text{F}$ ,  $T_S=90^\circ\text{F}$ , and  $T_C=120^\circ\text{F}$  for a mortar intrusion of 3.5 in and a CTE of  $6.5 \times 10^{-6}/^\circ\text{F}$ . ..... 140

Figure A113. Longitudinal shear cracking model in which  $T_M=110^\circ\text{F}$ ,  $T_S=100^\circ\text{F}$ , and  $T_C=110^\circ\text{F}$  for a mortar intrusion of 3.5 in and a CTE of  $6.5 \times 10^{-6}/^\circ\text{F}$ . ..... 140

Figure A114. Longitudinal shear cracking model in which  $T_M=110^\circ\text{F}$ ,  $T_S=70^\circ\text{F}$ , and  $T_C=110^\circ\text{F}$  for a mortar intrusion of 3.5 in and a CTE of  $6.5 \times 10^{-6}/^\circ\text{F}$ . ..... 141

Figure A115. Longitudinal shear cracking model in which  $T_M=110^\circ\text{F}$ ,  $T_S=70^\circ\text{F}$ , and  $T_C=120^\circ\text{F}$  for a mortar intrusion of 3.5 in and a CTE of  $6.5 \times 10^{-6}/^\circ\text{F}$ . ..... 141

Figure A116. Longitudinal shear cracking model in which $T_M=110^\circ\text{F}$ , $T_S=80^\circ\text{F}$ , and $T_C=110^\circ\text{F}$ for a mortar intrusion of 3.5 in and a CTE of $6.5 \times 10^{-6}/^\circ\text{F}$ .	142
Figure A117. Longitudinal shear cracking model in which $T_M=110^\circ\text{F}$ , $T_S=80^\circ\text{F}$ , and $T_C=120^\circ\text{F}$ for a mortar intrusion of 3.5 in and a CTE of $6.5 \times 10^{-6}/^\circ\text{F}$ .	142
Figure A118. Longitudinal shear cracking model in which $T_M=110^\circ\text{F}$ , $T_S=90^\circ\text{F}$ , and $T_C=110^\circ\text{F}$ for a mortar intrusion of 3.5 in and a CTE of $6.5 \times 10^{-6}/^\circ\text{F}$ .	143
Figure A119. Longitudinal shear cracking model in which $T_M=110^\circ\text{F}$ , $T_S=90^\circ\text{F}$ , and $T_C=120^\circ\text{F}$ for a mortar intrusion of 3.5 in and a CTE of $6.5 \times 10^{-6}/^\circ\text{F}$ .	143
Figure A120. Longitudinal shear cracking model in which $T_M=120^\circ\text{F}$ , $T_S=100^\circ\text{F}$ , and $T_C=120^\circ\text{F}$ for a mortar intrusion of 3.5 in and a CTE of $6.5 \times 10^{-6}/^\circ\text{F}$ .	144
Figure A121. Longitudinal shear cracking model in which $T_M=120^\circ\text{F}$ , $T_S=110^\circ\text{F}$ , and $T_C=120^\circ\text{F}$ for a mortar intrusion of 3.5 in and a CTE of $6.5 \times 10^{-6}/^\circ\text{F}$ .	144
Figure A122. Longitudinal shear cracking model in which $T_M=120^\circ\text{F}$ , $T_S=70^\circ\text{F}$ , and $T_C=120^\circ\text{F}$ for a mortar intrusion of 3.5 in and a CTE of $6.5 \times 10^{-6}/^\circ\text{F}$ .	145
Figure A123. Longitudinal shear cracking model in which $T_M=120^\circ\text{F}$ , $T_S=80^\circ\text{F}$ , and $T_C=120^\circ\text{F}$ for a mortar intrusion of 3.5 in and a CTE of $6.5 \times 10^{-6}/^\circ\text{F}$ .	145
Figure A124. Longitudinal shear cracking model in which $T_M=120^\circ\text{F}$ , $T_S=90^\circ\text{F}$ , and $T_C=120^\circ\text{F}$ for a mortar intrusion of 3.5 in and a CTE of $6.5 \times 10^{-6}/^\circ\text{F}$ .	146
Figure A125. Longitudinal shear cracking model in which $T_M=80^\circ\text{F}$ , $T_S=70^\circ\text{F}$ , and $T_C=100^\circ\text{F}$ for a mortar intrusion of 3.5 in and a CTE of $6.5 \times 10^{-6}/^\circ\text{F}$ .	146
Figure A126. Longitudinal shear cracking model in which $T_M=80^\circ\text{F}$ , $T_S=70^\circ\text{F}$ , and $T_C=110^\circ\text{F}$ for a mortar intrusion of 3.5 in and a CTE of $6.5 \times 10^{-6}/^\circ\text{F}$ .	147
Figure A127. Longitudinal shear cracking model in which $T_M=80^\circ\text{F}$ , $T_S=70^\circ\text{F}$ , and $T_C=120^\circ\text{F}$ for a mortar intrusion of 3.5 in and a CTE of $6.5 \times 10^{-6}/^\circ\text{F}$ .	147
Figure A128. Longitudinal shear cracking model in which $T_M=80^\circ\text{F}$ , $T_S=70^\circ\text{F}$ , and $T_C=80^\circ\text{F}$ for a mortar intrusion of 3.5 in and a CTE of $6.5 \times 10^{-6}/^\circ\text{F}$ .	148
Figure A129. Longitudinal shear cracking model in which $T_M=80^\circ\text{F}$ , $T_S=70^\circ\text{F}$ , and $T_C=90^\circ\text{F}$ for a mortar intrusion of 3.5 in and a CTE of $6.5 \times 10^{-6}/^\circ\text{F}$ .	148
Figure A130. Longitudinal shear cracking model in which $T_M=90^\circ\text{F}$ , $T_S=70^\circ\text{F}$ , and $T_C=100^\circ\text{F}$ for a mortar intrusion of 3.5 in and a CTE of $6.5 \times 10^{-6}/^\circ\text{F}$ .	149

Figure A131. Longitudinal shear cracking model in which $T_M=90^\circ\text{F}$ , $T_S=70^\circ\text{F}$ , and $T_C=110^\circ\text{F}$ for a mortar intrusion of 3.5 in and a CTE of $6.5 \times 10^{-6}/^\circ\text{F}$ .....	149
Figure A132. Longitudinal shear cracking model in which $T_M=90^\circ\text{F}$ , $T_S=70^\circ\text{F}$ , and $T_C=120^\circ\text{F}$ for a mortar intrusion of 3.5 in and a CTE of $6.5 \times 10^{-6}/^\circ\text{F}$ .....	150
Figure A133. Longitudinal shear cracking model in which $T_M=90^\circ\text{F}$ , $T_S=70^\circ\text{F}$ , and $T_C=90^\circ\text{F}$ for a mortar intrusion of 3.5 in and a CTE of $6.5 \times 10^{-6}/^\circ\text{F}$ .....	150
Figure A134. Longitudinal shear cracking model in which $T_M=90^\circ\text{F}$ , $T_S=80^\circ\text{F}$ , and $T_C=100^\circ\text{F}$ for a mortar intrusion of 3.5 in and a CTE of $6.5 \times 10^{-6}/^\circ\text{F}$ .....	151
Figure A135. Longitudinal shear cracking model in which $T_M=90^\circ\text{F}$ , $T_S=80^\circ\text{F}$ , and $T_C=110^\circ\text{F}$ for a mortar intrusion of 3.5 in and a CTE of $6.5 \times 10^{-6}/^\circ\text{F}$ .....	151
Figure A136. Longitudinal shear cracking model in which $T_M=90^\circ\text{F}$ , $T_S=80^\circ\text{F}$ , and $T_C=120^\circ\text{F}$ for a mortar intrusion of 3.5 in and a CTE of $6.5 \times 10^{-6}/^\circ\text{F}$ .....	152
Figure A137. Longitudinal shear cracking model in which $T_M=90^\circ\text{F}$ , $T_S=80^\circ\text{F}$ , and $T_C=90^\circ\text{F}$ for a mortar intrusion of 3.5 in and a CTE of $6.5 \times 10^{-6}/^\circ\text{F}$ .....	152
Figure A138. Longitudinal shear cracking model in which $T_M=110^\circ\text{F}$ , $T_S=100^\circ\text{F}$ , and $T_C=120^\circ\text{F}$ for a mortar intrusion of 3.5 in and a CTE of $6.5 \times 10^{-6}/^\circ\text{F}$ .....	153
Figure A139. Longitudinal shear cracking model in which $T_M=80^\circ\text{F}$ , $T_S=70^\circ\text{F}$ , and $T_C=80^\circ\text{F}$ for a mortar intrusion of 7 in and a CTE of $4 \times 10^{-6}/^\circ\text{F}$ .....	153
Figure A140. Longitudinal shear cracking model in which $T_M=100^\circ\text{F}$ , $T_S=70^\circ\text{F}$ , and $T_C=100^\circ\text{F}$ for a mortar intrusion of 7 in and a CTE of $4 \times 10^{-6}/^\circ\text{F}$ .....	154
Figure A141. Longitudinal shear cracking model in which $T_M=100^\circ\text{F}$ , $T_S=70^\circ\text{F}$ , and $T_C=110^\circ\text{F}$ for a mortar intrusion of 7 in and a CTE of $4 \times 10^{-6}/^\circ\text{F}$ .....	154
Figure A142. Longitudinal shear cracking model in which $T_M=100^\circ\text{F}$ , $T_S=70^\circ\text{F}$ , and $T_C=120^\circ\text{F}$ for a mortar intrusion of 7 in and a CTE of $4 \times 10^{-6}/^\circ\text{F}$ .....	155
Figure A143. Longitudinal shear cracking model in which $T_M=100^\circ\text{F}$ , $T_S=80^\circ\text{F}$ , and $T_C=100^\circ\text{F}$ for a mortar intrusion of 7 in and a CTE of $4 \times 10^{-6}/^\circ\text{F}$ .....	155
Figure A144. Longitudinal shear cracking model in which $T_M=100^\circ\text{F}$ , $T_S=80^\circ\text{F}$ , and $T_C=110^\circ\text{F}$ for a mortar intrusion of 7 in and a CTE of $4 \times 10^{-6}/^\circ\text{F}$ .....	156
Figure A145. Longitudinal shear cracking model in which $T_M=100^\circ\text{F}$ , $T_S=80^\circ\text{F}$ , and $T_C=120^\circ\text{F}$ for a mortar intrusion of 7 in and a CTE of $4 \times 10^{-6}/^\circ\text{F}$ .....	156

Figure A146. Longitudinal shear cracking model in which $T_M=100^\circ\text{F}$ , $T_S=90^\circ\text{F}$ , and $T_C=100^\circ\text{F}$ for a mortar intrusion of 7 in and a CTE of $4 \times 10^{-6}/^\circ\text{F}$ . .....	157
Figure A147. Longitudinal shear cracking model in which $T_M=100^\circ\text{F}$ , $T_S=90^\circ\text{F}$ , and $T_C=110^\circ\text{F}$ for a mortar intrusion of 7 in and a CTE of $4 \times 10^{-6}/^\circ\text{F}$ . .....	157
Figure A148. Longitudinal shear cracking model in which $T_M=100^\circ\text{F}$ , $T_S=90^\circ\text{F}$ , and $T_C=120^\circ\text{F}$ for a mortar intrusion of 7 in and a CTE of $4 \times 10^{-6}/^\circ\text{F}$ . .....	158
Figure A149. Longitudinal shear cracking model in which $T_M=110^\circ\text{F}$ , $T_S=100^\circ\text{F}$ , and $T_C=110^\circ\text{F}$ for a mortar intrusion of 7 in and a CTE of $4 \times 10^{-6}/^\circ\text{F}$ . .....	158
Figure A150. Longitudinal shear cracking model in which $T_M=110^\circ\text{F}$ , $T_S=100^\circ\text{F}$ , and $T_C=120^\circ\text{F}$ for a mortar intrusion of 7 in and a CTE of $4 \times 10^{-6}/^\circ\text{F}$ . .....	159
Figure A151. Longitudinal shear cracking model in which $T_M=110^\circ\text{F}$ , $T_S=70^\circ\text{F}$ , and $T_C=110^\circ\text{F}$ for a mortar intrusion of 7 in and a CTE of $4 \times 10^{-6}/^\circ\text{F}$ . .....	159
Figure A152. Longitudinal shear cracking model in which $T_M=110^\circ\text{F}$ , $T_S=70^\circ\text{F}$ , and $T_C=120^\circ\text{F}$ for a mortar intrusion of 7 in and a CTE of $4 \times 10^{-6}/^\circ\text{F}$ . .....	160
Figure A153. Longitudinal shear cracking model in which $T_M=110^\circ\text{F}$ , $T_S=80^\circ\text{F}$ , and $T_C=110^\circ\text{F}$ for a mortar intrusion of 7 in and a CTE of $4 \times 10^{-6}/^\circ\text{F}$ . .....	160
Figure A154. Longitudinal shear cracking model in which $T_M=110^\circ\text{F}$ , $T_S=80^\circ\text{F}$ , and $T_C=120^\circ\text{F}$ for a mortar intrusion of 7 in and a CTE of $4 \times 10^{-6}/^\circ\text{F}$ . .....	161
Figure A155. Longitudinal shear cracking model in which $T_M=110^\circ\text{F}$ , $T_S=90^\circ\text{F}$ , and $T_C=110^\circ\text{F}$ for a mortar intrusion of 7 in and a CTE of $4 \times 10^{-6}/^\circ\text{F}$ . .....	161
Figure A156. Longitudinal shear cracking model in which $T_M=110^\circ\text{F}$ , $T_S=90^\circ\text{F}$ , and $T_C=120^\circ\text{F}$ for a mortar intrusion of 7 in and a CTE of $4 \times 10^{-6}/^\circ\text{F}$ . .....	162
Figure A157. Longitudinal shear cracking model in which $T_M=120^\circ\text{F}$ , $T_S=100^\circ\text{F}$ , and $T_C=120^\circ\text{F}$ for a mortar intrusion of 7 in and a CTE of $4 \times 10^{-6}/^\circ\text{F}$ . .....	162
Figure A158. Longitudinal shear cracking model in which $T_M=120^\circ\text{F}$ , $T_S=110^\circ\text{F}$ , and $T_C=120^\circ\text{F}$ for a mortar intrusion of 7 in and a CTE of $4 \times 10^{-6}/^\circ\text{F}$ . .....	163
Figure A159. Longitudinal shear cracking model in which $T_M=120^\circ\text{F}$ , $T_S=70^\circ\text{F}$ , and $T_C=120^\circ\text{F}$ for a mortar intrusion of 7 in and a CTE of $4 \times 10^{-6}/^\circ\text{F}$ . .....	163
Figure A160. Longitudinal shear cracking model in which $T_M=120^\circ\text{F}$ , $T_S=80^\circ\text{F}$ , and $T_C=120^\circ\text{F}$ for a mortar intrusion of 7 in and a CTE of $4 \times 10^{-6}/^\circ\text{F}$ . .....	164

Figure A161. Longitudinal shear cracking model in which $T_M=120^\circ\text{F}$ , $T_S=90^\circ\text{F}$ , and $T_C=120^\circ\text{F}$ for a mortar intrusion of 7 in and a CTE of $4 \times 10^{-6}/^\circ\text{F}$ .	164
Figure A162. Longitudinal shear cracking model in which $T_M=80^\circ\text{F}$ , $T_S=70^\circ\text{F}$ , and $T_C=100^\circ\text{F}$ for a mortar intrusion of 7 in and a CTE of $4 \times 10^{-6}/^\circ\text{F}$ .	165
Figure A163. Longitudinal shear cracking model in which $T_M=80^\circ\text{F}$ , $T_S=70^\circ\text{F}$ , and $T_C=110^\circ\text{F}$ for a mortar intrusion of 7 in and a CTE of $4 \times 10^{-6}/^\circ\text{F}$ .	165
Figure A164. Longitudinal shear cracking model in which $T_M=80^\circ\text{F}$ , $T_S=70^\circ\text{F}$ , and $T_C=120^\circ\text{F}$ for a mortar intrusion of 7 in and a CTE of $4 \times 10^{-6}/^\circ\text{F}$ .	166
Figure A165. Longitudinal shear cracking model in which $T_M=80^\circ\text{F}$ , $T_S=70^\circ\text{F}$ , and $T_C=90^\circ\text{F}$ for a mortar intrusion of 7 in and a CTE of $4 \times 10^{-6}/^\circ\text{F}$ .	166
Figure A166. Longitudinal shear cracking model in which $T_M=90^\circ\text{F}$ , $T_S=70^\circ\text{F}$ , and $T_C=100^\circ\text{F}$ for a mortar intrusion of 7 in and a CTE of $4 \times 10^{-6}/^\circ\text{F}$ .	167
Figure A167. Longitudinal shear cracking model in which $T_M=90^\circ\text{F}$ , $T_S=70^\circ\text{F}$ , and $T_C=110^\circ\text{F}$ for a mortar intrusion of 7 in and a CTE of $4 \times 10^{-6}/^\circ\text{F}$ .	167
Figure A168. Longitudinal shear cracking model in which $T_M=90^\circ\text{F}$ , $T_S=70^\circ\text{F}$ , and $T_C=120^\circ\text{F}$ for a mortar intrusion of 7 in and a CTE of $4 \times 10^{-6}/^\circ\text{F}$ .	168
Figure A169. Longitudinal shear cracking model in which $T_M=90^\circ\text{F}$ , $T_S=70^\circ\text{F}$ , and $T_C=90^\circ\text{F}$ for a mortar intrusion of 7 in and a CTE of $4 \times 10^{-6}/^\circ\text{F}$ .	168
Figure A170. Longitudinal shear cracking model in which $T_M=90^\circ\text{F}$ , $T_S=80^\circ\text{F}$ , and $T_C=100^\circ\text{F}$ for a mortar intrusion of 7 in and a CTE of $4 \times 10^{-6}/^\circ\text{F}$ .	169
Figure A171. Longitudinal shear cracking model in which $T_M=90^\circ\text{F}$ , $T_S=80^\circ\text{F}$ , and $T_C=110^\circ\text{F}$ for a mortar intrusion of 7 in and a CTE of $4 \times 10^{-6}/^\circ\text{F}$ .	169
Figure A172. Longitudinal shear cracking model in which $T_M=90^\circ\text{F}$ , $T_S=80^\circ\text{F}$ , and $T_C=120^\circ\text{F}$ for a mortar intrusion of 7 in and a CTE of $4 \times 10^{-6}/^\circ\text{F}$ .	170
Figure A173. Longitudinal shear cracking model in which $T_M=90^\circ\text{F}$ , $T_S=80^\circ\text{F}$ , and $T_C=90^\circ\text{F}$ for a mortar intrusion of 7 in and a CTE of $4 \times 10^{-6}/^\circ\text{F}$ .	170
Figure A174. Longitudinal shear cracking model in which $T_M=100^\circ\text{F}$ , $T_S=70^\circ\text{F}$ , and $T_C=100^\circ\text{F}$ for a mortar intrusion of 7 in and a CTE of $6.5 \times 10^{-6}/^\circ\text{F}$ .	171
Figure A175. Longitudinal shear cracking model in which $T_M=100^\circ\text{F}$ , $T_S=70^\circ\text{F}$ , and $T_C=110^\circ\text{F}$ for a mortar intrusion of 7 in and a CTE of $6.5 \times 10^{-6}/^\circ\text{F}$ .	171

Figure A176. Longitudinal shear cracking model in which $T_M=100^\circ\text{F}$ , $T_S=70^\circ\text{F}$ , and $T_C=120^\circ\text{F}$ for a mortar intrusion of 7 in and a CTE of $6.5 \times 10^{-6}/^\circ\text{F}$ .	172
Figure A177. Longitudinal shear cracking model in which $T_M=100^\circ\text{F}$ , $T_S=80^\circ\text{F}$ , and $T_C=100^\circ\text{F}$ for a mortar intrusion of 7 in and a CTE of $6.5 \times 10^{-6}/^\circ\text{F}$ .	172
Figure A178. Longitudinal shear cracking model in which $T_M=100^\circ\text{F}$ , $T_S=80^\circ\text{F}$ , and $T_C=110^\circ\text{F}$ for a mortar intrusion of 7 in and a CTE of $6.5 \times 10^{-6}/^\circ\text{F}$ .	173
Figure A179. Longitudinal shear cracking model in which $T_M=100^\circ\text{F}$ , $T_S=80^\circ\text{F}$ , and $T_C=120^\circ\text{F}$ for a mortar intrusion of 7 in and a CTE of $6.5 \times 10^{-6}/^\circ\text{F}$ .	173
Figure A180. Longitudinal shear cracking model in which $T_M=100^\circ\text{F}$ , $T_S=90^\circ\text{F}$ , and $T_C=100^\circ\text{F}$ for a mortar intrusion of 7 in and a CTE of $6.5 \times 10^{-6}/^\circ\text{F}$ .	174
Figure A181. Longitudinal shear cracking model in which $T_M=100^\circ\text{F}$ , $T_S=90^\circ\text{F}$ , and $T_C=110^\circ\text{F}$ for a mortar intrusion of 7 in and a CTE of $6.5 \times 10^{-6}/^\circ\text{F}$ .	174
Figure A182. Longitudinal shear cracking model in which $T_M=100^\circ\text{F}$ , $T_S=90^\circ\text{F}$ , and $T_C=120^\circ\text{F}$ for a mortar intrusion of 7 in and a CTE of $6.5 \times 10^{-6}/^\circ\text{F}$ .	175
Figure A183. Longitudinal shear cracking model in which $T_M=110^\circ\text{F}$ , $T_S=100^\circ\text{F}$ , and $T_C=110^\circ\text{F}$ for a mortar intrusion of 7 in and a CTE of $6.5 \times 10^{-6}/^\circ\text{F}$ .	175
Figure A184. Longitudinal shear cracking model in which $T_M=110^\circ\text{F}$ , $T_S=100^\circ\text{F}$ , and $T_C=120^\circ\text{F}$ for a mortar intrusion of 7 in and a CTE of $6.5 \times 10^{-6}/^\circ\text{F}$ .	176
Figure A185. Longitudinal shear cracking model in which $T_M=110^\circ\text{F}$ , $T_S=70^\circ\text{F}$ , and $T_C=110^\circ\text{F}$ for a mortar intrusion of 7 in and a CTE of $6.5 \times 10^{-6}/^\circ\text{F}$ .	176
Figure A186. Longitudinal shear cracking model in which $T_M=110^\circ\text{F}$ , $T_S=70^\circ\text{F}$ , and $T_C=120^\circ\text{F}$ for a mortar intrusion of 7 in and a CTE of $6.5 \times 10^{-6}/^\circ\text{F}$ .	177
Figure A187. Longitudinal shear cracking model in which $T_M=110^\circ\text{F}$ , $T_S=80^\circ\text{F}$ , and $T_C=110^\circ\text{F}$ for a mortar intrusion of 7 in and a CTE of $6.5 \times 10^{-6}/^\circ\text{F}$ .	177
Figure A188. Longitudinal shear cracking model in which $T_M=110^\circ\text{F}$ , $T_S=80^\circ\text{F}$ , and $T_C=120^\circ\text{F}$ for a mortar intrusion of 7 in and a CTE of $6.5 \times 10^{-6}/^\circ\text{F}$ .	178
Figure A189. Longitudinal shear cracking model in which $T_M=110^\circ\text{F}$ , $T_S=90^\circ\text{F}$ , and $T_C=110^\circ\text{F}$ for a mortar intrusion of 7 in and a CTE of $6.5 \times 10^{-6}/^\circ\text{F}$ .	178
Figure A190. Longitudinal shear cracking model in which $T_M=110^\circ\text{F}$ , $T_S=90^\circ\text{F}$ , and $T_C=120^\circ\text{F}$ for a mortar intrusion of 7 in and a CTE of $6.5 \times 10^{-6}/^\circ\text{F}$ .	179

Figure A191. Longitudinal shear cracking model in which $T_M=120^\circ\text{F}$ , $T_S=100^\circ\text{F}$ , and $T_C=120^\circ\text{F}$ for a mortar intrusion of 7 in and a CTE of $6.5 \times 10^{-6}/^\circ\text{F}$ .	179
Figure A192. Longitudinal shear cracking model in which $T_M=120^\circ\text{F}$ , $T_S=110^\circ\text{F}$ , and $T_C=120^\circ\text{F}$ for a mortar intrusion of 7 in and a CTE of $6.5 \times 10^{-6}/^\circ\text{F}$ .	180
Figure A193. Longitudinal shear cracking model in which $T_M=120^\circ\text{F}$ , $T_S=70^\circ\text{F}$ , and $T_C=120^\circ\text{F}$ for a mortar intrusion of 7 in and a CTE of $6.5 \times 10^{-6}/^\circ\text{F}$ .	180
Figure A194. Longitudinal shear cracking model in which $T_M=120^\circ\text{F}$ , $T_S=80^\circ\text{F}$ , and $T_C=120^\circ\text{F}$ for a mortar intrusion of 7 in and a CTE of $6.5 \times 10^{-6}/^\circ\text{F}$ .	181
Figure A195. Longitudinal shear cracking model in which $T_M=120^\circ\text{F}$ , $T_S=90^\circ\text{F}$ , and $T_C=120^\circ\text{F}$ for a mortar intrusion of 7 in and a CTE of $6.5 \times 10^{-6}/^\circ\text{F}$ .	181
Figure A196. Longitudinal shear cracking model in which $T_M=80^\circ\text{F}$ , $T_S=70^\circ\text{F}$ , and $T_C=100^\circ\text{F}$ for a mortar intrusion of 7 in and a CTE of $6.5 \times 10^{-6}/^\circ\text{F}$ .	182
Figure A197. Longitudinal shear cracking model in which $T_M=80^\circ\text{F}$ , $T_S=70^\circ\text{F}$ , and $T_C=110^\circ\text{F}$ for a mortar intrusion of 7 in and a CTE of $6.5 \times 10^{-6}/^\circ\text{F}$ .	182
Figure A198. Longitudinal shear cracking model in which $T_M=80^\circ\text{F}$ , $T_S=70^\circ\text{F}$ , and $T_C=120^\circ\text{F}$ for a mortar intrusion of 7 in and a CTE of $6.5 \times 10^{-6}/^\circ\text{F}$ .	183
Figure A199. Longitudinal shear cracking model in which $T_M=80^\circ\text{F}$ , $T_S=70^\circ\text{F}$ , and $T_C=80^\circ\text{F}$ for a mortar intrusion of 7 in and a CTE of $6.5 \times 10^{-6}/^\circ\text{F}$ .	183
Figure A200. Longitudinal shear cracking model in which $T_M=0^\circ\text{F}$ , $T_S=70^\circ\text{F}$ , and $T_C=90^\circ\text{F}$ for a mortar intrusion of 7 in and a CTE of $6.5 \times 10^{-6}/^\circ\text{F}$ .	184
Figure A201. Longitudinal shear cracking model in which $T_M=90^\circ\text{F}$ , $T_S=70^\circ\text{F}$ , and $T_C=100^\circ\text{F}$ for a mortar intrusion of 7 in and a CTE of $6.5 \times 10^{-6}/^\circ\text{F}$ .	184
Figure A202. Longitudinal shear cracking model in which $T_M=90^\circ\text{F}$ , $T_S=70^\circ\text{F}$ , and $T_C=110^\circ\text{F}$ for a mortar intrusion of 7 in and a CTE of $6.5 \times 10^{-6}/^\circ\text{F}$ .	185
Figure A203. Longitudinal shear cracking model in which $T_M=90^\circ\text{F}$ , $T_S=70^\circ\text{F}$ , and $T_C=120^\circ\text{F}$ for a mortar intrusion of 7 in and a CTE of $6.5 \times 10^{-6}/^\circ\text{F}$ .	185
Figure A204. Longitudinal shear cracking model in which $T_M=90^\circ\text{F}$ , $T_S=70^\circ\text{F}$ , and $T_C=90^\circ\text{F}$ for a mortar intrusion of 7 in and a CTE of $6.5 \times 10^{-6}/^\circ\text{F}$ .	186
Figure A205. Longitudinal shear cracking model in which $T_M=90^\circ\text{F}$ , $T_S=80^\circ\text{F}$ , and $T_C=100^\circ\text{F}$ for a mortar intrusion of 7 in and a CTE of $6.5 \times 10^{-6}/^\circ\text{F}$ .	186

Figure A206. Longitudinal shear cracking model in which $T_M=90^\circ\text{F}$ , $T_S=80^\circ\text{F}$ , and $T_C=110^\circ\text{F}$ for a mortar intrusion of 7 in and a CTE of $6.5 \times 10^{-6}/^\circ\text{F}$ .	187
Figure A207. Longitudinal shear cracking model in which $T_M=90^\circ\text{F}$ , $T_S=80^\circ\text{F}$ , and $T_C=120^\circ\text{F}$ for a mortar intrusion of 7 in and a CTE of $6.5 \times 10^{-6}/^\circ\text{F}$ .	187
Figure A208. Longitudinal shear cracking model in which $T_M=90^\circ\text{F}$ , $T_S=80^\circ\text{F}$ , and $T_C=90^\circ\text{F}$ for a mortar intrusion of 7 in and a CTE of $6.5 \times 10^{-6}/^\circ\text{F}$ .	188
Figure A209. Longitudinal shear cracking model in which $T_M=100^\circ\text{F}$ , $T_S=70^\circ\text{F}$ , and $T_C$ =positive 1.37 gradient with a $110^\circ\text{F}$ weighted average for a mortar intrusion of 3.5 in and a CTE of $6.5 \times 10^{-6}/^\circ\text{F}$ .	188
Figure A210. Longitudinal shear cracking model in which $T_M=100^\circ\text{F}$ , $T_S=70^\circ\text{F}$ , and $T_C$ =negative 1.37 gradient with a $110^\circ\text{F}$ weighted average for a mortar intrusion of 3.5 in and a CTE of $6.5 \times 10^{-6}/^\circ\text{F}$ .	189
Figure A211. Longitudinal shear cracking model in which $T_M=100^\circ\text{F}$ , $T_S=80^\circ\text{F}$ , and $T_C$ =positive 1.37 gradient with a $110^\circ\text{F}$ weighted average for a mortar intrusion of 3.5 in and a CTE of $6.5 \times 10^{-6}/^\circ\text{F}$ .	189
Figure A212. Longitudinal shear cracking model in which $T_M=100^\circ\text{F}$ , $T_S=80^\circ\text{F}$ , and $T_C$ =negative 1.37 gradient with a $110^\circ\text{F}$ weighted average for a mortar intrusion of 3.5 in and a CTE of $6.5 \times 10^{-6}/^\circ\text{F}$ .	190
Figure A213. Longitudinal shear cracking model in which $T_M=100^\circ\text{F}$ , $T_S=90^\circ\text{F}$ , and $T_C$ =positive 1.37 gradient with a $110^\circ\text{F}$ weighted average for a mortar intrusion of 3.5 in and a CTE of $6.5 \times 10^{-6}/^\circ\text{F}$ .	190
Figure A214. Longitudinal shear cracking model in which $T_M=100^\circ\text{F}$ , $T_S=90^\circ\text{F}$ , and $T_C$ =negative 1.37 gradient with a $110^\circ\text{F}$ weighted average for a mortar intrusion of 3.5 in and a CTE of $6.5 \times 10^{-6}/^\circ\text{F}$ .	191
Figure A215. Longitudinal shear cracking model in which $T_M=80^\circ\text{F}$ , $T_S=70^\circ\text{F}$ , and $T_C$ =positive 1.37 gradient with a $100^\circ\text{F}$ weighted average for a mortar intrusion of 3.5 in and a CTE of $6.5 \times 10^{-6}/^\circ\text{F}$ .	191
Figure A216. Longitudinal shear cracking model in which $T_M=80^\circ\text{F}$ , $T_S=70^\circ\text{F}$ , and $T_C$ =positive 1.37 gradient with a $90^\circ\text{F}$ weighted average for a mortar intrusion of 3.5 in and a CTE of $6.5 \times 10^{-6}/^\circ\text{F}$ .	192
Figure A217. Longitudinal shear cracking model in which $T_M=80^\circ\text{F}$ , $T_S=70^\circ\text{F}$ , and $T_C$ =negative 1.37 gradient with a $100^\circ\text{F}$ weighted average for a mortar intrusion of 3.5 in and a CTE of $6.5 \times 10^{-6}/^\circ\text{F}$ .	192

Figure A218. Longitudinal shear cracking model in which $T_M=80^\circ\text{F}$ , $T_S=70^\circ\text{F}$ , and $T_C=\text{negative}$ 1.37 gradient with a $90^\circ\text{F}$ weighted average for a mortar intrusion of 3.5 in and a CTE of $6.5 \times 10^{-6}/^\circ\text{F}$ .	193
Figure A219. Longitudinal shear cracking model in which $T_M=90^\circ\text{F}$ , $T_S=70^\circ\text{F}$ , and $T_C=\text{positive}$ 1.37 gradient with a $100^\circ\text{F}$ weighted average for a mortar intrusion of 3.5 in and a CTE of $6.5 \times 10^{-6}/^\circ\text{F}$ .	193
Figure A220. Longitudinal shear cracking model in which $T_M=90^\circ\text{F}$ , $T_S=70^\circ\text{F}$ , and $T_C=\text{negative}$ 1.37 gradient with a $100^\circ\text{F}$ weighted average for a mortar intrusion of 3.5 in and a CTE of $6.5 \times 10^{-6}/^\circ\text{F}$ .	194
Figure A221. Longitudinal shear cracking model in which $T_M=90^\circ\text{F}$ , $T_S=80^\circ\text{F}$ , and $T_C=\text{positive}$ 1.37 gradient with a $100^\circ\text{F}$ weighted average for a mortar intrusion of 3.5 in and a CTE of $6.5 \times 10^{-6}/^\circ\text{F}$ .	194
Figure A222. Longitudinal shear cracking model in which $T_M=90^\circ\text{F}$ , $T_S=80^\circ\text{F}$ , and $T_C=\text{negative}$ 1.37 gradient with a $100^\circ\text{F}$ weighted average for a mortar intrusion of 3.5 in and a CTE of $6.5 \times 10^{-6}/^\circ\text{F}$ .	195
Figure B1. 10-ft shoulder transverse cracking model where $T_M=80^\circ\text{F}$ , $T_S=100^\circ\text{F}$ , and $T_C=50^\circ\text{F}$ , for a CTE of $4.5 \times 10^{-6}/^\circ\text{F}$ and a stiffness of $2.8 \times 10^6$ psi.	196
Figure B2. 10-ft shoulder transverse cracking model where $T_M=80^\circ\text{F}$ , $T_S=100^\circ\text{F}$ , and $T_C=50^\circ\text{F}$ , for a CTE of $4.5 \times 10^{-6}/^\circ\text{F}$ and a stiffness of $3.3 \times 10^6$ psi.	197
Figure B3. 2-ft shoulder transverse cracking model where $T_M=80^\circ\text{F}$ , $T_S=100^\circ\text{F}$ , and $T_C=50^\circ\text{F}$ , for a CTE of $4.5 \times 10^{-6}/^\circ\text{F}$ and a stiffness of $2.8 \times 10^6$ psi.	197
Figure B4. 5-ft shoulder transverse cracking model where $T_M=80^\circ\text{F}$ , $T_S=100^\circ\text{F}$ , and $T_C=50^\circ\text{F}$ , for a CTE of $4.5 \times 10^{-6}/^\circ\text{F}$ and a stiffness of $2.8 \times 10^6$ psi.	198
Figure B5. 5-ft shoulder transverse cracking model where $T_M=80^\circ\text{F}$ , $T_S=100^\circ\text{F}$ , and $T_C=50^\circ\text{F}$ , for a CTE of $4.5 \times 10^{-6}/^\circ\text{F}$ and a stiffness of $3.3 \times 10^6$ psi.	198
Figure B6. 10-ft shoulder transverse cracking model where $T_M=80^\circ\text{F}$ , $T_S=100^\circ\text{F}$ , and $T_C=60^\circ\text{F}$ , for a CTE of $4.5 \times 10^{-6}/^\circ\text{F}$ and a stiffness of $2.8 \times 10^6$ psi.	199
Figure B7. 10-ft shoulder transverse cracking model where $T_M=80^\circ\text{F}$ , $T_S=100^\circ\text{F}$ , and $T_C=60^\circ\text{F}$ , for a CTE of $4.5 \times 10^{-6}/^\circ\text{F}$ and a stiffness of $3.3 \times 10^6$ psi.	199
Figure B8. 2-ft shoulder transverse cracking model where $T_M=80^\circ\text{F}$ , $T_S=100^\circ\text{F}$ , and $T_C=60^\circ\text{F}$ , for a CTE of $4.5 \times 10^{-6}/^\circ\text{F}$ and a stiffness of $2.8 \times 10^6$ psi.	200
Figure B9. 5-ft shoulder transverse cracking model where $T_M=80^\circ\text{F}$ , $T_S=100^\circ\text{F}$ , and $T_C=60^\circ\text{F}$ , for a CTE of $4.5 \times 10^{-6}/^\circ\text{F}$ and a stiffness of $2.8 \times 10^6$ psi.	200



Figure B25. 5-ft shoulder transverse cracking model where $T_M=80^\circ\text{F}$ , $T_S=110^\circ\text{F}$ , and $T_C=50^\circ\text{F}$ , for a CTE of $4.5 \times 10^{-6}/^\circ\text{F}$ and a stiffness of $2.8 \times 10^6$ psi.....	208
Figure B26. 5-ft shoulder transverse cracking model where $T_M=80^\circ\text{F}$ , $T_S=110^\circ\text{F}$ , and $T_C=50^\circ\text{F}$ , for a CTE of $4.5 \times 10^{-6}/^\circ\text{F}$ and a stiffness of $3.3 \times 10^6$ psi.....	209
Figure B27. 10-ft shoulder transverse cracking model where $T_M=80^\circ\text{F}$ , $T_S=110^\circ\text{F}$ , and $T_C=60^\circ\text{F}$ , for a CTE of $4.5 \times 10^{-6}/^\circ\text{F}$ and a stiffness of $2.8 \times 10^6$ psi.....	209
Figure B28. 10-ft shoulder transverse cracking model where $T_M=80^\circ\text{F}$ , $T_S=110^\circ\text{F}$ , and $T_C=60^\circ\text{F}$ , for a CTE of $4.5 \times 10^{-6}/^\circ\text{F}$ and a stiffness of $3.3 \times 10^6$ psi.....	210
Figure B29. 2-ft shoulder transverse cracking model where $T_M=80^\circ\text{F}$ , $T_S=110^\circ\text{F}$ , and $T_C=60^\circ\text{F}$ , for a CTE of $4.5 \times 10^{-6}/^\circ\text{F}$ and a stiffness of $2.8 \times 10^6$ psi.....	210
Figure B30. 5-ft shoulder transverse cracking model where $T_M=80^\circ\text{F}$ , $T_S=110^\circ\text{F}$ , and $T_C=60^\circ\text{F}$ , for a CTE of $4.5 \times 10^{-6}/^\circ\text{F}$ and a stiffness of $2.8 \times 10^6$ psi.....	211
Figure B31. 5-ft shoulder transverse cracking model where $T_M=80^\circ\text{F}$ , $T_S=110^\circ\text{F}$ , and $T_C=60^\circ\text{F}$ , for a CTE of $4.5 \times 10^{-6}/^\circ\text{F}$ and a stiffness of $3.3 \times 10^6$ psi.....	211
Figure B32. 10-ft shoulder transverse cracking model where $T_M=80^\circ\text{F}$ , $T_S=110^\circ\text{F}$ , and $T_C=70^\circ\text{F}$ , for a CTE of $4.5 \times 10^{-6}/^\circ\text{F}$ and a stiffness of $2.8 \times 10^6$ psi.....	212
Figure B33. 10-ft shoulder transverse cracking model where $T_M=80^\circ\text{F}$ , $T_S=110^\circ\text{F}$ , and $T_C=70^\circ\text{F}$ , for a CTE of $4.5 \times 10^{-6}/^\circ\text{F}$ and a stiffness of $3.3 \times 10^6$ psi.....	212
Figure B34. 2-ft shoulder transverse cracking model where $T_M=80^\circ\text{F}$ , $T_S=110^\circ\text{F}$ , and $T_C=70^\circ\text{F}$ , for a CTE of $4.5 \times 10^{-6}/^\circ\text{F}$ and a stiffness of $2.8 \times 10^6$ psi.....	213
Figure B35. 5-ft shoulder transverse cracking model where $T_M=80^\circ\text{F}$ , $T_S=110^\circ\text{F}$ , and $T_C=70^\circ\text{F}$ , for a CTE of $4.5 \times 10^{-6}/^\circ\text{F}$ and a stiffness of $2.8 \times 10^6$ psi.....	213
Figure B36. 5-ft shoulder transverse cracking model where $T_M=80^\circ\text{F}$ , $T_S=110^\circ\text{F}$ , and $T_C=70^\circ\text{F}$ , for a CTE of $4.5 \times 10^{-6}/^\circ\text{F}$ and a stiffness of $3.3 \times 10^6$ psi.....	214
Figure B37. 10-ft shoulder transverse cracking model where $T_M=80^\circ\text{F}$ , $T_S=110^\circ\text{F}$ , and $T_C=80^\circ\text{F}$ , for a CTE of $4.5 \times 10^{-6}/^\circ\text{F}$ and a stiffness of $2.8 \times 10^6$ psi.....	214
Figure B38. 10-ft shoulder transverse cracking model where $T_M=80^\circ\text{F}$ , $T_S=110^\circ\text{F}$ , and $T_C=80^\circ\text{F}$ , for a CTE of $4.5 \times 10^{-6}/^\circ\text{F}$ and a stiffness of $3.3 \times 10^6$ psi.....	215
Figure B39. 2-ft shoulder transverse cracking model where $T_M=80^\circ\text{F}$ , $T_S=110^\circ\text{F}$ , and $T_C=80^\circ\text{F}$ , for a CTE of $4.5 \times 10^{-6}/^\circ\text{F}$ and a stiffness of $2.8 \times 10^6$ psi.....	215

Figure B40. 5-ft shoulder transverse cracking model where $T_M=80^\circ\text{F}$ , $T_S=110^\circ\text{F}$ , and $T_C=80^\circ\text{F}$ , for a CTE of $4.5 \times 10^{-6}/^\circ\text{F}$ and a stiffness of $2.8 \times 10^6$ psi.....	216
Figure B41. 5-ft shoulder transverse cracking model where $T_M=80^\circ\text{F}$ , $T_S=110^\circ\text{F}$ , and $T_C=80^\circ\text{F}$ , for a CTE of $4.5 \times 10^{-6}/^\circ\text{F}$ and a stiffness of $3.3 \times 10^6$ psi.....	216
Figure B42. 10-ft shoulder transverse cracking model where $T_M=80^\circ\text{F}$ , $T_S=90^\circ\text{F}$ , and $T_C=50^\circ\text{F}$ , for a CTE of $4.5 \times 10^{-6}/^\circ\text{F}$ and a stiffness of $2.8 \times 10^6$ psi.....	217
Figure B43. 10-ft shoulder transverse cracking model where $T_M=80^\circ\text{F}$ , $T_S=90^\circ\text{F}$ , and $T_C=50^\circ\text{F}$ , for a CTE of $4.5 \times 10^{-6}/^\circ\text{F}$ and a stiffness of $3.3 \times 10^6$ psi.....	217
Figure B44. 2-ft shoulder transverse cracking model where $T_M=80^\circ\text{F}$ , $T_S=90^\circ\text{F}$ , and $T_C=50^\circ\text{F}$ , for a CTE of $4.5 \times 10^{-6}/^\circ\text{F}$ and a stiffness of $2.8 \times 10^6$ psi.....	218
Figure B45. 5-ft shoulder transverse cracking model where $T_M=80^\circ\text{F}$ , $T_S=90^\circ\text{F}$ , and $T_C=50^\circ\text{F}$ , for a CTE of $4.5 \times 10^{-6}/^\circ\text{F}$ and a stiffness of $2.8 \times 10^6$ psi.....	218
Figure B46. 5-ft shoulder transverse cracking model where $T_M=80^\circ\text{F}$ , $T_S=90^\circ\text{F}$ , and $T_C=50^\circ\text{F}$ , for a CTE of $4.5 \times 10^{-6}/^\circ\text{F}$ and a stiffness of $3.3 \times 10^6$ psi.....	219
Figure B47. 10-ft shoulder transverse cracking model where $T_M=80^\circ\text{F}$ , $T_S=90^\circ\text{F}$ , and $T_C=60^\circ\text{F}$ , for a CTE of $4.5 \times 10^{-6}/^\circ\text{F}$ and a stiffness of $2.8 \times 10^6$ psi.....	219
Figure B48. 10-ft shoulder transverse cracking model where $T_M=80^\circ\text{F}$ , $T_S=90^\circ\text{F}$ , and $T_C=60^\circ\text{F}$ , for a CTE of $4.5 \times 10^{-6}/^\circ\text{F}$ and a stiffness of $3.3 \times 10^6$ psi.....	220
Figure B49. 2-ft shoulder transverse cracking model where $T_M=80^\circ\text{F}$ , $T_S=90^\circ\text{F}$ , and $T_C=60^\circ\text{F}$ , for a CTE of $4.5 \times 10^{-6}/^\circ\text{F}$ and a stiffness of $2.8 \times 10^6$ psi.....	220
Figure B50. 5-ft shoulder transverse cracking model where $T_M=80^\circ\text{F}$ , $T_S=90^\circ\text{F}$ , and $T_C=60^\circ\text{F}$ , for a CTE of $4.5 \times 10^{-6}/^\circ\text{F}$ and a stiffness of $2.8 \times 10^6$ psi.....	221
Figure B51. 5-ft shoulder transverse cracking model where $T_M=80^\circ\text{F}$ , $T_S=90^\circ\text{F}$ , and $T_C=60^\circ\text{F}$ , for a CTE of $4.5 \times 10^{-6}/^\circ\text{F}$ and a stiffness of $3.3 \times 10^6$ psi.....	221
Figure B52. 10-ft shoulder transverse cracking model where $T_M=80^\circ\text{F}$ , $T_S=90^\circ\text{F}$ , and $T_C=70^\circ\text{F}$ , for a CTE of $4.5 \times 10^{-6}/^\circ\text{F}$ and a stiffness of $2.8 \times 10^6$ psi.....	222
Figure B53. 10-ft shoulder transverse cracking model where $T_M=80^\circ\text{F}$ , $T_S=90^\circ\text{F}$ , and $T_C=70^\circ\text{F}$ , for a CTE of $4.5 \times 10^{-6}/^\circ\text{F}$ and a stiffness of $3.3 \times 10^6$ psi.....	222
Figure B54. 2-ft shoulder transverse cracking model where $T_M=80^\circ\text{F}$ , $T_S=90^\circ\text{F}$ , and $T_C=70^\circ\text{F}$ , for a CTE of $4.5 \times 10^{-6}/^\circ\text{F}$ and a stiffness of $2.8 \times 10^6$ psi.....	223



Figure B70. 2-ft shoulder transverse cracking model where $T_M=80^\circ\text{F}$ , $T_S=90^\circ\text{F}$ , and $T_C=60^\circ\text{F}$ , for a CTE of $4.5 \times 10^{-6}/^\circ\text{F}$ and a stiffness of $3.3 \times 10^6$ psi.....	231
Figure B71. 2-ft shoulder transverse cracking model where $T_M=80^\circ\text{F}$ , $T_S=90^\circ\text{F}$ , and $T_C=70^\circ\text{F}$ , for a CTE of $4.5 \times 10^{-6}/^\circ\text{F}$ and a stiffness of $3.3 \times 10^6$ psi.....	231
Figure B72. 2-ft shoulder transverse cracking model where $T_M=80^\circ\text{F}$ , $T_S=90^\circ\text{F}$ , and $T_C=80^\circ\text{F}$ , for a CTE of $4.5 \times 10^{-6}/^\circ\text{F}$ and a stiffness of $3.3 \times 10^6$ psi.....	232
Figure B73. 10-ft shoulder transverse cracking model where $T_M=80^\circ\text{F}$ , $T_S=100^\circ\text{F}$ , and $T_C=50^\circ\text{F}$ , for a CTE of $5.5 \times 10^{-6}/^\circ\text{F}$ and a stiffness of $2.8 \times 10^6$ psi.....	232
Figure B74. 10-ft shoulder transverse cracking model where $T_M=80^\circ\text{F}$ , $T_S=100^\circ\text{F}$ , and $T_C=50^\circ\text{F}$ , for a CTE of $5.5 \times 10^{-6}/^\circ\text{F}$ and a stiffness of $3.3 \times 10^6$ psi.....	233
Figure B75. 2-ft shoulder transverse cracking model where $T_M=80^\circ\text{F}$ , $T_S=100^\circ\text{F}$ , and $T_C=50^\circ\text{F}$ , for a CTE of $5.5 \times 10^{-6}/^\circ\text{F}$ and a stiffness of $2.8 \times 10^6$ psi.....	233
Figure B76. 2-ft shoulder transverse cracking model where $T_M=80^\circ\text{F}$ , $T_S=100^\circ\text{F}$ , and $T_C=50^\circ\text{F}$ , for a CTE of $5.5 \times 10^{-6}/^\circ\text{F}$ and a stiffness of $3.3 \times 10^6$ psi.....	234
Figure B77. 5-ft shoulder transverse cracking model where $T_M=80^\circ\text{F}$ , $T_S=100^\circ\text{F}$ , and $T_C=50^\circ\text{F}$ , for a CTE of $5.5 \times 10^{-6}/^\circ\text{F}$ and a stiffness of $2.8 \times 10^6$ psi.....	234
Figure B78. 5-ft shoulder transverse cracking model where $T_M=80^\circ\text{F}$ , $T_S=100^\circ\text{F}$ , and $T_C=50^\circ\text{F}$ , for a CTE of $5.5 \times 10^{-6}/^\circ\text{F}$ and a stiffness of $3.3 \times 10^6$ psi.....	235
Figure B79. 10-ft shoulder transverse cracking model where $T_M=80^\circ\text{F}$ , $T_S=100^\circ\text{F}$ , and $T_C=60^\circ\text{F}$ , for a CTE of $5.5 \times 10^{-6}/^\circ\text{F}$ and a stiffness of $2.8 \times 10^6$ psi.....	235
Figure B80. 10-ft shoulder transverse cracking model where $T_M=80^\circ\text{F}$ , $T_S=100^\circ\text{F}$ , and $T_C=60^\circ\text{F}$ , for a CTE of $5.5 \times 10^{-6}/^\circ\text{F}$ and a stiffness of $3.3 \times 10^6$ psi.....	236
Figure B81. 2-ft shoulder transverse cracking model where $T_M=80^\circ\text{F}$ , $T_S=100^\circ\text{F}$ , and $T_C=60^\circ\text{F}$ , for a CTE of $5.5 \times 10^{-6}/^\circ\text{F}$ and a stiffness of $2.8 \times 10^6$ psi.....	236
Figure B82. 2-ft shoulder transverse cracking model where $T_M=80^\circ\text{F}$ , $T_S=100^\circ\text{F}$ , and $T_C=60^\circ\text{F}$ , for a CTE of $5.5 \times 10^{-6}/^\circ\text{F}$ and a stiffness of $3.3 \times 10^6$ psi.....	237
Figure B83. 5-ft shoulder transverse cracking model where $T_M=80^\circ\text{F}$ , $T_S=100^\circ\text{F}$ , and $T_C=60^\circ\text{F}$ , for a CTE of $5.5 \times 10^{-6}/^\circ\text{F}$ and a stiffness of $2.8 \times 10^6$ psi.....	237
Figure B84. 5-ft shoulder transverse cracking model where $T_M=80^\circ\text{F}$ , $T_S=100^\circ\text{F}$ , and $T_C=60^\circ\text{F}$ , for a CTE of $5.5 \times 10^{-6}/^\circ\text{F}$ and a stiffness of $3.3 \times 10^6$ psi.....	238

Figure B85. 10-ft shoulder transverse cracking model where $T_M=80^\circ\text{F}$ , $T_S=100^\circ\text{F}$ , and $T_C=70^\circ\text{F}$ , for a CTE of $5.5 \times 10^{-6}/^\circ\text{F}$ and a stiffness of $2.8 \times 10^6$ psi.....	238
Figure B86. 10-ft shoulder transverse cracking model where $T_M=80^\circ\text{F}$ , $T_S=100^\circ\text{F}$ , and $T_C=70^\circ\text{F}$ , for a CTE of $5.5 \times 10^{-6}/^\circ\text{F}$ and a stiffness of $3.3 \times 10^6$ psi.....	239
Figure B87. 2-ft shoulder transverse cracking model where $T_M=80^\circ\text{F}$ , $T_S=100^\circ\text{F}$ , and $T_C=70^\circ\text{F}$ , for a CTE of $5.5 \times 10^{-6}/^\circ\text{F}$ and a stiffness of $2.8 \times 10^6$ psi.....	239
Figure B88. 2-ft shoulder transverse cracking model where $T_M=80^\circ\text{F}$ , $T_S=100^\circ\text{F}$ , and $T_C=70^\circ\text{F}$ , for a CTE of $5.5 \times 10^{-6}/^\circ\text{F}$ and a stiffness of $3.3 \times 10^6$ psi.....	240
Figure B89. 5-ft shoulder transverse cracking model where $T_M=80^\circ\text{F}$ , $T_S=100^\circ\text{F}$ , and $T_C=70^\circ\text{F}$ , for a CTE of $5.5 \times 10^{-6}/^\circ\text{F}$ and a stiffness of $2.8 \times 10^6$ psi.....	240
Figure B90. 5-ft shoulder transverse cracking model where $T_M=80^\circ\text{F}$ , $T_S=100^\circ\text{F}$ , and $T_C=70^\circ\text{F}$ , for a CTE of $5.5 \times 10^{-6}/^\circ\text{F}$ and a stiffness of $3.3 \times 10^6$ psi.....	241
Figure B91. 10-ft shoulder transverse cracking model where $T_M=80^\circ\text{F}$ , $T_S=100^\circ\text{F}$ , and $T_C=80^\circ\text{F}$ , for a CTE of $5.5 \times 10^{-6}/^\circ\text{F}$ and a stiffness of $2.8 \times 10^6$ psi.....	241
Figure B92. 10-ft shoulder transverse cracking model where $T_M=80^\circ\text{F}$ , $T_S=100^\circ\text{F}$ , and $T_C=80^\circ\text{F}$ , for a CTE of $5.5 \times 10^{-6}/^\circ\text{F}$ and a stiffness of $3.3 \times 10^6$ psi.....	242
Figure B93. 2-ft shoulder transverse cracking model where $T_M=80^\circ\text{F}$ , $T_S=100^\circ\text{F}$ , and $T_C=80^\circ\text{F}$ , for a CTE of $5.5 \times 10^{-6}/^\circ\text{F}$ and a stiffness of $2.8 \times 10^6$ psi.....	242
Figure B94. 2-ft shoulder transverse cracking model where $T_M=80^\circ\text{F}$ , $T_S=100^\circ\text{F}$ , and $T_C=80^\circ\text{F}$ , for a CTE of $5.5 \times 10^{-6}/^\circ\text{F}$ and a stiffness of $3.3 \times 10^6$ psi.....	243
Figure B95. 5-ft shoulder transverse cracking model where $T_M=80^\circ\text{F}$ , $T_S=100^\circ\text{F}$ , and $T_C=80^\circ\text{F}$ , for a CTE of $5.5 \times 10^{-6}/^\circ\text{F}$ and a stiffness of $2.8 \times 10^6$ psi.....	243
Figure B96. 5-ft shoulder transverse cracking model where $T_M=80^\circ\text{F}$ , $T_S=100^\circ\text{F}$ , and $T_C=80^\circ\text{F}$ , for a CTE of $5.5 \times 10^{-6}/^\circ\text{F}$ and a stiffness of $3.3 \times 10^6$ psi.....	244
Figure B97. 10-ft shoulder transverse cracking model where $T_M=80^\circ\text{F}$ , $T_S=110^\circ\text{F}$ , and $T_C=50^\circ\text{F}$ , for a CTE of $5.5 \times 10^{-6}/^\circ\text{F}$ and a stiffness of $2.8 \times 10^6$ psi.....	244
Figure B98. 10-ft shoulder transverse cracking model where $T_M=80^\circ\text{F}$ , $T_S=110^\circ\text{F}$ , and $T_C=50^\circ\text{F}$ , for a CTE of $5.5 \times 10^{-6}/^\circ\text{F}$ and a stiffness of $3.3 \times 10^6$ psi.....	245
Figure B99. 2-ft shoulder transverse cracking model where $T_M=80^\circ\text{F}$ , $T_S=110^\circ\text{F}$ , and $T_C=50^\circ\text{F}$ , for a CTE of $5.5 \times 10^{-6}/^\circ\text{F}$ and a stiffness of $2.8 \times 10^6$ psi.....	245



Figure B115. 10-ft shoulder transverse cracking model where $T_M=80^\circ\text{F}$ , $T_S=110^\circ\text{F}$ , and $T_C=80^\circ\text{F}$ , for a CTE of $5.5 \times 10^{-6}/^\circ\text{F}$ and a stiffness of $2.8 \times 10^6$ psi.....	253
Figure B116. 10-ft shoulder transverse cracking model where $T_M=80^\circ\text{F}$ , $T_S=110^\circ\text{F}$ , and $T_C=80^\circ\text{F}$ , for a CTE of $5.5 \times 10^{-6}/^\circ\text{F}$ and a stiffness of $3.3 \times 10^6$ psi.....	254
Figure B117. 2-ft shoulder transverse cracking model where $T_M=80^\circ\text{F}$ , $T_S=110^\circ\text{F}$ , and $T_C=80^\circ\text{F}$ , for a CTE of $5.5 \times 10^{-6}/^\circ\text{F}$ and a stiffness of $2.8 \times 10^6$ psi.....	254
Figure B118. 2-ft shoulder transverse cracking model where $T_M=80^\circ\text{F}$ , $T_S=110^\circ\text{F}$ , and $T_C=80^\circ\text{F}$ , for a CTE of $5.5 \times 10^{-6}/^\circ\text{F}$ and a stiffness of $3.3 \times 10^6$ psi.....	255
Figure B119. 5-ft shoulder transverse cracking model where $T_M=80^\circ\text{F}$ , $T_S=110^\circ\text{F}$ , and $T_C=80^\circ\text{F}$ , for a CTE of $5.5 \times 10^{-6}/^\circ\text{F}$ and a stiffness of $2.8 \times 10^6$ psi.....	255
Figure B120. 5-ft shoulder transverse cracking model where $T_M=80^\circ\text{F}$ , $T_S=110^\circ\text{F}$ , and $T_C=80^\circ\text{F}$ , for a CTE of $5.5 \times 10^{-6}/^\circ\text{F}$ and a stiffness of $3.3 \times 10^6$ psi.....	256
Figure B121. 10-ft shoulder transverse cracking model where $T_M=80^\circ\text{F}$ , $T_S=90^\circ\text{F}$ , and $T_C=50^\circ\text{F}$ , for a CTE of $5.5 \times 10^{-6}/^\circ\text{F}$ and a stiffness of $2.8 \times 10^6$ psi.....	256
Figure B122. 10-ft shoulder transverse cracking model where $T_M=80^\circ\text{F}$ , $T_S=90^\circ\text{F}$ , and $T_C=50^\circ\text{F}$ , for a CTE of $5.5 \times 10^{-6}/^\circ\text{F}$ and a stiffness of $3.3 \times 10^6$ psi.....	257
Figure B123. 3-ft shoulder transverse cracking model where $T_M=80^\circ\text{F}$ , $T_S=90^\circ\text{F}$ , and $T_C=50^\circ\text{F}$ , for a CTE of $5.5 \times 10^{-6}/^\circ\text{F}$ and a stiffness of $2.8 \times 10^6$ psi.....	257
Figure B124. 2-ft shoulder transverse cracking model where $T_M=80^\circ\text{F}$ , $T_S=90^\circ\text{F}$ , and $T_C=50^\circ\text{F}$ , for a CTE of $5.5 \times 10^{-6}/^\circ\text{F}$ and a stiffness of $3.3 \times 10^6$ psi.....	258
Figure B125. 5-ft shoulder transverse cracking model where $T_M=80^\circ\text{F}$ , $T_S=90^\circ\text{F}$ , and $T_C=50^\circ\text{F}$ , for a CTE of $5.5 \times 10^{-6}/^\circ\text{F}$ and a stiffness of $2.8 \times 10^6$ psi.....	258
Figure B126. 5-ft shoulder transverse cracking model where $T_M=80^\circ\text{F}$ , $T_S=90^\circ\text{F}$ , and $T_C=50^\circ\text{F}$ , for a CTE of $5.5 \times 10^{-6}/^\circ\text{F}$ and a stiffness of $3.3 \times 10^6$ psi.....	259
Figure B127. 10-ft shoulder transverse cracking model where $T_M=80^\circ\text{F}$ , $T_S=90^\circ\text{F}$ , and $T_C=60^\circ\text{F}$ , for a CTE of $5.5 \times 10^{-6}/^\circ\text{F}$ and a stiffness of $2.8 \times 10^6$ psi.....	259
Figure B128. 10-ft shoulder transverse cracking model where $T_M=80^\circ\text{F}$ , $T_S=90^\circ\text{F}$ , and $T_C=60^\circ\text{F}$ , for a CTE of $5.5 \times 10^{-6}/^\circ\text{F}$ and a stiffness of $3.3 \times 10^6$ psi.....	260
Figure B129. 2-ft shoulder transverse cracking model where $T_M=80^\circ\text{F}$ , $T_S=90^\circ\text{F}$ , and $T_C=60^\circ\text{F}$ , for a CTE of $5.5 \times 10^{-6}/^\circ\text{F}$ and a stiffness of $2.8 \times 10^6$ psi.....	260

Figure B130. 2-ft shoulder transverse cracking model where $T_M=80^\circ\text{F}$ , $T_S=90^\circ\text{F}$ , and $T_C=60^\circ\text{F}$ , for a CTE of $5.5 \times 10^{-6}/^\circ\text{F}$ and a stiffness of $3.3 \times 10^6$ psi.....	261
Figure B131. 5-ft shoulder transverse cracking model where $T_M=80^\circ\text{F}$ , $T_S=90^\circ\text{F}$ , and $T_C=60^\circ\text{F}$ , for a CTE of $5.5 \times 10^{-6}/^\circ\text{F}$ and a stiffness of $2.8 \times 10^6$ psi.....	261
Figure B132. 5-ft shoulder transverse cracking model where $T_M=80^\circ\text{F}$ , $T_S=90^\circ\text{F}$ , and $T_C=60^\circ\text{F}$ , for a CTE of $5.5 \times 10^{-6}/^\circ\text{F}$ and a stiffness of $3.3 \times 10^6$ psi.....	262
Figure B133. 10-ft shoulder transverse cracking model where $T_M=80^\circ\text{F}$ , $T_S=90^\circ\text{F}$ , and $T_C=70^\circ\text{F}$ , for a CTE of $5.5 \times 10^{-6}/^\circ\text{F}$ and a stiffness of $2.8 \times 10^6$ psi.....	262
Figure B134. 10-ft shoulder transverse cracking model where $T_M=80^\circ\text{F}$ , $T_S=90^\circ\text{F}$ , and $T_C=70^\circ\text{F}$ , for a CTE of $5.5 \times 10^{-6}/^\circ\text{F}$ and a stiffness of $3.3 \times 10^6$ psi.....	263
Figure B135. 2-ft shoulder transverse cracking model where $T_M=80^\circ\text{F}$ , $T_S=90^\circ\text{F}$ , and $T_C=70^\circ\text{F}$ , for a CTE of $5.5 \times 10^{-6}/^\circ\text{F}$ and a stiffness of $2.8 \times 10^6$ psi.....	263
Figure B136. 2-ft shoulder transverse cracking model where $T_M=80^\circ\text{F}$ , $T_S=90^\circ\text{F}$ , and $T_C=70^\circ\text{F}$ , for a CTE of $5.5 \times 10^{-6}/^\circ\text{F}$ and a stiffness of $3.3 \times 10^6$ psi.....	264
Figure B137. 5-ft shoulder transverse cracking model where $T_M=80^\circ\text{F}$ , $T_S=90^\circ\text{F}$ , and $T_C=70^\circ\text{F}$ , for a CTE of $5.5 \times 10^{-6}/^\circ\text{F}$ and a stiffness of $2.8 \times 10^6$ psi.....	264
Figure B138. 5-ft shoulder transverse cracking model where $T_M=80^\circ\text{F}$ , $T_S=90^\circ\text{F}$ , and $T_C=70^\circ\text{F}$ , for a CTE of $5.5 \times 10^{-6}/^\circ\text{F}$ and a stiffness of $3.3 \times 10^6$ psi.....	265
Figure B139. 10-ft shoulder transverse cracking model where $T_M=80^\circ\text{F}$ , $T_S=90^\circ\text{F}$ , and $T_C=80^\circ\text{F}$ , for a CTE of $5.5 \times 10^{-6}/^\circ\text{F}$ and a stiffness of $2.8 \times 10^6$ psi.....	265
Figure B140. 10-ft shoulder transverse cracking model where $T_M=80^\circ\text{F}$ , $T_S=90^\circ\text{F}$ , and $T_C=90^\circ\text{F}$ , for a CTE of $5.5 \times 10^{-6}/^\circ\text{F}$ and a stiffness of $3.3 \times 10^6$ psi.....	266
Figure B141. 2-ft shoulder transverse cracking model where $T_M=80^\circ\text{F}$ , $T_S=90^\circ\text{F}$ , and $T_C=80^\circ\text{F}$ , for a CTE of $5.5 \times 10^{-6}/^\circ\text{F}$ and a stiffness of $2.8 \times 10^6$ psi.....	266
Figure B142. 2-ft shoulder transverse cracking model where $T_M=80^\circ\text{F}$ , $T_S=90^\circ\text{F}$ , and $T_C=80^\circ\text{F}$ , for a CTE of $5.5 \times 10^{-6}/^\circ\text{F}$ and a stiffness of $3.3 \times 10^6$ psi.....	267
Figure B143. 5-ft shoulder transverse cracking model where $T_M=80^\circ\text{F}$ , $T_S=90^\circ\text{F}$ , and $T_C=80^\circ\text{F}$ , for a CTE of $5.5 \times 10^{-6}/^\circ\text{F}$ and a stiffness of $2.8 \times 10^6$ psi.....	267
Figure B144. 5-ft shoulder transverse cracking model where $T_M=80^\circ\text{F}$ , $T_S=90^\circ\text{F}$ , and $T_C=80^\circ\text{F}$ , for a CTE of $5.5 \times 10^{-6}/^\circ\text{F}$ and a stiffness of $3.3 \times 10^6$ psi.....	268





Figure B175. 2-ft shoulder transverse cracking model where $T_M=80^\circ\text{F}$ , $T_S=90^\circ\text{F}$ , and $T_C=60^\circ\text{F}$ , for a CTE of $7.5 \times 10^{-6}/^\circ\text{F}$ and a stiffness of $2.8 \times 10^6$ psi.....	283
Figure B176. 5-ft shoulder transverse cracking model where $T_M=80^\circ\text{F}$ , $T_S=90^\circ\text{F}$ , and $T_C=60^\circ\text{F}$ , for a CTE of $7.5 \times 10^{-6}/^\circ\text{F}$ and a stiffness of $2.8 \times 10^6$ psi.....	284
Figure B177. 10-ft shoulder transverse cracking model where $T_M=80^\circ\text{F}$ , $T_S=90^\circ\text{F}$ , and $T_C=70^\circ\text{F}$ , for a CTE of $7.5 \times 10^{-6}/^\circ\text{F}$ and a stiffness of $2.8 \times 10^6$ psi.....	284
Figure B178. 2-ft shoulder transverse cracking model where $T_M=80^\circ\text{F}$ , $T_S=90^\circ\text{F}$ , and $T_C=70^\circ\text{F}$ , for a CTE of $7.5 \times 10^{-6}/^\circ\text{F}$ and a stiffness of $2.8 \times 10^6$ psi.....	285
Figure B179. 5-ft shoulder transverse cracking model where $T_M=80^\circ\text{F}$ , $T_S=90^\circ\text{F}$ , and $T_C=70^\circ\text{F}$ , for a CTE of $7.5 \times 10^{-6}/^\circ\text{F}$ and a stiffness of $2.8 \times 10^6$ psi.....	285
Figure B180. 10-ft shoulder transverse cracking model where $T_M=80^\circ\text{F}$ , $T_S=90^\circ\text{F}$ , and $T_C=80^\circ\text{F}$ , for a CTE of $7.5 \times 10^{-6}/^\circ\text{F}$ and a stiffness of $2.8 \times 10^6$ psi.....	286
Figure B181. 2-ft shoulder transverse cracking model where $T_M=80^\circ\text{F}$ , $T_S=90^\circ\text{F}$ , and $T_C=80^\circ\text{F}$ , for a CTE of $7.5 \times 10^{-6}/^\circ\text{F}$ and a stiffness of $2.8 \times 10^6$ psi.....	286
Figure B182. 5-ft shoulder transverse cracking model where $T_M=80^\circ\text{F}$ , $T_S=90^\circ\text{F}$ , and $T_C=80^\circ\text{F}$ , for a CTE of $7.5 \times 10^{-6}/^\circ\text{F}$ and a stiffness of $2.8 \times 10^6$ psi.....	287
Figure B183. 10-ft shoulder transverse cracking model where $T_M=80^\circ\text{F}$ , $T_S=110^\circ\text{F}$ , and $T_C=-0.38$ linear gradient for a CTE of $5.5 \times 10^{-6}/^\circ\text{F}$ and a stiffness of $2.8 \times 10^6$ psi.....	287
Figure B184. 2-ft shoulder transverse cracking model where $T_M=80^\circ\text{F}$ , $T_S=110^\circ\text{F}$ , and $T_C=-0.38$ linear gradient for a CTE of $5.5 \times 10^{-6}/^\circ\text{F}$ and a stiffness of $2.8 \times 10^6$ psi.....	288
Figure B185. 10-ft shoulder transverse cracking model where $T_M=80^\circ\text{F}$ , $T_S=110^\circ\text{F}$ , and $T_C=-0.75$ linear gradient for a CTE of $5.5 \times 10^{-6}/^\circ\text{F}$ and a stiffness of $2.8 \times 10^6$ psi.....	288
Figure B186. 2-ft shoulder transverse cracking model where $T_M=80^\circ\text{F}$ , $T_S=110^\circ\text{F}$ , and $T_C=-0.75$ linear gradient for a CTE of $5.5 \times 10^{-6}/^\circ\text{F}$ and a stiffness of $2.8 \times 10^6$ psi.....	289
Figure B187. 10-ft shoulder transverse cracking model where $T_M=80^\circ\text{F}$ , $T_S=110^\circ\text{F}$ , and $T_C=-1.5$ linear gradient for a CTE of $5.5 \times 10^{-6}/^\circ\text{F}$ and a stiffness of $2.8 \times 10^6$ psi.....	289
Figure B188. 2-ft shoulder transverse cracking model where $T_M=80^\circ\text{F}$ , $T_S=110^\circ\text{F}$ , and $T_C=-1.5$ linear gradient for a CTE of $5.5 \times 10^{-6}/^\circ\text{F}$ and a stiffness of $2.8 \times 10^6$ psi.....	290
Figure B189. 10-ft shoulder transverse cracking model where $T_M=80^\circ\text{F}$ , $T_S=90^\circ\text{F}$ , and $T_C=+0.38$ linear gradient for a CTE of $5.5 \times 10^{-6}/^\circ\text{F}$ and a stiffness of $2.8 \times 10^6$ psi.....	290

Figure B190. 2-ft shoulder transverse cracking model where $T_M=80^\circ\text{F}$ , $T_S=90^\circ\text{F}$ , and $T_C=+0.38$ linear gradient for a CTE of $5.5 \times 10^{-6}/^\circ\text{F}$ and a stiffness of $2.8 \times 10^6$ psi.....	291
Figure B191. 10-ft shoulder transverse cracking model where $T_M=80^\circ\text{F}$ , $T_S=90^\circ\text{F}$ , and $T_C=+0.75$ linear gradient for a CTE of $5.5 \times 10^{-6}/^\circ\text{F}$ and a stiffness of $2.8 \times 10^6$ psi.....	291
Figure B192. 2-ft shoulder transverse cracking model where $T_M=80^\circ\text{F}$ , $T_S=90^\circ\text{F}$ , and $T_C=+0.75$ linear gradient for a CTE of $5.5 \times 10^{-6}/^\circ\text{F}$ and a stiffness of $2.8 \times 10^6$ psi.....	292
Figure B193. 10-ft shoulder transverse cracking model where $T_M=80^\circ\text{F}$ , $T_S=90^\circ\text{F}$ , and $T_C=+1.5$ linear gradient for a CTE of $5.5 \times 10^{-6}/^\circ\text{F}$ and a stiffness of $2.8 \times 10^6$ psi.....	292
Figure B194. 2-ft shoulder transverse cracking model where $T_M=80^\circ\text{F}$ , $T_S=90^\circ\text{F}$ , and $T_C=+1.5$ linear gradient for a CTE of $5.5 \times 10^{-6}/^\circ\text{F}$ and a stiffness of $2.8 \times 10^6$ psi.....	293
Figure B195. 10-ft shoulder transverse cracking model where $T_M=80^\circ\text{F}$ , $T_S=90^\circ\text{F}$ , and $T_C=-0.38$ linear gradient for a CTE of $5.5 \times 10^{-6}/^\circ\text{F}$ and a stiffness of $2.8 \times 10^6$ psi.....	293
Figure B196. 2-ft shoulder transverse cracking model where $T_M=80^\circ\text{F}$ , $T_S=90^\circ\text{F}$ , and $T_C=-0.38$ linear gradient for a CTE of $5.5 \times 10^{-6}/^\circ\text{F}$ and a stiffness of $2.8 \times 10^6$ psi.....	294
Figure B197. 10-ft shoulder transverse cracking model where $T_M=80^\circ\text{F}$ , $T_S=90^\circ\text{F}$ , and $T_C=-0.75$ linear gradient for a CTE of $5.5 \times 10^{-6}/^\circ\text{F}$ and a stiffness of $2.8 \times 10^6$ psi.....	294
Figure B198. 2-ft shoulder transverse cracking model where $T_M=80^\circ\text{F}$ , $T_S=90^\circ\text{F}$ , and $T_C=-0.75$ linear gradient for a CTE of $5.5 \times 10^{-6}/^\circ\text{F}$ and a stiffness of $2.8 \times 10^6$ psi.....	295
Figure B199. 10-ft shoulder transverse cracking model where $T_M=80^\circ\text{F}$ , $T_S=90^\circ\text{F}$ , and $T_C=-1.5$ linear gradient for a CTE of $5.5 \times 10^{-6}/^\circ\text{F}$ and a stiffness of $2.8 \times 10^6$ psi.....	295
Figure B200. 2-ft shoulder transverse cracking model where $T_M=80^\circ\text{F}$ , $T_S=90^\circ\text{F}$ , and $T_C=-1.5$ linear gradient for a CTE of $5.5 \times 10^{-6}/^\circ\text{F}$ and a stiffness of $2.8 \times 10^6$ psi.....	296

## **PREFACE**

Firstly, I would like to thank my advisor, Dr. Julie Vandebossche, for her guidance, support, and encouragement. I greatly appreciate her dedication to my education. She taught me everything I know about how to conduct research and view things with a critical eye. Without her faith in me, none of this would have ever been possible.

I would like to thank my committee which comprises Dr. John Brigham and Dr. Jeen-Shang Lin for taking time out of their busy schedules to review my thesis. I would like to express extreme gratitude to all of the graduate students who assisted me in this journey. A special thanks goes out to Mr. Feng Mu who helped me not only with this research but was a great friend and mentor throughout the entire process, constantly encouraging and pushing me forward.

Last but not least, I would like to thank my friends and family for supporting me throughout this endeavor. Special thanks to A.J. for staying by my side and putting up with me when things got rough over the past few years.

## **1.0 INTRODUCTION**

### **1.1 BACKGROUND**

When constructing concrete pavements, it is not unusual to construct adjacent lanes at different times. An entire year could go by before concrete shoulders are tied on to the mainline. Often during construction, it is not possible to finish paving all of the constituents (lanes, shoulders, etc.) during the same construction season because of time, money and unforeseen circumstances. Therefore, it is necessary to construct the adjacent lanes at a different time than when the original lanes were constructed.

If lanes are going to be tied on during different seasons, different times of the day, or with a different mixture design, it is important to factor these differences into the design; otherwise, it is possible for premature cracking to occur in the newly paved lane, the existing lane, or both. Cracking can develop in concrete pavements even before traffic loads are applied because of thermal loads. If factors such as materials, structure, and climate are not taken into consideration when tying on adjacent lanes, a variety of problems can arise in the newly paved lane, as well as the adjacent lane. The objective of the following study is to provide guidelines for professionals so that problems associated with delayed lane construction can be avoided.

## **1.2 OBJECTIVE**

The primary objective of this research is to develop guidelines to protect against premature cracking from paving adjacent lanes at separate times. These guidelines will be based on field work, and a parametric study using the finite element (FE) method. Critical combinations of stresses due to climate, structure, and materials that cause newly paved concrete to exhibit stress prematurely will be identified.

## **1.3 RESEARCH APPROACH**

This research consists of gathering information about problems associated with paving adjacent lanes at separate times and developing guidelines to prevent these problems in the future. It should be noted that an adjacent lane can also refer to an adjacent shoulder. The goal is that this thesis will serve as a reference for professionals who face the situations outlined in the sections below. Several scenarios highlighting different construction sequences will be identified. For example, one sequence will consist of a mainline placed in the summer with an adjacent lane in the fall. For each construction sequence, a parametric study will be conducted using parameters known to induce stress in pavements. Within each sequence, a range of conditions will be looked at and the most critical ones will be identified and used to develop guidelines.

Several examples of distresses caused by delayed lane construction will be presented in Chapter 2 as well as a literature review of work that has previously been done in the area. The purpose of the examples is to validate the existence of problems due to delayed lane construction. Several factors that influence distress due to delayed lane construction will be used

to create a parametric study identifying critical scenarios. The parametric study is introduced in Chapter 2 and is carried out using a FE analysis. The FE analysis is presented in Chapter 3. Chapter 4 presents the results and analysis from the FE analysis and Chapter 5 provides the final guidelines and recommendations.

## **2.0 LITERATURE REVIEW**

This chapter presents a review of current information pertaining to problems associated with delayed lane construction. Several distresses have been identified when an adjacent lane, typically a shoulder, was paved at a different time from the mainline, namely longitudinal shear cracking and transverse cracking. In general, these distresses manifest within a year of paving the adjacent lane. Three categories have been identified as sources of these distresses: structure, materials and construction. Critical combinations of parameters within those categories have been identified and a parametric study has been developed keeping them in mind. The parametric study will be the basis for which the finite element analysis is to be conducted.

### **2.1 DOCUMENTED DISTRESSES**

#### **2.1.1 Longitudinal Shear Cracking**

In August 2004, the American Concrete Paving Association (ACPA) released a Research and Technology (R&T) update with the title, “Cause, Prevention, and Repair of Longitudinal Shear Cracking.” The report documents a form of premature cracking that resembles the shape of a smile. A typical crack pattern can be seen in Figure 2.3.

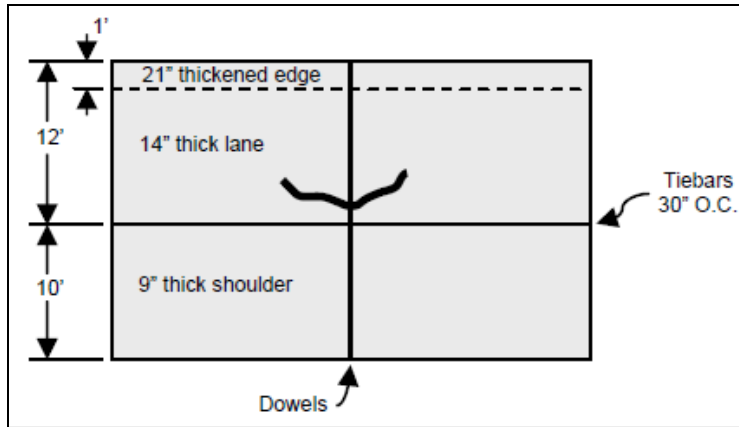


**Figure 2.1.** Typical crack pattern documented by the ACPA (copied from ACPA R&T Update).

A detailed study of a pavement with this type of cracking is documented in the report. The pavement is a curved section of a ramp connecting two interstates. The existing ramp pavement consists of one lane of continuously reinforced concrete pavement (CRCP). A new 12-ft wide, 14-in thick jointed-plain concrete pavement (JPCP) with a 1-ft wide, 21-in thickened longitudinal edge was placed adjacent to the CRCP. The thickened edge tapered over 3 ft to the design thickness of 14 in. Joints were spaced every 15 ft and included dowel bars. The base underneath of the 12-ft lane consists of cement-stabilized recycled concrete topped with a 1-in asphalt bond-breaker. Adjacent to the 12-ft lane, a 10-ft wide, 9-in thick concrete shoulder was placed. The base under the shoulder consists of compacted aggregates. The 12-ft lane was paved in September 2003 which saw an average temperature of 72°F and the shoulder was placed in January 2004 which saw an average temperature of 42°F. The dowels were found to be aligned properly via pavement excavation. Cores were taken at the affected transverse joints 1.5 ft and 1.5 in from the longitudinal shoulder joint. The cores that were taken at 1.5 ft were normal while the cores taken 1.5 in from the joint had mortar and saw slurry in the initial saw-cut. All of the cores showed that the joints were working (cracked).

The cracks occurred only in the 12-ft lane at about every 4th joint. The cracks were slightly curved in nature (see Figure 2.1). The following list explains all of the possible causes thought to lead to this type of distress. A schematic of the factors can be seen in Figure 2.2.

1. The different ambient temperatures seen during the placement of the 12-ft lane and the 10-ft shoulder resulted in different zero-stress temperatures.
2. The thickened longitudinal edge (lug) and the stabilized base restrained the pavement from moving which is why only every 4th joint cracked.
3. The granular base underneath of the shoulder provides for more freedom in movement which leads to more working joints.
4. The tie-bars along the lane/shoulder joint may be causing the corners of the slab to lock and preventing the opened joints in the 12-ft lane from closing.
5. The horizontal curve adds to the stress built up by the high-friction stabilized base and the lug (American Concrete Pavement Association).

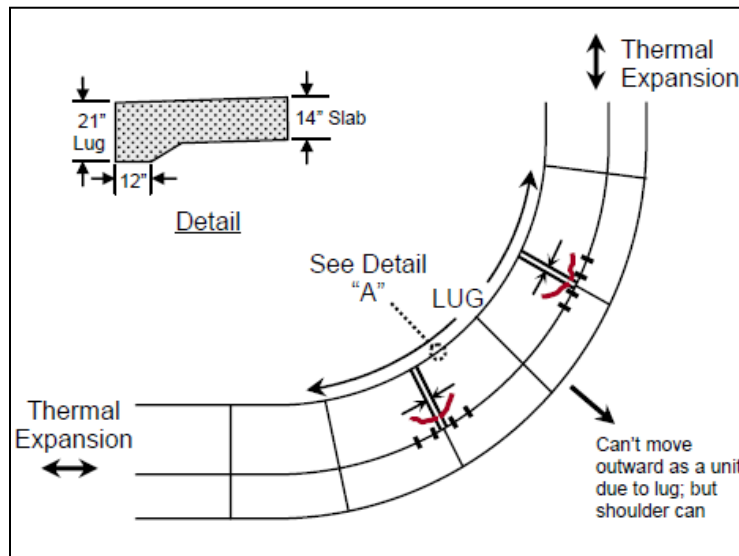


**Figure 2.2.** Schematic of factors leading to cracking (copied from ACPA R&T Update).

The conclusion to the report states that uncontrolled cracking is typically due to a combination of several factors. The authors of the report believe that the cracks on the 12-ft lane

of the curved ramp were due to the combination of the lug, the high friction base, the compacted aggregate base, the horizontal curved ramp section, the tie-bar design, and mortar intrusion.

Construction Technology Laboratories conducted an investigation of premature cracking along a section of Interstate-81 in Franklin County, Pennsylvania. This section consists of two 12-ft lanes which were placed in October 2001. The transverse joints were constructed with 1.5-in dowel bars and spaced at 18 ft. Concrete shoulders were placed in December 2001. The inside shoulder was 4-ft wide and the outside shoulder was 10-ft wide. A schematic of the pavement can be seen in Figure 2.3 along with the typical cracking pattern.

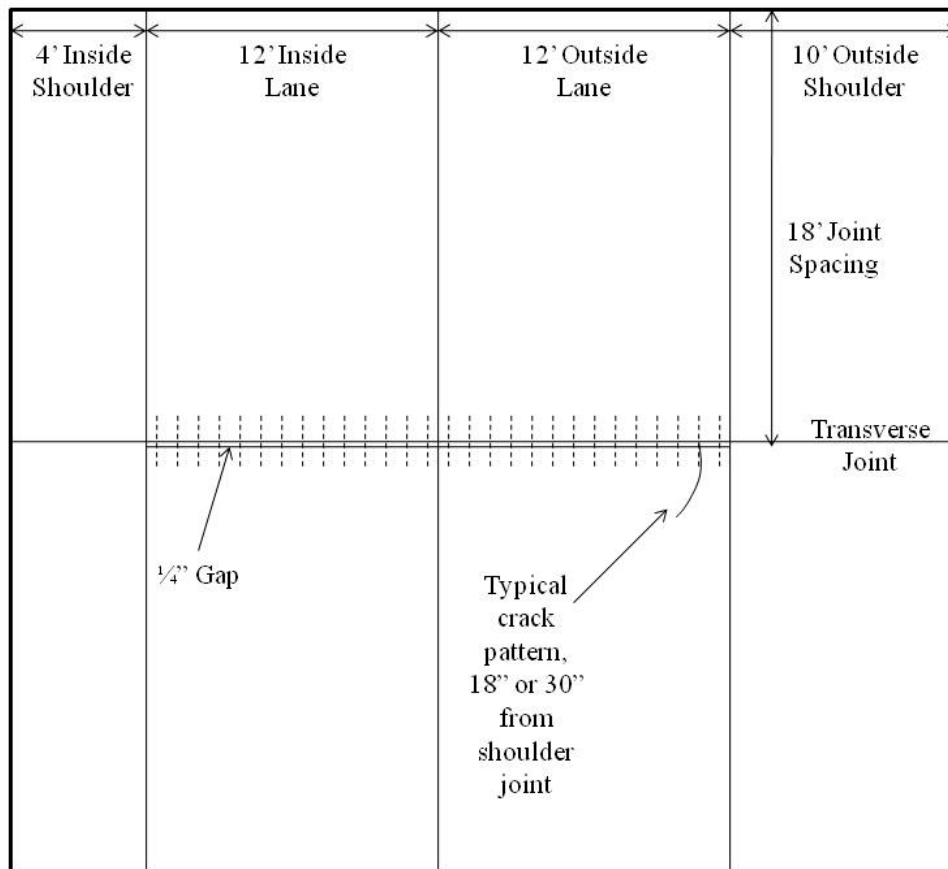


**Figure 2.3.** Interstate 81, Franklin County pavement layout.

Some time before the shoulders were placed, it was reported that only every third or fourth joint had opened. When the shoulders were placed, the joints that had opened were open

wide due to the low ambient temperatures and drying shrinkage. When the concrete shoulders set, the joints were closed tight; however, the mainline joints were opened 0.125 to 0.25 in. Two cores were pulled in April 2003 and September 2003 confirmed this. In Franklin County, warm temperatures can cause the temperature of the concrete to reach 120°F. The summer following the paving of the mainline and shoulders, when the concrete wants to expand, the shoulder joints closed first at about 70 to 75°F. The joints in the mainline were not closed at this time and still wanted to expand; however, they were restrained by the shoulders. This was observed from a core location in September 2003. Approximately 95 locations along the section have premature cracking. There were several ideas pertaining to the cause of the premature cracking (Tayabji & Lotfi, 2003):

1. Dissimilar joint openings in the mainline and shoulder joints caused the cracking to occur.
2. The cracking is due to shear type failure that initiates at a weak point at the transverse joint.
3. The weak fracture locations could be the dowel bar locations, since that is where the cracks initiated.

Due to a short amount of time, a simplified finite element analysis was performed to test the hypotheses stated above. The finite element program SAP2000 was used. The simplified analysis supports the first hypothesis. The cracking was due to high tensile stresses that developed in the mainline due to the restraint imposed by the shoulder. The restraint was caused by the shoulder joints closing at a lower temperature than the mainline, which continues to expand after the shoulder joints were closed.

In June 1988, an 11-mile stretch of I-64 in West Virginia, that had yet to be opened to traffic, had longitudinal cracking on both sides of the transverse joints. The cracks were scattered throughout the 11-mile section that had concrete shoulders tied to jointed reinforced concrete pavement (JRCP). The section had been paved in 1987 and consisted of a 12-in JRCP with a 40-ft joint spacing that contained dowel bars. The highway consisted of two travel lanes with an occasional truck climbing lane. The Portland cement concrete (PCC) shoulders were 10-in thick, contained no reinforcement, and had a 20-ft joint spacing. They were tied to the mainline using hook bolts. The entire pavement structure had an aggregate base containing No. 57 stone which was treated with 2 percent asphalt by weight. According to the report, the mainline was paved in warm weather while the shoulders were placed during cooler weather.

The State had concerns prior to the placement of the PCC shoulder about adequate consolidation of the concrete at the mainline/shoulder joint. During the time of the shoulder placement, the joints in the mainline were open wide due to the fact that they were placed during warm weather. The combination of open joints and a fear of improper consolidation caused mortar to flow into the joints of the mainline. The following summer when temperatures started to rise again, the mainline tried to expand and was restricted due to the hardened mortar in the joints (Federal Highway Administration, 1988). Longitudinal cracking occurred as a result. The cracks were typically 12- to 18-in long and approximately 9- to 12-in away from the mainline/shoulder longitudinal joint. The cracks were always present on both sides of the transverse joint. A schematic of a typical cracking pattern can be seen in Figure 2.4.

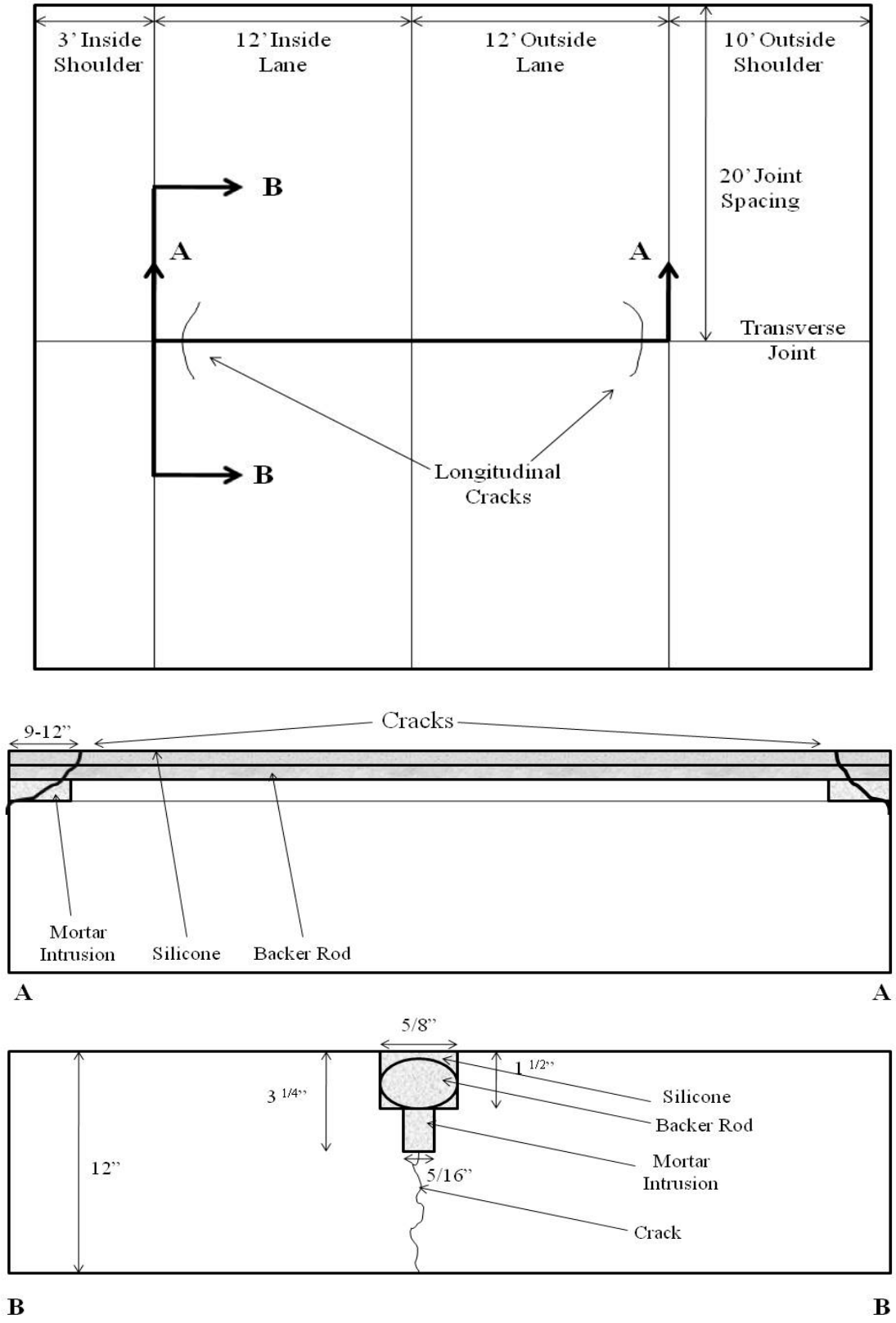


**Figure 2.4.** Typical longitudinal cracking pattern on Interstate 64 West Virginia.

The solution to the problem involved re-sawing every joint, whether or not a longitudinal crack existed. It was recommended that the State seal the sides of the joints prior to shoulder placement in order to avoid this type of problem from occurring again. This would prevent mortar from entering the joint and hardening.

### **2.1.2 Transverse Cracking**

A new construction project just outside of Blairsville, PA on US-22 experienced premature transverse cracking in the shoulder. The project consists of two 12-ft lanes in each direction with a 10-ft outside tied PCC shoulder and a 2-ft inside PCC shoulder. The directions are separated by a curb and gutter system. The pavement mainline was constructed in October 2008 and a series of 2-ft shoulders were constructed in July 2009. One week after the 2-ft shoulders were paved, mid-panel cracks were noticed by Pennsylvania Department of Transportation (PennDOT) engineers. During the week of paving the 20-ft shoulders, several of the days were extremely hot followed by colder nights.

An examination of all of the 2-ft shoulder sections were made to quantify the cracking in the shoulder. No other distresses were found during the distress survey. On average, the cracks in the shoulder occurred at mid-panel. A typical crack can be seen in Figure 2.5. The majority of the cracks propagated across the full width of the shoulder; however, there were a few that partially traversed the width of the slab. The cracks were more open along the free edge and tight at the edge adjacent to the mainline. All of the cracks were wider at the top than at the bottom indicating top-down cracking. Based on those two observations, the cracks initiated at the top, outer edge of the shoulder.

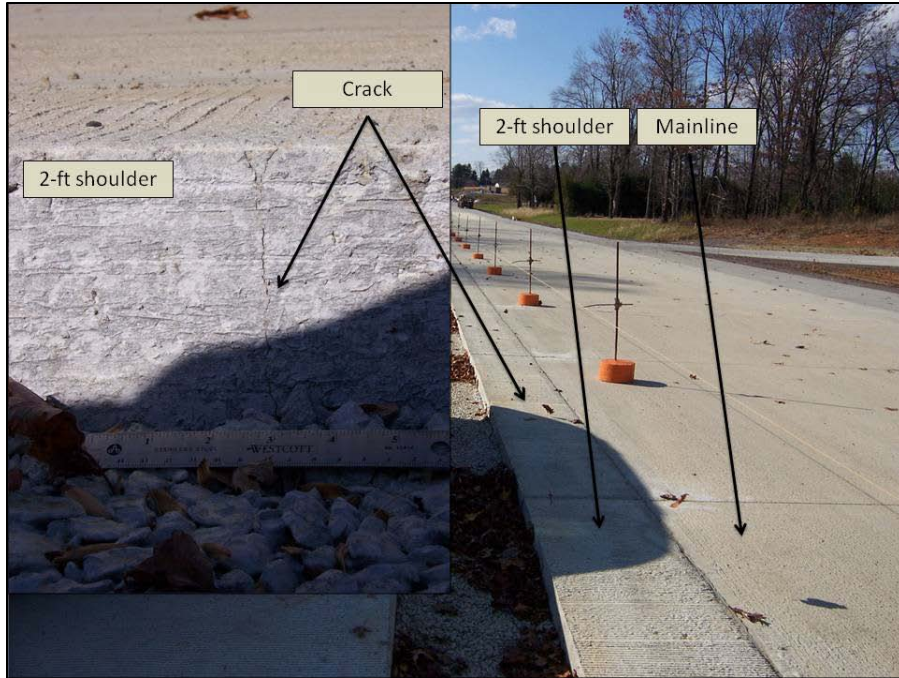


**Figure 2.5.** Typical crack found in 2-ft shoulder at US 22 Clyde.

A total of 19 cores were pulled from the project at various locations. Nine of the cores were pulled from mid-panel of the mainline, five were pulled from a non-cracked shoulder, two were pulled from a non-cracked area of a cracked shoulder, two were pulled from a full length crack of a cracked shoulder and one was pulled from a partial length crack of a cracked shoulder. Ten of the cores were tested for compressive strength, six were tested for tensile strength and ten of the cores were tested for elastic modulus and Poisson's ratio. Additionally, six cores were tested for coefficient of thermal expansion (CTE), three from the mainline and three from the shoulder. This was to check for thermal incompatibility. A summary of the testing results can be seen in Table 2.1. The values in the table reflect average values from testing.

**Table 2.1.** Summary of compressive strengths and elastic moduli for each core.

Material Property	Mainline	Shoulder
Compressive strength, psi	7,300	6,600
Split tensile strength, psi	670	550
Elastic modulus, $10^6$ psi	4.8	4.5
Coefficient of thermal expansion, $10^{-6}/^{\circ}\text{F}$	6.0	6.0

## **2.2 FACTORS THAT INFLUENCE DISTRESS DUE TO DELAYED LANE CONSTRUCTION**

Distresses caused by delayed lane construction can be generalized into three categories: structure, materials and construction. There are several distresses associated with delayed shoulder construction, namely longitudinal shear cracking in the mainline and transverse cracking in the adjacent lane. Relatively speaking, longitudinal shear cracking is a newly documented distress. The ACPA was the first professional organization to characterize this distress in literature. It typically manifests in the outer driving lane, parallel to the lane/shoulder longitudinal joint and resembles the shape of a smile. Transverse cracking in the shoulder can either be due to late saw cutting or an excessive amount of tensile stress caused by volume changes in the mainline.

### **2.2.1 Structure**

The structure of a pavement provides the support for the entire system. The ultimate goal of a pavement structure is to carry traffic and withstand climatic loadings. Factors such as PCC slab

dimensions (lane and shoulder), tie bar size and spacing, and shoulder type are all important parameters to consider when constructing the mainline and adjacent shoulder separately. The combination of tie bar layout and shoulder width dictate the level of restraint seen by the mainline slabs and ultimately the amount of stress build up. The thicker the tie bar and smaller the spacing, the more restraint is provided by the shoulder. Additionally, a larger shoulder will also provide more restraint.

### **2.2.1.1 Geometry**

The dimensions of a concrete slab are important when determining the effects of axial expansion and contraction. When large slab dimensions are combined with high CTE values, high stress concentrations develop due to the expansion and contraction of the slab caused by daily and seasonal variations in temperature. If the slab is restrained, stresses build up in the longitudinal and transverse directions. In the ACPA report, which discusses longitudinal shear cracking, the geometry of the horizontal curve, seen in Figure 2.2, added to the buildup of stress when the slabs tried to expand. The mainline was restrained due to the lug, while the shoulder was free to move.

The geometry of a pavement structure also needs to be able to withstand forces from the expansion and contraction of adjacent slabs. Often times, a shoulder is paved when the adjacent mainline has had enough time to gain adequate stiffness. Shortly after a shoulder is paved, it is a slave to the movement of the adjacent mainline since it has not yet gained sufficient stiffness. The smaller the width of the shoulder, the more likely it is for an adjacent slab to push/drag the shoulder when expanding/contracting. A hypothesis for the transverse cracking on US-22 is that the combination of the stiffness and width of the 2-ft shoulder was not sufficient to resist the expansion of the adjacent mainline. It is possible that the shoulder failed in flexure, which could

be the case since the dimensions of the shoulder slabs are relatively small compared to a typical slab. Additionally, the shoulder slabs had not yet gained sufficient stiffness since the cracks were noticed a week after paving.

### **2.2.1.2 Shoulder Type**

Concrete shoulders, which are tied to the mainline with tie bars, provide structural support and can reduce edge deflections. They can also prevent moisture and debris from penetrating into the pavement structure. On highways, it is recommended by the Federal Highway Administration (FHWA) that the base type, joint spacing and thickness of the shoulder match that of the mainline pavement; however, that is not always the case. Sometimes the shoulder varies from the mainline structurally. In the ACPA report, the shoulder has a different thickness and base type from the mainline. On I-64 in WV, the shoulder had a different thickness and contained no reinforcement like the JRC pavement adjacent to it. It is important to keep conditions uniform. If the thickness of the adjacent shoulder does not match that of the mainline, the structural capacity at the lane/shoulder interface may be inadequate. If the base type of the shoulder is different than the mainline, non-uniform support conditions can exist as well as differences in drainage characteristics (Federal Highway Administration, 1990).

### **2.2.1.3 Tie Bar Layout**

The size and spacing of tie bars dictate the level of restraint seen by the mainline slabs and ultimately, the amount of stress build up. The thicker the tie bar and smaller the spacing, the more restraint is provided by the shoulder. Typically, agencies use the same tie bar layout when constructing interstates. In the cases which discuss longitudinal shear cracking, the restraint provided by the tie bars prevented open joints in the mainline from closing due to the thermal

incompatibility of the shoulder and mainline. In the case with premature transverse cracking in the shoulder, the tie bars were 30-in long and spaced 30 in apart. Even though the shoulder was only 24 in wide, the tie bars were embedded into the shoulder 15 in. More than half of the 2-ft shoulder contained tie bars. Essentially, the shoulder was completely attached to the mainline and had very little freedom to move.

#### **2.2.1.4 Base Type**

In this study, the importance of base type has to do with the amount of friction generated between the concrete and the base. Friction at the slab/base interface causes restraint when the slab tries to expand and contract due to changes in temperature. This restraint causes stresses to develop at the interface and throughout the depth of the slab. The tensile stress that develops in the concrete due to the restraint at the interface is proportional to the slab length, the unit weight of the concrete and the coefficient of friction between the slab and the base (Huang, 2004). In the case of the transverse cracking that occurred at US-22, the lean concrete base provided enough resistance for stress to build up when the shoulder was being dragged by the mainline.

In the ACPA report, the mainline had a stabilized base and the shoulder had a granular base, which allowed for more freedom in movement. The increase in freedom led to more working joints in the shoulder. Only every third or fourth joint opened in the mainline by the time the shoulder was paved. This is due to the stabilized base. Similarly, at the project on I-81, which also had a stabilized base, every third or fourth joint had opened at the time the shoulder was paved.

## **2.2.2 Materials**

### **2.2.2.1 Portland Cement Concrete**

The CTE of concrete, which describes how the concrete changes in size when subjected to a change in temperature, is an extremely important parameter when characterizing stress development in pavements. Large CTE values result in large deformations. When those deformations are restrained by the base, tie bars, and other slabs, large stresses develop. The CTE is primarily a function of the aggregate since cement paste has a relatively constant CTE. Potentially high CTE values were part of the cause in the cases where longitudinal shear cracking occurred. At I-81 and I-64, wide joints allowed slurry from the newly paved shoulder to penetrate into the mainline. The following summer, when the mainline was trying to expand, the shoulder joints closed first. Due to the slurry in the joints, stresses built up in the mainline causing the cracking. The mainline continued to expand after the shoulder joints were closed. Additionally, the geometry of the horizontal curve, seen in Figure 2.1, in combination with the CTE caused the buildup of stress in the mainline, eventually causing it to crack.

#### ***Stiffness and Strength Development***

The stiffness of the concrete determines the magnitude of induced stresses and deflections. The strength and fracture properties control when the concrete cracks (Ruiz, Rasmussen, Chang, Dick, & Nelson, 2005). In mechanistic pavement response analysis, the PCC elastic modulus has a strong effect on pavement deflection and stresses throughout the pavement structure. The modulus of elasticity is significantly influenced by mixture design parameters such as w/c ratio and proportions of paste and aggregate, as well as the aggregate type, (ARA Inc., ERES Consultants Division, 2004).

In terms of distress in PCC shoulders, strength development is very important. Early strength gain can be achieved by curing at higher temperatures; however, this will lower the ultimate strength of the concrete. The first week after paving, when the concrete has yet to gain sufficient strength, shoulders that are tied on to the mainline have a tendency to be dragged/pushed when the mainline is expanding/contracting. In the case of the transverse cracking in the 2-ft shoulders, it is believed that shoulder had not achieved sufficient strength when it was being pushed by the mainline. Since the cracking was noticed at an early age, drying shrinkage could not have been a cause for the cracks.

### **2.2.3 Construction**

#### **2.2.3.1 Built in Construction Gradient**

Concrete set time represents the time when the concrete reaches a solid state, the transition from a plastic to a solid (Ruiz, Rasmussen, Chang, Dick, & Nelson, 2005). In general, set time is coupled with the time stresses begin to develop and volume changes occur due to changes in temperature and moisture. Under typical paving conditions, the top of the slabs are exposed to higher temperatures than the bottom of the slab, exposing the slab to a positive built-in gradient. A built in construction gradient is defined as the gradient present in the slab at the time of set (Wells, 2005). The temperature gradient of the slab just before the time of set is known as the zero-stress temperature gradient. Whenever the temperature profile of the slab is the same magnitude as the zero-stress gradient, the slab will be flat and experience no stress (Asbahan, 2009). Whenever the temperature gradient present in the slab is larger than the zero-stress gradient, the slab will curl downwards. The slab will curl up when the temperature gradient is lower than the zero-stress gradient.

### 2.2.3.2 Zero-Stress Temperature

The zero-stress temperature is a weighted average of the temperature profile of the zero-stress gradient. For simplicity, the zero-stress temperature is sometimes used instead of the zero-stress gradient. It is possible to estimate the zero-stress temperature in the Mechanistic Empirical Pavement Design Guide (MEPDG) using Equation 2.1:

$$T_z = [(CC * 0.59328 * H(0.5 * 1000 * 1.8))/(1.1 * 2400)] + MMT \quad (\text{Equation 2.1})$$

where,

$T_z$  = temperature at which the PCC layer exhibits zero thermal stress, °F

CC = Cementitious content, lb/yd<sup>3</sup>

$H = -0.0787 + 0.007 * MMT - 0.00003 * MMT^2$

MMT = mean monthly temperature for month of construction, °F.

According to PennDOT specifications, paving operations are only performed when the ambient temperature is between 50°F and 90°F which corresponds to a zero-stress temperature range of 70°F to 130°F.

### 2.2.3.3 Construction Sequence

If a mainline is paved in the summer and the shoulders are paved the following fall, there is a possibility for the difference in zero-stress temperatures to exceed 30°F. When thermal incompatibility exists between the mainline and the shoulder, the rates at which volume changes occur relative to each other could induce stress in the mainline, shoulder or both. Thermal incompatibility between the mainline and the shoulder is believed to be a significant factor in longitudinal shear cracking and transverse cracking in the shoulder. In all three of the longitudinal shear cracking cases, the mainline was paved in warm fall weather and the shoulders

were paved in the winter. In the case of the transverse cracking in the 2-ft shoulder, it can be determined that the zero-stress temperature of the mainline was more than 20°F lower than that of the shoulder. The environmental conditions under which concrete slabs are paved have a significant influence on the performance. As discussed above, the sequence in which the different concrete components (mainline, shoulder) are paved has a significant effect on the build-up of stress.

#### **2.2.3.4 Mortar Intrusion**

If shoulders are paved at lower temperatures than the mainline, it is likely that the transverse joints in the mainline will be open wide, especially if not all of the joints are working. Since the joint widths are larger than normal, it is possible for mortar to penetrate the transverse joints in the mainline when the shoulder is being paved. Once this happens, the transverse joints in the mainline are unable to close once the temperatures rise. This occurred in several of the cases where longitudinal shear cracking occurred.

## **3.0 PARAMETRIC STUDIES**

### **3.1 INTRODUCTION**

Parametric studies were developed for evaluating the potential for the development of longitudinal shear cracking and shoulder transverse cracking with the objective of identifying critical combinations of parameters that would lead to each type of distress. The studies were developed based on the review of information presented in Chapter 2.

ABAQUS Version 6.9 was used to create models to analyze the potential for each distress and carry out the parametric studies. ABAQUS is general purpose finite element software and is widely used in areas such as structural and geotechnical engineering, materials engineering, mechanical engineering, and biomedical engineering.

It is important to choose the appropriate element and mesh fineness in order to achieve accurate results. Several studies have been previously performed using different elements and mesh finenesses and then comparing them to the Westergaard equations. These studies have shown that an 8-node linear element, which is an 8-node brick, does not predict acceptable results in comparison to Westergaard's solution, even with a very fine mesh (Kuo, 1994). Westergaard developed closed-form solutions for different loading conditions for slab-on-grade pavements (Westergaard, 1927). The solutions are an industry standard and are often used to validate research. The 20- and 27-node quadratic brick elements were also evaluated as potential

element candidates to be used in the models. With a fine mesh, both elements do a good job in predicting Westergaard's solutions; however, the execution time of the 27-node element is 60 percent more than the 20-node element (Lee, Wu, & Yen, 2004). The reduced integration 20-node quadratic brick element was chosen to be used throughout both models, even for tie bars and dowel bars. The mesh for each model was verified by decreasing the mesh fineness until it converged to Westergaard's solution.

## **3.2 PARAMETRIC STUDIES**

### **3.2.1 Longitudinal Shear Cracking**

There are several parameters that were found to be critical the development of longitudinal shear cracking. Those parameters consist of CTE, depth of mortar intrusion, and construction sequence. The construction sequence refers to the time sequence in which the mainline and shoulder are paved. A typical construction sequence consists of paving the mainline in the summer and paving the shoulder in the fall. The construction sequence is important because if the month of paving is known, a zero-stress temperature can be determined using Equation 2.1. It is thought that the difference in zero-stress temperatures between the mainline and shoulder is one of the major factors that contribute to longitudinal shear cracking (American Concrete Pavement Association).

The following variables have been defined to aid in explaining the parametric study for longitudinal shear cracking:

$T_S$ = Zero-stress temperature, which corresponds to time shoulder was placed, °F

$T_M$ = Zero-stress temperature, which corresponds to time mainline was placed, °F

$T_C$ = Pavement temperature at a point in time after paving is completed, °F

In every case studied presented in Section 2.1.1,  $T_S$  is less than  $T_M$ . Additionally, it appears that the distress manifests when  $T_C$  is greater than or equal to  $T_M$ . Merging those two limitations, the combinations for  $T_S$ ,  $T_M$  and  $T_D$  are limited to the following expression:  $T_C \geq T_M > T_S$ . As previously mentioned, PennDOT specifications state that paving will take place when the ambient temperature is between 50°F and 90°F, which corresponds to zero-stress temperatures of 70°F to 130°F, respectively using Equation 2.1. Combining the expression and range of zero-stress temperatures of 70°F to 130°F, the following table can be generated, which displays all of the critical combinations for construction sequence.

**Table 3.1.** Combination of construction sequences critical to longitudinal shear cracking.

$T_M$ , °F	$T_S$ , °F	$T_C$ , °F
80	70	80,90,100,110,120
90	80	90,100,110,120
90	80	90,100,110,120
100	90	100,110,120
100	80	100,110,120
100	70	100,110,120
110	100	110,120
110	90	110,120
110	80	110,120
110	70	110,120
120	110,100,90,80,70	120

The value of 130°F is not used in this parametric study because it is highly unlikely that pavement temperatures will reach values of that magnitude. In Pennsylvania, the only time a pavement would see a temperature of that magnitude is if the set time coincided with the peak temperature on the hottest day of the year. Since  $T_C$  must be greater than or equal to  $T_M$ , the

value of 130°F will not be used. Table 3.1 represents 35 different construction sequence combinations. These combinations will be used with two different CTE values, two different shoulder widths and three different mortar intrusion depths.

**Table 3.2.** Varied parameters not related to construction sequence for longitudinal shear cracking.

Parameter	Value		
CTE, $10^{-6} / ^\circ\text{F}$	4	6.5	
Depth of mortar intrusion, in	0	3.5	7

Table 3.2 presents the values chosen for the parameters not related to construction sequence. The values of 4 and  $6.5 \times 10^{-6} / ^\circ\text{F}$  were chosen because they represent values above and below the CTE of  $5.2 \times 10^{-6} / ^\circ\text{F}$  commonly observed for the aggregate types typical of those in Pennsylvania. The CTE is an important parameter to include because of its affect of the expansion and contraction of concrete. The depth of mortar intrusion represents a maximum, minimum and average value from the case studies mentioned in Section 2.1.1.

### 3.2.2 Shoulder Transverse Cracking

The parameters that were found to be critical to transverse cracking in the shoulder consist of CTE, stiffness of the shoulder, shoulder width, and construction sequence. Similar to longitudinal shear cracking, it is thought that the difference in zero-stress temperatures of the mainline and shoulder is one of the major factors that contribute to longitudinal shear cracking.

The same variables that were defined for the longitudinal shear cracking model apply to this model. The variables have been repeated below as a reminder.

$T_S$ = Zero-stress temperature, which corresponds to time shoulder was placed, °F

$T_M$ = Zero-stress temperature, which corresponds to time mainline was placed, °F

$T_C$ = Pavement temperature at a point in time after paving is completed, °F

The case study described in Section 2.1.2 is the focus of this parametric study. The climatic, material and structural conditions present in the case study will be used as a basis for establishing the parameters. The mainline was paved in October, which corresponds to a zero-stress temperature of approximately 80°F using Equation 2.1. The 2-ft shoulder was paved the following July, which corresponds to a zero-stress temperature ranging from 90°F to 110°F. During the week after paving, the ambient temperature ranged from 50°F to 80°F. The combination of construction sequences are presented in Table 3.3.

**Table 3.3.** Combination of construction sequences critical to shoulder transverse cracking.

$T_M$ , °F	$T_S$ , °F	$T_C$ , °F
80	90, 100, 110	50, 60, 70, 80

These combinations will be used with three different CTE values, three different shoulder widths and two different concrete ages. Table 3.4 presents the values selected for the parameters not related to construction sequence. The values of 4.5, 5.5 and 7.5 x 10<sup>-6</sup> /°F were chosen because they represent three typical CTE values. Two different stiffnesses were chosen to represent 1-day and 7-day strengths of the shoulder. Shoulder widths of 2, 5 and 10 ft were chosen to be included in the study. A 2-ft shoulder was present in the case study described. It is thought that one of the factors causing the 2-ft shoulder to crack is because of the width of the shoulder. Two additional shoulder widths of 5 and 10 ft were chosen to test this theory.

**Table 3.4.** Varied parameters not related to construction sequence for shoulder transverse cracking.

Parameter	Value		
Stiffness, psi	2,800,000	3,300,000	
CTE, 10 <sup>-6</sup> /°F	4.5	5.5	7.5
Shoulder width, ft	2	5	10

### 3.3 LONGITUDINAL SHEAR CRACKING MODEL

#### 3.3.1 Overview

The first model was developed to establish the failure criteria for longitudinal shear cracking. It was set up using a 45-ft by 24-ft mainline, a 10-ft outside shoulder and a 2-ft inside shoulder assuming that every third joint in the mainline had opened and no joints in the newly paved shoulder were open. The 45-ft by 24-ft mainline represents two lanes, typically 12-ft wide, and two transverse joints, typically spaced 15-ft apart. In the mainline, the joints that had opened were open wide while the shoulder joints remained closed.

An overall view of the model can be seen in Figure 3.1. It contains approximately 40,000, 20-node reduced integration 3-D quadratic brick elements. The outside edge is where the cracking was observed, which is why the mesh in that region is very fine. The mesh in the rest of the model is coarse to reduce computation time. The mesh fineness at the outside edge was reduced until the nodal stresses converged to a single value.

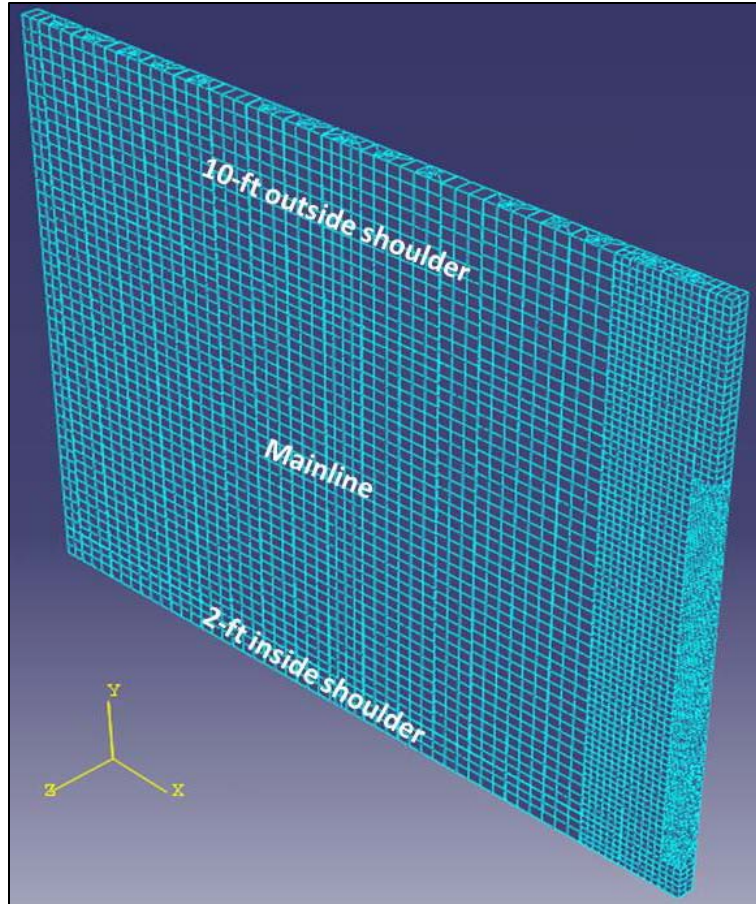


**Figure 3.1.** Overall view of longitudinal shear cracking model.

### **3.3.2 Parts and Material Properties**

The model consists of several sections. Within each section, there are several parts. The sections include the inside shoulder, the outside shoulder, the mainline and the tie bars. In ABAQUS, defining the geometry, by creating parts, is the basis for which the mesh is created. The various parts used to create the model can be seen in Figure 3.2.

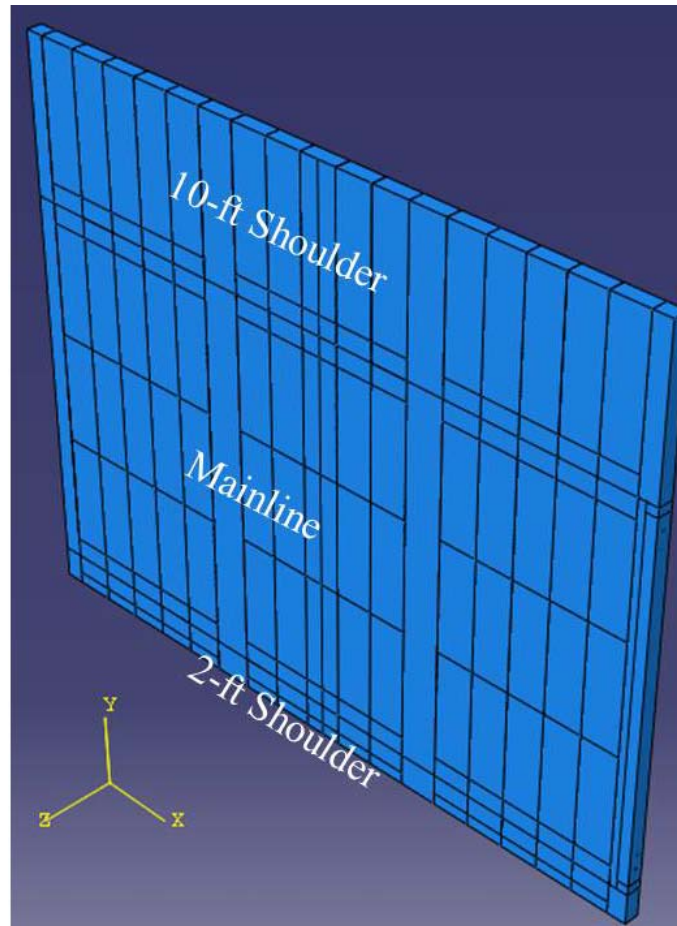


**Figure 3.2.** Overall view of parts that make up longitudinal shear cracking model.

The material properties used in the longitudinal shear cracking model can be found in Table 3.4. The elastic modulus and Poisson’s ratio values were chosen to represent typical values for a concrete pavement that has reached its ultimate strength. As previously mentioned, the CTE values of concrete in the pavement structure were varied between 4 and  $6.5 \times 10^{-6}/^{\circ}\text{F}$ . The unit weight of 0.084 pci corresponds to a typical value of 145 pcf.

**Table 3.5.** Material properties for longitudinal shear cracking model.

	Elastic modulus, psi	Poisson's ratio	CTE, $10^{-6}/^{\circ}\text{F}$	Unit weight, pci
Mainline	4,500,000	0.17	4 and 6.5	0.084
Shoulder	4,500,000	0.17	4 and 6.5	0.084
Tie bar	29,000,000	0.3	n/a	0.28
Dowel bar	29,000,000	0.3	n/a	0.28

### **3.3.2.1 Inside 2-ft Shoulder Section**

The inside 2-ft shoulder contains tie bars and runs along the inside edge of the pavement. The overall dimensions of the 2-ft shoulder section are 24 x 540 x 12 in.

### **3.3.2.2 Outside 10-ft Shoulder Section**

The outside 10-ft shoulder also contains tie bars and runs along the outside edge of the pavement. The overall dimensions of the 10-ft shoulder section are 120 x 540 x 12 in.

### **3.3.2.3 Mainline Section**

The mainline contains tie bars and dowel bars and is located in between the inside and outside shoulders. The overall dimensions of the mainline section are 288 x 540 x 12 in.

### **3.3.2.4 Steel Section**

The pavement section modeled included both tie bars and dowel bars. The tie bars are 30-in long with a diameter of 0.625 in. The dowel bars are 9-in long with a diameter of 1.5 in.

## **3.3.3 Contact Interactions**

Two contact interactions were used in the model. The first is between the slab and the supporting foundation and the second is between the mainline and the shoulders.

### **3.3.3.1 Elastic Foundation**

A Winkler foundation was used to model the granular material beneath the PCC slab. With a Winkler foundation, the slab rests on a bed of springs, which release when the slab deforms

upward thereby putting the spring in tension. The interaction is defined in the initial step and is carried out through the entire analysis (ABAQUS/CAE, 2007). The stiffness of the foundation is defined by setting the stiffness of the spring equal to the modulus of subgrade reaction (k-value) representing the composite stiffness of all layers beneath the slab. A k-value of 100 pci was used, which is a typical value for a granular base. A model of the slab resting on a Winkler foundation can be found in Figure 3.3.

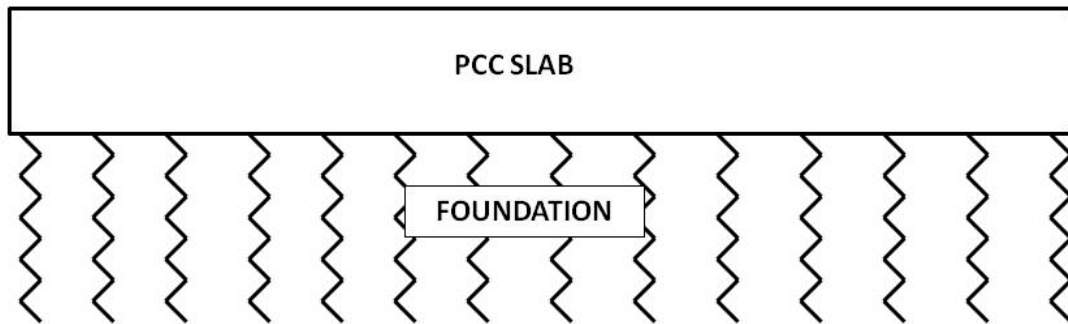


**Figure 3.3.** Model of slab resting on Winkler foundation.

### 3.3.3.2 Surface-to-Surface Contact

Contact between the mainline and both shoulders is defined by a surface-to-surface contact. In ABAQUS, surface-to-surface contacts are necessary to model interactions between two deformable bodies. A discretization method and sliding formulation must be chosen to yield the most accurate results. When selecting the surfaces of the interaction, one surface must be defined as the master surface and the other must be defined as the slave surface.

Choosing the proper discretization method is important so that the interaction between the surfaces is accurately modeled. The user can either choose surface-to-surface or node-to-surface. In the node-to-surface contact discretization, each slave node interacts with a group of nodes on the master surface. In theory, the slave nodes do not penetrate the master surface; however, it is possible if there are dissimilar meshes with irregular geometries. In a surface-to-

surface contact discretization, the contact is imposed over the slave surface and not at discrete points. In general, the surface-to-surface discretization is more accurate than node-to-surface in terms of pressure and stress results, especially if the geometry is representative. However, it usually requires more computational time (ABAQUS/CAE, 2007). Since the geometry of both models is representative of what is seen in the field, surface-to-surface discretization was chosen in order to yield the most accurate results.

There are two approaches for defining the relative motion between two surfaces in ABAQUS, finite-sliding and small-sliding. The most general approach, finite-sliding, allows the contact surfaces to undergo separation, sliding and rotation. In the small sliding approach, it is assumed that there will be little to no sliding between the surfaces. Slave nodes should slide less than an element length from their corresponding anchor point and still be contacting their local tangent plane (ABAQUS/CAE, 2007). A definition of the anchor point and local tangent plane from the ABAQUS User Manual can be seen in Figure 3.4. Small sliding was used in both models since the amount of sliding expected is less than an element length.

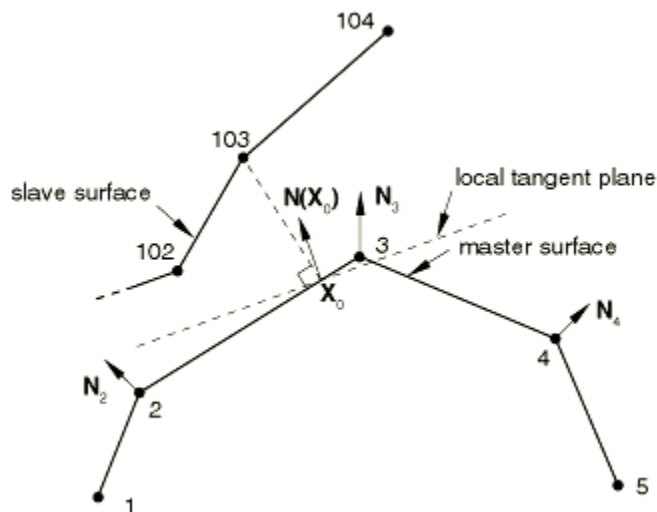


**Figure 3.4.** Definition of anchor point and local tangent plane for small sliding (ABAQUS/CAE, 2007).

There are a few general guidelines provided by ABAQUS for selecting the master and slave surfaces. For a surface-to-surface discretization with small sliding, the choice of the master and slave surfaces is not very sensitive. In both models, the master and slave surfaces have similar geometries and meshes. Therefore, choosing which surface to define as master was not as crucial as it is in some models. For this contact interaction, the mainline was chosen as the master surface and the shoulders were chosen as the slave surface.

Once the contact interaction is defined, a contact interaction property must be defined. In the case of the mainline and shoulder interactions, “hard” contact, no separation and no friction was chosen. Hard contact implies that the surfaces transmit no contact pressure unless the nodes of the slave surface contact the master surface. Also, there is no limit to the magnitude of contact pressure that can be transmitted when the surfaces are in contact (ABAQUS/CAE, 2007). Initially, the contact between the lane and shoulder joint was modeled with coulomb friction. However, that led to an extreme build-up of pressure at the interface. By modeling the surfaces to be frictionless, more reasonable results were obtained. This is also more reasonable since this surface is modeling a cold joint.

### **3.3.4 Loading**

ABAQUS allows the user to define a sequence of one or more analysis steps. By dividing the analysis into steps, it provides a convenient way to capture changes in the loading and boundary conditions of the model, changes in the way parts of the model interact with each other, and any other changes that may occur in the model during the course of the analysis (ABAQUS/CAE, 2007). When modeling longitudinal shear cracking, the loading was applied in two steps. In the

first step, the self weight of the model was applied using a gravity load. In the second step, a temperature was applied throughout the entire model.

#### **3.3.4.1 Gravity Load**

In ABAQUS, a gravity load can be applied if the density of the material is defined. The density for the concrete is defined as 0.084 lb/in<sup>3</sup> and the density for the steel is 0.28 lb/in<sup>3</sup>. The load, which has a magnitude of 386.4 in/s<sup>2</sup>, is applied in the z-direction throughout the entire model.

#### **3.3.4.2 Temperature Load**

Nodal temperatures can be applied as an initial condition or in any analysis step. In order for expansion or contraction to occur due to a change in temperature, a coefficient of thermal expansion must be defined. Temperatures can be applied via direct specification or through the use of an analytical field. Applying a temperature via direct specification allows the user to assign a uniform temperature to any part. An analytical field is a mathematical function that defines spatially varying parameters, like temperature. If the temperature distribution throughout a slab is known, a linear or quadratic function can be used to define the distribution and apply it to the model through an analytical field. Using an analytical field to define a temperature distribution requires significantly more computational time in comparison to using direct specification to apply a uniform temperature.

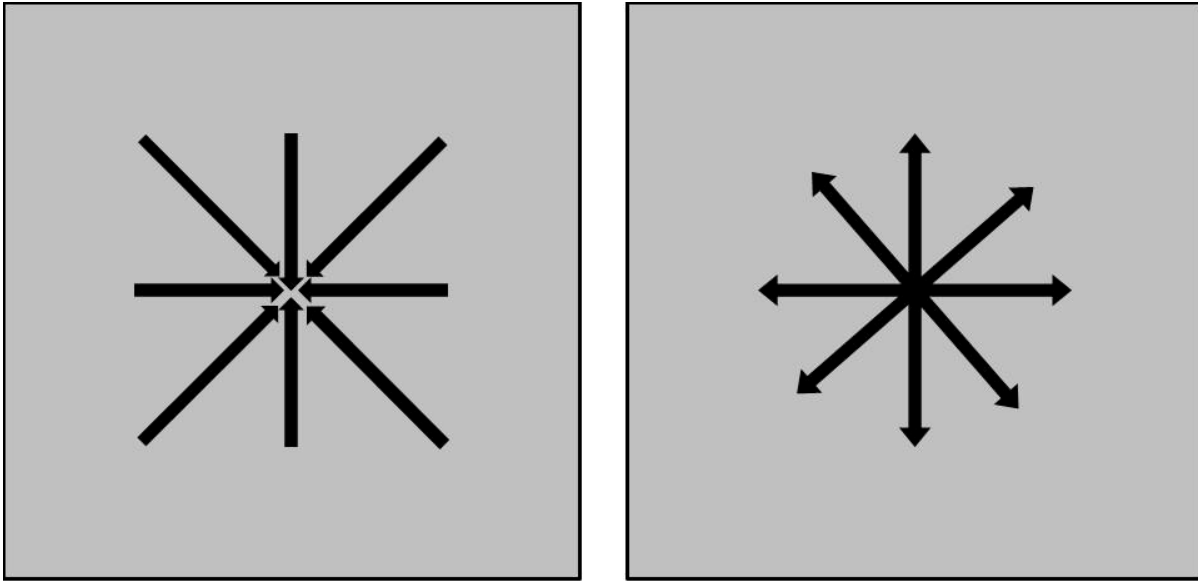
Temperature data came from several sources. When applying a uniform temperature, the data came from mean monthly temperatures typical for Pennsylvania. Predicted temperature gradients from the enhanced integrated climatic model, which is a one-dimensional coupled heat and moisture flow model, were used to see the effect of temperature gradients on each model. The enhanced integrated climatic model (EICM) is used to predict changes in behavior and

characteristics of pavement and unbound materials in conjunction with environmental conditions (Zapata & Houston, 2008). When validating the model, measured temperature data from thermocouples installed in a smart pavement at US-22 in Murrysville, Pennsylvania was used. Data collected from this project includes over five years of temperature data. It is an excellent representation of typical temperature distributions encountered in Pennsylvania.

In the initial step, a uniform temperature was applied to each slab representing the zero-stress temperature. During the second step, either a uniform temperature or temperature gradient was applied representing the transient temperature in the slab at a point in time after paving.

#### **3.3.4.3 Surface Traction**

The base was modeled using a surface traction force. Since the traction force is applied over a surface, the units are psi. By modeling the base this way, the computational time was significantly decreased because a separate base did not have to be meshed. If the slab is expanding, the surface traction force is applied radially inward and if the slab is contracting, the surface traction force is applied radially outward. This can be seen in Figure 3.5.



Expansion

Contraction

**Figure 3.5.** Surface traction applied to bottom of slab to represent base.

The surface traction force was calculated by determining the force required to drag the slab across a base and then dividing that force by the surface area of the bottom of the slab. Equation 3.1 was used to determine the surface traction force.

$$\text{SurfaceTraction} = \frac{\text{Forcerequiredtodragslabacrossbase}}{\text{SurfaceAreaofBottomofSlab}} \quad (\text{Equation 3.1})$$

The force required to drag a slab across a base is presented in Equation 3.2.

$$F = L * W * H * UW * \mu \quad (\text{Equation 3.2})$$

Where:

F=Force required to drag slab across base, lb

L=Length of slab, in

W=Width of slab, in

H=Slab thickness, in

UW=Unit weight of slab, pci

$\mu$ =Coefficient of friction

A study was performed at the Indian Institute of Technology that established coefficients of friction between the concrete slab and the underlying base. The study determined that once the initial bond between the concrete slab and base was broken, the coefficient of friction significantly decreased (Maitra, Reddy, & Ramachandra, 2009). Based on the findings presented, a coefficient of friction of 0.8 was selected. Using Equation 3.1, the surface traction force for a stabilized base is 0.8 psi.

### **3.3.5 Boundary Conditions**

The boundary conditions in the longitudinal shear cracking model can be seen in Figure 3.6 and Figure 3.7. Figure 3.6 shows the boundary conditions for the cases where there is no mortar intrusion and Figure 3.7 shows the boundary conditions for the cases where there is mortar intrusion. By restricting the shoulder movement in the x-direction and allowing the mainline to be free, this simulates closed shoulder joints and open mainline joints. Since a gravity load has been applied, the entire model is free in the z-direction.

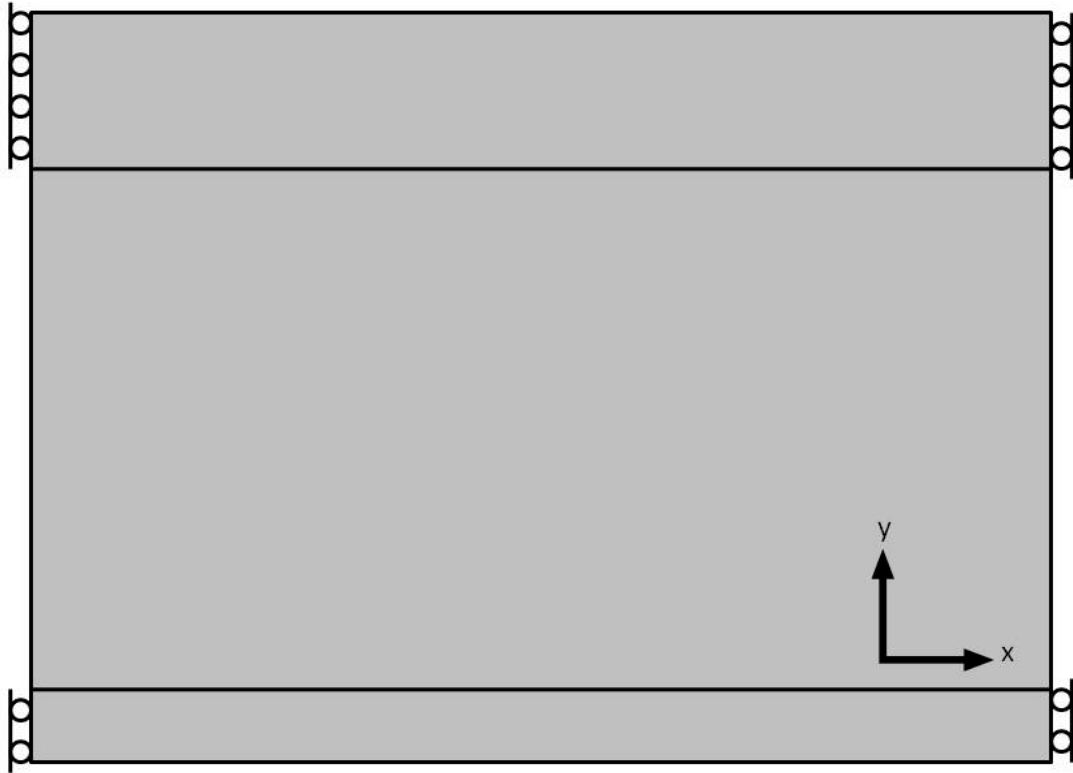


**Figure 3.6.** Longitudinal shear cracking boundary conditions with no mortar intrusion.

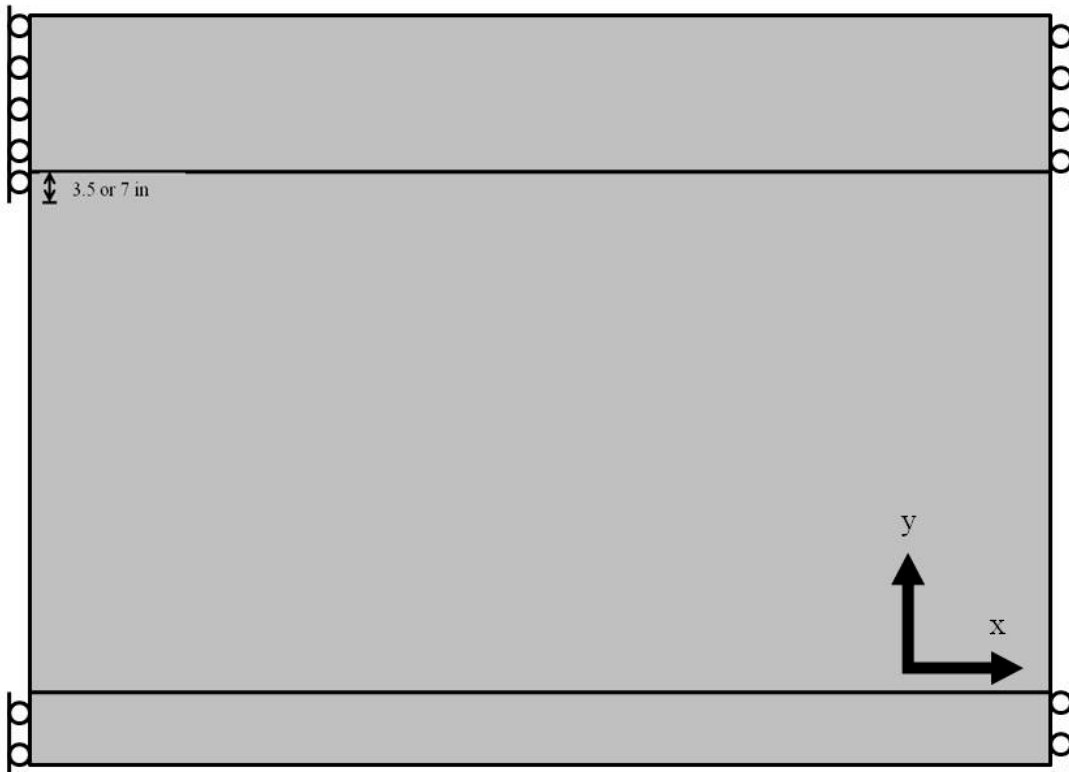


**Figure 3.7.** Longitudinal shear cracking boundary conditions with mortar intrusion.

### **3.3.6 Mesh**

Since there are several geometric discontinuities throughout the model, i.e. tie bars and dowel bars, difficulties can arise when meshing since brick elements are being used and the geometries are incompatible. Elements can have large aspect ratios and interior angles that are less than 60° and greater than 120°. By creating partitions in the model, the majority of the problems that are encountered while creating a mesh can be eliminated. As previously mentioned, 20-node quadratic, reduced integration brick elements were used throughout the model, including tie bars and dowel bars.

## **3.4 SHOULDER TRANSVERSE CRACKING MODEL**

### **3.4.1 Overview**

A model was developed to evaluate the potential for the development of transverse cracking in the shoulder. It consisted of a 15-ft by 12-ft mainline and shoulder widths ranging from 2, 5 and 10 ft wide.

An overall view of the model can be seen in Figure 3.11. It contains approximately 6,500, 20-node reduced integration 3-D quadratic brick elements. The mesh fineness at the outside edge was reduced until the nodal stresses converged to a single value.

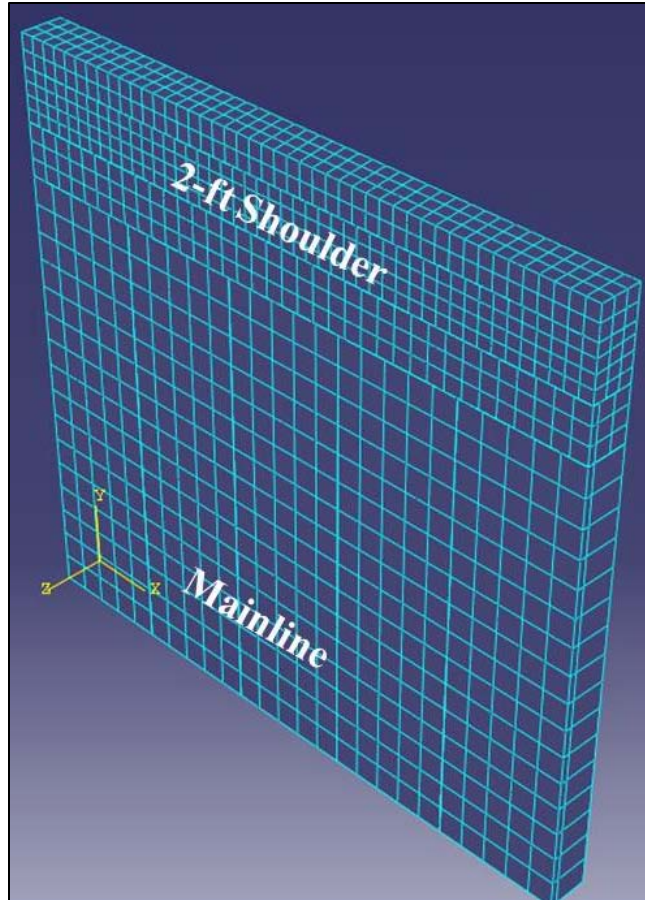


**Figure 3.8.** Overall view of shoulder transverse cracking model.

### **3.4.2 Parts and Material Properties**

The model is made up of several sections. The sections include the shoulder, the mainline and the tie bars. The various parts used to create the model can be seen in Figure 3.9.

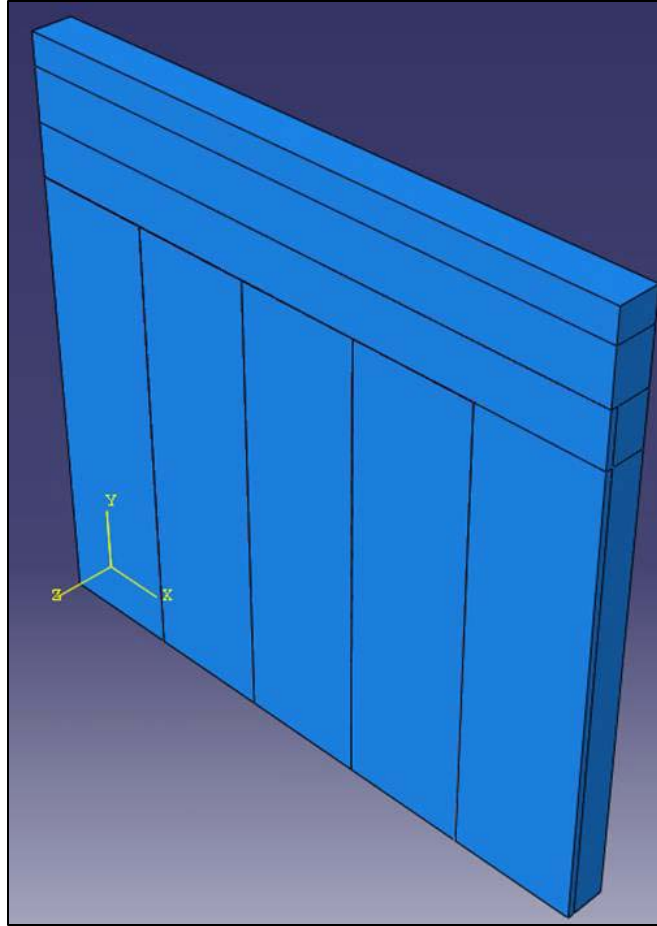


**Figure 3.9.** Overall view of parts that make up shoulder transverse cracking model.

The material properties used in the shoulder transverse cracking model can be found in Table 3.6. The elastic modulus and Poisson's ratio of the mainline represent the values of the concrete cores tested in the laboratory. The elastic modulus of the shoulder was varied between 2.8 and 3.3 million psi to represent 1-day and 7-day strengths. Chapter 4 discusses how these values were established. As previously mentioned, the CTE values of concrete in the pavement structure were varied between  $4.5, 5.5$  and  $7.5 \times 10^{-6}/^{\circ}\text{F}$ . The unit weight of the concrete is 0.084 pci, which corresponds to a typical value of 145 pcf.

**Table 3.6.** Material properties for shoulder transverse cracking model.

	Elastic modulus, 10 <sup>6</sup> psi	Poisson's ratio	CTE, 10 <sup>-6</sup> /°F	Unit weight, pci
Mainline	4.5	0.17	3.5, 4.5, 5.5	0.084
Shoulder	2.8 and 3.3	0.17	3.5, 4.5, 5.5	0.084
Tie bar	29	0.3	n/a	0.28

### **3.4.2.1 Shoulder Section**

For the 2-ft shoulder, the overall dimensions of the shoulder section are 24 x 180 x 12 in. The width of the shoulder increases to 60 in and 120 in for the wider shoulder widths considered.

### **3.4.2.2 Mainline Section**

The overall dimensions of the mainline section are 144 x 180 x 12 in.

### **3.4.2.3 Steel Section**

The steel section is made up of tie bars. The tie bars are 30-in long with a diameter of 0.625 in.

## **3.4.3 Contact Interactions**

The same contact interactions that were used in the longitudinal shear cracking model are used in this model. The k-value of 100 pci was again used as the stiffness for the Winkler foundation. The surface to surface contact between the mainline and the shoulder is modeled in the same manner as model used for evaluating the potential of longitudinal shear cracking in Section 3.3.3.

### **3.4.4 Loading**

Similar to the longitudinal shear cracking model, loading was applied in two steps. In the first step, the self weight of the model was applied using a gravity load with a magnitude of 386.4 in/s<sup>2</sup>. In the second step, a temperature was applied throughout the entire model.

#### **3.4.4.1 Gravity Load**

The density for the concrete is defined as 0.084 lb/in<sup>3</sup> and the density for the steel is 0.28 lb/in<sup>3</sup>. The gravity load, which has a magnitude of 386.4 in/s<sup>2</sup>, is applied throughout the entire model.

#### **3.4.4.2 Temperature Load**

In the initial step, a uniform temperature was applied to each slab representing the zero-stress temperature. During the second step, either a uniform temperature or temperature gradient was applied representing the transient temperature in the slab at a point in time after paving. Temperature data was obtained from the same sources as in Section 3.3.4.2.

#### **3.4.4.3 Surface Traction**

The base was modeled using a surface traction force, similar to the longitudinal shear cracking model. Using Equation 3.1, the surface traction force for a stabilized base is 1.8 psi and 1.5 psi for an unstabilized base.

### 3.4.5 Boundary Conditions

The boundary conditions in the shoulder transverse cracking model can be seen in Figure 3.10. Since the adjacent lane is tied to the mainline, to simulate this, the outer edge of the mainline is restricted. A symmetry boundary condition is applied in the y-direction. This makes the effective length of the model 90 in. With this type of boundary condition, the computational time is cut in half with no loss in accuracy. Since a gravity load has been applied, the entire model is free in the z-direction.

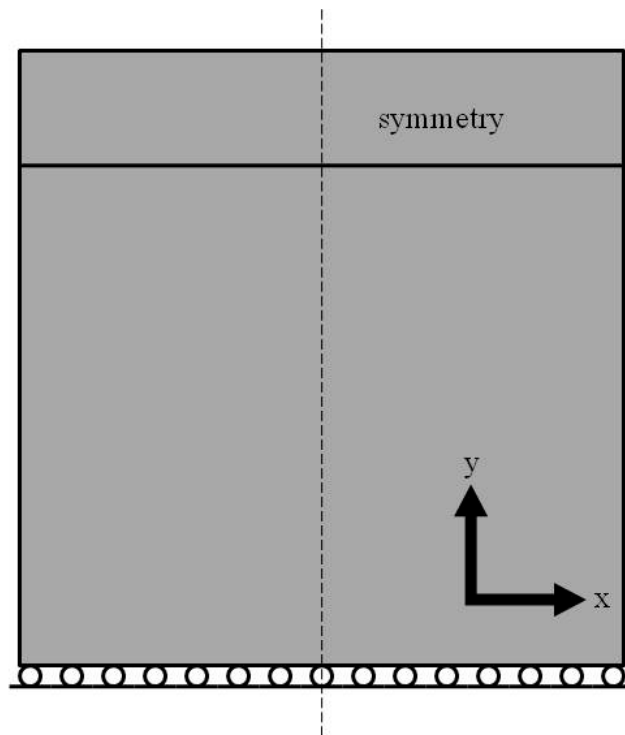


**Figure 3.10.** Shoulder transverse cracking boundary conditions.

### 3.4.6 Mesh

The mesh for this model was created in the same manner as the model for evaluating longitudinal shear cracking. Since there are several geometric discontinuities throughout the model, i.e. tie

bars, difficulties can arise when meshing since brick elements are being used and the geometries are incompatible. By creating partitions in the model, the majority of the problems that are encountered while creating a mesh can be eliminated. As previously mentioned, 20-node quadratic, reduced integration brick elements were used throughout the model, including tie bars.

### 3.5 VALIDATION

Both finite element models were validated using field data collected from vibrating wire strain gages located at three different depths throughout the pavement. Strains measured in the field due to changes in temperature are compared to the strains predicted using the finite element method. The zero-stress temperature profile for the pavement in the field, which was established by Asbahan (2009), was used to establish the initial condition in ABAQUS. Later on in the analysis, a different temperature profile was introduced into the model to represent a point in time after paving. Twenty-two different temperature profiles were chosen to validate the model. The profiles include equivalent linear temperature gradients ranging from  $-0.8$  °F/in to  $1.86$  °F/in. The equivalent linear zero-stress temperature gradient is  $0.32$  °F/in. The accuracy of the model is evaluated using a statistical analysis. The predicted strain is plotted against the measured strain for all of the temperature profiles. The results from the validation study can be seen in Figure 3.11, Figure 3.12, and Figure 3.13, which represent the strains at the top, middle and bottom of the slab, respectively. The correlation coefficient ( $R^2$ ) between predicted and measured is equal to 0.96, 0.997, and 0.91 for the top middle and bottom of the slab, respectively. This indicates that the models accurately reflect the response of the pavement measured in the field for 22 different temperature loading conditions.

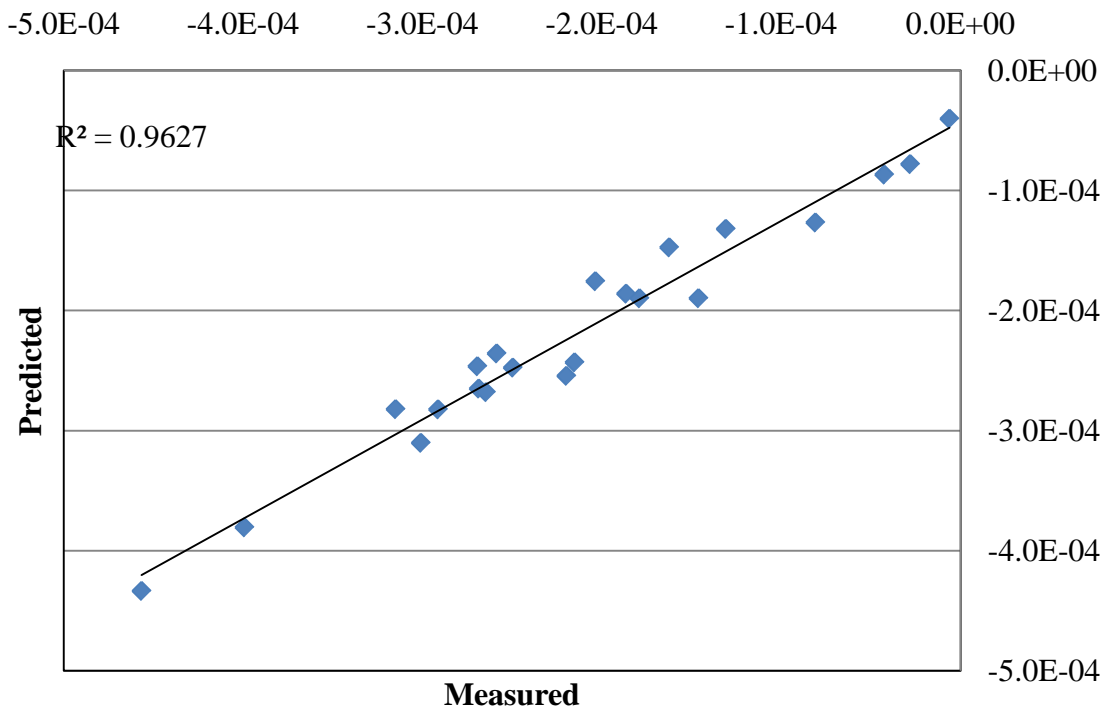


**Figure 3.11.** Predicted vs. measured strains for the top of the slab.

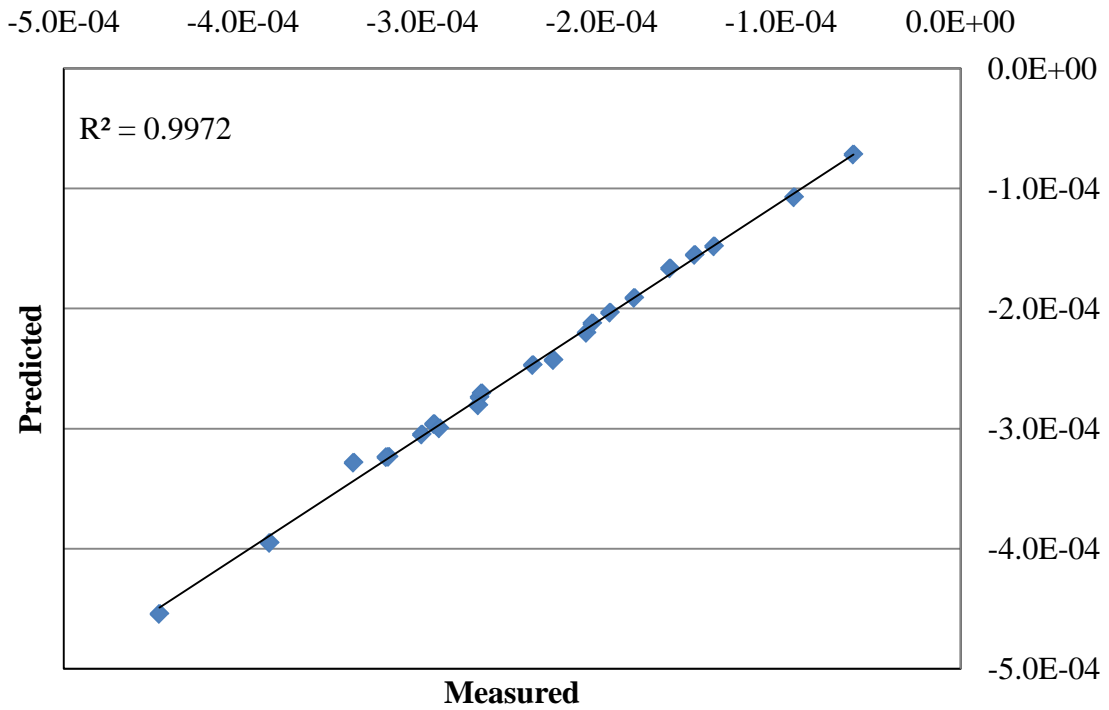


**Figure 3.12.** Predicted vs. measured strains for the middle of the slab.

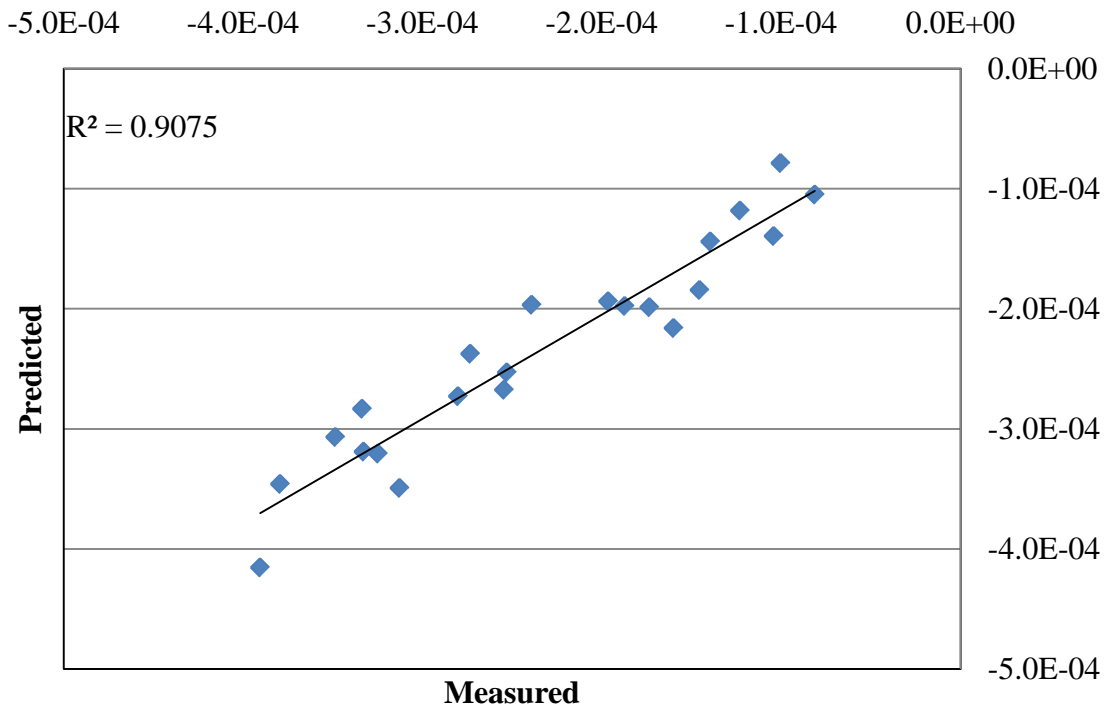


**Figure 3.13.** Predicted vs. measured strains for the bottom of the slab.

## 4.0 PARAMETRIC STUDY RESULTS

As mentioned in Section 3.3.2 and Section 3.4.2, concrete was modeled by defining the elastic modulus, Poisson's ratio, unit weight and coefficient of thermal expansion. Since the elastic modulus and the strength of the concrete are correlated material properties, the defined strengths were used to establish the elastic modulus.

When analyzing the development of transverse cracking in the shoulder, 7- and 28-day compressive strength cylinders that were cast during construction were available. These compressive strengths were correlated to the elastic modulus of the concrete and split tensile strength. While the elastic modulus was used in the FE analysis, the split tensile strength was used to establish the level of stress at which cracking would develop in the shoulder. In the longitudinal shear cracking study, the elastic modulus was assumed based on typical values and correlations were then used to define the split tensile strength. The methods used to establish these values are described below.

Equation 4.1 was used to estimate the split tensile strength based on the measured compressive strength. The elastic modulus was also estimated based on the compressive strength. The following procedure was used to establish the elastic modulus and split tensile strength based on the compressive strength. The first step is to use the compressive strength to estimate the split tensile strength using Equation 4.1.

$$f'_{sp} = 4.34 f'_c{}^{0.55} \quad (\text{Equation 4.1})$$

where,

$f'_{sp}$  = split tensile strength, psi

$f'_c$  = compressive strength at 28 days, psi

Using Equation 4.2, the elastic modulus can be estimated for a given compressive strength.

$$E_c = 33\rho^{3/2}\sqrt{f'_c} \quad (\text{Equation 4.2})$$

where,

$E_c$  = PCC elastic modulus, psi

$\rho$  = unit weight of concrete, lb/ft<sup>3</sup>

$f'_c$  = PCC compressive strength at 28 days, psi

Using the procedure outlined above, the split tensile strength was determined for each analysis. Any location in the model where the tensile stress is greater than the strength, there is potential for a crack to develop. For the longitudinal shear cracking model, the tensile strength of the concrete is 650 psi. For the shoulder transverse cracking model, the tensile strength of the concrete is 300 psi for a stiffness of 2.8 million psi and 350 psi for a stiffness of 3.3 million psi.

#### 4.1 LONGITUDINAL SHEAR CRACKING MODEL

As the name states in the literature, this type of distress is caused by a shear failure; however, the results from the model show that the crack initiates due to a tensile failure. It is possible that

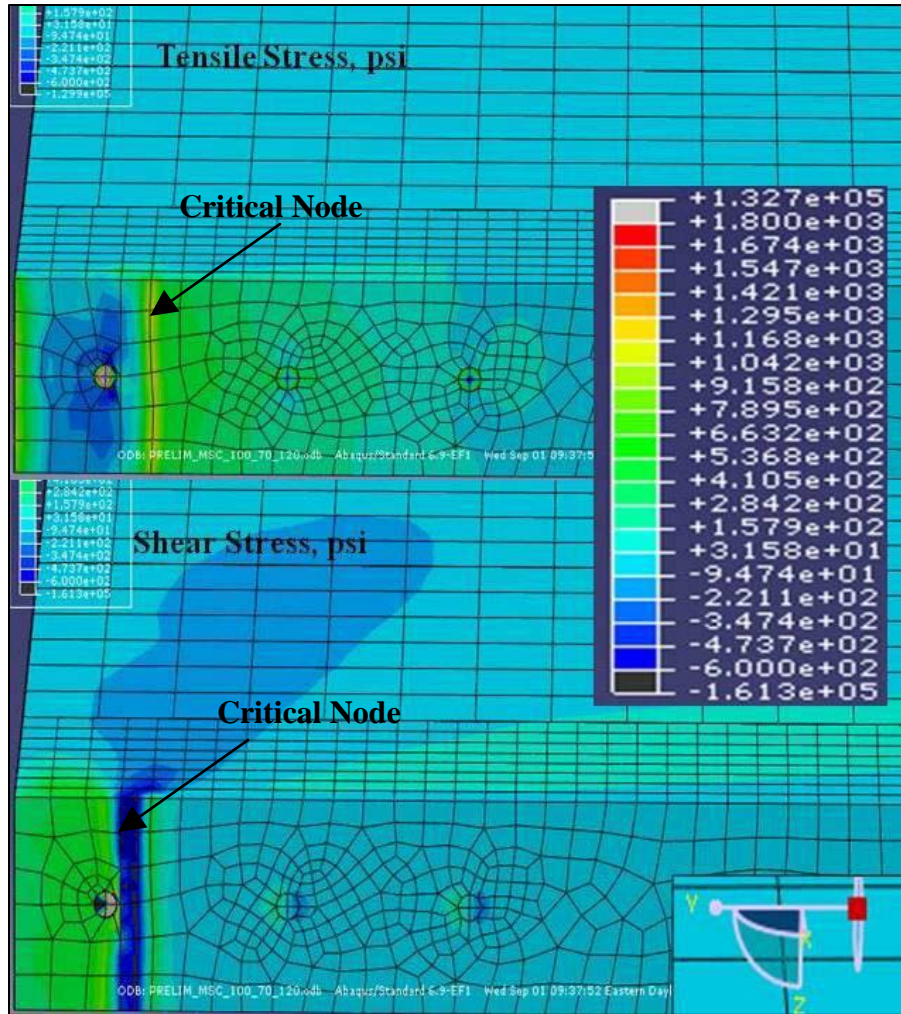
once the crack initiates, the resulting propagation is caused by shear stresses. The propagation of the crack is beyond the scope of this analysis.

Figure 4.1 compares the shear stresses with the tensile stresses for an analysis in which there is a strong possibility that a crack will form. Only the contour for the  $\sigma_{xy}$  is shown in the Figure 4.1, because the  $\sigma_{xz}$  and  $\sigma_{yz}$  are nearly zero.

The critical zone for the shear stress can be easily identified using the contour plot in Figure 4.1. This analysis showed that the critical mode of failure was in tension since the stress to strength ratio in tension was always higher than in compression.

After examining a node in the critical zone for tensile stress (shown in Figure 4.1), the maximum and minimum principle stresses were found to be approximately 1,200 and 50 psi, respectively. According to Kupfer et al. (1969), the tensile strength of concrete under biaxial tension is not affected by its multiaxial state of stress (Kupfer, Hilsdorf, & Rusch, 1969). Therefore, the tensile strength of the concrete (modulus of rupture), which was correlated from the elastic modulus and calculated to be 750 psi, can be compared to the maximum principle stress, which in this case would result in a tensile failure.

Although it was first hypothesized that the cracks were due to a shear failure they actually occur due to a tensile failure. For each analysis, the tensile stresses in the transverse direction ( $\sigma_y$ ) were used to determine the presence of a crack. Recall that in Figure 2.1 the crack initially forms in the longitudinal direction. Since the tensile stresses in the transverse direction ( $\sigma_y$ ) are larger than the tensile stresses in the longitudinal direction ( $\sigma_x$ ), a longitudinal crack would form because cracks initiate perpendicular to the maximum stress.



**Figure 4.1.** Comparison of shear stresses and tensile stresses for longitudinal shear cracking model.

#### 4.1.1 Construction Sequence

Recall that the construction sequence refers to the time sequence in which the mainline and shoulder are paved. A typical construction sequence consists of paving the mainline in the summer and paving the shoulder in the fall.

As a reminder, the variables that have been defined for this model are repeated below with one additional variable. The new variable,  $T_D$ , was created to highlight the importance of

the difference in zero-stress temperatures of the mainline and shoulder and its influence on the distress.

$T_S$ = Zero-stress temperature which corresponds to time shoulder was placed, °F

$T_M$ = Zero-stress temperature which corresponds to time mainline was placed, °F

$T_C$ = Pavement temperature at a point in time after paving is completed, °F

$T_D = T_M - T_S$ , °F

Figure 4.2 shows the overall results for this parametric study. The x-axis consists of a range of values of  $T_C$  for different CTE values, depth of mortar intrusion and values of  $T_D$ . As seen in Figure 4.2, regardless of the magnitude of  $T_S$  and  $T_M$ , the influence of  $T_D$  remains the same. A construction sequence in which  $T_M = 100^\circ\text{F}$  and  $T_S = 80^\circ\text{F}$  will exhibit the same magnitude of stress as a construction sequence where  $T_M = 90^\circ\text{F}$  and  $T_S = 70^\circ\text{F}$ . As  $T_D$  increases, the probability of a crack developing increases as well. Figure 4.2 shows  $T_D$  versus tensile stress for all cases with no mortar intrusion. If the CTE is somewhat low, the critical value of  $T_D$  is approximately  $30^\circ\text{F}$ . If the CTE is somewhat high, the critical value of  $T_D$  is approximately  $20^\circ\text{F}$ . These are only approximate values since a change in concrete stiffness, CTE or another parameter could change the critical  $T_D$  value. Figure 4.2 also highlights the importance of the  $T_C$  parameter. For cases where there is no mortar intrusion,  $T_C$  is not significant. When there is mortar intrusion, the tensile stress tends to increase when  $T_C$  increases.

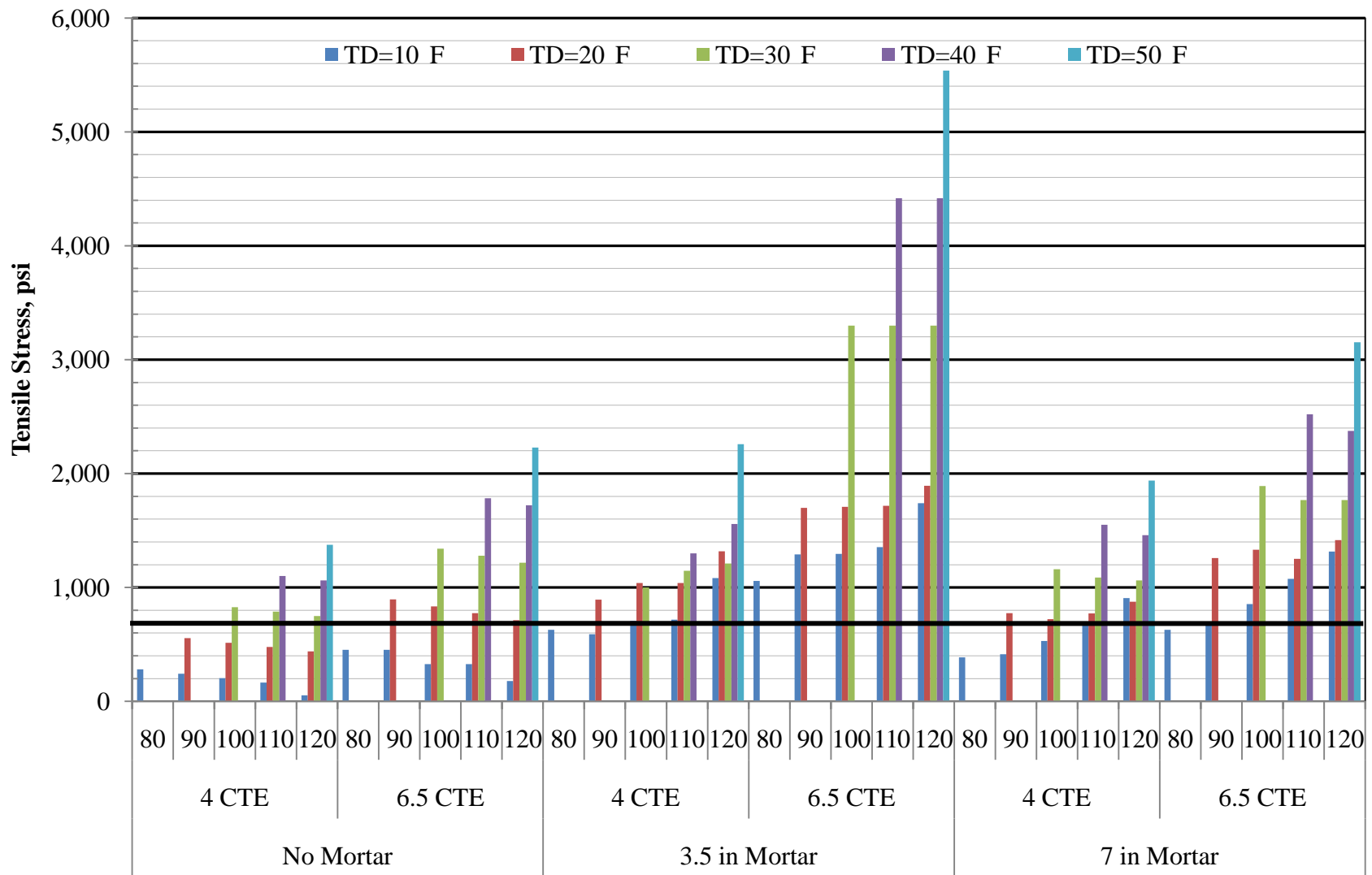
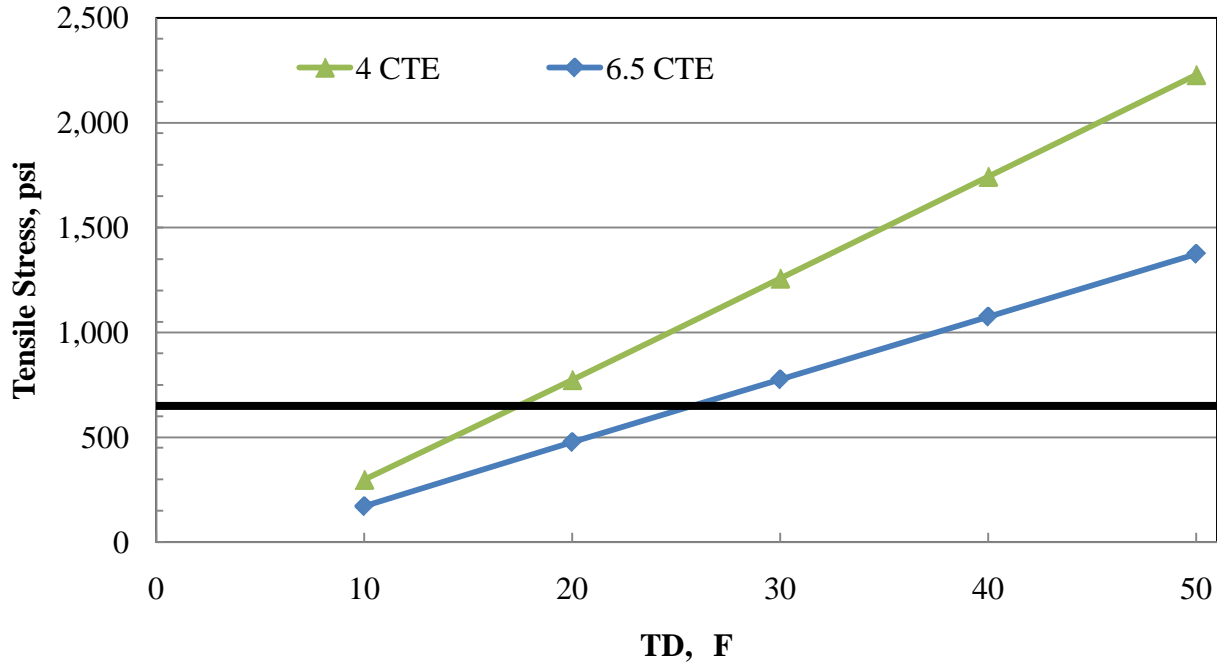


Figure 4.2. Summary of construction sequence results for longitudinal shear cracking.



**Figure 4.3.**  $T_D$  versus stress with no mortar intrusion in longitudinal shear cracking model.

Table 4.1 presents a review of the cases discussed in Section 2.1.1 so that the field observations could be compared to the results of the FE study. The values of  $T_M$  and  $T_S$  were estimated using Equation 2.1 for each study. The exact temperatures at the time of paving are unknown. It is possible that  $T_M$  and  $T_S$  could be higher or lower by  $10^\circ\text{F}$  or more due to variability in daily temperatures. In each study,  $T_D$  is greater than the critical value of  $30^\circ\text{F}$ . The field observations agree with the FE results, even if there is variability in the value of  $T_D$ .

**Table 4.1.** Review of field observations for longitudinal shear cracking model.

Study	$T_M, ^\circ\text{F}$	$T_S, ^\circ\text{F}$	$T_D, ^\circ\text{F}$	Notes
ACPA Report	104	61	43	Mortar intrusion $\geq 1.5$ in
I-81 Pennsylvania	80	45	35	Mortar intrusion unknown
1-64 West Virginia	110	65	45	Mortar intrusion $\geq 4.5$ in

Table 4.2 shows the value of  $T_D$  for different construction sequences in Pennsylvania. The cells that are highlighted in yellow represent construction sequences where there might be a

risk for a longitudinal shear crack to develop for the range of conditions considered in this study. The gray cells represent construction sequences that do not meet paving PennDOT paving specifications. If the MMT is known for a particular region, this table can be generated and used to determine which construction sequences are suitable for paving.

Based on this study, if the mainline is constructed outside of the May to September time window, the contractor should wait to tie on the shoulder until the value of  $T_D$  can be lower. To estimate the best times for paving in other climatic regions, Equation 2.1 can be used to determine the difference in zero-stress temperatures for each month.

**Table 4.2.** Guidelines for choosing appropriate construction sequence in Pennsylvania for longitudinal shear cracking.

		<b>Month of Mainline Paving</b>											
		<b>Jan</b>	<b>Feb</b>	<b>Mar</b>	<b>Apr</b>	<b>May</b>	<b>Jun</b>	<b>Jul</b>	<b>Aug</b>	<b>Sept</b>	<b>Oct</b>	<b>Nov</b>	<b>Dec</b>
<b>Month of Shoulder Paving</b>	<b>Jan</b>												
	<b>Feb</b>												
	<b>Mar</b>												
	<b>Apr</b>				0	13	27	30	29	16	2		
	<b>May</b>				13	0	13	17	16	3	15		
	<b>Jun</b>				27	13	0	4	3	10	29		
	<b>Jul</b>				30	17	4	0	1	14	32		
	<b>Aug</b>				29	16	3	1	0	13	31		
	<b>Sept</b>				16	3	10	14	13	0	18		
	<b>Oct</b>				2	15	29	32	31	18	0		
	<b>Nov</b>												
	<b>Dec</b>												

#### 4.1.2 Coefficient of Thermal Expansion

Figure 4.2 shows the effects of CTE has on the magnitude of stress. As expected, a larger CTE results in a higher potential for cracking to occur while a lower CTE reduces the potential of

cracking. The CTE can be estimated using Equation 4.3 and Table 4.3. If the CTE turns out to be high, extra precautions should be taken to decrease the value of  $T_D$ .

$$\alpha_{PCC} = \alpha_{agg} * V_{agg} + \alpha_{paste} * V_{paste} \quad (\text{Equation 4.3})$$

where,

$\alpha_{PCC}$  = Coefficient of thermal expansion of concrete.

$\alpha_{agg}$  = Coefficient of thermal expansion of aggregate.

$V_{agg}$  = Volumetric proportion of the aggregate in the PCC mix.

$\alpha_{paste}$  = Coefficient of thermal expansion of paste.

$V_{paste}$  = Volumetric proportion of the paste in the PCC mix.

**Table 4.3.** Typical coefficient of thermal expansion ranges for common aggregates and concrete (ARA Inc., ERES Consultants Division, 2004).

Material Type	Coefficient of Thermal Expansion, $10^{-6}/^{\circ}\text{F}$	Concrete Coefficient of Thermal Expansion (made from this material), $10^{-6}/^{\circ}\text{F}$
<b>Aggregates</b>		
Marbles	2.2-3.9	2.3
Limestones	2.0-3.6	3.4-5.1
Granites & Gneisses	3.2-5.3	3.8-5.3
Syenites, Diorites, Andesite, Basalt, Gabbros, Diabase	3.0-4.5	4.4-5.3
Dolomites	3.9-5.5	5.1-6.4*
Blast Furnace Slag		5.1-5.9
Sandstones	5.6-6.7	5.6-6.5
Quartz Sands & Gravels	5.5-7.1	6.0-8.7
Quartzite, Cherts	6.1-7.0	6.6-7.1
<b>Cement Paste (saturated)</b>		
w/c = 0.4 to 0.6	10-11	--
<b>Concrete Cores</b>		
Cores from LTPP pavement sections, many of which were used in calibration	N/A	$4.0*10^{-6}$ – $5.5*10^{-6}$ – $7.2*10^{-6}$ (Min – Mean – Max)

### **4.1.3 Depth of Mortar Intrusion**

Figure 4.2 illustrates the influence that mortar intrusion has on the potential for longitudinal shear cracks to develop. When the depth of mortar intrusion was varied, it was assumed that the greatest depth of mortar intrusion would result in the highest potential for a crack to occur. As it turns out, a mortar intrusion of 3.5 in yields higher tensile stresses than a mortar intrusion of 7 in. This phenomenon can be seen in Figure 4.2, which compares two identical models that have different depths of mortar intrusion. It is believed that the cause for this increase in tensile stress is due to the dowel bars and the discontinuity introduced by their presence. The center of the first dowel bar is located 6 in from the edge of the pavement. The first 3.5 in of the mainline are restrained from expanding and the first discontinuity (dowel bar) is found approximately 2 in away from the edge of the restraint. The highest tensile stresses can be seen in the vicinity of the first dowel bar. For the 7 in mortar intrusion, the first dowel bar is restrained and does not seem to cause a buildup of tensile stress. The next discontinuity is approximately 10 in away. It appears that the discontinuity introduced by the dowel is the reason that the 3.5 in mortar intrusion has such high tensile stresses.

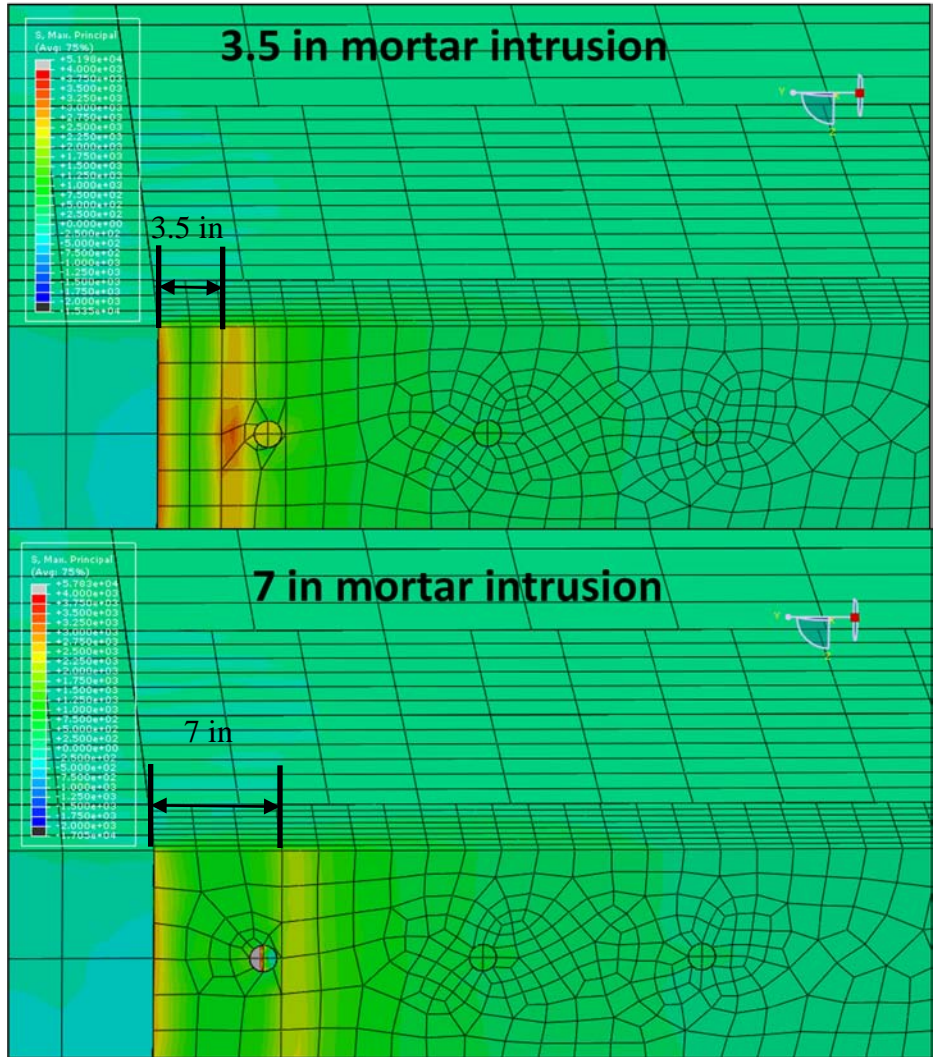


**Figure 4.4.** Comparison of 3.5-in mortar intrusion and 7-in mortar intrusion for the longitudinal shear cracking model.

Regardless of the depth of mortar intrusion, the corner of the mainline slab has a high stress concentration as seen in Figure 4.5. The reason for the high tensile stress concentration is because there is a part of the mainline that extends beyond the shoulder due to the boundary conditions specified. Recall that the entire pavement structure is expanding due to an increase in temperature. The shoulder is restrained from moving in the x-direction and the mainline is free to expand, which is why part of the mainline is extended beyond the shoulder. The part of the mainline that extends beyond the shoulder is still expanding in all directions. In the y-direction,

it is restrained by the presence of the shoulder, which is the reason for the high tensile stress concentration.

In Figure 4.6, the shoulder has been removed so that the distribution of tensile stress in the mainline can be seen more clearly. Based on this figure, it is clear that the tensile stress concentration is due to the overhanging part of the mainline. It was originally thought that the tensile stress concentration could be due to the adjacent tie bar; however, Figure 4.6 disproves this theory. In reality, this high tensile stress concentration would probably not exist because there would be an adjacent slab preventing the expansion in the y-direction.

Figure 4.7 is showing Figure 4.6 zoomed out. In this figure, there is a tensile stress concentration originating from the first tie bar and the first dowel bar (indicated by arrow). The shape of this stress concentration is somewhat similar to the shape of the cracks typically seen in longitudinal shear cracking examples. Refer to Figure 2.1.

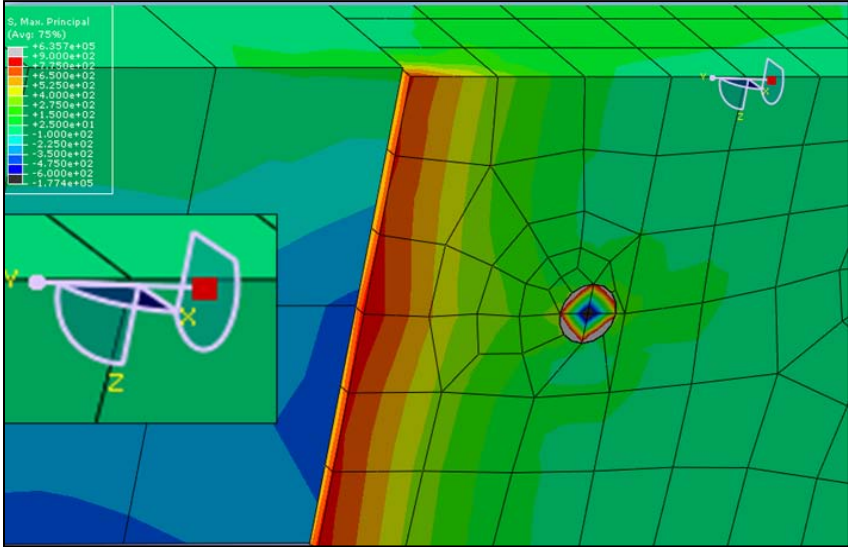


**Figure 4.5.** Close-up of lane-shoulder longitudinal joint where the mainline extends beyond the shoulder in longitudinal shear cracking model.

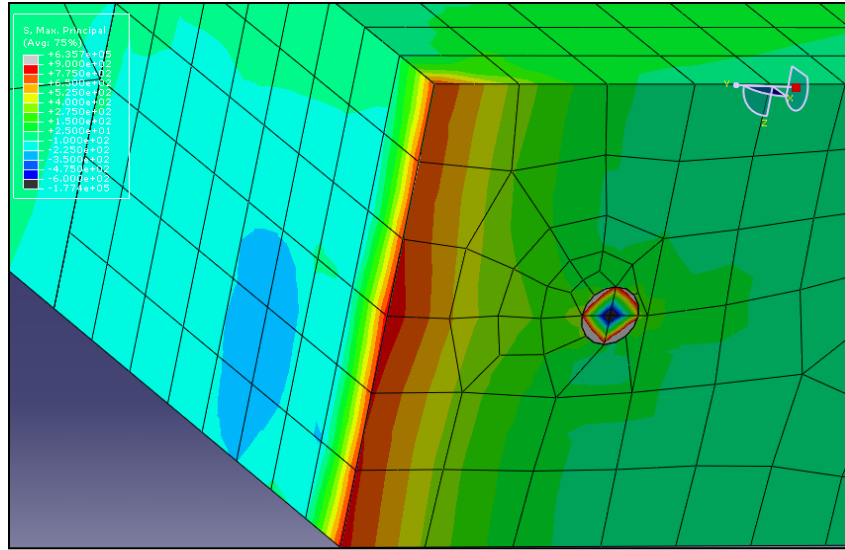


**Figure 4.6.** Close-up of lane-shoulder longitudinal joint with the shoulder removed for the longitudinal shear cracking model.

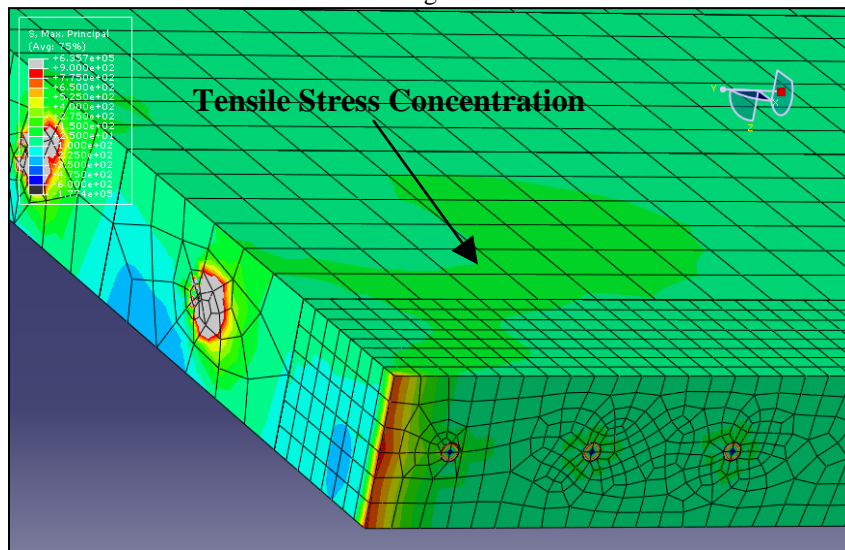


**Figure 4.7.** Overall view of lane-shoulder longitudinal joint with the shoulder removed for the longitudinal shear cracking model.

In Table 4.4, which summarizes the field observations in terms of this parametric study, two out of the three studies had mortar and saw slurry in the transverse joints. In the other study, cores were not pulled so it is unknown whether mortar had penetrated in to the transverse joint.

#### 4.1.4 Gradients

Positive and negative linear gradients with a magnitude of 1.37 were run using different weighted averages. The distribution of the gradients still satisfied the expression of  $T_C \geq T_M > T_S$ . A total of 14 different scenarios were run. A summary of the different construction sequences simulated using gradients is summarized in Table 4.4.

**Table 4.4.** Summary of construction sequences simulated using gradients.

Weighted Average of Gradient, °F	Magnitude of Gradient	Construction Sequence ( $T_M$ - $T_S$ )
110	-1.37	100_70, 100_80, 100_90
110	1.37	100_70, 100_80, 100_90
100	-1.37	80_70, 90_80, 90_70
100	1.37	80_70, 90_80, 90_70
90	-1.37	80_70
90	1.37	80_70

A summary of the results for the different construction sequences simulated using gradients can be seen in Figure 4.8. For each construction sequence, the positive and negative gradients are compared with the construction sequence that has a  $T_C$  value equal to the weighted average of the gradient. For the positive gradients, the magnitude of the stress is taken from the bottom of the slab where the critical stress is located. For the negative gradients, the magnitude of the tensile stress is taken from the top of the slab where the critical stress is located. This was done so that an equivalent comparison could be made.

According to Figure 4.7, when a gradient is applied to the model, there is an increase in the magnitude of the tensile stress when compared to a uniform temperature. It seems that the presence of a gradient, whether negative or positive, will not cause or prevent a crack from occurring.

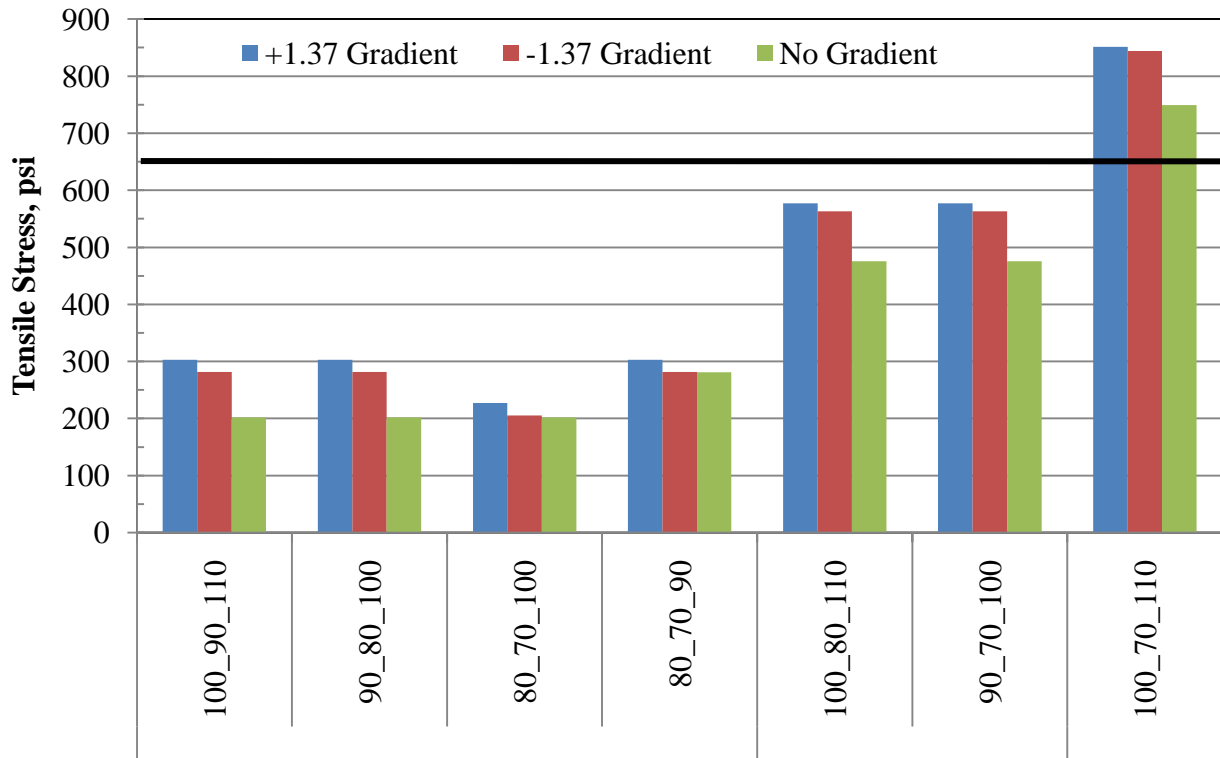


**Figure 4.8.** Summary of effect of positive and negative gradients in comparison to uniform temperature for longitudinal shear cracking model.

When the model was being validated, a variety of gradients were applied to the slab. In comparison to the measured strain, little error was observed in the predicted strain for gradients that were similar to the zero-stress gradient. When gradients started to diverge from the zero-stress gradient, more error existed between the measured and predicted strain values. Based on Figure 4.9, which illustrates the error encountered in ABAQUS when using gradients, the -1.37 linear gradient that was applied to the model has a percent error approaching 20 percent. The

+1.37 gradient applied to the slab showed little to no error. This is one possible explanation for the impact that gradients have on the tensile stress in the slab.

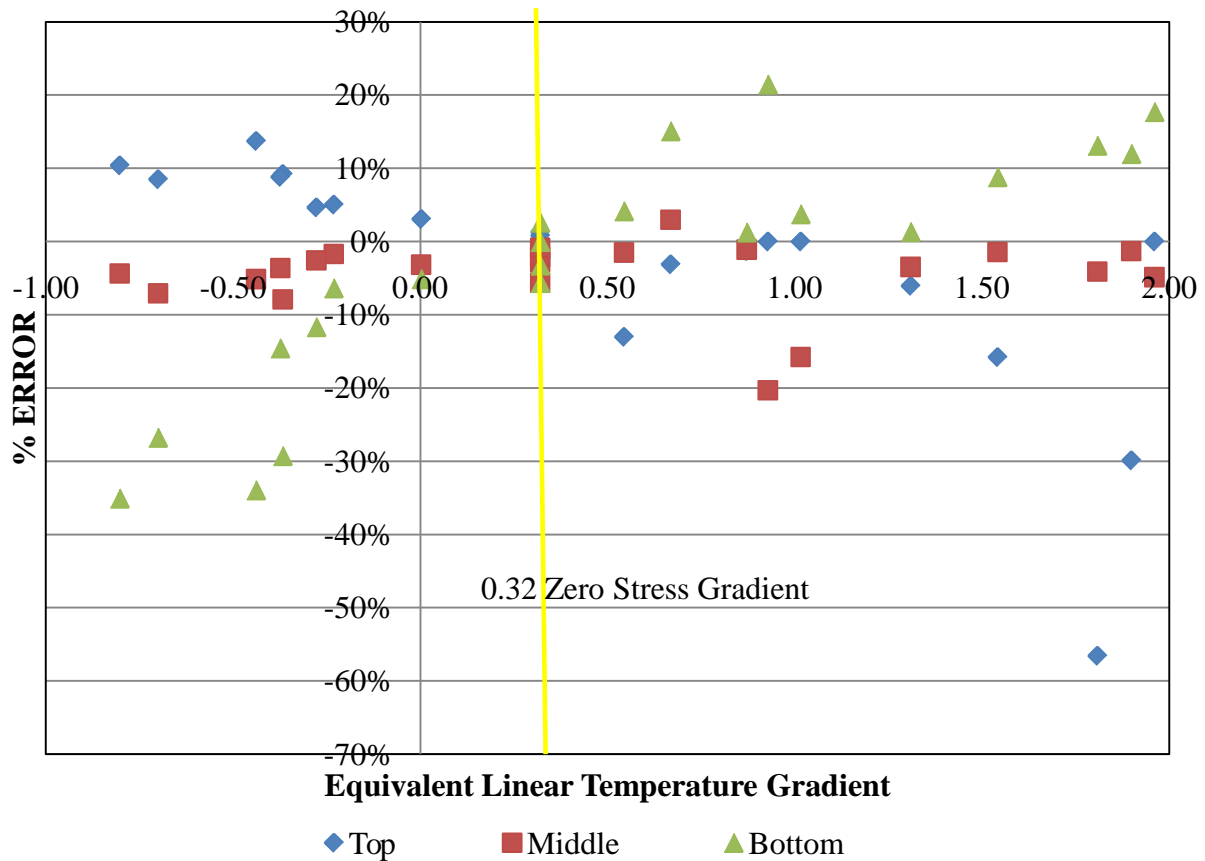


**Figure 4.9.** Observed error when using positive and negative gradients in ABAQUS.

Figure 4.10 through Figure 4.15 show the positive and negative gradients in comparison to the corresponding construction sequence throughout the depth of the pavement.

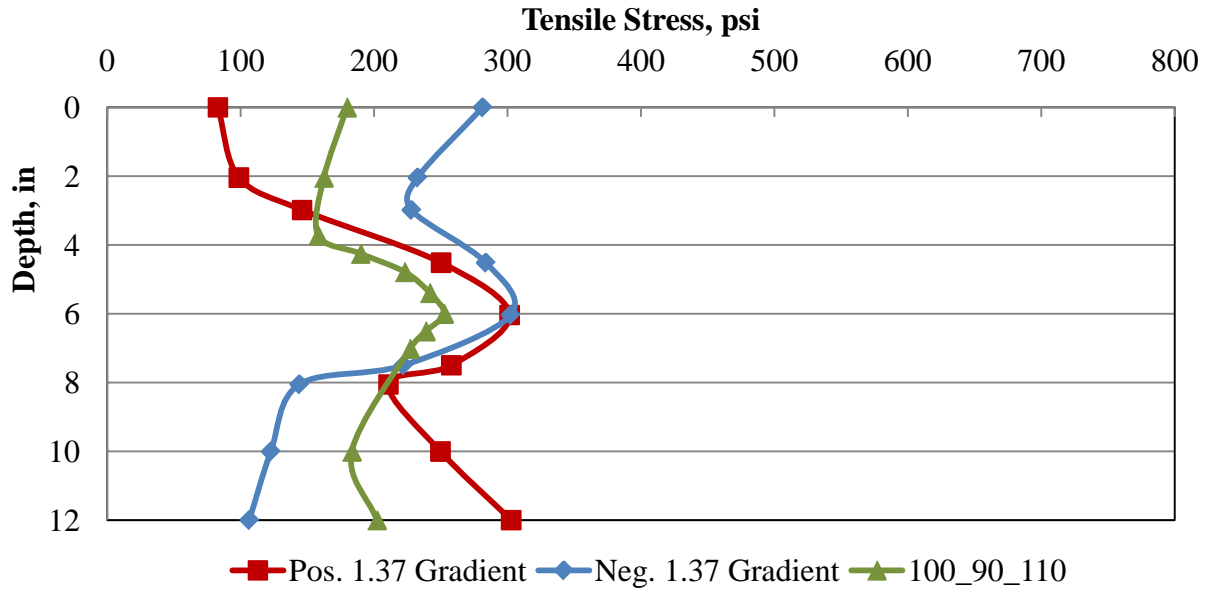


**Figure 4.10.** Effect of positive and negative gradient throughout the depth of the mainline for  $T_M=100^\circ\text{F}$ ,  $T_S=90^\circ\text{F}$  and  $T_C=110^\circ\text{F}$  for longitudinal shear cracking model.

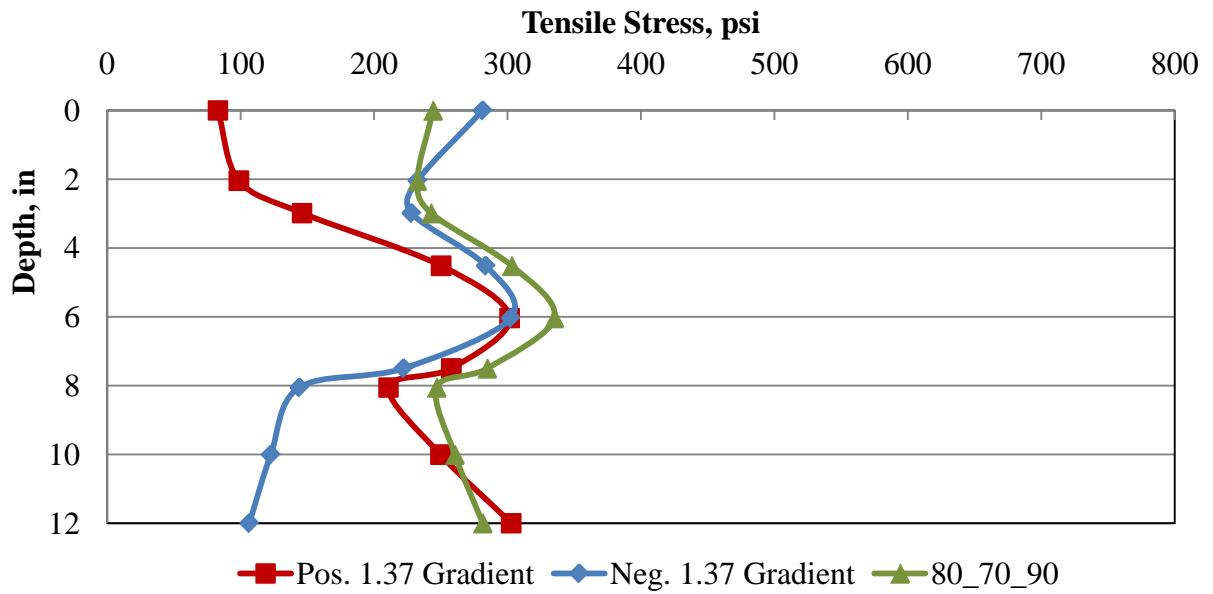


**Figure 4.11.** Effect of positive and negative gradient throughout the depth of the mainline for  $T_M=80^\circ\text{F}$ ,  $T_S=70^\circ\text{F}$  and  $T_C=90^\circ\text{F}$  for longitudinal shear cracking model.

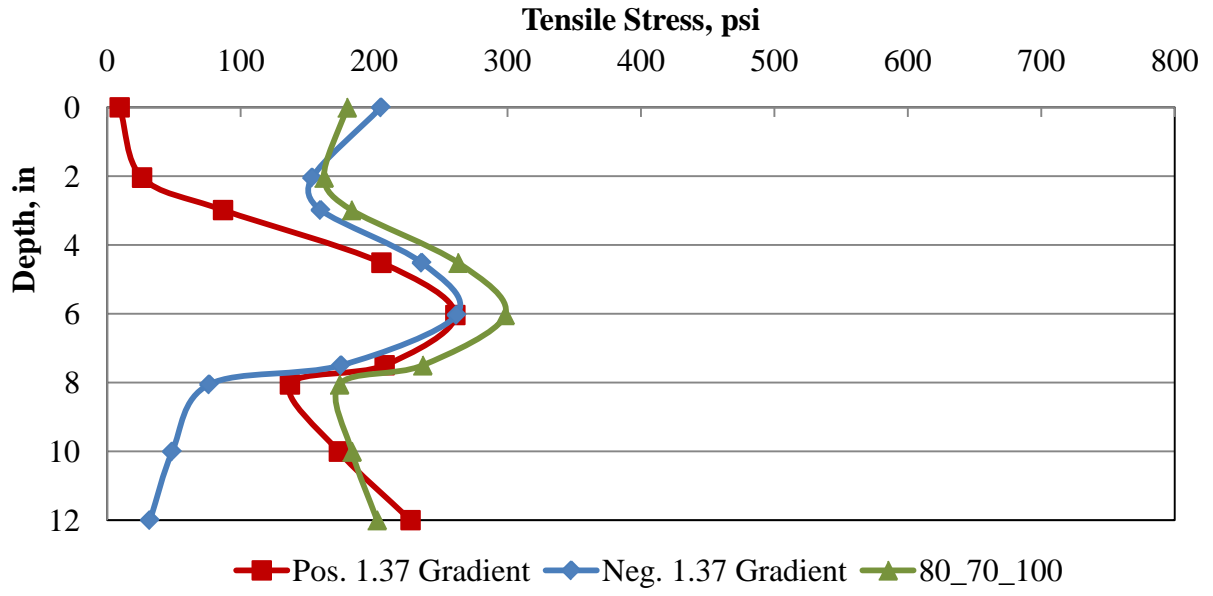


**Figure 4.12.** Effect of positive and negative gradient throughout the depth of the mainline for  $T_M=80^\circ\text{F}$ ,  $T_S=70^\circ\text{F}$  and  $T_C=100^\circ\text{F}$  for longitudinal shear cracking model.

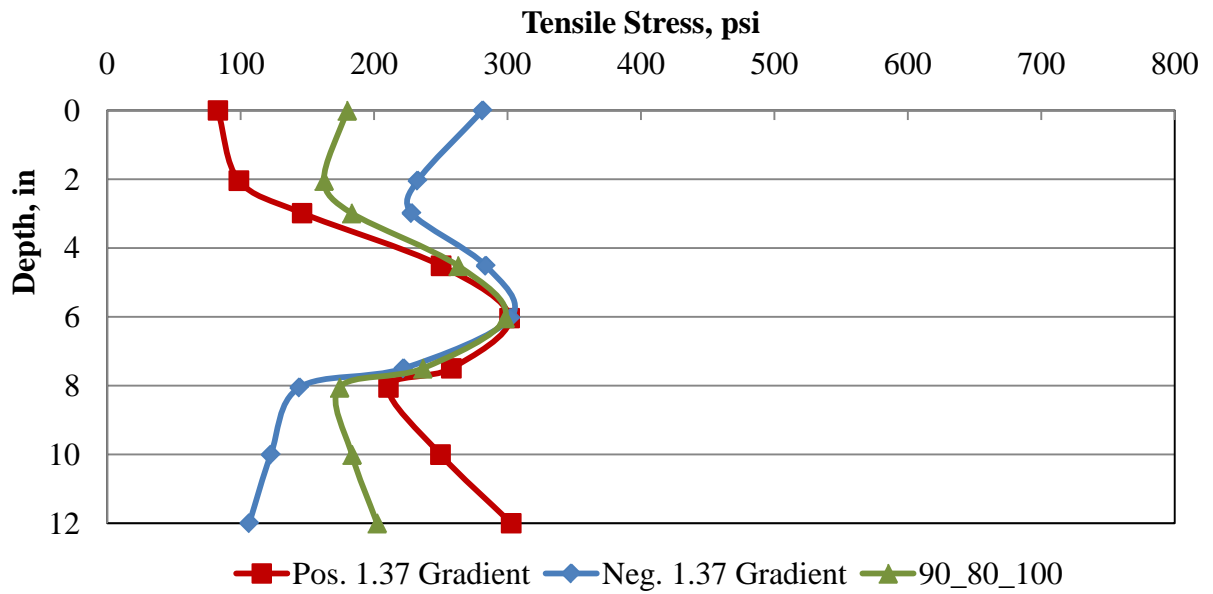


**Figure 4.13.** Effect of positive and negative gradient throughout the depth of the mainline for  $T_M=90^\circ\text{F}$ ,  $T_S=80^\circ\text{F}$  and  $T_C=100^\circ\text{F}$  for longitudinal shear cracking model.

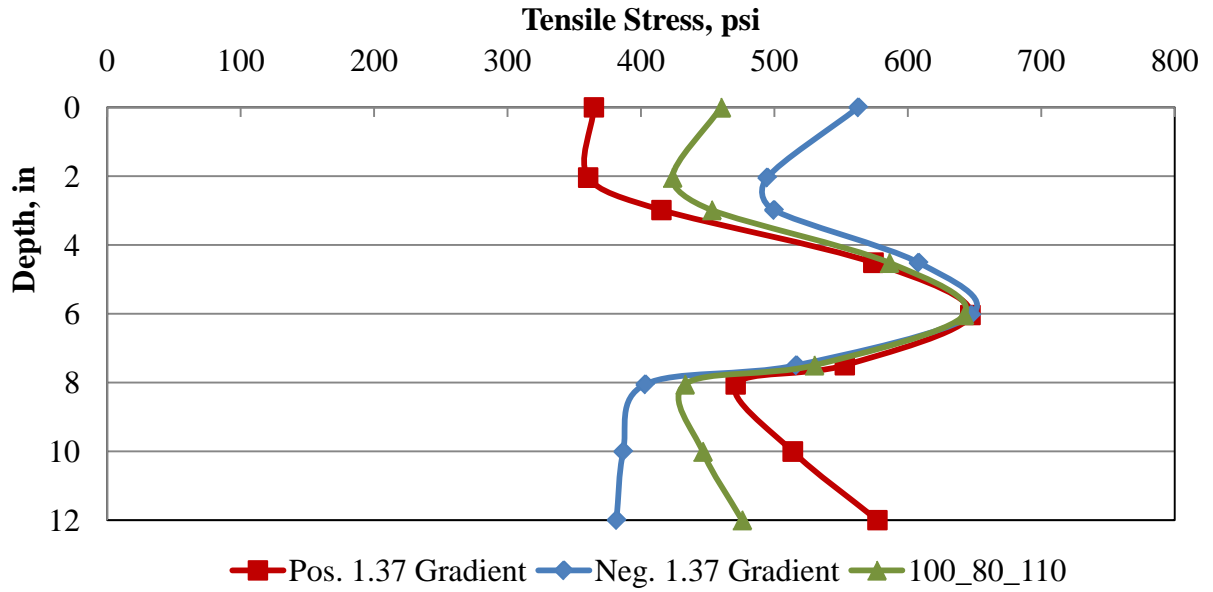


**Figure 4.14.** Effect of positive and negative gradient throughout the depth of the mainline for  $T_M=100^\circ\text{F}$ ,  $T_S=80^\circ\text{F}$  and  $T_C=110^\circ\text{F}$  for longitudinal shear cracking model.

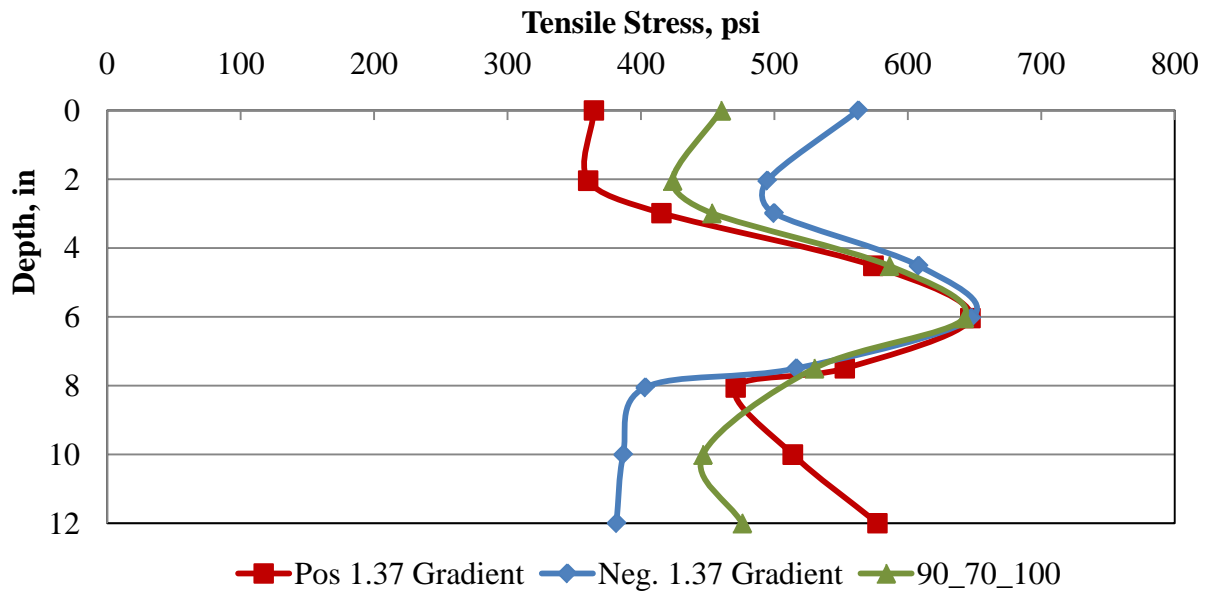


**Figure 4.15.** Effect of positive and negative gradient throughout the depth of the mainline for  $T_M=90^\circ\text{F}$ ,  $T_S=70^\circ\text{F}$  and  $T_C=100^\circ\text{F}$  for longitudinal shear cracking model.

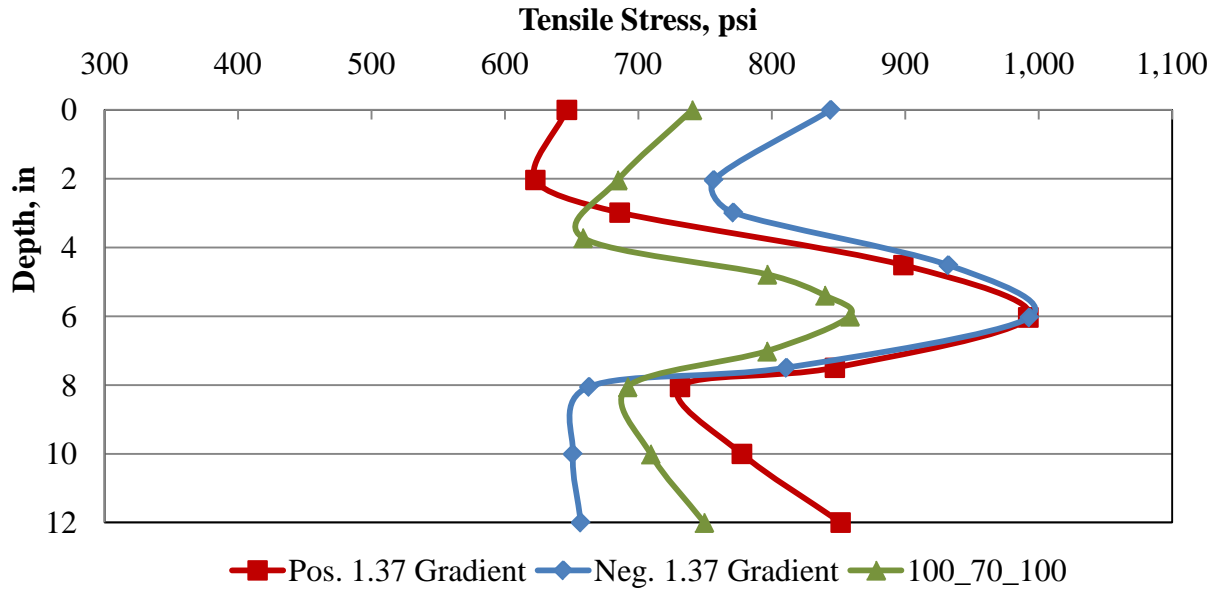


**Figure 4.16.** Effect of positive and negative gradient throughout the depth of the mainline for  $T_M=100^\circ\text{F}$ ,  $T_S=70^\circ\text{F}$  and  $T_C=110^\circ\text{F}$  for longitudinal shear cracking model.

#### 4.1.5 Overall Conclusions

The following conclusions were made based on the results of this parametric study:

- The results from the model show that the crack initiates due to a tensile failure. It is possible that the crack propagates later on due to a shear failure.
- If large gaps of time are present between paving the mainline and the shoulder, every effort should be made to pave the shoulder on a day similar in temperature to when the mainline was paved. The difference in ambient temperatures between the paving days should not exceed  $20^\circ\text{F}$ .
- A large CTE provides a greater chance for a crack to occur.
- Mortar intrusion increases the chance for a crack to occur.

- The presence of a positive gradient increases the tensile stresses seen at the bottom of the slab and the presence of a negative gradient increases the tensile stresses seen at the top of the slab.
- Based on this study, if the mainline is constructed outside of the May to September time window, the contractor should wait to tie on the shoulder until the value of  $T_D$  can be lower. To estimate the best times for paving in other climatic regions, Equation 2.1 can be used to determine the difference in zero-stress temperatures for each month.

## **4.2 SHOULDER TRANSVERSE CRACKING MODEL**

The CTE, shoulder width, and concrete age are all variables included in the parametric study carried out as described in the previous chapter. The following sections will discuss each parameter and the influence it has on the development of transverse cracking in the shoulder. The final section will present overall conclusions and provide a table which can be used to predict whether or not cracks will occur given paving conditions.

### **4.2.1 Construction Sequence**

Recall that the construction sequence refers to the time sequence in which the mainline and shoulder are paved. A typical construction sequence consists of paving the mainline in the summer and paving the shoulder in the fall.

As a reminder, the variables that have been defined for this model are repeated below with one additional variable.

$T_S$ = Zero-stress temperature which corresponds to time when shoulder was paved, °F

$T_M$ = Zero-stress temperature which corresponds to time when mainline was paved, °F

$T_C$ = Pavement temperature at a point in time after paving is completed, °F

$T_D = T_M - T_S$ , °F

$T_A = T_S - T_C$ , °F

Similar to the longitudinal shear cracking model, the value of  $T_D$  proved to be a critical parameter; however, for this distress, the value of  $T_C$  proved to be significant as well. A new variable was defined in order to better describe the critical scenarios under which this distress occurs. The variable,  $T_A$ , is the difference of the zero-stress temperature at the time the shoulder was placed,  $T_S$ , and the pavement temperature at a point in time after paving is completed,  $T_C$ .

The region in which the shoulder transverse cracking occurred is in a mountainous portion of Pennsylvania where daily temperature variations of 30°F or more are not uncommon. During the time when the shoulder was being paved, the daily temperature variation was approximately 30°F. While the temperatures in the afternoon reached the 80s, the temperature dropped to the 50s during the night. This scenario results in values of  $T_A$  reaching upwards of 60°F. The cracking was identified within the first week after paving the shoulder.

Figure 4.1 shows a summary of the results for the transverse shoulder cracking model. This summary is only for a stiffness of 2.8 million psi, which corresponds to a 1-day strength. As shown in the figure, a crack is likely to occur for any value larger than 500 psi.

Whether or not a crack will occur depends on the values of  $T_D$  and  $T_A$ . Assuming a CTE of  $5.5 \times 10^{-6}/^\circ\text{F}$  and 1-day strengths, a  $T_D$  of -10°F will not result in cracking unless the value of

$T_A$  is 60°F or more. A  $T_D$  of -20°F will not produce cracking if  $T_A$  is less than 40°F. A  $T_D$  of -30°F will result in cracking if  $T_A$  is less than 25°F. Table 4.1 presents guidelines for determining the potential for a shoulder to develop transverse cracking based on the construction sequence and CTE. A graphical representation of these results can be found in Figure 4.1.

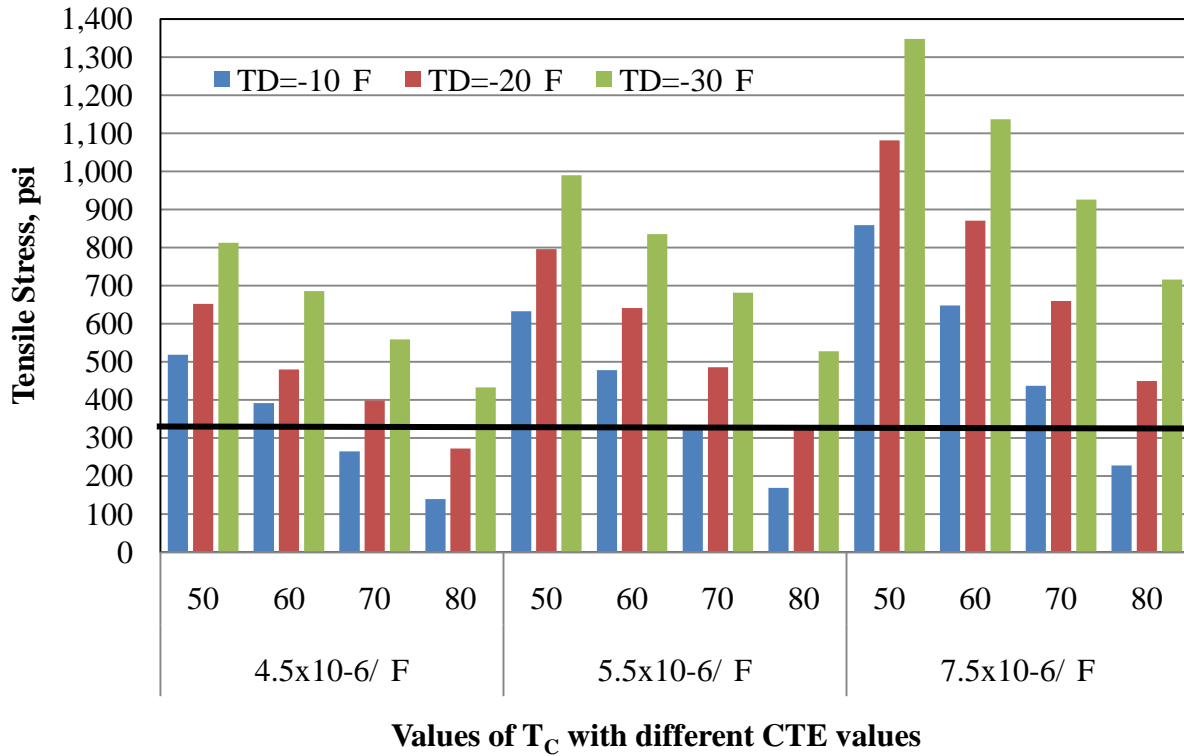


**Figure 4.17.** Critical value of  $T_C$  for different CTE values with a trigger value of 450 psi.

**Table 4.5.** Guidelines for determining crack potential based on construction sequence and CTE.

<b>CTE 4.5</b>				
<b>T<sub>C</sub>, °F</b>				
<b>T<sub>D</sub>, °F</b>	<b>50</b>	<b>60</b>	<b>70</b>	<b>80</b>
<b>-30</b>				
<b>-20</b>				
<b>-10</b>				
<b>CTE 5.5</b>				
<b>T<sub>C</sub>, °F</b>				
<b>T<sub>D</sub>, °F</b>	<b>50</b>	<b>60</b>	<b>70</b>	<b>80</b>
<b>-30</b>				
<b>-20</b>				
<b>-10</b>				
<b>CTE 7.5</b>				
<b>T<sub>C</sub>, °F</b>				
<b>T<sub>D</sub>, °F</b>	<b>50</b>	<b>60</b>	<b>70</b>	<b>80</b>
<b>-30</b>				
<b>-20</b>				
<b>-10</b>				

\*Highlighted cell indicates risk for a crack

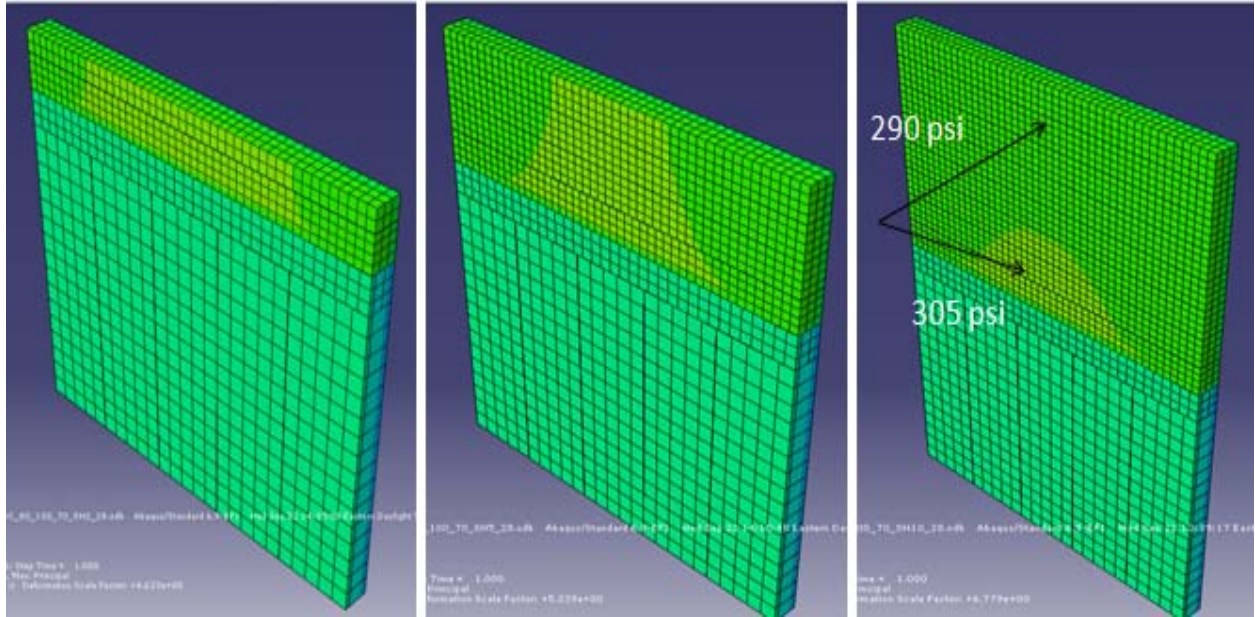
Based on this study, the best months to construct the mainline and shoulder separately in Pennsylvania are from May to September. If the mainline is constructed outside of this time window, the contractor should wait to tie on the shoulder until the value of TD meets the criteria in Table 4.5. It is possible to pave in April and October as long as the ambient temperature is higher than normal. To estimate the best times for paving in other climatic regions, Equation 2.1 can be used to determine the difference in zero-stress temperatures for each month. For this study, it is also important to consider the value of T<sub>A</sub>, use Table 4.5 for guidance.

## 4.2.2 Coefficient of Thermal Expansion

Figure 4.1 shows the effect that CTE has on transverse cracking in the shoulder. As expected, a larger CTE results in a higher chance for the distress to occur. A lower CTE reduces the chance for a crack. If a CTE value is unknown, which is common, a value can be estimated using (Equation 4.4 and Table 4.3 (Section 4.1.2) to determine if the coefficient of thermal expansion is on the high or low end of typical ranges.

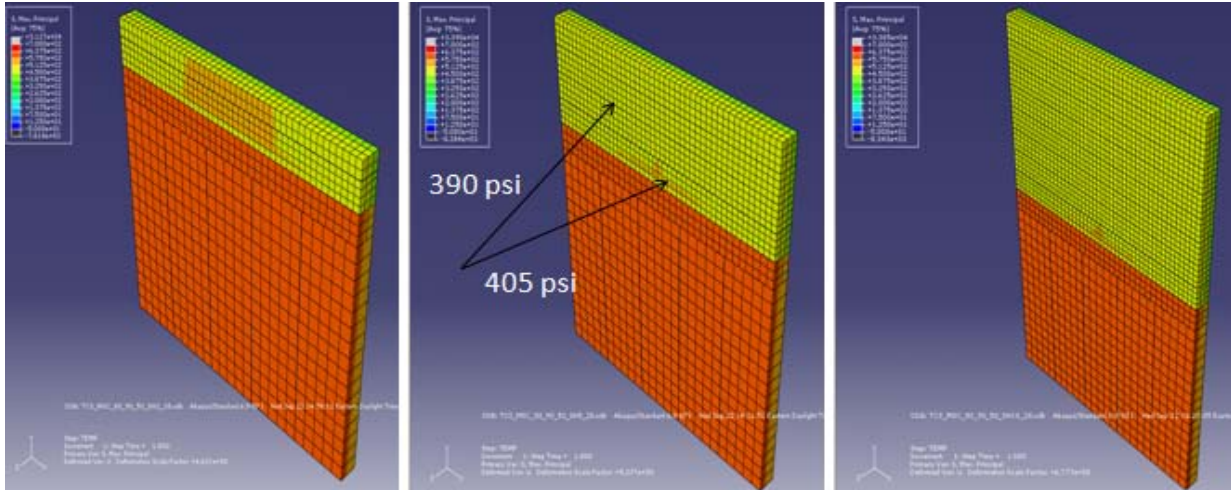
## 4.2.3 Shoulder Width

Figure 4.18, Figure 4.19 and Figure 4.20 show screen shots of the bottom of the slab from three models that are identical except for the shoulder width. In Figure 4.18, the three models have a CTE of  $4.5 \times 10^{-6}/^{\circ}\text{F}$  and a stiffness of 2.8 million psi. There is no crack present and at first glance, it would appear as if there is no difference between the three different shoulder widths. However, the distribution of tensile stress in the shoulder is different among them. In the 2-ft shoulder, there is an area of higher tensile stress that is located in the center of the shoulder and extends across the entire width. In the 5-ft shoulder, that same area of higher tensile stress still extends across the entire width of the shoulder. However, the area of higher stress begins to taper as it reaches the outside edge. In the 10-ft shoulder, the area of higher tensile stress extends only a few feet across the shoulder. The tie bars have a major influence on the area of higher tensile stress. Along the length of the shoulder, the area of higher stress begins where the first tie bar is located and ends where the last tie bar is located. Figure 4.21 illustrates this point.



**Figure 4.18.** Influence of shoulder width when  $T_D=-20^{\circ}\text{F}$  and  $T_A=30^{\circ}\text{F}$  for the shoulder transverse cracking model.

In Figure 4.19, the three models have a CTE of  $4.5 \times 10^{-6}/^{\circ}\text{F}$  and a stiffness of 2.8 million psi. The calculated tensile stress in this figure is less than the tensile strength of the concrete. It should be noted that for the color schemes within the same figure, areas represented by the same color share the same magnitude of stress. These same comparisons cannot be made between different figures because colors represent different magnitudes of stress for different figures. The distribution of stress in the shoulder is different among the three models. Similar to Figure 4.18, there is an area of higher stress in the 2-ft shoulder that is located in the center of the shoulder at the bottom of the slab and extends across the entire width. In the 5-ft and 10-ft shoulder, the area of higher tensile stress diminished significantly and extends only a foot across the shoulder.



**Figure 4.19.** Influence of shoulder width when  $T_D = -10^\circ\text{F}$  and  $T_A = 60^\circ\text{F}$  for the shoulder transverse cracking model.

In Figure 4.20, the three models have a CTE of  $7.5 \times 10^{-6}/^\circ\text{F}$  and a stiffness of 2.8 million psi. In all three of the models, the predicted tensile stresses exceed the defined strength of the concrete. There is a crack present in all three of the models. In the 2-ft shoulder, there is an area of higher tensile stress that is located in the center of the shoulder and extends across the entire width. In the 5-ft shoulder that same area of higher tensile stress still extends across the entire width of the shoulder; however, it begins to thin out as it reaches the outside edge. In the model with the 10-ft shoulder, the area of higher tensile stress extends only a few feet across the shoulder. In all three of the models, the area of the shoulder that has a high tensile stress concentration around the tie bars.

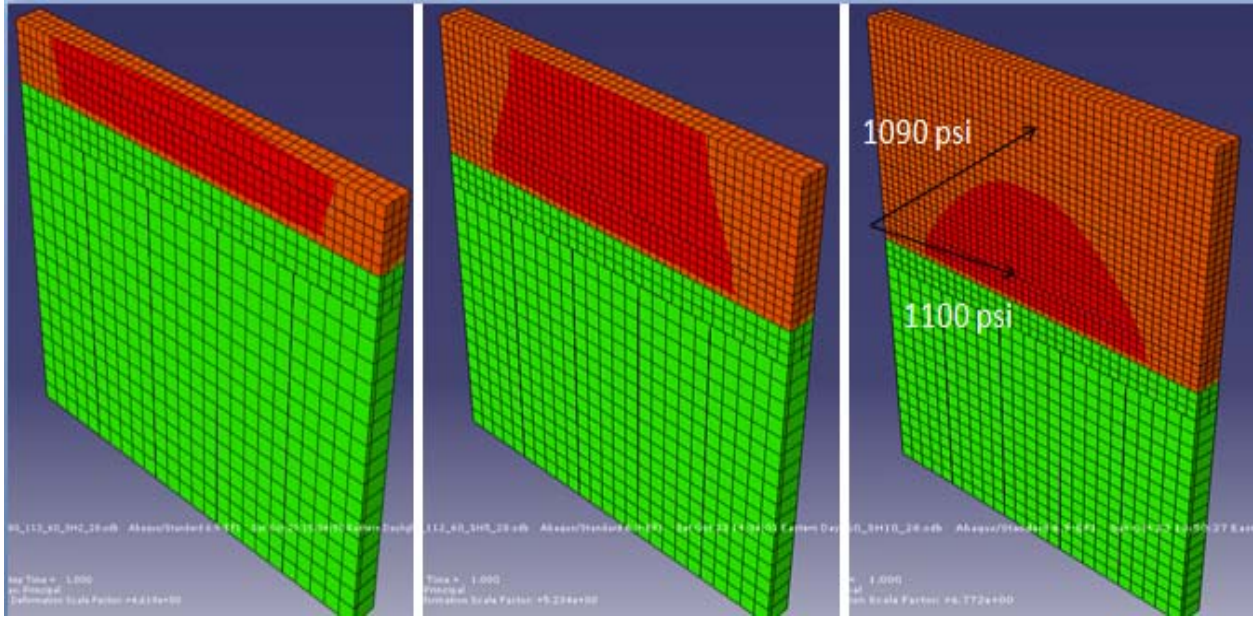


**Figure 4.20.** Influence of shoulder width when  $T_D=-30^\circ\text{F}$  and  $T_A=50^\circ\text{F}$  for the shoulder transverse cracking model.

Figure 4.21 illustrates the concentration of stress surrounding the tie bars. This is a model that is sliced in the z-direction so that the tie bars are visible. The larger tensile stresses clearly begin to form around the tie bars. This holds true for all of the cases in the parametric study.

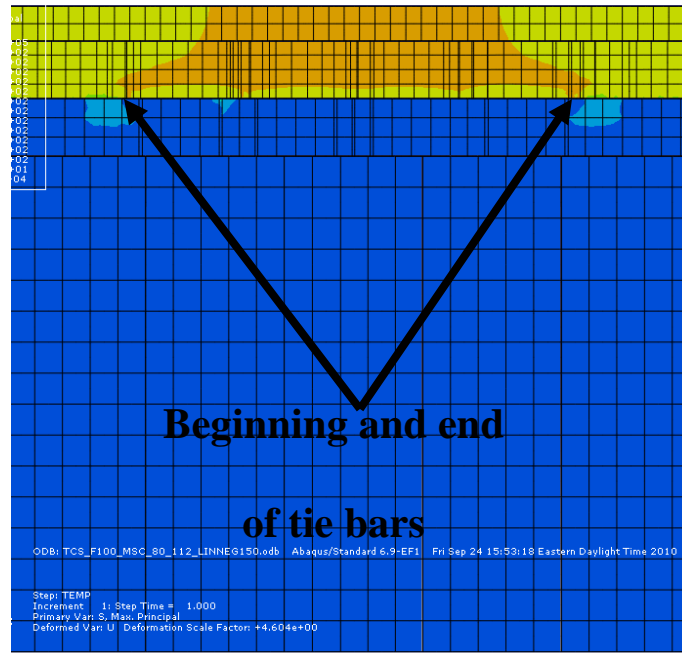


**Figure 4.21.** Illustration of tensile stress concentration surrounding tie bars in shoulder transverse cracking model.

It is unknown if there are any cases where this distress occurs in a shoulder that has a width greater than 2 ft. It is believed that if this distress commonly occurred in larger shoulders, it would have already been studied and documented since 5- and 10-ft shoulders are much more common than 2-ft shoulders. Since there is no known documentation of this distress that is specific to shoulders, it might be unique to 2-ft shoulders.

Because the area of high stress concentration does not extend all the way across the 10-ft shoulder, it is believed that a micro crack will form around the tie bars relieving the stress in the area causing the stresses to redistribute. It is possible that the restraint from the tie bars will hold the crack tight preventing it from propagating across the slab.

In Figure 4.18, Figure 4.19 and Figure 4.20, the area of high stress concentration initiates at the bottom of the slab. It is likely that the restraint from the base could prevent the crack from propagating to the top of the slab. It is unknown at what point the observed cracks in the 2-ft shoulders propagated to the top of the slab.

#### 4.2.4 Stiffness

In ABAQUS, the strength properties of the concrete were only defined using the elastic modulus and Poisson’s ratio. By increasing the stiffness, the trigger value also increases. Figure 4.22 shows 12 different scenarios with two different stiffnesses. The stiffness of 2.8 million psi represents a 1-day strength and 3.3 million psi represents a 7-day strength. The tensile stresses seen with a 3.3 million psi stiffness are larger than the stresses seen with a 2.8 million psi stiffness; however, the strength for the stiffer concrete increases. Based on the results from Figure 4.21, it can be concluded that the transverse cracks in the shoulder occurred within the first few days.

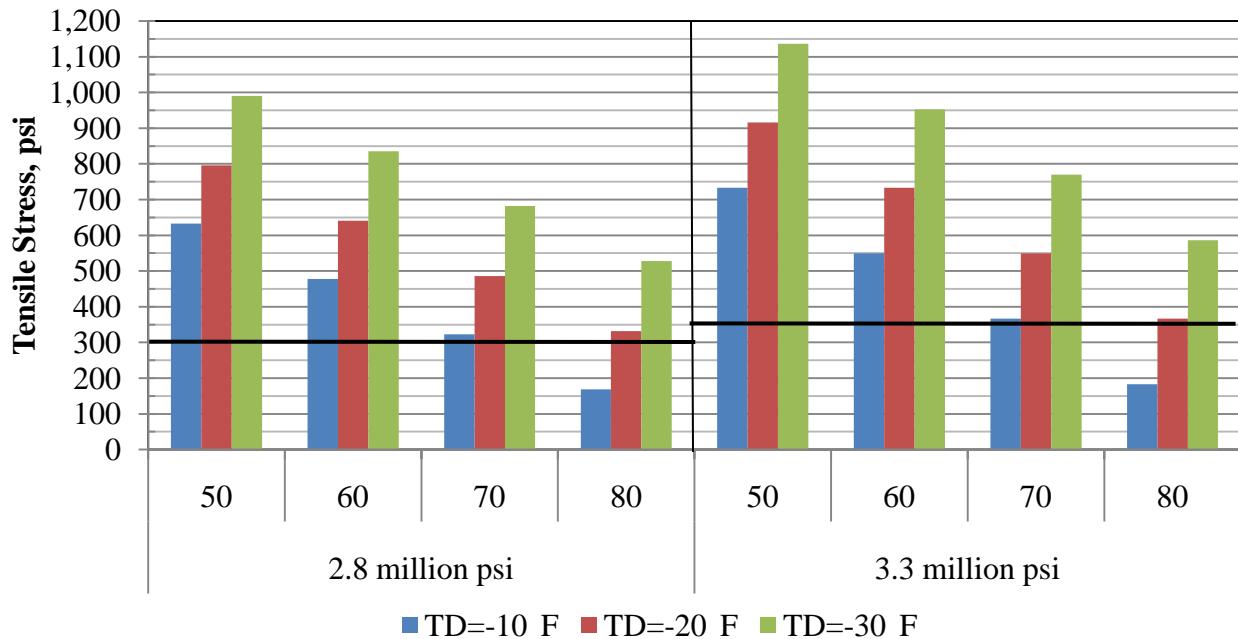


Figure 4.22. Influence of concrete stiffness on the shoulder transverse cracking model.

## 4.2.5 Gradients

The parametric study was carried out assuming that the temperature throughout the slab is uniform. By doing this, the stress due to changes in volume caused by uniform temperature change is isolated. By introducing a gradient, the tensile stress due to the slabs change in shape is highlighted in addition to the tensile stress due to uniform temperature change. Six different linear temperature gradients were used with two different values of  $T_S$  in order to evaluate the effect that gradients have on stresses in the shoulder. A linear temperature gradient was chosen and all six of the gradients have the same average temperature of 60°F. The six gradients that were used along with their temperature distribution throughout the slab can be seen in Table 4.6.

**Table 4.6.** Temperature distributions for gradients used in shoulder transverse cracking model.

Gradient °F/in	Depth, in					
	0	2.5	5	7.5	10	12
<b>-0.38</b>	56	57	58	59	60	61
<b>-0.75</b>	54	56	58	60	62	64
<b>-1.5</b>	50	54	58	62	66	69
<b>0.38</b>	61	60	59	58	57	56
<b>0.75</b>	64	62	60	58	56	54
<b>1.5</b>	66	62	58	54	50	47

Figure 4.7 shows the effect of a positive and negative gradient in comparison to a uniform temperature for a  $T_D$  of -10°F and -30°F. In general, the critical stress location for a positive gradient is at the bottom of the slab and the top of the slab for a negative gradient. For the negative gradient, the tensile stress shown is at the top of the slab and at the bottom of the slab for the positive gradient. When there is no gradient present, the critical stress location is at the bottom of the slab.

As shown in the figure, a negative gradient does not have a significant effect on the magnitude of stress when compared to a situation with no gradient. This is because the critical stress location of the negative gradient is at the top while the critical stress location of the model with no gradient is at the bottom of the slab. It appears that these stresses offset each other, which is why there is no increase in stress. If there is a positive gradient present in the slab, the stresses at the bottom of the slab are magnified, even for the smaller gradient of 0.38 °F/in.

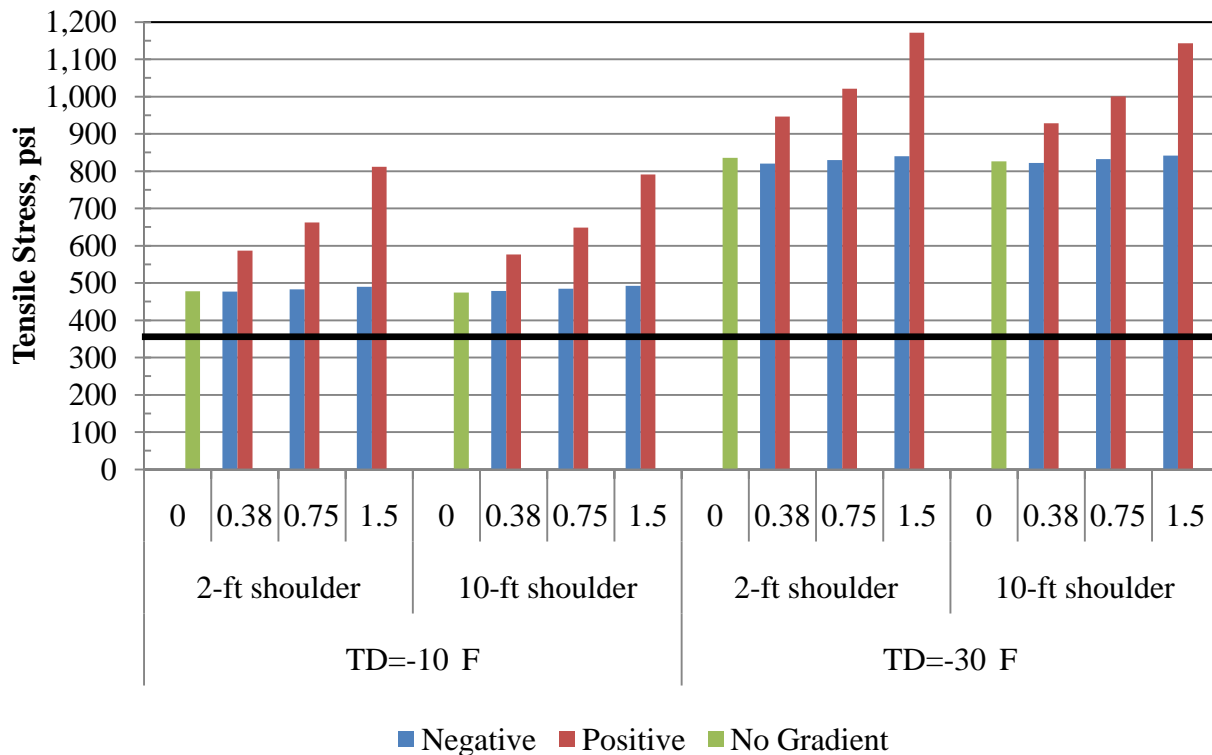


**Figure 4.23.** Effect of gradients when  $T_s = 110$  °F in the shoulder transverse cracking model.

#### 4.2.6 Overall Conclusions

The following conclusions were made based on the results of this parametric study:

- This distress develops within one week of paving.
- The cracks initiate at the bottom of the slab close to the tie bar

- The values of  $T_D$  and  $T_A$  should satisfy the guidelines found in Table 4.5
- A large CTE increases the probability that a crack will develop.
- A 2-ft shoulder increases the probability that a crack will develop because the tie bars extend over half the width of the slab. The source of the high tensile stress concentration is localized around the tie bars.
- The presence of a positive gradient magnifies the effect of a uniform temperature change and increases the probability that a crack will develop.
- In the case studied in Section 2.1.2, only three out of the seven sections had transverse cracks in the shoulder. This is because some of the sections were paved in the morning, which would bring down the value of the zero-stress temperature and cause the value of  $T_D$  to be around 10°F resulting in a small chance for a crack.
- To estimate the best times for paving in other climatic regions, Equation 2.1 can be used to determine the difference in zero-stress temperatures for each month. For this study, it is also important to consider the value of  $T_A$ , use Table 4.5 for guidance.

## **5.0 CONCLUSIONS AND RECOMMENDATIONS**

This research has provided a better understanding of distresses that develop due to delayed shoulder construction for PCC pavements. Field data collected from several sources allowed FE models to be developed. The instrumented pavement sections at US-22 were used to validate the models which were then used to effectively characterize the distresses seen in the field. The following sections provide conclusions drawn from this study as it pertains to each analysis. A section discussing recommendations for further research follows the conclusions.

### **5.1 CONCLUSIONS**

#### **5.1.1 General**

The following general conclusions were developed based on the findings of this study:

- Thermal incompatibility is the cause for distresses associated with delayed shoulder construction.
- If  $T_M > T_S$  there is a chance for longitudinal shear cracking to occur. If  $T_M < T_S$  there is a change for transverse cracking in the shoulder to occur.

### 5.1.2 Longitudinal Shear Cracking

The following conclusions regarding longitudinal shear cracking were made based on the findings of this study:

- Dissimilar joint openings, due to thermal incompatibility, can cause cracking when joints in the shoulder close before the mainline or vice-versa (Section 2.1.1).
- Base type does not appear to be significant since all of the longitudinal shear cracking examples had different base types (Section 2.1.1).
- The sides of the joints should be sealed to prevent mortar intrusion. When paving the shoulder, it is possible for mortar to intrude if a vibrator in the paver is close to the longitudinal joint (Section 2.1.1).
- Longitudinal shear cracks can develop in a variety of different shoulder widths (Section 2.1.1).
- Using a concrete having a lower CTE will help to reduce the potential for the development of shear cracks if mainline and the shoulder are to be paved during the different seasons (Section 4.1.2).
- The presence of a gradient does not reduce or enhance the tensile stresses caused by a uniform temperature change (Section 4.1.4).
- The parameter that has the largest influence on the development of a crack is construction sequence. It is recommended that the value of  $T_D$  be less than 20°F (Section 4.1.1).

- Based on this study, if the mainline is constructed outside of the May to September time window, the contractor should wait to tie on the shoulder until the value of  $T_D$  can be lower. To estimate the best times for paving in other climatic regions, Equation 2.1 can be used to determine the difference in zero-stress temperatures for each month.

### 5.1.3 Shoulder Transverse Cracking

The following conclusions were made regarding the development of transverse cracking in the shoulder based on the findings of this study:

- In addition to the value of  $T_D$ ,  $T_C$  is a very sensitive parameter. If paving in a region where large daily swings in temperature are common, it is recommended that the mainline and shoulder be paved during the same season to reduce the value of  $T_D$  below 20°F. (Section 4.2.1).
- The values of  $T_D$  and  $T_A$  should follow the guidelines proposed in Table 3.3. When at all possible, both values should be kept to a minimum (Section 4.2.1).
- Shoulders widths less than 5 ft are more likely to crack than shoulders larger than 5 ft because of the depth of tie bar penetration. Since the tensile stresses concentrate around the tie bars, a larger distance between the end of the tie bars and the edge of the shoulder reduces the potential for a crack to develop (Section 4.2.3).
- Using a concrete having a lower CTE will help to reduce the potential for the development of cracks if mainline and the shoulder are to be paved during the different seasons (Section 4.2.2).

- Positive gradients increase the chance for a crack to develop. When there is no gradient, the critical stress is located at the bottom of the slab. The addition of a positive gradient, which increase the tensile at the bottom of the slab, increases the combined tensile stress due to the gradient and a uniform temperature change (Section 4.2.5).

## **5.2 RECOMMENDATIONS**

The following recommendations were developed based on the findings of this study:

- Research should be performed to further evaluate conditions under which longitudinal shear cracks and transverse cracks in the shoulder develop. The range of construction sequences, support conditions and material properties considered in this study should be expanded upon to evaluate a broader range of conditions.
- Further research is needed in determining the effect of different effective slab lengths, curved pavement sections and vehicle loads.

## APPENDIX A

### LONGITUDINAL SHEAR CRACKING SCREEN SHOTS



**Figure A1.** Longitudinal shear cracking model in which  $T_M=100^\circ\text{F}$ ,  $T_S=70^\circ\text{F}$ , and  $T_C=100^\circ\text{F}$  for a mortar intrusion of 0 in and a CTE of  $4 \times 10^{-6}/^\circ\text{F}$ .

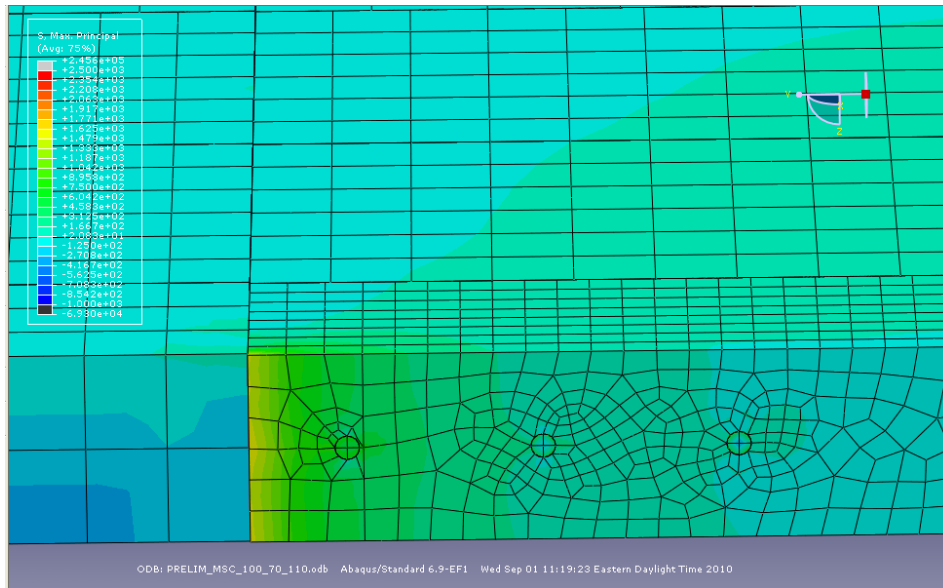


**Figure A2.** Longitudinal shear cracking model in which  $T_M=100^\circ\text{F}$ ,  $T_S=70^\circ\text{F}$ , and  $T_C=110^\circ\text{F}$  for a mortar intrusion of 0 in and a CTE of  $4 \times 10^{-6}/^\circ\text{F}$ .

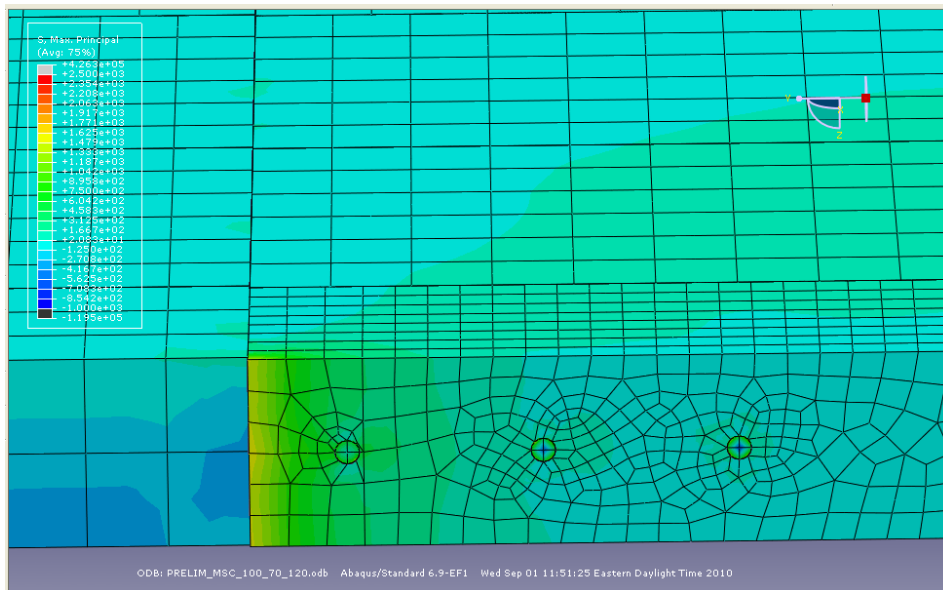


**Figure A3.** Longitudinal shear cracking model in which  $T_M=100^\circ\text{F}$ ,  $T_S=70^\circ\text{F}$ , and  $T_C=120^\circ\text{F}$  for a mortar intrusion of 0 in and a CTE of  $4 \times 10^{-6}/^\circ\text{F}$ .

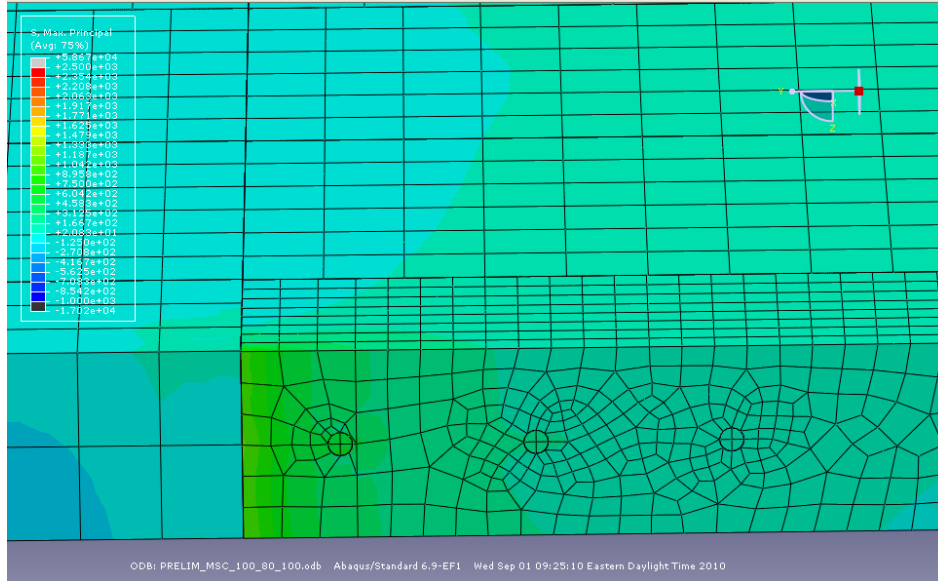


**Figure A4.** Longitudinal shear cracking model in which  $T_M=100^\circ\text{F}$ ,  $T_S=80^\circ\text{F}$ , and  $T_C=100^\circ\text{F}$  for a mortar intrusion of 0 in and a CTE of  $4 \times 10^{-6}/^\circ\text{F}$ .

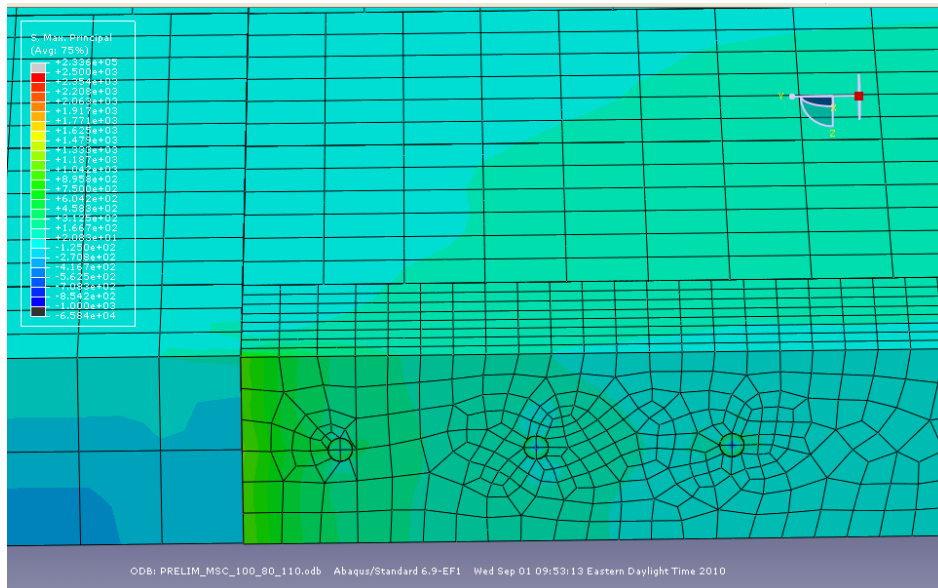


**Figure A5.** Longitudinal shear cracking model in which  $T_M=100^\circ\text{F}$ ,  $T_S=80^\circ\text{F}$ , and  $T_C=110^\circ\text{F}$  for a mortar intrusion of 0 in and a CTE of  $4 \times 10^{-6}/^\circ\text{F}$ .

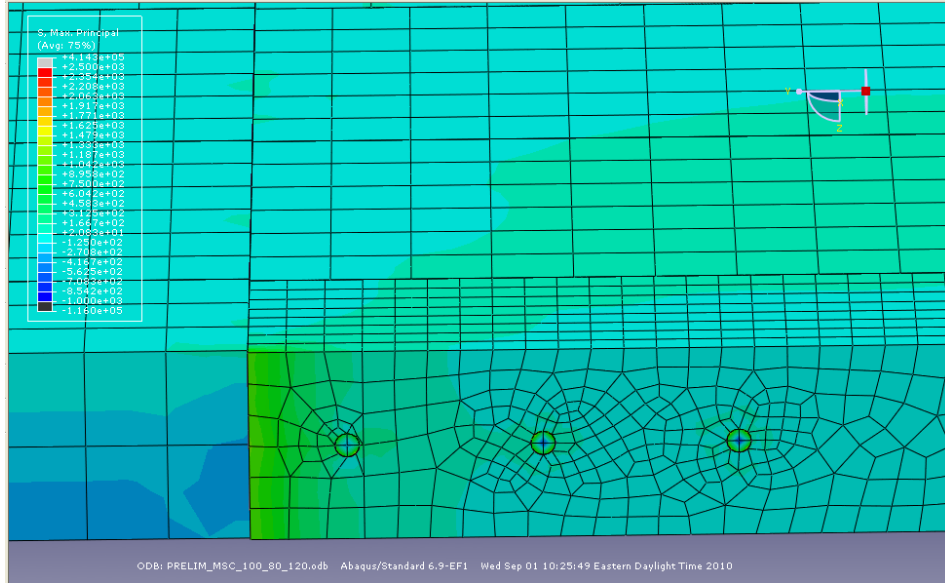


**Figure A6.** Longitudinal shear cracking model in which  $T_M=100^\circ\text{F}$ ,  $T_S=80^\circ\text{F}$ , and  $T_C=120^\circ\text{F}$  for a mortar intrusion of 0 in and a CTE of  $4 \times 10^{-6}/^\circ\text{F}$ .

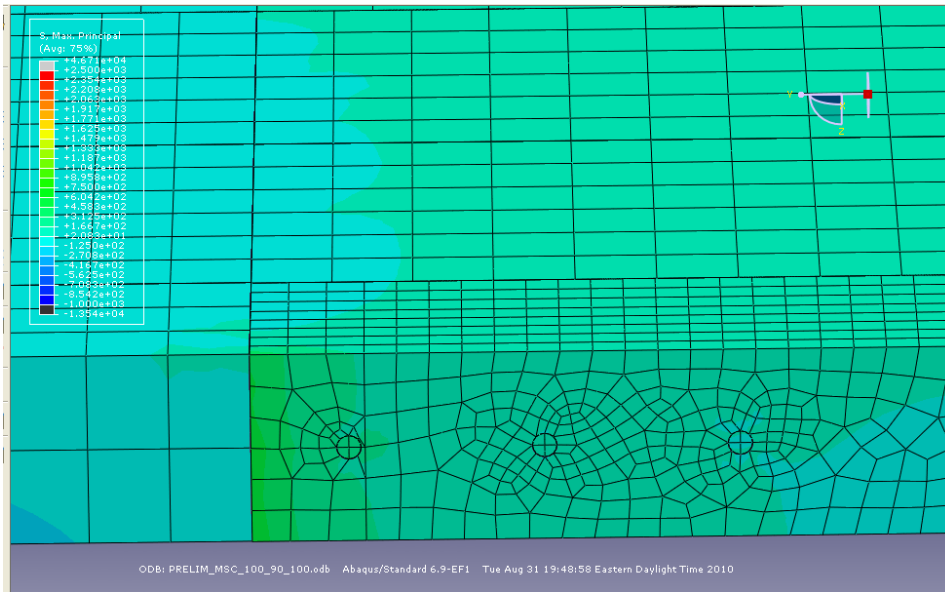


**Figure A7.** Longitudinal shear cracking model in which  $T_M=100^\circ\text{F}$ ,  $T_S=90^\circ\text{F}$ , and  $T_C=100^\circ\text{F}$  for a mortar intrusion of 0 in and a CTE of  $4 \times 10^{-6}/^\circ\text{F}$ .

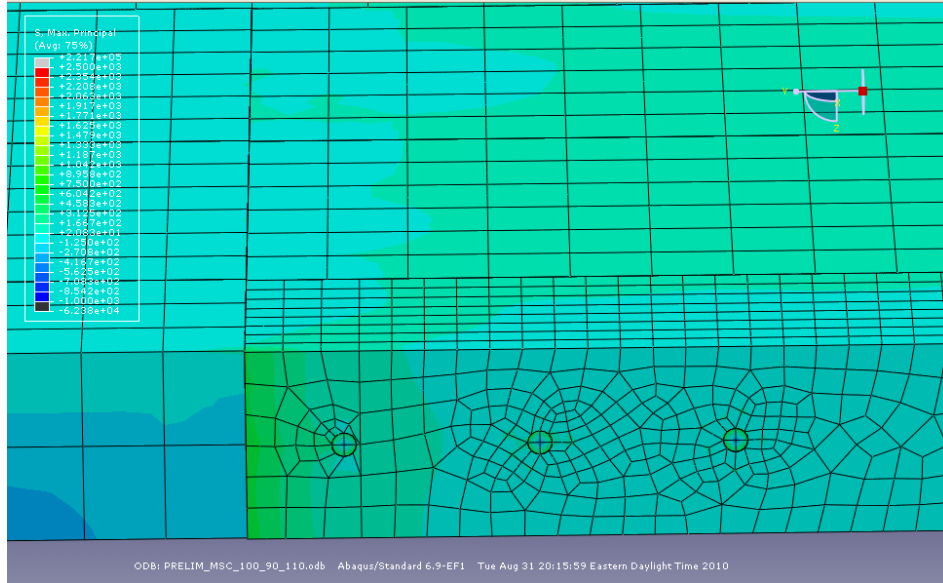


**Figure A8.** Longitudinal shear cracking model in which  $T_M=100^\circ\text{F}$ ,  $T_S=90^\circ\text{F}$ , and  $T_C=110^\circ\text{F}$  for a mortar intrusion of 0 in and a CTE of  $4 \times 10^{-6}/^\circ\text{F}$ .

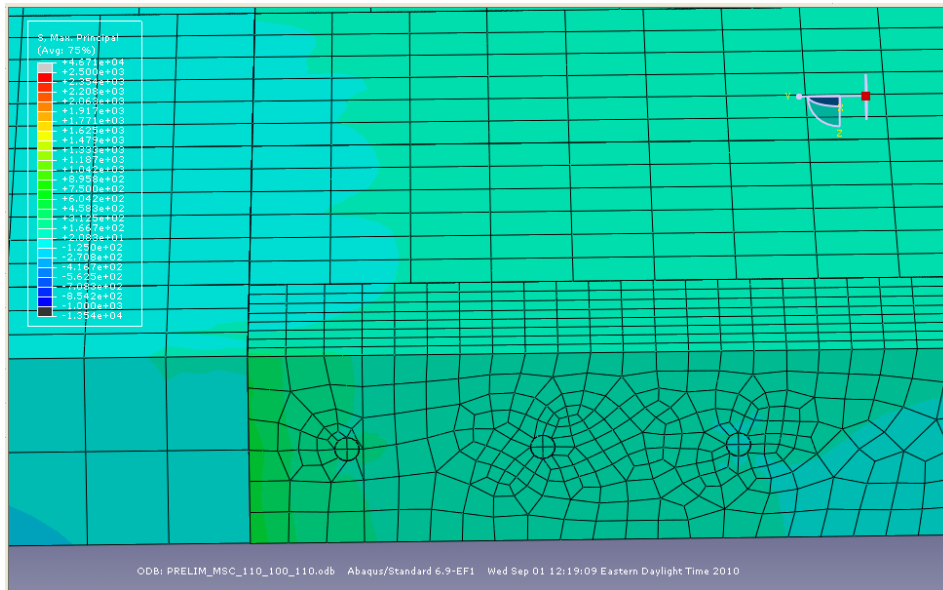


**Figure A9.** Longitudinal shear cracking model in which  $T_M=110^\circ\text{F}$ ,  $T_S=100^\circ\text{F}$ , and  $T_C=110^\circ\text{F}$  for a mortar intrusion of 0 in and a CTE of  $4 \times 10^{-6}/^\circ\text{F}$ .

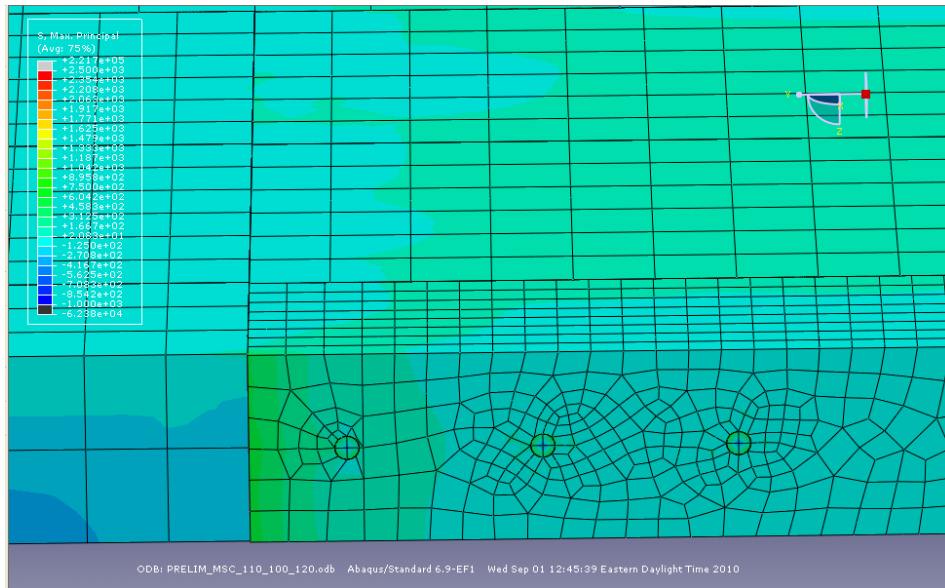


**Figure A10.** Longitudinal shear cracking model in which  $T_M=110^\circ\text{F}$ ,  $T_S=100^\circ\text{F}$ , and  $T_C=120^\circ\text{F}$  for a mortar intrusion of 0 in and a CTE of  $4 \times 10^{-6}/^\circ\text{F}$ .

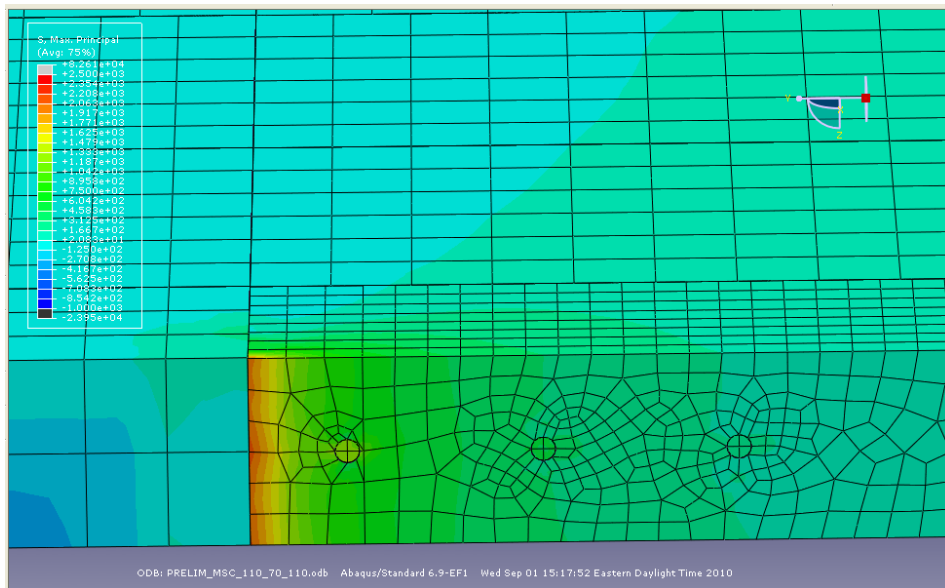


**Figure A11.** Longitudinal shear cracking model in which  $T_M=110^\circ\text{F}$ ,  $T_S=70^\circ\text{F}$ , and  $T_C=110^\circ\text{F}$  for a mortar intrusion of 0 in and a CTE of  $4 \times 10^{-6}/^\circ\text{F}$ .

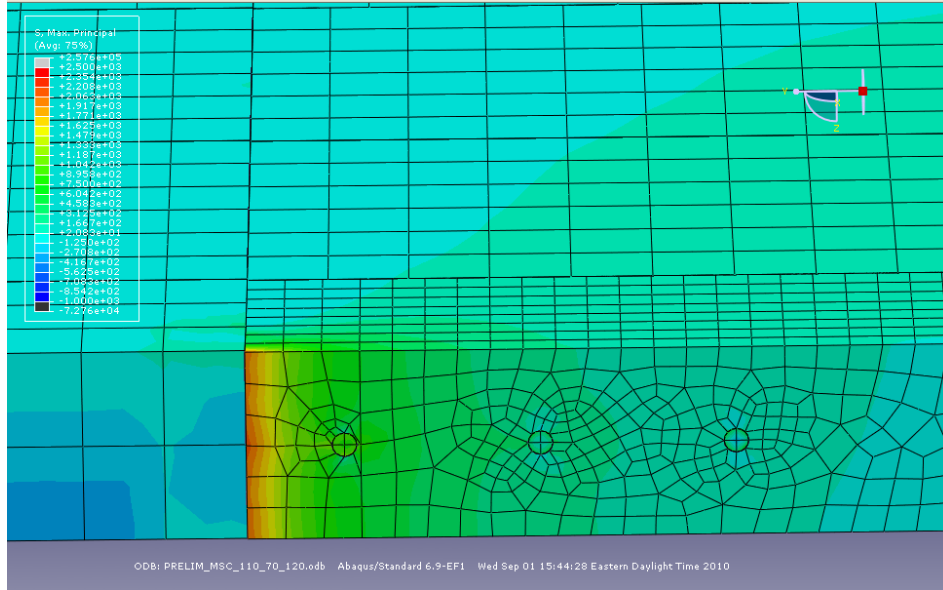


**Figure A12.** Longitudinal shear cracking model in which  $T_M=110^\circ\text{F}$ ,  $T_S=70^\circ\text{F}$ , and  $T_C=120^\circ\text{F}$  for a mortar intrusion of 0 in and a CTE of  $4 \times 10^{-6}/^\circ\text{F}$ .

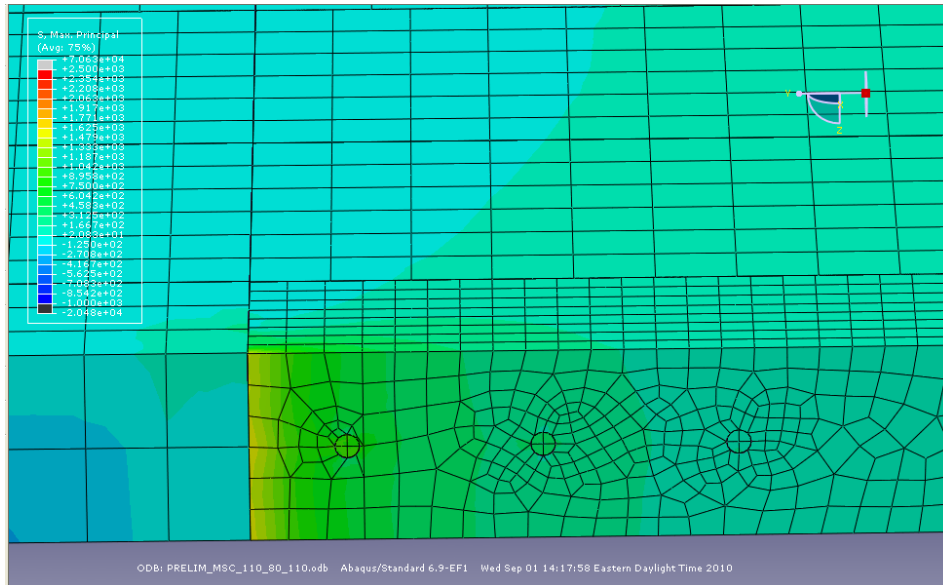


**Figure A13.** Longitudinal shear cracking model in which  $T_M=110^\circ\text{F}$ ,  $T_S=80^\circ\text{F}$ , and  $T_C=110^\circ\text{F}$  for a mortar intrusion of 0 in and a CTE of  $4 \times 10^{-6}/^\circ\text{F}$ .

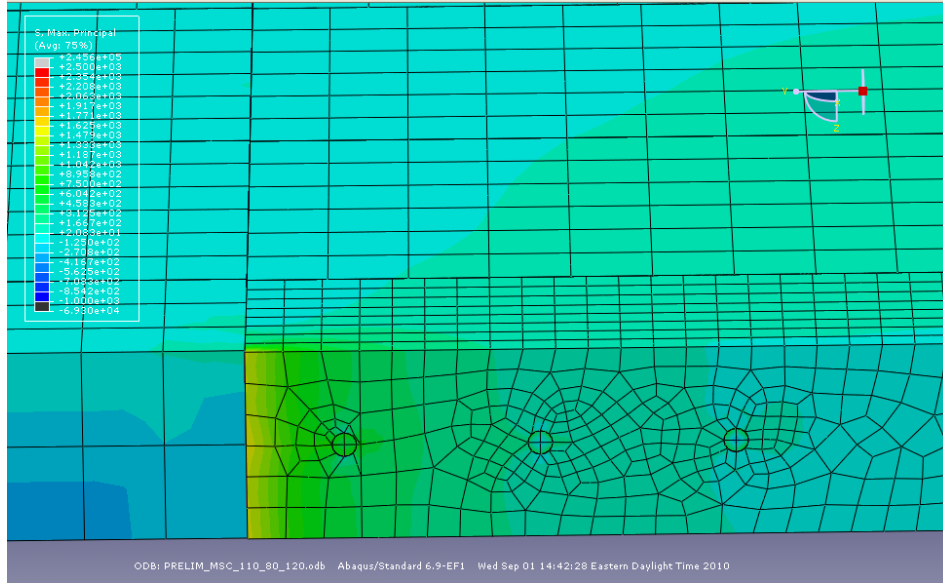


**Figure A14.** Longitudinal shear cracking model in which  $T_M=110^\circ\text{F}$ ,  $T_S=80^\circ\text{F}$ , and  $T_C=120^\circ\text{F}$  for a mortar intrusion of 0 in and a CTE of  $4 \times 10^{-6}/^\circ\text{F}$ .



**Figure A15.** Longitudinal shear cracking model in which  $T_M=110^\circ\text{F}$ ,  $T_S=90^\circ\text{F}$ , and  $T_C=110^\circ\text{F}$  for a mortar intrusion of 0 in and a CTE of  $4 \times 10^{-6}/^\circ\text{F}$ .

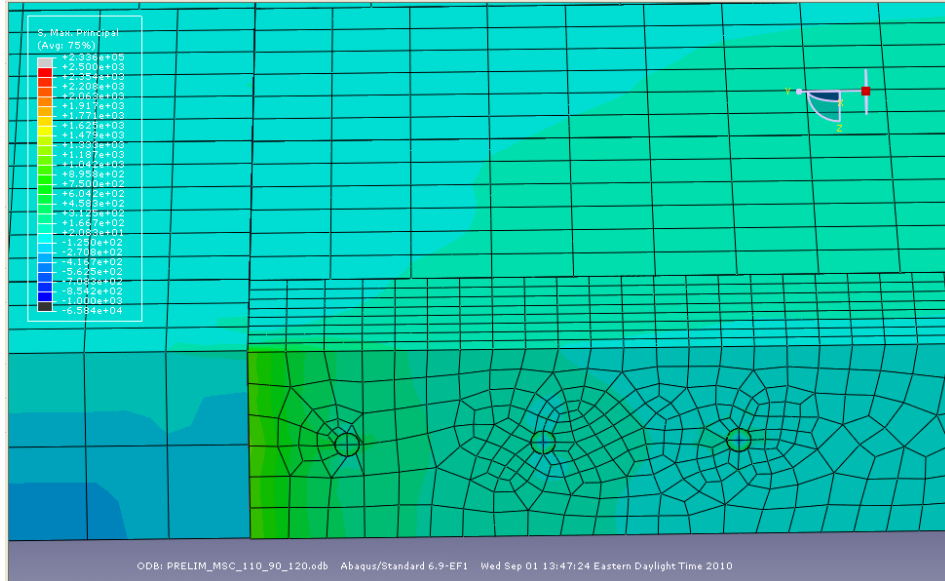


**Figure A16.** Longitudinal shear cracking model in which  $T_M=110^\circ\text{F}$ ,  $T_S=90^\circ\text{F}$ , and  $T_C=120^\circ\text{F}$  for a mortar intrusion of 0 in and a CTE of  $4 \times 10^{-6}/^\circ\text{F}$ .

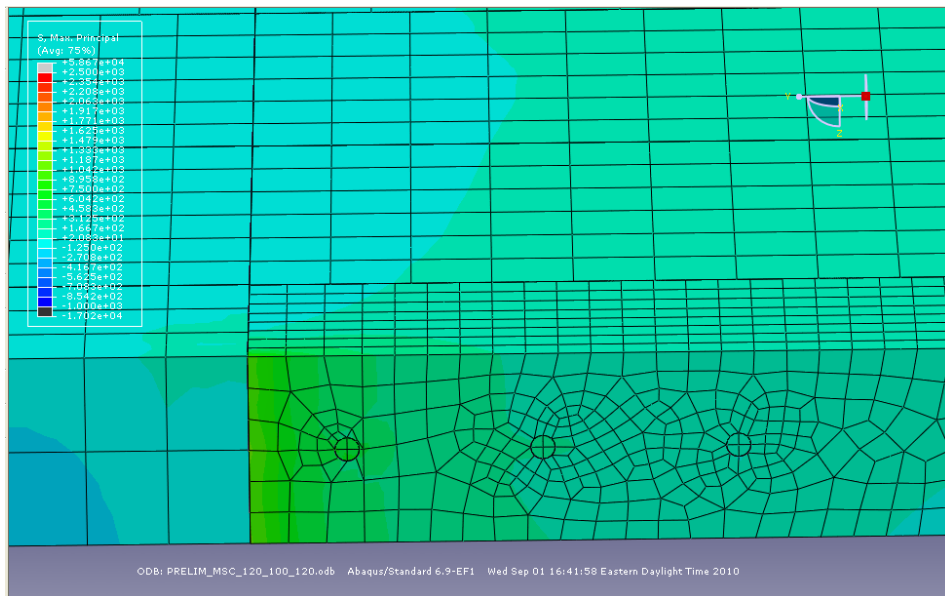


**Figure A17.** Longitudinal shear cracking model in which  $T_M=120^\circ\text{F}$ ,  $T_S=100^\circ\text{F}$ , and  $T_C=120^\circ\text{F}$  for a mortar intrusion of 0 in and a CTE of  $4 \times 10^{-6}/^\circ\text{F}$ .

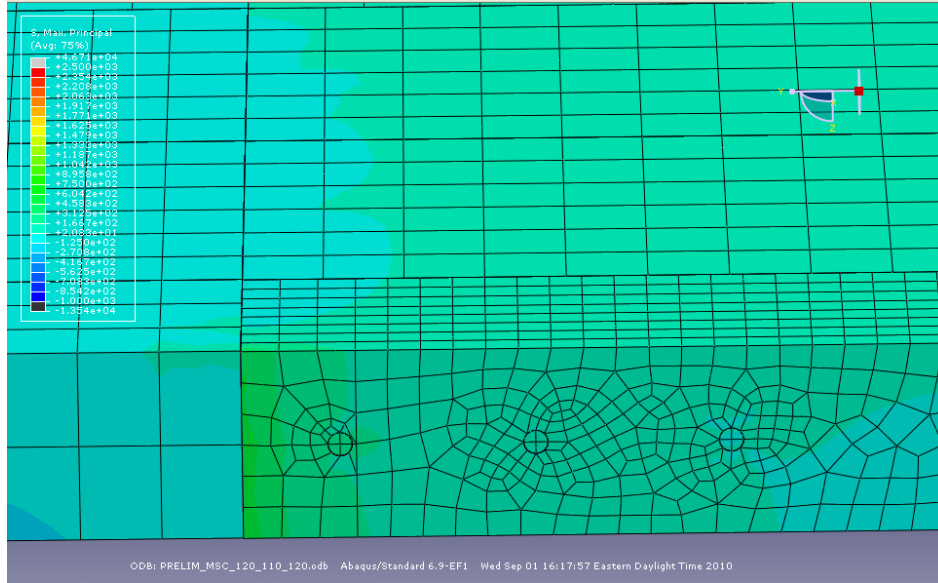


**Figure A18.** Longitudinal shear cracking model in which  $T_M=120^\circ\text{F}$ ,  $T_S=110^\circ\text{F}$ , and  $T_C=120^\circ\text{F}$  for a mortar intrusion of 0 in and a CTE of  $4 \times 10^{-6}/^\circ\text{F}$ .

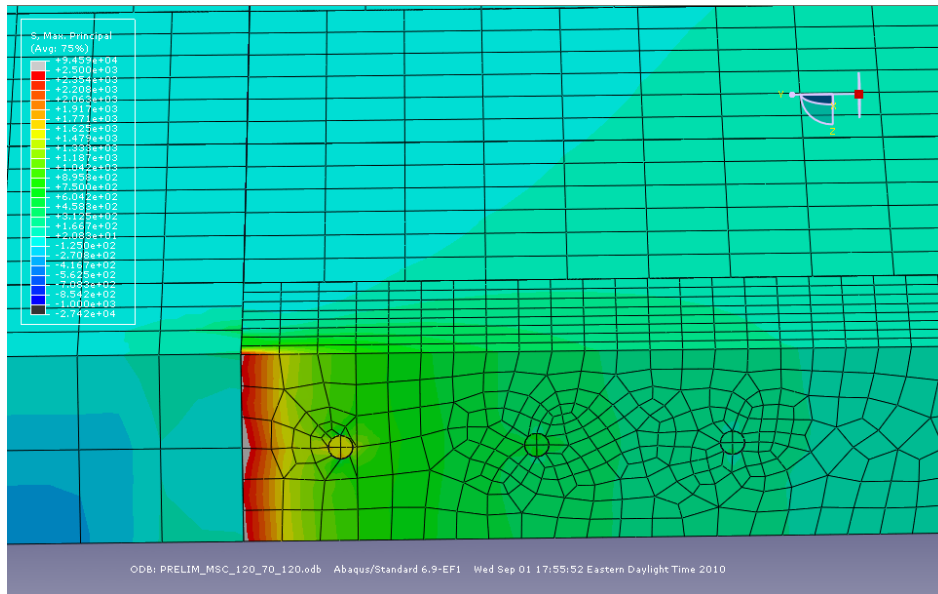


**Figure A19.** Longitudinal shear cracking model in which  $T_M=120^\circ\text{F}$ ,  $T_S=70^\circ\text{F}$ , and  $T_C=120^\circ\text{F}$  for a mortar intrusion of 0 in and a CTE of  $4 \times 10^{-6}/^\circ\text{F}$ .

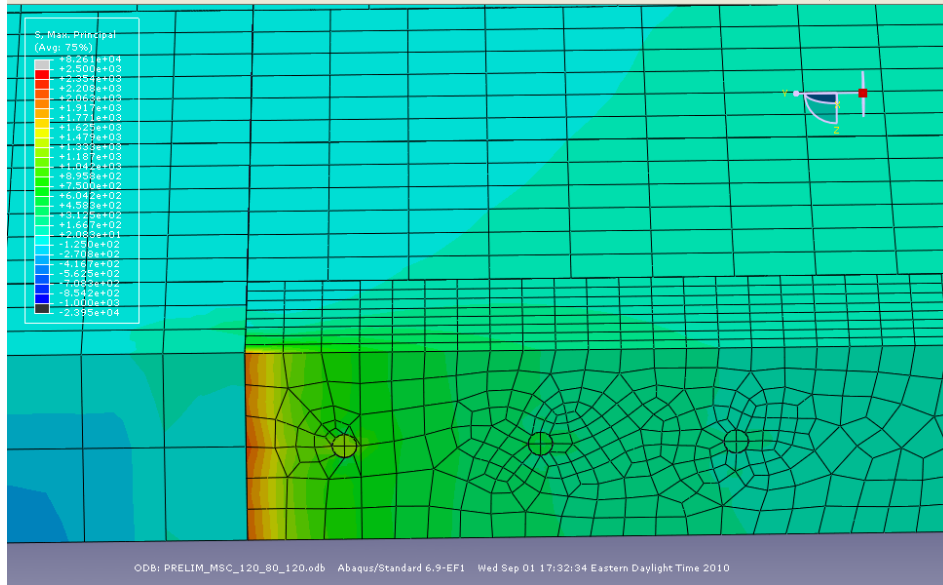


**Figure A20.** Longitudinal shear cracking model in which  $T_M=120^\circ\text{F}$ ,  $T_S=80^\circ\text{F}$ , and  $T_C=120^\circ\text{F}$  for a mortar intrusion of 0 in and a CTE of  $4 \times 10^{-6}/^\circ\text{F}$ .

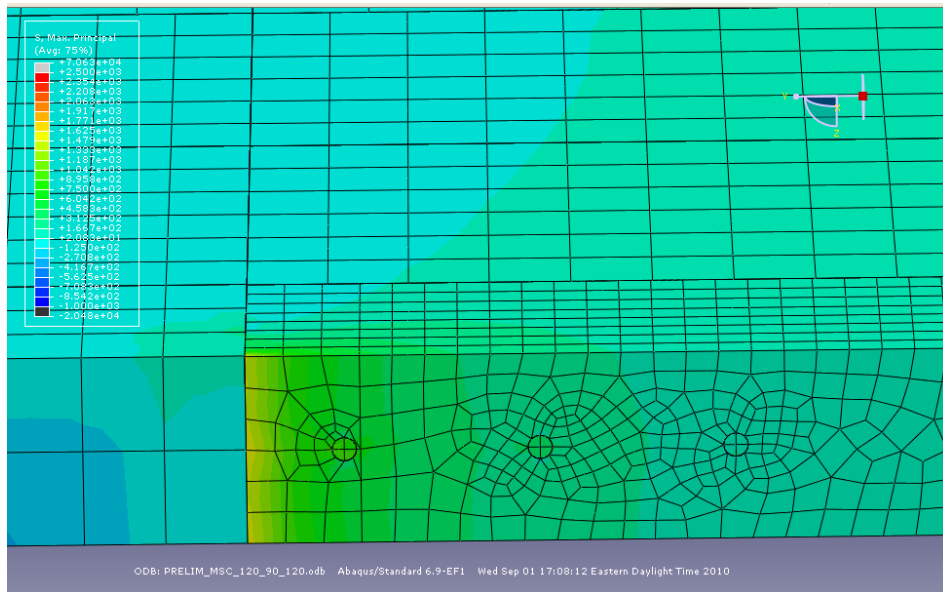


**Figure A21.** Longitudinal shear cracking model in which  $T_M=120^\circ\text{F}$ ,  $T_S=90^\circ\text{F}$ , and  $T_C=120^\circ\text{F}$  for a mortar intrusion of 0 in and a CTE of  $4 \times 10^{-6}/^\circ\text{F}$ .

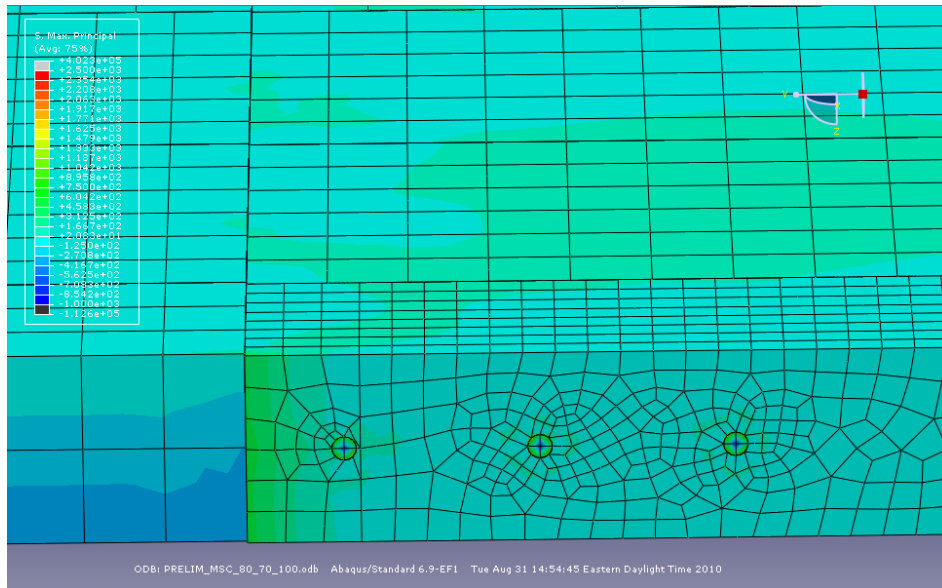


**Figure A22.** Longitudinal shear cracking model in which  $T_M=80^\circ\text{F}$ ,  $T_S=70^\circ\text{F}$ , and  $T_C=100^\circ\text{F}$  for a mortar intrusion of 0 in and a CTE of  $4 \times 10^{-6}/^\circ\text{F}$ .

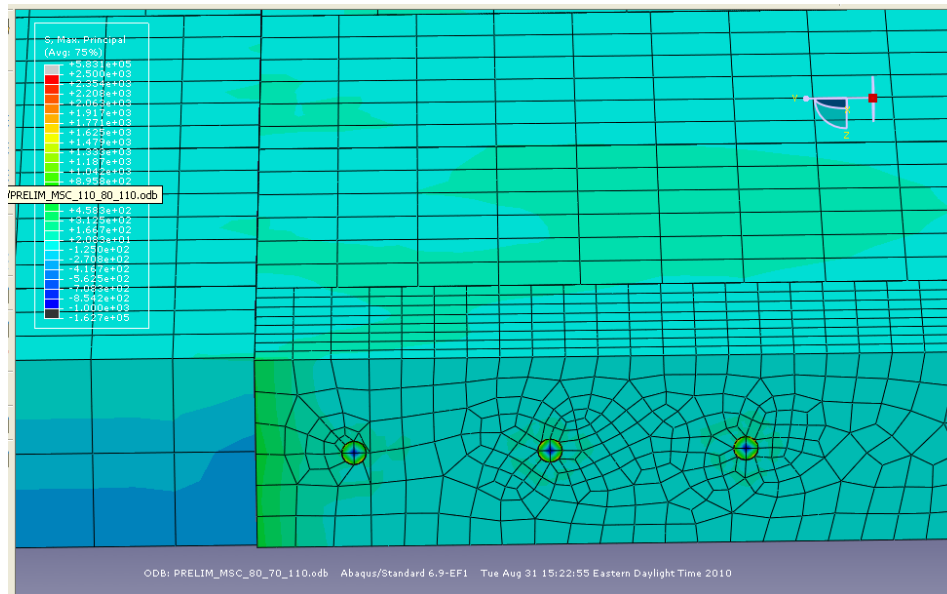


**Figure A23.** Longitudinal shear cracking model in which  $T_M=80^\circ\text{F}$ ,  $T_S=70^\circ\text{F}$ , and  $T_C=110^\circ\text{F}$  for a mortar intrusion of 0 in and a CTE of  $4 \times 10^{-6}/^\circ\text{F}$ .

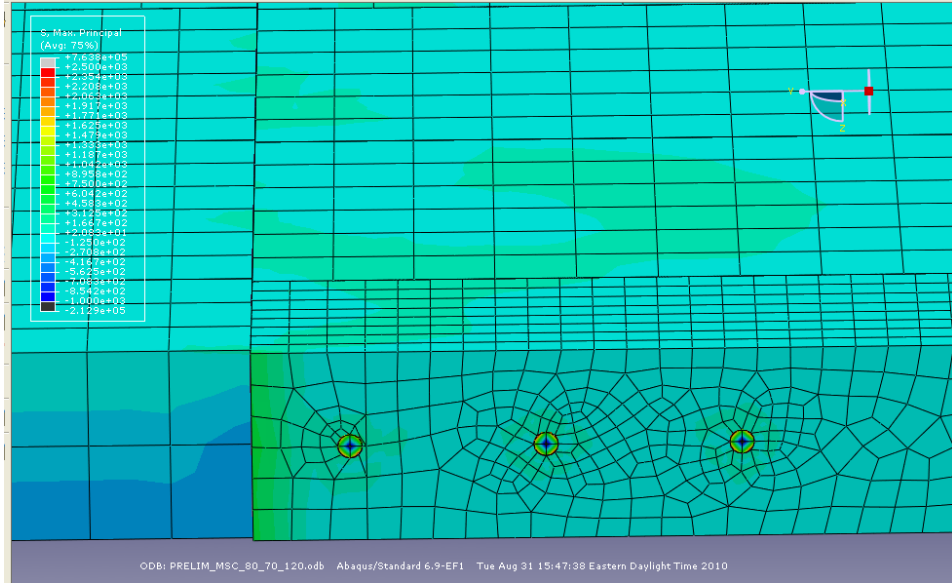


**Figure A24.** Longitudinal shear cracking model in which  $T_M=80^\circ\text{F}$ ,  $T_S=70^\circ\text{F}$ , and  $T_C=120^\circ\text{F}$  for a mortar intrusion of 0 in and a CTE of  $4 \times 10^{-6}/^\circ\text{F}$ .

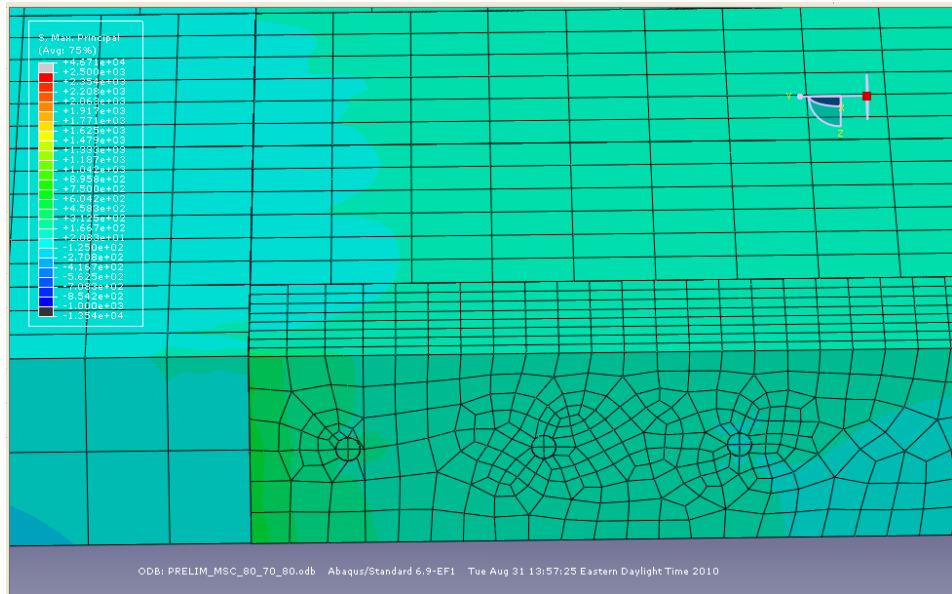


**Figure A25.** Longitudinal shear cracking model in which  $T_M=80^\circ\text{F}$ ,  $T_S=70^\circ\text{F}$ , and  $T_C=80^\circ\text{F}$  for a mortar intrusion of 0 in and a CTE of  $4 \times 10^{-6}/^\circ\text{F}$ .

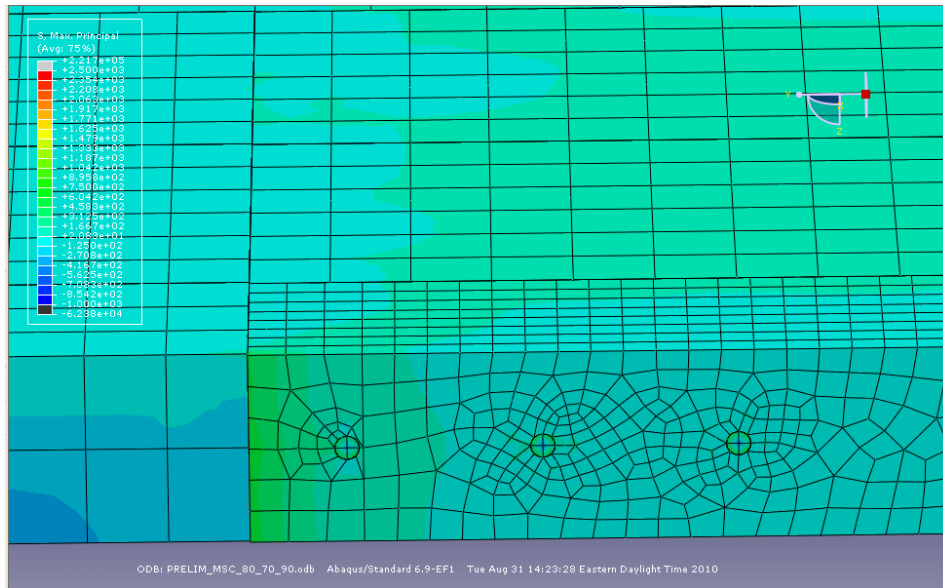


**Figure A26.** Longitudinal shear cracking model in which  $T_M=80^\circ\text{F}$ ,  $T_S=70^\circ\text{F}$ , and  $T_C=90^\circ\text{F}$  for a mortar intrusion of 0 in and a CTE of  $4 \times 10^{-6}/^\circ\text{F}$ .

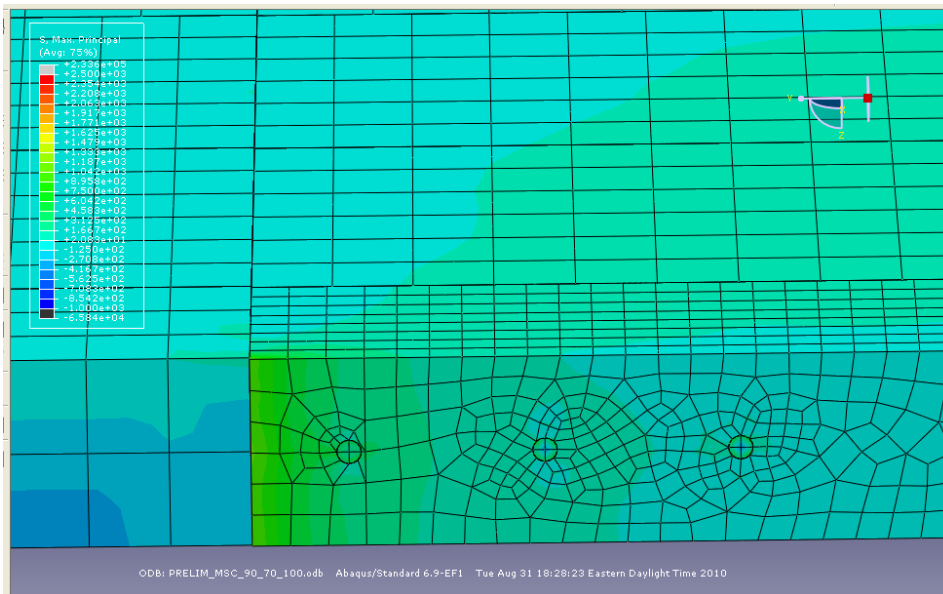


**Figure A27.** Longitudinal shear cracking model in which  $T_M=90^\circ\text{F}$ ,  $T_S=70^\circ\text{F}$ , and  $T_C=100^\circ\text{F}$  for a mortar intrusion of 0 in and a CTE of  $4 \times 10^{-6}/^\circ\text{F}$ .

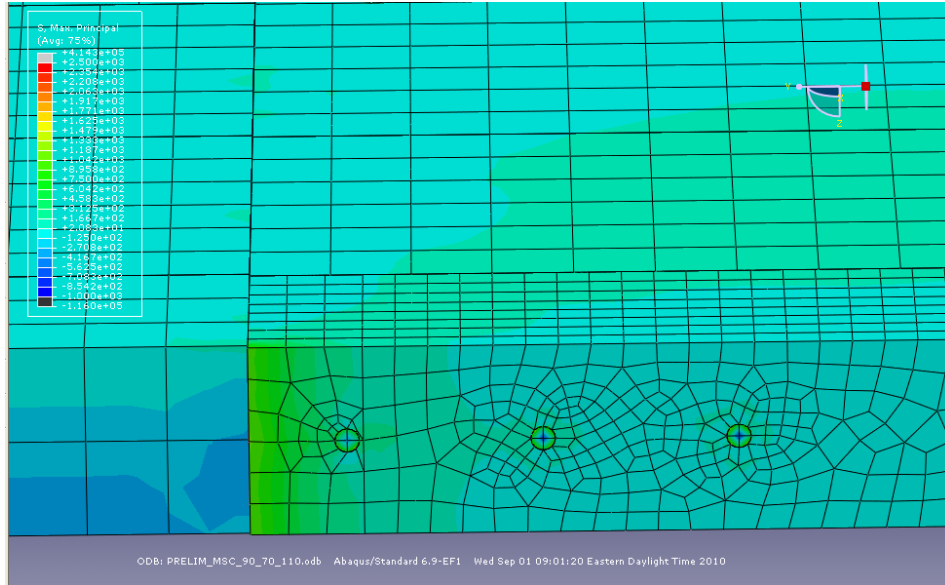


**Figure A28.** Longitudinal shear cracking model in which  $T_M=90^\circ\text{F}$ ,  $T_S=70^\circ\text{F}$ , and  $T_C=110^\circ\text{F}$  for a mortar intrusion of 0 in and a CTE of  $4 \times 10^{-6}/^\circ\text{F}$ .

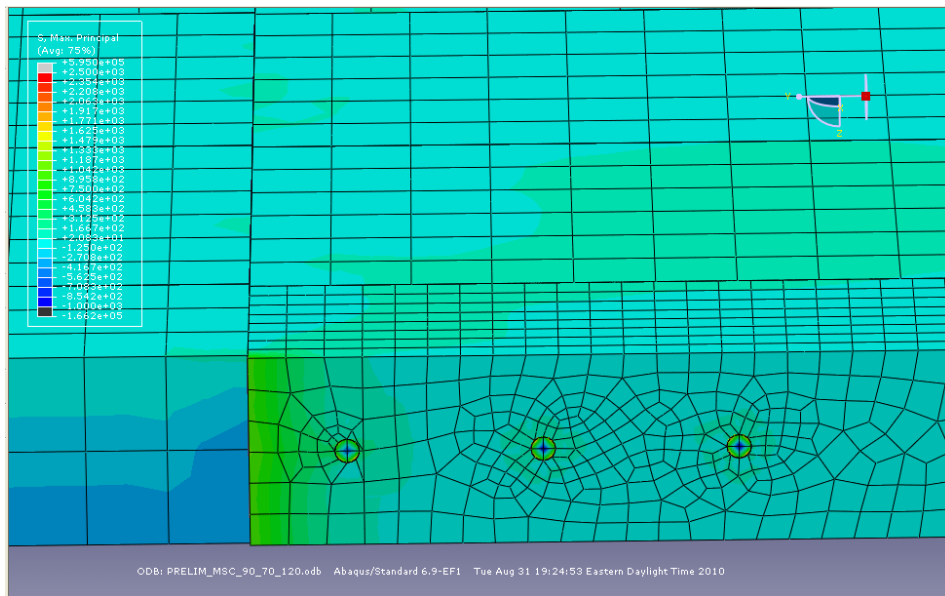


**Figure A29.** Longitudinal shear cracking model in which  $T_M=90^\circ\text{F}$ ,  $T_S=70^\circ\text{F}$ , and  $T_C=120^\circ\text{F}$  for a mortar intrusion of 0 in and a CTE of  $4 \times 10^{-6}/^\circ\text{F}$ .

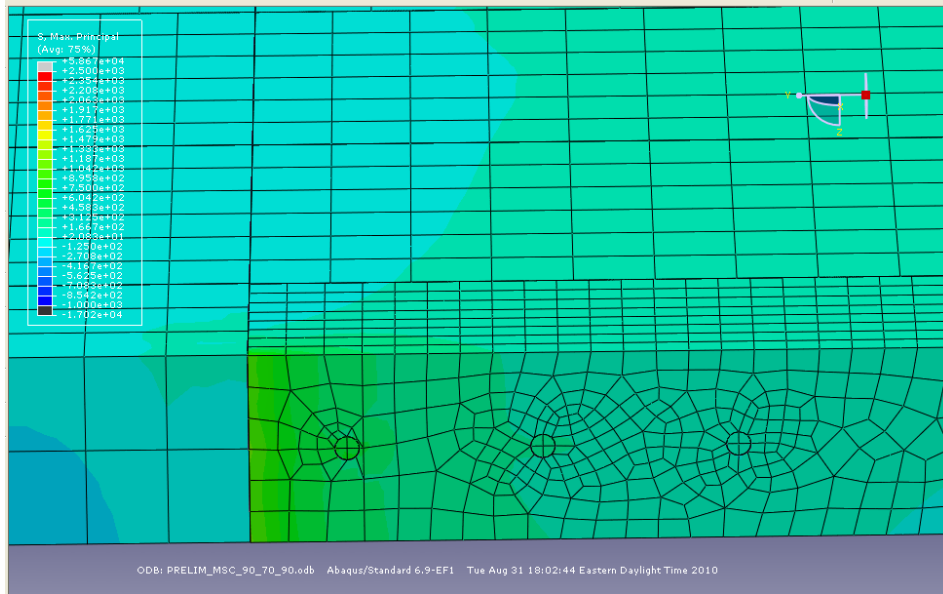


**Figure A30.** Longitudinal shear cracking model in which  $T_M=90^\circ\text{F}$ ,  $T_S=70^\circ\text{F}$ , and  $T_C=90^\circ\text{F}$  for a mortar intrusion of 0 in and a CTE of  $4 \times 10^{-6}/^\circ\text{F}$ .

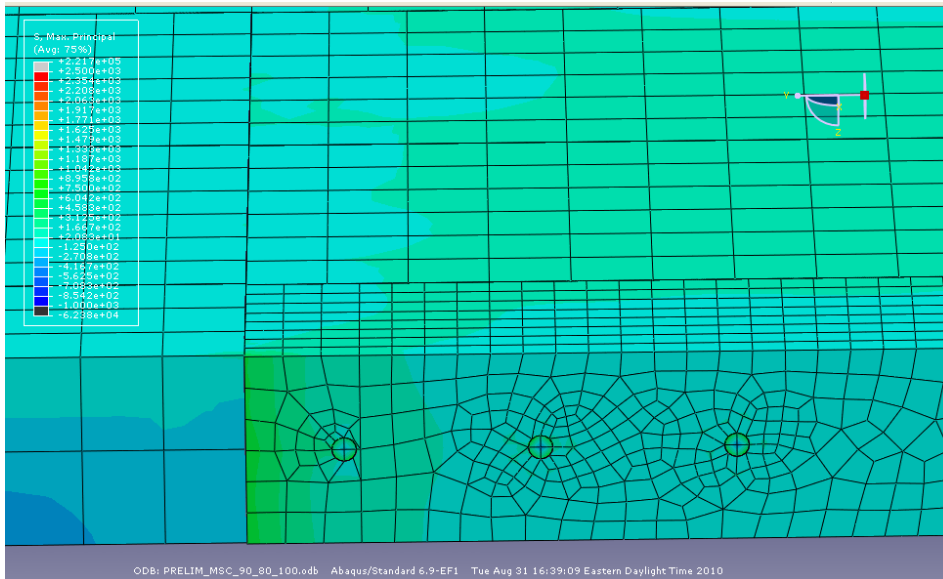


**Figure A31.** Longitudinal shear cracking model in which  $T_M=90^\circ\text{F}$ ,  $T_S=80^\circ\text{F}$ , and  $T_C=100^\circ\text{F}$  for a mortar intrusion of 0 in and a CTE of  $4 \times 10^{-6}/^\circ\text{F}$ .

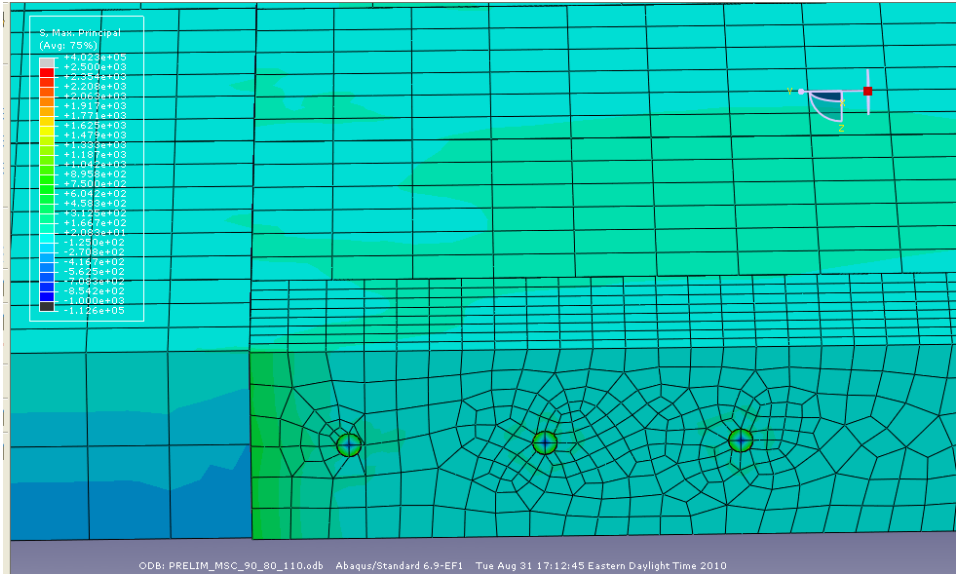


**Figure A32.** Longitudinal shear cracking model in which  $T_M=90^\circ\text{F}$ ,  $T_S=80^\circ\text{F}$ , and  $T_C=110^\circ\text{F}$  for a mortar intrusion of 0 in and a CTE of  $4 \times 10^{-6}/^\circ\text{F}$ .

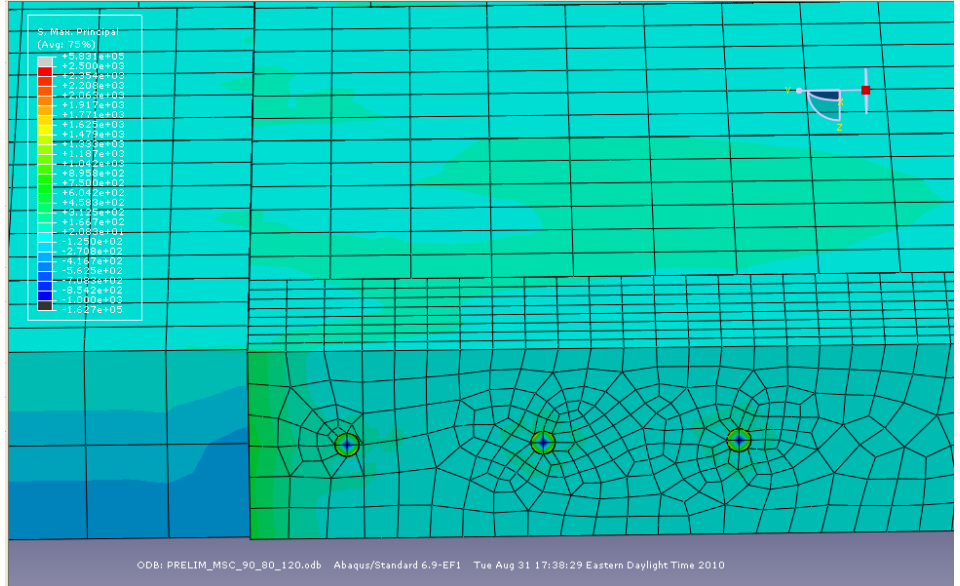


**Figure A33.** Longitudinal shear cracking model in which  $T_M=90^\circ\text{F}$ ,  $T_S=80^\circ\text{F}$ , and  $T_C=120^\circ\text{F}$  for a mortar intrusion of 0 in and a CTE of  $4 \times 10^{-6}/^\circ\text{F}$ .

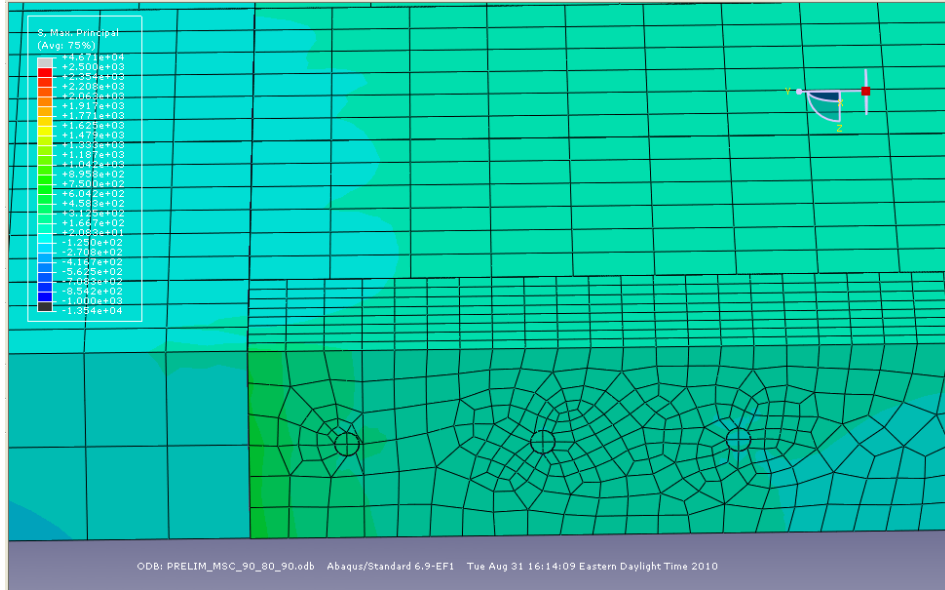


**Figure A34.** Longitudinal shear cracking model in which  $T_M=90^\circ\text{F}$ ,  $T_S=80^\circ\text{F}$ , and  $T_C=90^\circ\text{F}$  for a mortar intrusion of 0 in and a CTE of  $4 \times 10^{-6}/^\circ\text{F}$ .

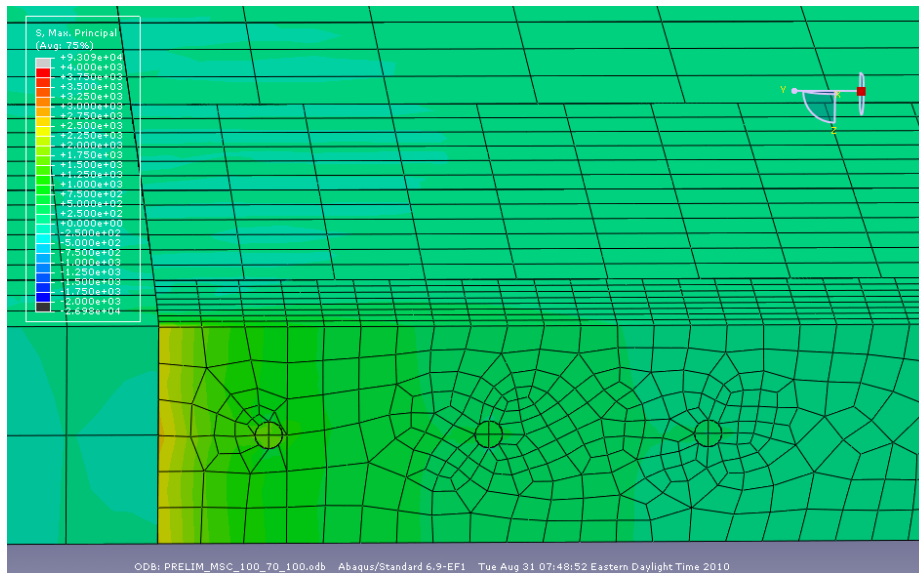


**Figure A35.** Longitudinal shear cracking model in which  $T_M=100^\circ\text{F}$ ,  $T_S=70^\circ\text{F}$ , and  $T_C=100^\circ\text{F}$  for a mortar intrusion of 0 in and a CTE of  $6.5 \times 10^{-6}/^\circ\text{F}$ .

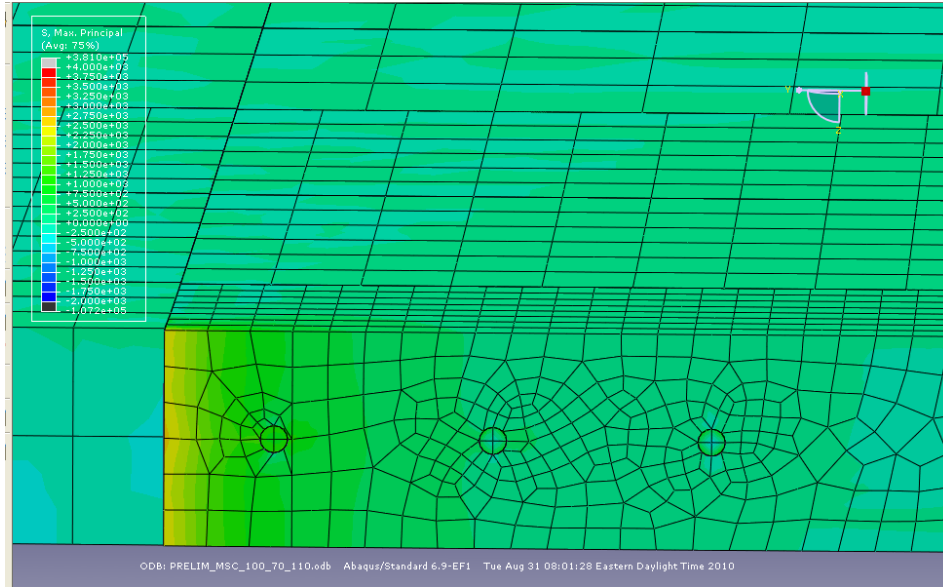


**Figure A36.** Longitudinal shear cracking model in which  $T_M=100^\circ\text{F}$ ,  $T_S=70^\circ\text{F}$ , and  $T_C=110^\circ\text{F}$  for a mortar intrusion of 0 in and a CTE of  $6.5 \times 10^{-6}/^\circ\text{F}$ .

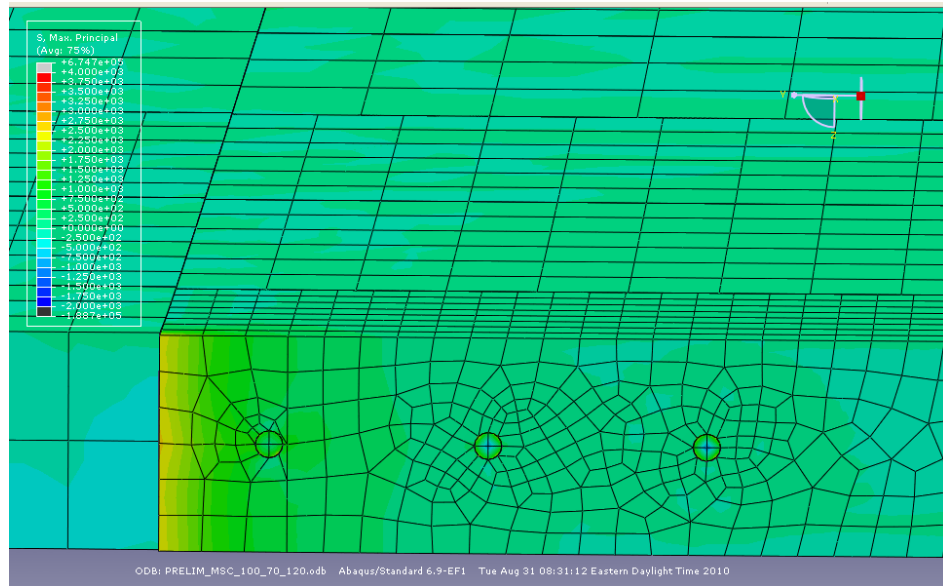


**Figure A37.** Longitudinal shear cracking model in which  $T_M=100^\circ\text{F}$ ,  $T_S=70^\circ\text{F}$ , and  $T_C=120^\circ\text{F}$  for a mortar intrusion of 0 in and a CTE of  $6.5 \times 10^{-6}/^\circ\text{F}$ .

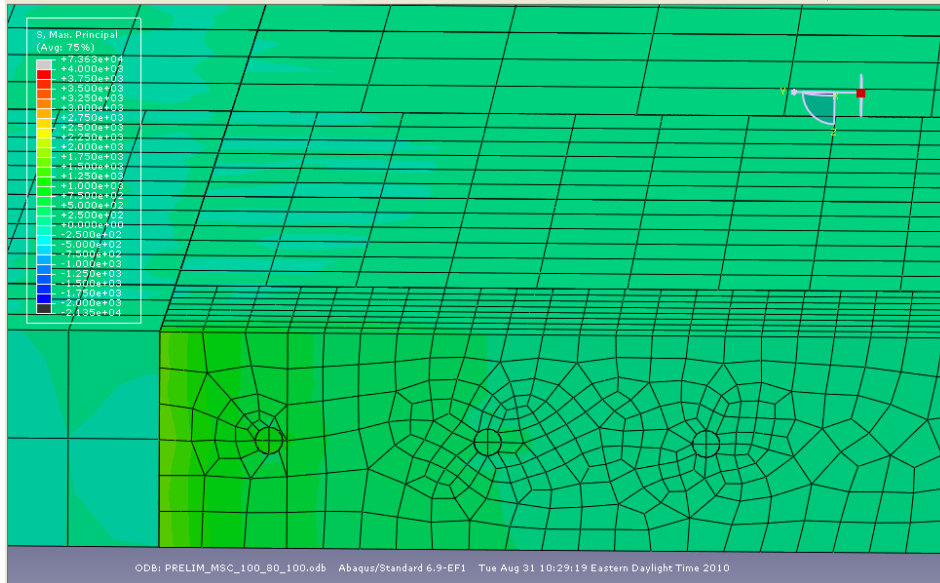


**Figure A38.** Longitudinal shear cracking model in which  $T_M=100^\circ\text{F}$ ,  $T_S=80^\circ\text{F}$ , and  $T_C=100^\circ\text{F}$  for a mortar intrusion of 0 in and a CTE of  $6.5 \times 10^{-6}/^\circ\text{F}$ .

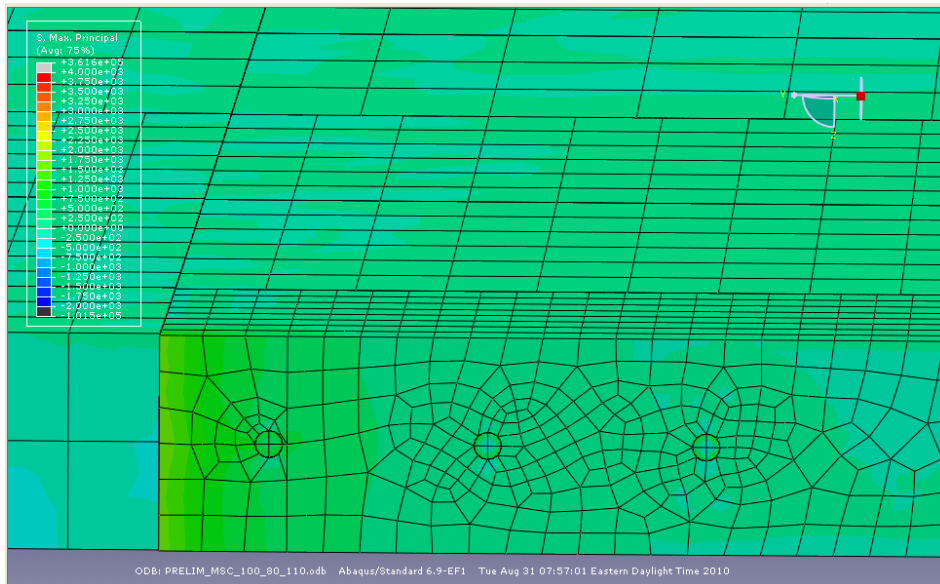


**Figure A39.** Longitudinal shear cracking model in which  $T_M=100^\circ\text{F}$ ,  $T_S=80^\circ\text{F}$ , and  $T_C=110^\circ\text{F}$  for a mortar intrusion of 0 in and a CTE of  $6.5 \times 10^{-6}/^\circ\text{F}$ .

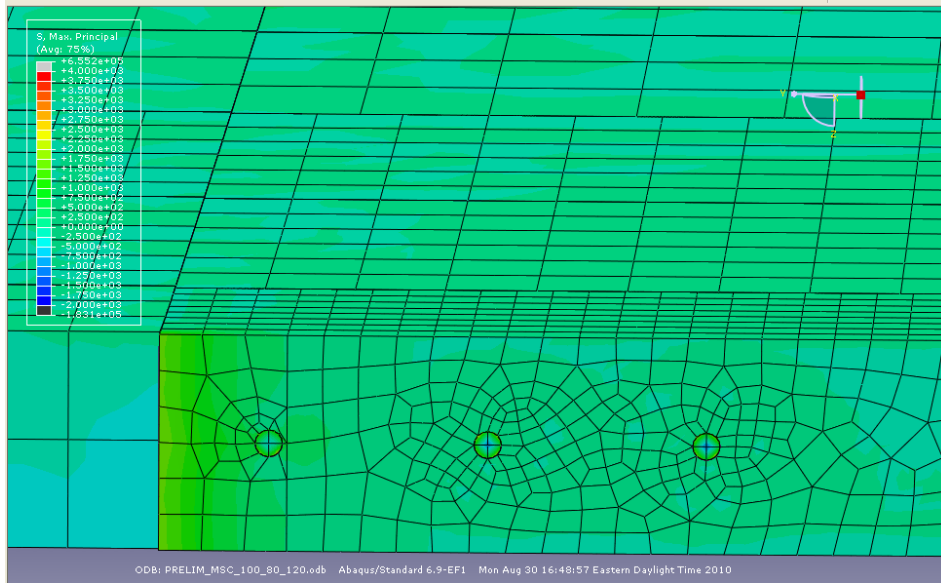


**Figure A40.** Longitudinal shear cracking model in which  $T_M=100^\circ\text{F}$ ,  $T_S=80^\circ\text{F}$ , and  $T_C=120^\circ\text{F}$  for a mortar intrusion of 0 in and a CTE of  $6.5 \times 10^{-6}/^\circ\text{F}$ .

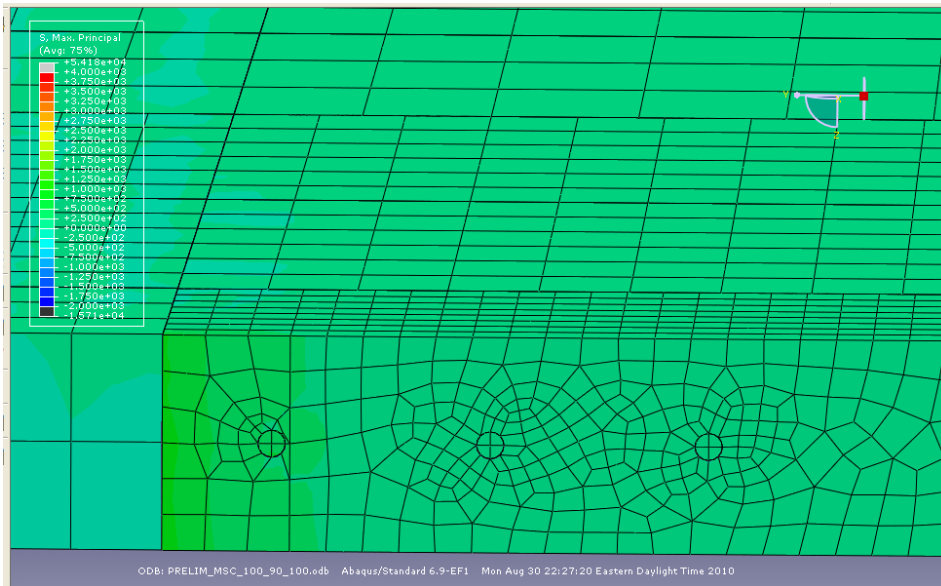


**Figure A41.** Longitudinal shear cracking model in which  $T_M=100^\circ\text{F}$ ,  $T_S=90^\circ\text{F}$ , and  $T_C=100^\circ\text{F}$  for a mortar intrusion of 0 in and a CTE of  $6.5 \times 10^{-6}/^\circ\text{F}$ .

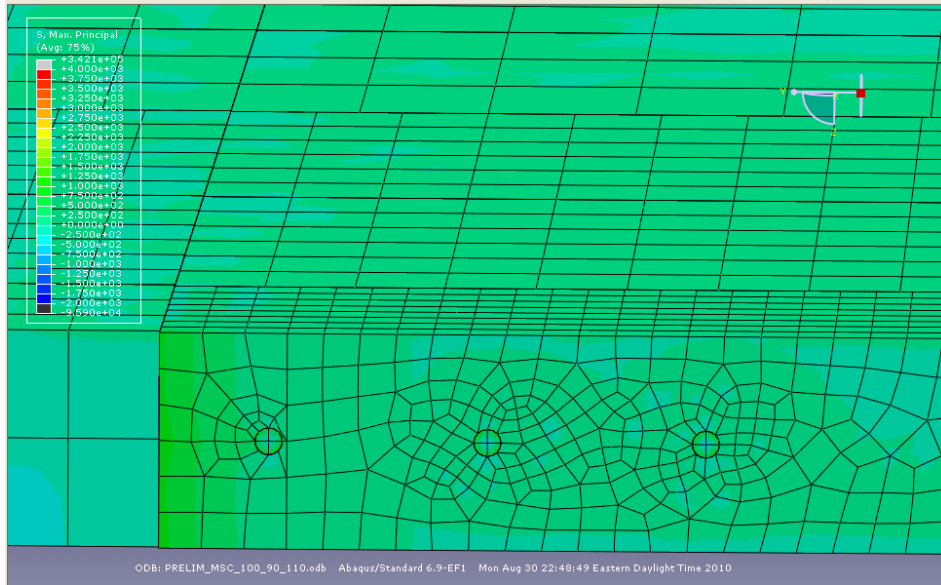


**Figure A42.** Longitudinal shear cracking model in which  $T_M=100^\circ\text{F}$ ,  $T_S=90^\circ\text{F}$ , and  $T_C=110^\circ\text{F}$  for a mortar intrusion of 0 in and a CTE of  $6.5 \times 10^{-6}/^\circ\text{F}$ .

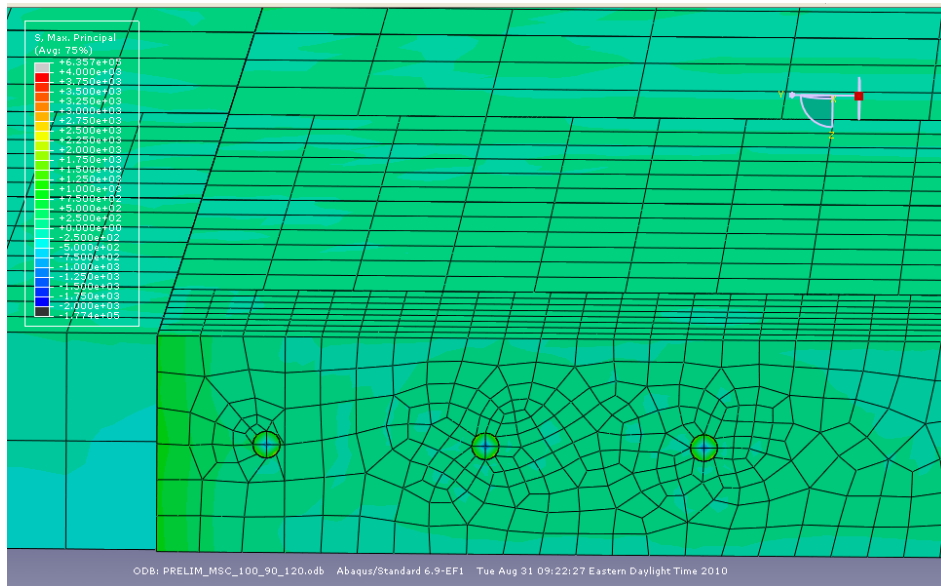


**Figure A43.** Longitudinal shear cracking model in which  $T_M=100^\circ\text{F}$ ,  $T_S=90^\circ\text{F}$ , and  $T_C=120^\circ\text{F}$  for a mortar intrusion of 0 in and a CTE of  $6.5 \times 10^{-6}/^\circ\text{F}$ .

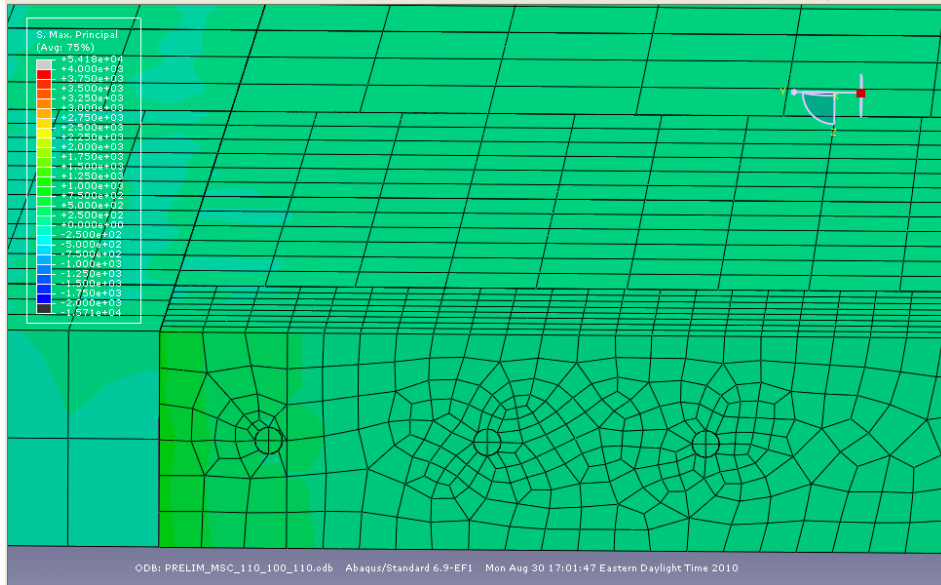


**Figure A44.** Longitudinal shear cracking model in which  $T_M=110^\circ\text{F}$ ,  $T_S=100^\circ\text{F}$ , and  $T_C=110^\circ\text{F}$  for a mortar intrusion of 0 in and a CTE of  $6.5 \times 10^{-6}/^\circ\text{F}$ .

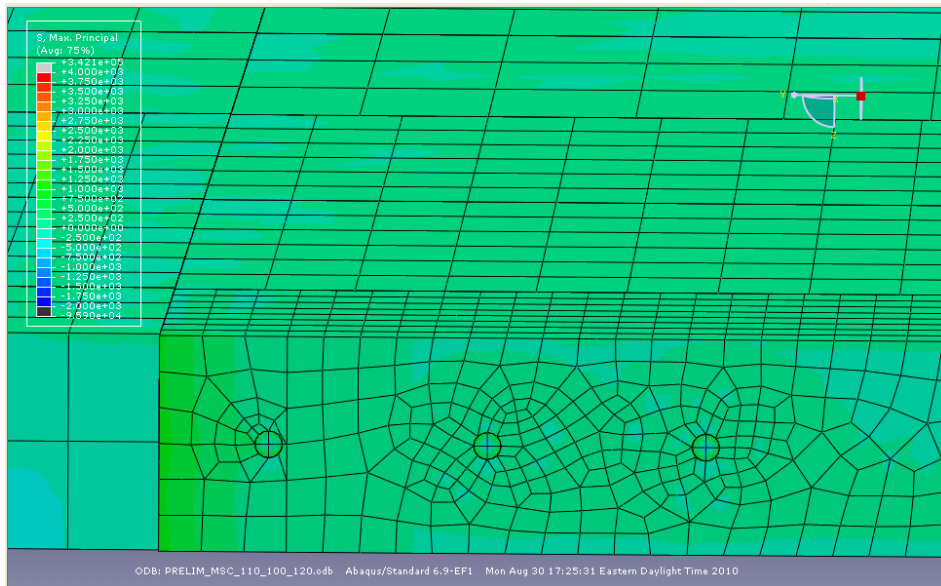


**Figure A45.** Longitudinal shear cracking model in which  $T_M=110^\circ\text{F}$ ,  $T_S=100^\circ\text{F}$ , and  $T_C=120^\circ\text{F}$  for a mortar intrusion of 0 in and a CTE of  $6.5 \times 10^{-6}/^\circ\text{F}$ .

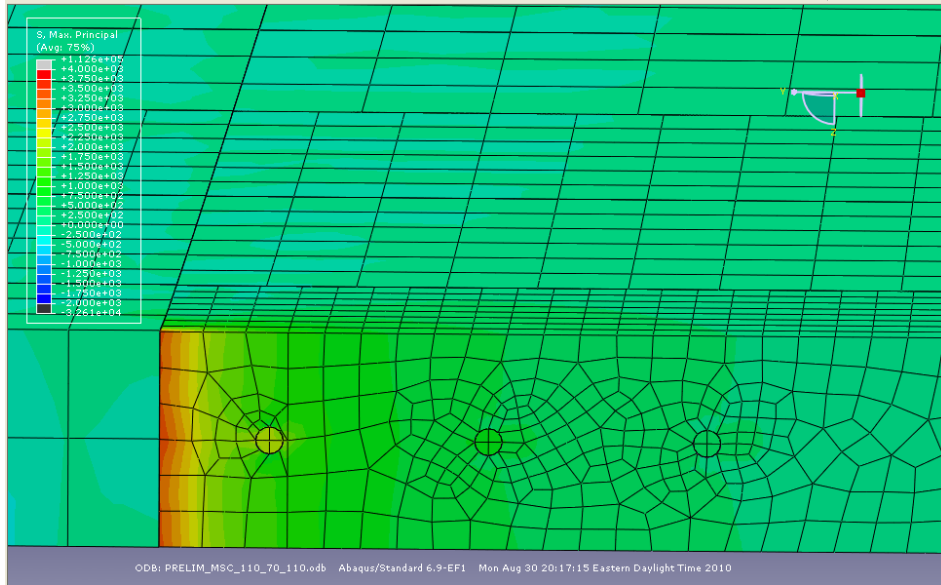


**Figure A46.** Longitudinal shear cracking model in which  $T_M=110^\circ\text{F}$ ,  $T_S=70^\circ\text{F}$ , and  $T_C=110^\circ\text{F}$  for a mortar intrusion of 0 in and a CTE of  $6.5 \times 10^{-6}/^\circ\text{F}$ .

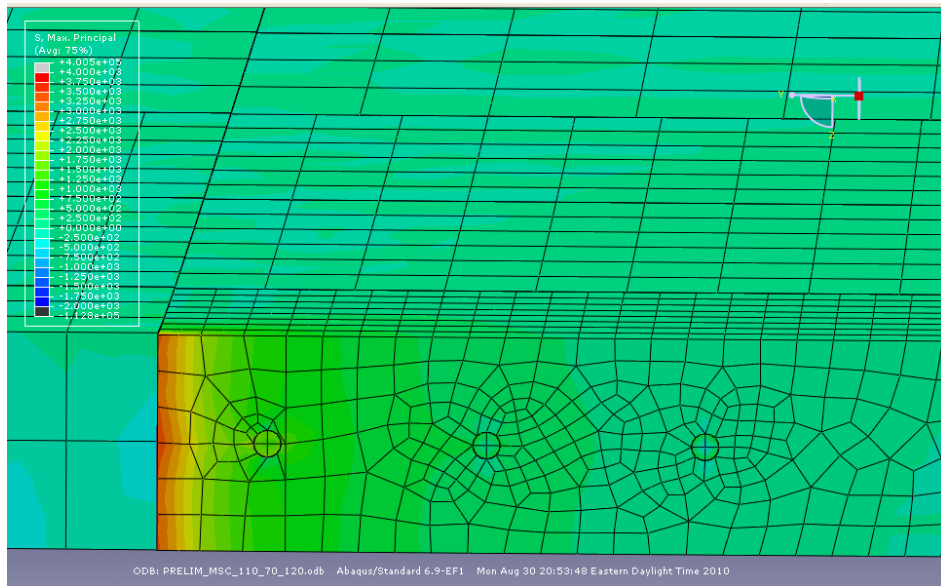


**Figure A47.** Longitudinal shear cracking model in which  $T_M=110^\circ\text{F}$ ,  $T_S=70^\circ\text{F}$ , and  $T_C=120^\circ\text{F}$  for a mortar intrusion of 0 in and a CTE of  $6.5 \times 10^{-6}/^\circ\text{F}$ .

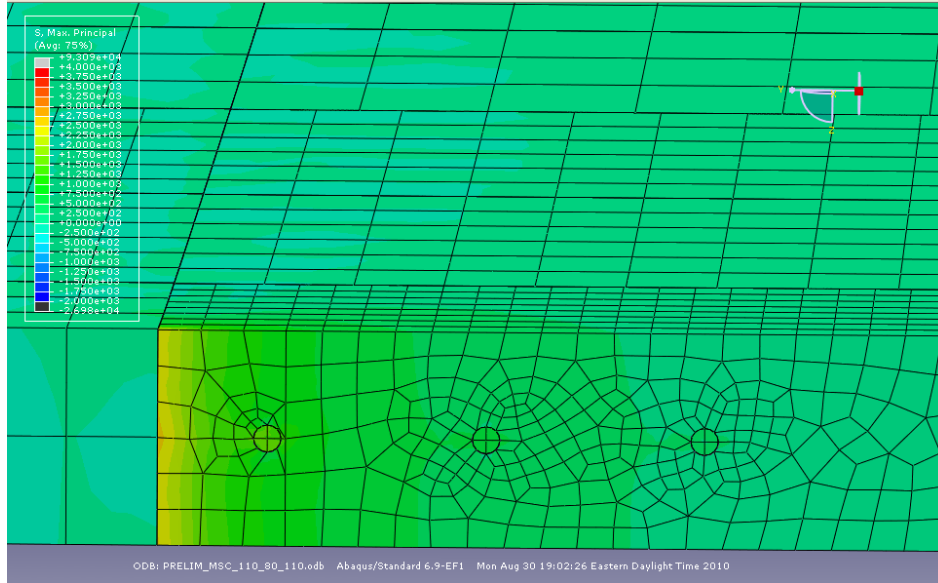


**Figure A48.** Longitudinal shear cracking model in which  $T_M=110^\circ\text{F}$ ,  $T_S=80^\circ\text{F}$ , and  $T_C=110^\circ\text{F}$  for a mortar intrusion of 0 in and a CTE of  $6.5 \times 10^{-6}/^\circ\text{F}$ .

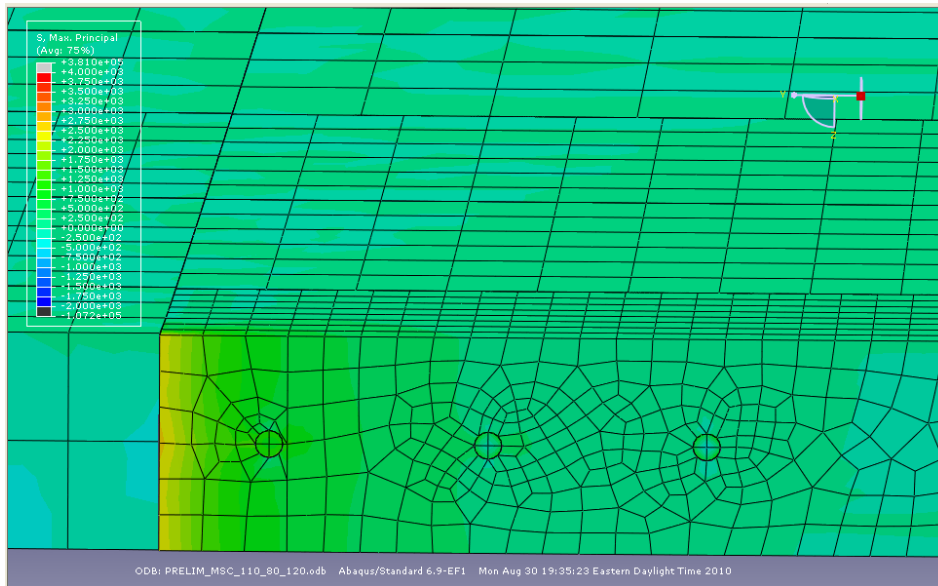


**Figure A49.** Longitudinal shear cracking model in which  $T_M=110^\circ\text{F}$ ,  $T_S=80^\circ\text{F}$ , and  $T_C=120^\circ\text{F}$  for a mortar intrusion of 0 in and a CTE of  $6.5 \times 10^{-6}/^\circ\text{F}$ .

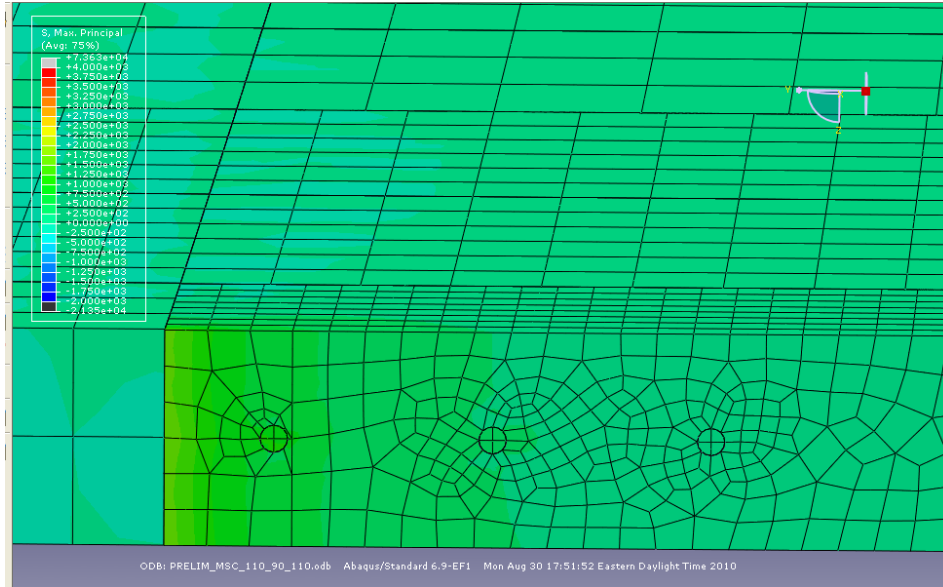


**Figure A50.** Longitudinal shear cracking model in which  $T_M=110^\circ\text{F}$ ,  $T_S=90^\circ\text{F}$ , and  $T_C=110^\circ\text{F}$  for a mortar intrusion of 0 in and a CTE of  $6.5 \times 10^{-6}/^\circ\text{F}$ .

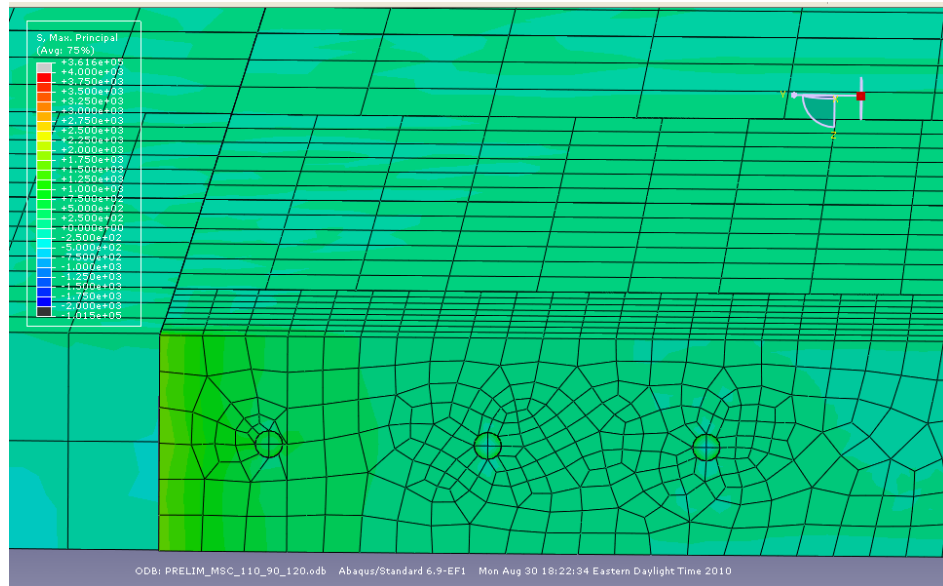


**Figure A51.** Longitudinal shear cracking model in which  $T_M=110^\circ\text{F}$ ,  $T_S=90^\circ\text{F}$ , and  $T_C=120^\circ\text{F}$  for a mortar intrusion of 0 in and a CTE of  $6.5 \times 10^{-6}/^\circ\text{F}$ .

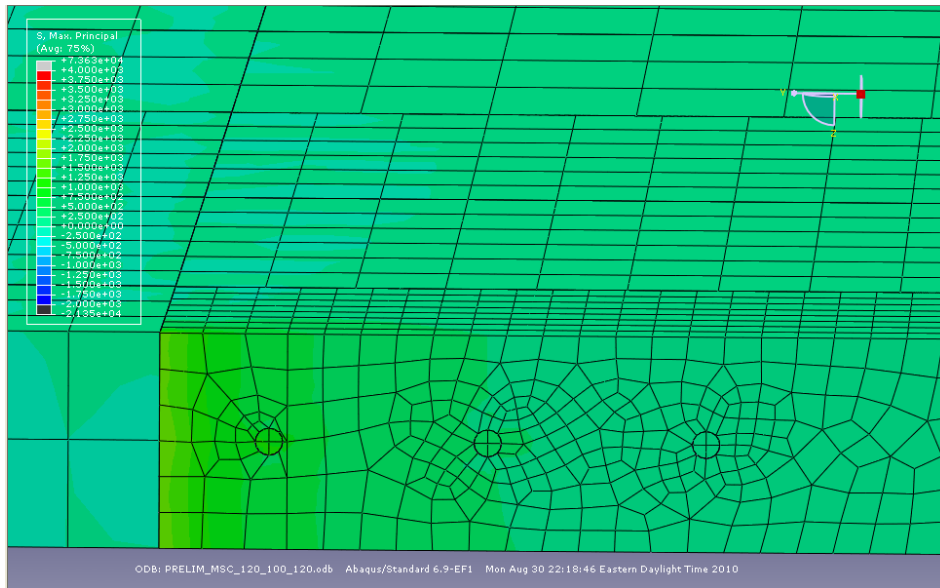


**Figure A52.** Longitudinal shear cracking model in which  $T_M=120^\circ\text{F}$ ,  $T_S=100^\circ\text{F}$ , and  $T_C=120^\circ\text{F}$  for a mortar intrusion of 0 in and a CTE of  $6.5 \times 10^{-6}/^\circ\text{F}$ .

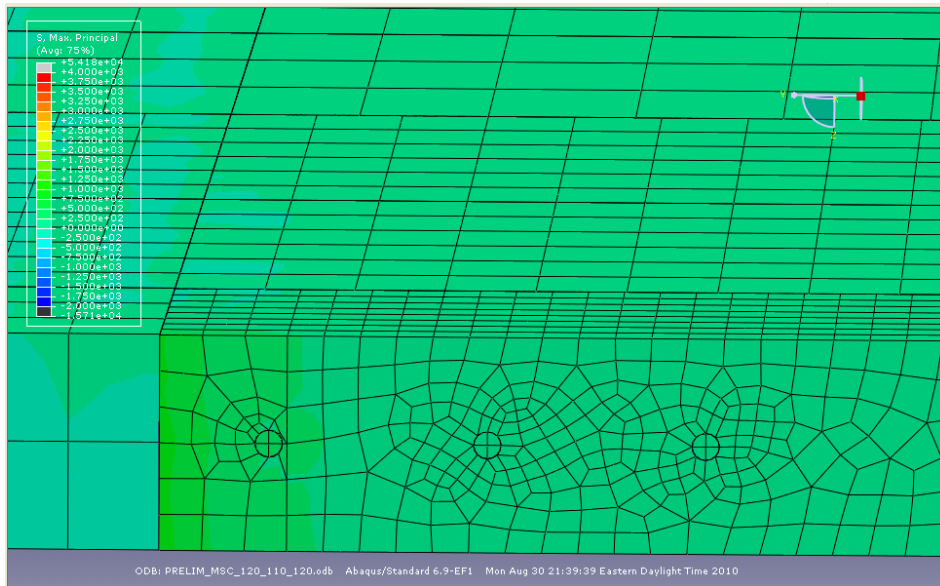


**Figure A53.** Longitudinal shear cracking model in which  $T_M=120^\circ\text{F}$ ,  $T_S=110^\circ\text{F}$ , and  $T_C=120^\circ\text{F}$  for a mortar intrusion of 0 in and a CTE of  $6.5 \times 10^{-6}/^\circ\text{F}$ .

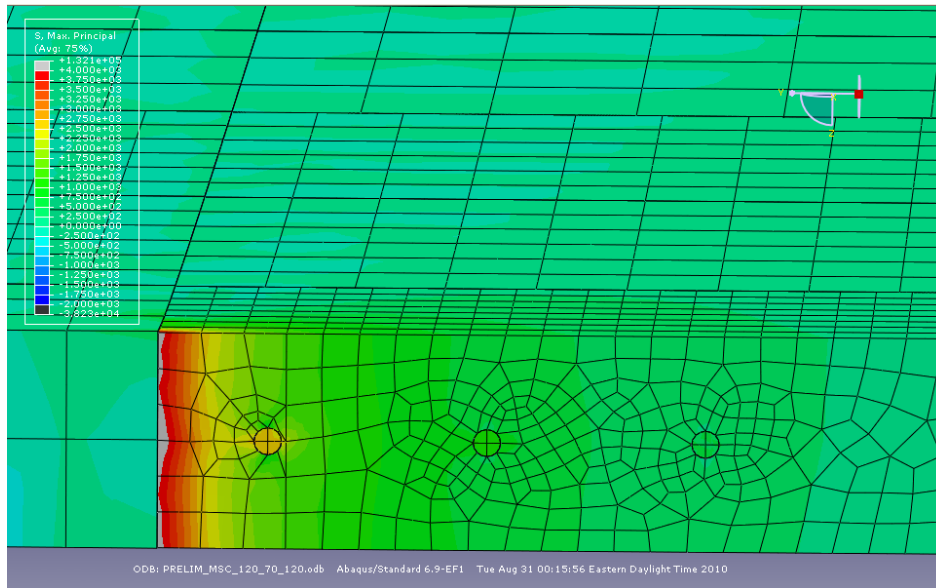


**Figure A54.** Longitudinal shear cracking model in which  $T_M=120^\circ\text{F}$ ,  $T_S=70^\circ\text{F}$ , and  $T_C=120^\circ\text{F}$  for a mortar intrusion of 0 in and a CTE of  $6.5 \times 10^{-6}/^\circ\text{F}$ .

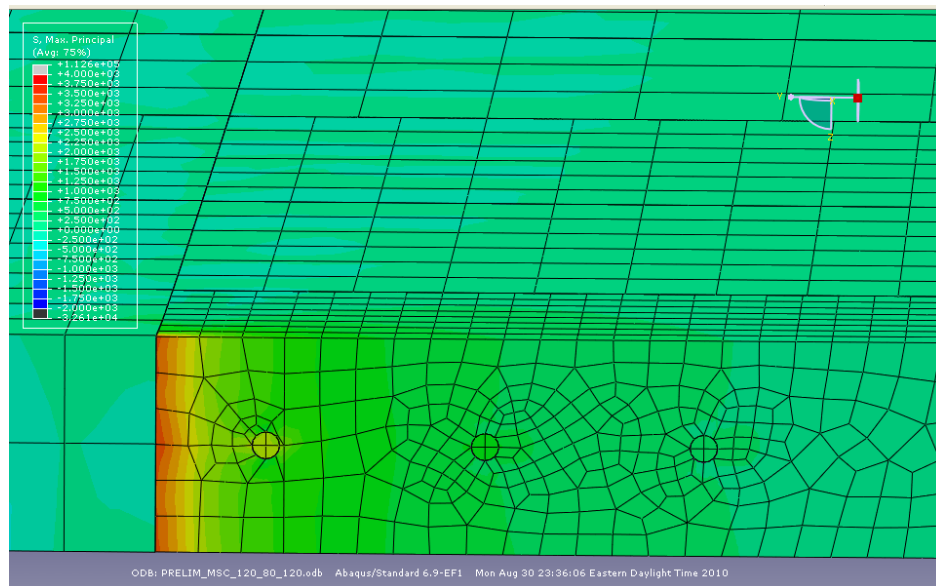


**Figure A55.** Longitudinal shear cracking model in which  $T_M=120^\circ\text{F}$ ,  $T_S=80^\circ\text{F}$ , and  $T_C=120^\circ\text{F}$  for a mortar intrusion of 0 in and a CTE of  $6.5 \times 10^{-6}/^\circ\text{F}$ .

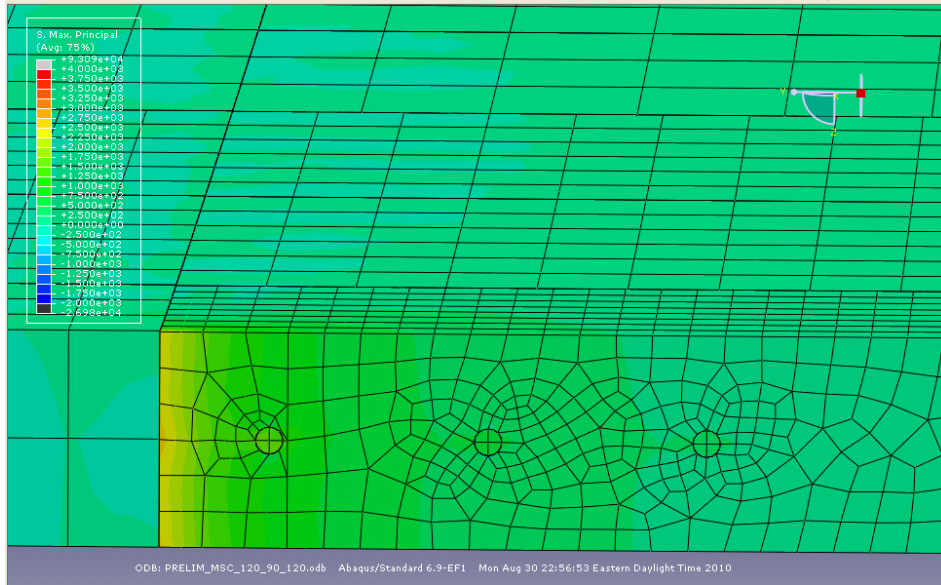


**Figure A56.** Longitudinal shear cracking model in which  $T_M=120^\circ\text{F}$ ,  $T_S=90^\circ\text{F}$ , and  $T_C=120^\circ\text{F}$  for a mortar intrusion of 0 in and a CTE of  $6.5 \times 10^{-6}/^\circ\text{F}$ .

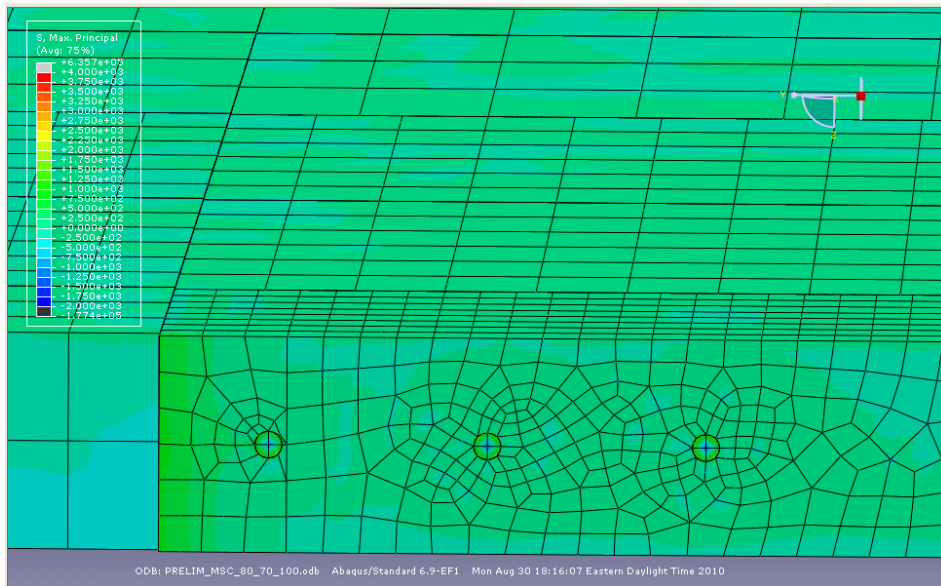


**Figure A57.** Longitudinal shear cracking model in which  $T_M=80^\circ\text{F}$ ,  $T_S=70^\circ\text{F}$ , and  $T_C=100^\circ\text{F}$  for a mortar intrusion of 0 in and a CTE of  $6.5 \times 10^{-6}/^\circ\text{F}$ .

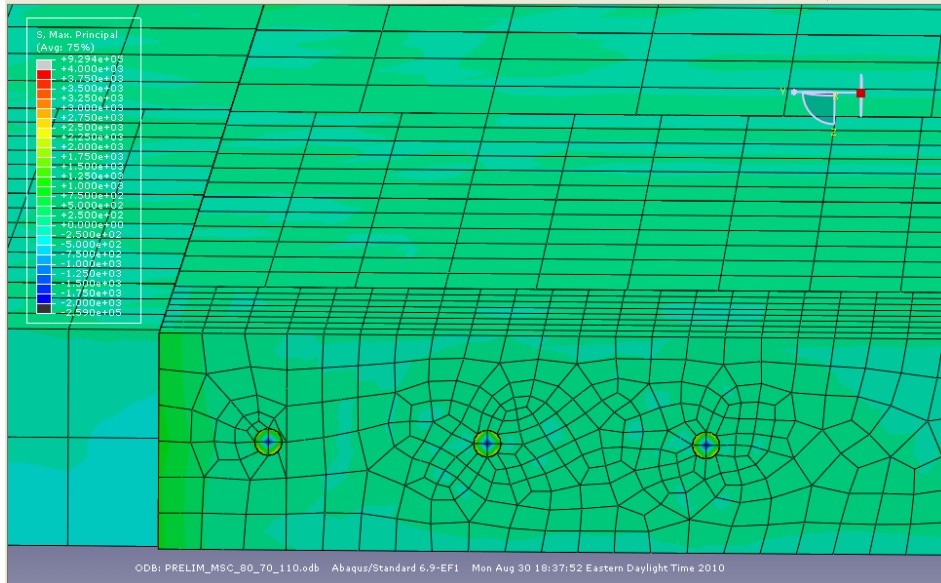


**Figure A58.** Longitudinal shear cracking model in which  $T_M=80^\circ\text{F}$ ,  $T_S=70^\circ\text{F}$ , and  $T_C=110^\circ\text{F}$  for a mortar intrusion of 0 in and a CTE of  $6.5 \times 10^{-6}/^\circ\text{F}$ .

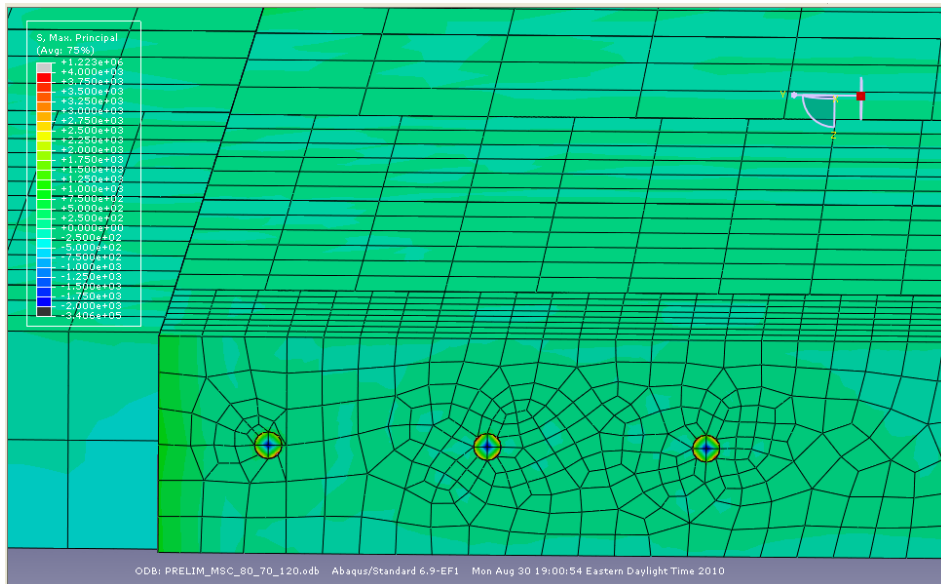


**Figure A59.** Longitudinal shear cracking model in which  $T_M=80^\circ\text{F}$ ,  $T_S=70^\circ\text{F}$ , and  $T_C=120^\circ\text{F}$  for a mortar intrusion of 0 in and a CTE of  $6.5 \times 10^{-6}/^\circ\text{F}$ .

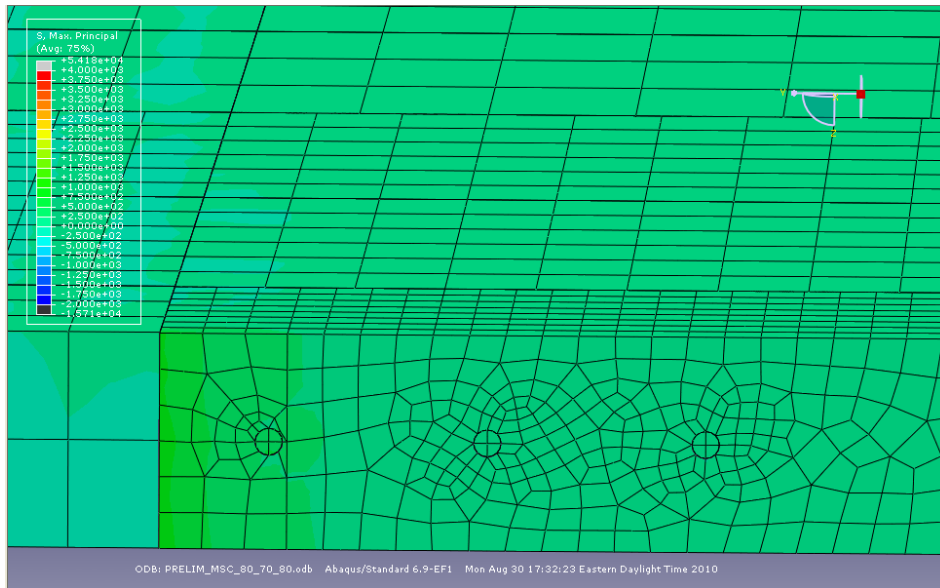


**Figure A60.** Longitudinal shear cracking model in which  $T_M=80^\circ\text{F}$ ,  $T_S=70^\circ\text{F}$ , and  $T_C=80^\circ\text{F}$  for a mortar intrusion of 0 in and a CTE of  $6.5 \times 10^{-6}/^\circ\text{F}$ .

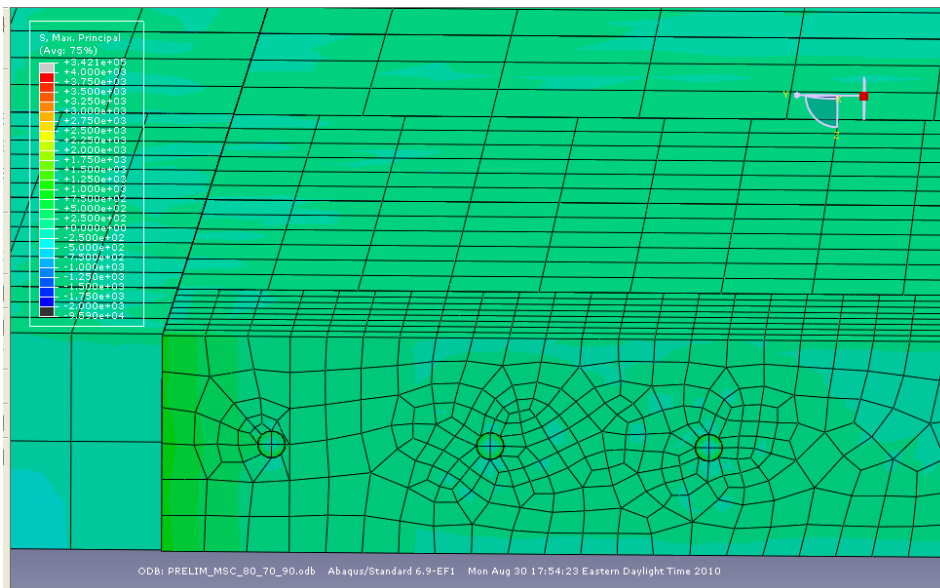


**Figure A61.** Longitudinal shear cracking model in which  $T_M=80^\circ\text{F}$ ,  $T_S=70^\circ\text{F}$ , and  $T_C=90^\circ\text{F}$  for a mortar intrusion of 0 in and a CTE of  $6.5 \times 10^{-6}/^\circ\text{F}$ .

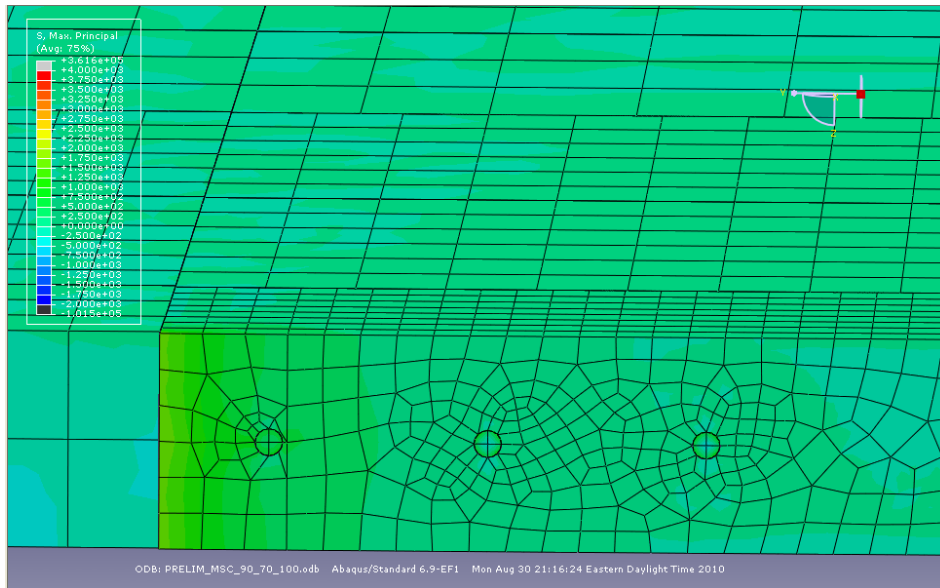


**Figure A62.** Longitudinal shear cracking model in which  $T_M=90^\circ\text{F}$ ,  $T_S=70^\circ\text{F}$ , and  $T_C=100^\circ\text{F}$  for a mortar intrusion of 0 in and a CTE of  $6.5 \times 10^{-6}/^\circ\text{F}$ .

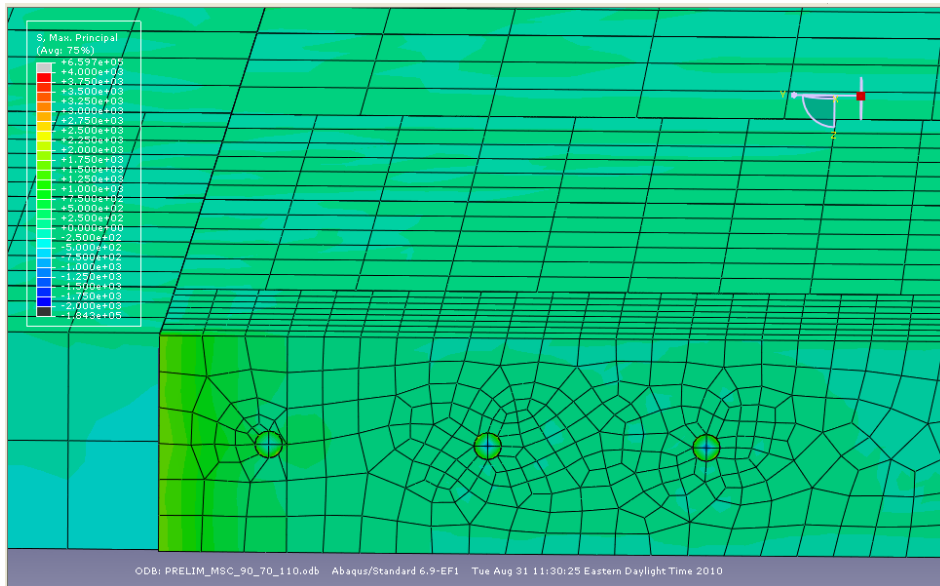


**Figure A63.** Longitudinal shear cracking model in which  $T_M=90^\circ\text{F}$ ,  $T_S=70^\circ\text{F}$ , and  $T_C=110^\circ\text{F}$  for a mortar intrusion of 0 in and a CTE of  $6.5 \times 10^{-6}/^\circ\text{F}$ .

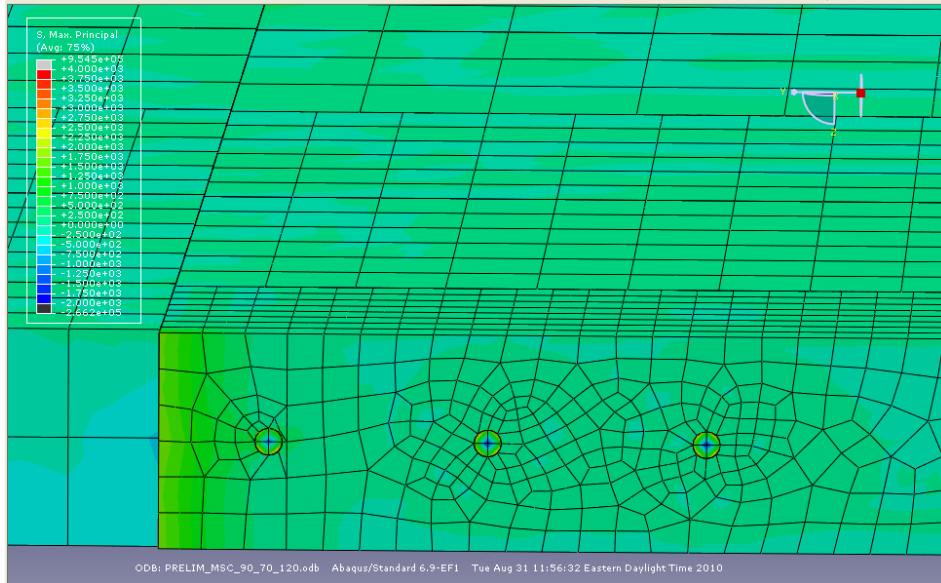


**Figure A64.** Longitudinal shear cracking model in which  $T_M=90^\circ\text{F}$ ,  $T_S=70^\circ\text{F}$ , and  $T_C=120^\circ\text{F}$  for a mortar intrusion of 0 in and a CTE of  $6.5 \times 10^{-6}/^\circ\text{F}$ .

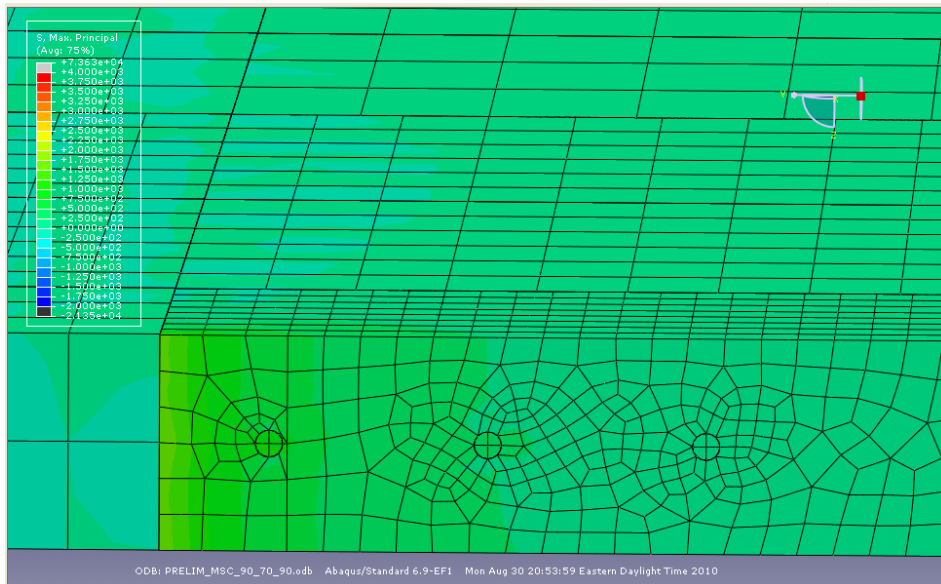


**Figure A65.** Longitudinal shear cracking model in which  $T_M=90^\circ\text{F}$ ,  $T_S=70^\circ\text{F}$ , and  $T_C=90^\circ\text{F}$  for a mortar intrusion of 0 in and a CTE of  $6.5 \times 10^{-6}/^\circ\text{F}$ .

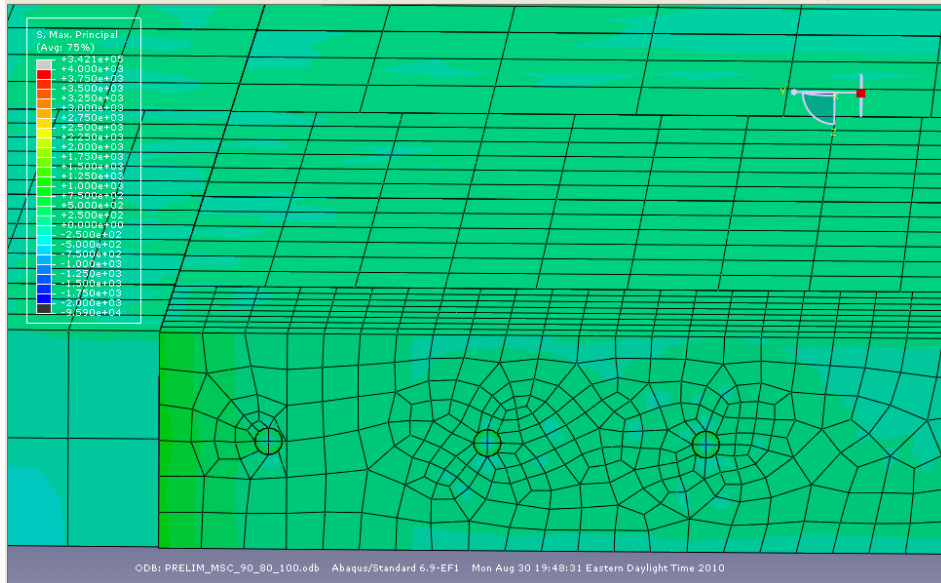


**Figure A66.** Longitudinal shear cracking model in which  $T_M=90^\circ\text{F}$ ,  $T_S=80^\circ\text{F}$ , and  $T_C=100^\circ\text{F}$  for a mortar intrusion of 0 in and a CTE of  $6.5 \times 10^{-6}/^\circ\text{F}$ .

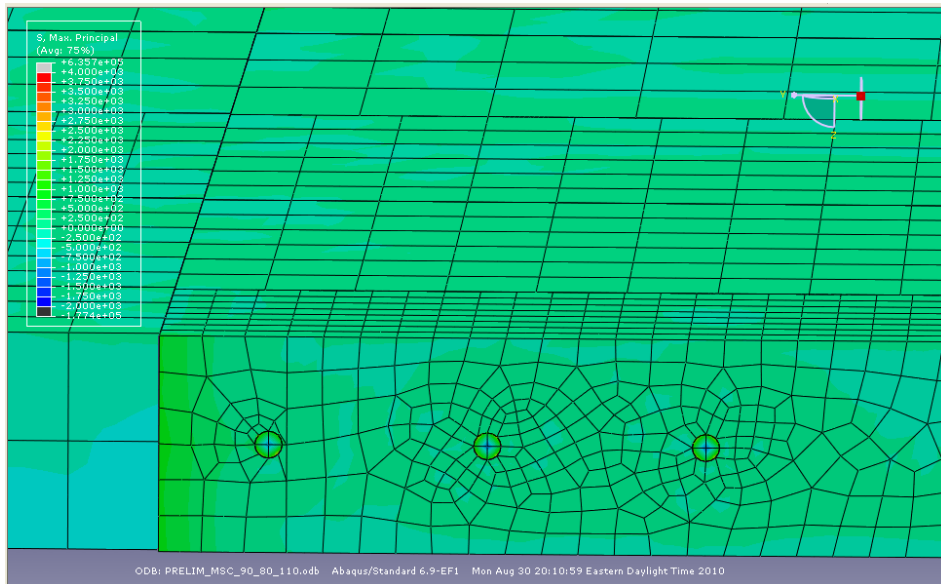


**Figure A67.** Longitudinal shear cracking model in which  $T_M=90^\circ\text{F}$ ,  $T_S=80^\circ\text{F}$ , and  $T_C=110^\circ\text{F}$  for a mortar intrusion of 0 in and a CTE of  $6.5 \times 10^{-6}/^\circ\text{F}$ .

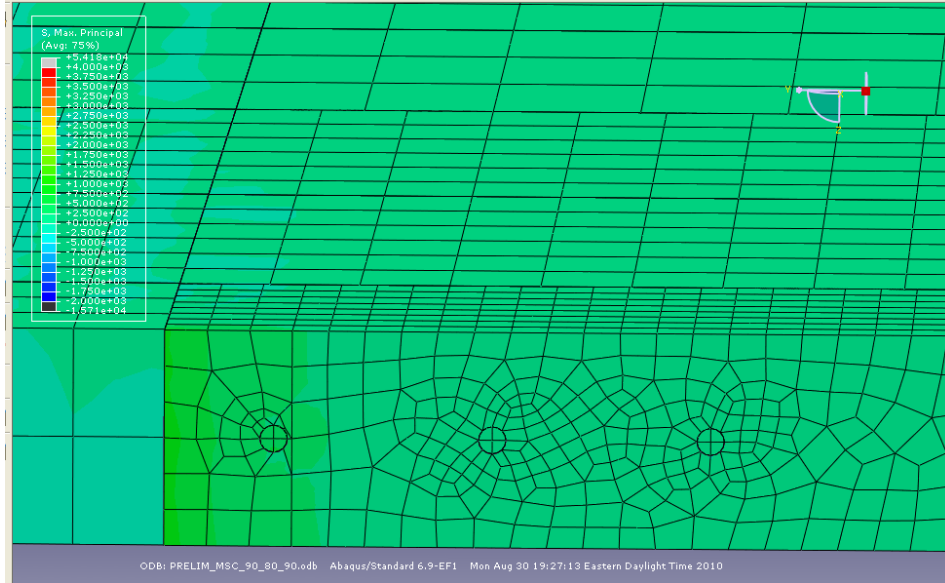


**Figure A68.** Longitudinal shear cracking model in which  $T_M=90^\circ\text{F}$ ,  $T_S=80^\circ\text{F}$ , and  $T_C=90^\circ\text{F}$  for a mortar intrusion of 0 in and a CTE of  $6.5 \times 10^{-6}/^\circ\text{F}$ .

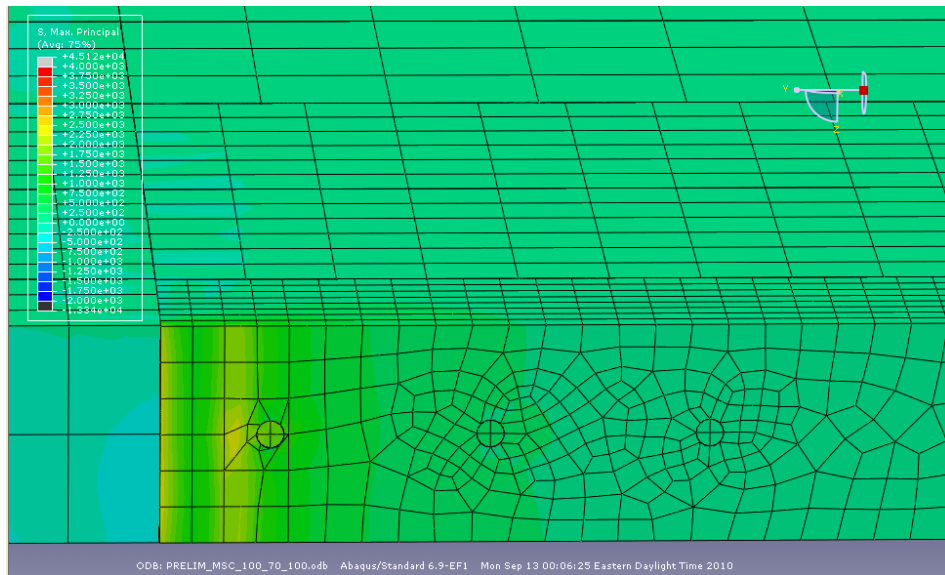


**Figure A69.** Longitudinal shear cracking model in which  $T_M=100^\circ\text{F}$ ,  $T_S=70^\circ\text{F}$ , and  $T_C=100^\circ\text{F}$  for a mortar intrusion of 3.5 in and a CTE of  $4 \times 10^{-6}/^\circ\text{F}$ .

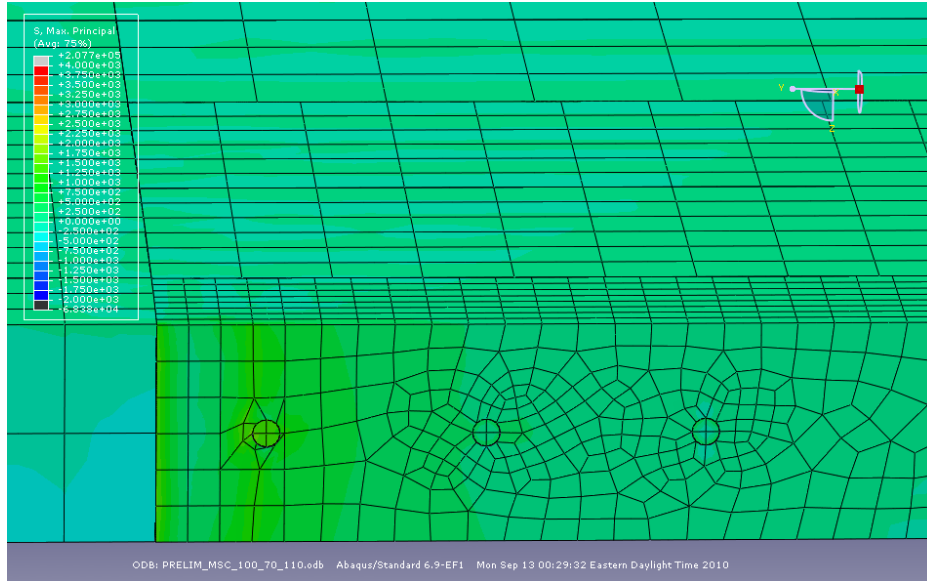


**Figure A70.** Longitudinal shear cracking model in which  $T_M=100^\circ\text{F}$ ,  $T_S=70^\circ\text{F}$ , and  $T_C=100^\circ\text{F}$  for a mortar intrusion of 3.5 in and a CTE of  $4 \times 10^{-6}/^\circ\text{F}$ .

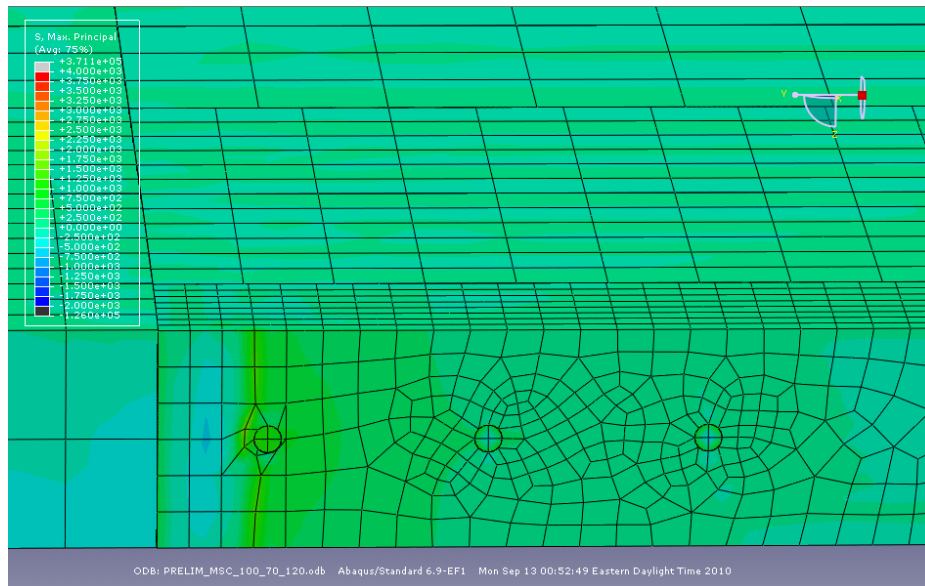


**Figure A71.** Longitudinal shear cracking model in which  $T_M=100^\circ\text{F}$ ,  $T_S=70^\circ\text{F}$ , and  $T_C=120^\circ\text{F}$  for a mortar intrusion of 3.5 in and a CTE of  $4 \times 10^{-6}/^\circ\text{F}$ .

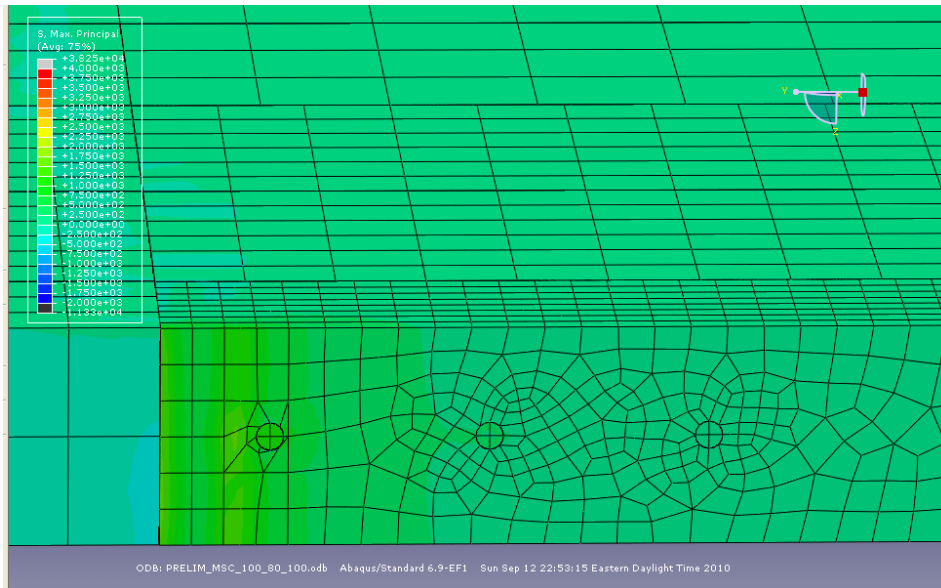


**Figure A72.** Longitudinal shear cracking model in which  $T_M=100^\circ\text{F}$ ,  $T_S=80^\circ\text{F}$ , and  $T_C=100^\circ\text{F}$  for a mortar intrusion of 3.5 in and a CTE of  $4 \times 10^{-6}/^\circ\text{F}$ .

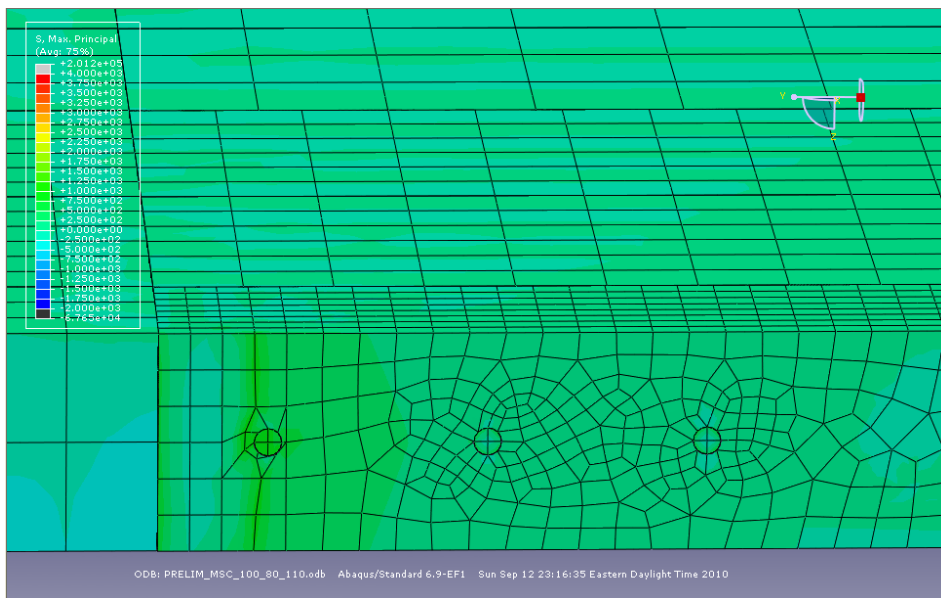


**Figure A73.** Longitudinal shear cracking model in which  $T_M=100^\circ\text{F}$ ,  $T_S=80^\circ\text{F}$ , and  $T_C=120^\circ\text{F}$  for a mortar intrusion of 3.5 in and a CTE of  $4 \times 10^{-6}/^\circ\text{F}$ .

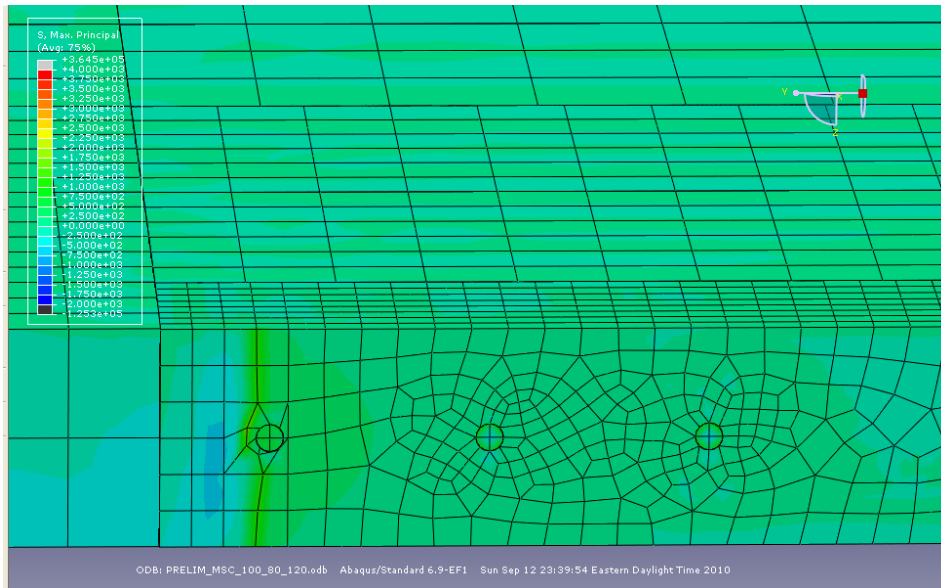


**Figure A74.** Longitudinal shear cracking model in which  $T_M=100^\circ\text{F}$ ,  $T_S=80^\circ\text{F}$ , and  $T_C=120^\circ\text{F}$  for a mortar intrusion of 3.5 in and a CTE of  $4 \times 10^{-6}/^\circ\text{F}$ .

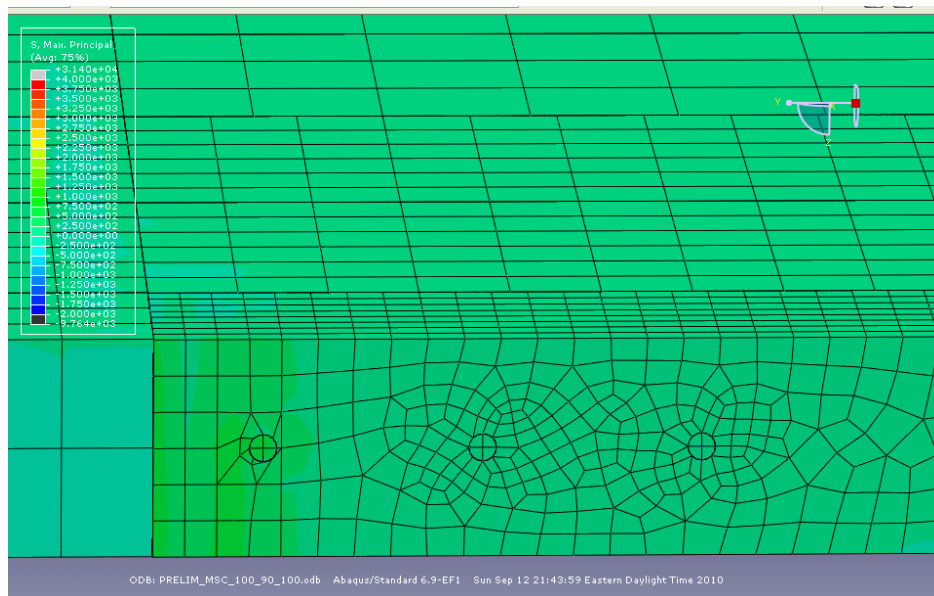


**Figure A75.** Longitudinal shear cracking model in which  $T_M=100^\circ\text{F}$ ,  $T_S=90^\circ\text{F}$ , and  $T_C=100^\circ\text{F}$  for a mortar intrusion of 3.5 in and a CTE of  $4 \times 10^{-6}/^\circ\text{F}$ .

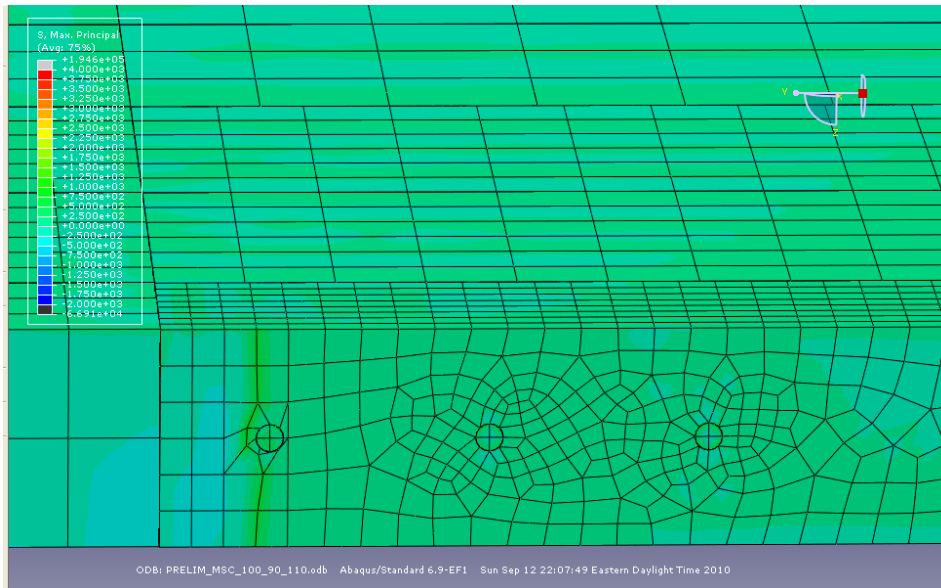


**Figure A76.** Longitudinal shear cracking model in which  $T_M=100^\circ\text{F}$ ,  $T_S=90^\circ\text{F}$ , and  $T_C=110^\circ\text{F}$  for a mortar intrusion of 3.5 in and a CTE of  $4 \times 10^{-6}/^\circ\text{F}$ .

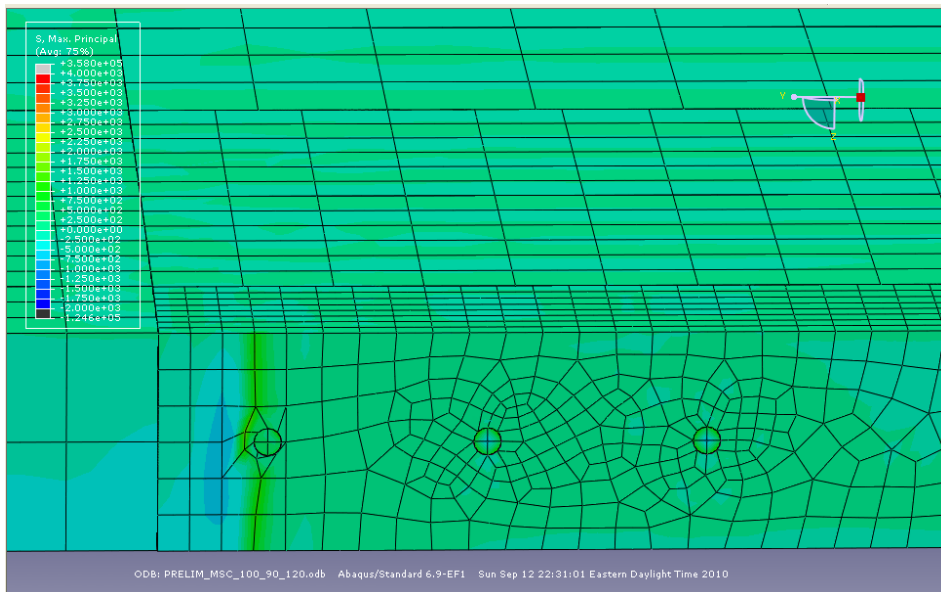


**Figure A77.** Longitudinal shear cracking model in which  $T_M=100^\circ\text{F}$ ,  $T_S=90^\circ\text{F}$ , and  $T_C=120^\circ\text{F}$  for a mortar intrusion of 3.5 in and a CTE of  $4 \times 10^{-6}/^\circ\text{F}$ .

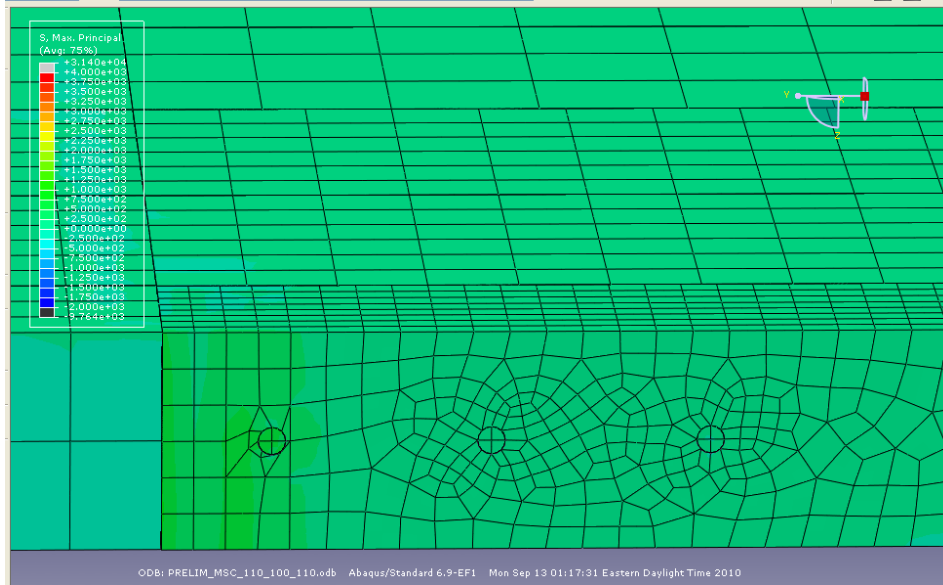


**Figure A78.** Longitudinal shear cracking model in which  $T_M=110^\circ\text{F}$ ,  $T_S=100^\circ\text{F}$ , and  $T_C=110^\circ\text{F}$  for a mortar intrusion of 3.5 in and a CTE of  $4 \times 10^{-6}/^\circ\text{F}$ .

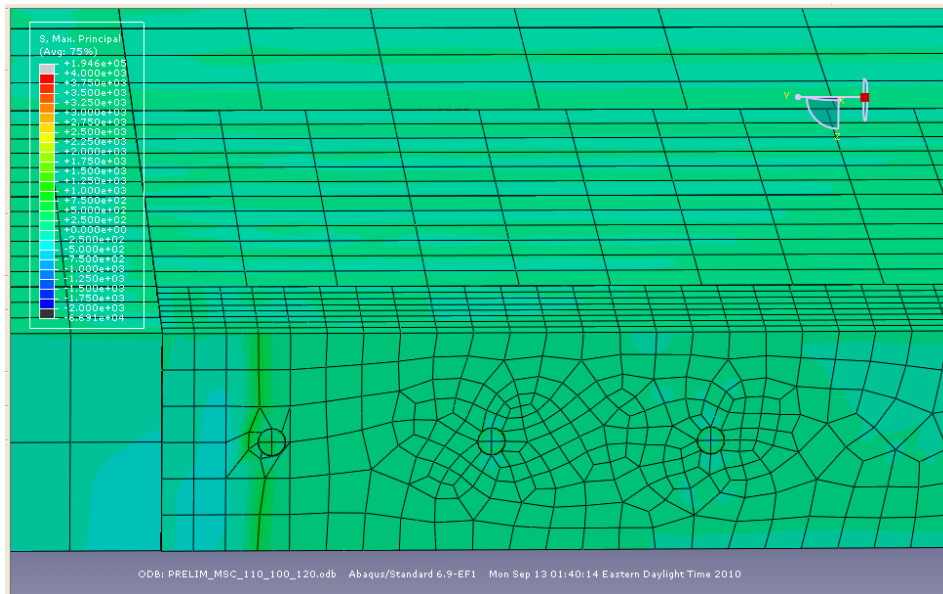


**Figure A79.** Longitudinal shear cracking model in which  $T_M=110^\circ\text{F}$ ,  $T_S=100^\circ\text{F}$ , and  $T_C=120^\circ\text{F}$  for a mortar intrusion of 3.5 in and a CTE of  $4 \times 10^{-6}/^\circ\text{F}$ .

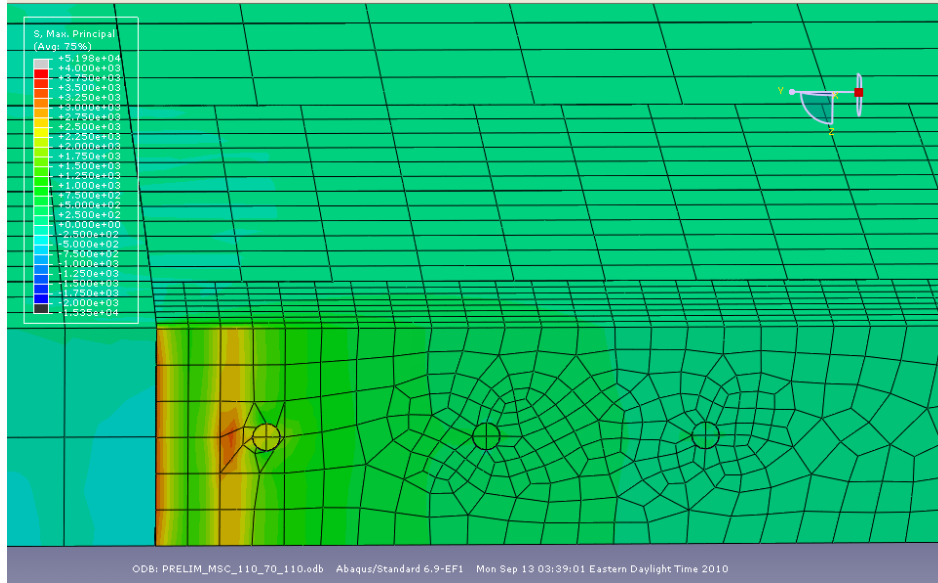


**Figure A80.** Longitudinal shear cracking model in which  $T_M=110^\circ\text{F}$ ,  $T_S=70^\circ\text{F}$ , and  $T_C=110^\circ\text{F}$  for a mortar intrusion of 3.5 in and a CTE of  $4 \times 10^{-6}/^\circ\text{F}$ .

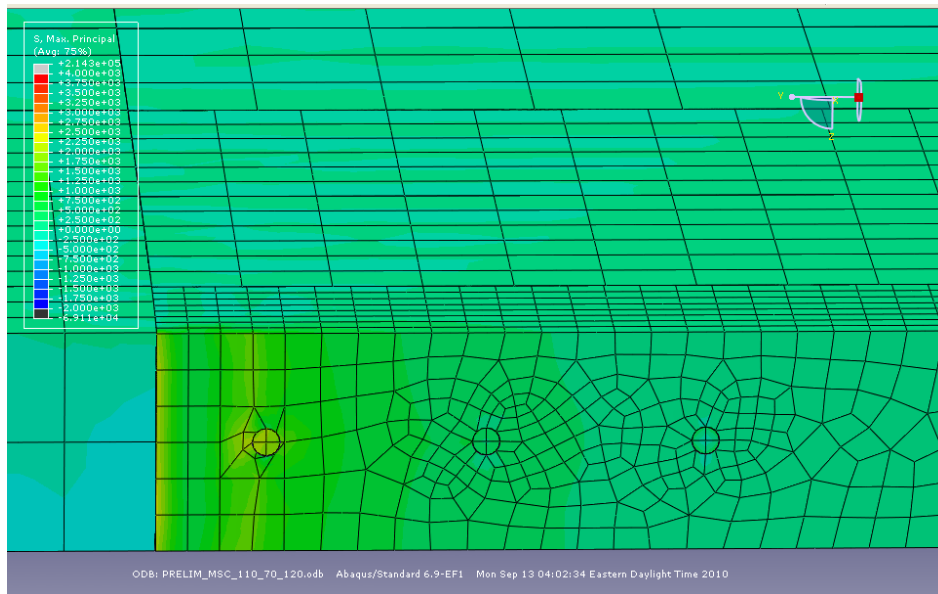


**Figure A81.** Longitudinal shear cracking model in which  $T_M=110^\circ\text{F}$ ,  $T_S=70^\circ\text{F}$ , and  $T_C=120^\circ\text{F}$  for a mortar intrusion of 3.5 in and a CTE of  $4 \times 10^{-6}/^\circ\text{F}$ .

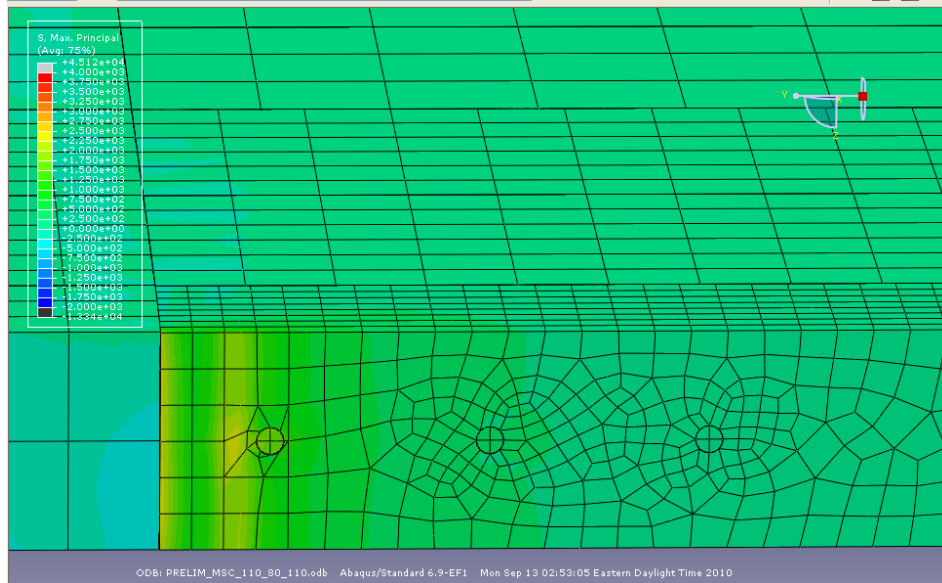


**Figure A82.** Longitudinal shear cracking model in which  $T_M=110^\circ\text{F}$ ,  $T_S=80^\circ\text{F}$ , and  $T_C=110^\circ\text{F}$  for a mortar intrusion of 3.5 in and a CTE of  $4 \times 10^{-6}/^\circ\text{F}$ .

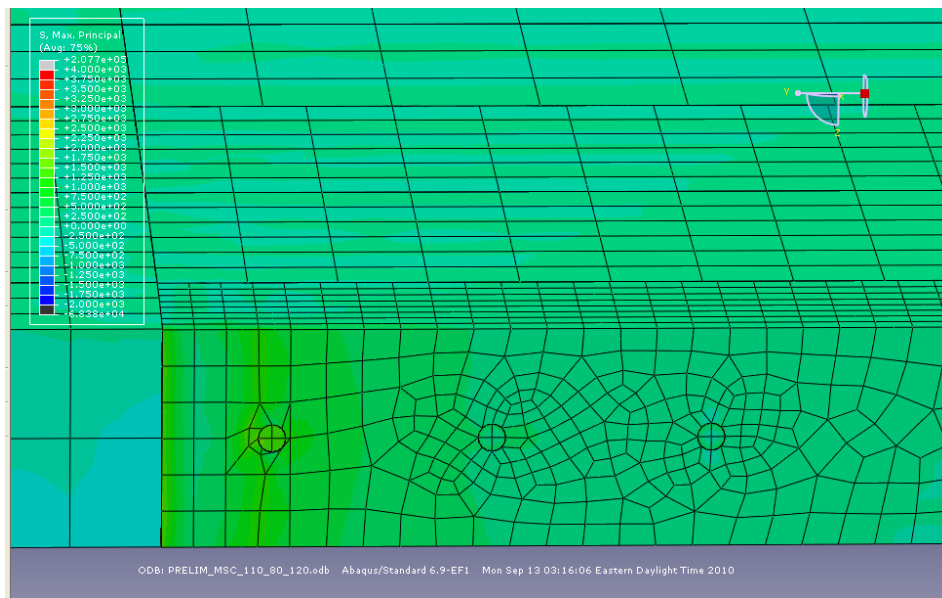


**Figure A83.** Longitudinal shear cracking model in which  $T_M=110^\circ\text{F}$ ,  $T_S=80^\circ\text{F}$ , and  $T_C=120^\circ\text{F}$  for a mortar intrusion of 3.5 in and a CTE of  $4 \times 10^{-6}/^\circ\text{F}$ .

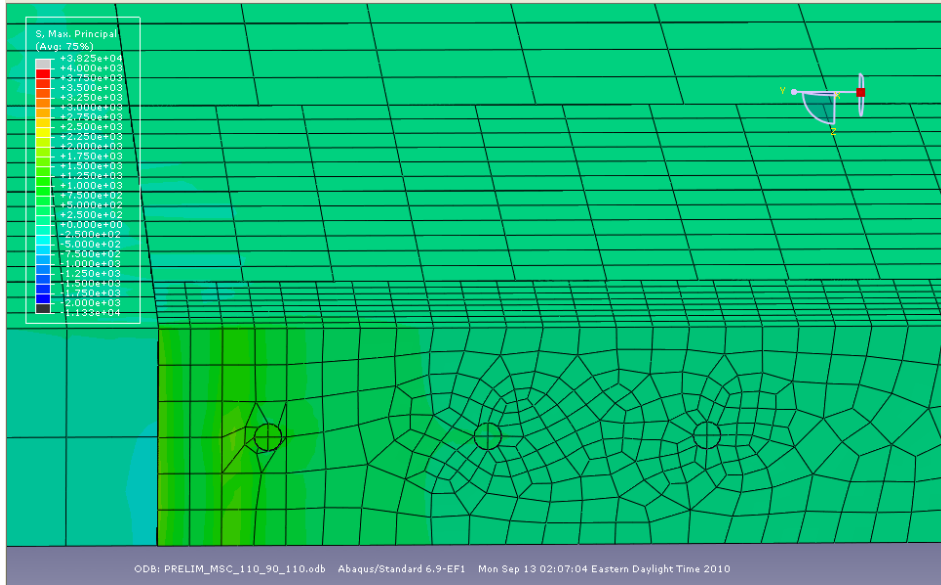


**Figure A84.** Longitudinal shear cracking model in which  $T_M=110^\circ\text{F}$ ,  $T_S=90^\circ\text{F}$ , and  $T_C=110^\circ\text{F}$  for a mortar intrusion of 3.5 in and a CTE of  $4 \times 10^{-6}/^\circ\text{F}$ .

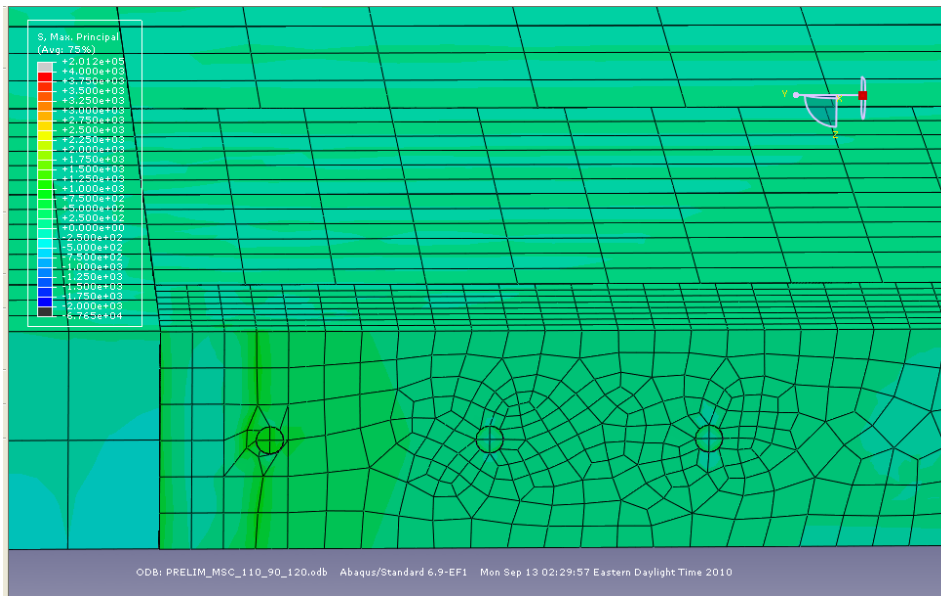


**Figure A85.** Longitudinal shear cracking model in which  $T_M=110^\circ\text{F}$ ,  $T_S=90^\circ\text{F}$ , and  $T_C=120^\circ\text{F}$  for a mortar intrusion of 3.5 in and a CTE of  $4 \times 10^{-6}/^\circ\text{F}$ .

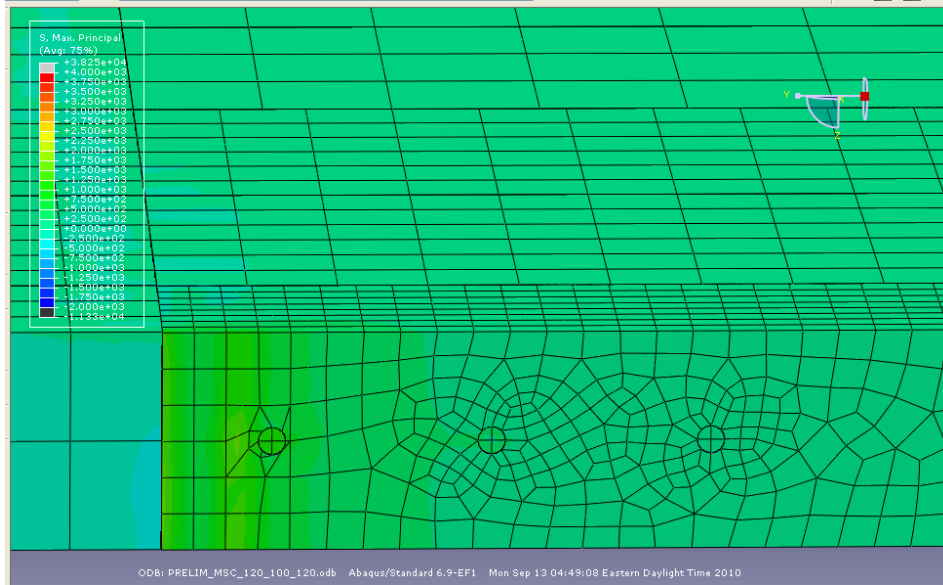


**Figure A86.** Longitudinal shear cracking model in which  $T_M=120^\circ\text{F}$ ,  $T_S=100^\circ\text{F}$ , and  $T_C=120^\circ\text{F}$  for a mortar intrusion of 3.5 in and a CTE of  $4 \times 10^{-6}/^\circ\text{F}$ .

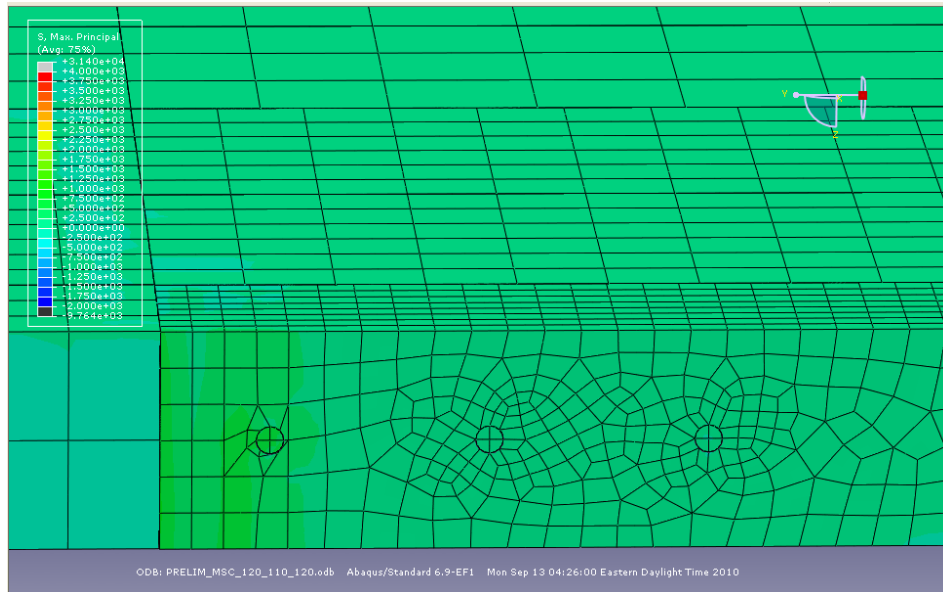


**Figure A87.** Longitudinal shear cracking model in which  $T_M=120^\circ\text{F}$ ,  $T_S=110^\circ\text{F}$ , and  $T_C=120^\circ\text{F}$  for a mortar intrusion of 3.5 in and a CTE of  $4 \times 10^{-6}/^\circ\text{F}$ .

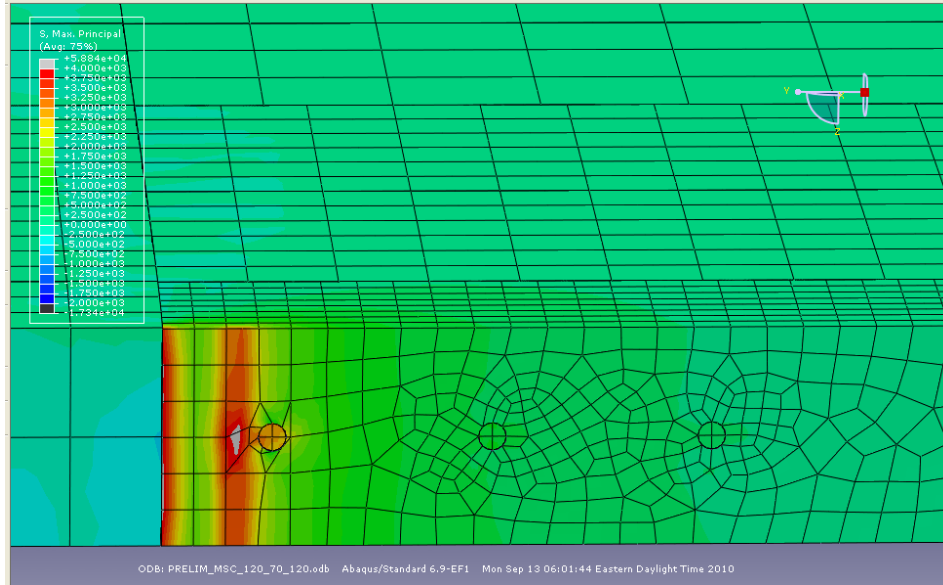


**Figure A88.** Longitudinal shear cracking model in which  $T_M=120^\circ\text{F}$ ,  $T_S=70^\circ\text{F}$ , and  $T_C=120^\circ\text{F}$  for a mortar intrusion of 3.5 in and a CTE of  $4 \times 10^{-6}/^\circ\text{F}$ .

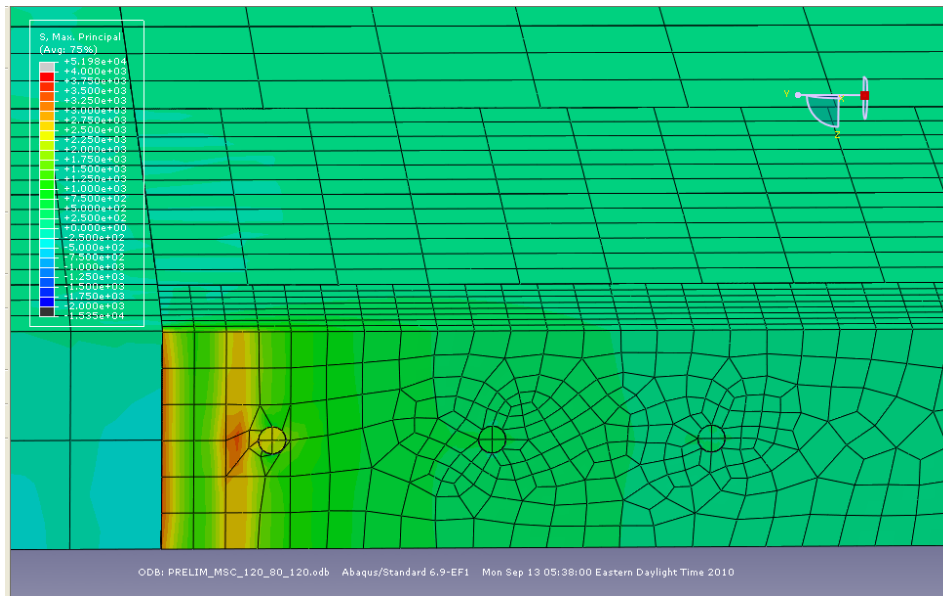


**Figure A89.** Longitudinal shear cracking model in which  $T_M=120^\circ\text{F}$ ,  $T_S=80^\circ\text{F}$ , and  $T_C=120^\circ\text{F}$  for a mortar intrusion of 3.5 in and a CTE of  $4 \times 10^{-6}/^\circ\text{F}$ .

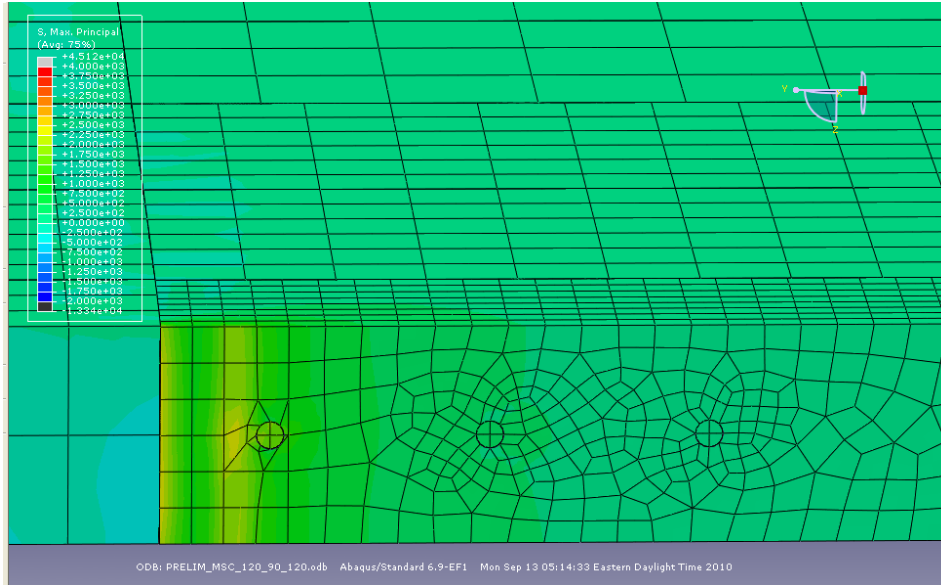


**Figure A90.** Longitudinal shear cracking model in which  $T_M=120^\circ\text{F}$ ,  $T_S=90^\circ\text{F}$ , and  $T_C=120^\circ\text{F}$  for a mortar intrusion of 3.5 in and a CTE of  $4 \times 10^{-6}/^\circ\text{F}$ .

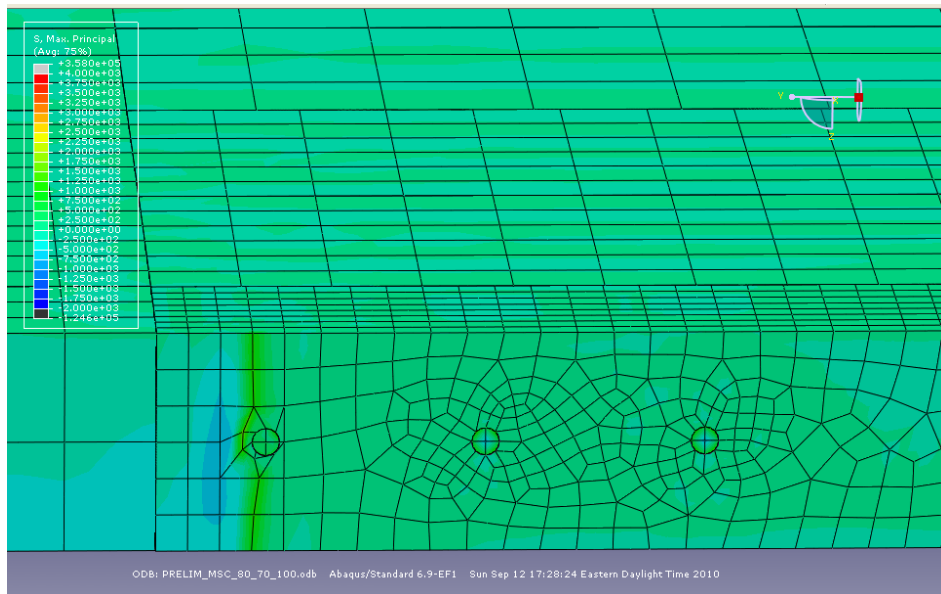


**Figure A91.** Longitudinal shear cracking model in which  $T_M=80^\circ\text{F}$ ,  $T_S=70^\circ\text{F}$ , and  $T_C=100^\circ\text{F}$  for a mortar intrusion of 3.5 in and a CTE of  $4 \times 10^{-6}/^\circ\text{F}$ .

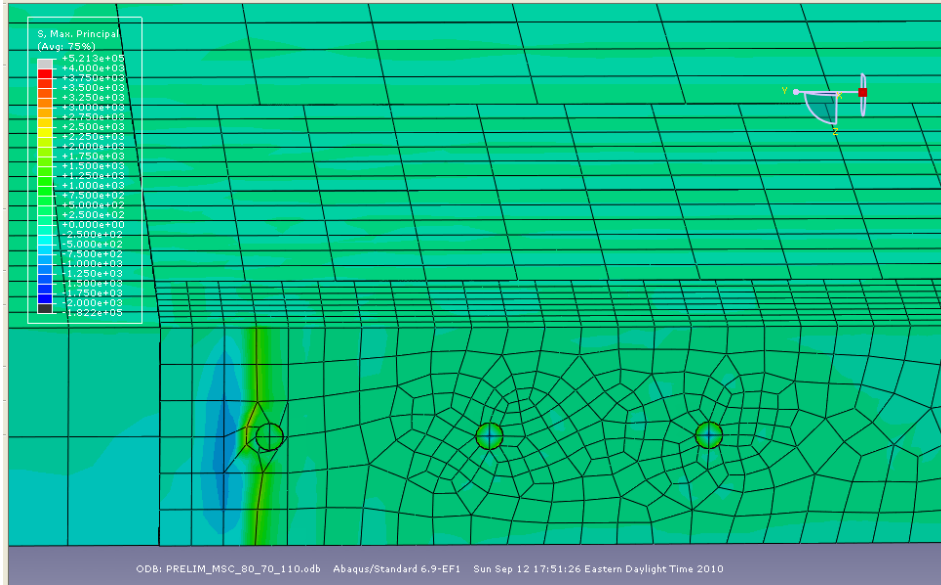


**Figure A92.** Longitudinal shear cracking model in which  $T_M=80^\circ\text{F}$ ,  $T_S=70^\circ\text{F}$ , and  $T_C=110^\circ\text{F}$  for a mortar intrusion of 3.5 in and a CTE of  $4 \times 10^{-6}/^\circ\text{F}$ .

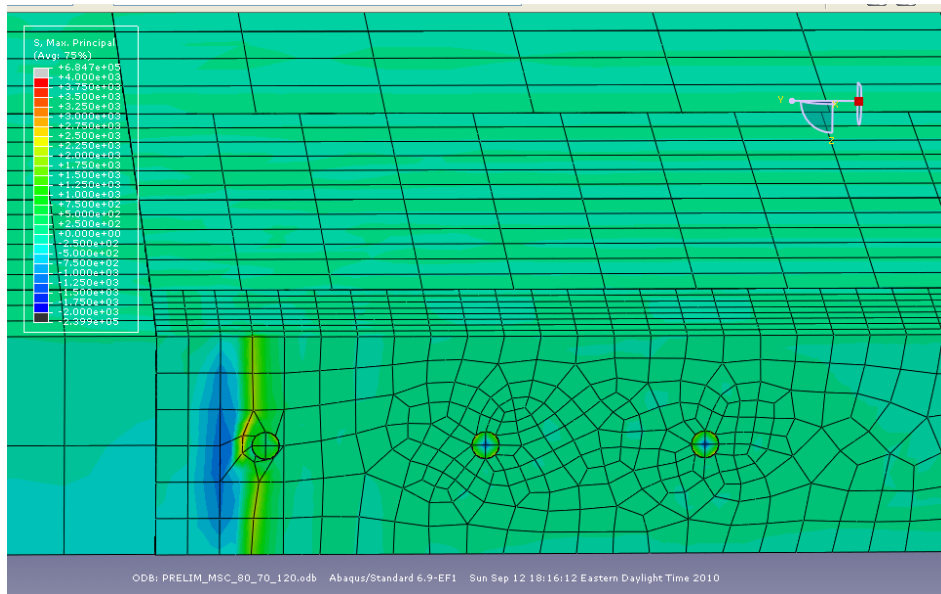


**Figure A93.** Longitudinal shear cracking model in which  $T_M=80^\circ\text{F}$ ,  $T_S=70^\circ\text{F}$ , and  $T_C=120^\circ\text{F}$  for a mortar intrusion of 3.5 in and a CTE of  $4 \times 10^{-6}/^\circ\text{F}$ .

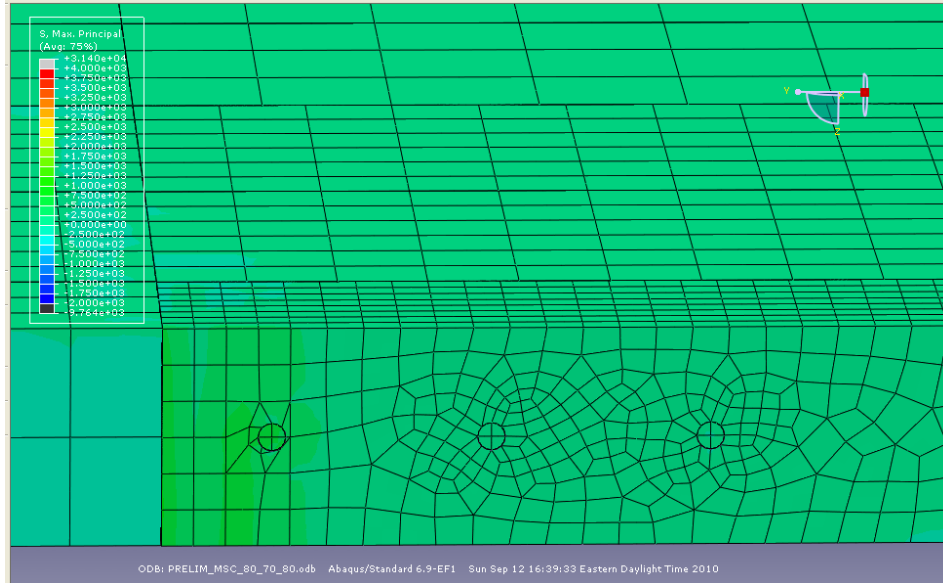


**Figure A94.** Longitudinal shear cracking model in which  $T_M=80^\circ\text{F}$ ,  $T_S=70^\circ\text{F}$ , and  $T_C=80^\circ\text{F}$  for a mortar intrusion of 3.5 in and a CTE of  $4 \times 10^{-6}/^\circ\text{F}$ .

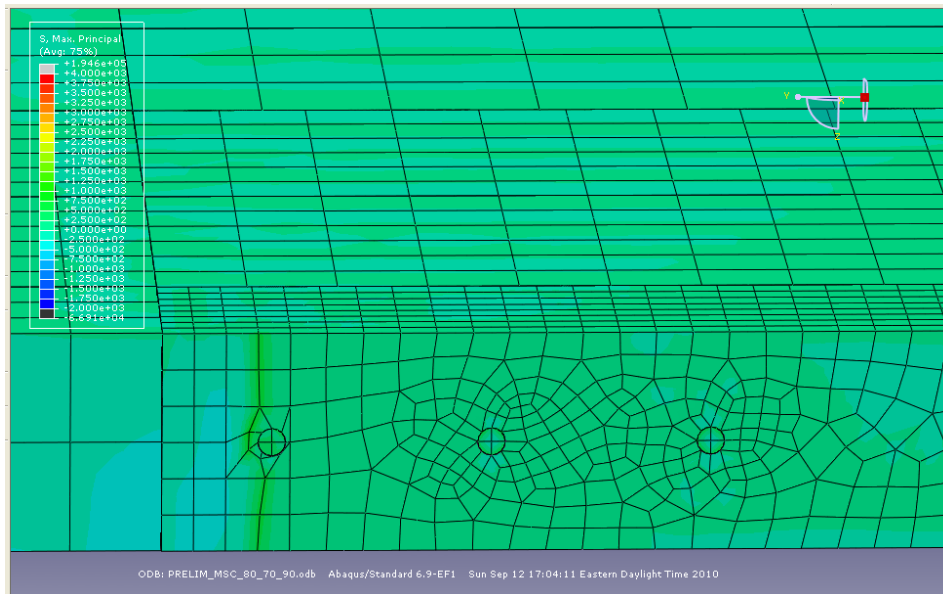


**Figure A95.** Longitudinal shear cracking model in which  $T_M=80^\circ\text{F}$ ,  $T_S=70^\circ\text{F}$ , and  $T_C=90^\circ\text{F}$  for a mortar intrusion of 3.5 in and a CTE of  $4 \times 10^{-6}/^\circ\text{F}$ .

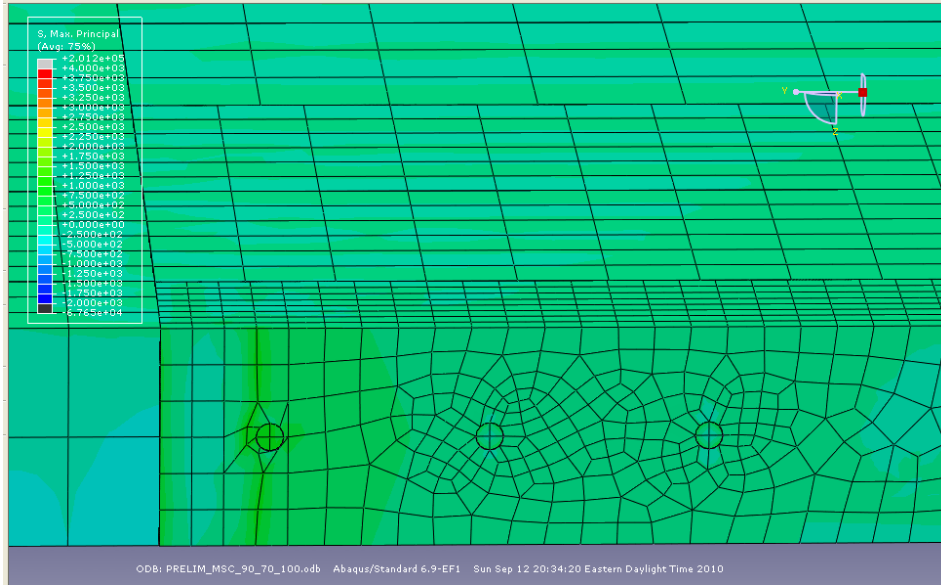


**Figure A96.** Longitudinal shear cracking model in which  $T_M=90^\circ\text{F}$ ,  $T_S=70^\circ\text{F}$ , and  $T_C=100^\circ\text{F}$  for a mortar intrusion of 3.5 in and a CTE of  $4 \times 10^{-6}/^\circ\text{F}$ .

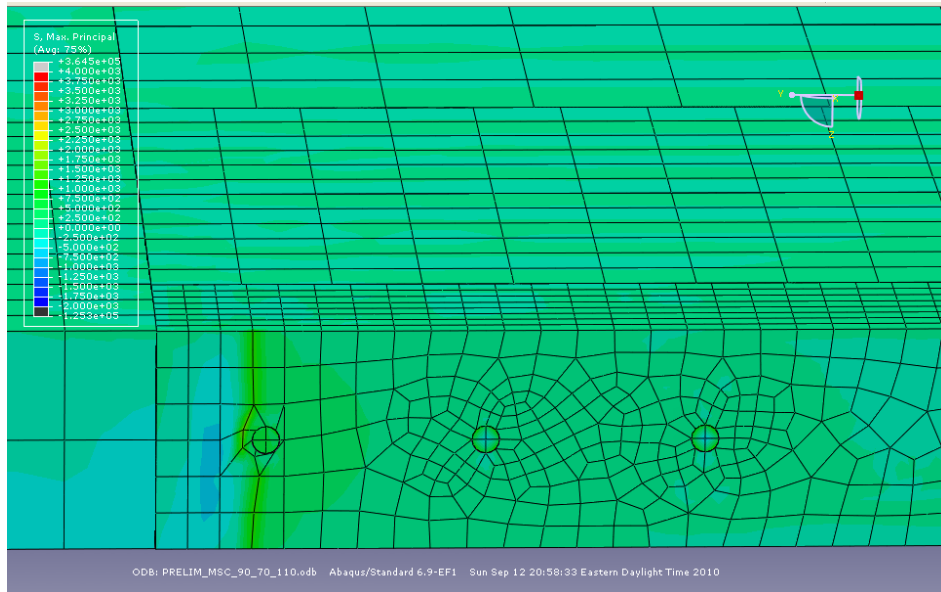


**Figure A97.** Longitudinal shear cracking model in which  $T_M=90^\circ\text{F}$ ,  $T_S=70^\circ\text{F}$ , and  $T_C=110^\circ\text{F}$  for a mortar intrusion of 3.5 in and a CTE of  $4 \times 10^{-6}/^\circ\text{F}$ .

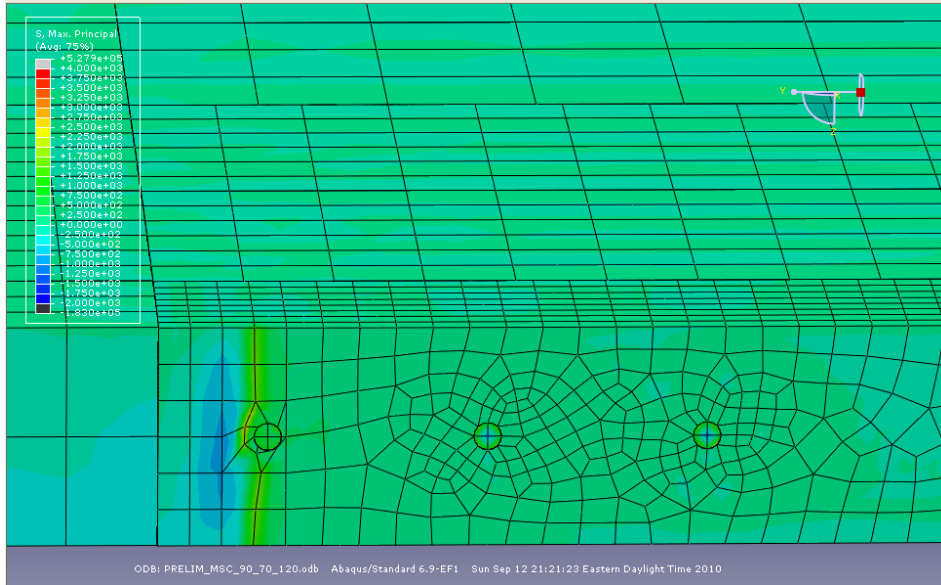


**Figure A98.** Longitudinal shear cracking model in which  $T_M=90^\circ\text{F}$ ,  $T_S=70^\circ\text{F}$ , and  $T_C=120^\circ\text{F}$  for a mortar intrusion of 3.5 in and a CTE of  $4 \times 10^{-6}/^\circ\text{F}$ .

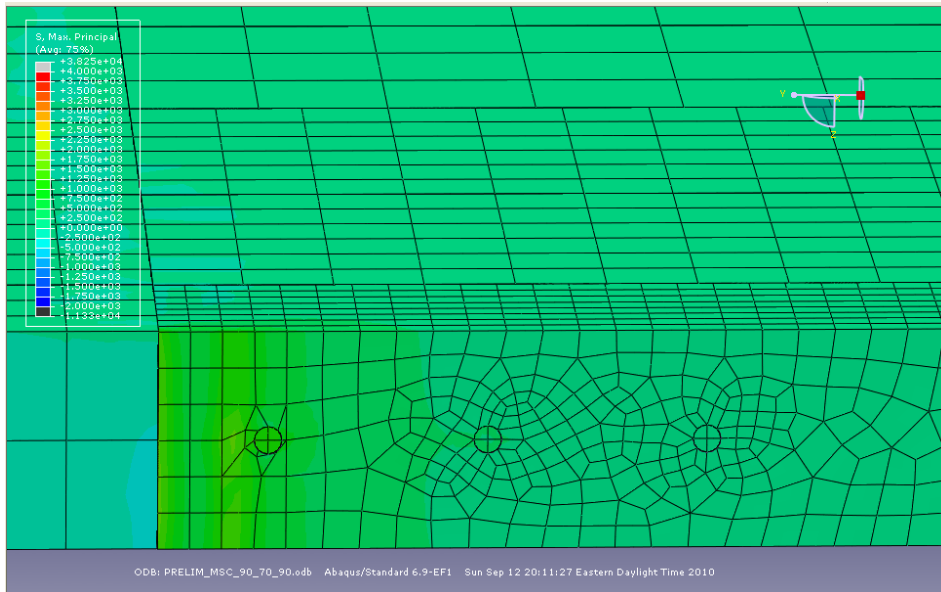


**Figure A99.** Longitudinal shear cracking model in which  $T_M=90^\circ\text{F}$ ,  $T_S=70^\circ\text{F}$ , and  $T_C=90^\circ\text{F}$  for a mortar intrusion of 3.5 in and a CTE of  $4 \times 10^{-6}/^\circ\text{F}$ .

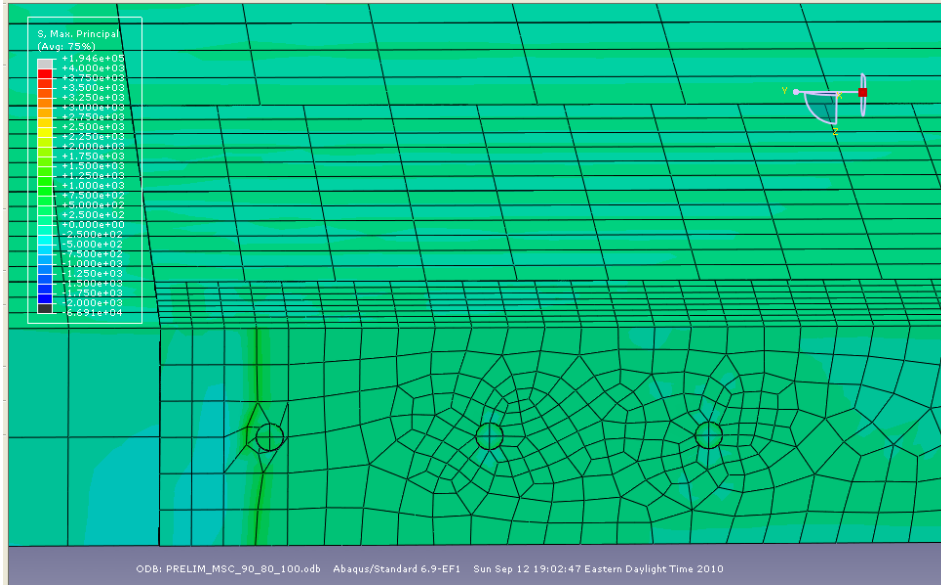


**Figure A100.** Longitudinal shear cracking model in which  $T_M=90^\circ\text{F}$ ,  $T_S=80^\circ\text{F}$ , and  $T_C=100^\circ\text{F}$  for a mortar intrusion of 3.5 in and a CTE of  $4 \times 10^{-6}/^\circ\text{F}$ .

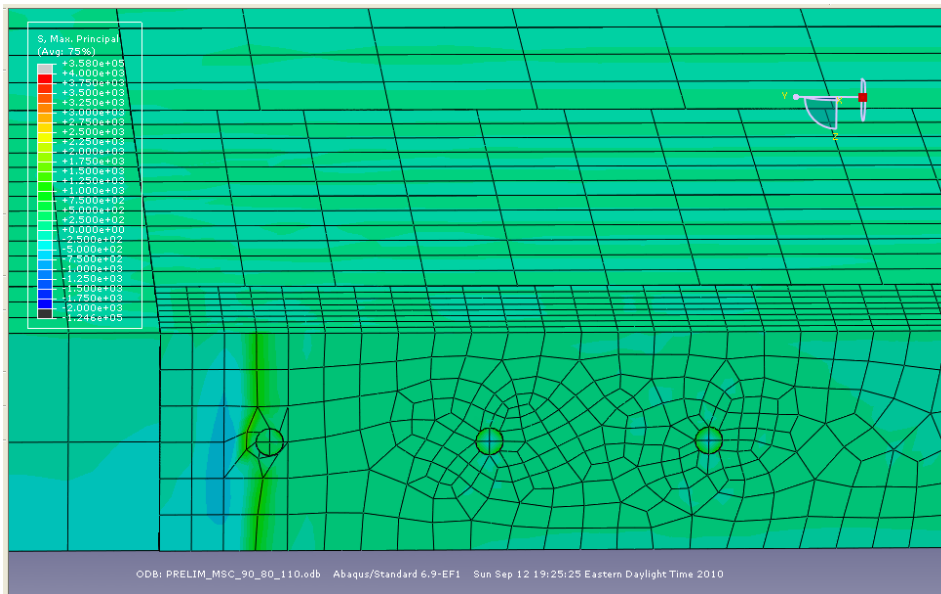


**Figure A101.** Longitudinal shear cracking model in which  $T_M=90^\circ\text{F}$ ,  $T_S=80^\circ\text{F}$ , and  $T_C=110^\circ\text{F}$  for a mortar intrusion of 3.5 in and a CTE of  $4 \times 10^{-6}/^\circ\text{F}$ .

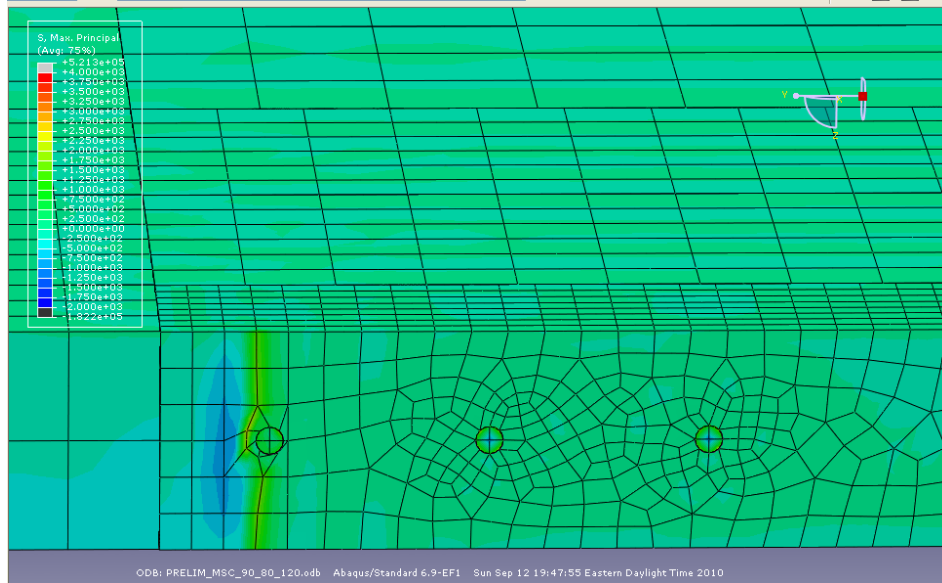


**Figure A102.** Longitudinal shear cracking model in which  $T_M=90^\circ\text{F}$ ,  $T_S=80^\circ\text{F}$ , and  $T_C=120^\circ\text{F}$  for a mortar intrusion of 3.5 in and a CTE of  $4 \times 10^{-6}/^\circ\text{F}$ .

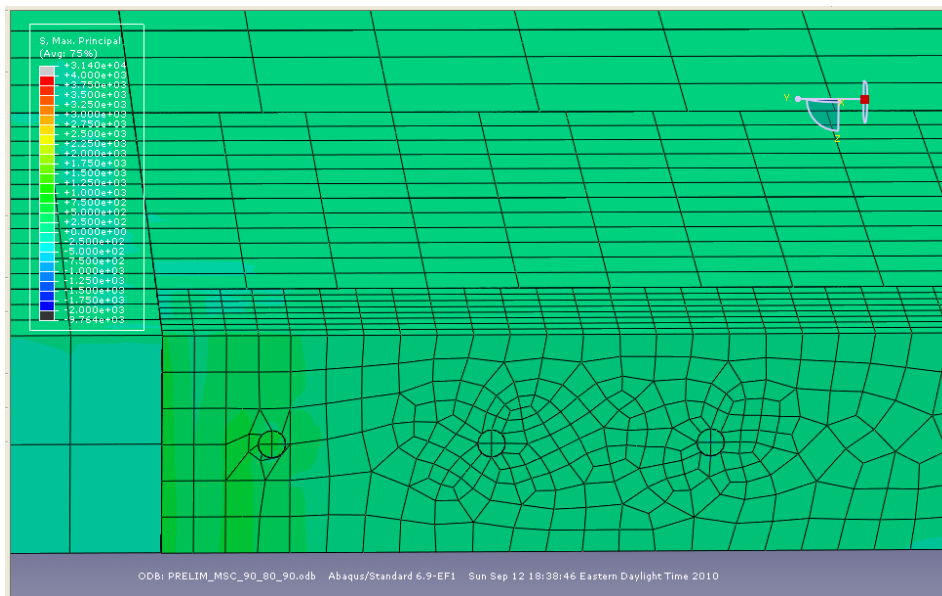


**Figure A103.** Longitudinal shear cracking model in which  $T_M=90^\circ\text{F}$ ,  $T_S=80^\circ\text{F}$ , and  $T_C=90^\circ\text{F}$  for a mortar intrusion of 3.5 in and a CTE of  $4 \times 10^{-6}/^\circ\text{F}$ .

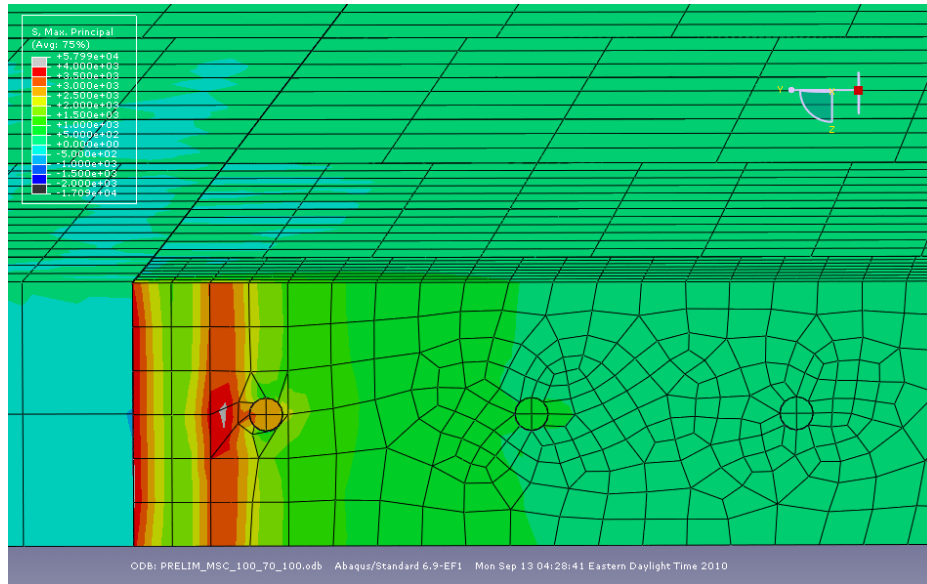


**Figure A104.** Longitudinal shear cracking model in which  $T_M=100^\circ\text{F}$ ,  $T_S=70^\circ\text{F}$ , and  $T_C=100^\circ\text{F}$  for a mortar intrusion of 3.5 in and a CTE of  $6.5 \times 10^{-6}/^\circ\text{F}$ .

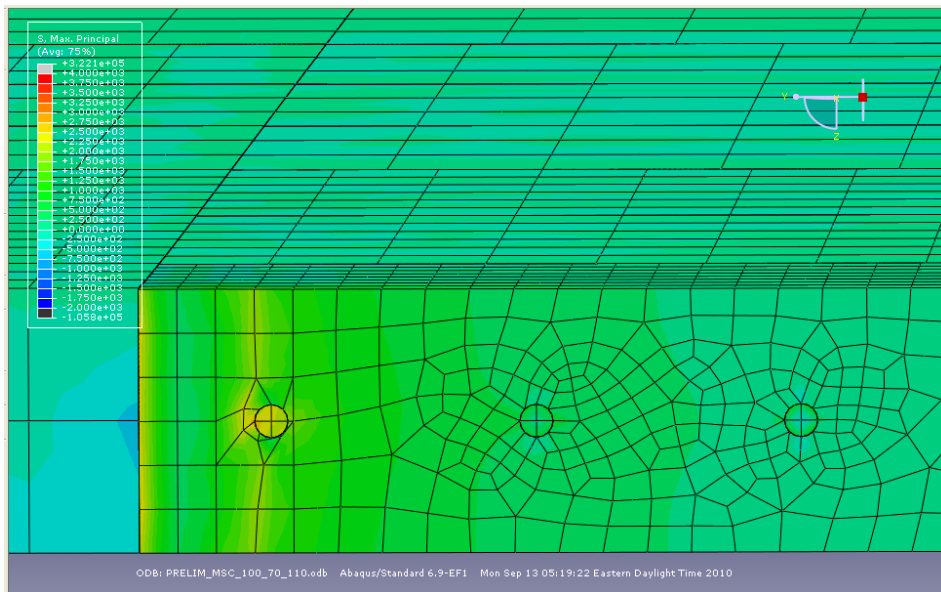


**Figure A105.** Longitudinal shear cracking model in which  $T_M=100^\circ\text{F}$ ,  $T_S=70^\circ\text{F}$ , and  $T_C=110^\circ\text{F}$  for a mortar intrusion of 3.5 in and a CTE of  $6.5 \times 10^{-6}/^\circ\text{F}$ .

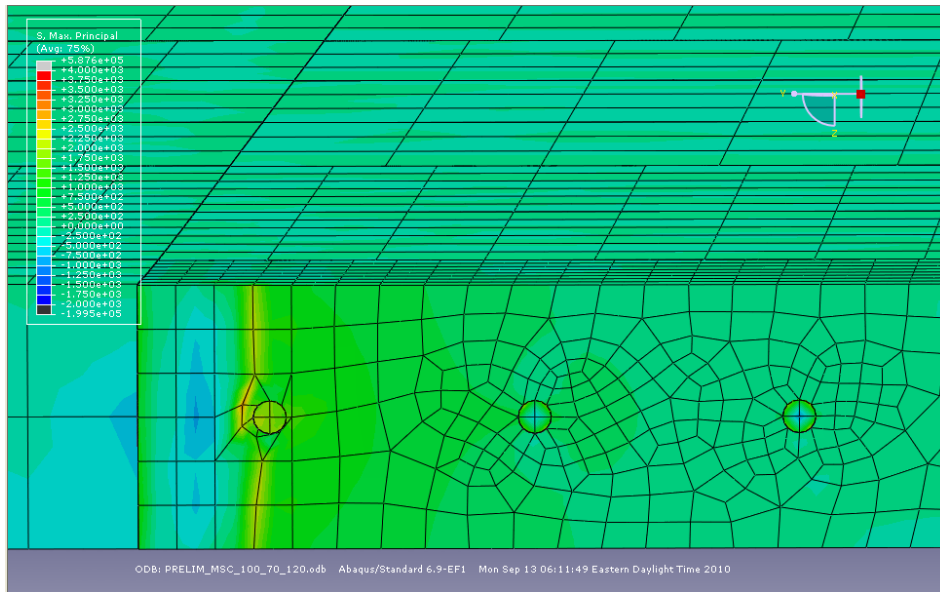


**Figure A106.** Longitudinal shear cracking model in which  $T_M=100^\circ\text{F}$ ,  $T_S=70^\circ\text{F}$ , and  $T_C=120^\circ\text{F}$  for a mortar intrusion of 3.5 in and a CTE of  $6.5 \times 10^{-6}/^\circ\text{F}$ .

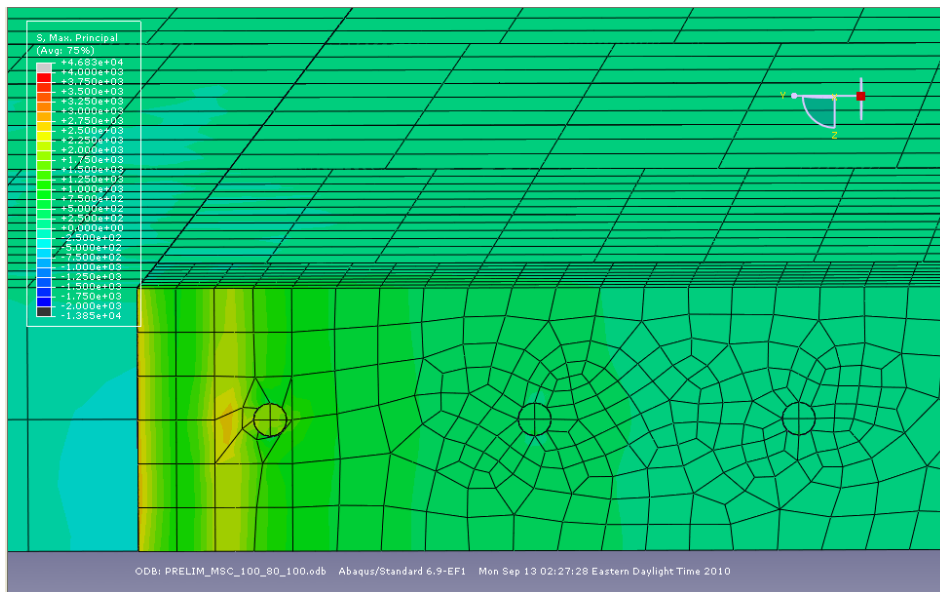


**Figure A107.** Longitudinal shear cracking model in which  $T_M=100^\circ\text{F}$ ,  $T_S=80^\circ\text{F}$ , and  $T_C=100^\circ\text{F}$  for a mortar intrusion of 3.5 in and a CTE of  $6.5 \times 10^{-6}/^\circ\text{F}$ .

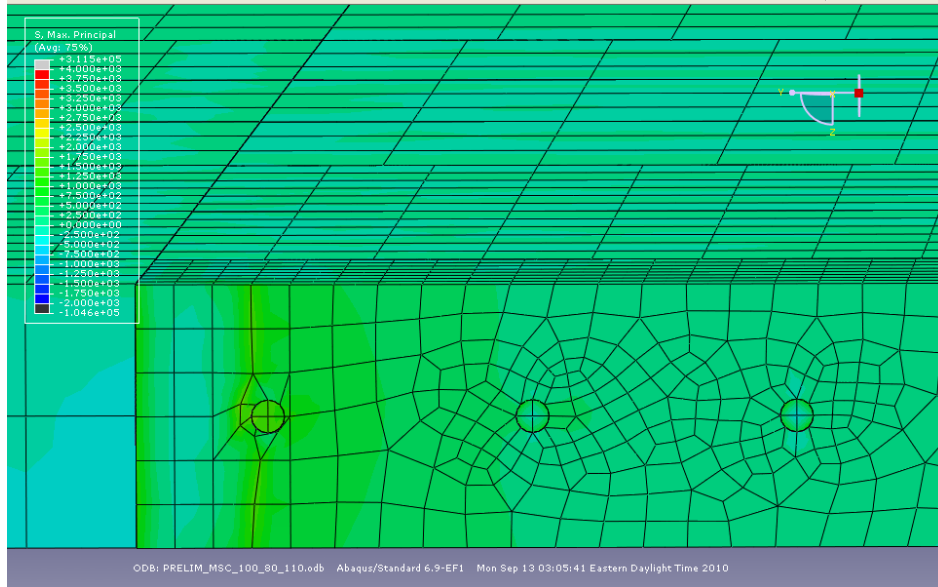


**Figure A108.** Longitudinal shear cracking model in which  $T_M=100^\circ\text{F}$ ,  $T_S=80^\circ\text{F}$ , and  $T_C=110^\circ\text{F}$  for a mortar intrusion of 3.5 in and a CTE of  $6.5 \times 10^{-6}/^\circ\text{F}$ .

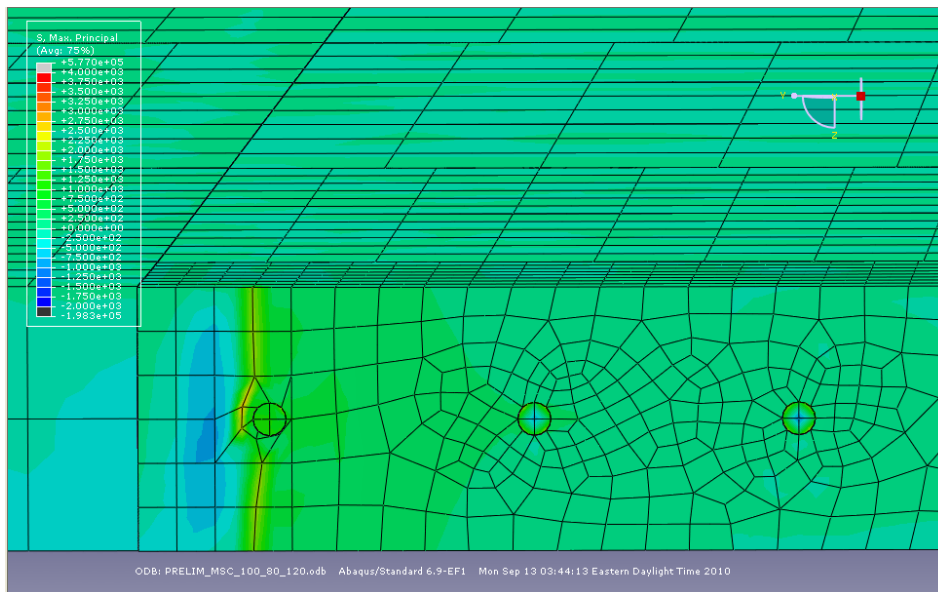


**Figure A109.** Longitudinal shear cracking model in which  $T_M=100^\circ\text{F}$ ,  $T_S=80^\circ\text{F}$ , and  $T_C=120^\circ\text{F}$  for a mortar intrusion of 3.5 in and a CTE of  $6.5 \times 10^{-6}/^\circ\text{F}$ .



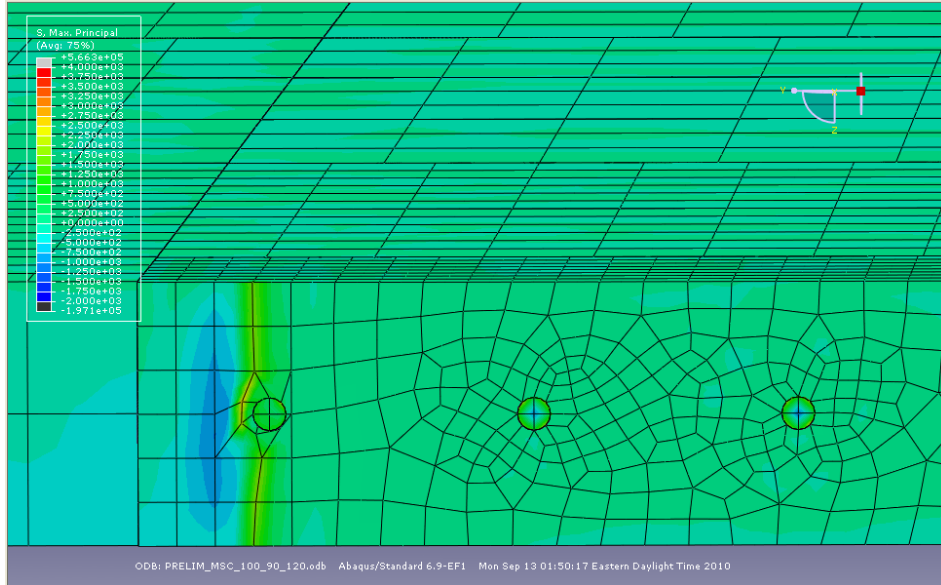


**Figure A112.** Longitudinal shear cracking model in which  $T_M=100^\circ\text{F}$ ,  $T_S=90^\circ\text{F}$ , and  $T_C=120^\circ\text{F}$  for a mortar intrusion of 3.5 in and a CTE of  $6.5 \times 10^{-6}/^\circ\text{F}$ .

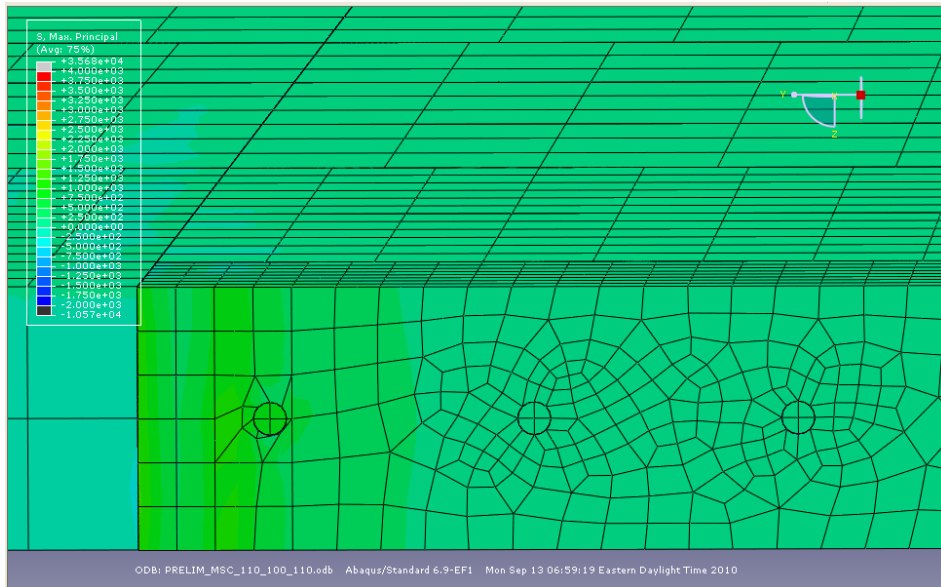


**Figure A113.** Longitudinal shear cracking model in which  $T_M=110^\circ\text{F}$ ,  $T_S=100^\circ\text{F}$ , and  $T_C=110^\circ\text{F}$  for a mortar intrusion of 3.5 in and a CTE of  $6.5 \times 10^{-6}/^\circ\text{F}$ .

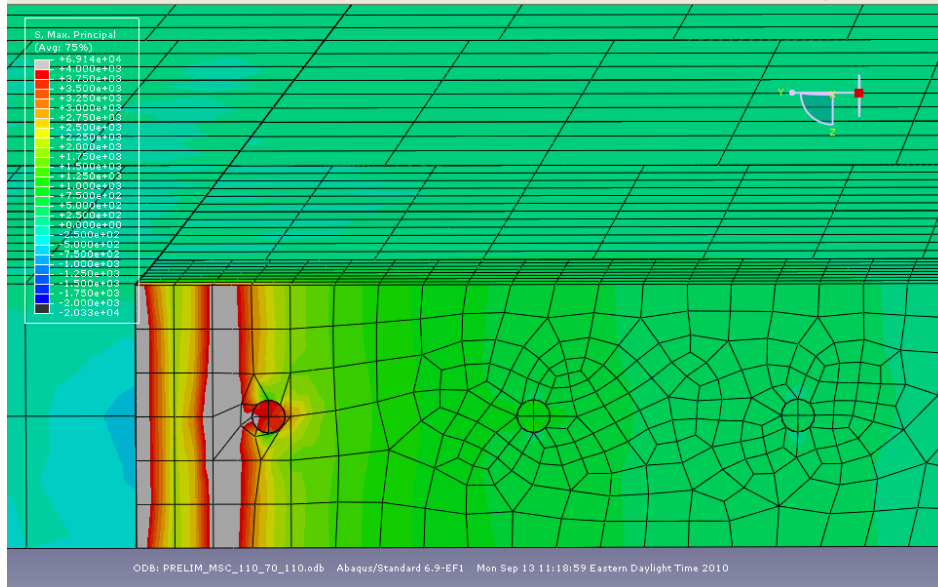


**Figure A114.** Longitudinal shear cracking model in which  $T_M=110^\circ\text{F}$ ,  $T_S=70^\circ\text{F}$ , and  $T_C=110^\circ\text{F}$  for a mortar intrusion of 3.5 in and a CTE of  $6.5 \times 10^{-6}/^\circ\text{F}$ .

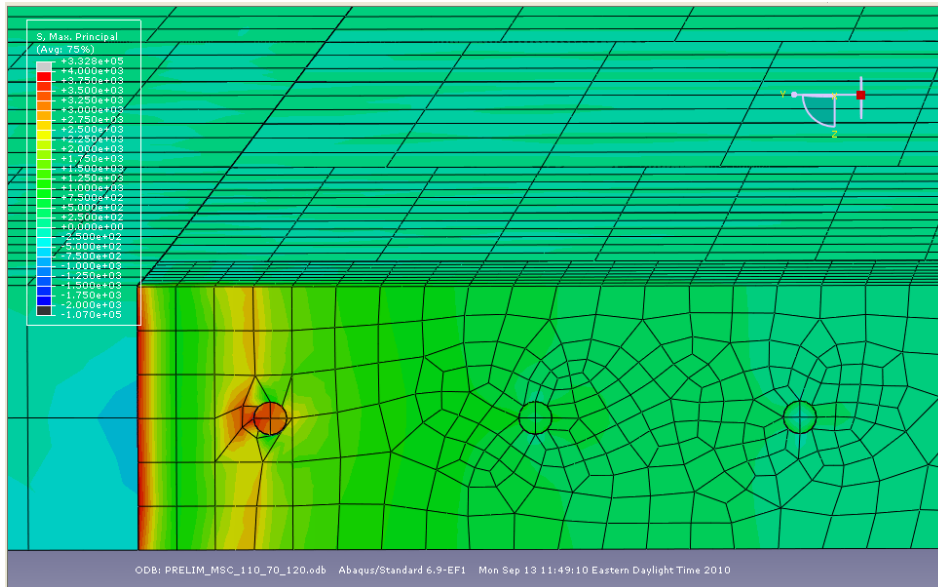


**Figure A115.** Longitudinal shear cracking model in which  $T_M=110^\circ\text{F}$ ,  $T_S=70^\circ\text{F}$ , and  $T_C=120^\circ\text{F}$  for a mortar intrusion of 3.5 in and a CTE of  $6.5 \times 10^{-6}/^\circ\text{F}$ .

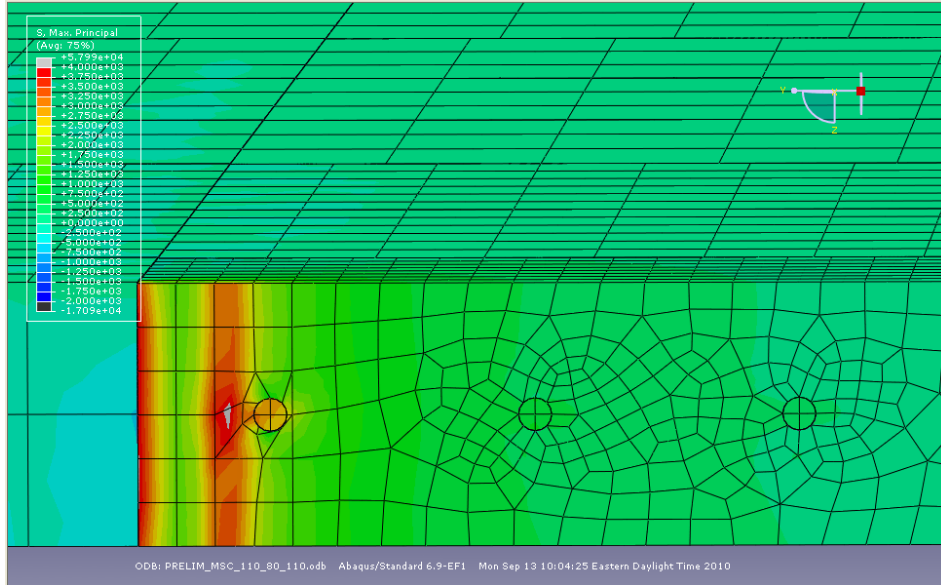


**Figure A116.** Longitudinal shear cracking model in which  $T_M=110^\circ\text{F}$ ,  $T_S=80^\circ\text{F}$ , and  $T_C=110^\circ\text{F}$  for a mortar intrusion of 3.5 in and a CTE of  $6.5 \times 10^{-6}/^\circ\text{F}$ .

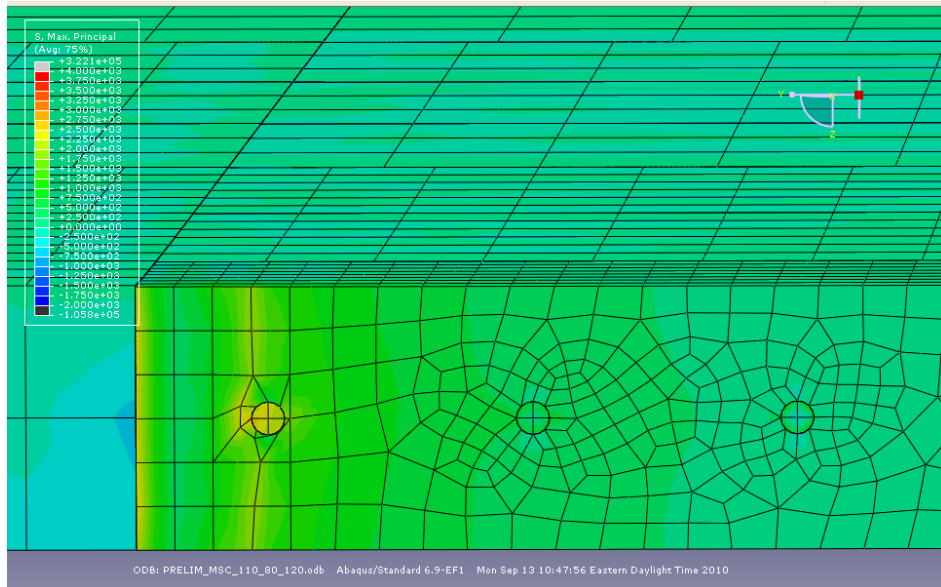


**Figure A117.** Longitudinal shear cracking model in which  $T_M=110^\circ\text{F}$ ,  $T_S=80^\circ\text{F}$ , and  $T_C=120^\circ\text{F}$  for a mortar intrusion of 3.5 in and a CTE of  $6.5 \times 10^{-6}/^\circ\text{F}$ .

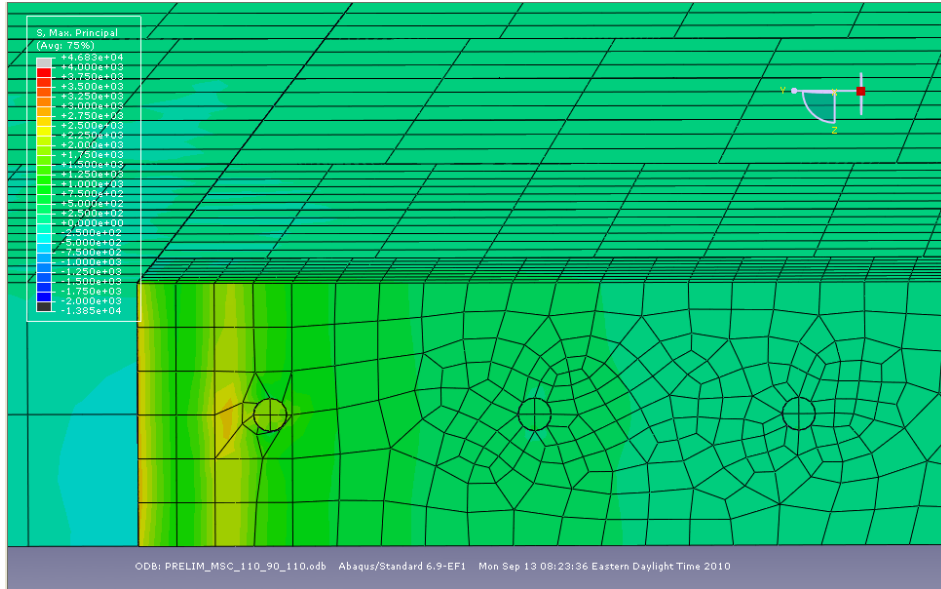


**Figure A118.** Longitudinal shear cracking model in which  $T_M=110^\circ\text{F}$ ,  $T_S=90^\circ\text{F}$ , and  $T_C=110^\circ\text{F}$  for a mortar intrusion of 3.5 in and a CTE of  $6.5 \times 10^{-6}/^\circ\text{F}$ .

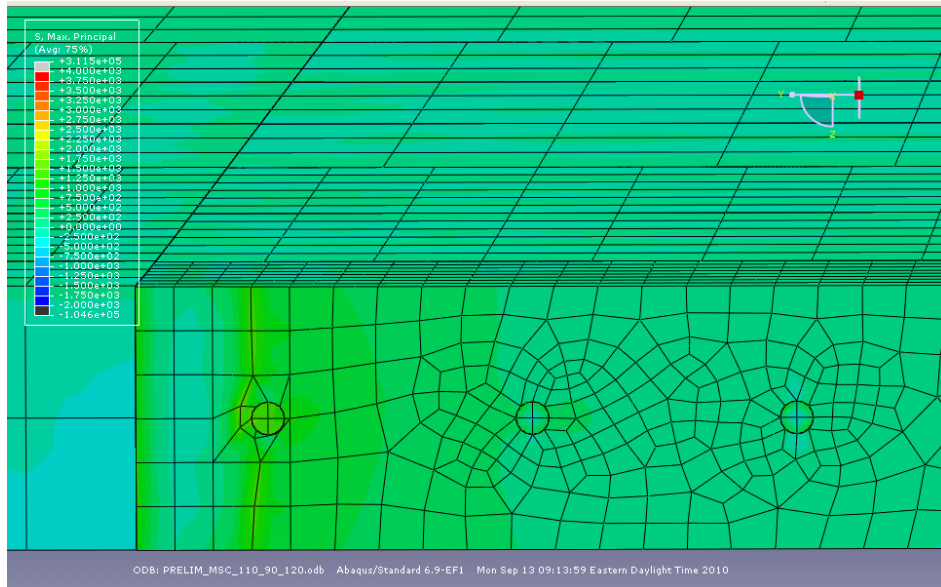


**Figure A119.** Longitudinal shear cracking model in which  $T_M=110^\circ\text{F}$ ,  $T_S=90^\circ\text{F}$ , and  $T_C=120^\circ\text{F}$  for a mortar intrusion of 3.5 in and a CTE of  $6.5 \times 10^{-6}/^\circ\text{F}$ .

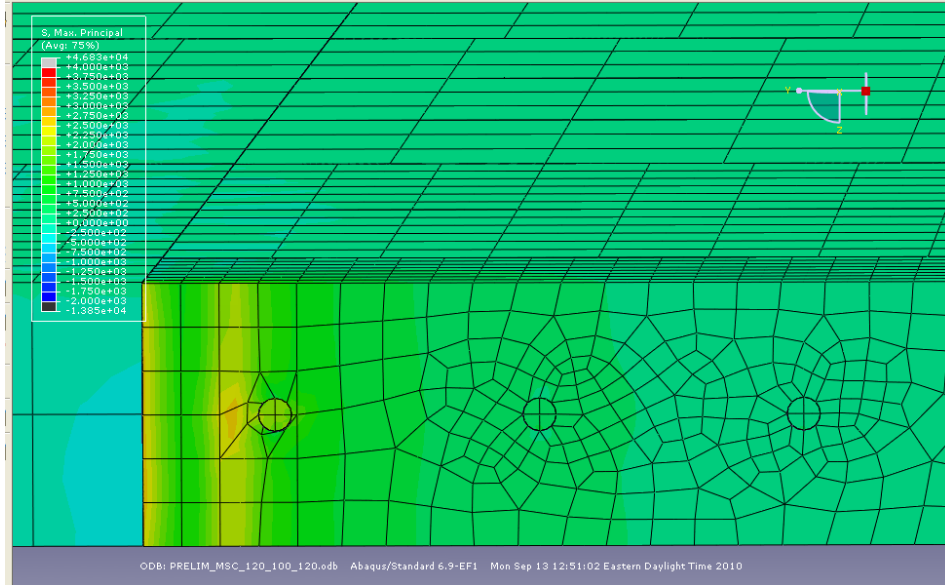


**Figure A120.** Longitudinal shear cracking model in which  $T_M=120^\circ\text{F}$ ,  $T_S=100^\circ\text{F}$ , and  $T_C=120^\circ\text{F}$  for a mortar intrusion of 3.5 in and a CTE of  $6.5 \times 10^{-6}/^\circ\text{F}$ .

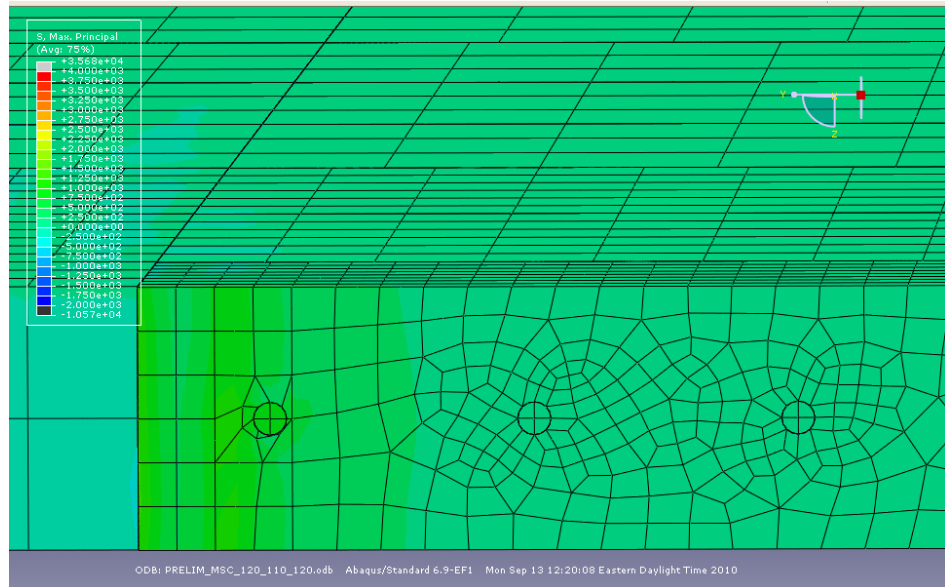


**Figure A121.** Longitudinal shear cracking model in which  $T_M=120^\circ\text{F}$ ,  $T_S=110^\circ\text{F}$ , and  $T_C=120^\circ\text{F}$  for a mortar intrusion of 3.5 in and a CTE of  $6.5 \times 10^{-6}/^\circ\text{F}$ .

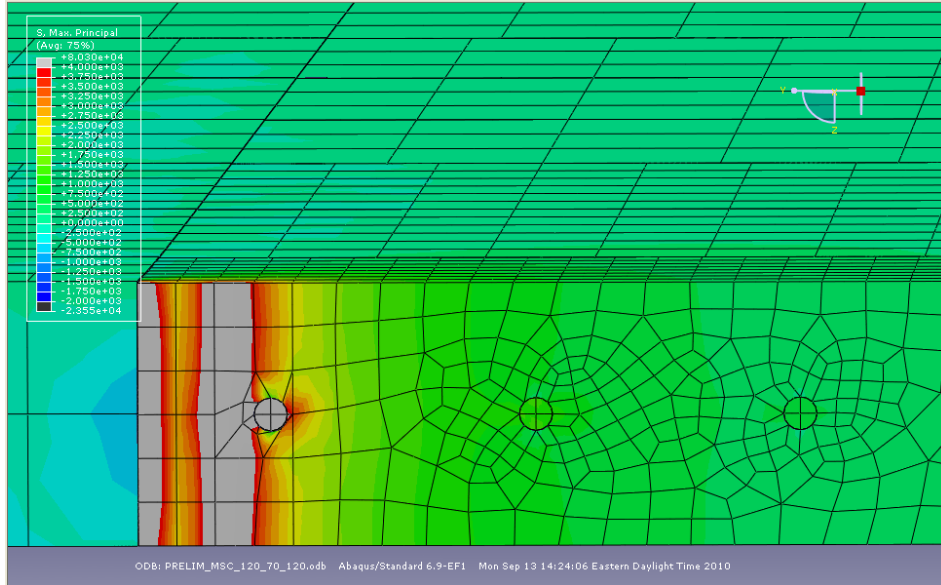


**Figure A122.** Longitudinal shear cracking model in which  $T_M=120^\circ\text{F}$ ,  $T_S=70^\circ\text{F}$ , and  $T_C=120^\circ\text{F}$  for a mortar intrusion of 3.5 in and a CTE of  $6.5 \times 10^{-6}/^\circ\text{F}$ .

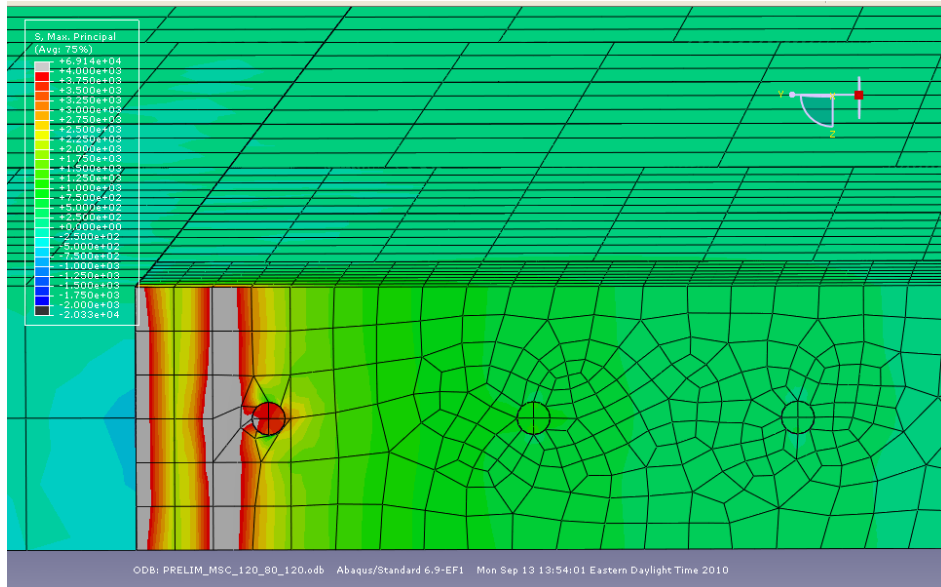


**Figure A123.** Longitudinal shear cracking model in which  $T_M=120^\circ\text{F}$ ,  $T_S=80^\circ\text{F}$ , and  $T_C=120^\circ\text{F}$  for a mortar intrusion of 3.5 in and a CTE of  $6.5 \times 10^{-6}/^\circ\text{F}$ .

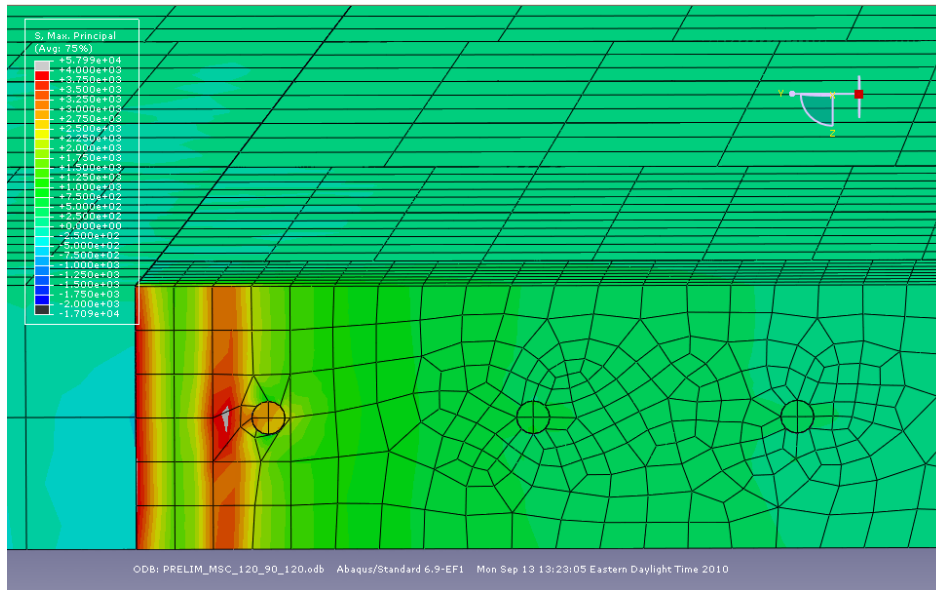


**Figure A124.** Longitudinal shear cracking model in which  $T_M=120^\circ\text{F}$ ,  $T_S=90^\circ\text{F}$ , and  $T_C=120^\circ\text{F}$  for a mortar intrusion of 3.5 in and a CTE of  $6.5 \times 10^{-6}/^\circ\text{F}$ .

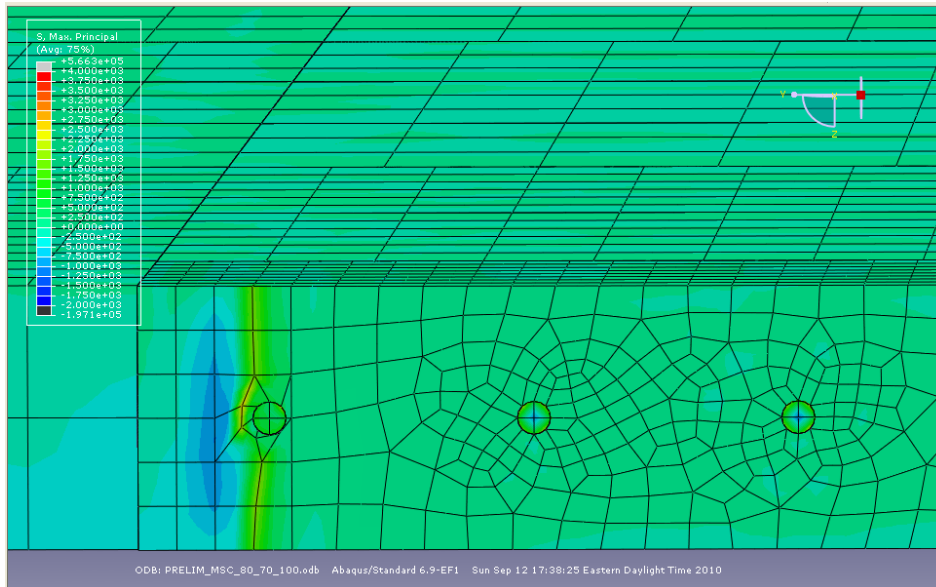


**Figure A125.** Longitudinal shear cracking model in which  $T_M=80^\circ\text{F}$ ,  $T_S=70^\circ\text{F}$ , and  $T_C=100^\circ\text{F}$  for a mortar intrusion of 3.5 in and a CTE of  $6.5 \times 10^{-6}/^\circ\text{F}$ .

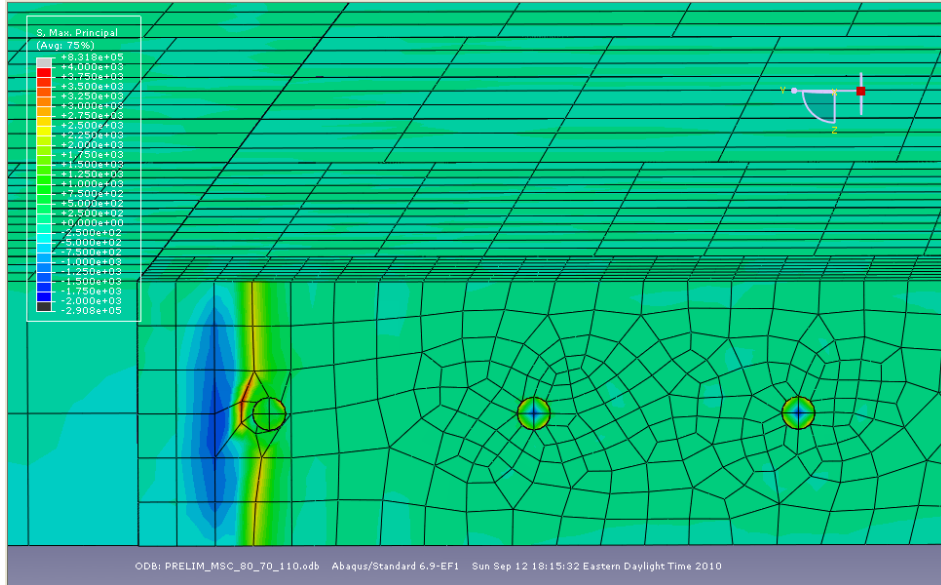


**Figure A126.** Longitudinal shear cracking model in which  $T_M=80^\circ\text{F}$ ,  $T_S=70^\circ\text{F}$ , and  $T_C=110^\circ\text{F}$  for a mortar intrusion of 3.5 in and a CTE of  $6.5 \times 10^{-6}/^\circ\text{F}$ .

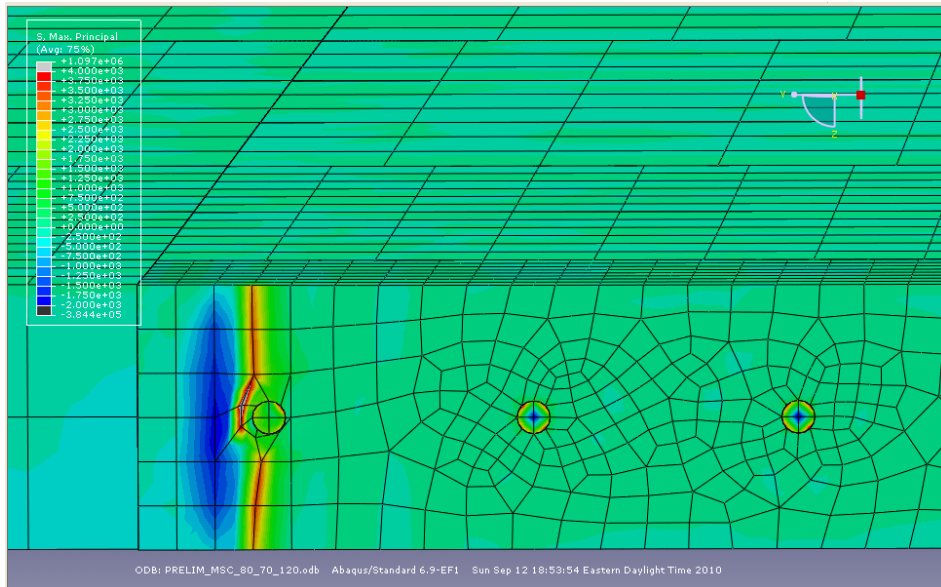


**Figure A127.** Longitudinal shear cracking model in which  $T_M=80^\circ\text{F}$ ,  $T_S=70^\circ\text{F}$ , and  $T_C=120^\circ\text{F}$  for a mortar intrusion of 3.5 in and a CTE of  $6.5 \times 10^{-6}/^\circ\text{F}$ .

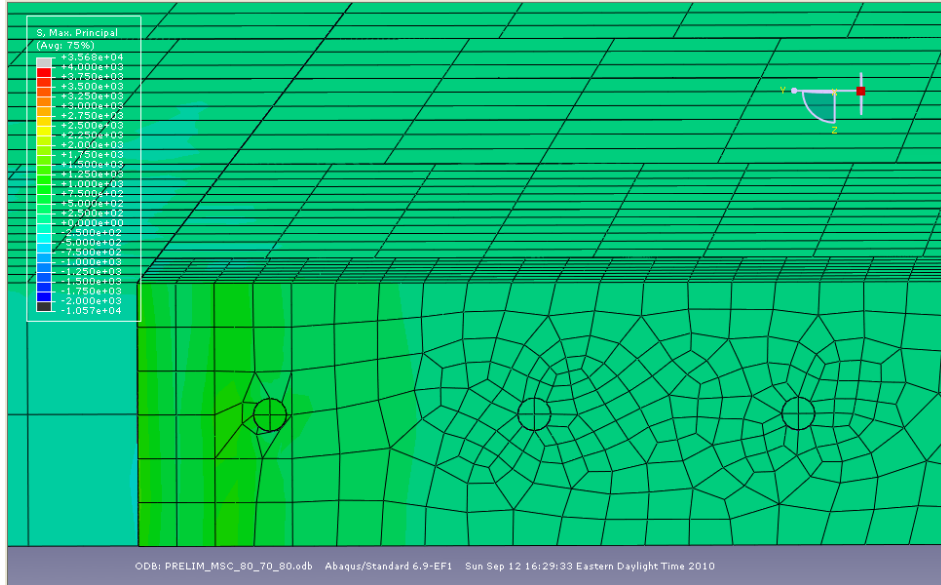


**Figure A128.** Longitudinal shear cracking model in which  $T_M=80^\circ\text{F}$ ,  $T_S=70^\circ\text{F}$ , and  $T_C=80^\circ\text{F}$  for a mortar intrusion of 3.5 in and a CTE of  $6.5 \times 10^{-6}/^\circ\text{F}$ .

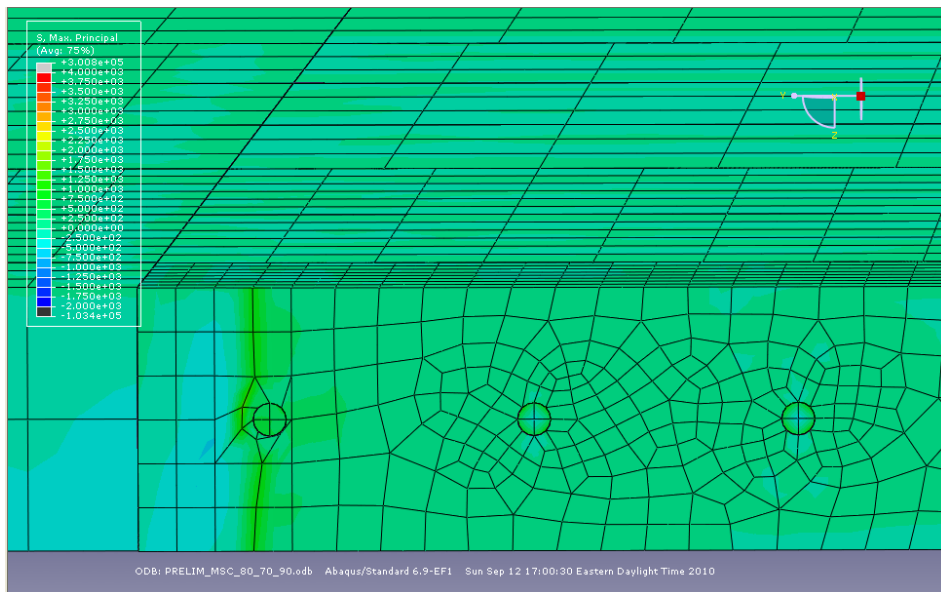


**Figure A129.** Longitudinal shear cracking model in which  $T_M=80^\circ\text{F}$ ,  $T_S=70^\circ\text{F}$ , and  $T_C=90^\circ\text{F}$  for a mortar intrusion of 3.5 in and a CTE of  $6.5 \times 10^{-6}/^\circ\text{F}$ .

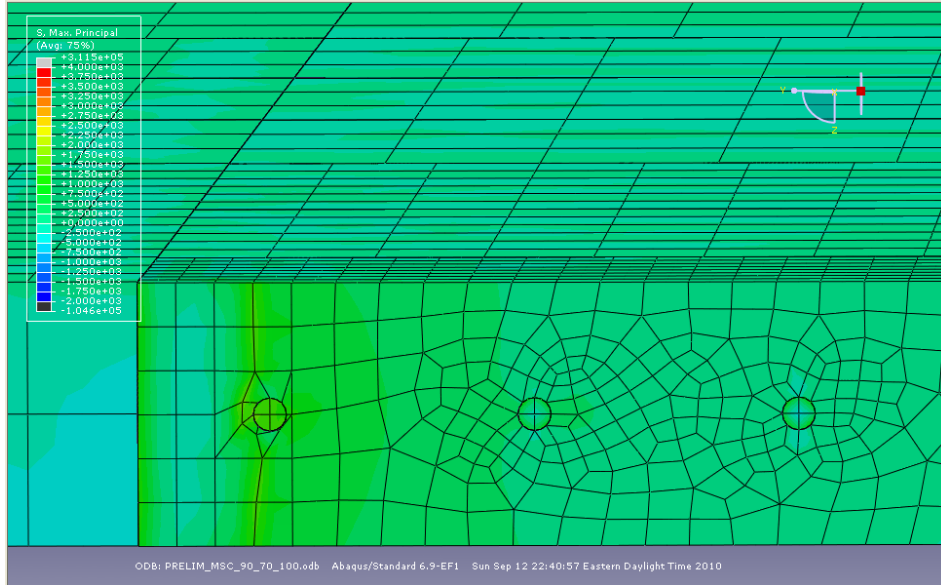


**Figure A130.** Longitudinal shear cracking model in which  $T_M=90^\circ\text{F}$ ,  $T_S=70^\circ\text{F}$ , and  $T_C=100^\circ\text{F}$  for a mortar intrusion of 3.5 in and a CTE of  $6.5 \times 10^{-6}/^\circ\text{F}$ .

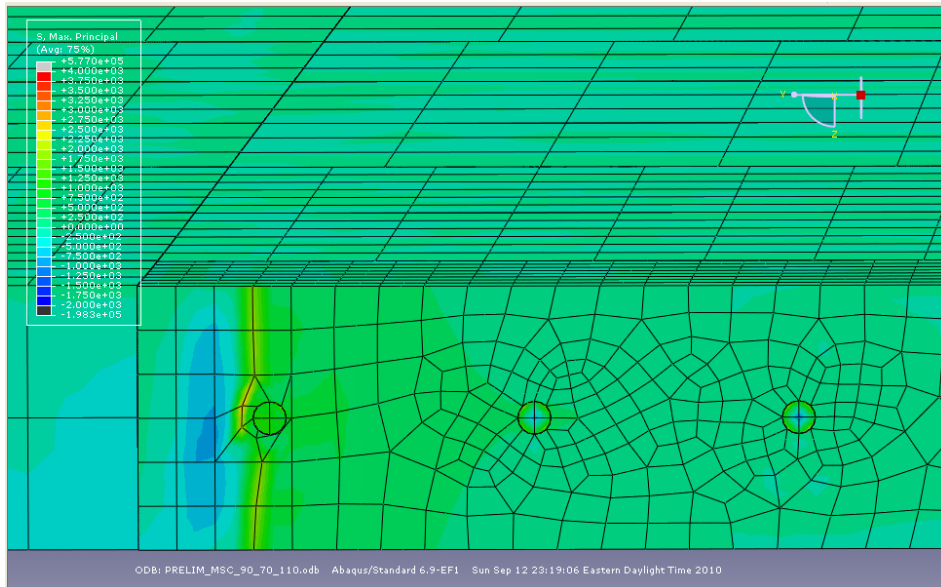


**Figure A131.** Longitudinal shear cracking model in which  $T_M=90^\circ\text{F}$ ,  $T_S=70^\circ\text{F}$ , and  $T_C=110^\circ\text{F}$  for a mortar intrusion of 3.5 in and a CTE of  $6.5 \times 10^{-6}/^\circ\text{F}$ .

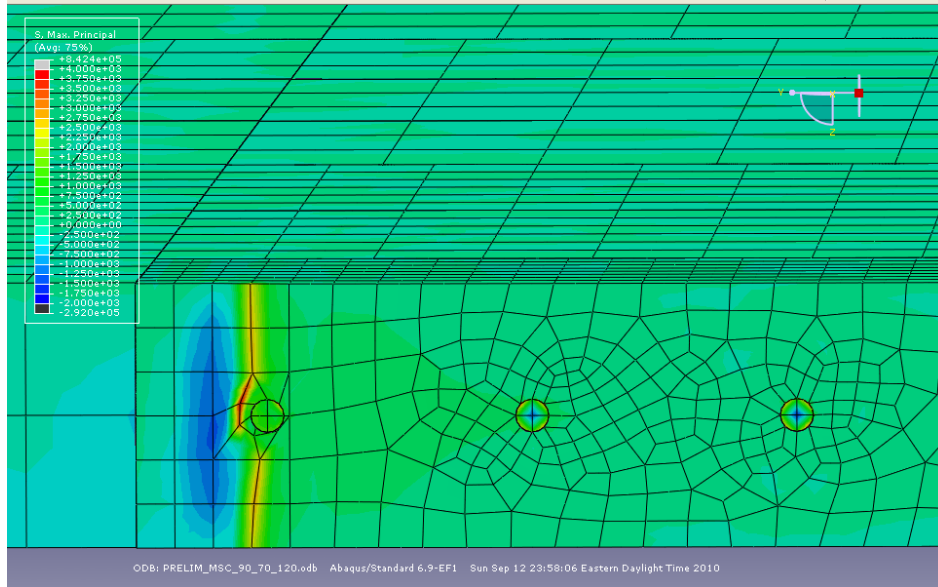


**Figure A132.** Longitudinal shear cracking model in which  $T_M=90^\circ\text{F}$ ,  $T_S=70^\circ\text{F}$ , and  $T_C=120^\circ\text{F}$  for a mortar intrusion of 3.5 in and a CTE of  $6.5 \times 10^{-6}/^\circ\text{F}$ .

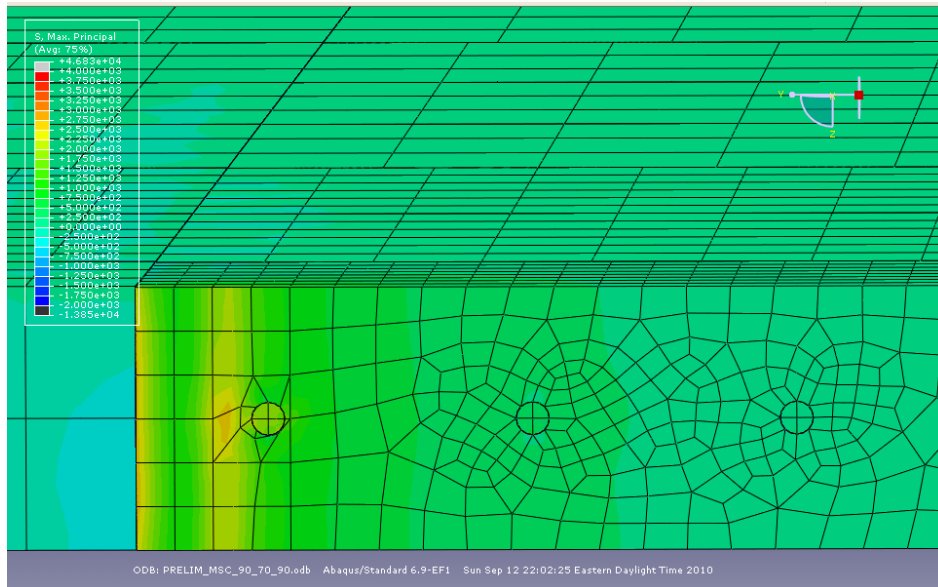


**Figure A133.** Longitudinal shear cracking model in which  $T_M=90^\circ\text{F}$ ,  $T_S=70^\circ\text{F}$ , and  $T_C=90^\circ\text{F}$  for a mortar intrusion of 3.5 in and a CTE of  $6.5 \times 10^{-6}/^\circ\text{F}$ .

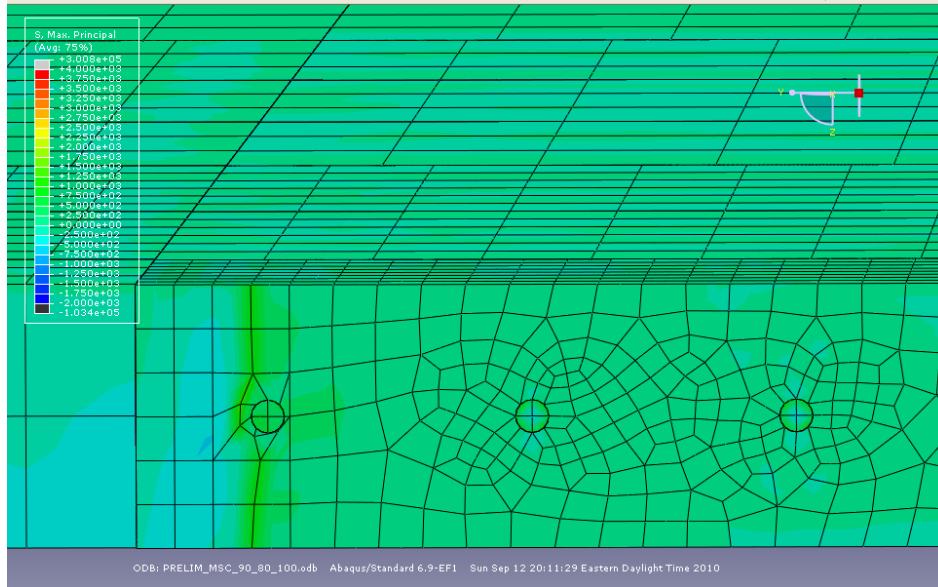


**Figure A134.** Longitudinal shear cracking model in which  $T_M=90^\circ\text{F}$ ,  $T_S=80^\circ\text{F}$ , and  $T_C=100^\circ\text{F}$  for a mortar intrusion of 3.5 in and a CTE of  $6.5 \times 10^{-6}/^\circ\text{F}$ .

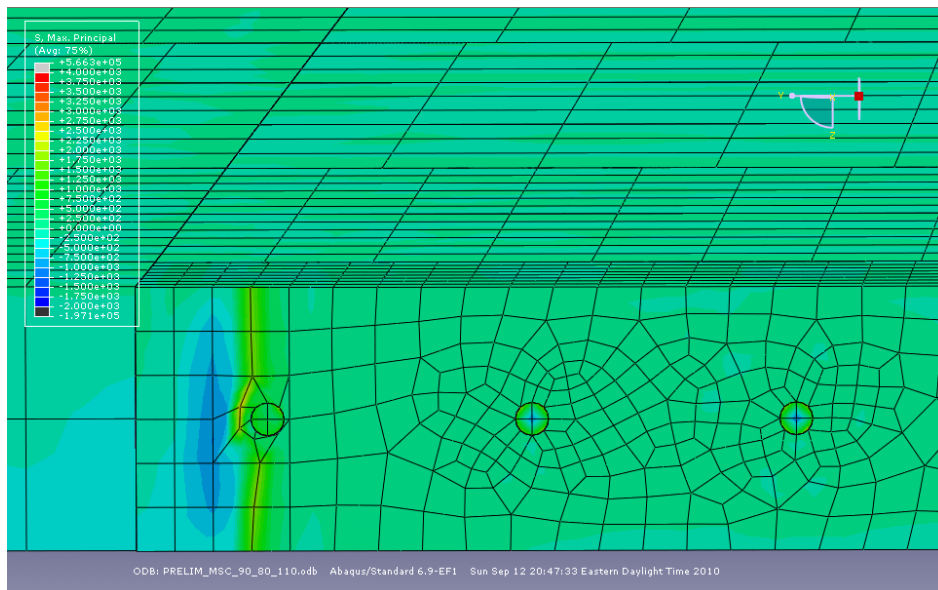


**Figure A135.** Longitudinal shear cracking model in which  $T_M=90^\circ\text{F}$ ,  $T_S=80^\circ\text{F}$ , and  $T_C=110^\circ\text{F}$  for a mortar intrusion of 3.5 in and a CTE of  $6.5 \times 10^{-6}/^\circ\text{F}$ .

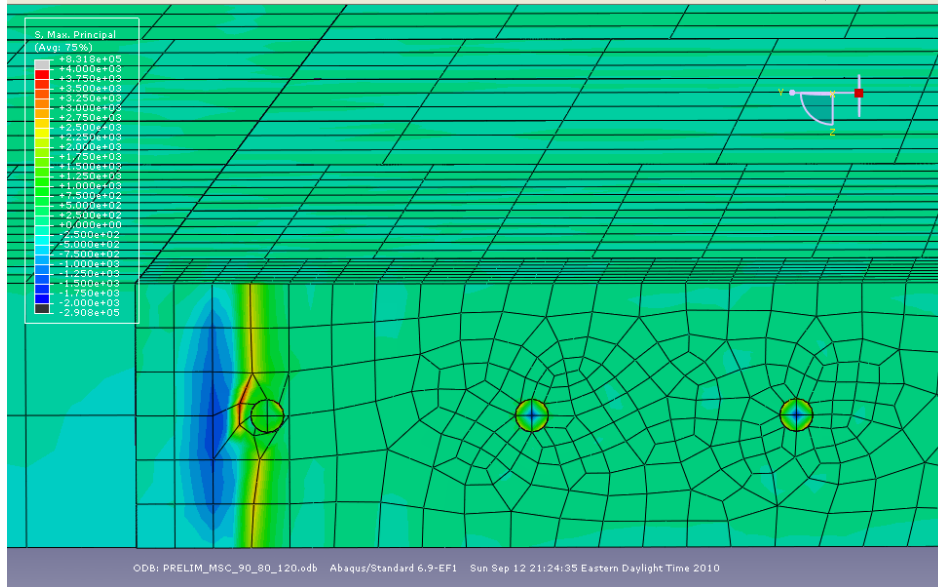


**Figure A136.** Longitudinal shear cracking model in which  $T_M=90^\circ\text{F}$ ,  $T_S=80^\circ\text{F}$ , and  $T_C=120^\circ\text{F}$  for a mortar intrusion of 3.5 in and a CTE of  $6.5 \times 10^{-6}/^\circ\text{F}$ .

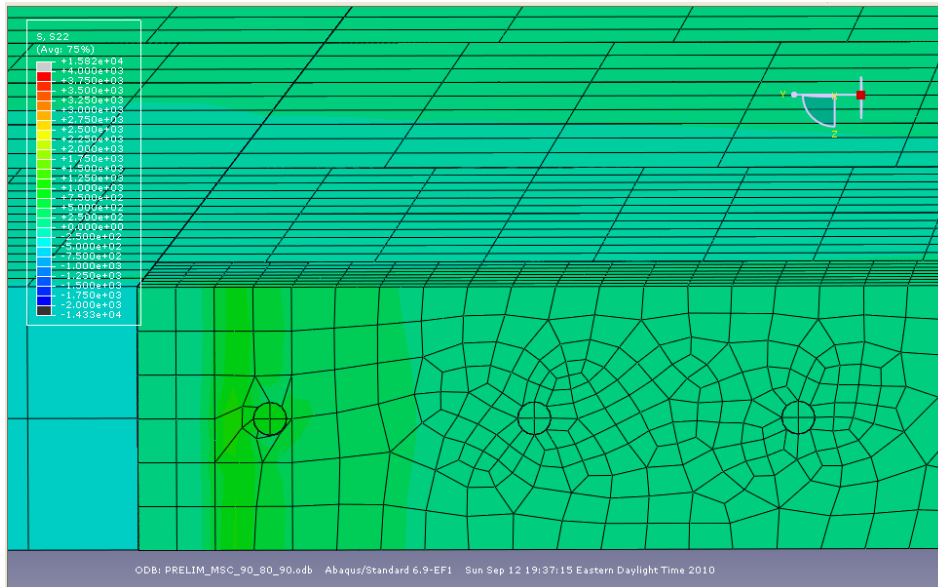


**Figure A137.** Longitudinal shear cracking model in which  $T_M=90^\circ\text{F}$ ,  $T_S=80^\circ\text{F}$ , and  $T_C=90^\circ\text{F}$  for a mortar intrusion of 3.5 in and a CTE of  $6.5 \times 10^{-6}/^\circ\text{F}$ .

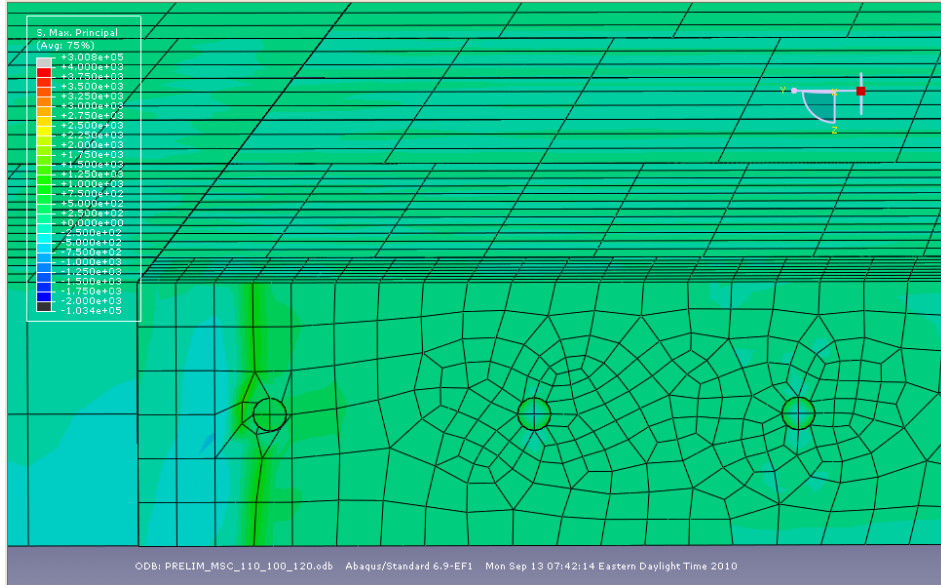


**Figure A138.** Longitudinal shear cracking model in which  $T_M=110^\circ\text{F}$ ,  $T_S=100^\circ\text{F}$ , and  $T_C=120^\circ\text{F}$  for a mortar intrusion of 3.5 in and a CTE of  $6.5 \times 10^{-6}/^\circ\text{F}$ .

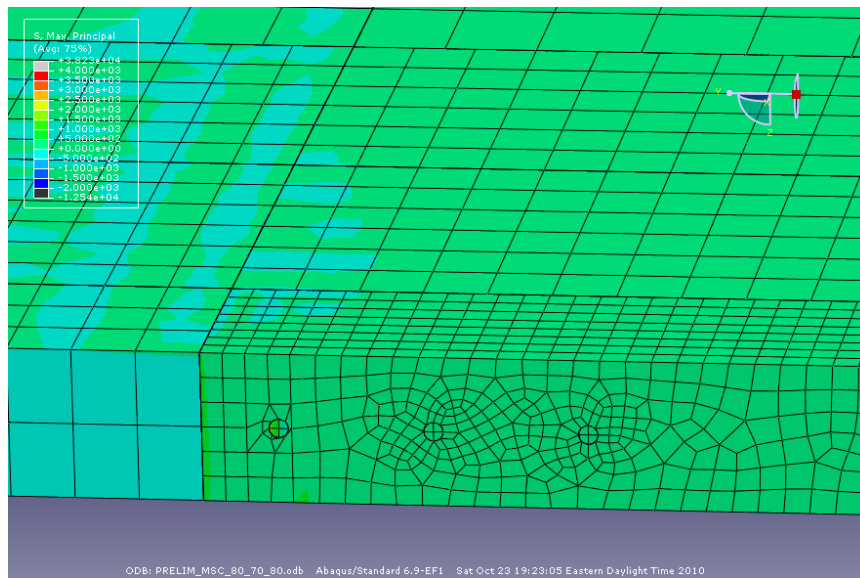


**Figure A139.** Longitudinal shear cracking model in which  $T_M=80^\circ\text{F}$ ,  $T_S=70^\circ\text{F}$ , and  $T_C=80^\circ\text{F}$  for a mortar intrusion of 7 in and a CTE of  $4 \times 10^{-6}/^\circ\text{F}$ .

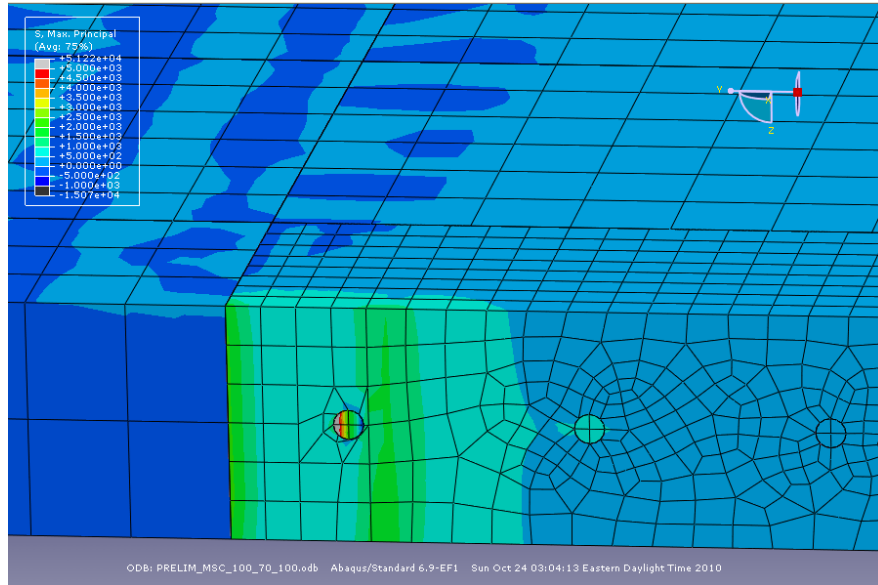


**Figure A140.** Longitudinal shear cracking model in which  $T_M=100^\circ\text{F}$ ,  $T_S=70^\circ\text{F}$ , and  $T_C=100^\circ\text{F}$  for a mortar intrusion of 7 in and a CTE of  $4 \times 10^{-6}/^\circ\text{F}$ .

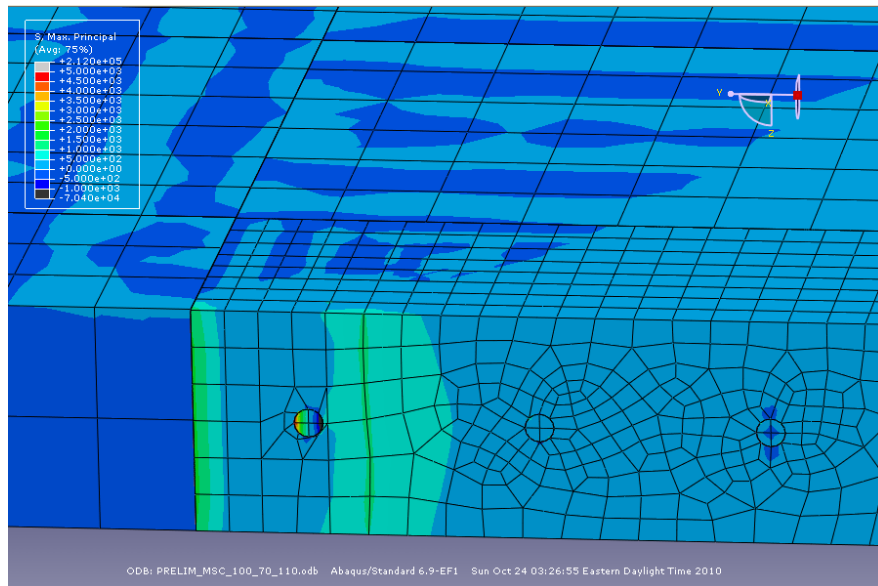


**Figure A141.** Longitudinal shear cracking model in which  $T_M=100^\circ\text{F}$ ,  $T_S=70^\circ\text{F}$ , and  $T_C=110^\circ\text{F}$  for a mortar intrusion of 7 in and a CTE of  $4 \times 10^{-6}/^\circ\text{F}$ .

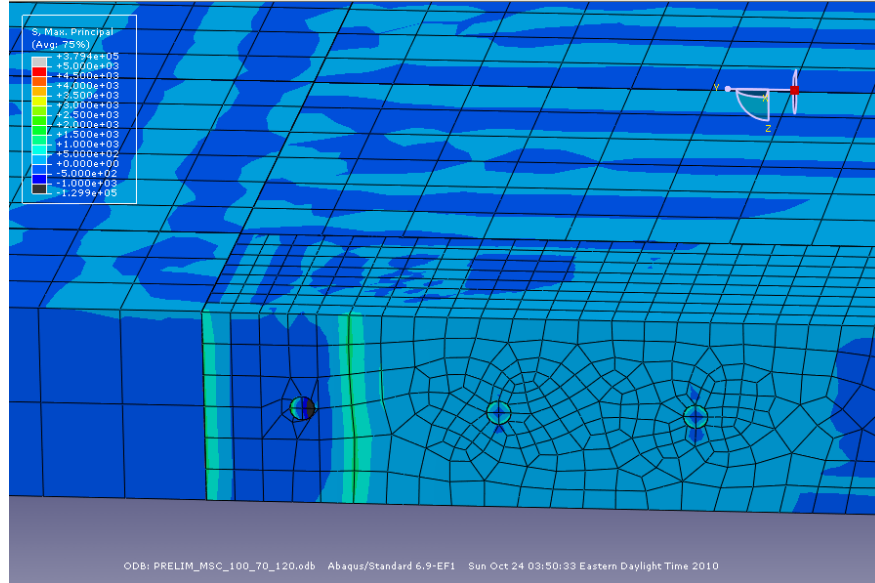


**Figure A142.** Longitudinal shear cracking model in which  $T_M=100^\circ\text{F}$ ,  $T_S=70^\circ\text{F}$ , and  $T_C=120^\circ\text{F}$  for a mortar intrusion of 7 in and a CTE of  $4 \times 10^{-6}/^\circ\text{F}$ .

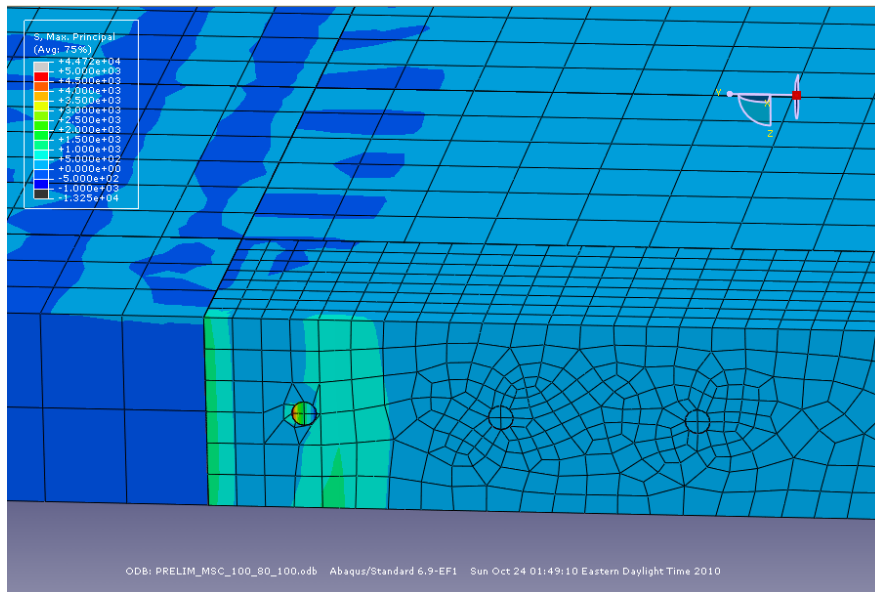


**Figure A143.** Longitudinal shear cracking model in which  $T_M=100^\circ\text{F}$ ,  $T_S=80^\circ\text{F}$ , and  $T_C=100^\circ\text{F}$  for a mortar intrusion of 7 in and a CTE of  $4 \times 10^{-6}/^\circ\text{F}$ .

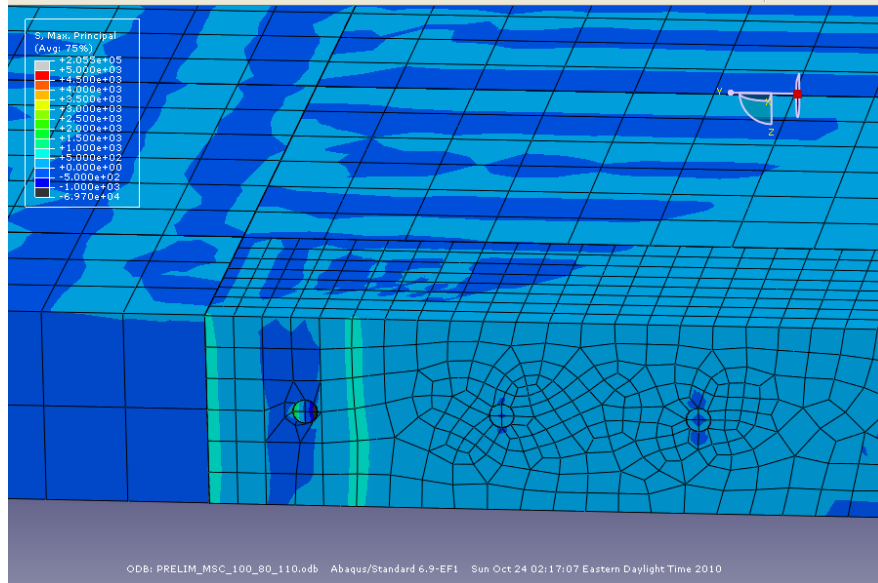


**Figure A144.** Longitudinal shear cracking model in which  $T_M=100^\circ\text{F}$ ,  $T_S=80^\circ\text{F}$ , and  $T_C=110^\circ\text{F}$  for a mortar intrusion of 7 in and a CTE of  $4 \times 10^{-6}/^\circ\text{F}$ .

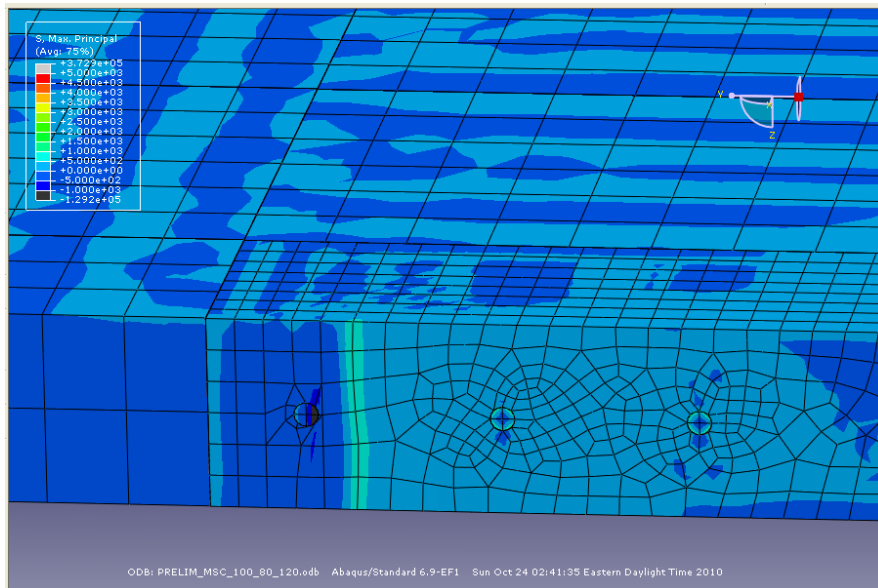


**Figure A145.** Longitudinal shear cracking model in which  $T_M=100^\circ\text{F}$ ,  $T_S=80^\circ\text{F}$ , and  $T_C=120^\circ\text{F}$  for a mortar intrusion of 7 in and a CTE of  $4 \times 10^{-6}/^\circ\text{F}$ .

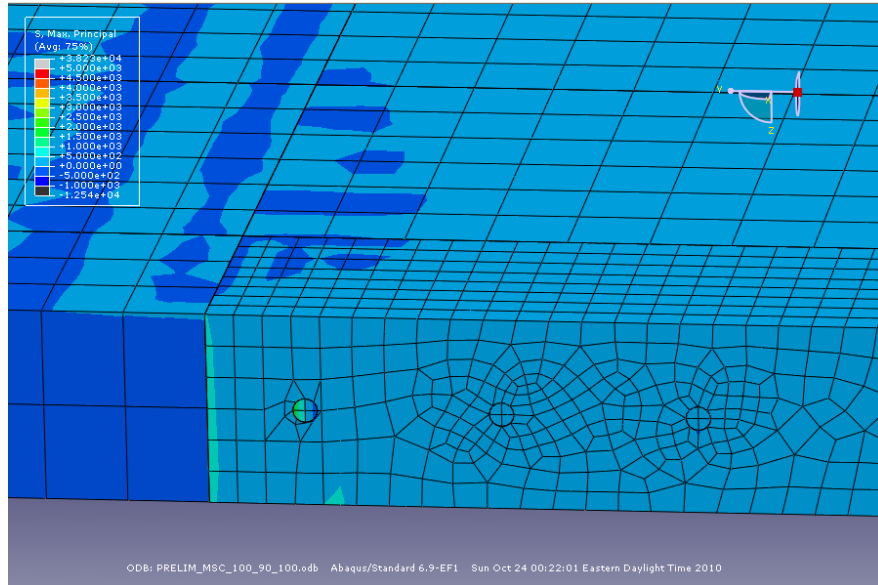


**Figure A146.** Longitudinal shear cracking model in which  $T_M=100^\circ\text{F}$ ,  $T_S=90^\circ\text{F}$ , and  $T_C=100^\circ\text{F}$  for a mortar intrusion of 7 in and a CTE of  $4 \times 10^{-6}/^\circ\text{F}$ .

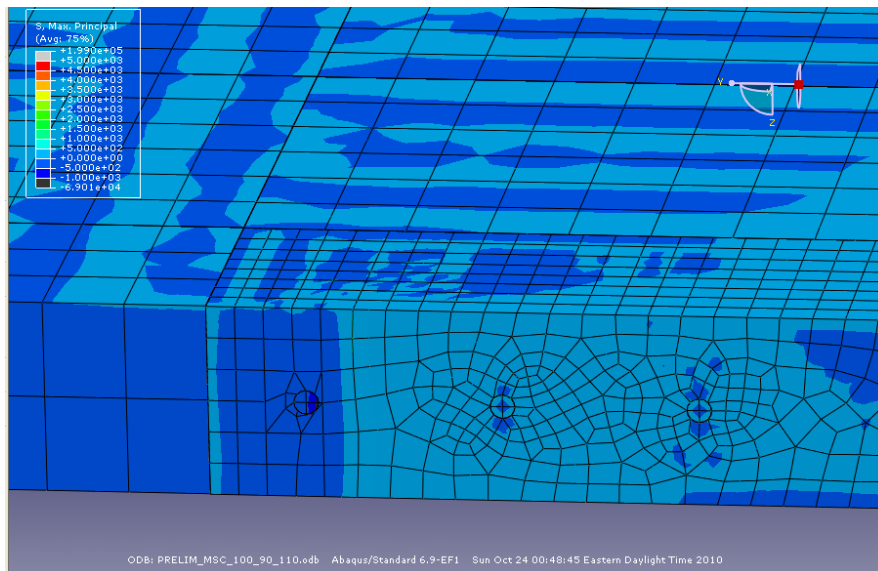


**Figure A147.** Longitudinal shear cracking model in which  $T_M=100^\circ\text{F}$ ,  $T_S=90^\circ\text{F}$ , and  $T_C=110^\circ\text{F}$  for a mortar intrusion of 7 in and a CTE of  $4 \times 10^{-6}/^\circ\text{F}$ .

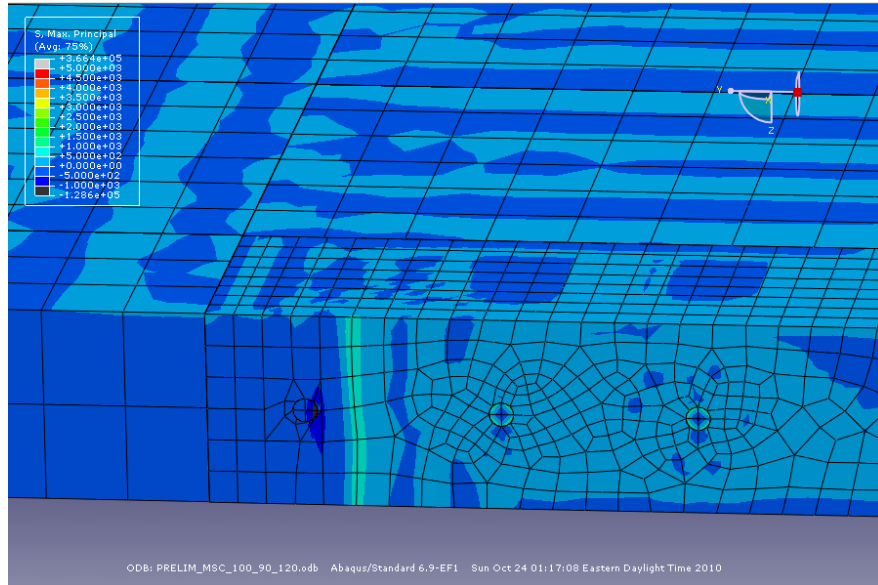


**Figure A148.** Longitudinal shear cracking model in which  $T_M=100^\circ\text{F}$ ,  $T_S=90^\circ\text{F}$ , and  $T_C=120^\circ\text{F}$  for a mortar intrusion of 7 in and a CTE of  $4 \times 10^{-6}/^\circ\text{F}$ .

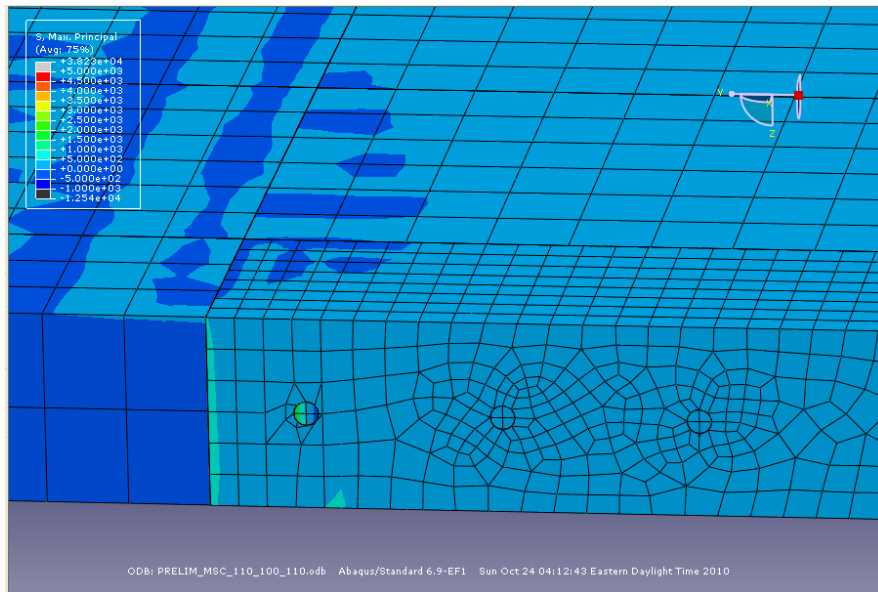


**Figure A149.** Longitudinal shear cracking model in which  $T_M=110^\circ\text{F}$ ,  $T_S=100^\circ\text{F}$ , and  $T_C=110^\circ\text{F}$  for a mortar intrusion of 7 in and a CTE of  $4 \times 10^{-6}/^\circ\text{F}$ .

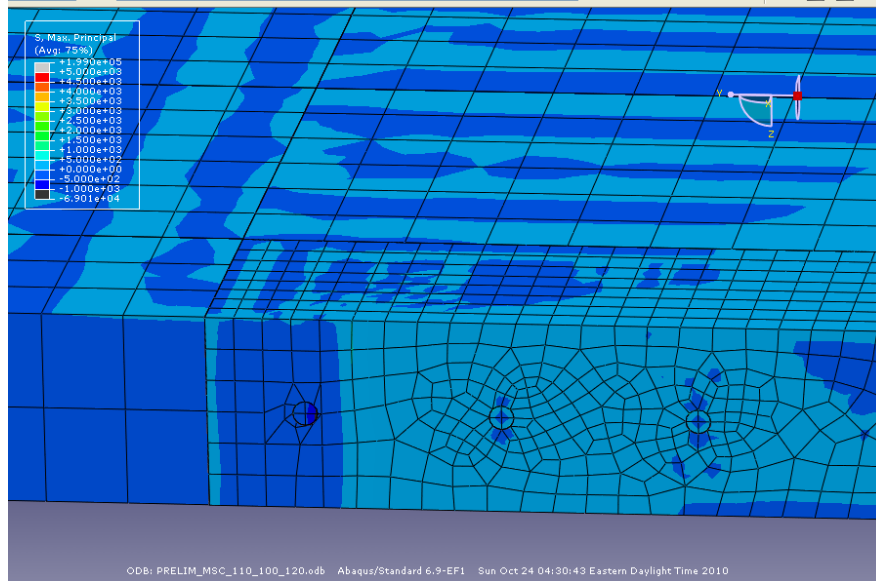


**Figure A150.** Longitudinal shear cracking model in which  $T_M=110^\circ\text{F}$ ,  $T_S=100^\circ\text{F}$ , and  $T_C=120^\circ\text{F}$  for a mortar intrusion of 7 in and a CTE of  $4 \times 10^{-6}/^\circ\text{F}$ .

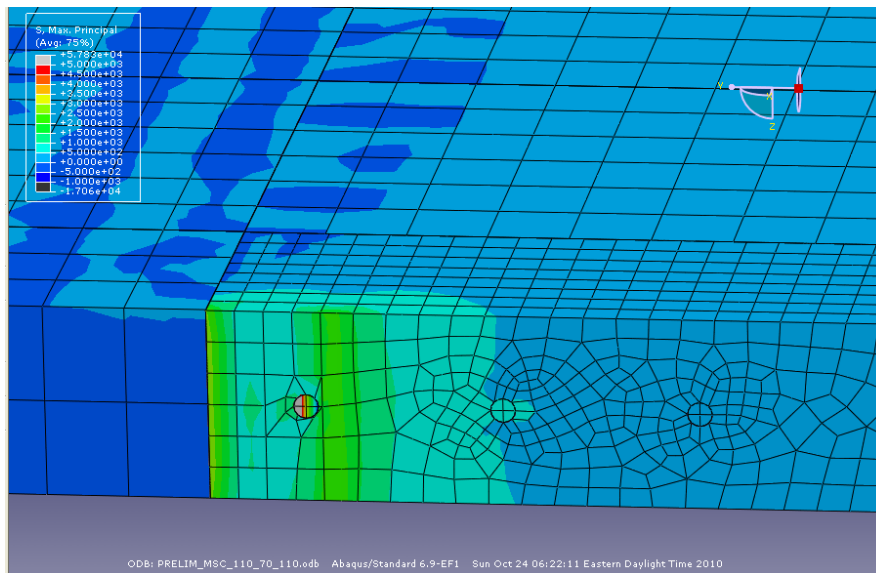


**Figure A151.** Longitudinal shear cracking model in which  $T_M=110^\circ\text{F}$ ,  $T_S=70^\circ\text{F}$ , and  $T_C=110^\circ\text{F}$  for a mortar intrusion of 7 in and a CTE of  $4 \times 10^{-6}/^\circ\text{F}$ .

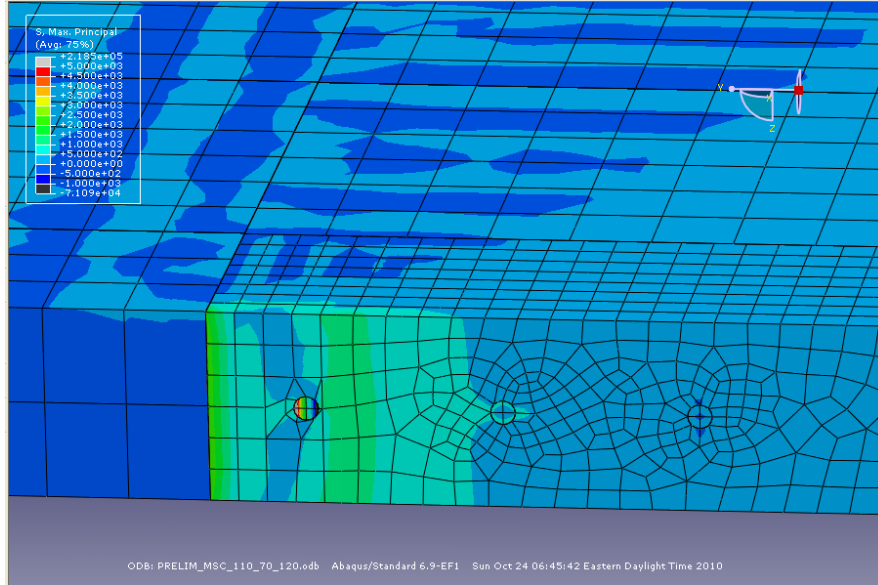


**Figure A152.** Longitudinal shear cracking model in which  $T_M=110^\circ\text{F}$ ,  $T_S=70^\circ\text{F}$ , and  $T_C=120^\circ\text{F}$  for a mortar intrusion of 7 in and a CTE of  $4 \times 10^{-6}/^\circ\text{F}$ .

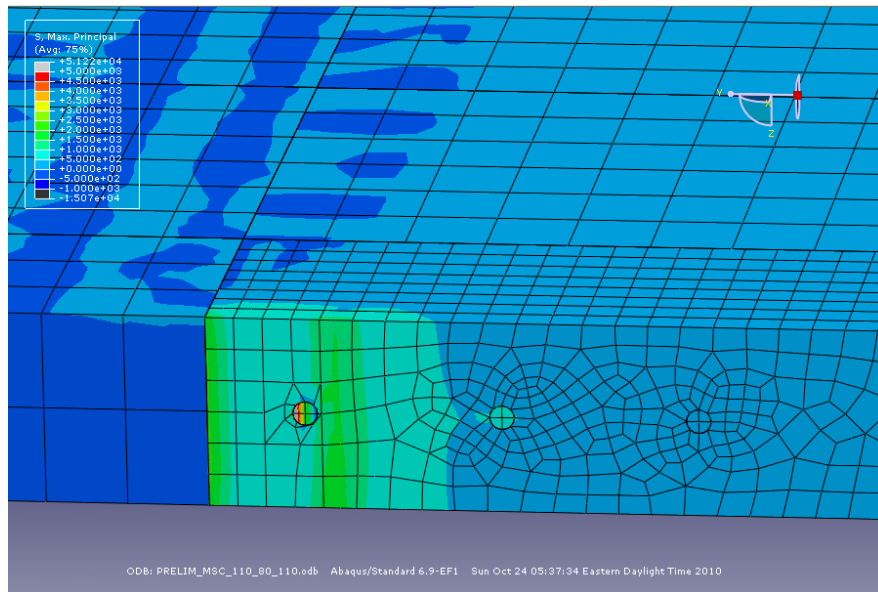


**Figure A153.** Longitudinal shear cracking model in which  $T_M=110^\circ\text{F}$ ,  $T_S=80^\circ\text{F}$ , and  $T_C=110^\circ\text{F}$  for a mortar intrusion of 7 in and a CTE of  $4 \times 10^{-6}/^\circ\text{F}$ .

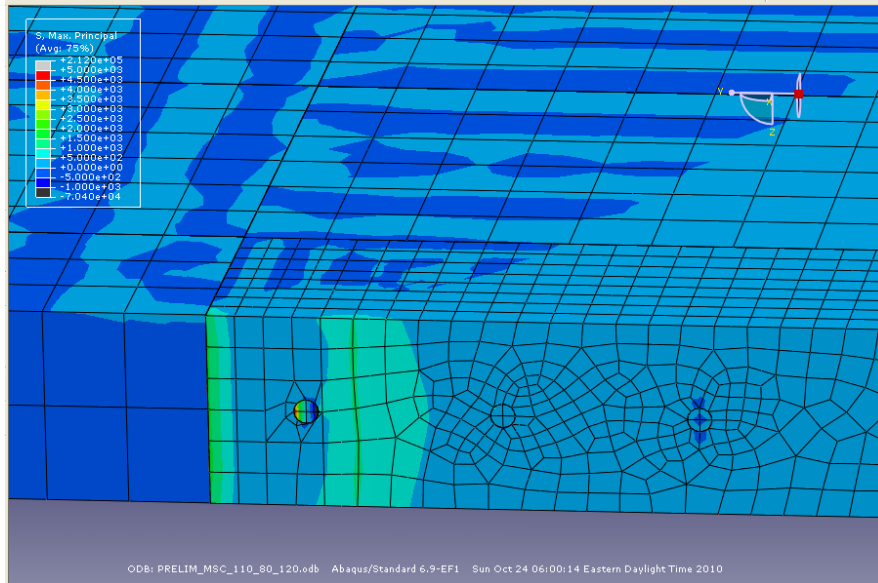


**Figure A154.** Longitudinal shear cracking model in which  $T_M=110^\circ\text{F}$ ,  $T_S=80^\circ\text{F}$ , and  $T_C=120^\circ\text{F}$  for a mortar intrusion of 7 in and a CTE of  $4 \times 10^{-6}/^\circ\text{F}$ .

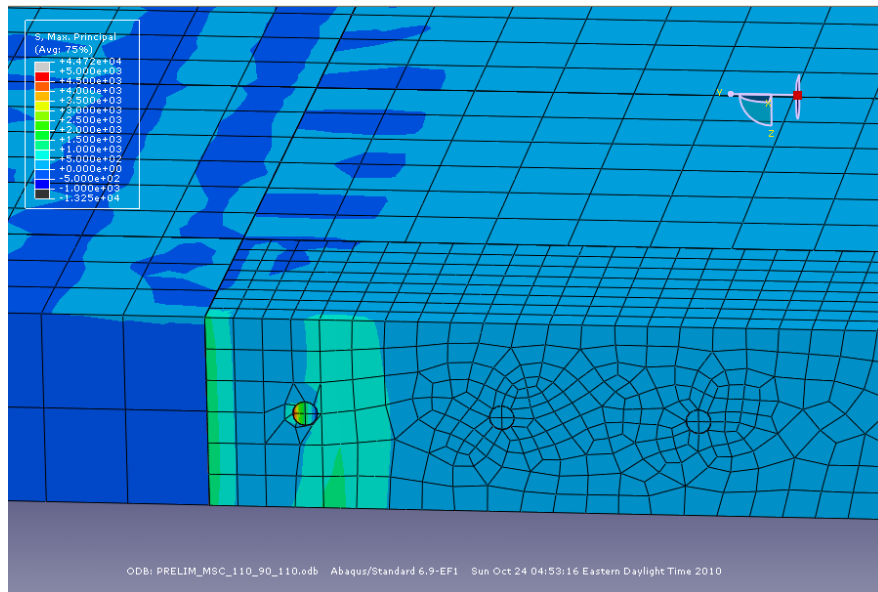


**Figure A155.** Longitudinal shear cracking model in which  $T_M=110^\circ\text{F}$ ,  $T_S=90^\circ\text{F}$ , and  $T_C=110^\circ\text{F}$  for a mortar intrusion of 7 in and a CTE of  $4 \times 10^{-6}/^\circ\text{F}$ .

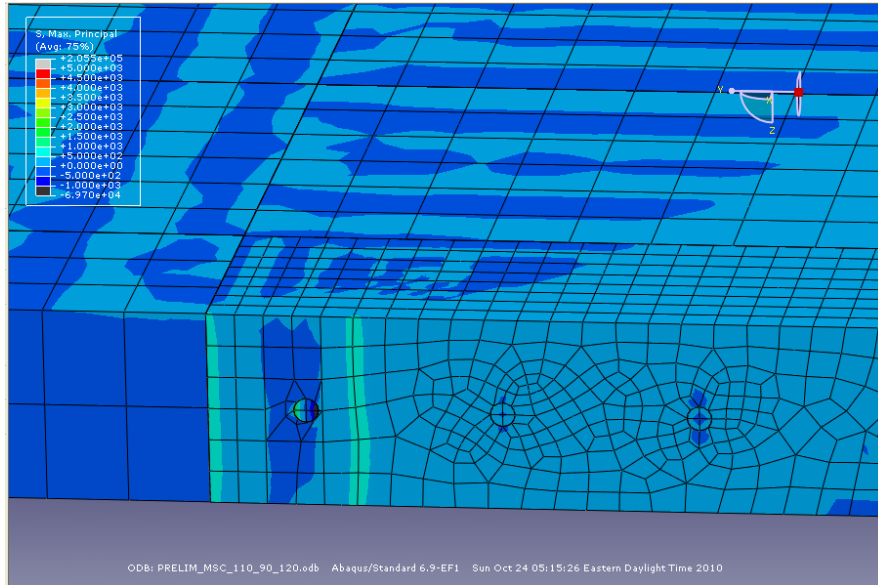


**Figure A156.** Longitudinal shear cracking model in which  $T_M=110^\circ\text{F}$ ,  $T_S=90^\circ\text{F}$ , and  $T_C=120^\circ\text{F}$  for a mortar intrusion of 7 in and a CTE of  $4 \times 10^{-6}/^\circ\text{F}$ .

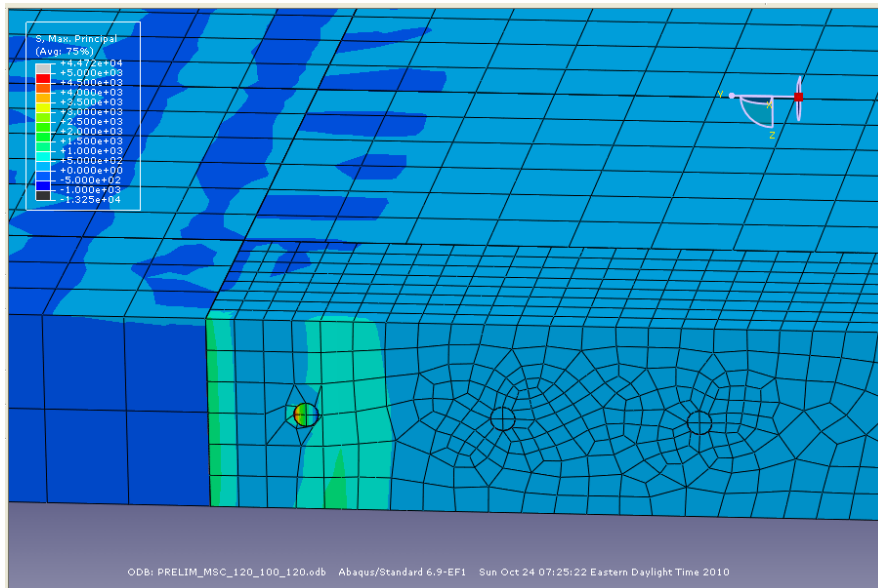


**Figure A157.** Longitudinal shear cracking model in which  $T_M=120^\circ\text{F}$ ,  $T_S=100^\circ\text{F}$ , and  $T_C=120^\circ\text{F}$  for a mortar intrusion of 7 in and a CTE of  $4 \times 10^{-6}/^\circ\text{F}$ .

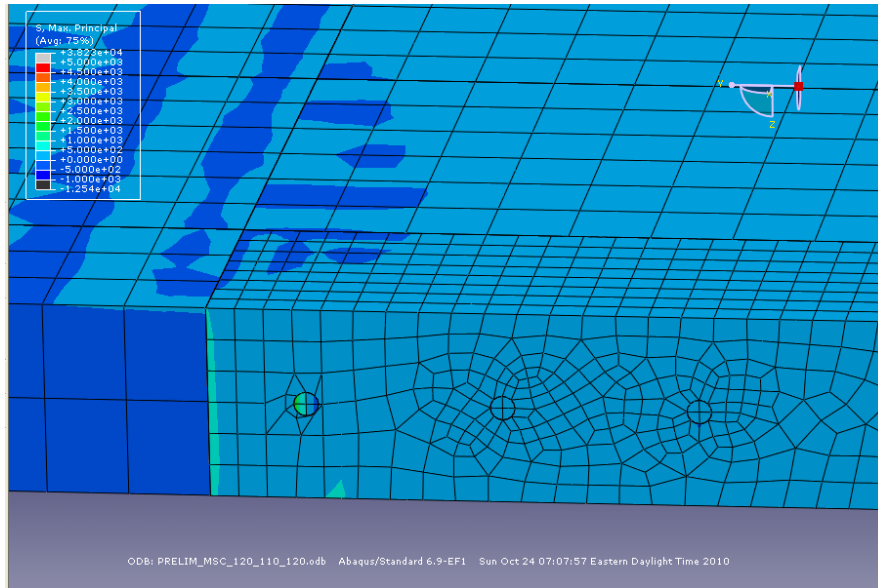


**Figure A158.** Longitudinal shear cracking model in which  $T_M=120^\circ\text{F}$ ,  $T_S=110^\circ\text{F}$ , and  $T_C=120^\circ\text{F}$  for a mortar intrusion of 7 in and a CTE of  $4 \times 10^{-6}/^\circ\text{F}$ .

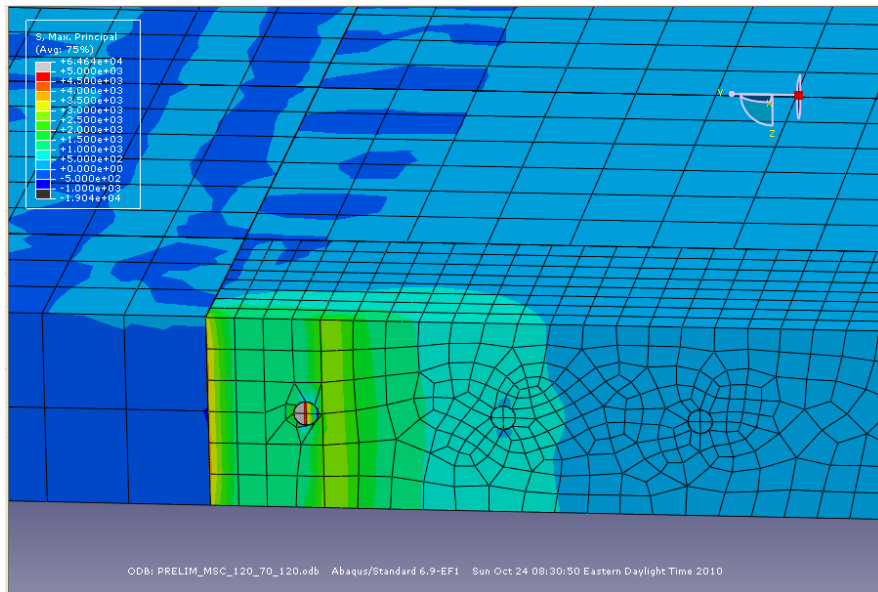


**Figure A159.** Longitudinal shear cracking model in which  $T_M=120^\circ\text{F}$ ,  $T_S=70^\circ\text{F}$ , and  $T_C=120^\circ\text{F}$  for a mortar intrusion of 7 in and a CTE of  $4 \times 10^{-6}/^\circ\text{F}$ .

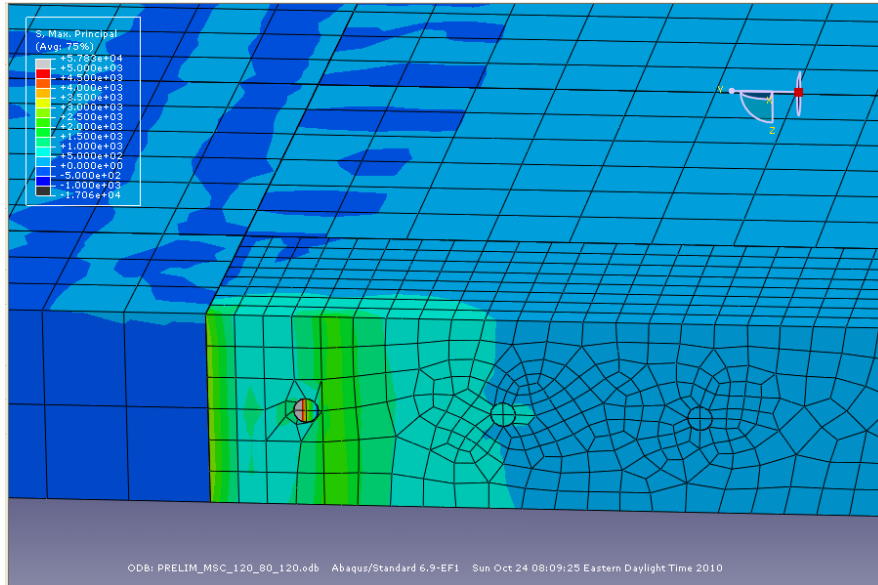


**Figure A160.** Longitudinal shear cracking model in which  $T_M=120^\circ\text{F}$ ,  $T_S=80^\circ\text{F}$ , and  $T_C=120^\circ\text{F}$  for a mortar intrusion of 7 in and a CTE of  $4 \times 10^{-6}/^\circ\text{F}$ .

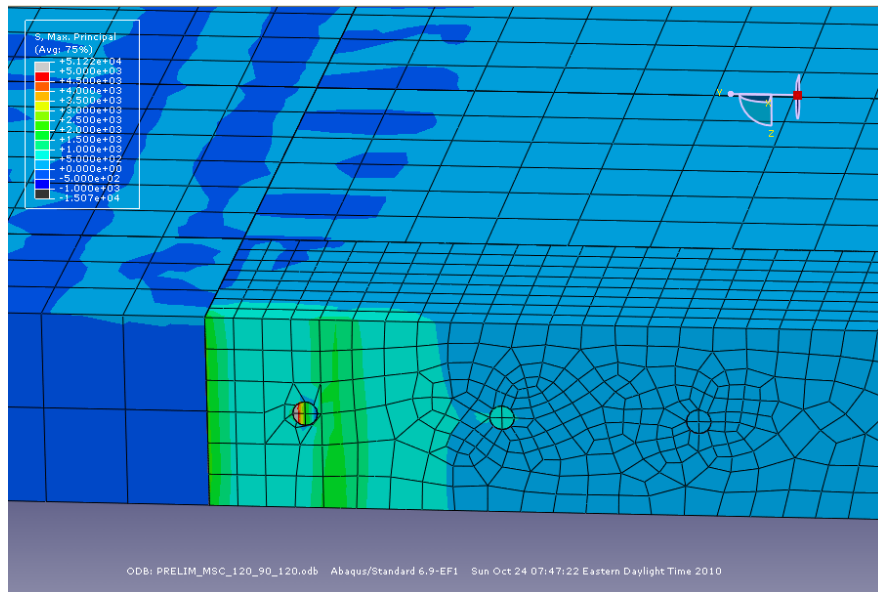


**Figure A161.** Longitudinal shear cracking model in which  $T_M=120^\circ\text{F}$ ,  $T_S=90^\circ\text{F}$ , and  $T_C=120^\circ\text{F}$  for a mortar intrusion of 7 in and a CTE of  $4 \times 10^{-6}/^\circ\text{F}$ .

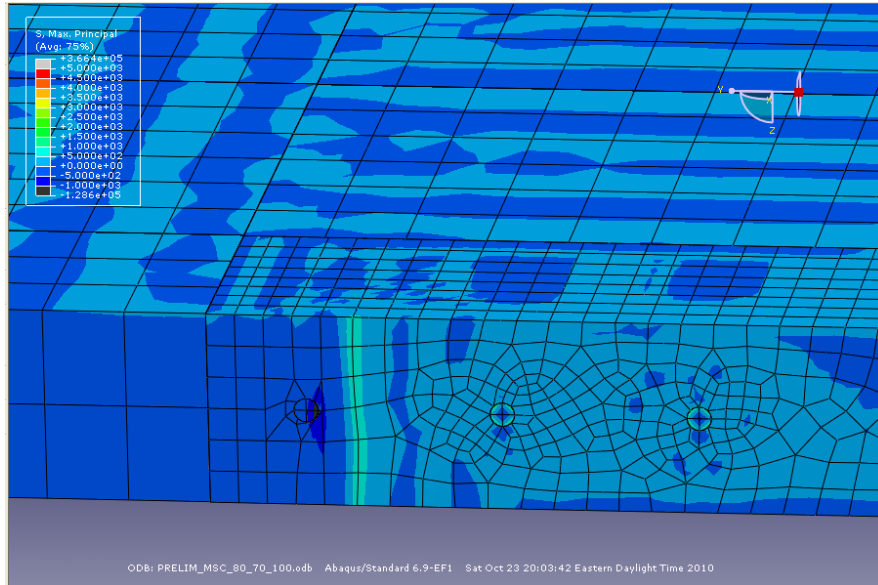


**Figure A162.** Longitudinal shear cracking model in which  $T_M=80^\circ\text{F}$ ,  $T_S=70^\circ\text{F}$ , and  $T_C=100^\circ\text{F}$  for a mortar intrusion of 7 in and a CTE of  $4 \times 10^{-6}/^\circ\text{F}$ .

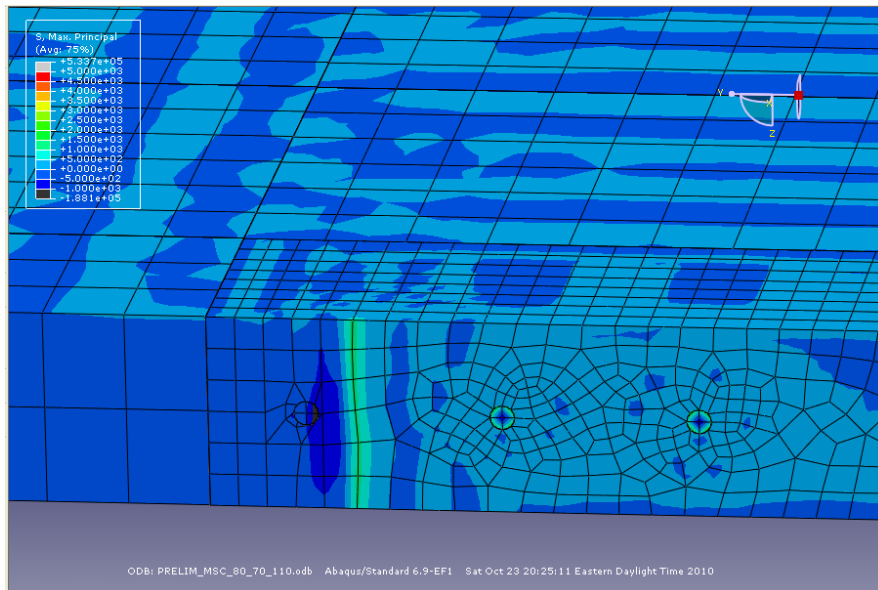


**Figure A163.** Longitudinal shear cracking model in which  $T_M=80^\circ\text{F}$ ,  $T_S=70^\circ\text{F}$ , and  $T_C=110^\circ\text{F}$  for a mortar intrusion of 7 in and a CTE of  $4 \times 10^{-6}/^\circ\text{F}$ .

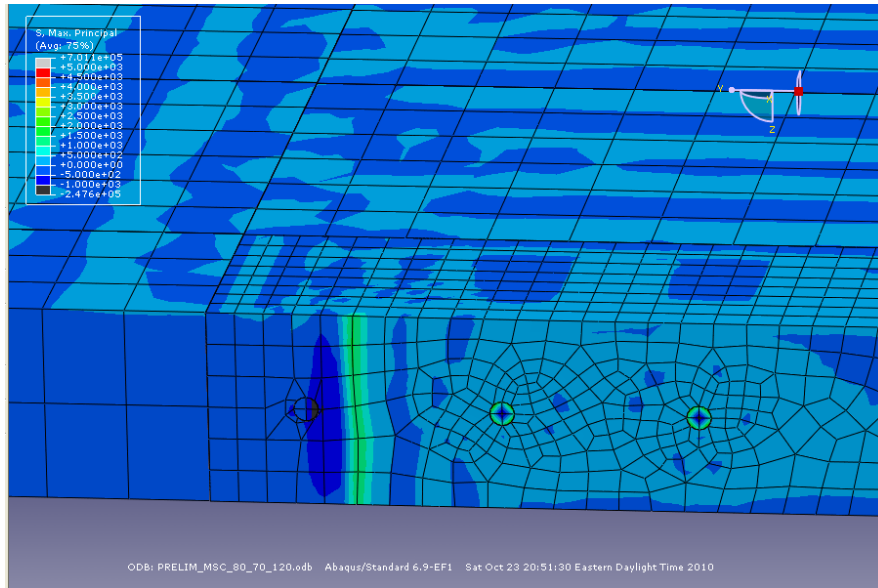


**Figure A164.** Longitudinal shear cracking model in which  $T_M=80^\circ\text{F}$ ,  $T_S=70^\circ\text{F}$ , and  $T_C=120^\circ\text{F}$  for a mortar intrusion of 7 in and a CTE of  $4 \times 10^{-6}/^\circ\text{F}$ .

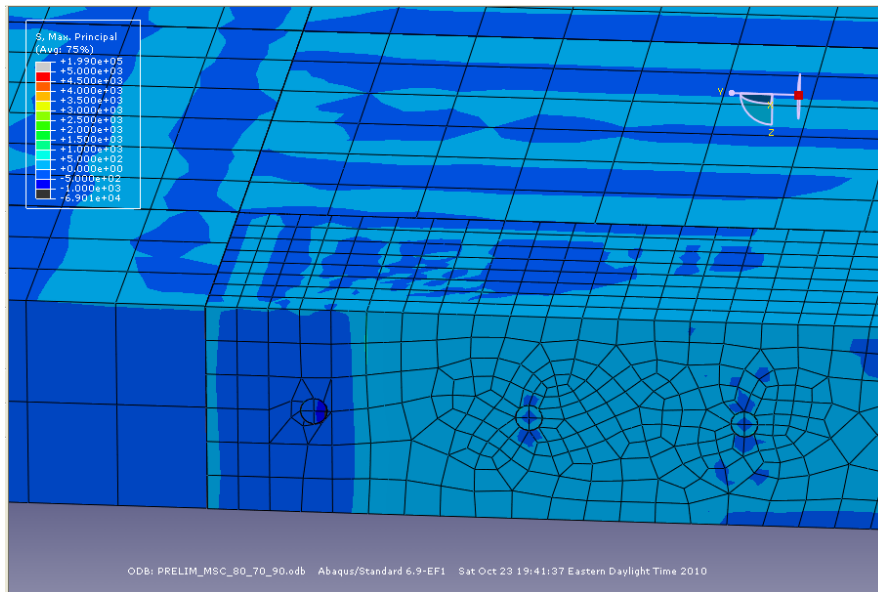


**Figure A165.** Longitudinal shear cracking model in which  $T_M=80^\circ\text{F}$ ,  $T_S=70^\circ\text{F}$ , and  $T_C=90^\circ\text{F}$  for a mortar intrusion of 7 in and a CTE of  $4 \times 10^{-6}/^\circ\text{F}$ .

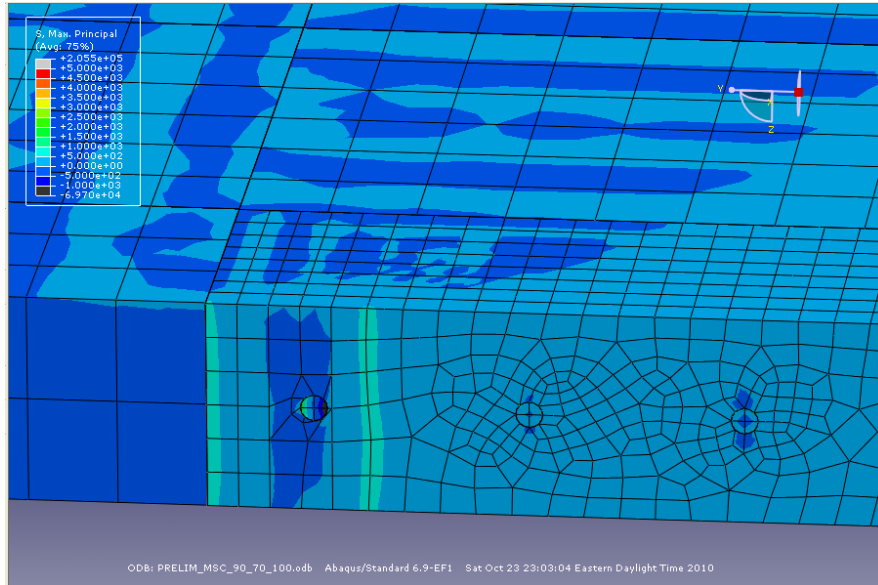


**Figure A166.** Longitudinal shear cracking model in which  $T_M=90^\circ\text{F}$ ,  $T_S=70^\circ\text{F}$ , and  $T_C=100^\circ\text{F}$  for a mortar intrusion of 7 in and a CTE of  $4 \times 10^{-6}/^\circ\text{F}$ .

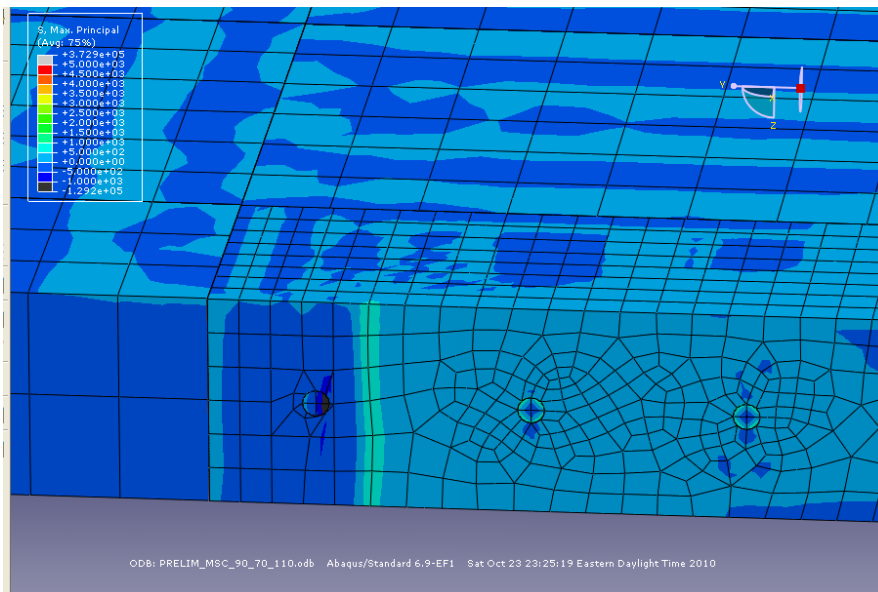


**Figure A167.** Longitudinal shear cracking model in which  $T_M=90^\circ\text{F}$ ,  $T_S=70^\circ\text{F}$ , and  $T_C=110^\circ\text{F}$  for a mortar intrusion of 7 in and a CTE of  $4 \times 10^{-6}/^\circ\text{F}$ .

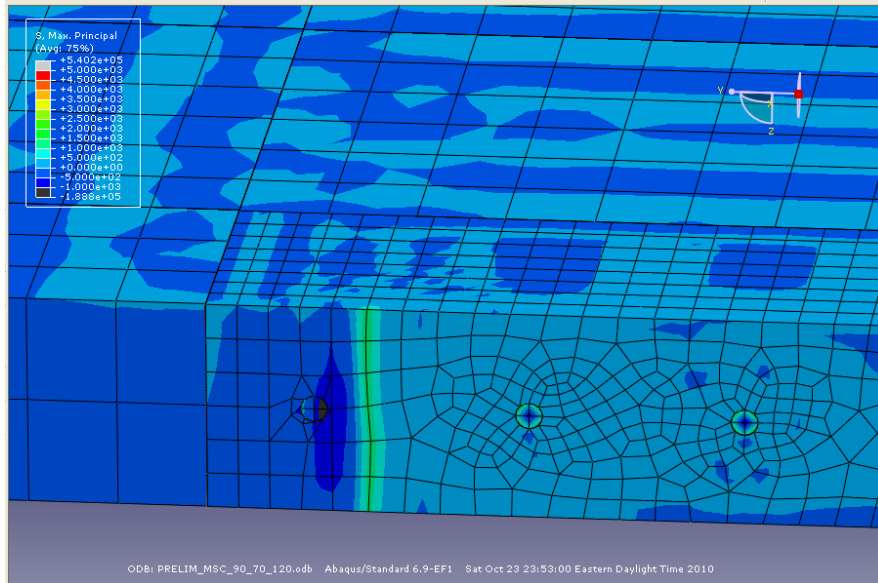


**Figure A168.** Longitudinal shear cracking model in which  $T_M=90^\circ\text{F}$ ,  $T_S=70^\circ\text{F}$ , and  $T_C=120^\circ\text{F}$  for a mortar intrusion of 7 in and a CTE of  $4 \times 10^{-6}/^\circ\text{F}$ .

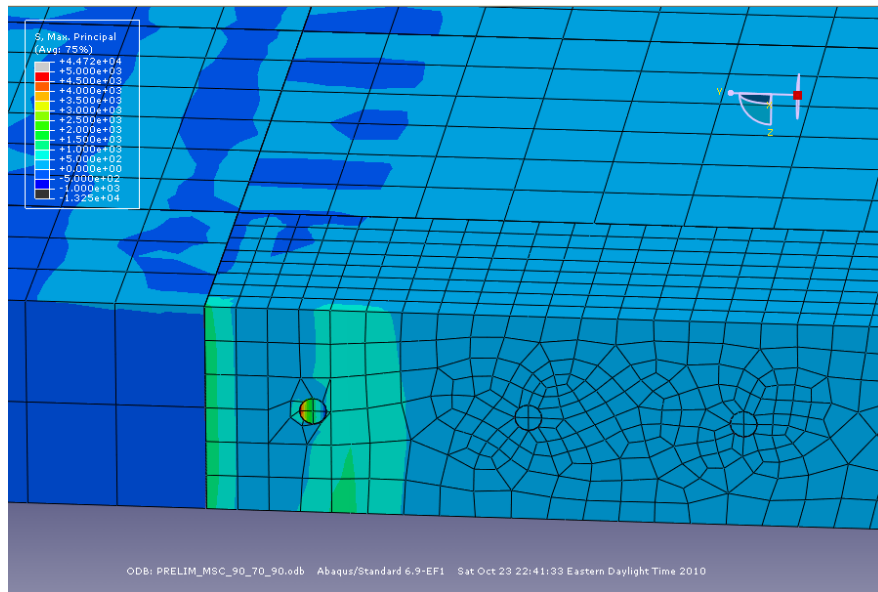


**Figure A169.** Longitudinal shear cracking model in which  $T_M=90^\circ\text{F}$ ,  $T_S=70^\circ\text{F}$ , and  $T_C=90^\circ\text{F}$  for a mortar intrusion of 7 in and a CTE of  $4 \times 10^{-6}/^\circ\text{F}$ .

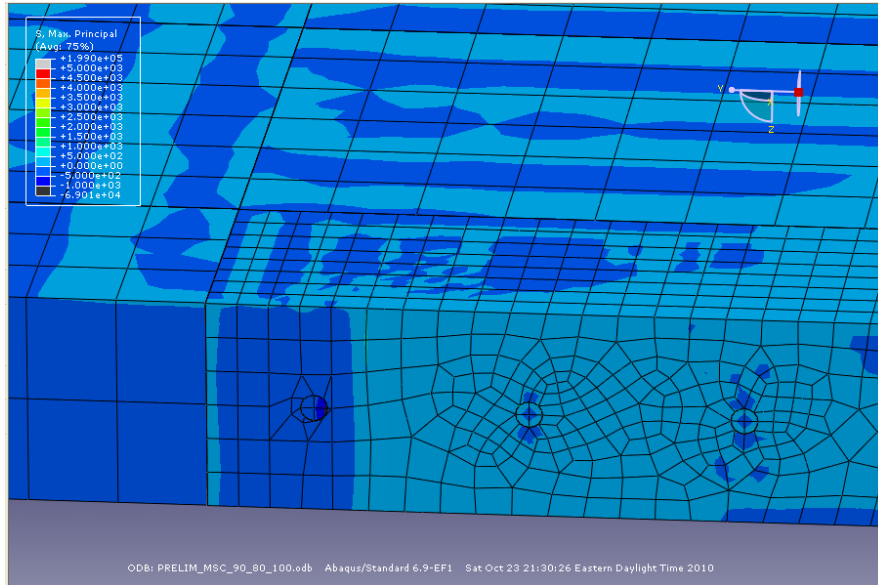


**Figure A170.** Longitudinal shear cracking model in which  $T_M=90^\circ\text{F}$ ,  $T_S=80^\circ\text{F}$ , and  $T_C=100^\circ\text{F}$  for a mortar intrusion of 7 in and a CTE of  $4 \times 10^{-6}/^\circ\text{F}$ .

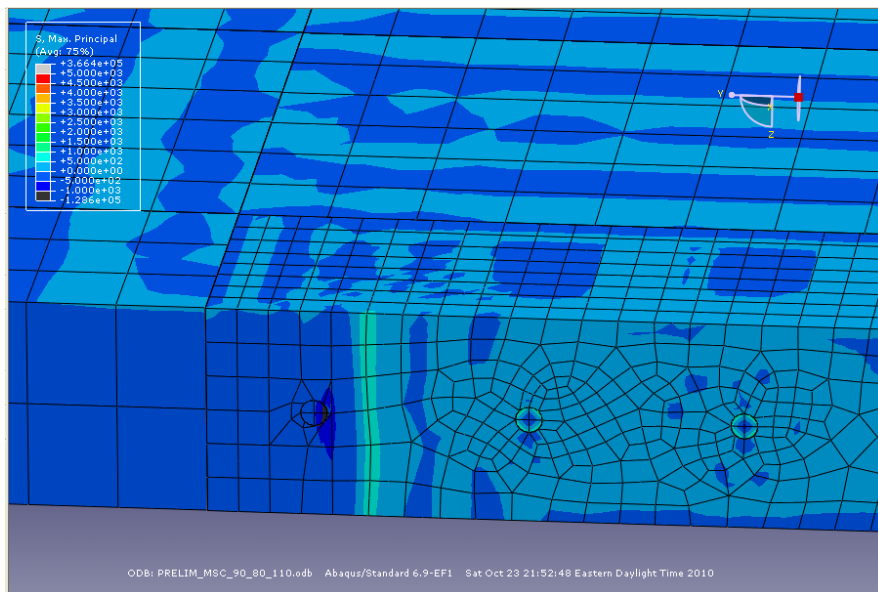


**Figure A171.** Longitudinal shear cracking model in which  $T_M=90^\circ\text{F}$ ,  $T_S=80^\circ\text{F}$ , and  $T_C=110^\circ\text{F}$  for a mortar intrusion of 7 in and a CTE of  $4 \times 10^{-6}/^\circ\text{F}$ .

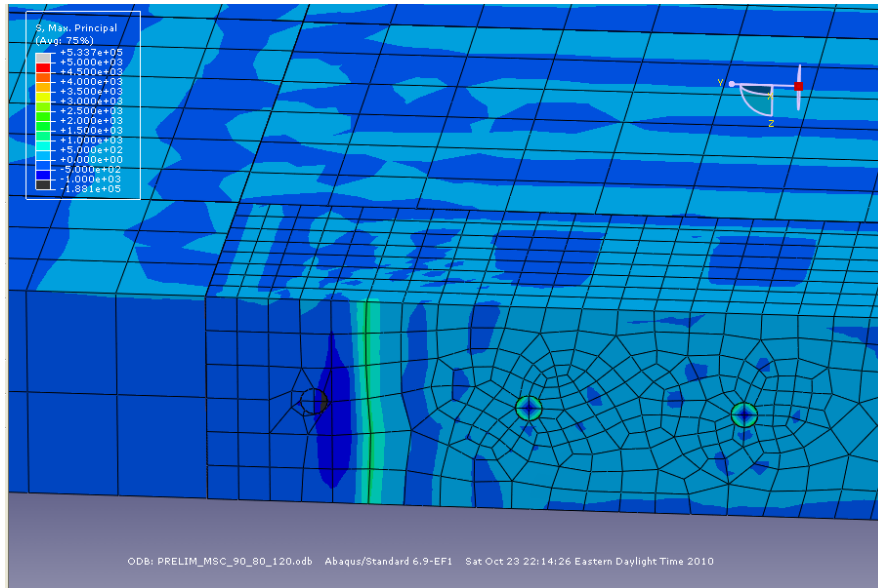


**Figure A172.** Longitudinal shear cracking model in which  $T_M=90^\circ\text{F}$ ,  $T_S=80^\circ\text{F}$ , and  $T_C=120^\circ\text{F}$  for a mortar intrusion of 7 in and a CTE of  $4 \times 10^{-6}/^\circ\text{F}$ .

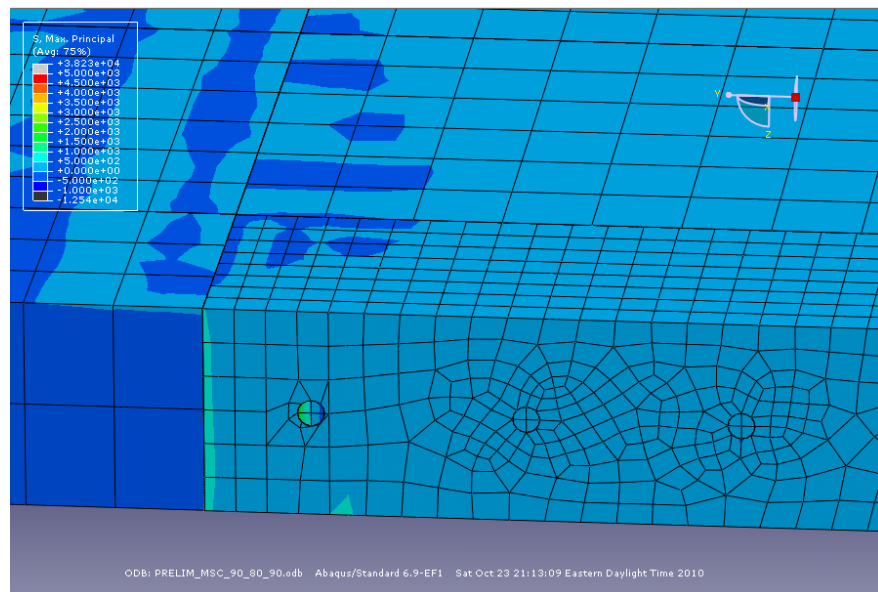


**Figure A173.** Longitudinal shear cracking model in which  $T_M=90^\circ\text{F}$ ,  $T_S=80^\circ\text{F}$ , and  $T_C=90^\circ\text{F}$  for a mortar intrusion of 7 in and a CTE of  $4 \times 10^{-6}/^\circ\text{F}$ .

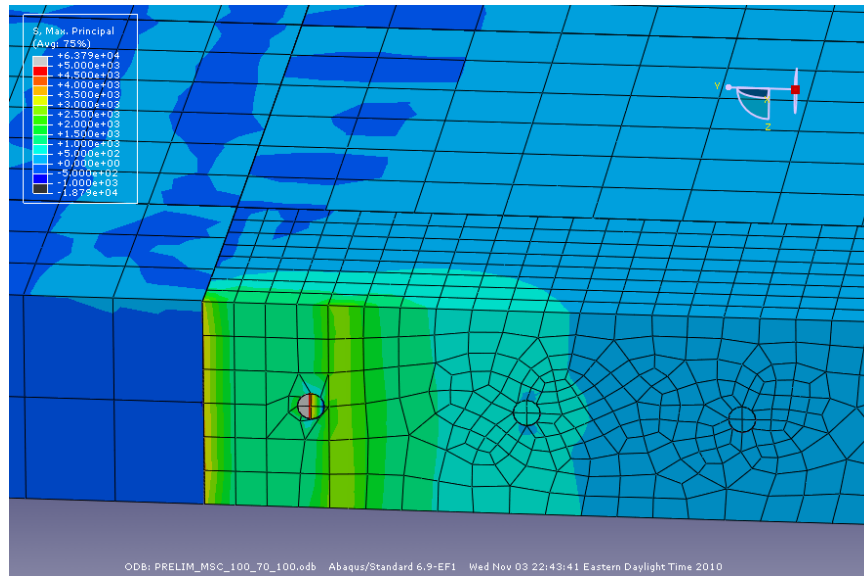


**Figure A174.** Longitudinal shear cracking model in which  $T_M=100^\circ\text{F}$ ,  $T_S=70^\circ\text{F}$ , and  $T_C=100^\circ\text{F}$  for a mortar intrusion of 7 in and a CTE of  $6.5 \times 10^{-6}/^\circ\text{F}$ .

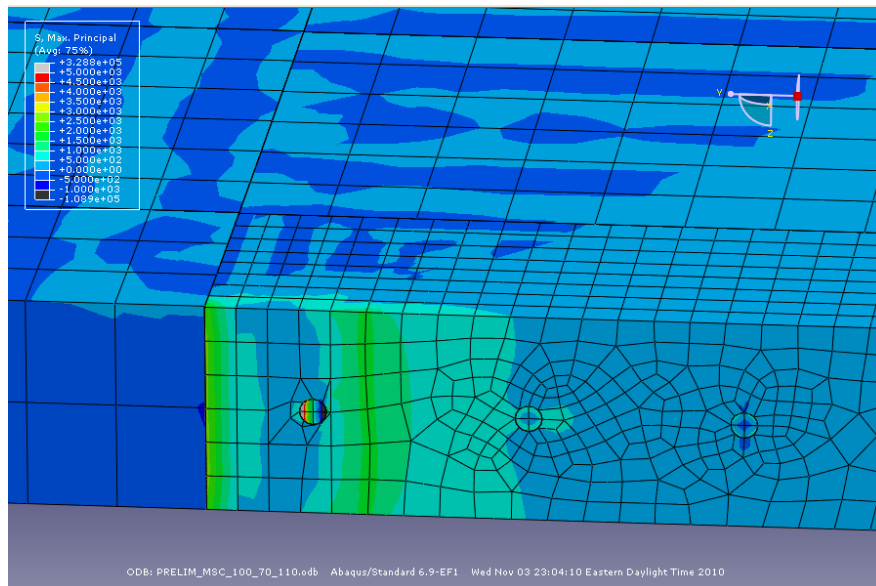


**Figure A175.** Longitudinal shear cracking model in which  $T_M=100^\circ\text{F}$ ,  $T_S=70^\circ\text{F}$ , and  $T_C=110^\circ\text{F}$  for a mortar intrusion of 7 in and a CTE of  $6.5 \times 10^{-6}/^\circ\text{F}$ .

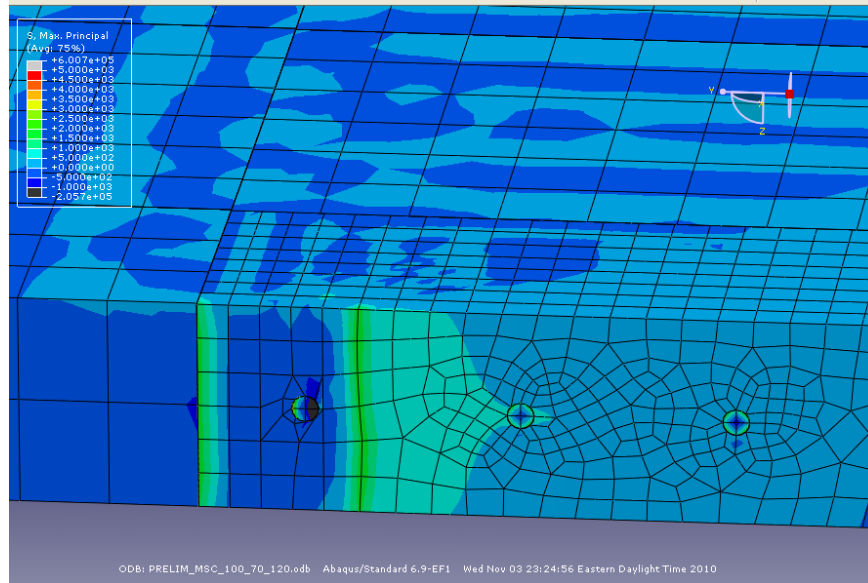


**Figure A176.** Longitudinal shear cracking model in which  $T_M=100^\circ\text{F}$ ,  $T_S=70^\circ\text{F}$ , and  $T_C=120^\circ\text{F}$  for a mortar intrusion of 7 in and a CTE of  $6.5 \times 10^{-6}/^\circ\text{F}$ .

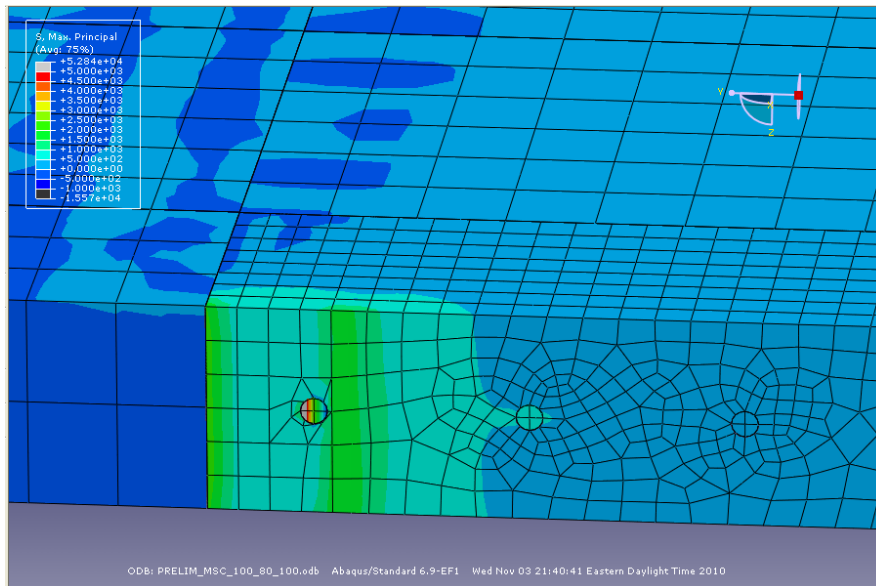


**Figure A177.** Longitudinal shear cracking model in which  $T_M=100^\circ\text{F}$ ,  $T_S=80^\circ\text{F}$ , and  $T_C=100^\circ\text{F}$  for a mortar intrusion of 7 in and a CTE of  $6.5 \times 10^{-6}/^\circ\text{F}$ .

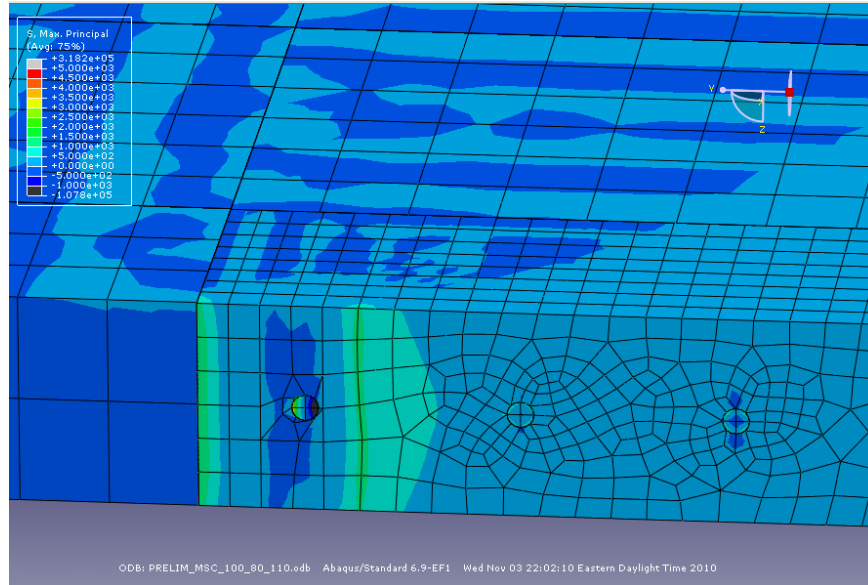


**Figure A178.** Longitudinal shear cracking model in which  $T_M=100^\circ\text{F}$ ,  $T_S=80^\circ\text{F}$ , and  $T_C=110^\circ\text{F}$  for a mortar intrusion of 7 in and a CTE of  $6.5 \times 10^{-6}/^\circ\text{F}$ .

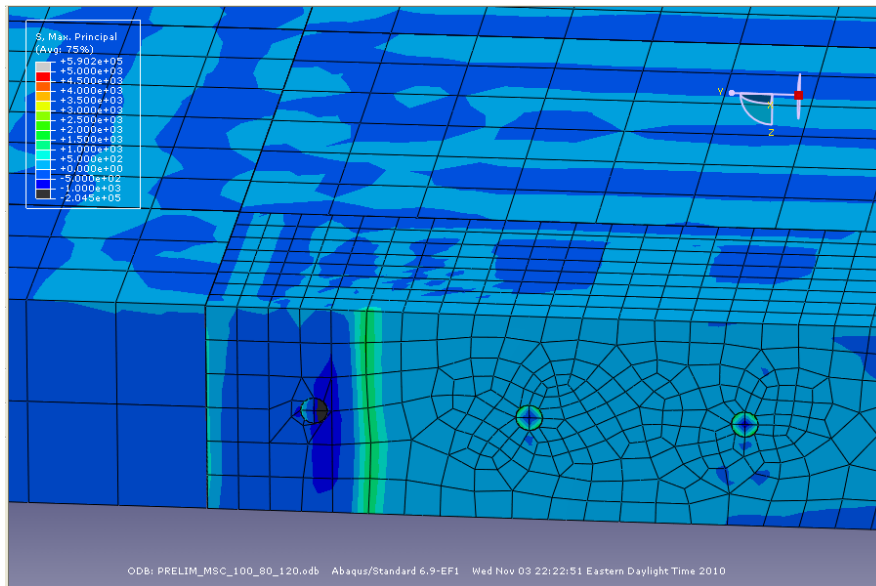


**Figure A179.** Longitudinal shear cracking model in which  $T_M=100^\circ\text{F}$ ,  $T_S=80^\circ\text{F}$ , and  $T_C=120^\circ\text{F}$  for a mortar intrusion of 7 in and a CTE of  $6.5 \times 10^{-6}/^\circ\text{F}$ .

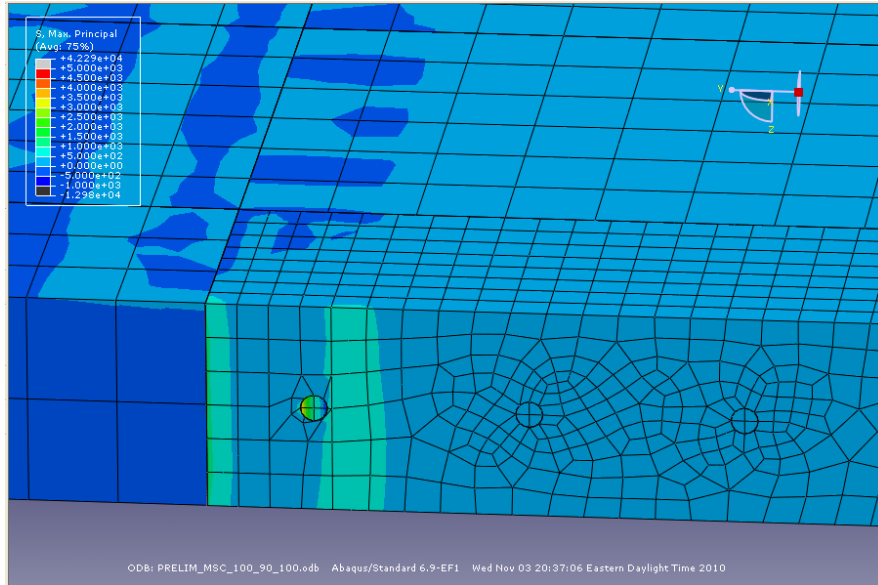


**Figure A180.** Longitudinal shear cracking model in which  $T_M=100^\circ\text{F}$ ,  $T_S=90^\circ\text{F}$ , and  $T_C=100^\circ\text{F}$  for a mortar intrusion of 7 in and a CTE of  $6.5 \times 10^{-6}/^\circ\text{F}$ .

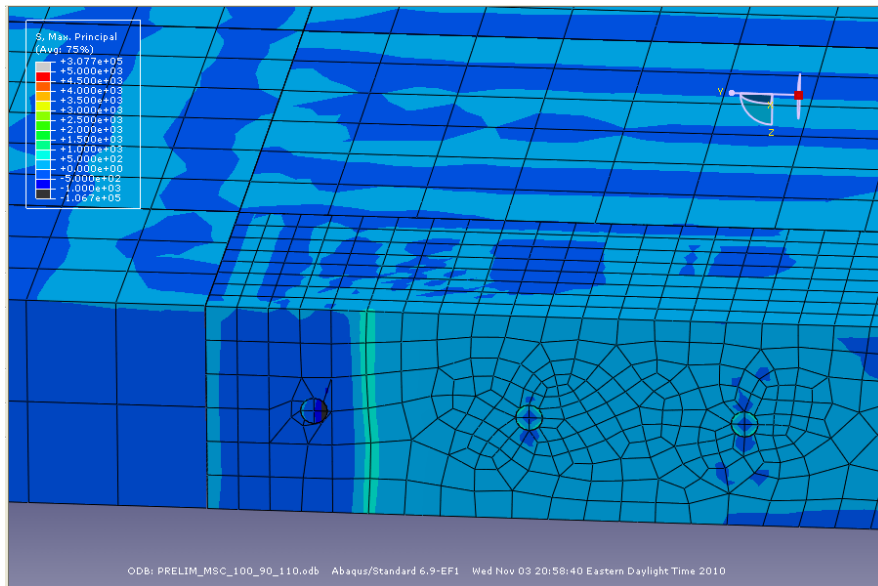


**Figure A181.** Longitudinal shear cracking model in which  $T_M=100^\circ\text{F}$ ,  $T_S=90^\circ\text{F}$ , and  $T_C=110^\circ\text{F}$  for a mortar intrusion of 7 in and a CTE of  $6.5 \times 10^{-6}/^\circ\text{F}$ .

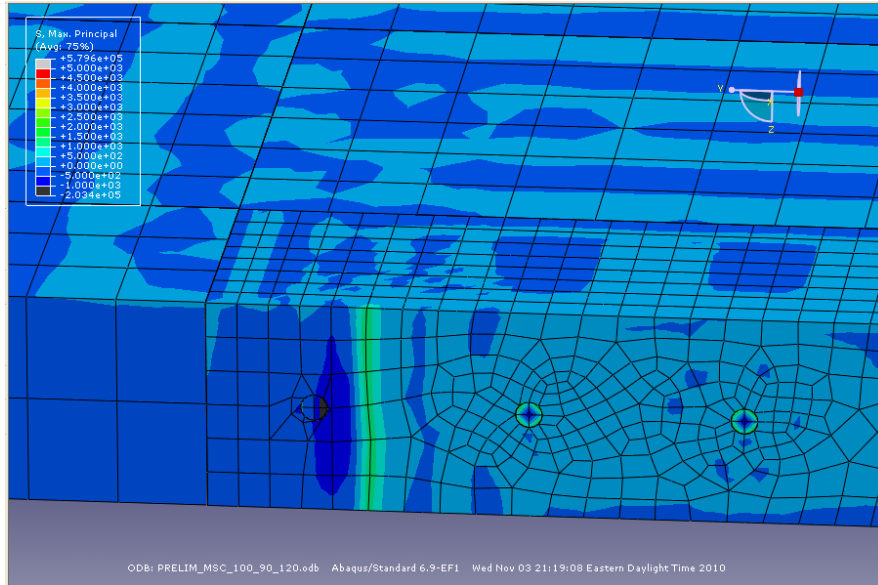


**Figure A182.** Longitudinal shear cracking model in which  $T_M=100^\circ\text{F}$ ,  $T_S=90^\circ\text{F}$ , and  $T_C=120^\circ\text{F}$  for a mortar intrusion of 7 in and a CTE of  $6.5 \times 10^{-6}/^\circ\text{F}$ .

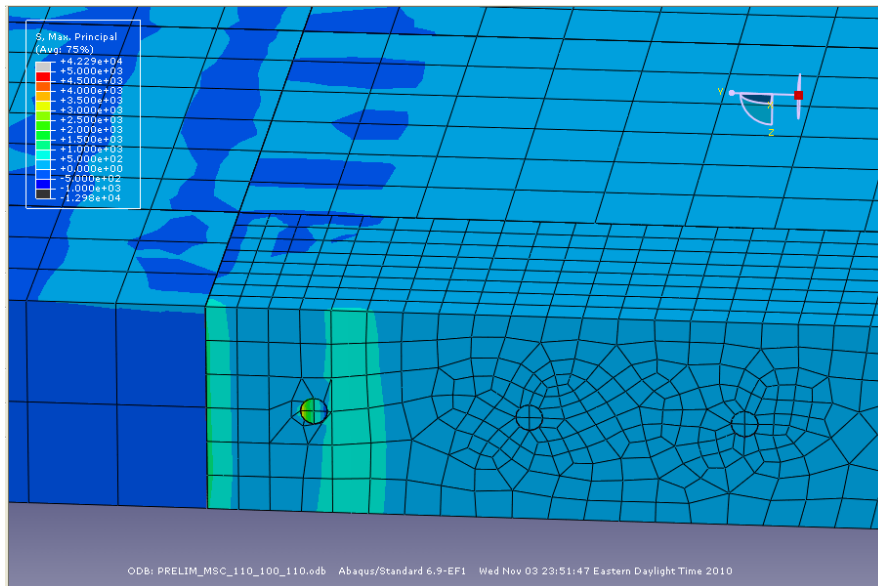


**Figure A183.** Longitudinal shear cracking model in which  $T_M=110^\circ\text{F}$ ,  $T_S=100^\circ\text{F}$ , and  $T_C=110^\circ\text{F}$  for a mortar intrusion of 7 in and a CTE of  $6.5 \times 10^{-6}/^\circ\text{F}$ .

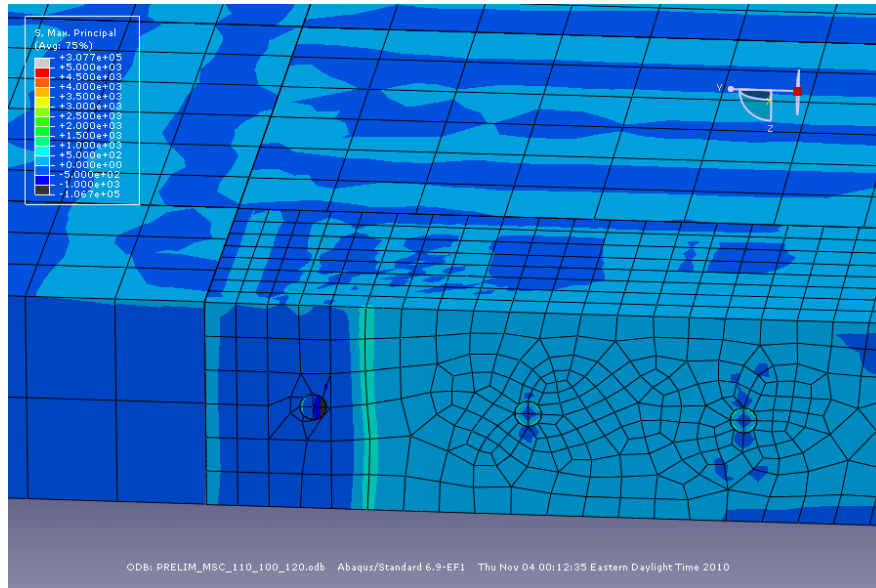


**Figure A184.** Longitudinal shear cracking model in which  $T_M=110^\circ\text{F}$ ,  $T_S=100^\circ\text{F}$ , and  $T_C=120^\circ\text{F}$  for a mortar intrusion of 7 in and a CTE of  $6.5 \times 10^{-6}/^\circ\text{F}$ .

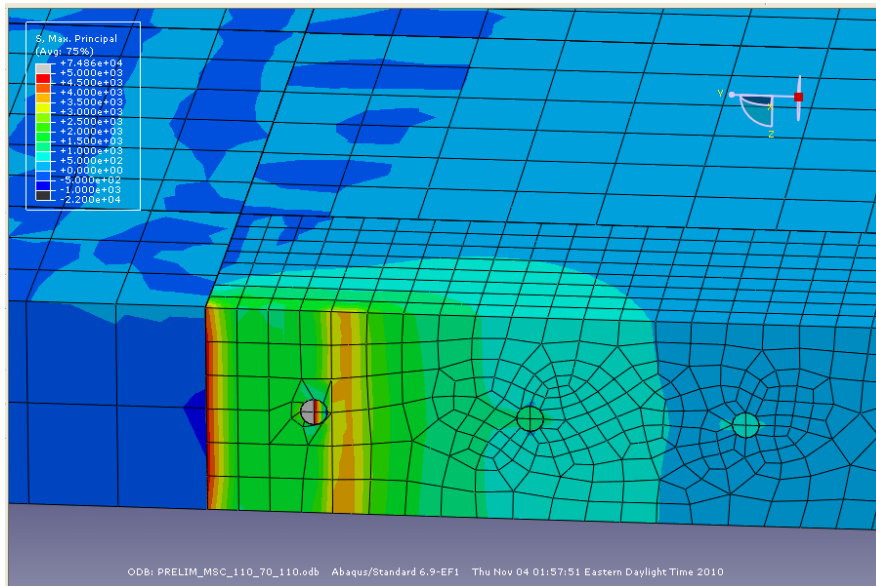


**Figure A185.** Longitudinal shear cracking model in which  $T_M=110^\circ\text{F}$ ,  $T_S=70^\circ\text{F}$ , and  $T_C=110^\circ\text{F}$  for a mortar intrusion of 7 in and a CTE of  $6.5 \times 10^{-6}/^\circ\text{F}$ .

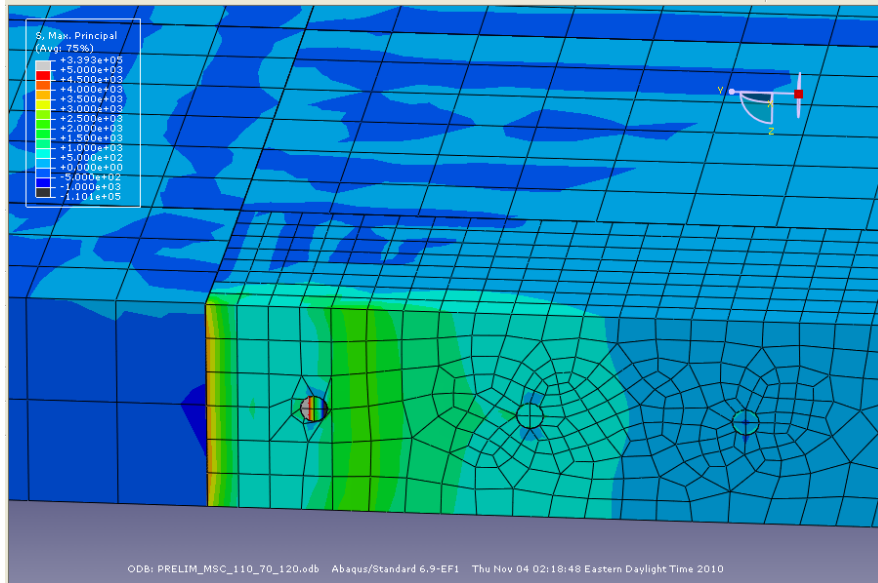


**Figure A186.** Longitudinal shear cracking model in which  $T_M=110^\circ\text{F}$ ,  $T_S=70^\circ\text{F}$ , and  $T_C=120^\circ\text{F}$  for a mortar intrusion of 7 in and a CTE of  $6.5 \times 10^{-6}/^\circ\text{F}$ .

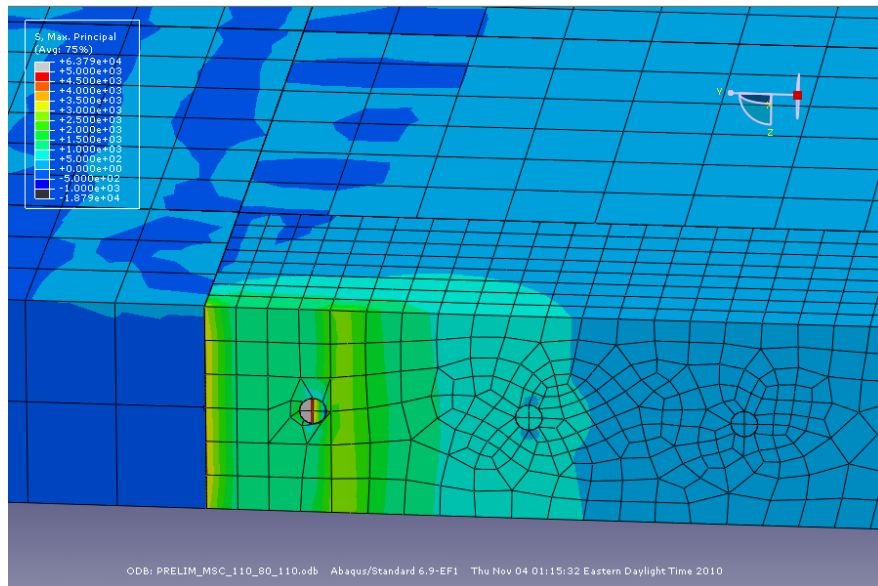


**Figure A187.** Longitudinal shear cracking model in which  $T_M=110^\circ\text{F}$ ,  $T_S=80^\circ\text{F}$ , and  $T_C=110^\circ\text{F}$  for a mortar intrusion of 7 in and a CTE of  $6.5 \times 10^{-6}/^\circ\text{F}$ .

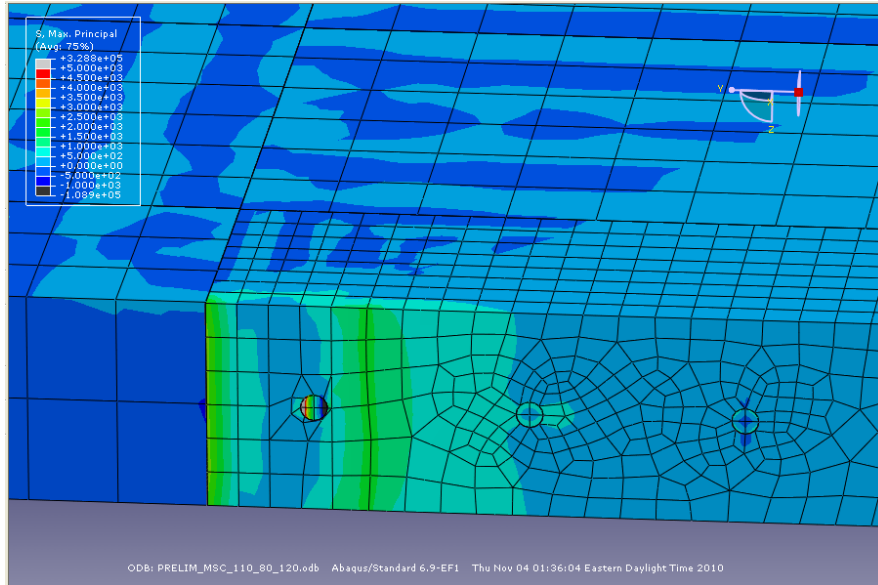


**Figure A188.** Longitudinal shear cracking model in which  $T_M=110^\circ\text{F}$ ,  $T_S=80^\circ\text{F}$ , and  $T_C=120^\circ\text{F}$  for a mortar intrusion of 7 in and a CTE of  $6.5 \times 10^{-6}/^\circ\text{F}$ .

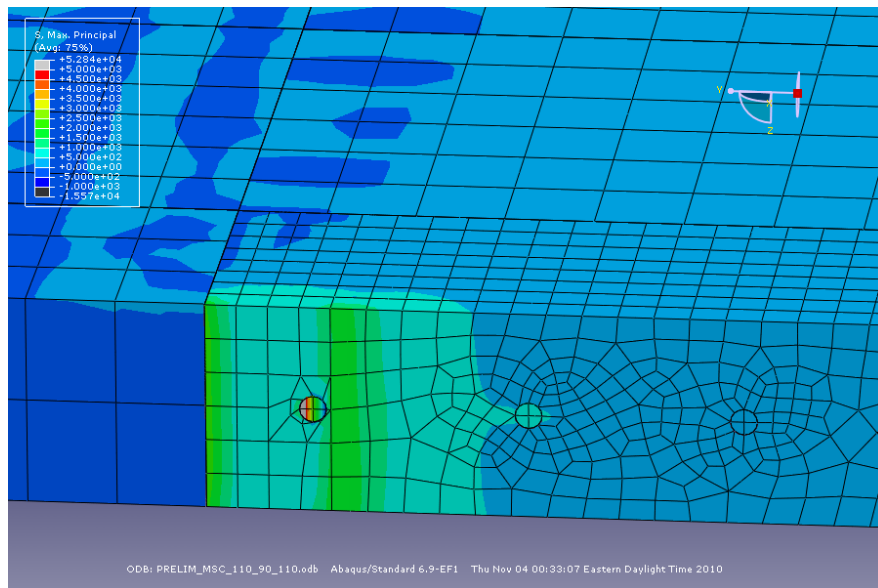


**Figure A189.** Longitudinal shear cracking model in which  $T_M=110^\circ\text{F}$ ,  $T_S=90^\circ\text{F}$ , and  $T_C=110^\circ\text{F}$  for a mortar intrusion of 7 in and a CTE of  $6.5 \times 10^{-6}/^\circ\text{F}$ .

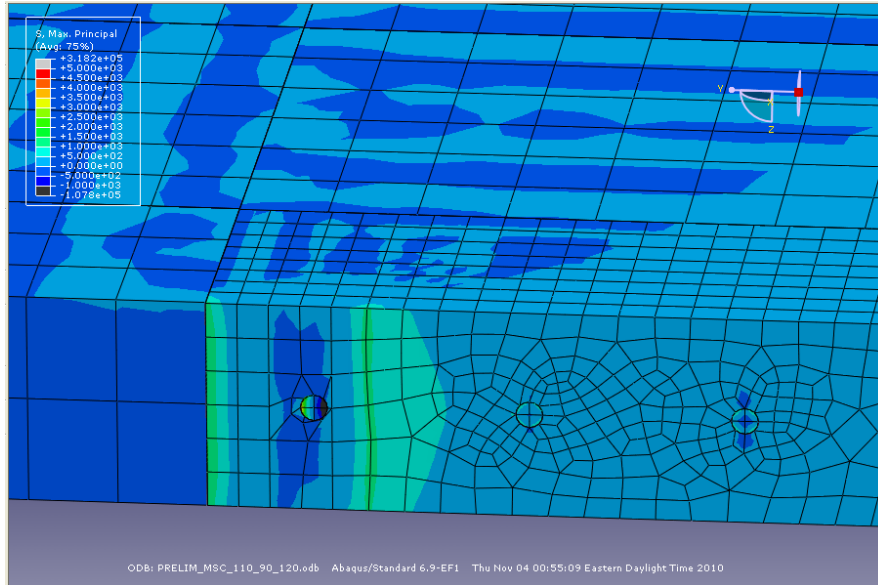


**Figure A190.** Longitudinal shear cracking model in which  $T_M=110^\circ\text{F}$ ,  $T_S=90^\circ\text{F}$ , and  $T_C=120^\circ\text{F}$  for a mortar intrusion of 7 in and a CTE of  $6.5 \times 10^{-6}/^\circ\text{F}$ .

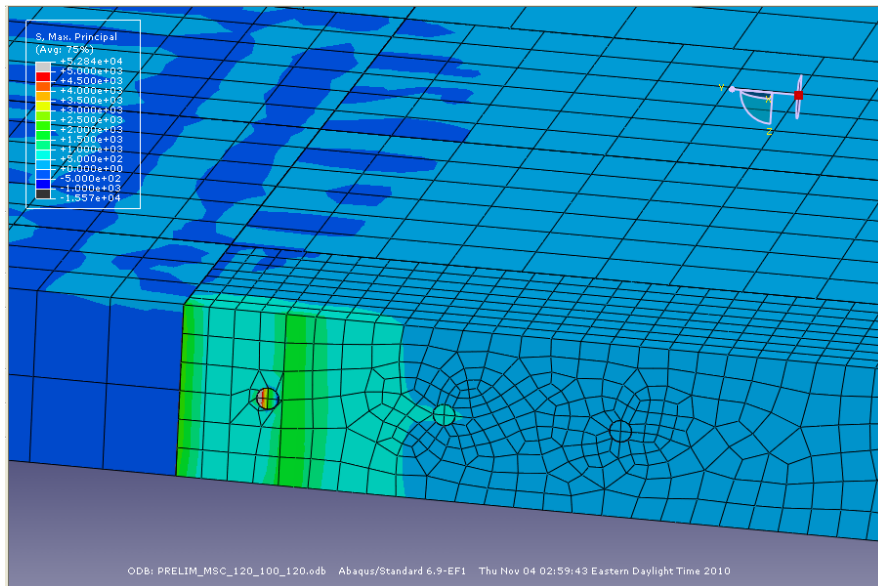


**Figure A191.** Longitudinal shear cracking model in which  $T_M=120^\circ\text{F}$ ,  $T_S=100^\circ\text{F}$ , and  $T_C=120^\circ\text{F}$  for a mortar intrusion of 7 in and a CTE of  $6.5 \times 10^{-6}/^\circ\text{F}$ .

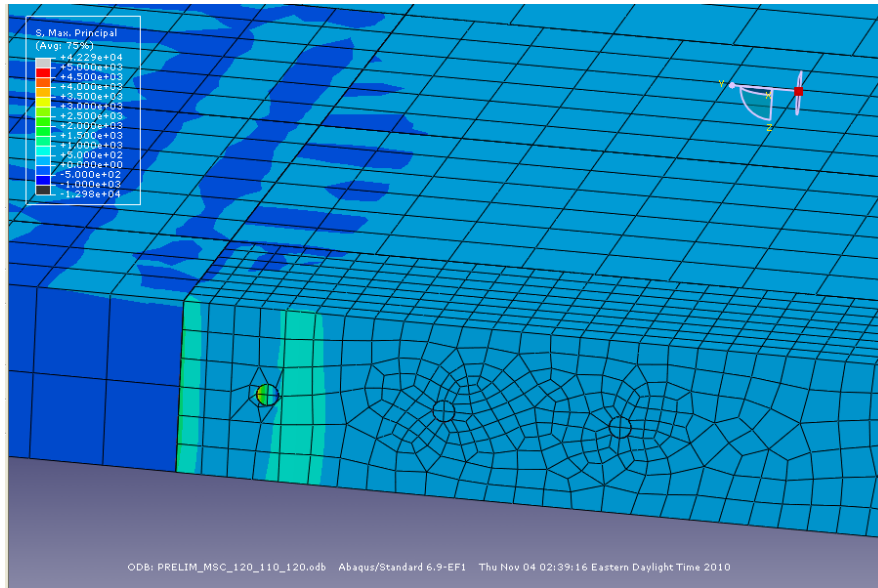


**Figure A192.** Longitudinal shear cracking model in which  $T_M=120^\circ\text{F}$ ,  $T_S=110^\circ\text{F}$ , and  $T_C=120^\circ\text{F}$  for a mortar intrusion of 7 in and a CTE of  $6.5 \times 10^{-6}/^\circ\text{F}$ .

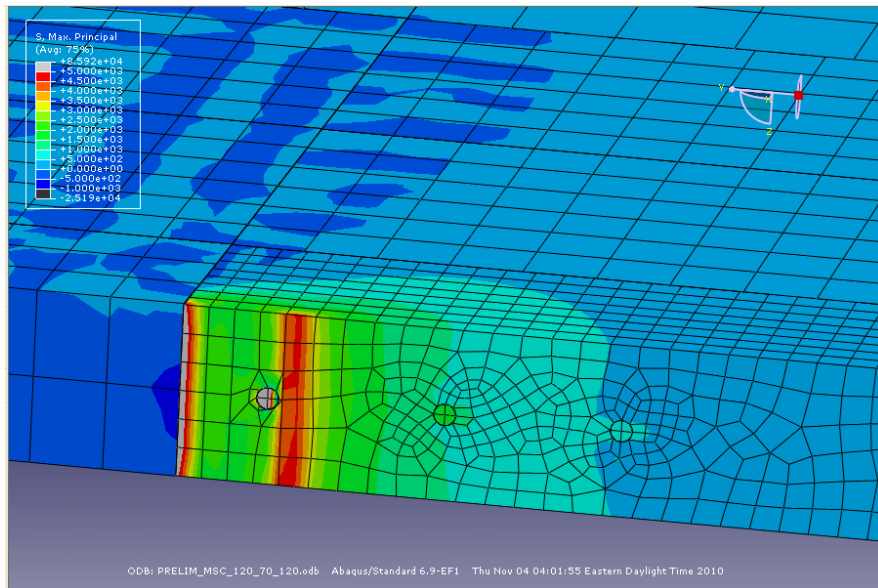


**Figure A193.** Longitudinal shear cracking model in which  $T_M=120^\circ\text{F}$ ,  $T_S=70^\circ\text{F}$ , and  $T_C=120^\circ\text{F}$  for a mortar intrusion of 7 in and a CTE of  $6.5 \times 10^{-6}/^\circ\text{F}$ .

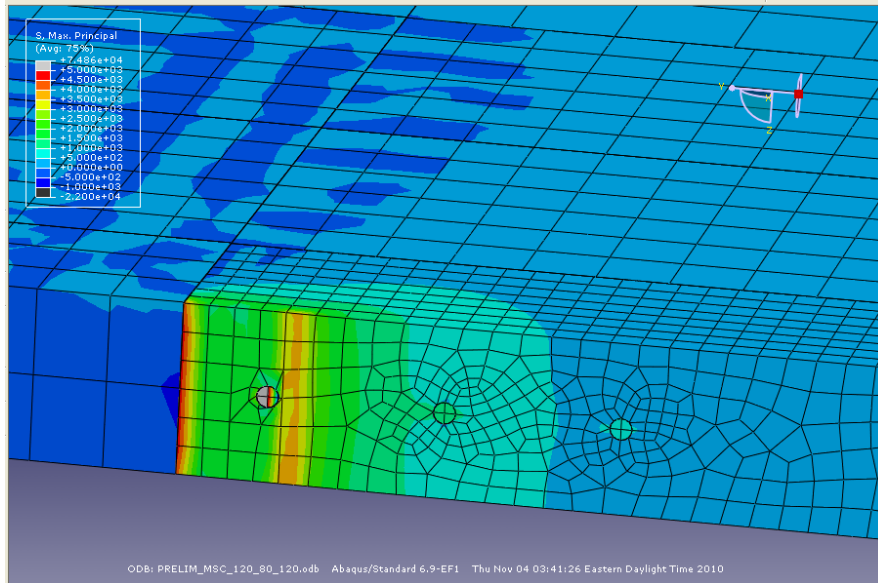


**Figure A194.** Longitudinal shear cracking model in which  $T_M=120^\circ\text{F}$ ,  $T_S=80^\circ\text{F}$ , and  $T_C=120^\circ\text{F}$  for a mortar intrusion of 7 in and a CTE of  $6.5 \times 10^{-6}/^\circ\text{F}$ .

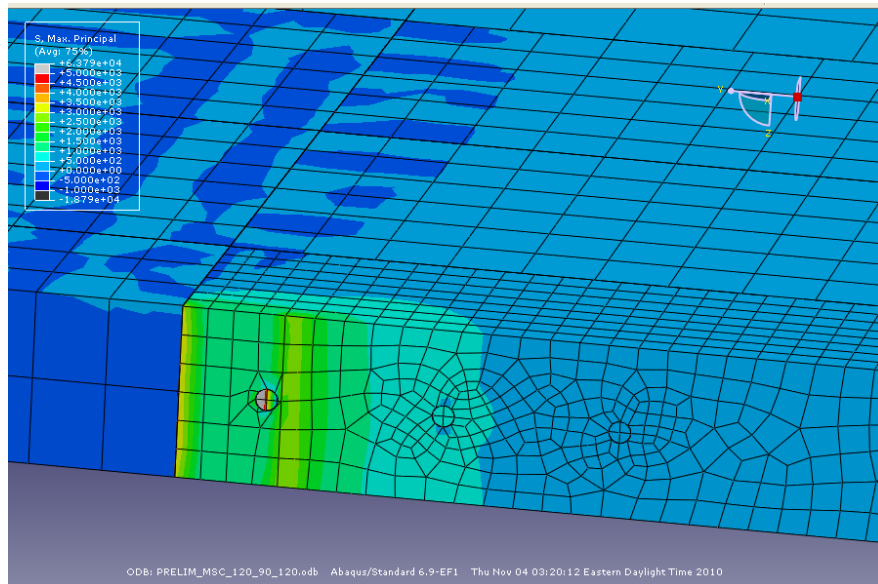


**Figure A195.** Longitudinal shear cracking model in which  $T_M=120^\circ\text{F}$ ,  $T_S=90^\circ\text{F}$ , and  $T_C=120^\circ\text{F}$  for a mortar intrusion of 7 in and a CTE of  $6.5 \times 10^{-6}/^\circ\text{F}$ .

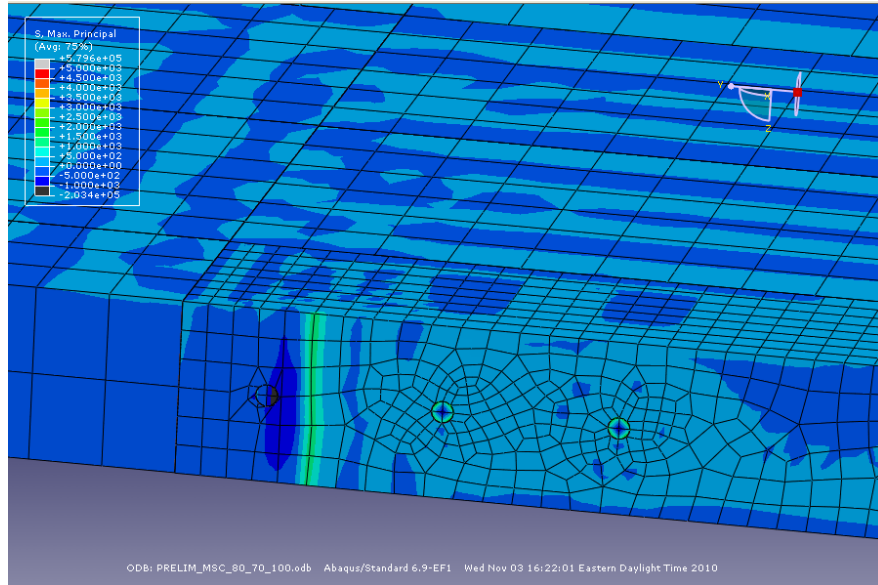


**Figure A196.** Longitudinal shear cracking model in which  $T_M=80^\circ\text{F}$ ,  $T_S=70^\circ\text{F}$ , and  $T_C=100^\circ\text{F}$  for a mortar intrusion of 7 in and a CTE of  $6.5 \times 10^{-6}/^\circ\text{F}$ .

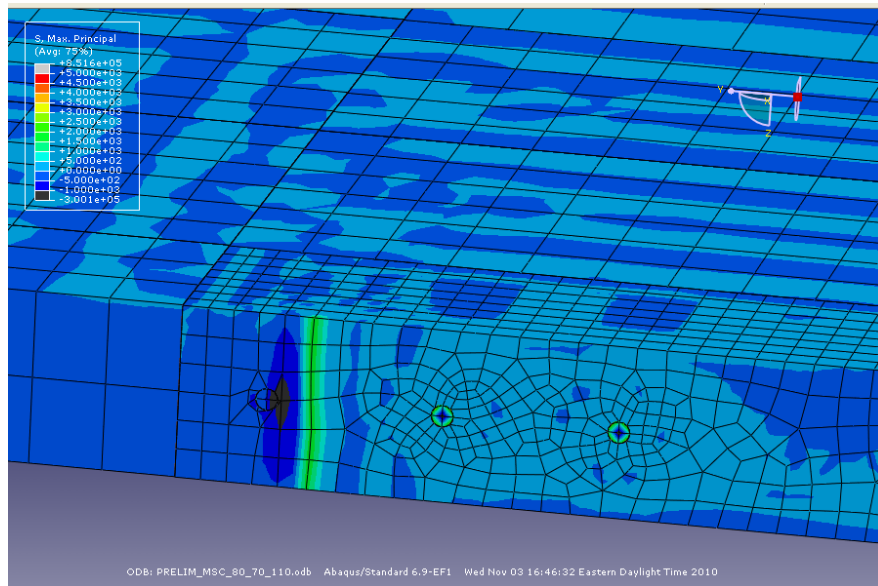


**Figure A197.** Longitudinal shear cracking model in which  $T_M=80^\circ\text{F}$ ,  $T_S=70^\circ\text{F}$ , and  $T_C=110^\circ\text{F}$  for a mortar intrusion of 7 in and a CTE of  $6.5 \times 10^{-6}/^\circ\text{F}$ .

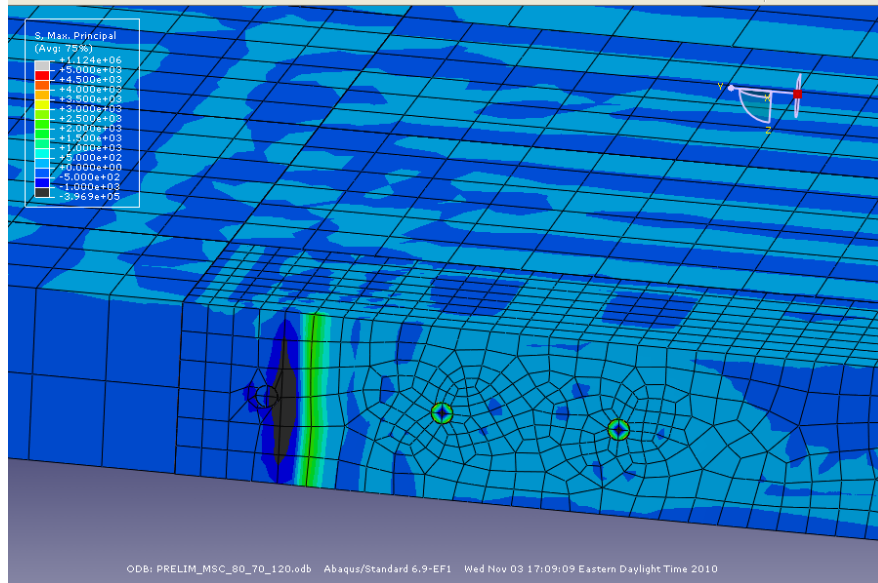


**Figure A198.** Longitudinal shear cracking model in which  $T_M=80^\circ\text{F}$ ,  $T_S=70^\circ\text{F}$ , and  $T_C=120^\circ\text{F}$  for a mortar intrusion of 7 in and a CTE of  $6.5 \times 10^{-6}/^\circ\text{F}$ .

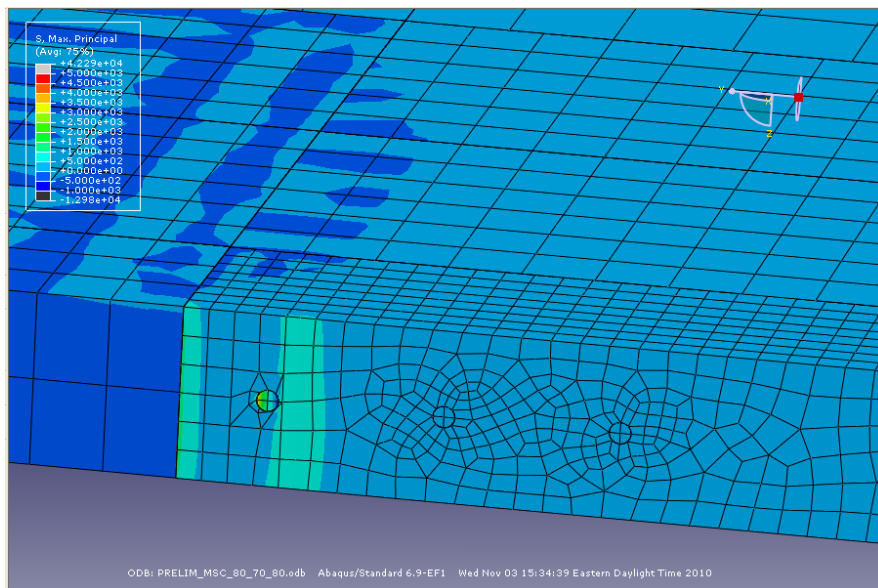


**Figure A199.** Longitudinal shear cracking model in which  $T_M=80^\circ\text{F}$ ,  $T_S=70^\circ\text{F}$ , and  $T_C=80^\circ\text{F}$  for a mortar intrusion of 7 in and a CTE of  $6.5 \times 10^{-6}/^\circ\text{F}$ .

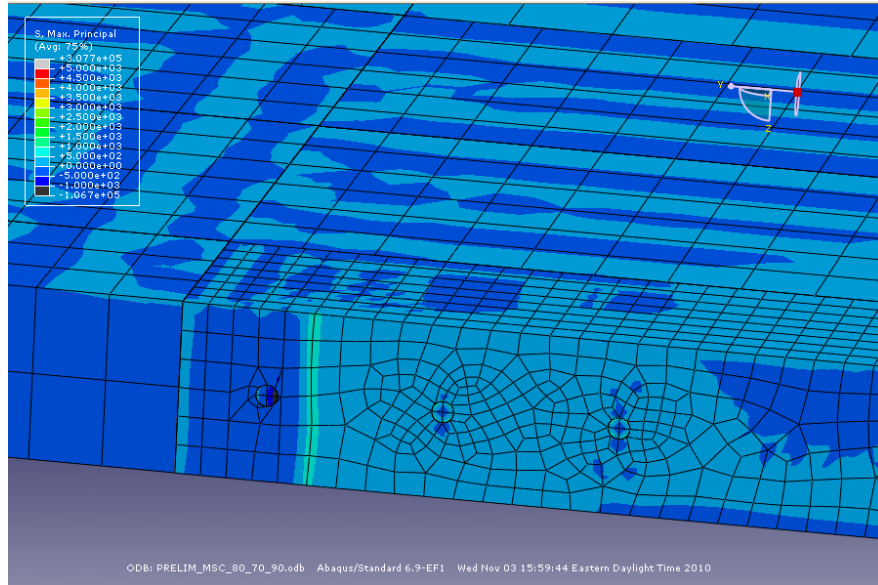


**Figure A200.** Longitudinal shear cracking model in which  $T_M=0^\circ\text{F}$ ,  $T_S=70^\circ\text{F}$ , and  $T_C=90^\circ\text{F}$  for a mortar intrusion of 7 in and a CTE of  $6.5 \times 10^{-6}/^\circ\text{F}$ .

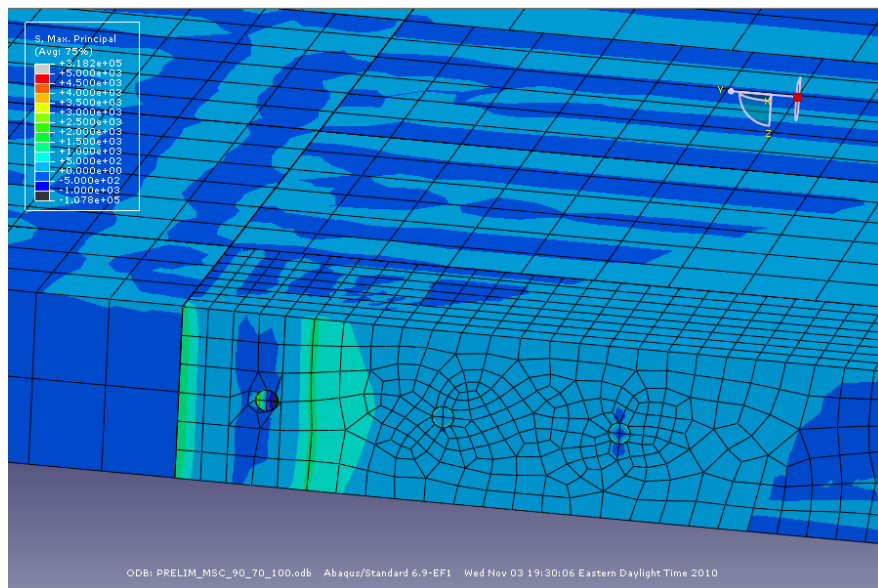


**Figure A201.** Longitudinal shear cracking model in which  $T_M=90^\circ\text{F}$ ,  $T_S=70^\circ\text{F}$ , and  $T_C=100^\circ\text{F}$  for a mortar intrusion of 7 in and a CTE of  $6.5 \times 10^{-6}/^\circ\text{F}$ .

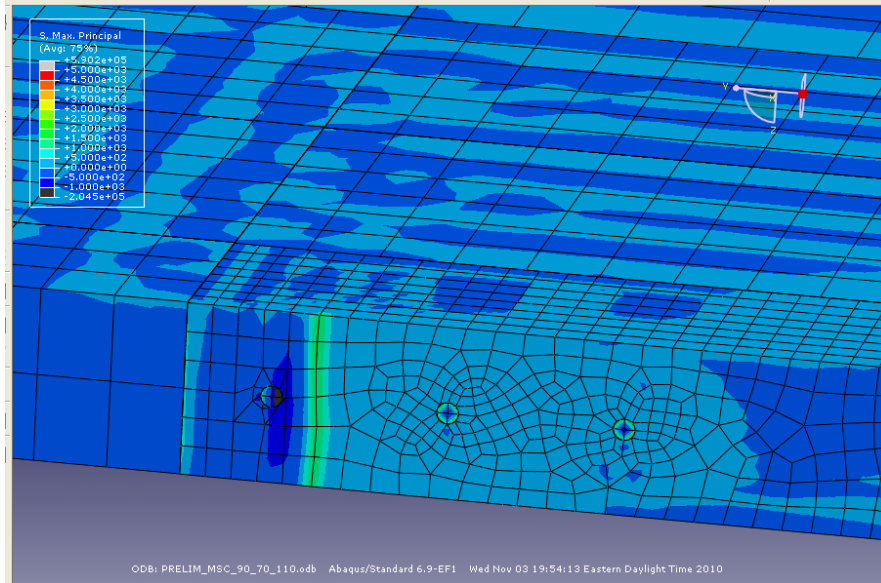


**Figure A202.** Longitudinal shear cracking model in which  $T_M=90^\circ\text{F}$ ,  $T_S=70^\circ\text{F}$ , and  $T_C=110^\circ\text{F}$  for a mortar intrusion of 7 in and a CTE of  $6.5 \times 10^{-6}/^\circ\text{F}$ .

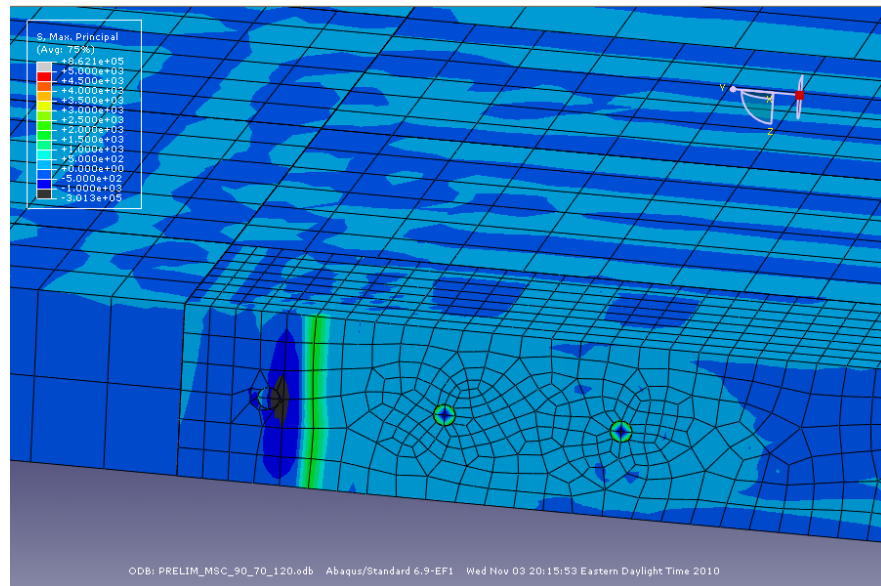


**Figure A203.** Longitudinal shear cracking model in which  $T_M=90^\circ\text{F}$ ,  $T_S=70^\circ\text{F}$ , and  $T_C=120^\circ\text{F}$  for a mortar intrusion of 7 in and a CTE of  $6.5 \times 10^{-6}/^\circ\text{F}$ .

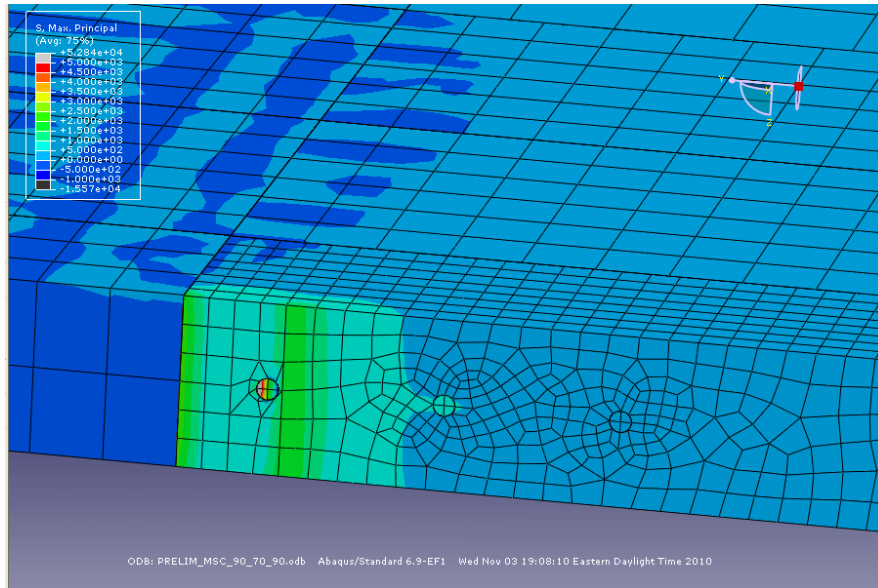


**Figure A204.** Longitudinal shear cracking model in which  $T_M=90^\circ\text{F}$ ,  $T_S=70^\circ\text{F}$ , and  $T_C=90^\circ\text{F}$  for a mortar intrusion of 7 in and a CTE of  $6.5 \times 10^{-6}/^\circ\text{F}$ .

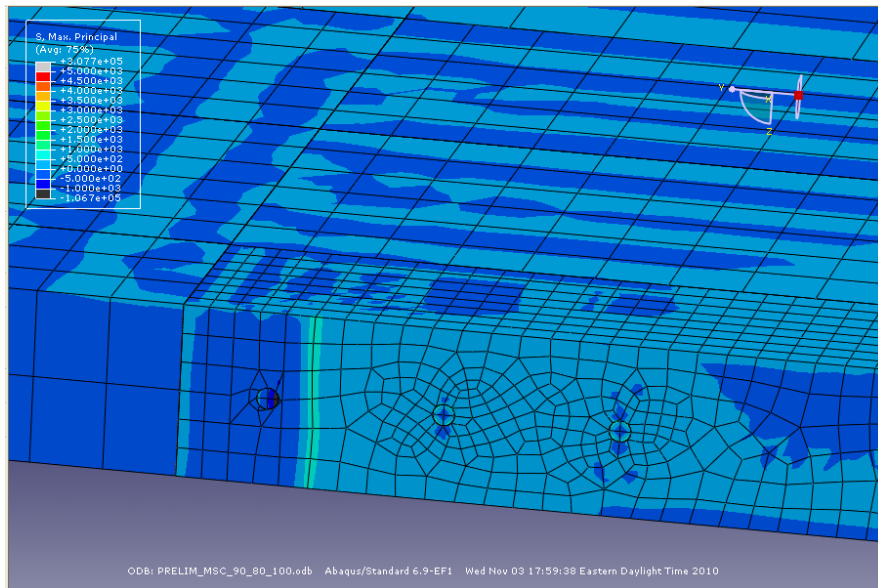


**Figure A205.** Longitudinal shear cracking model in which  $T_M=90^\circ\text{F}$ ,  $T_S=80^\circ\text{F}$ , and  $T_C=100^\circ\text{F}$  for a mortar intrusion of 7 in and a CTE of  $6.5 \times 10^{-6}/^\circ\text{F}$ .

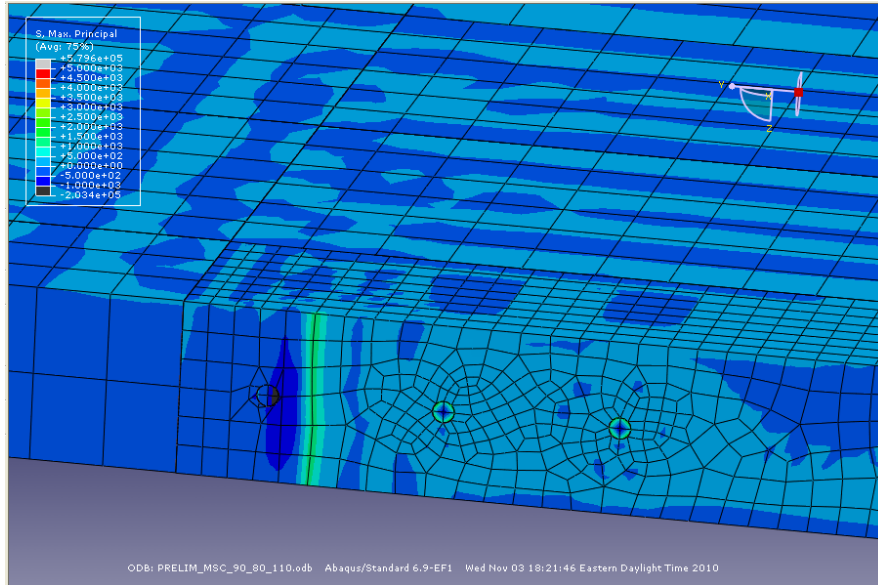


**Figure A206.** Longitudinal shear cracking model in which  $T_M=90^\circ\text{F}$ ,  $T_S=80^\circ\text{F}$ , and  $T_C=110^\circ\text{F}$  for a mortar intrusion of 7 in and a CTE of  $6.5 \times 10^{-6}/^\circ\text{F}$ .

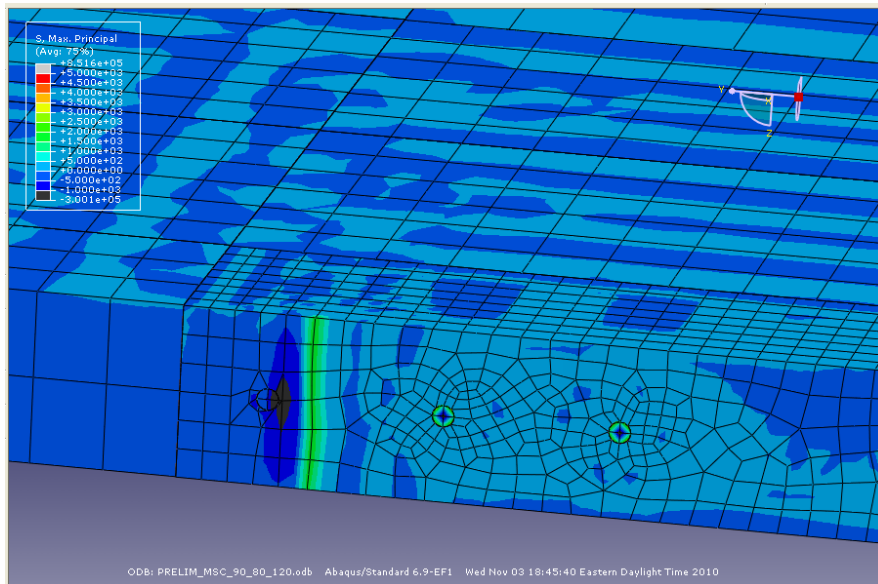


**Figure A207.** Longitudinal shear cracking model in which  $T_M=90^\circ\text{F}$ ,  $T_S=80^\circ\text{F}$ , and  $T_C=120^\circ\text{F}$  for a mortar intrusion of 7 in and a CTE of  $6.5 \times 10^{-6}/^\circ\text{F}$ .

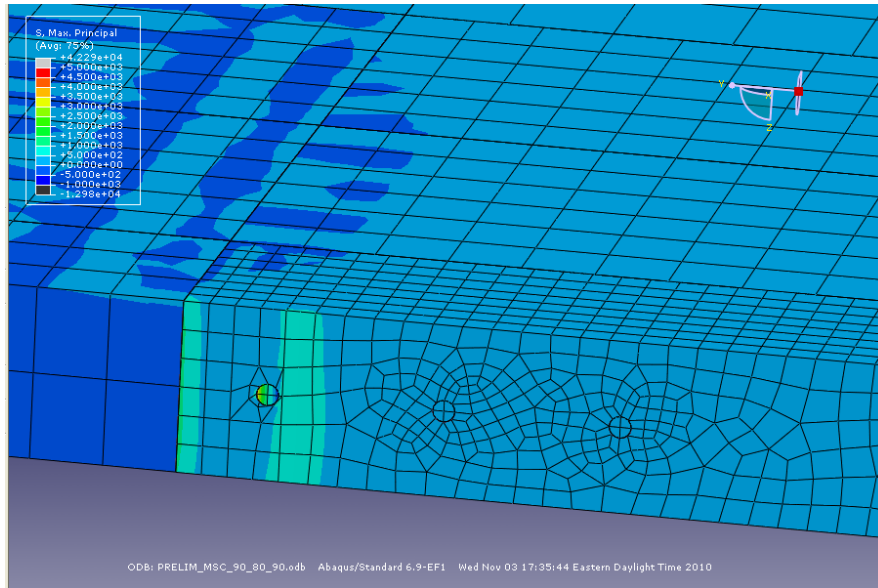


**Figure A208.** Longitudinal shear cracking model in which  $T_M=90^\circ\text{F}$ ,  $T_S=80^\circ\text{F}$ , and  $T_C=90^\circ\text{F}$  for a mortar intrusion of 7 in and a CTE of  $6.5 \times 10^{-6}/^\circ\text{F}$ .

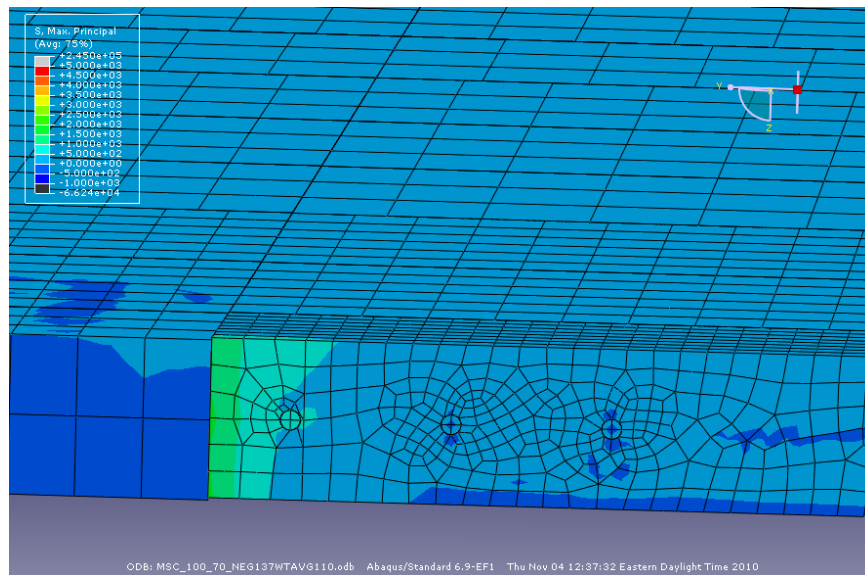


**Figure A209.** Longitudinal shear cracking model in which  $T_M=100^\circ\text{F}$ ,  $T_S=70^\circ\text{F}$ , and  $T_C=\text{positive } 1.37 \text{ gradient}$  with a  $110^\circ\text{F}$  weighted average for a mortar intrusion of 3.5 in and a CTE of  $6.5 \times 10^{-6}/^\circ\text{F}$ .

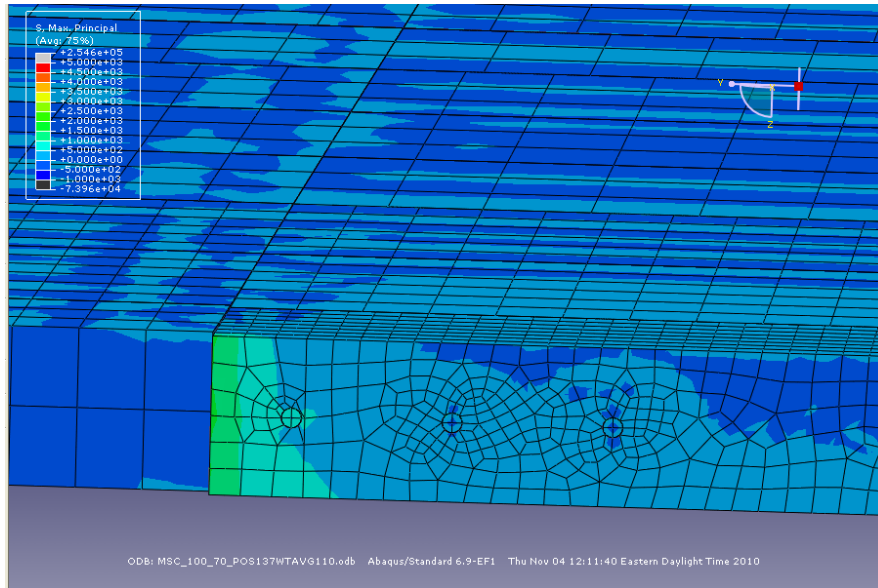


**Figure A210.** Longitudinal shear cracking model in which  $T_M=100^\circ\text{F}$ ,  $T_S=70^\circ\text{F}$ , and  $T_C=\text{negative } 1.37$  gradient with a  $110^\circ\text{F}$  weighted average for a mortar intrusion of 3.5 in and a CTE of  $6.5 \times 10^{-6}/^\circ\text{F}$ .

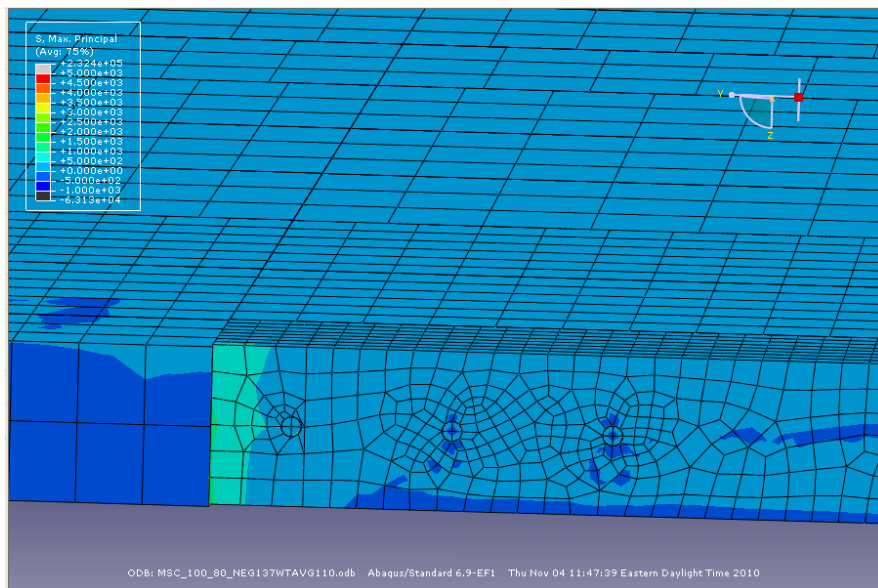


**Figure A211.** Longitudinal shear cracking model in which  $T_M=100^\circ\text{F}$ ,  $T_S=80^\circ\text{F}$ , and  $T_C=\text{positive } 1.37$  gradient with a  $110^\circ\text{F}$  weighted average for a mortar intrusion of 3.5 in and a CTE of  $6.5 \times 10^{-6}/^\circ\text{F}$ .

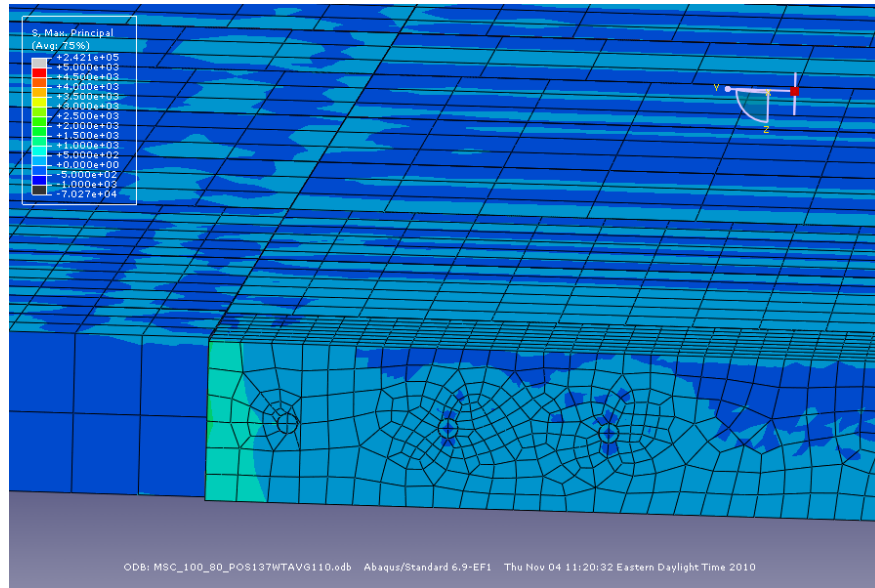


**Figure A212.** Longitudinal shear cracking model in which  $T_M=100^\circ\text{F}$ ,  $T_S=80^\circ\text{F}$ , and  $T_C=\text{negative } 1.37$  gradient with a  $110^\circ\text{F}$  weighted average for a mortar intrusion of 3.5 in and a CTE of  $6.5 \times 10^{-6}/^\circ\text{F}$ .

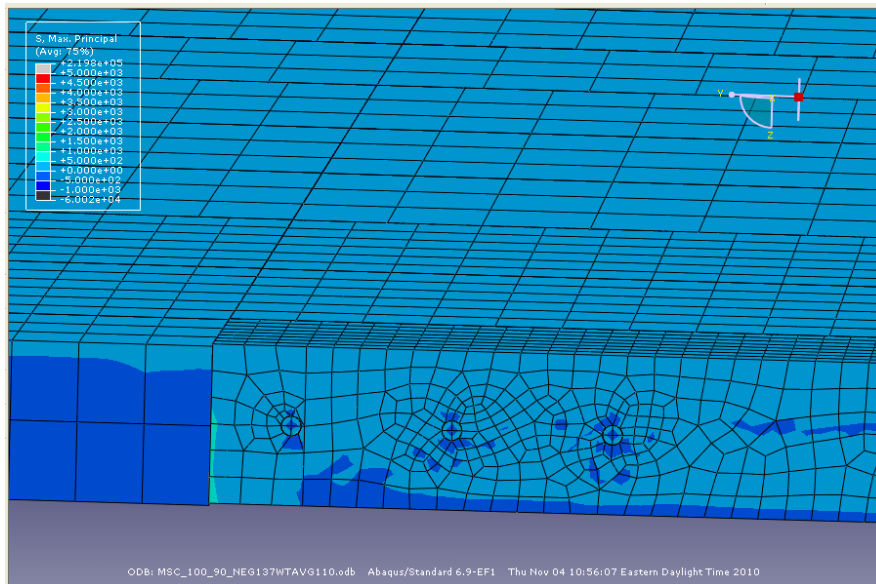


**Figure A213.** Longitudinal shear cracking model in which  $T_M=100^\circ\text{F}$ ,  $T_S=90^\circ\text{F}$ , and  $T_C=\text{positive } 1.37$  gradient with a  $110^\circ\text{F}$  weighted average for a mortar intrusion of 3.5 in and a CTE of  $6.5 \times 10^{-6}/^\circ\text{F}$ .

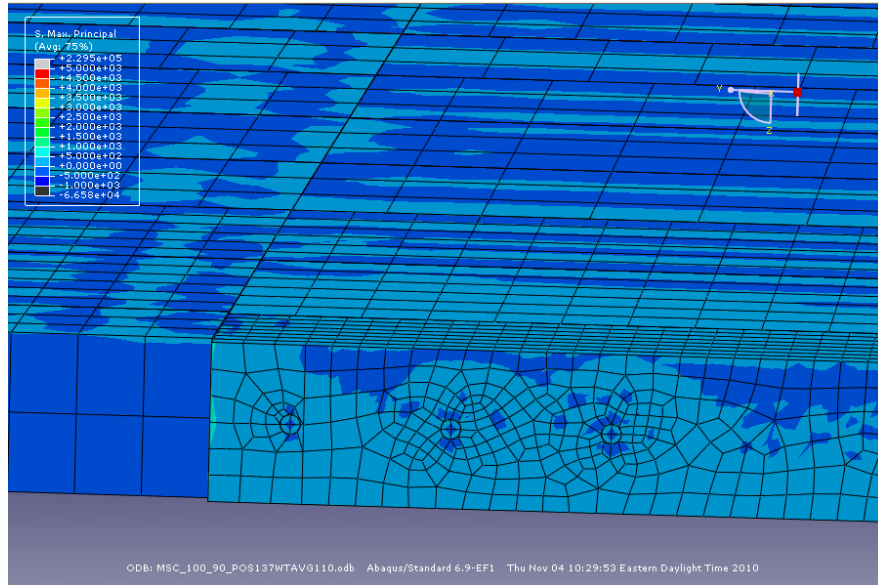


**Figure A214.** Longitudinal shear cracking model in which  $T_M=100^\circ\text{F}$ ,  $T_S=90^\circ\text{F}$ , and  $T_C=\text{negative } 1.37$  gradient with a  $110^\circ\text{F}$  weighted average for a mortar intrusion of 3.5 in and a CTE of  $6.5 \times 10^{-6}/^\circ\text{F}$ .

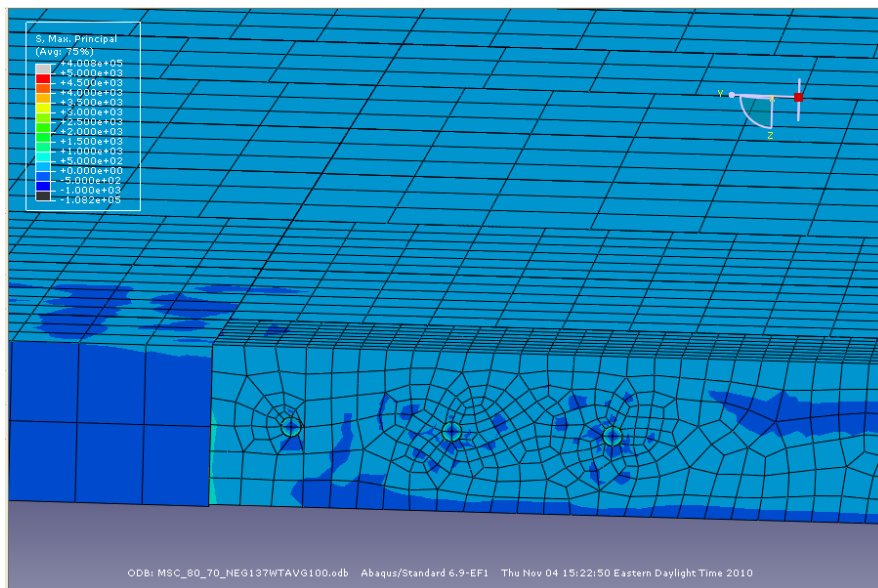


**Figure A215.** Longitudinal shear cracking model in which  $T_M=80^\circ\text{F}$ ,  $T_S=70^\circ\text{F}$ , and  $T_C=\text{positive } 1.37$  gradient with a  $100^\circ\text{F}$  weighted average for a mortar intrusion of 3.5 in and a CTE of  $6.5 \times 10^{-6}/^\circ\text{F}$ .

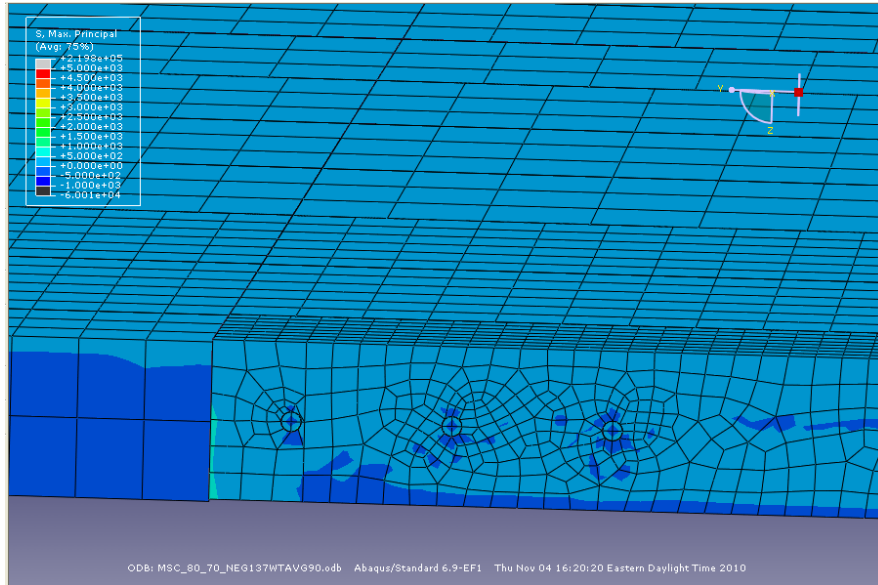


**Figure A216.** Longitudinal shear cracking model in which  $T_M=80^\circ\text{F}$ ,  $T_S=70^\circ\text{F}$ , and  $T_C=\text{positive } 1.37$  gradient with a  $90^\circ\text{F}$  weighted average for a mortar intrusion of 3.5 in and a CTE of  $6.5 \times 10^{-6}/^\circ\text{F}$ .

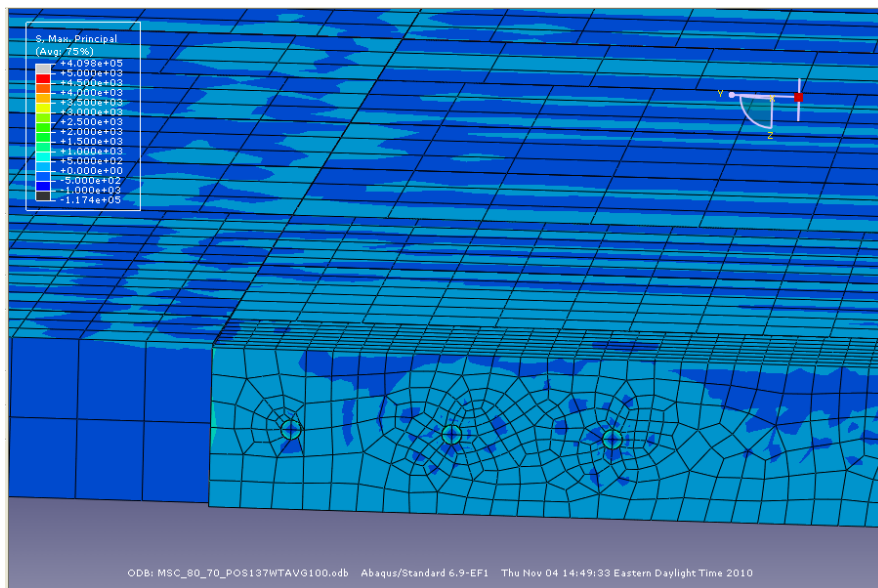


**Figure A217.** Longitudinal shear cracking model in which  $T_M=80^\circ\text{F}$ ,  $T_S=70^\circ\text{F}$ , and  $T_C=\text{negative } 1.37$  gradient with a  $100^\circ\text{F}$  weighted average for a mortar intrusion of 3.5 in and a CTE of  $6.5 \times 10^{-6}/^\circ\text{F}$ .

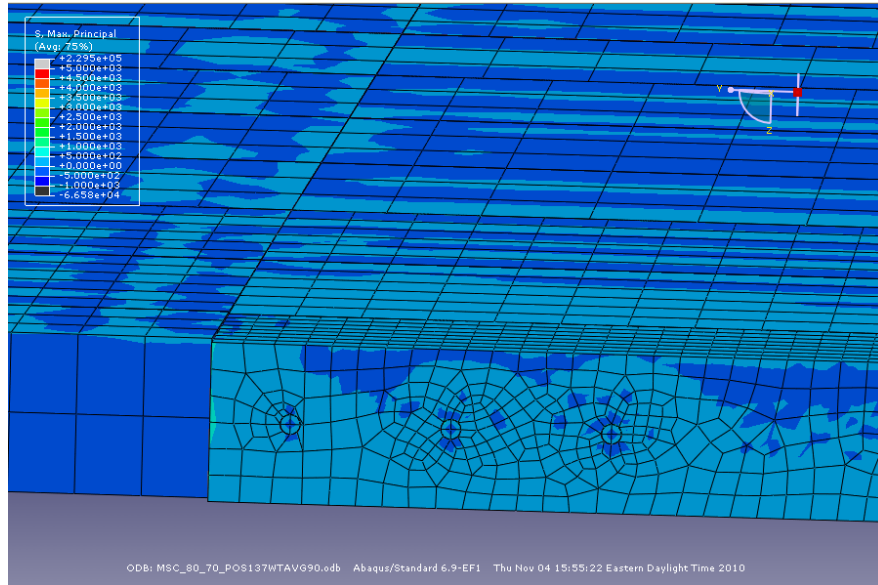


**Figure A218.** Longitudinal shear cracking model in which  $T_M=80^\circ\text{F}$ ,  $T_S=70^\circ\text{F}$ , and  $T_C=\text{negative } 1.37$  gradient with a  $90^\circ\text{F}$  weighted average for a mortar intrusion of 3.5 in and a CTE of  $6.5 \times 10^{-6}/^\circ\text{F}$ .

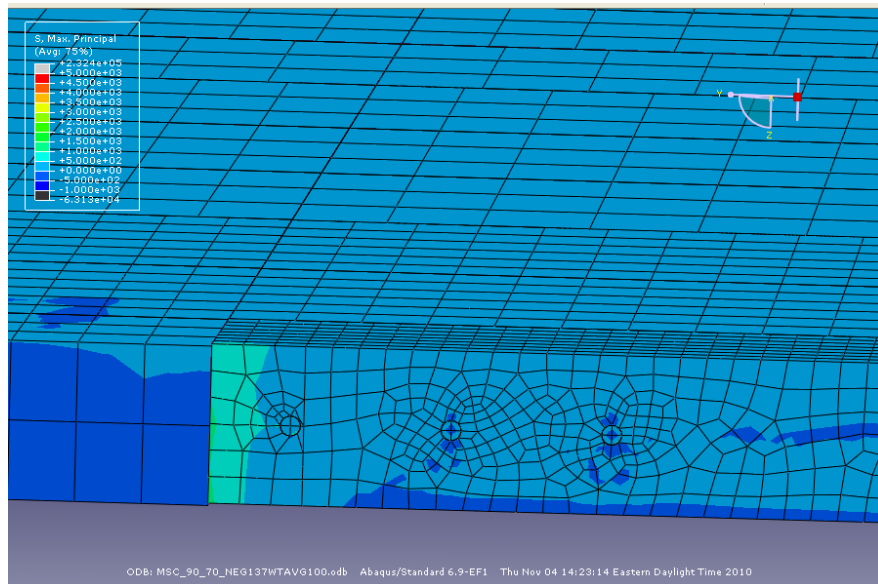


**Figure A219.** Longitudinal shear cracking model in which  $T_M=90^\circ\text{F}$ ,  $T_S=70^\circ\text{F}$ , and  $T_C=\text{positive } 1.37$  gradient with a  $100^\circ\text{F}$  weighted average for a mortar intrusion of 3.5 in and a CTE of  $6.5 \times 10^{-6}/^\circ\text{F}$ .

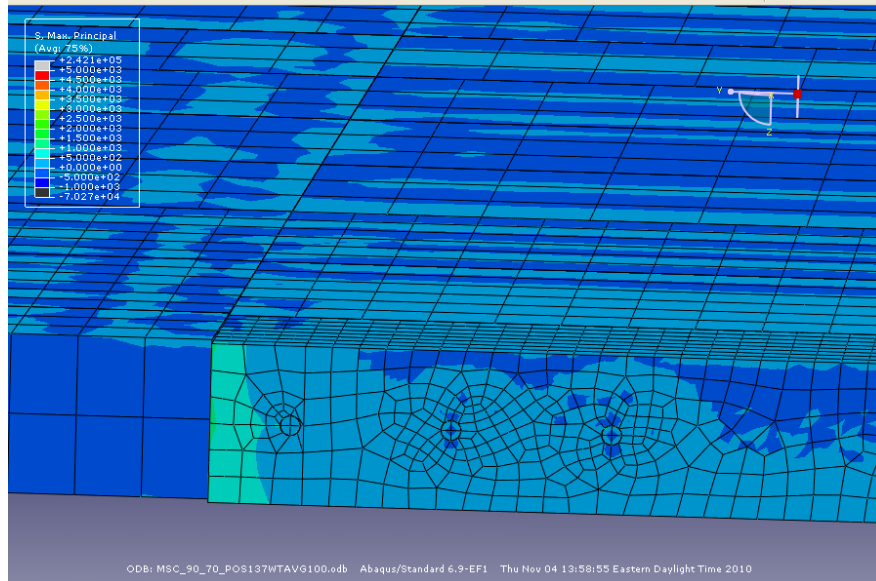


**Figure A220.** Longitudinal shear cracking model in which  $T_M=90^\circ\text{F}$ ,  $T_S=70^\circ\text{F}$ , and  $T_C=\text{negative } 1.37$  gradient with a  $100^\circ\text{F}$  weighted average for a mortar intrusion of 3.5 in and a CTE of  $6.5 \times 10^{-6}/^\circ\text{F}$ .

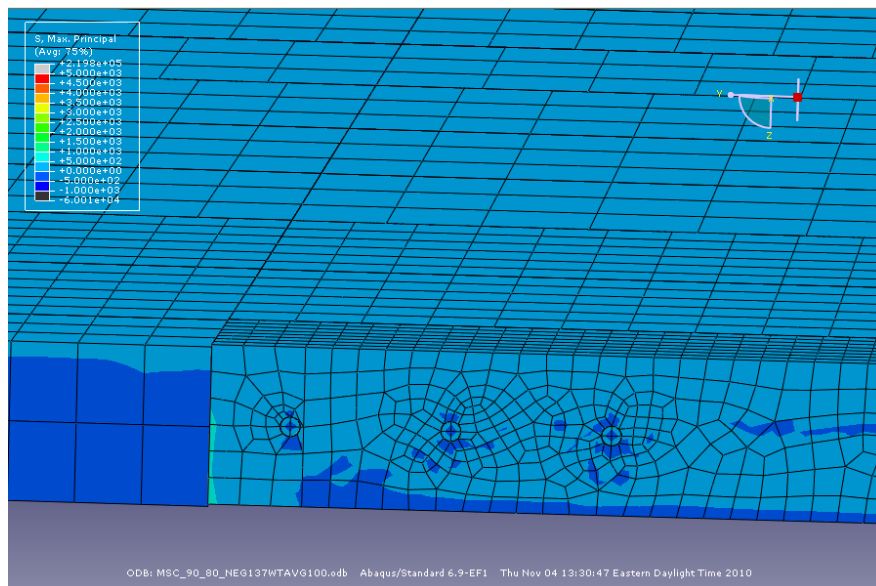


**Figure A221.** Longitudinal shear cracking model in which  $T_M=90^\circ\text{F}$ ,  $T_S=80^\circ\text{F}$ , and  $T_C=\text{positive } 1.37$  gradient with a  $100^\circ\text{F}$  weighted average for a mortar intrusion of 3.5 in and a CTE of  $6.5 \times 10^{-6}/^\circ\text{F}$ .

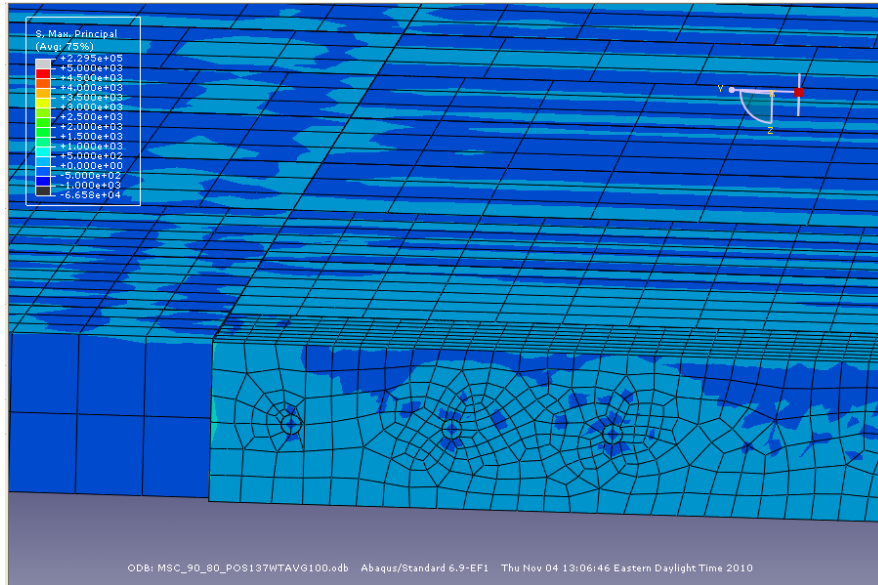


**Figure A222.** Longitudinal shear cracking model in which  $T_M=90^\circ\text{F}$ ,  $T_S=80^\circ\text{F}$ , and  $T_C=\text{negative } 1.37$  gradient with a  $100^\circ\text{F}$  weighted average for a mortar intrusion of 3.5 in and a CTE of  $6.5 \times 10^{-6}/^\circ\text{F}$ .

## APPENDIX B

### SHOULDER TRANSVERSE CRACKING SCREEN SHOTS

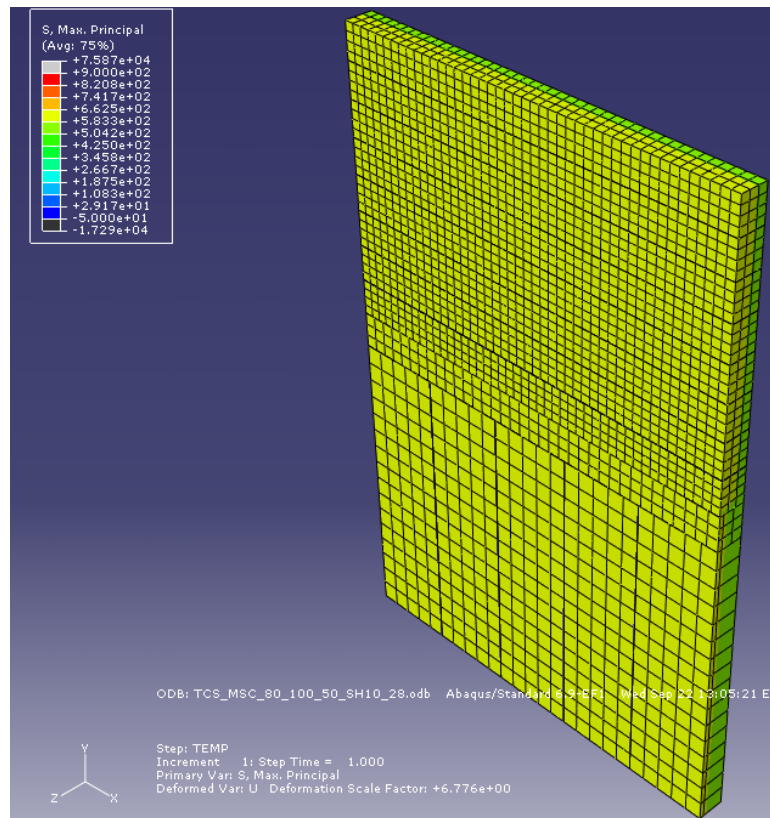


**Figure B223.** 10-ft shoulder transverse cracking model where  $T_M=80^\circ\text{F}$ ,  $T_S=100^\circ\text{F}$ , and  $T_C=50^\circ\text{F}$ , for a CTE of  $4.5 \times 10^{-6}/^\circ\text{F}$  and a stiffness of  $2.8 \times 10^6$  psi.

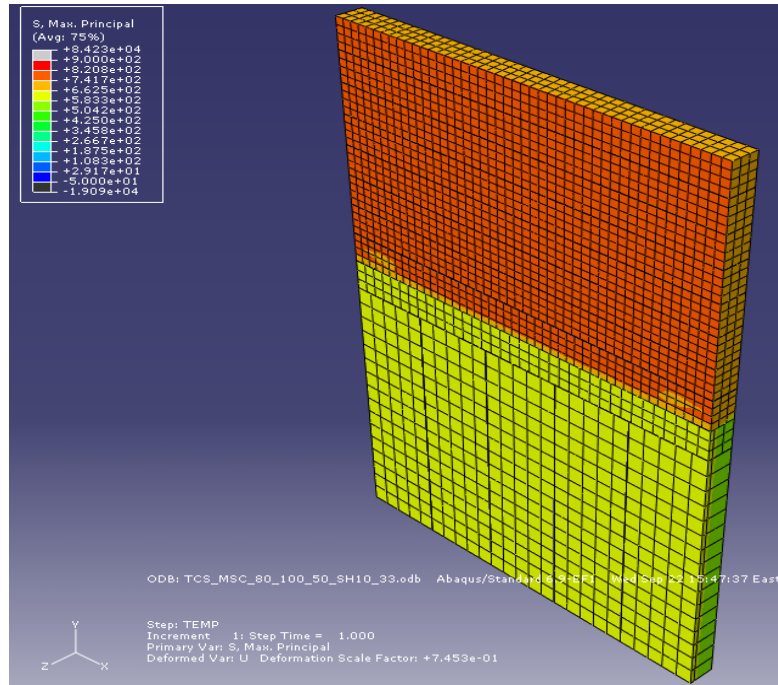


**Figure B224.** 10-ft shoulder transverse cracking model where  $T_M=80^\circ\text{F}$ ,  $T_S=100^\circ\text{F}$ , and  $T_C=50^\circ\text{F}$ , for a CTE of  $4.5 \times 10^{-6}/^\circ\text{F}$  and a stiffness of  $3.3 \times 10^6$  psi.

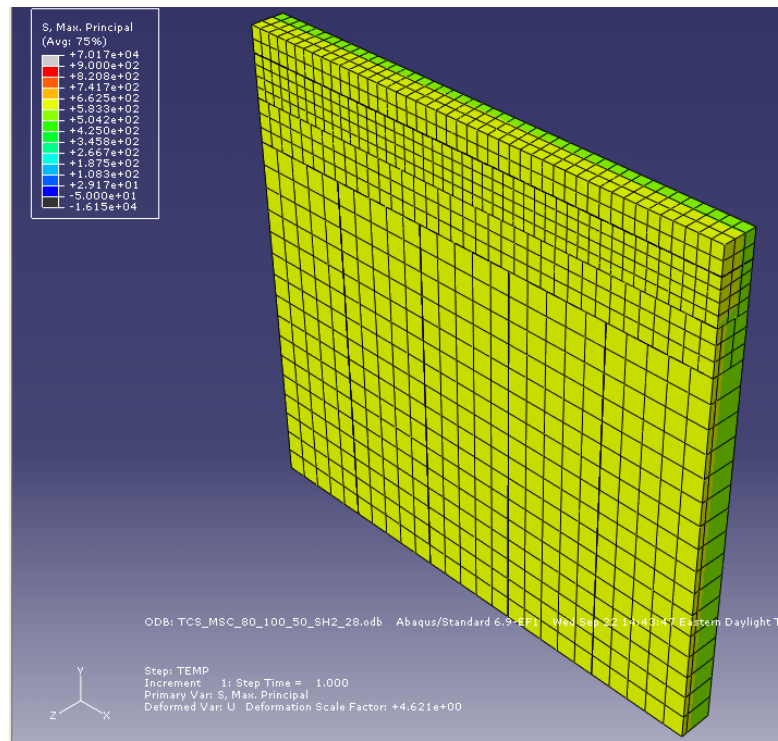


**Figure B225.** 2-ft shoulder transverse cracking model where  $T_M=80^\circ\text{F}$ ,  $T_S=100^\circ\text{F}$ , and  $T_C=50^\circ\text{F}$ , for a CTE of  $4.5 \times 10^{-6}/^\circ\text{F}$  and a stiffness of  $2.8 \times 10^6$  psi.

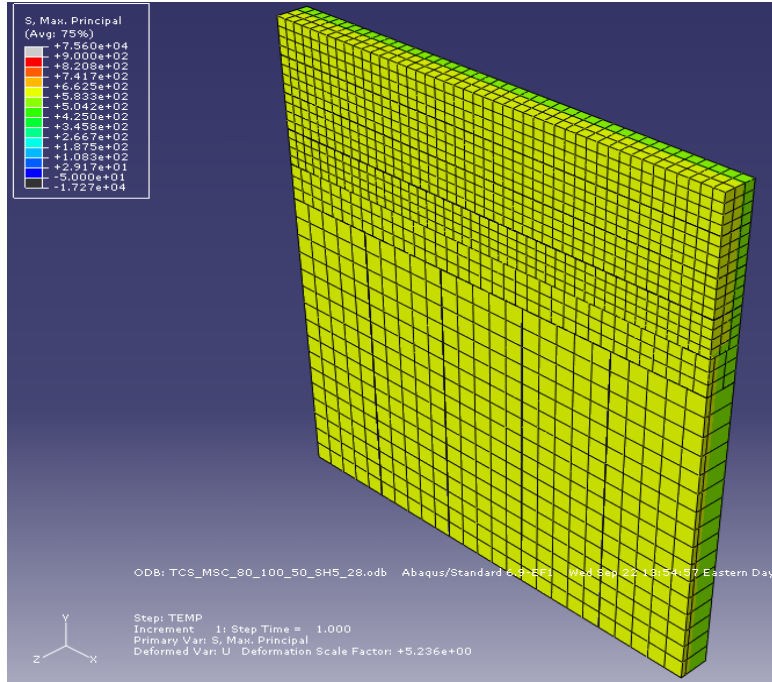


**Figure B226.** 5-ft shoulder transverse cracking model where  $T_M=80^\circ\text{F}$ ,  $T_S=100^\circ\text{F}$ , and  $T_C=50^\circ\text{F}$ , for a CTE of  $4.5 \times 10^{-6}/^\circ\text{F}$  and a stiffness of  $2.8 \times 10^6$  psi.

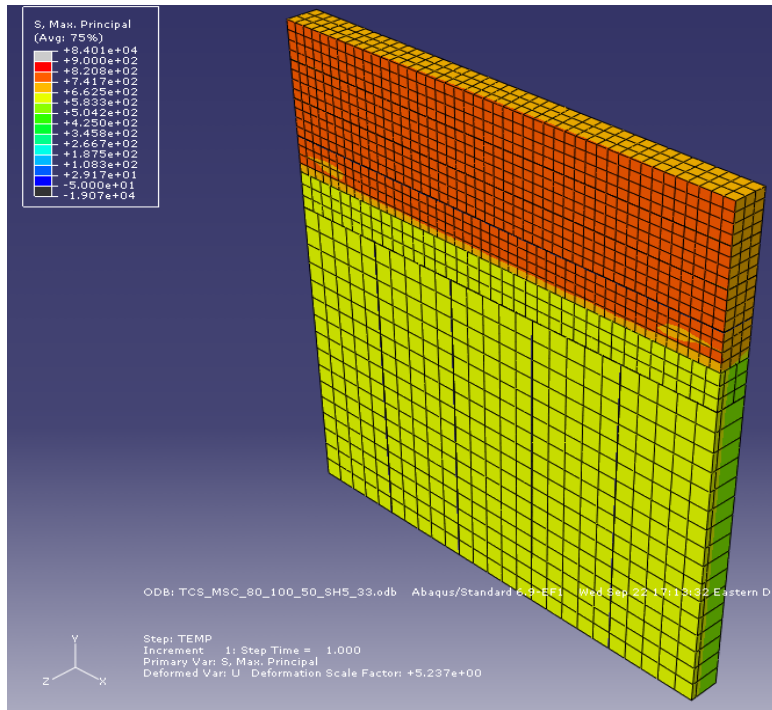


**Figure B227.** 5-ft shoulder transverse cracking model where  $T_M=80^\circ\text{F}$ ,  $T_S=100^\circ\text{F}$ , and  $T_C=50^\circ\text{F}$ , for a CTE of  $4.5 \times 10^{-6}/^\circ\text{F}$  and a stiffness of  $3.3 \times 10^6$  psi.

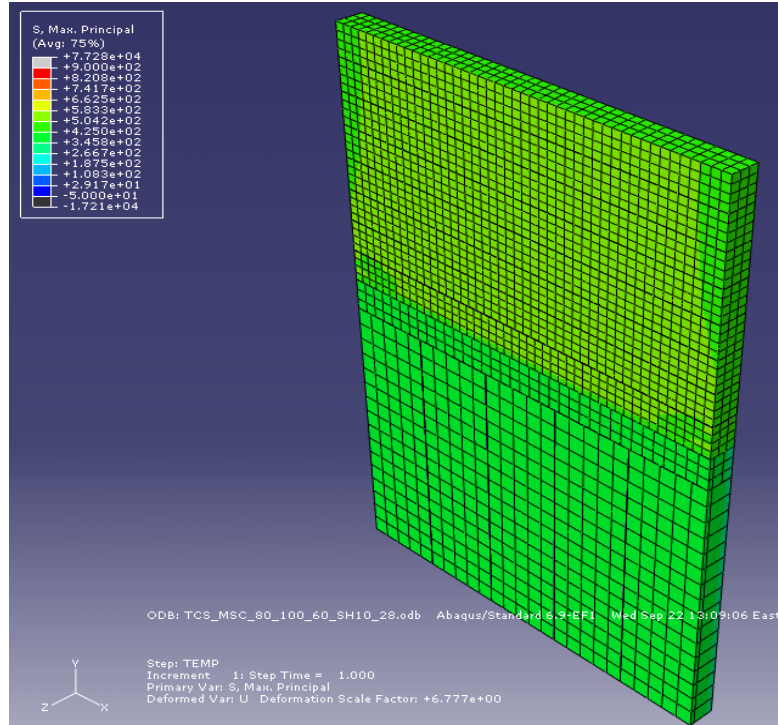


**Figure B228.** 10-ft shoulder transverse cracking model where  $T_M=80^\circ\text{F}$ ,  $T_S=100^\circ\text{F}$ , and  $T_C=60^\circ\text{F}$ , for a CTE of  $4.5 \times 10^{-6}/^\circ\text{F}$  and a stiffness of  $2.8 \times 10^6$  psi.

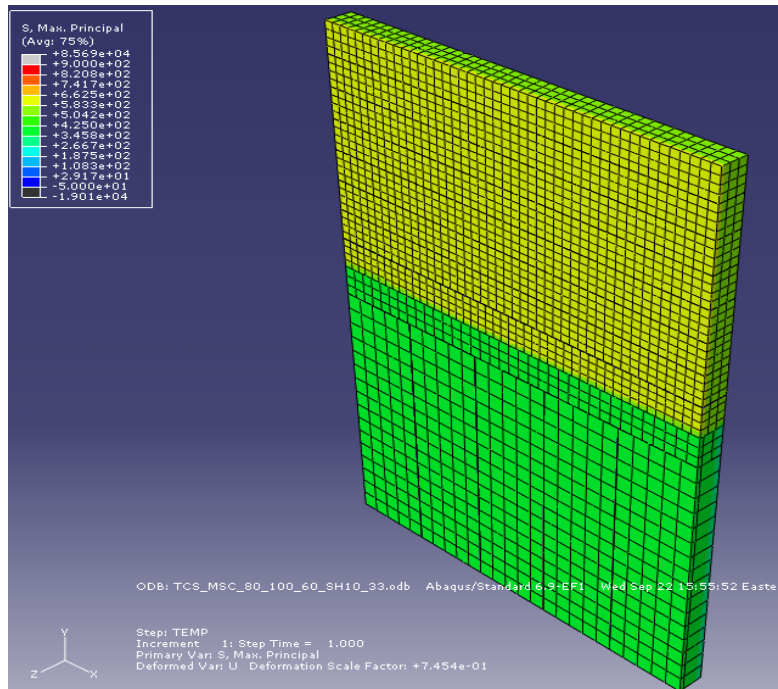


**Figure B229.** 10-ft shoulder transverse cracking model where  $T_M=80^\circ\text{F}$ ,  $T_S=100^\circ\text{F}$ , and  $T_C=60^\circ\text{F}$ , for a CTE of  $4.5 \times 10^{-6}/^\circ\text{F}$  and a stiffness of  $3.3 \times 10^6$  psi.

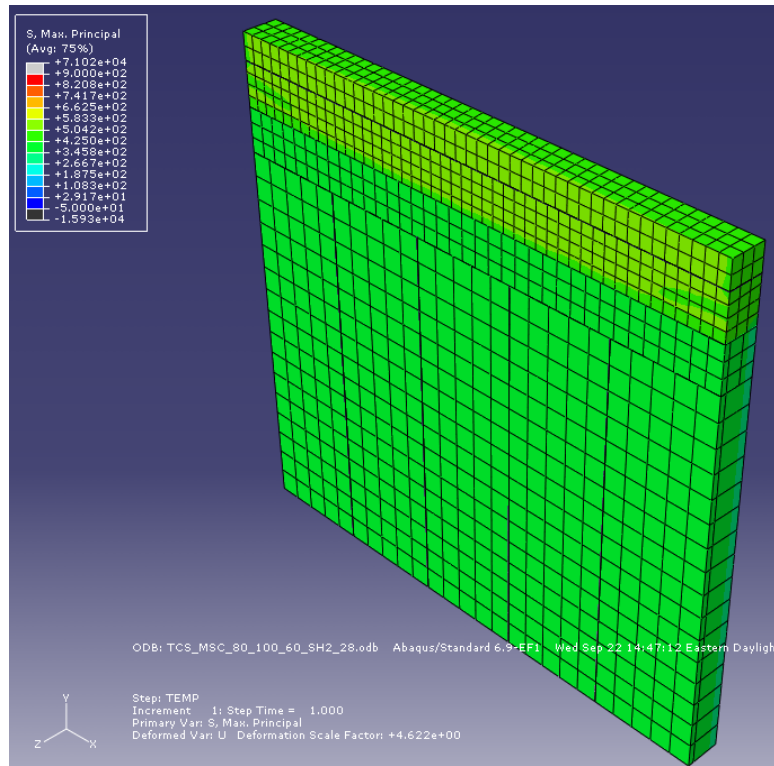


**Figure B230.** 2-ft shoulder transverse cracking model where  $T_M=80^\circ\text{F}$ ,  $T_S=100^\circ\text{F}$ , and  $T_C=60^\circ\text{F}$ , for a CTE of  $4.5 \times 10^{-6}/^\circ\text{F}$  and a stiffness of  $2.8 \times 10^6$  psi.

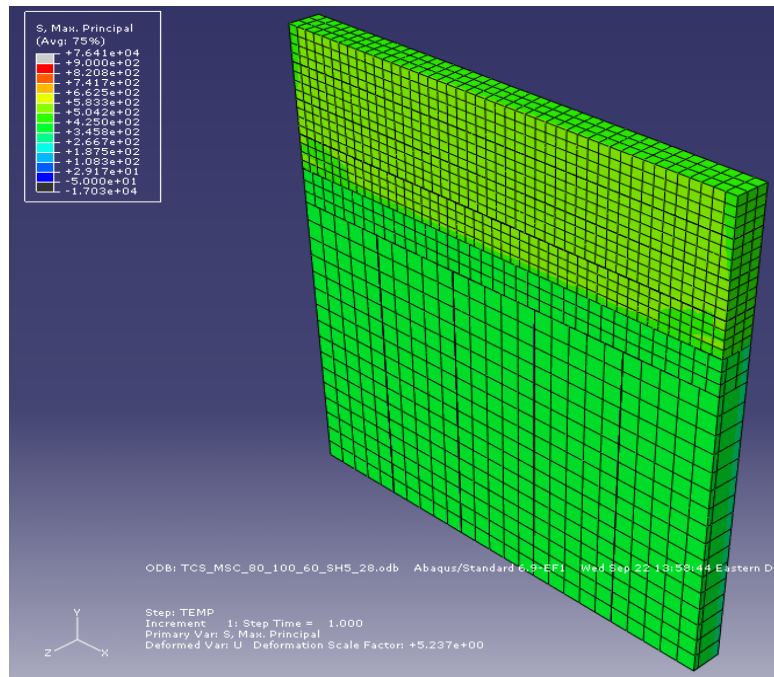


**Figure B231.** 5-ft shoulder transverse cracking model where  $T_M=80^\circ\text{F}$ ,  $T_S=100^\circ\text{F}$ , and  $T_C=60^\circ\text{F}$ , for a CTE of  $4.5 \times 10^{-6}/^\circ\text{F}$  and a stiffness of  $2.8 \times 10^6$  psi.

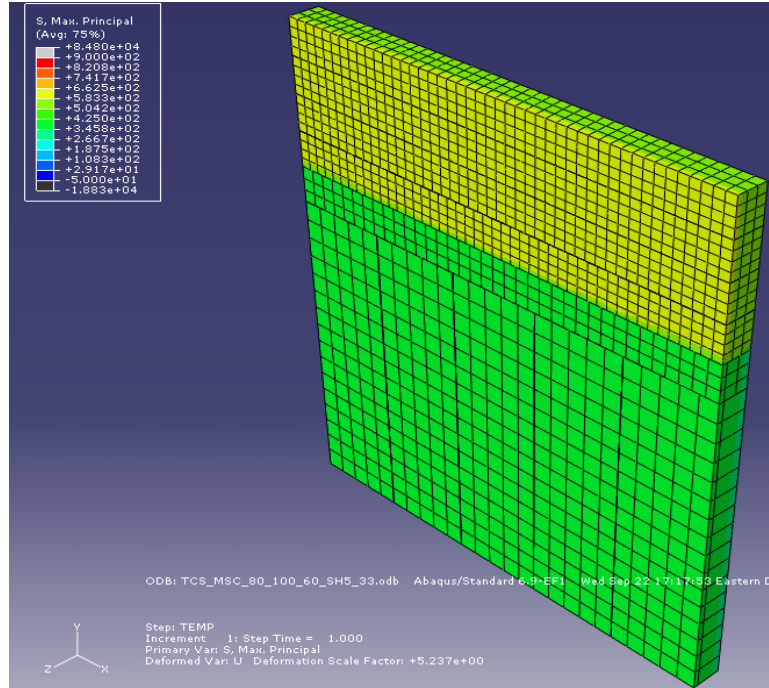


**Figure B232.** 5-ft shoulder transverse cracking model where  $T_M=80^\circ\text{F}$ ,  $T_S=100^\circ\text{F}$ , and  $T_C=60^\circ\text{F}$ , for a CTE of  $4.5 \times 10^{-6}/^\circ\text{F}$  and a stiffness of  $3.3 \times 10^6$  psi.

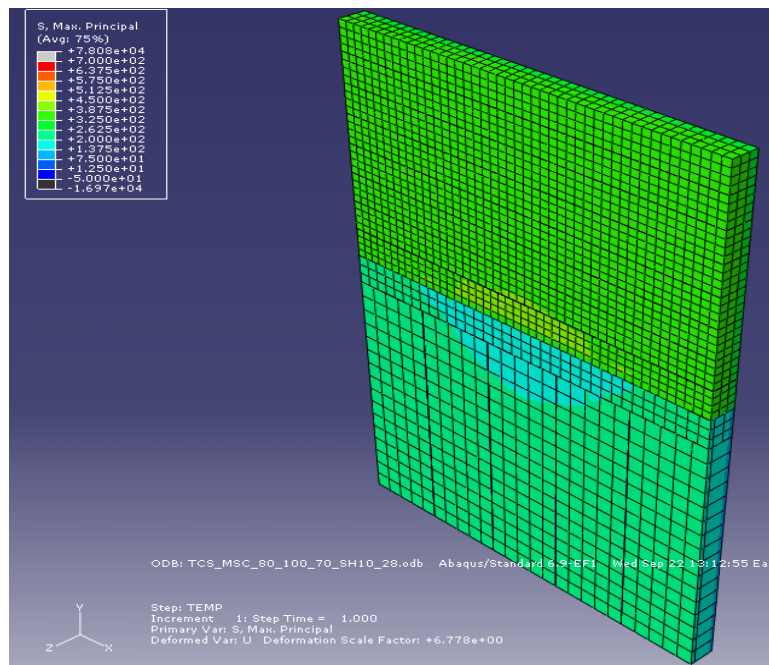


**Figure B233.** 10-ft shoulder transverse cracking model where  $T_M=80^\circ\text{F}$ ,  $T_S=100^\circ\text{F}$ , and  $T_C=70^\circ\text{F}$ , for a CTE of  $4.5 \times 10^{-6}/^\circ\text{F}$  and a stiffness of  $2.8 \times 10^6$  psi.

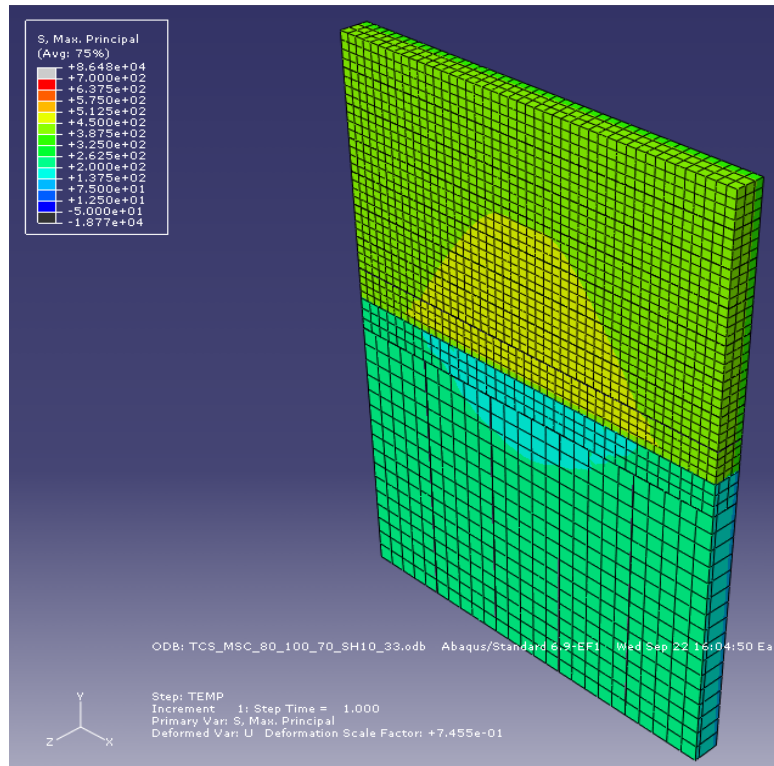


**Figure B234.** 10-ft shoulder transverse cracking model where  $T_M=80^\circ\text{F}$ ,  $T_S=100^\circ\text{F}$ , and  $T_C=70^\circ\text{F}$ , for a CTE of  $4.5 \times 10^{-6}/^\circ\text{F}$  and a stiffness of  $3.3 \times 10^6$  psi.

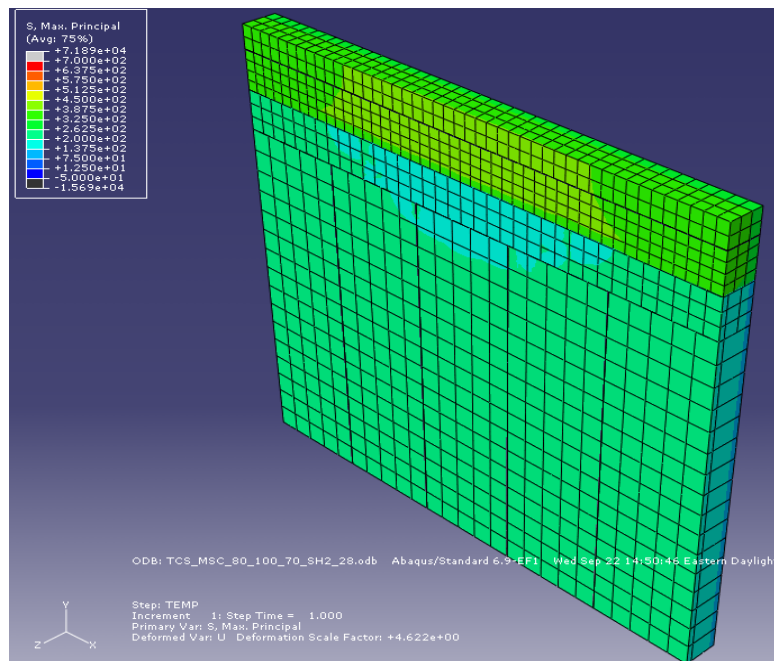


**Figure B235.** 2-ft shoulder transverse cracking model where  $T_M=80^\circ\text{F}$ ,  $T_S=100^\circ\text{F}$ , and  $T_C=70^\circ\text{F}$ , for a CTE of  $4.5 \times 10^{-6}/^\circ\text{F}$  and a stiffness of  $2.8 \times 10^6$  psi.

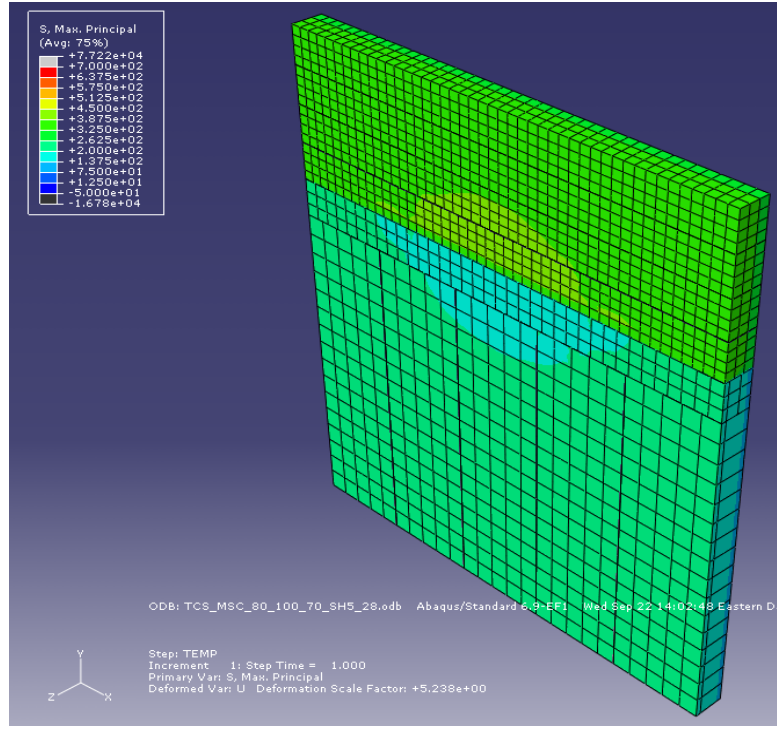


**Figure B236.** 5-ft shoulder transverse cracking model where  $T_M=80^\circ\text{F}$ ,  $T_S=100^\circ\text{F}$ , and  $T_C=70^\circ\text{F}$ , for a CTE of  $4.5 \times 10^{-6}/^\circ\text{F}$  and a stiffness of  $2.8 \times 10^6$  psi.

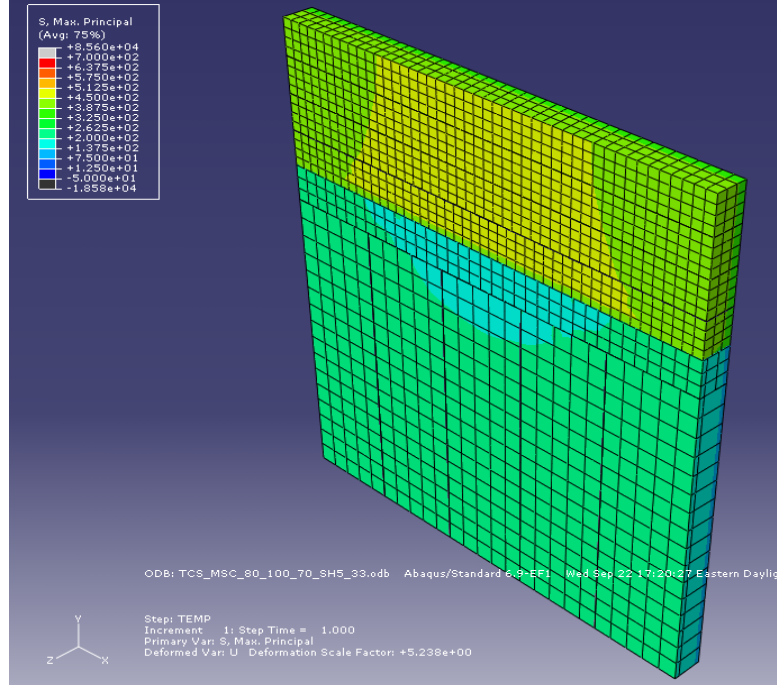


**Figure B237.** 5-ft shoulder transverse cracking model where  $T_M=80^\circ\text{F}$ ,  $T_S=100^\circ\text{F}$ , and  $T_C=70^\circ\text{F}$ , for a CTE of  $4.5 \times 10^{-6}/^\circ\text{F}$  and a stiffness of  $3.3 \times 10^6$  psi.

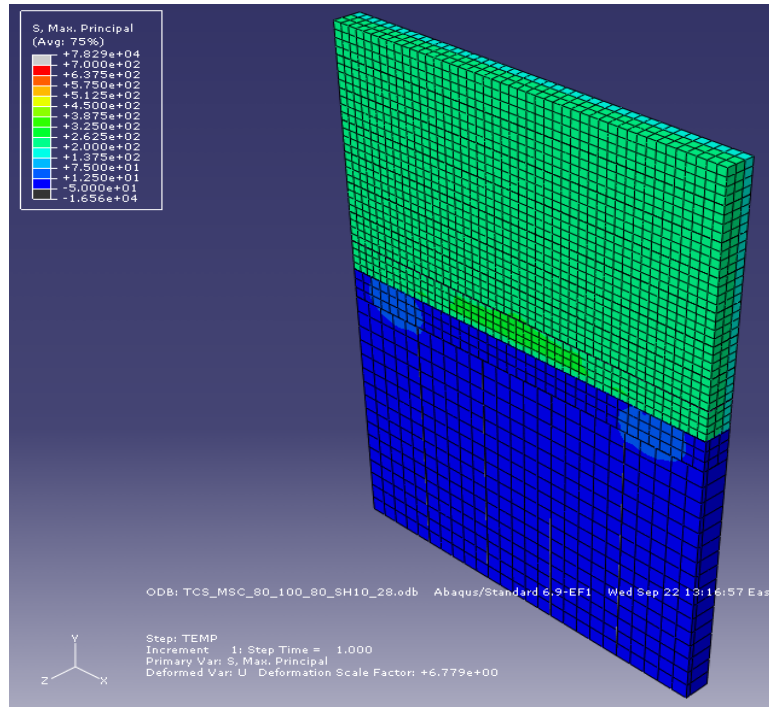


**Figure B238.** 10-ft shoulder transverse cracking model where  $T_M=80^\circ\text{F}$ ,  $T_S=100^\circ\text{F}$ , and  $T_C=80^\circ\text{F}$ , for a CTE of  $4.5 \times 10^{-6}/^\circ\text{F}$  and a stiffness of  $2.8 \times 10^6$  psi.

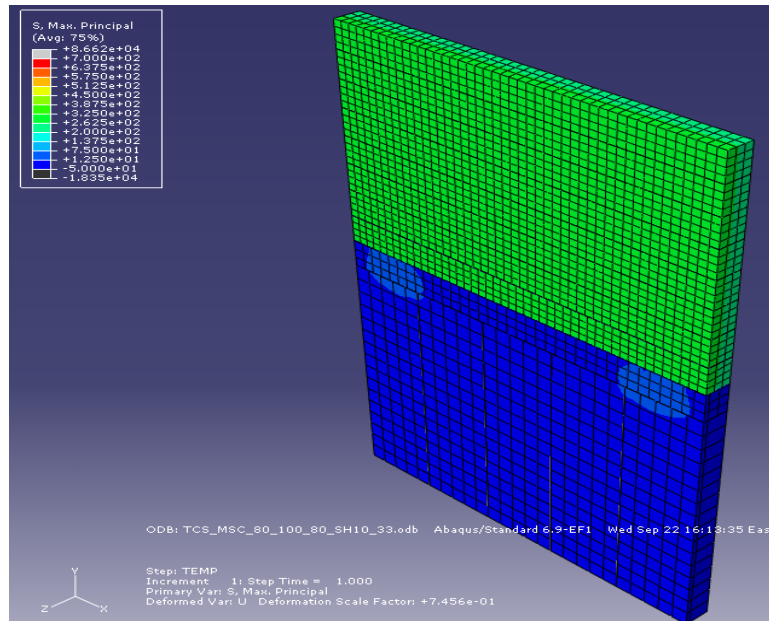


**Figure B239.** 10-ft shoulder transverse cracking model where  $T_M=80^\circ\text{F}$ ,  $T_S=100^\circ\text{F}$ , and  $T_C=80^\circ\text{F}$ , for a CTE of  $4.5 \times 10^{-6}/^\circ\text{F}$  and a stiffness of  $3.3 \times 10^6$  psi.

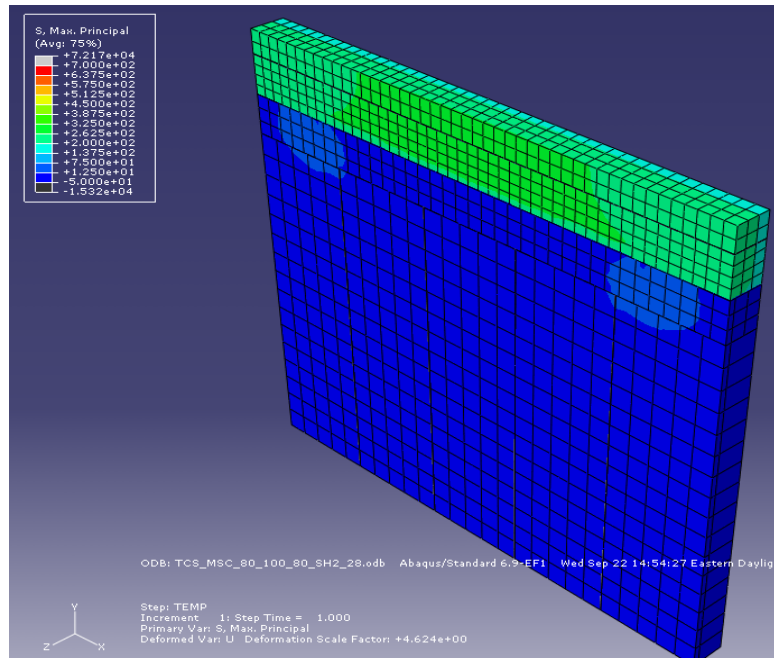


**Figure B240.** 2-ft shoulder transverse cracking model where  $T_M=80^\circ\text{F}$ ,  $T_S=100^\circ\text{F}$ , and  $T_C=80^\circ\text{F}$ , for a CTE of  $4.5 \times 10^{-6}/^\circ\text{F}$  and a stiffness of  $2.8 \times 10^6$  psi.

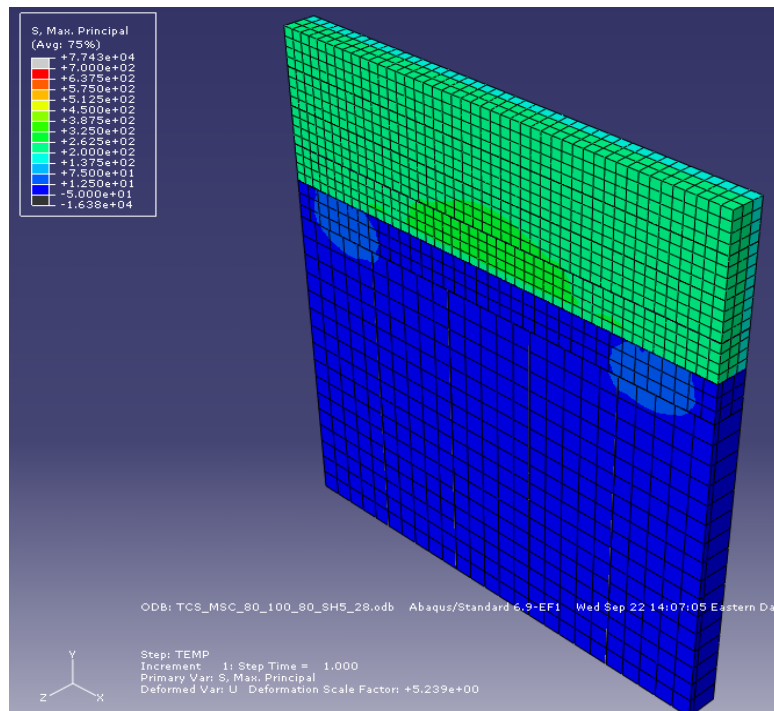


**Figure B241.** 5-ft shoulder transverse cracking model where  $T_M=80^\circ\text{F}$ ,  $T_S=100^\circ\text{F}$ , and  $T_C=80^\circ\text{F}$ , for a CTE of  $4.5 \times 10^{-6}/^\circ\text{F}$  and a stiffness of  $2.8 \times 10^6$  psi.

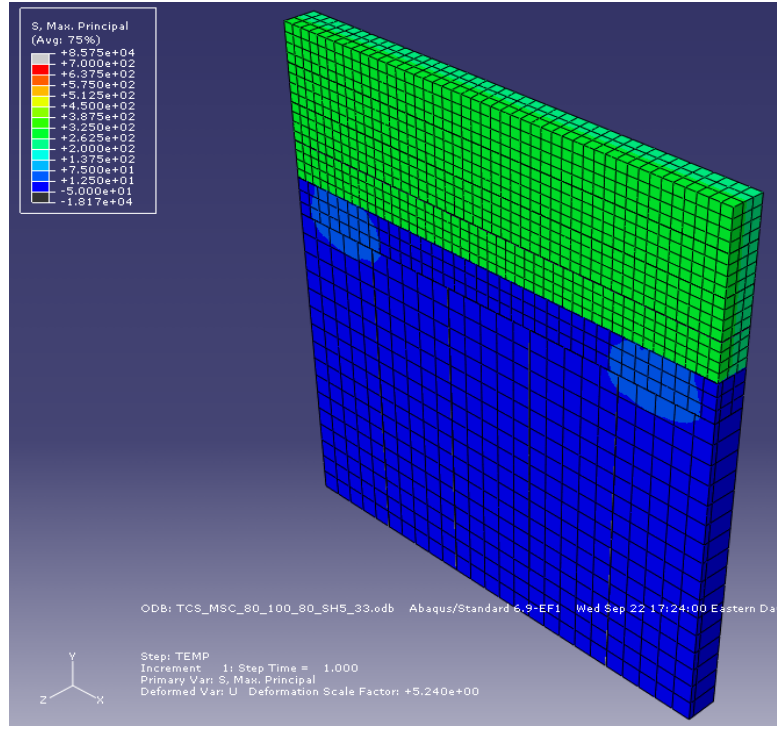


**Figure B242.** 5-ft shoulder transverse cracking model where  $T_M=80^\circ\text{F}$ ,  $T_S=100^\circ\text{F}$ , and  $T_C=80^\circ\text{F}$ , for a CTE of  $4.5 \times 10^{-6}/^\circ\text{F}$  and a stiffness of  $3.3 \times 10^6$  psi.

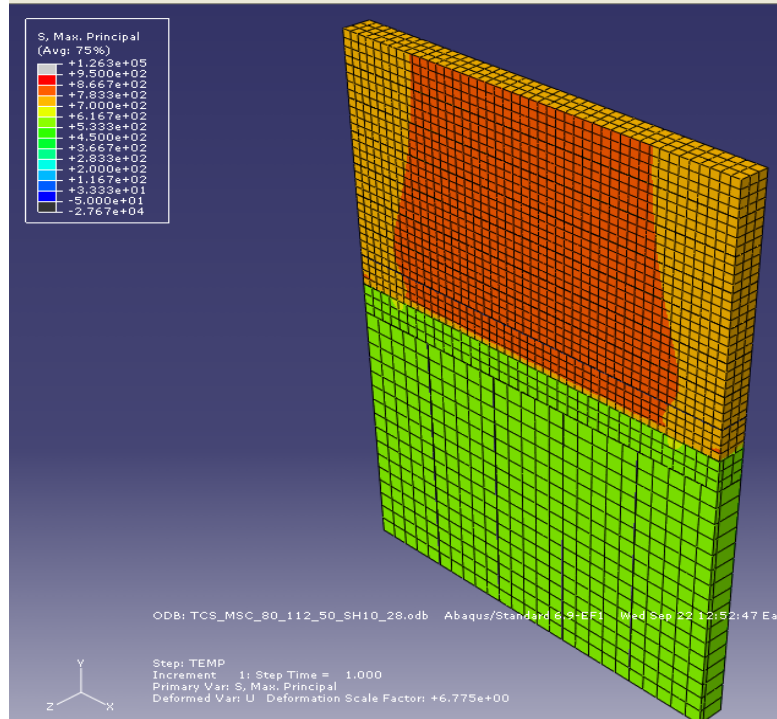


**Figure B243.** 10-ft shoulder transverse cracking model where  $T_M=80^\circ\text{F}$ ,  $T_S=110^\circ\text{F}$ , and  $T_C=50^\circ\text{F}$ , for a CTE of  $4.5 \times 10^{-6}/^\circ\text{F}$  and a stiffness of  $2.8 \times 10^6$  psi.

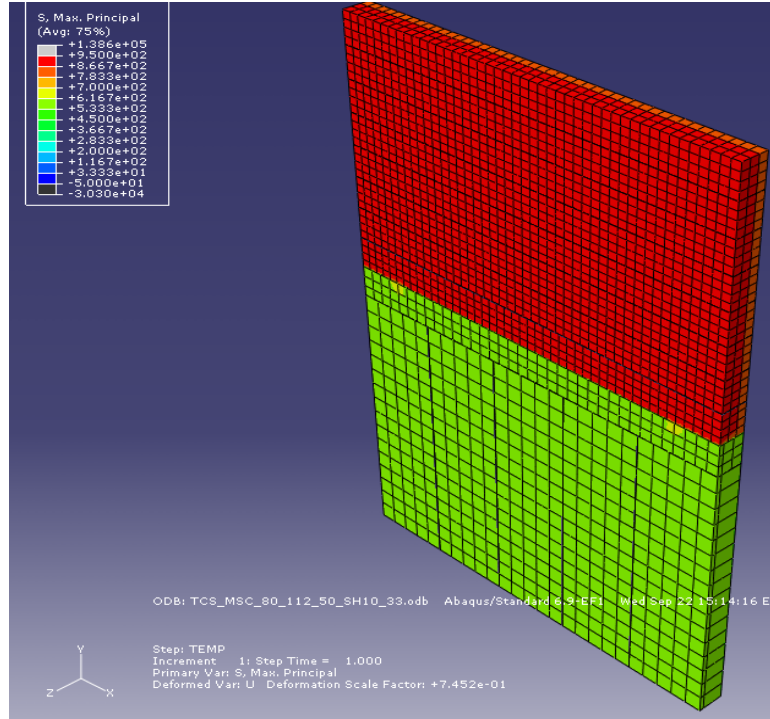


**Figure B244.** 10-ft shoulder transverse cracking model where  $T_M=80^\circ\text{F}$ ,  $T_S=110^\circ\text{F}$ , and  $T_C=50^\circ\text{F}$ , for a CTE of  $4.5 \times 10^{-6}/^\circ\text{F}$  and a stiffness of  $3.3 \times 10^6$  psi.

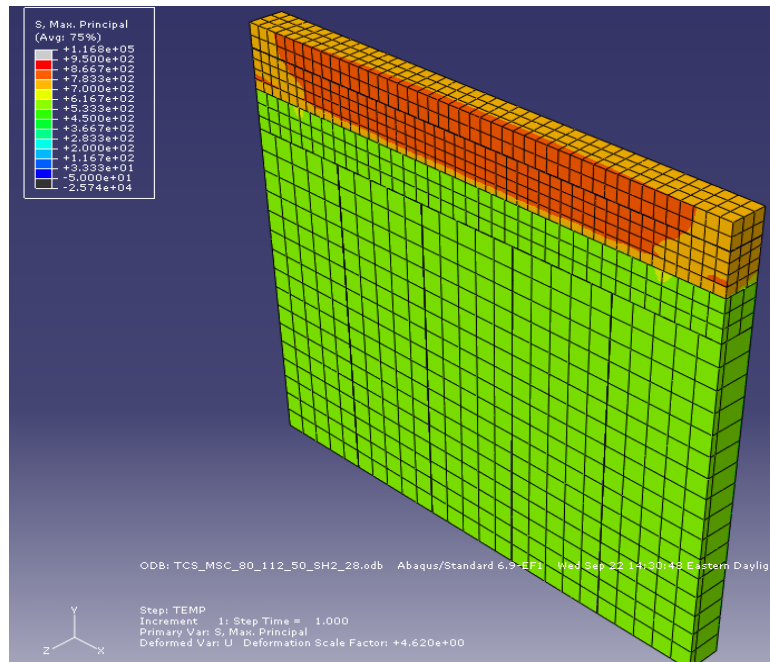


**Figure B245.** 2-ft shoulder transverse cracking model where  $T_M=80^\circ\text{F}$ ,  $T_S=110^\circ\text{F}$ , and  $T_C=50^\circ\text{F}$ , for a CTE of  $4.5 \times 10^{-6}/^\circ\text{F}$  and a stiffness of  $2.8 \times 10^6$  psi.

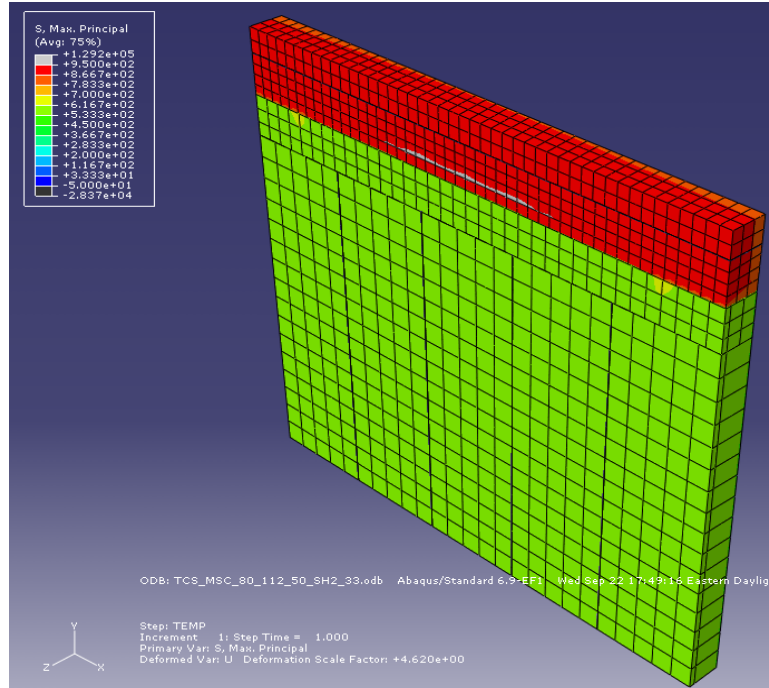


**Figure B246.** 2-ft shoulder transverse cracking model where  $T_M=80^\circ\text{F}$ ,  $T_S=110^\circ\text{F}$ , and  $T_C=50^\circ\text{F}$ , for a CTE of  $4.5 \times 10^{-6}/^\circ\text{F}$  and a stiffness of  $3.3 \times 10^6$  psi.

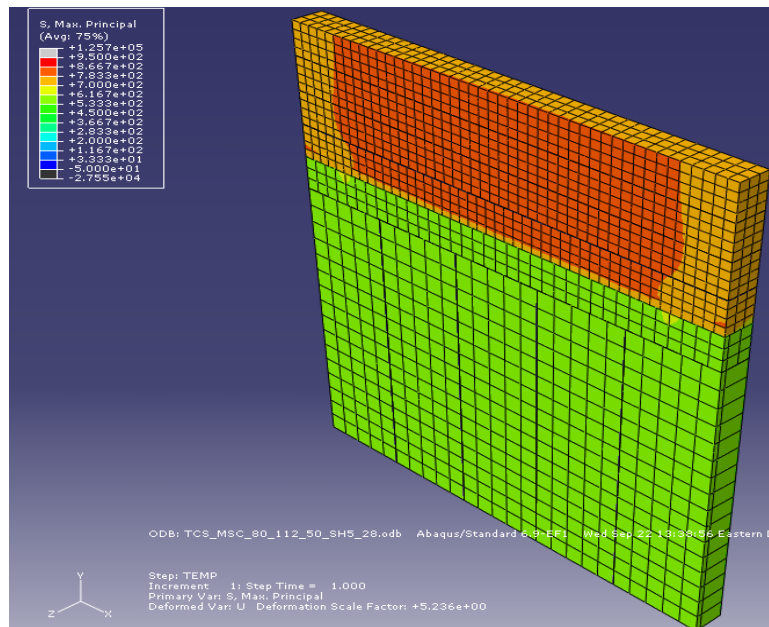


**Figure B247.** 5-ft shoulder transverse cracking model where  $T_M=80^\circ\text{F}$ ,  $T_S=110^\circ\text{F}$ , and  $T_C=50^\circ\text{F}$ , for a CTE of  $4.5 \times 10^{-6}/^\circ\text{F}$  and a stiffness of  $2.8 \times 10^6$  psi.

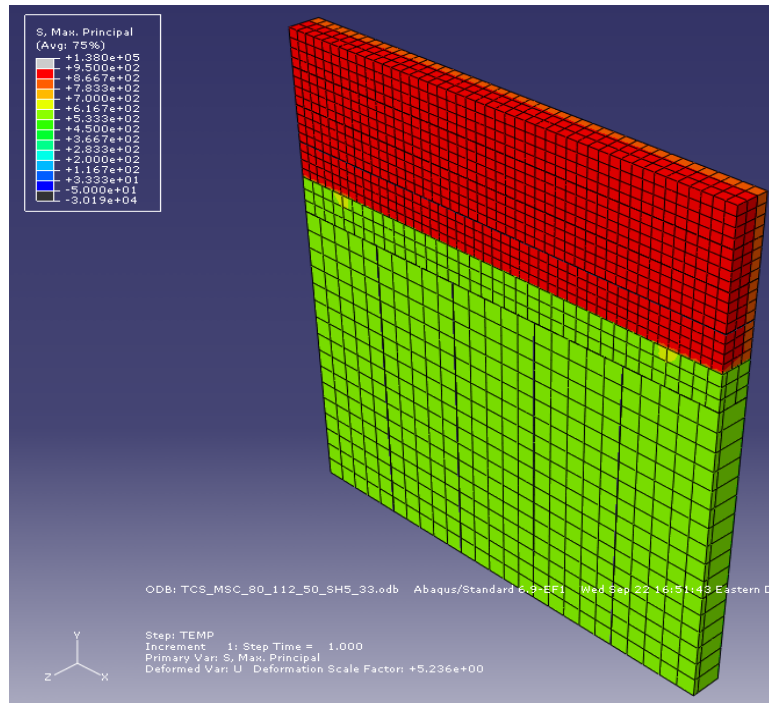


**Figure B248.** 5-ft shoulder transverse cracking model where  $T_M=80^\circ\text{F}$ ,  $T_S=110^\circ\text{F}$ , and  $T_C=50^\circ\text{F}$ , for a CTE of  $4.5 \times 10^{-6}/^\circ\text{F}$  and a stiffness of  $3.3 \times 10^6$  psi.

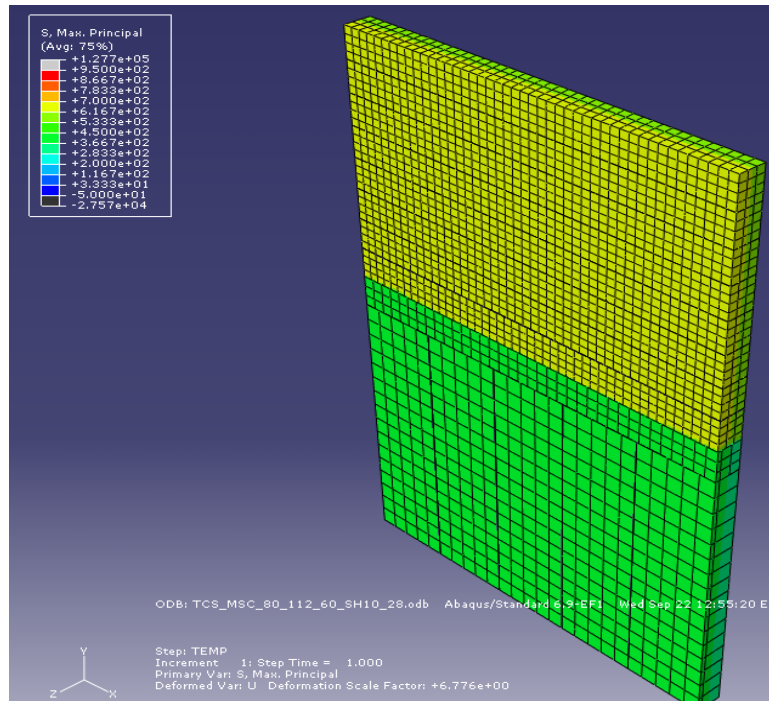


**Figure B249.** 10-ft shoulder transverse cracking model where  $T_M=80^\circ\text{F}$ ,  $T_S=110^\circ\text{F}$ , and  $T_C=60^\circ\text{F}$ , for a CTE of  $4.5 \times 10^{-6}/^\circ\text{F}$  and a stiffness of  $2.8 \times 10^6$  psi.

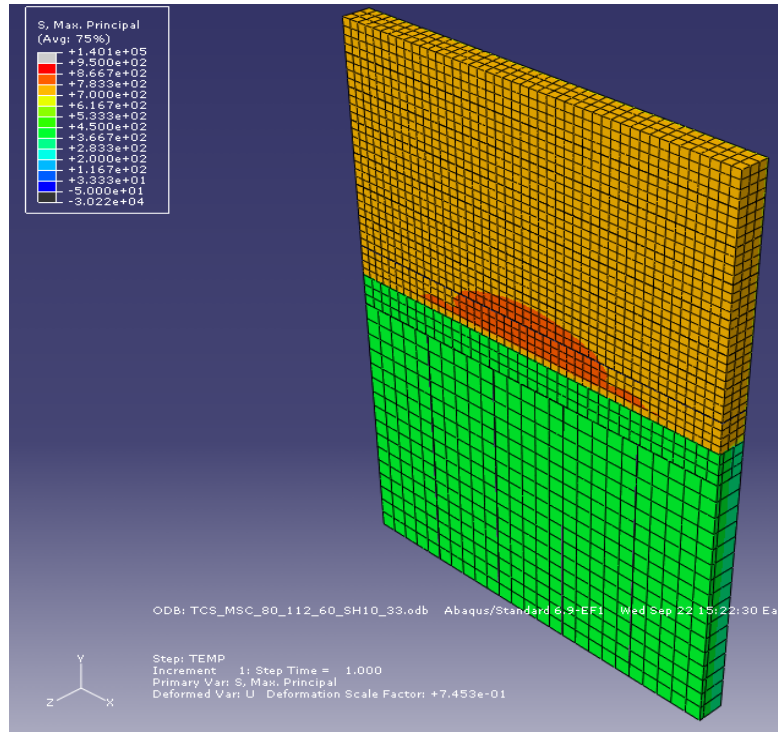


**Figure B250.** 10-ft shoulder transverse cracking model where  $T_M=80^\circ\text{F}$ ,  $T_S=110^\circ\text{F}$ , and  $T_C=60^\circ\text{F}$ , for a CTE of  $4.5 \times 10^{-6}/^\circ\text{F}$  and a stiffness of  $3.3 \times 10^6$  psi.

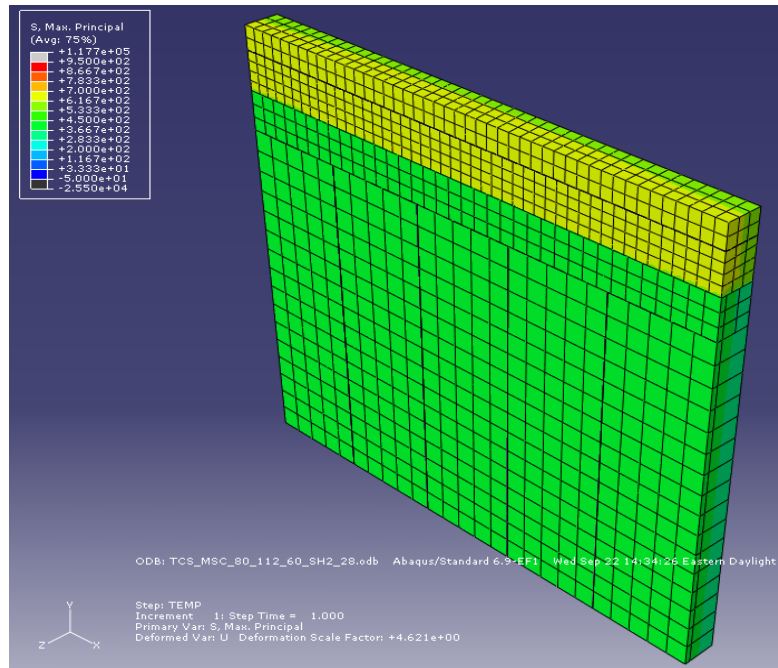


**Figure B251.** 2-ft shoulder transverse cracking model where  $T_M=80^\circ\text{F}$ ,  $T_S=110^\circ\text{F}$ , and  $T_C=60^\circ\text{F}$ , for a CTE of  $4.5 \times 10^{-6}/^\circ\text{F}$  and a stiffness of  $2.8 \times 10^6$  psi.

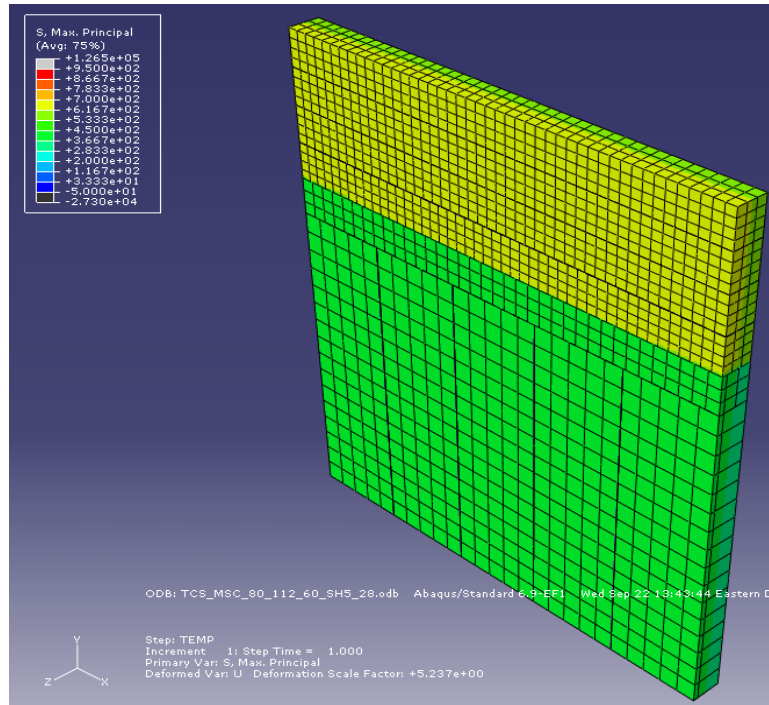


**Figure B252.** 5-ft shoulder transverse cracking model where  $T_M=80^\circ\text{F}$ ,  $T_S=110^\circ\text{F}$ , and  $T_C=60^\circ\text{F}$ , for a CTE of  $4.5 \times 10^{-6}/^\circ\text{F}$  and a stiffness of  $2.8 \times 10^6$  psi.

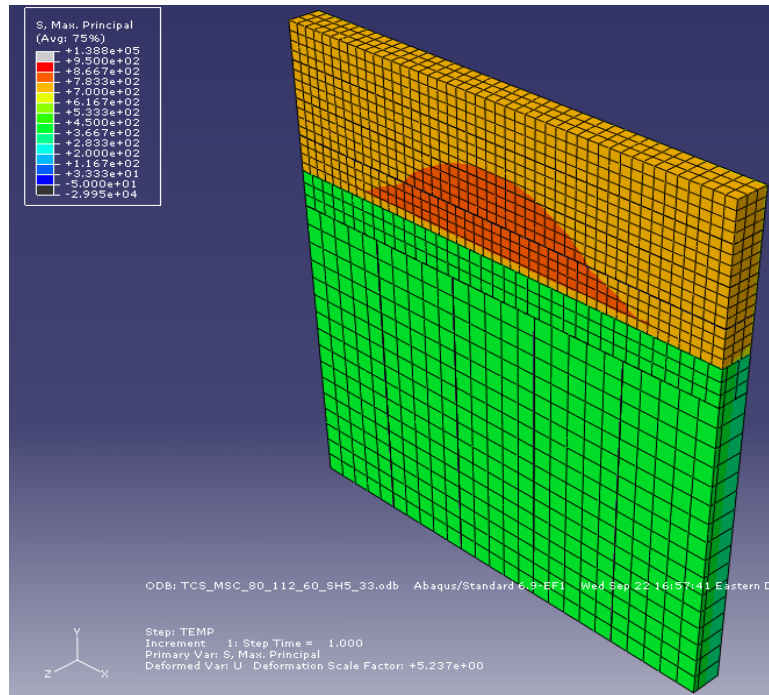


**Figure B253.** 5-ft shoulder transverse cracking model where  $T_M=80^\circ\text{F}$ ,  $T_S=110^\circ\text{F}$ , and  $T_C=60^\circ\text{F}$ , for a CTE of  $4.5 \times 10^{-6}/^\circ\text{F}$  and a stiffness of  $3.3 \times 10^6$  psi.

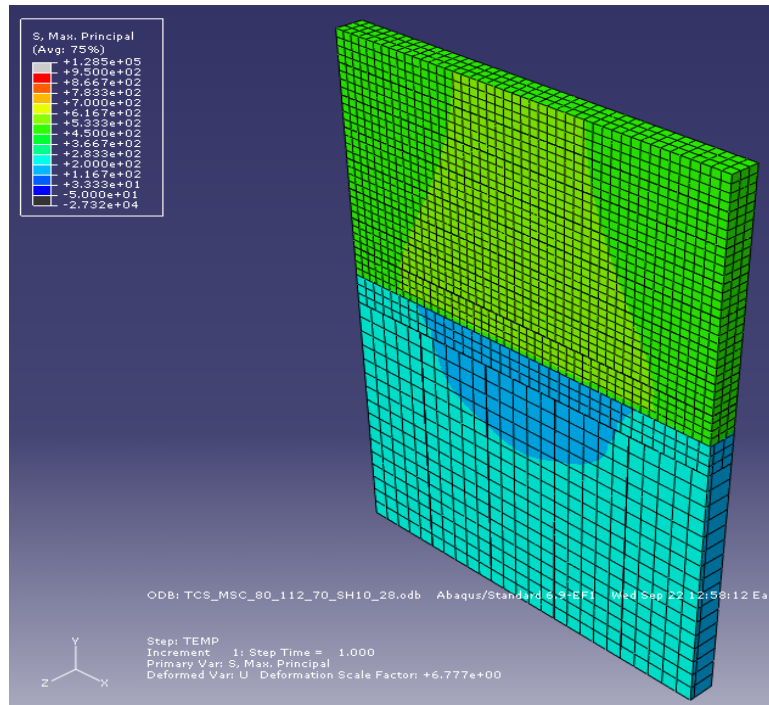


**Figure B254.** 10-ft shoulder transverse cracking model where  $T_M=80^\circ\text{F}$ ,  $T_S=110^\circ\text{F}$ , and  $T_C=70^\circ\text{F}$ , for a CTE of  $4.5 \times 10^{-6}/^\circ\text{F}$  and a stiffness of  $2.8 \times 10^6$  psi.

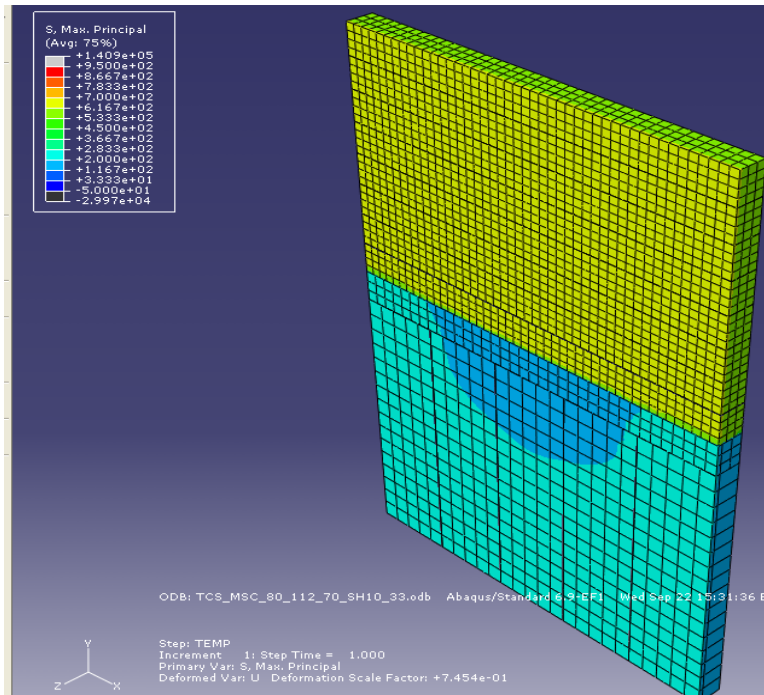


**Figure B255.** 10-ft shoulder transverse cracking model where  $T_M=80^\circ\text{F}$ ,  $T_S=110^\circ\text{F}$ , and  $T_C=70^\circ\text{F}$ , for a CTE of  $4.5 \times 10^{-6}/^\circ\text{F}$  and a stiffness of  $3.3 \times 10^6$  psi.

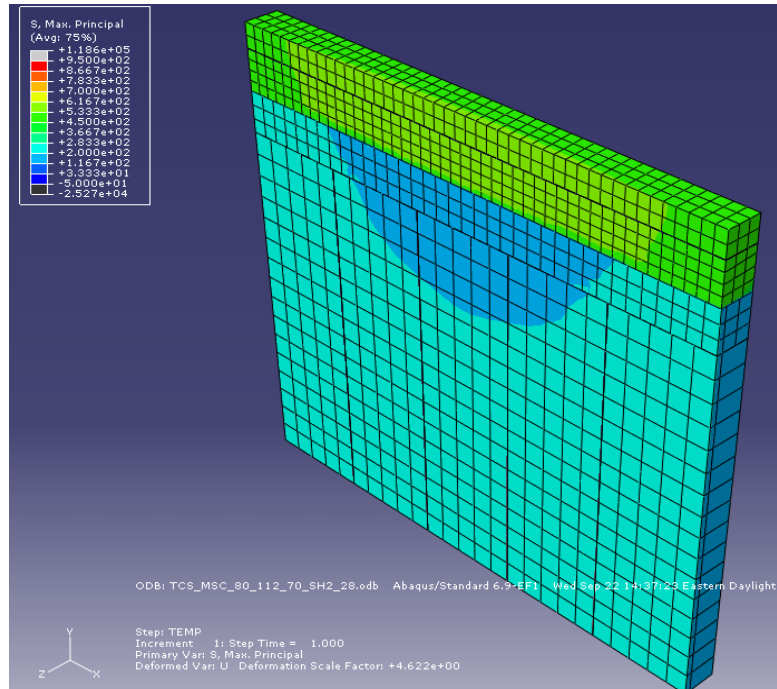


**Figure B256.** 2-ft shoulder transverse cracking model where  $T_M=80^\circ\text{F}$ ,  $T_S=110^\circ\text{F}$ , and  $T_C=70^\circ\text{F}$ , for a CTE of  $4.5 \times 10^{-6}/^\circ\text{F}$  and a stiffness of  $2.8 \times 10^6$  psi.

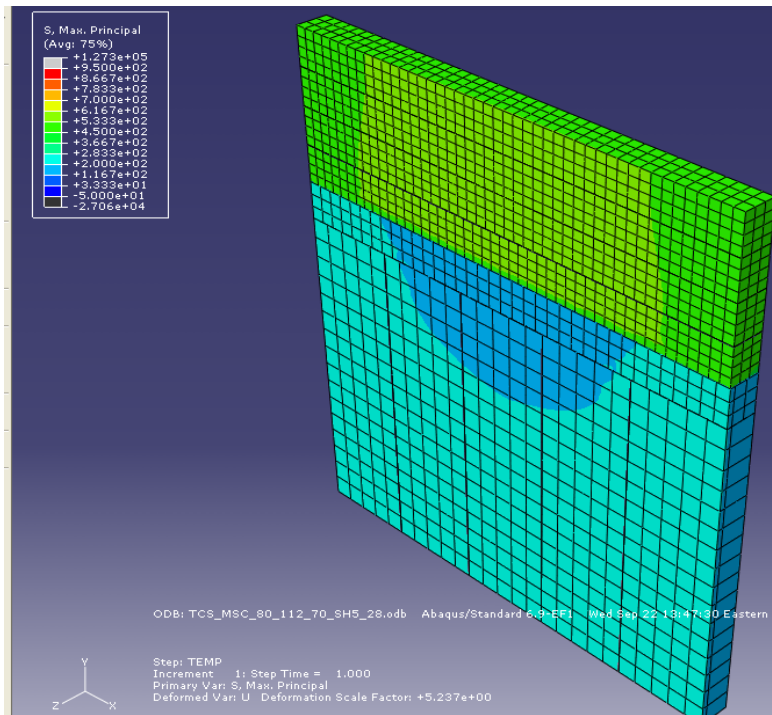


**Figure B257.** 5-ft shoulder transverse cracking model where  $T_M=80^\circ\text{F}$ ,  $T_S=110^\circ\text{F}$ , and  $T_C=70^\circ\text{F}$ , for a CTE of  $4.5 \times 10^{-6}/^\circ\text{F}$  and a stiffness of  $2.8 \times 10^6$  psi.

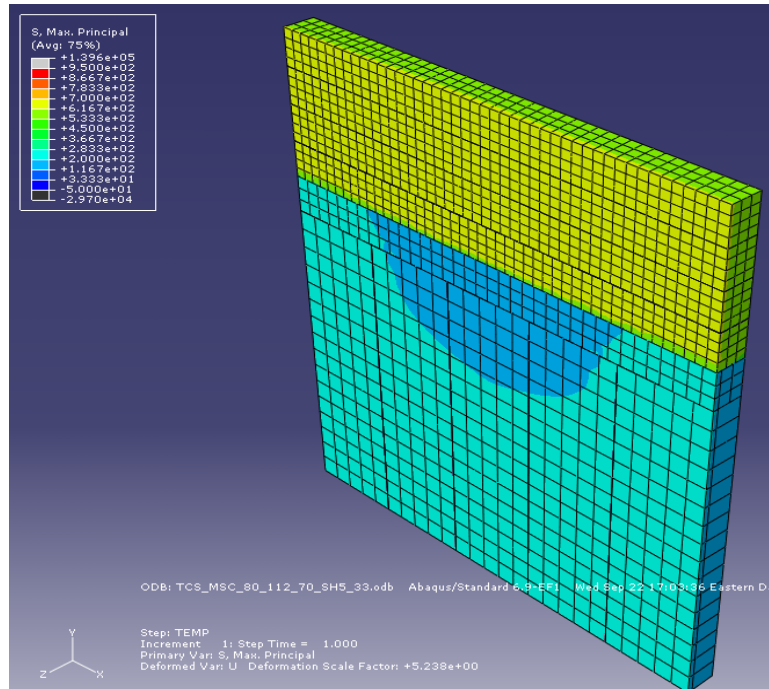


**Figure B258.** 5-ft shoulder transverse cracking model where  $T_M=80^\circ\text{F}$ ,  $T_S=110^\circ\text{F}$ , and  $T_C=70^\circ\text{F}$ , for a CTE of  $4.5 \times 10^{-6}/^\circ\text{F}$  and a stiffness of  $3.3 \times 10^6$  psi.

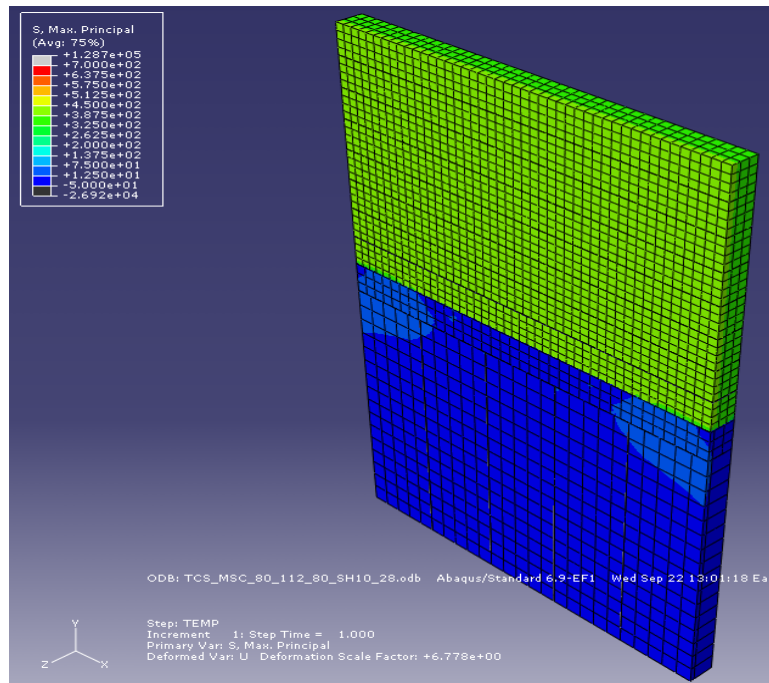


**Figure B259.** 10-ft shoulder transverse cracking model where  $T_M=80^\circ\text{F}$ ,  $T_S=110^\circ\text{F}$ , and  $T_C=80^\circ\text{F}$ , for a CTE of  $4.5 \times 10^{-6}/^\circ\text{F}$  and a stiffness of  $2.8 \times 10^6$  psi.

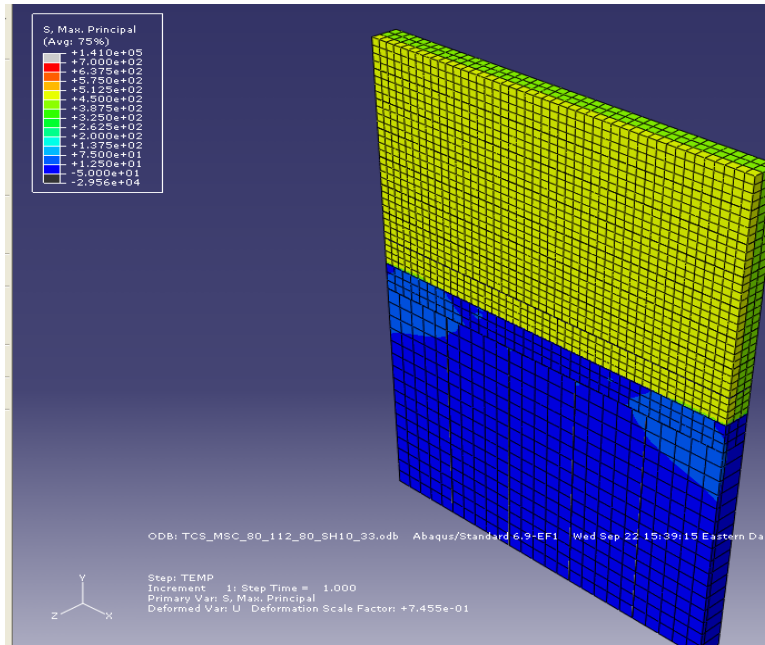


**Figure B260.** 10-ft shoulder transverse cracking model where  $T_M=80^\circ\text{F}$ ,  $T_S=110^\circ\text{F}$ , and  $T_C=80^\circ\text{F}$ , for a CTE of  $4.5 \times 10^{-6}/^\circ\text{F}$  and a stiffness of  $3.3 \times 10^6$  psi.

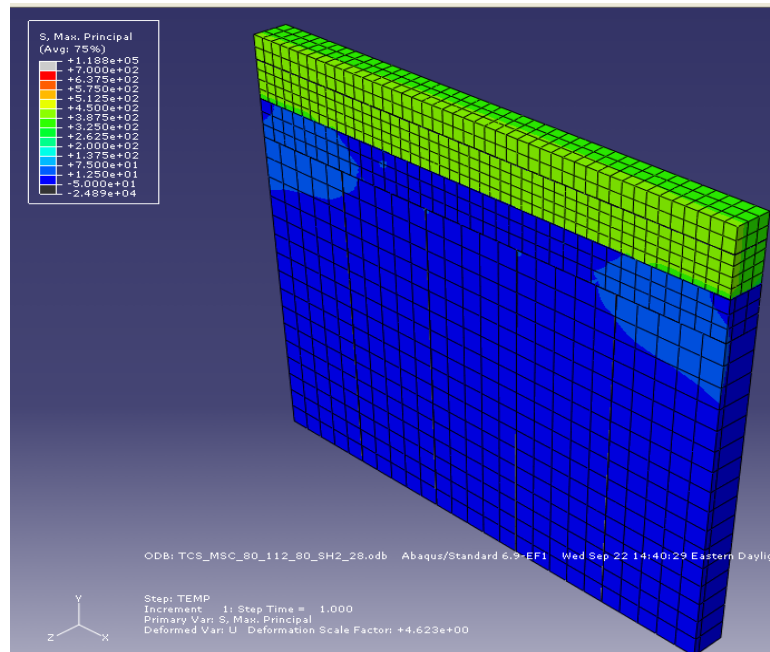


**Figure B261.** 2-ft shoulder transverse cracking model where  $T_M=80^\circ\text{F}$ ,  $T_S=110^\circ\text{F}$ , and  $T_C=80^\circ\text{F}$ , for a CTE of  $4.5 \times 10^{-6}/^\circ\text{F}$  and a stiffness of  $2.8 \times 10^6$  psi.

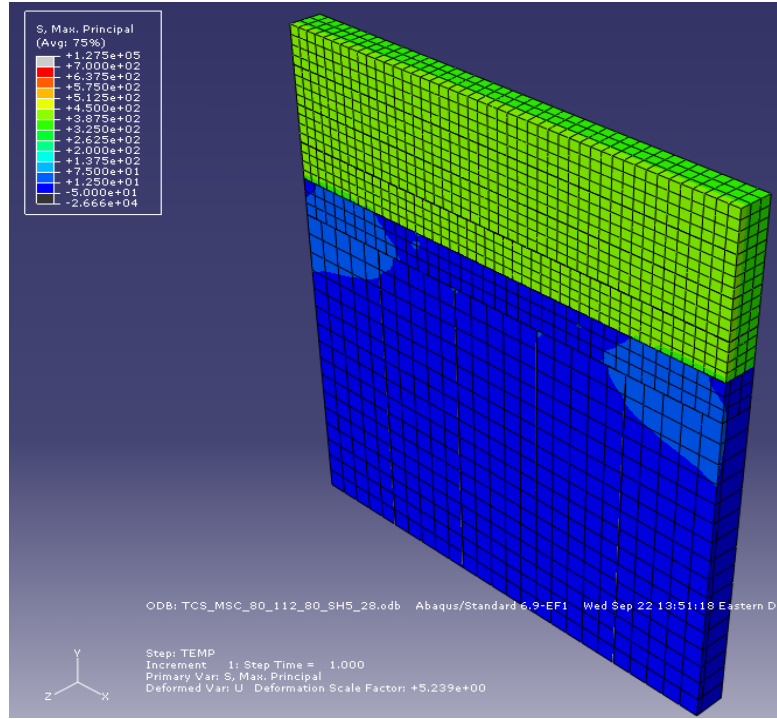


**Figure B262.** 5-ft shoulder transverse cracking model where  $T_M=80^\circ\text{F}$ ,  $T_S=110^\circ\text{F}$ , and  $T_C=80^\circ\text{F}$ , for a CTE of  $4.5 \times 10^{-6}/^\circ\text{F}$  and a stiffness of  $2.8 \times 10^6$  psi.

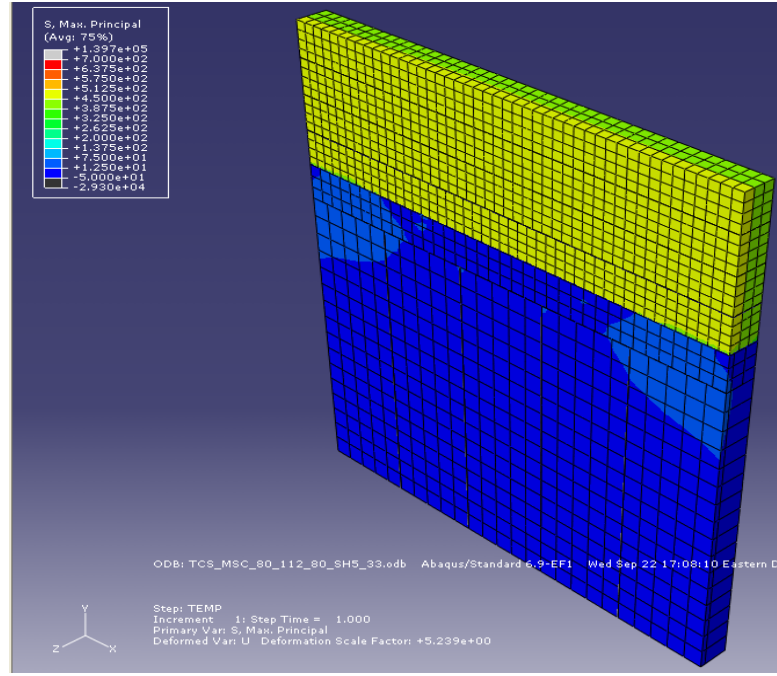


**Figure B263.** 5-ft shoulder transverse cracking model where  $T_M=80^\circ\text{F}$ ,  $T_S=110^\circ\text{F}$ , and  $T_C=80^\circ\text{F}$ , for a CTE of  $4.5 \times 10^{-6}/^\circ\text{F}$  and a stiffness of  $3.3 \times 10^6$  psi.

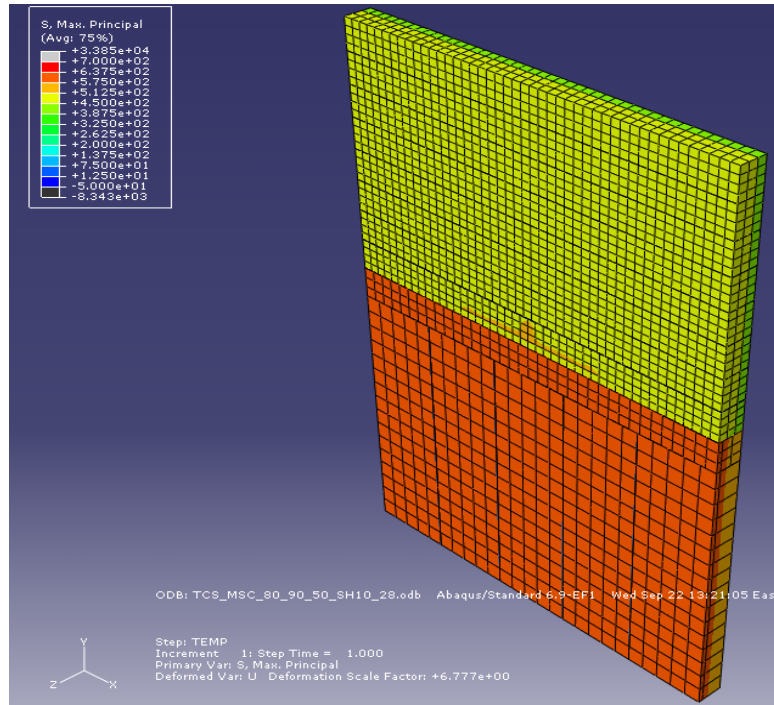


**Figure B264.** 10-ft shoulder transverse cracking model where  $T_M=80^\circ\text{F}$ ,  $T_S=90^\circ\text{F}$ , and  $T_C=50^\circ\text{F}$ , for a CTE of  $4.5 \times 10^{-6}/^\circ\text{F}$  and a stiffness of  $2.8 \times 10^6$  psi.

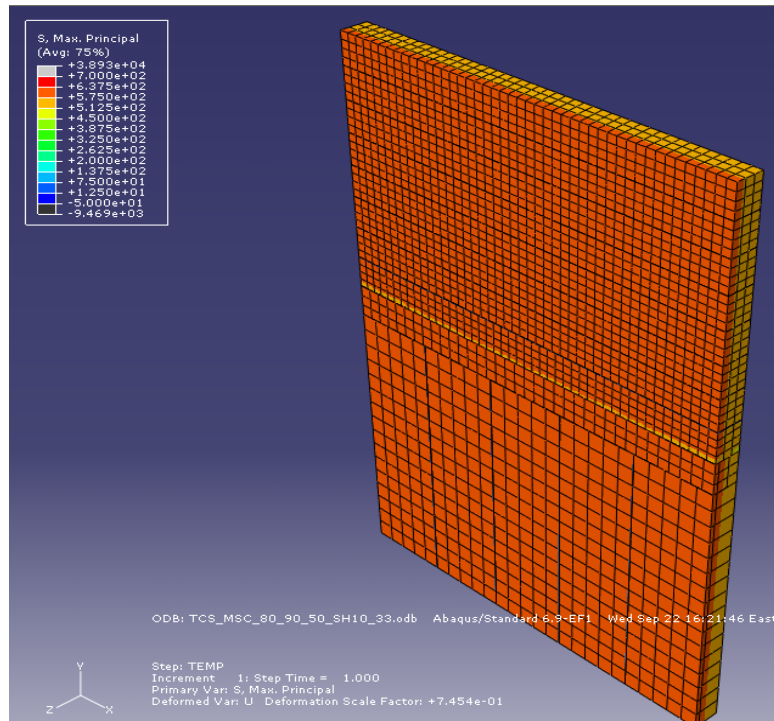


**Figure B265.** 10-ft shoulder transverse cracking model where  $T_M=80^\circ\text{F}$ ,  $T_S=90^\circ\text{F}$ , and  $T_C=50^\circ\text{F}$ , for a CTE of  $4.5 \times 10^{-6}/^\circ\text{F}$  and a stiffness of  $3.3 \times 10^6$  psi.

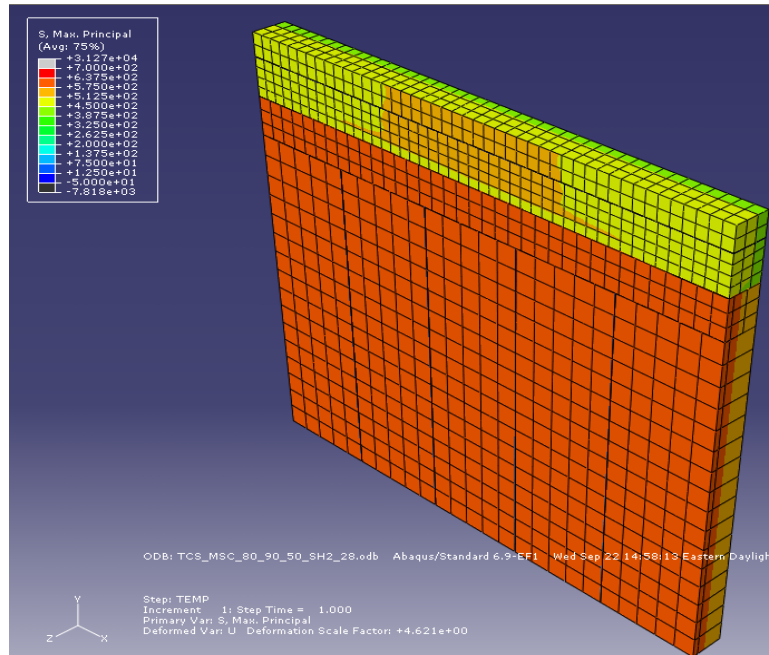


**Figure B266.** 2-ft shoulder transverse cracking model where  $T_M=80^\circ\text{F}$ ,  $T_S=90^\circ\text{F}$ , and  $T_C=50^\circ\text{F}$ , for a CTE of  $4.5 \times 10^{-6}/^\circ\text{F}$  and a stiffness of  $2.8 \times 10^6$  psi.

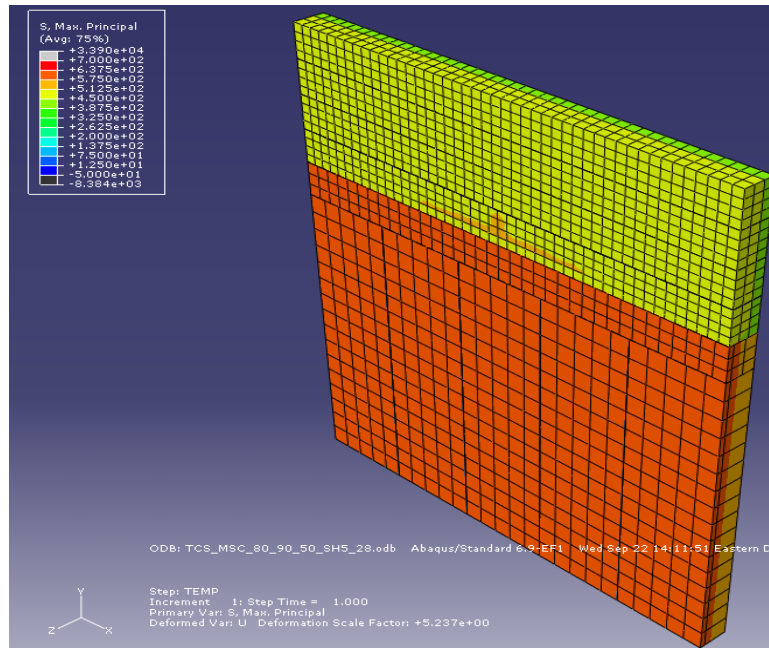


**Figure B267.** 5-ft shoulder transverse cracking model where  $T_M=80^\circ\text{F}$ ,  $T_S=90^\circ\text{F}$ , and  $T_C=50^\circ\text{F}$ , for a CTE of  $4.5 \times 10^{-6}/^\circ\text{F}$  and a stiffness of  $2.8 \times 10^6$  psi.

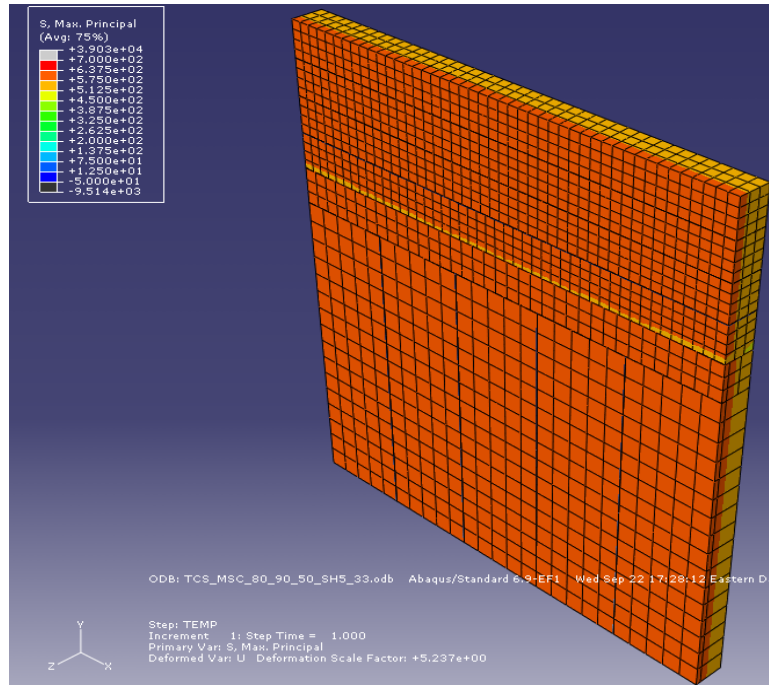


**Figure B268.** 5-ft shoulder transverse cracking model where  $T_M=80^\circ\text{F}$ ,  $T_S=90^\circ\text{F}$ , and  $T_C=50^\circ\text{F}$ , for a CTE of  $4.5 \times 10^{-6}/^\circ\text{F}$  and a stiffness of  $3.3 \times 10^6$  psi.

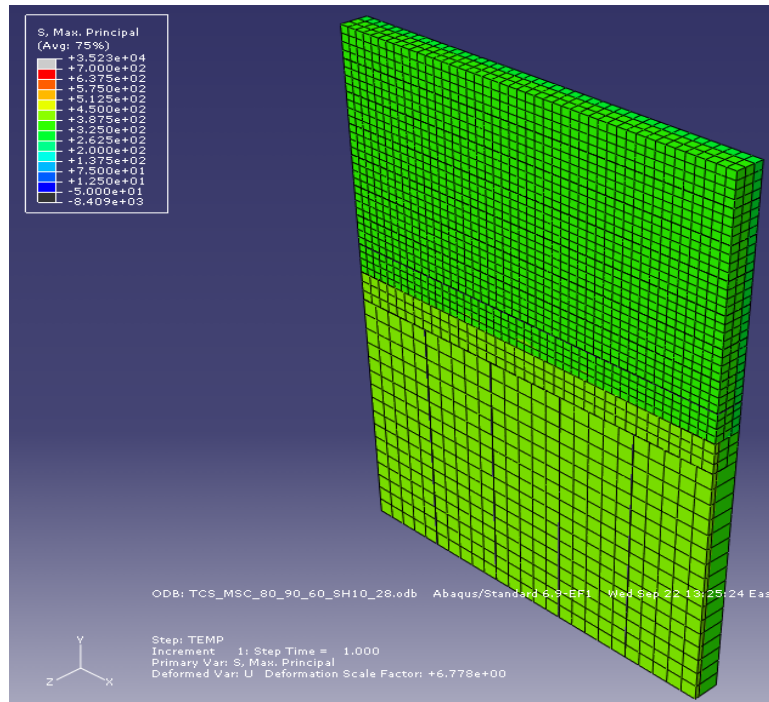


**Figure B269.** 10-ft shoulder transverse cracking model where  $T_M=80^\circ\text{F}$ ,  $T_S=90^\circ\text{F}$ , and  $T_C=60^\circ\text{F}$ , for a CTE of  $4.5 \times 10^{-6}/^\circ\text{F}$  and a stiffness of  $2.8 \times 10^6$  psi.

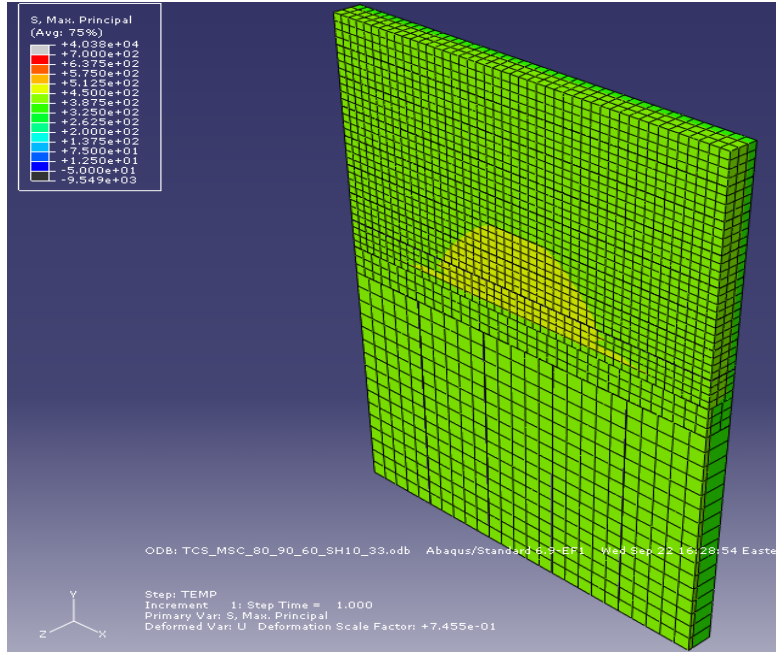


**Figure B270.** 10-ft shoulder transverse cracking model where  $T_M=80^\circ\text{F}$ ,  $T_S=90^\circ\text{F}$ , and  $T_C=60^\circ\text{F}$ , for a CTE of  $4.5 \times 10^{-6}/^\circ\text{F}$  and a stiffness of  $3.3 \times 10^6$  psi.

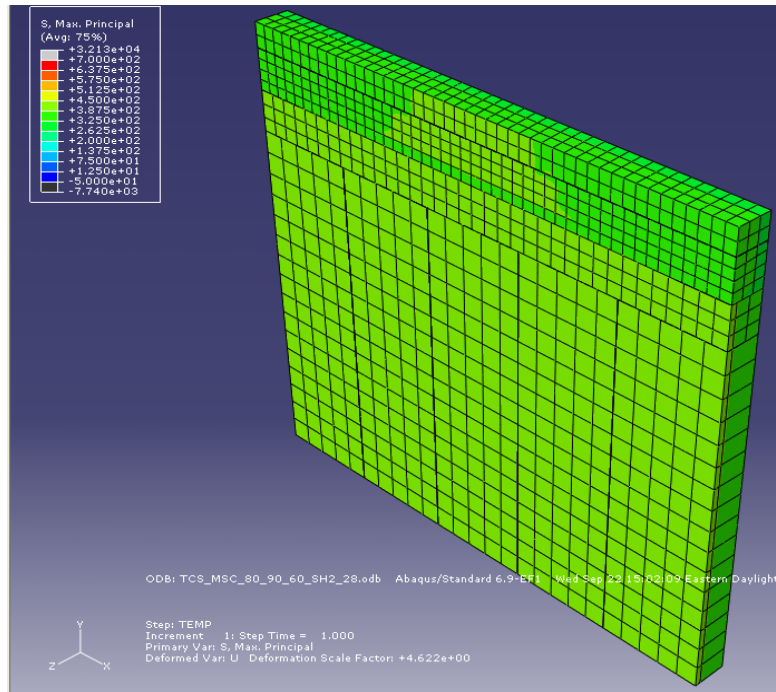


**Figure B271.** 2-ft shoulder transverse cracking model where  $T_M=80^\circ\text{F}$ ,  $T_S=90^\circ\text{F}$ , and  $T_C=60^\circ\text{F}$ , for a CTE of  $4.5 \times 10^{-6}/^\circ\text{F}$  and a stiffness of  $2.8 \times 10^6$  psi.

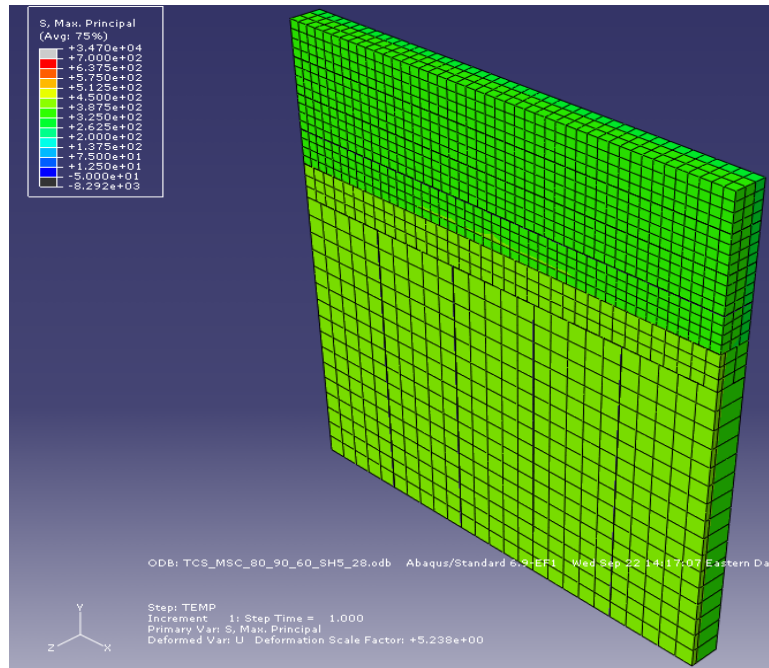


**Figure B272.** 5-ft shoulder transverse cracking model where  $T_M=80^\circ\text{F}$ ,  $T_S=90^\circ\text{F}$ , and  $T_C=60^\circ\text{F}$ , for a CTE of  $4.5 \times 10^{-6}/^\circ\text{F}$  and a stiffness of  $2.8 \times 10^6$  psi.

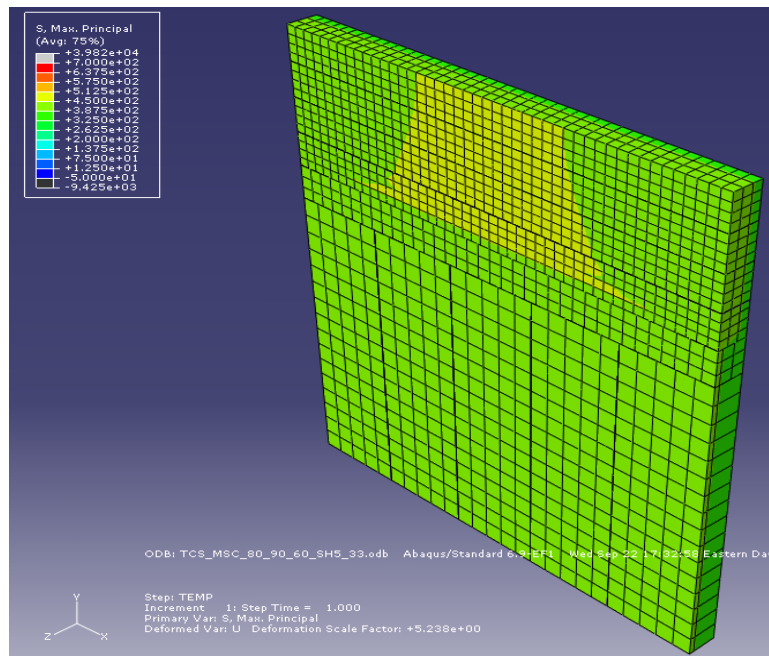


**Figure B273.** 5-ft shoulder transverse cracking model where  $T_M=80^\circ\text{F}$ ,  $T_S=90^\circ\text{F}$ , and  $T_C=60^\circ\text{F}$ , for a CTE of  $4.5 \times 10^{-6}/^\circ\text{F}$  and a stiffness of  $3.3 \times 10^6$  psi.

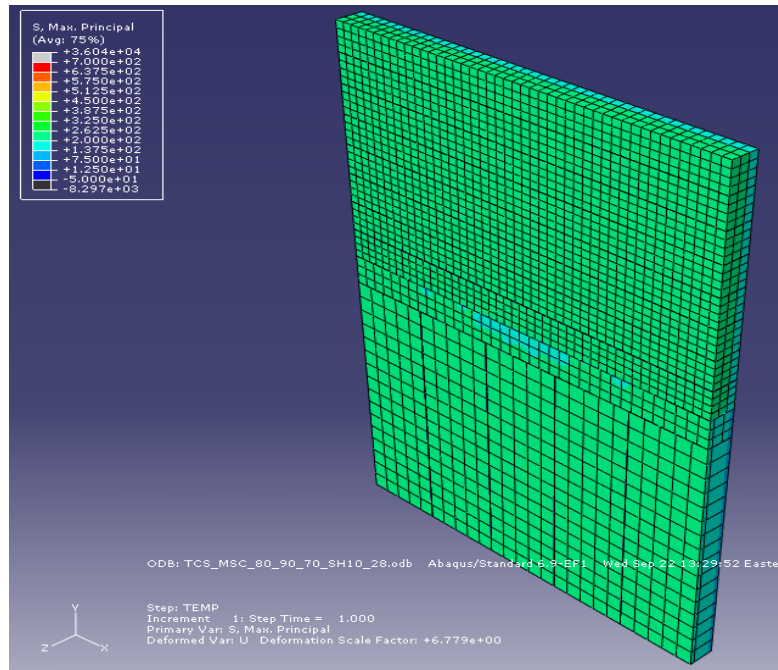


**Figure B274.** 10-ft shoulder transverse cracking model where  $T_M=80^\circ\text{F}$ ,  $T_S=90^\circ\text{F}$ , and  $T_C=70^\circ\text{F}$ , for a CTE of  $4.5 \times 10^{-6}/^\circ\text{F}$  and a stiffness of  $2.8 \times 10^6$  psi.

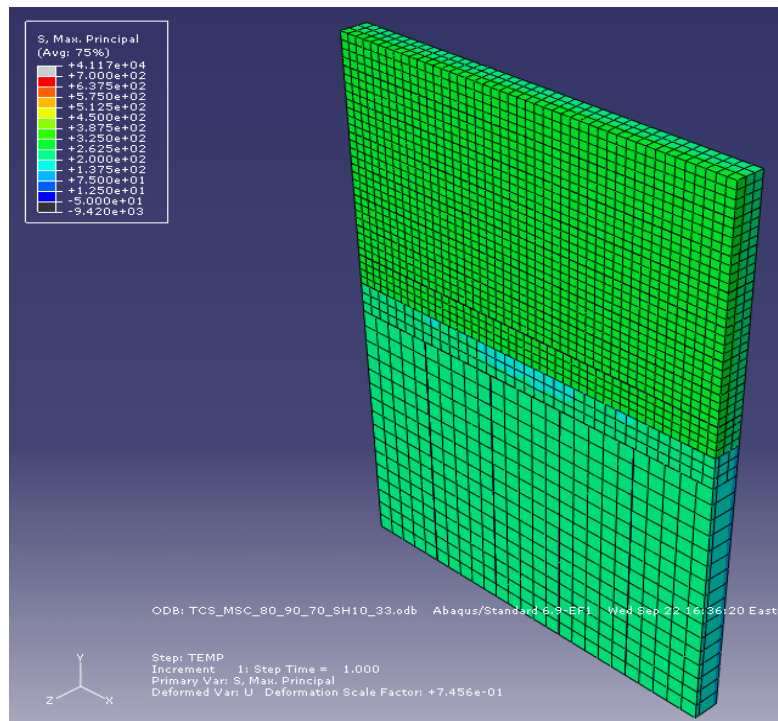


**Figure B275.** 10-ft shoulder transverse cracking model where  $T_M=80^\circ\text{F}$ ,  $T_S=90^\circ\text{F}$ , and  $T_C=70^\circ\text{F}$ , for a CTE of  $4.5 \times 10^{-6}/^\circ\text{F}$  and a stiffness of  $3.3 \times 10^6$  psi.

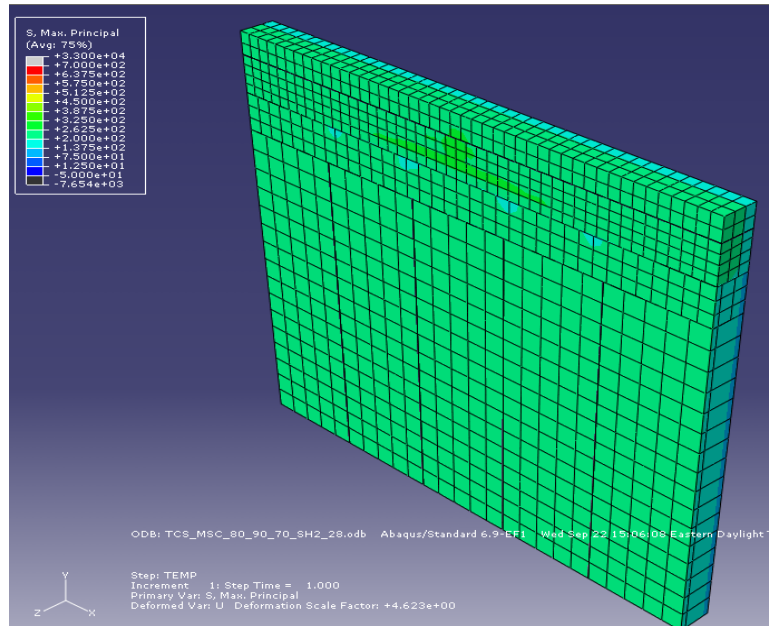


**Figure B276.** 2-ft shoulder transverse cracking model where  $T_M=80^\circ\text{F}$ ,  $T_S=90^\circ\text{F}$ , and  $T_C=70^\circ\text{F}$ , for a CTE of  $4.5 \times 10^{-6}/^\circ\text{F}$  and a stiffness of  $2.8 \times 10^6$  psi.

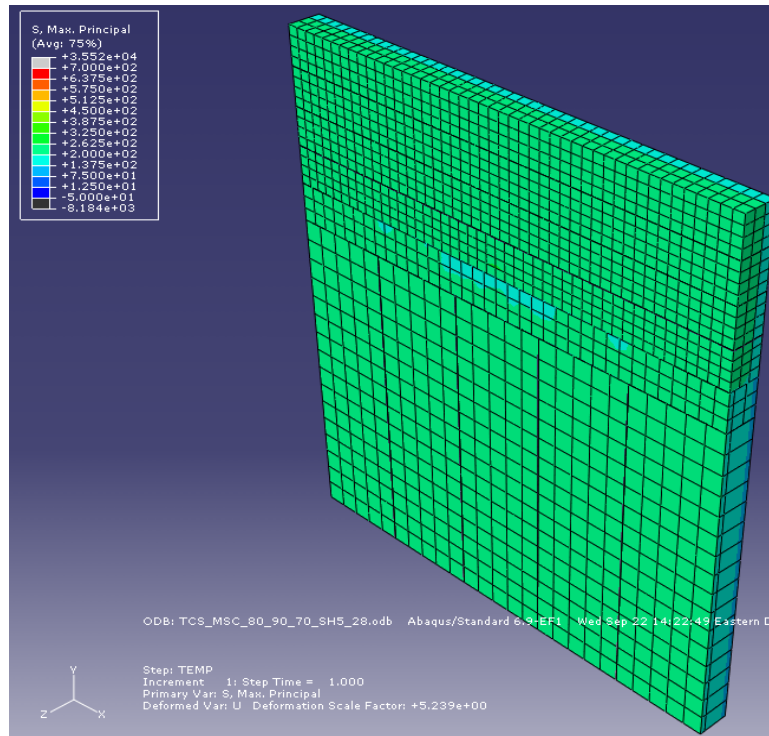


**Figure B277.** 5-ft shoulder transverse cracking model where  $T_M=80^\circ\text{F}$ ,  $T_S=90^\circ\text{F}$ , and  $T_C=70^\circ\text{F}$ , for a CTE of  $4.5 \times 10^{-6}/^\circ\text{F}$  and a stiffness of  $2.8 \times 10^6$  psi.

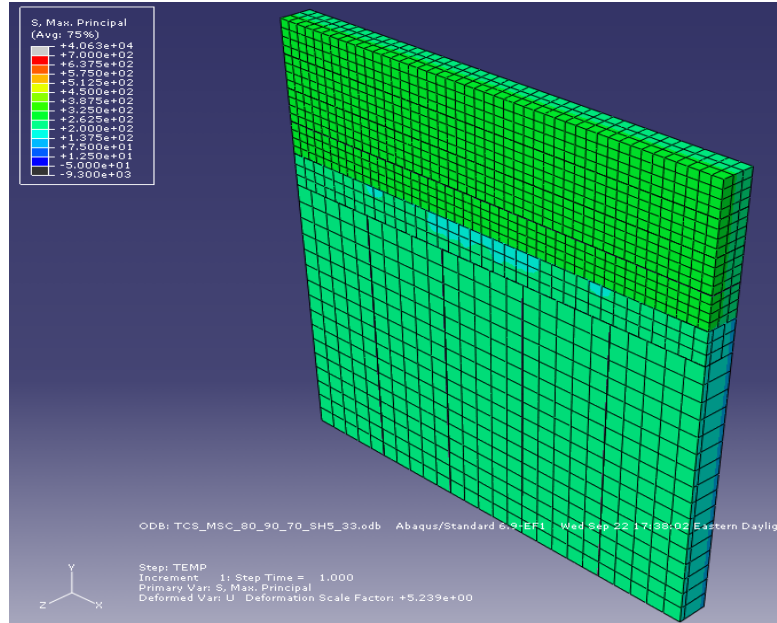


**Figure B278.** 5-ft shoulder transverse cracking model where  $T_M=80^\circ\text{F}$ ,  $T_S=90^\circ\text{F}$ , and  $T_C=70^\circ\text{F}$ , for a CTE of  $4.5 \times 10^{-6}/^\circ\text{F}$  and a stiffness of  $3.3 \times 10^6$  psi.

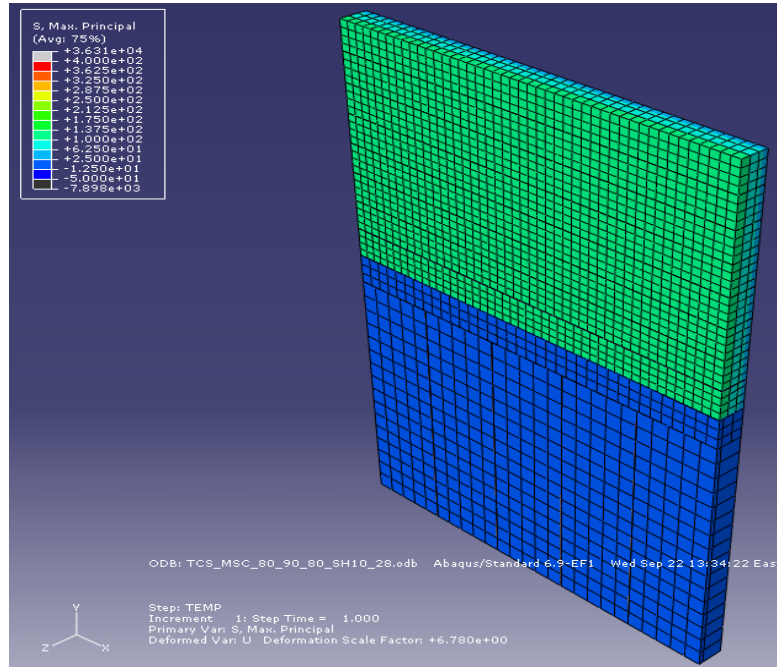


**Figure B279.** 10-ft shoulder transverse cracking model where  $T_M=80^\circ\text{F}$ ,  $T_S=90^\circ\text{F}$ , and  $T_C=80^\circ\text{F}$ , for a CTE of  $4.5 \times 10^{-6}/^\circ\text{F}$  and a stiffness of  $2.8 \times 10^6$  psi.

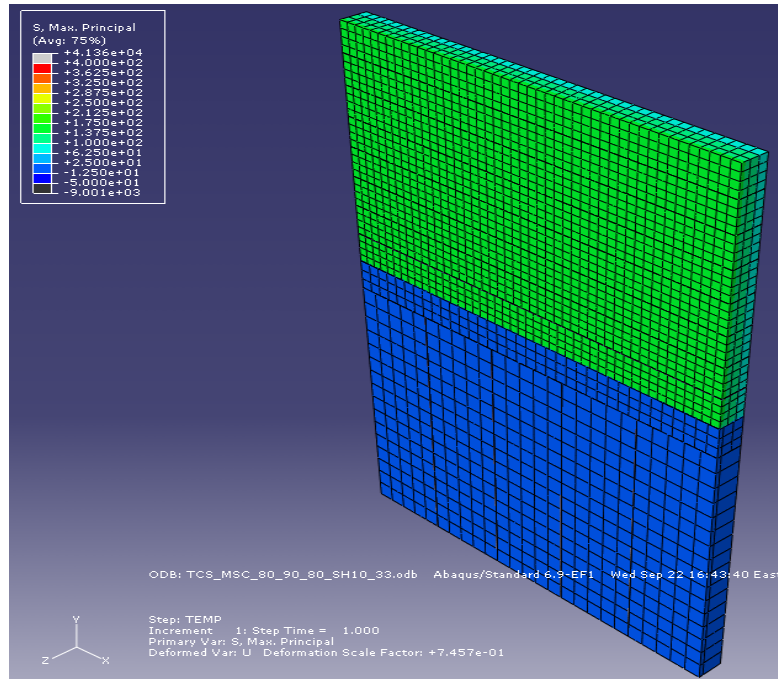


**Figure B280.** 10-ft shoulder transverse cracking model where  $T_M=80^\circ\text{F}$ ,  $T_S=90^\circ\text{F}$ , and  $T_C=80^\circ\text{F}$ , for a CTE of  $4.5 \times 10^{-6}/^\circ\text{F}$  and a stiffness of  $3.3 \times 10^6$  psi.

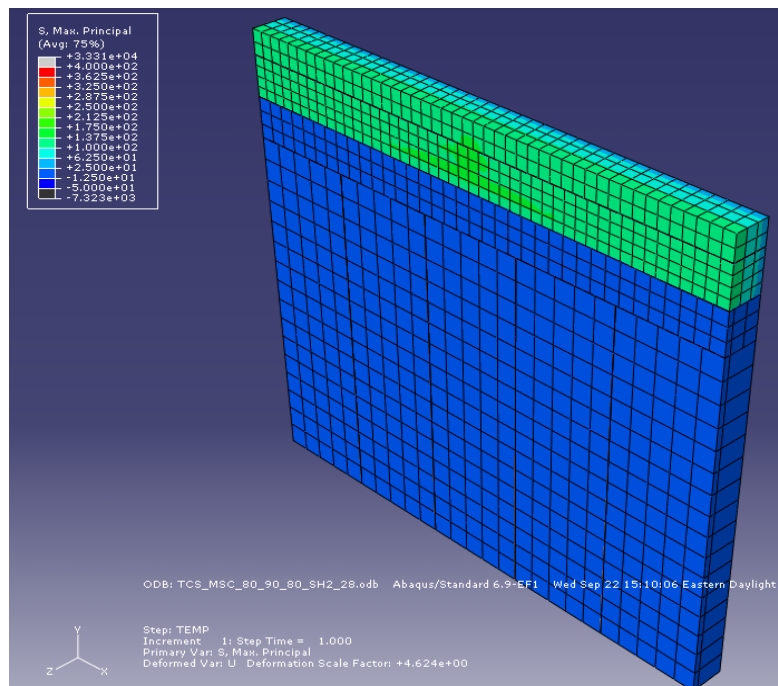


**Figure B281.** 2-ft shoulder transverse cracking model where  $T_M=80^\circ\text{F}$ ,  $T_S=90^\circ\text{F}$ , and  $T_C=80^\circ\text{F}$ , for a CTE of  $4.5 \times 10^{-6}/^\circ\text{F}$  and a stiffness of  $2.8 \times 10^6$  psi.

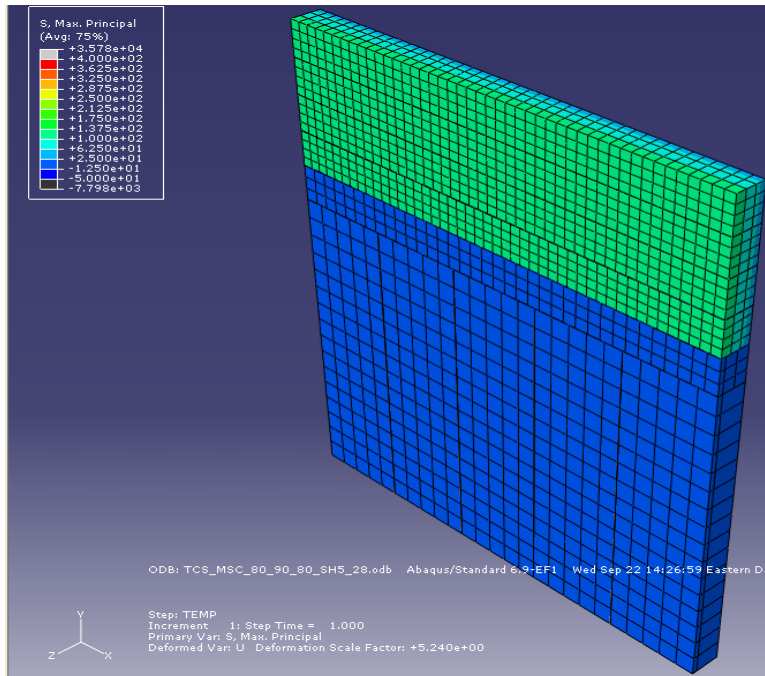


**Figure B282.** 5-ft shoulder transverse cracking model where  $T_M=80^\circ\text{F}$ ,  $T_S=90^\circ\text{F}$ , and  $T_C=80^\circ\text{F}$ , for a CTE of  $4.5 \times 10^{-6}/^\circ\text{F}$  and a stiffness of  $2.8 \times 10^6$  psi.

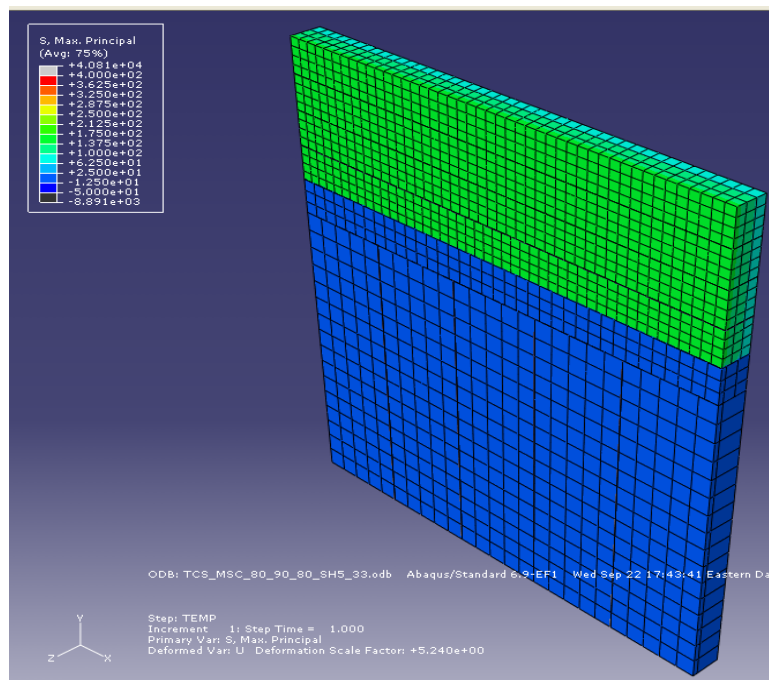


**Figure B283.** 5-ft shoulder transverse cracking model where  $T_M=80^\circ\text{F}$ ,  $T_S=90^\circ\text{F}$ , and  $T_C=80^\circ\text{F}$ , for a CTE of  $4.5 \times 10^{-6}/^\circ\text{F}$  and a stiffness of  $3.3 \times 10^6$  psi.

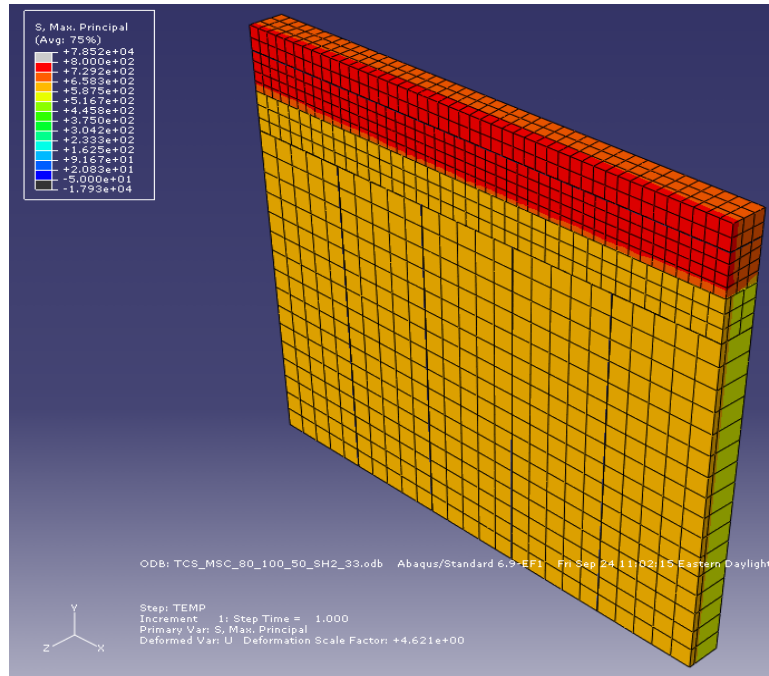


**Figure B284.** 2-ft shoulder transverse cracking model where  $T_M=80^\circ\text{F}$ ,  $T_S=100^\circ\text{F}$ , and  $T_C=50^\circ\text{F}$ , for a CTE of  $4.5 \times 10^{-6}/^\circ\text{F}$  and a stiffness of  $3.3 \times 10^6$  psi.

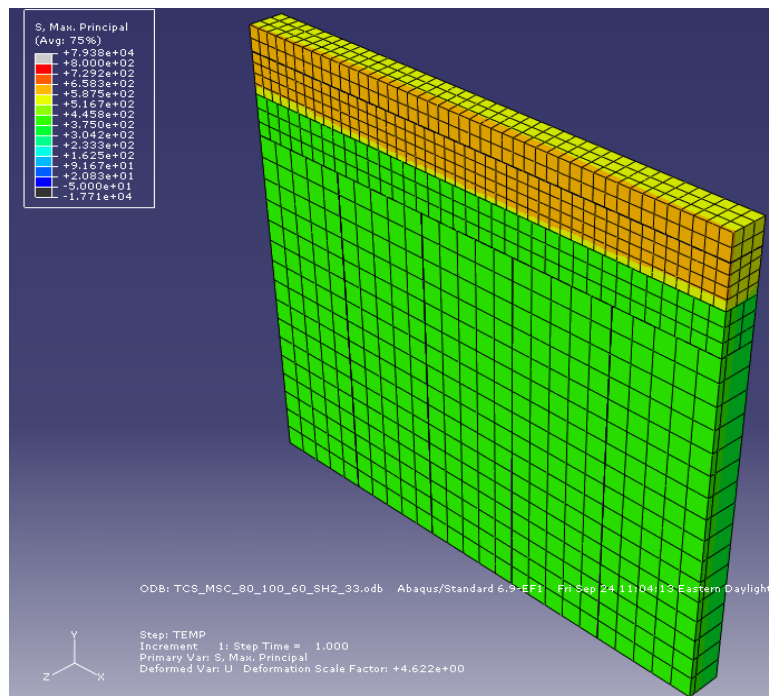


**Figure B285.** 2-ft shoulder transverse cracking model where  $T_M=80^\circ\text{F}$ ,  $T_S=100^\circ\text{F}$ , and  $T_C=60^\circ\text{F}$ , for a CTE of  $4.5 \times 10^{-6}/^\circ\text{F}$  and a stiffness of  $3.3 \times 10^6$  psi.

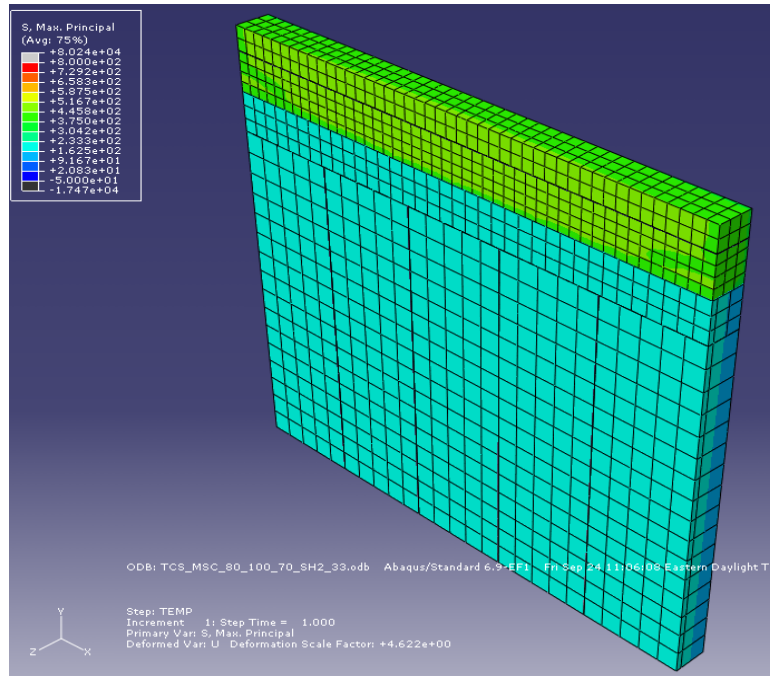


**Figure B286.** 2-ft shoulder transverse cracking model where  $T_M=80^\circ\text{F}$ ,  $T_S=100^\circ\text{F}$ , and  $T_C=70^\circ\text{F}$ , for a CTE of  $4.5 \times 10^{-6}/^\circ\text{F}$  and a stiffness of  $3.3 \times 10^6$  psi.

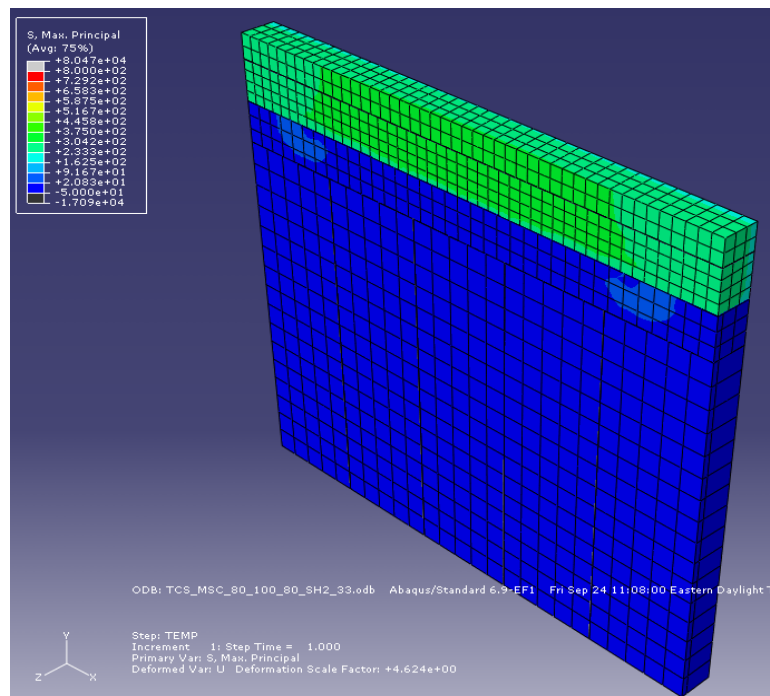


**Figure B287.** 2-ft shoulder transverse cracking model where  $T_M=80^\circ\text{F}$ ,  $T_S=100^\circ\text{F}$ , and  $T_C=80^\circ\text{F}$ , for a CTE of  $4.5 \times 10^{-6}/^\circ\text{F}$  and a stiffness of  $3.3 \times 10^6$  psi.

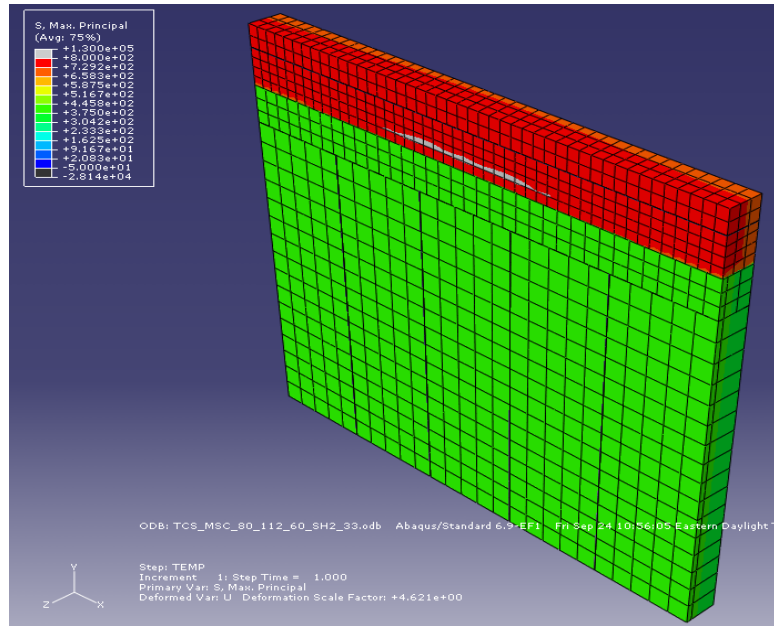


**Figure B288.** 2-ft shoulder transverse cracking model where  $T_M=80^\circ\text{F}$ ,  $T_S=110^\circ\text{F}$ , and  $T_C=60^\circ\text{F}$ , for a CTE of  $4.5 \times 10^{-6}/^\circ\text{F}$  and a stiffness of  $3.3 \times 10^6$  psi.

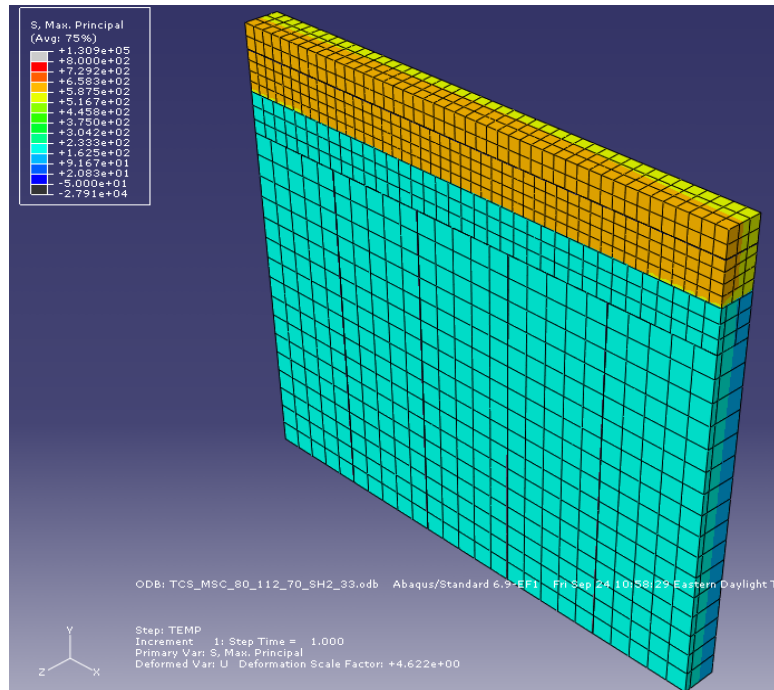


**Figure B289.** 2-ft shoulder transverse cracking model where  $T_M=80^\circ\text{F}$ ,  $T_S=110^\circ\text{F}$ , and  $T_C=70^\circ\text{F}$ , for a CTE of  $4.5 \times 10^{-6}/^\circ\text{F}$  and a stiffness of  $3.3 \times 10^6$  psi.

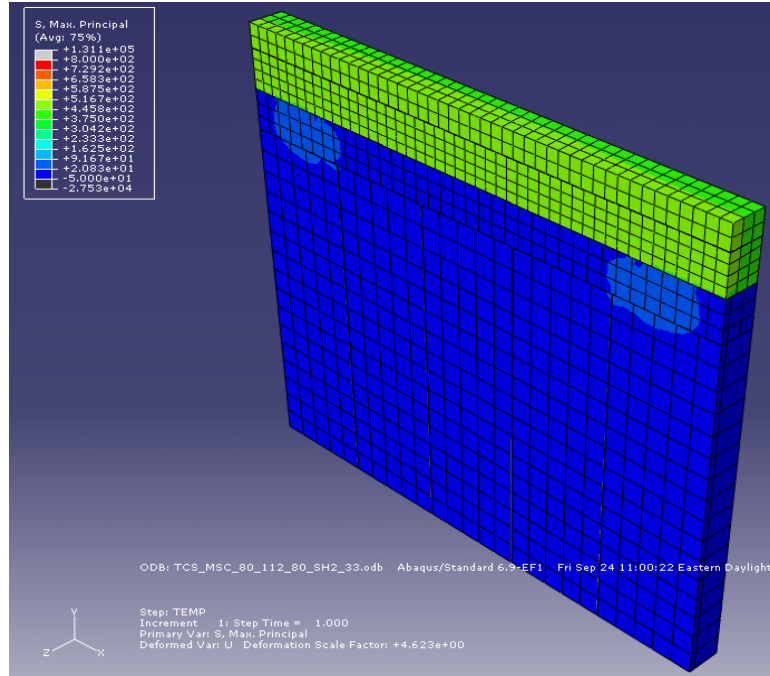


**Figure B290.** 2-ft shoulder transverse cracking model where  $T_M=80^\circ\text{F}$ ,  $T_S=110^\circ\text{F}$ , and  $T_C=80^\circ\text{F}$ , for a CTE of  $4.5 \times 10^{-6}/^\circ\text{F}$  and a stiffness of  $3.3 \times 10^6$  psi.

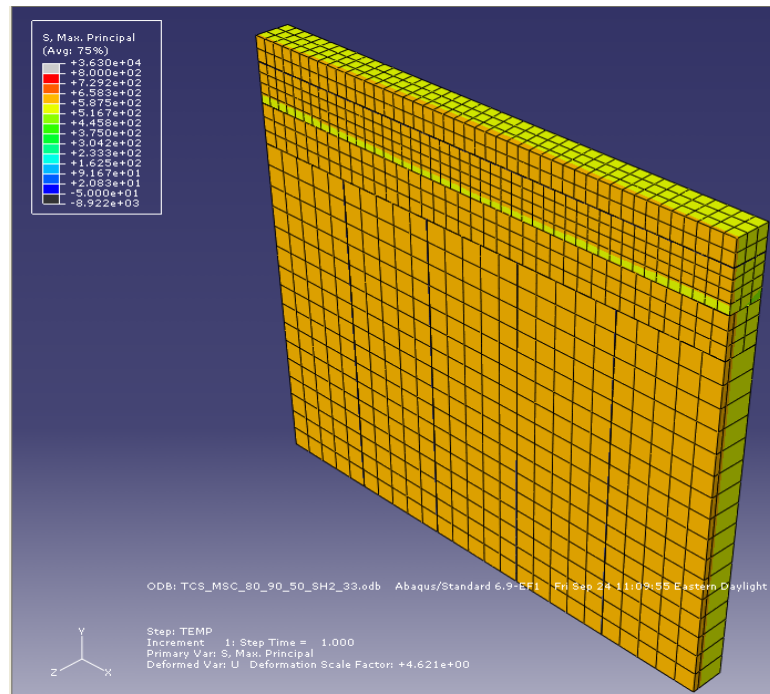


**Figure B291.** 2-ft shoulder transverse cracking model where  $T_M=80^\circ\text{F}$ ,  $T_S=90^\circ\text{F}$ , and  $T_C=50^\circ\text{F}$ , for a CTE of  $4.5 \times 10^{-6}/^\circ\text{F}$  and a stiffness of  $3.3 \times 10^6$  psi.

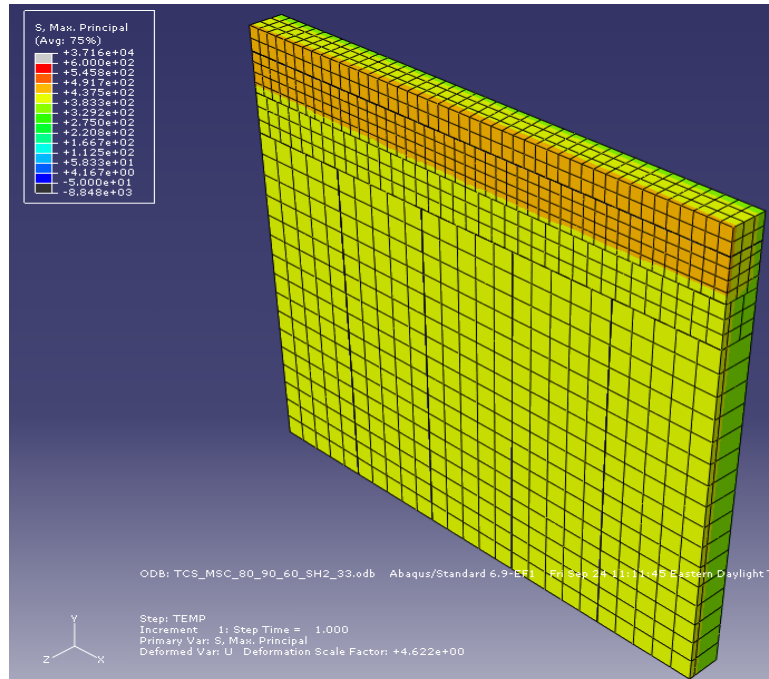


**Figure B292.** 2-ft shoulder transverse cracking model where  $T_M=80^\circ\text{F}$ ,  $T_S=90^\circ\text{F}$ , and  $T_C=60^\circ\text{F}$ , for a CTE of  $4.5 \times 10^{-6}/^\circ\text{F}$  and a stiffness of  $3.3 \times 10^6$  psi.

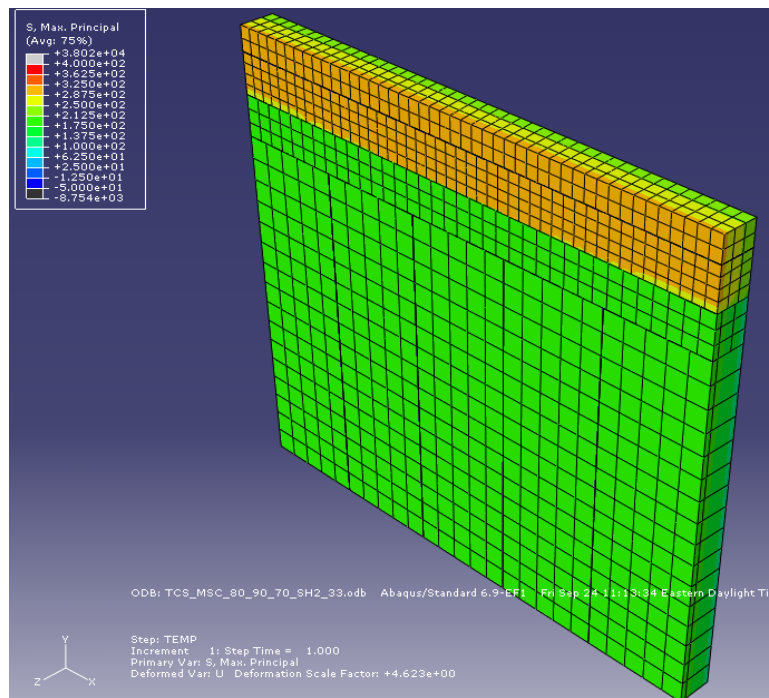


**Figure B293.** 2-ft shoulder transverse cracking model where  $T_M=80^\circ\text{F}$ ,  $T_S=90^\circ\text{F}$ , and  $T_C=70^\circ\text{F}$ , for a CTE of  $4.5 \times 10^{-6}/^\circ\text{F}$  and a stiffness of  $3.3 \times 10^6$  psi.

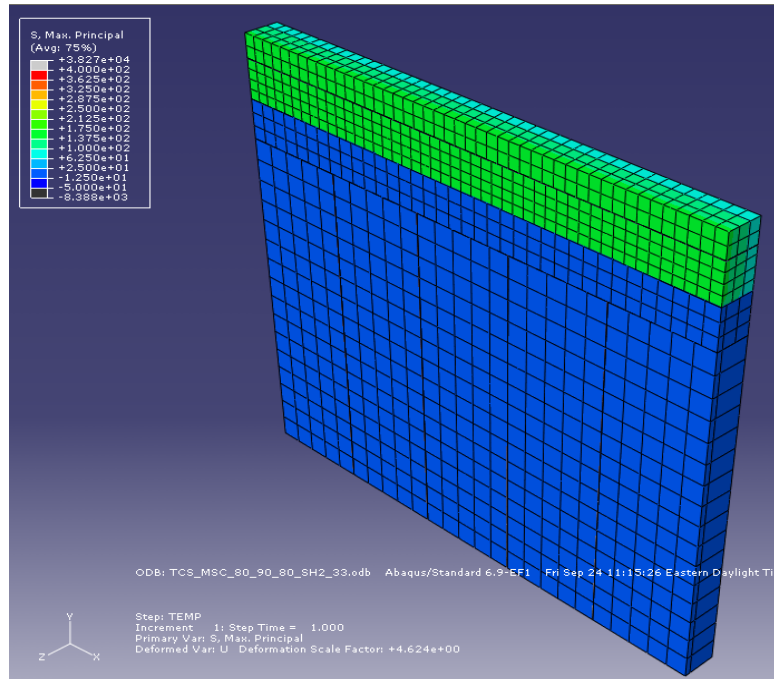


**Figure B294.** 2-ft shoulder transverse cracking model where  $T_M=80^\circ\text{F}$ ,  $T_S=90^\circ\text{F}$ , and  $T_C=80^\circ\text{F}$ , for a CTE of  $4.5 \times 10^{-6}/^\circ\text{F}$  and a stiffness of  $3.3 \times 10^6$  psi.

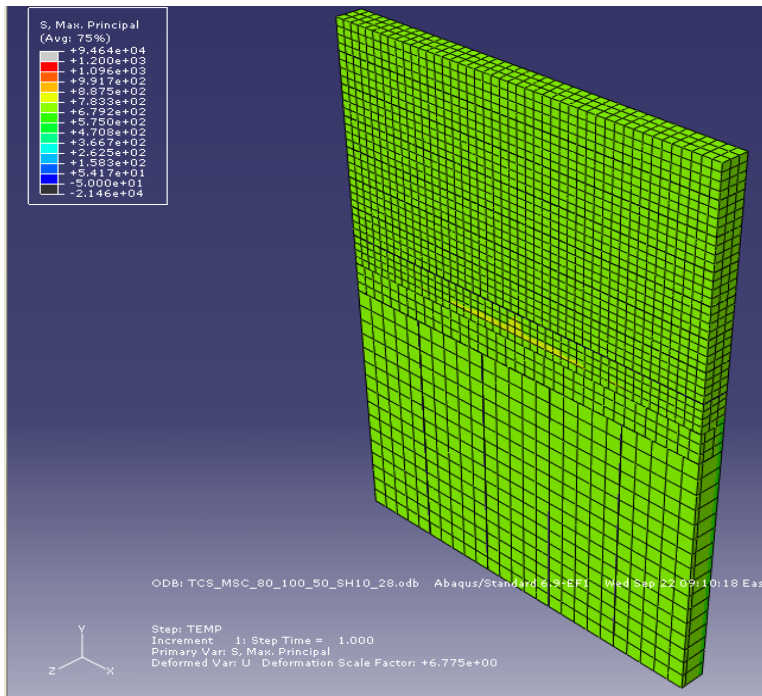


**Figure B295.** 10-ft shoulder transverse cracking model where  $T_M=80^\circ\text{F}$ ,  $T_S=100^\circ\text{F}$ , and  $T_C=50^\circ\text{F}$ , for a CTE of  $5.5 \times 10^{-6}/^\circ\text{F}$  and a stiffness of  $2.8 \times 10^6$  psi.

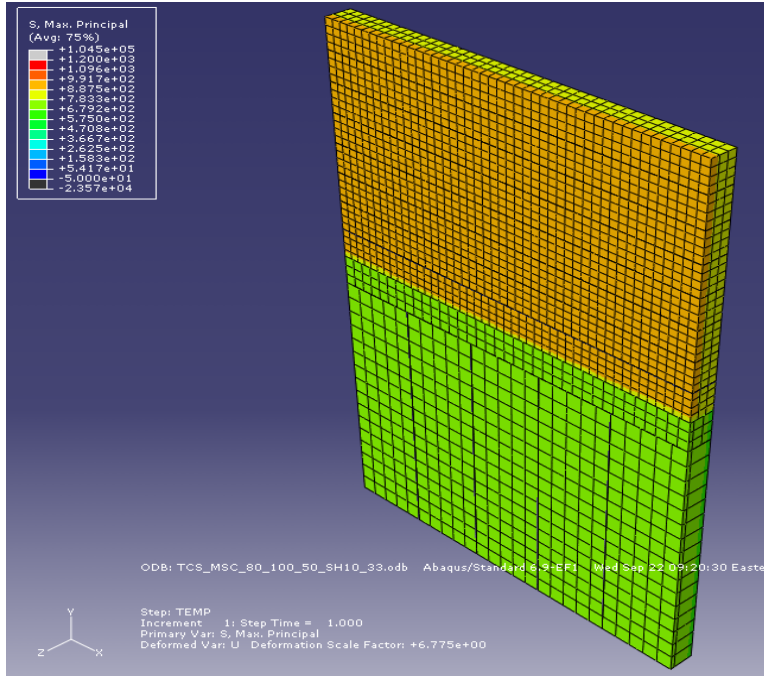


**Figure B296.** 10-ft shoulder transverse cracking model where  $T_M=80^\circ\text{F}$ ,  $T_S=100^\circ\text{F}$ , and  $T_C=50^\circ\text{F}$ , for a CTE of  $5.5 \times 10^{-6}/^\circ\text{F}$  and a stiffness of  $3.3 \times 10^6$  psi.

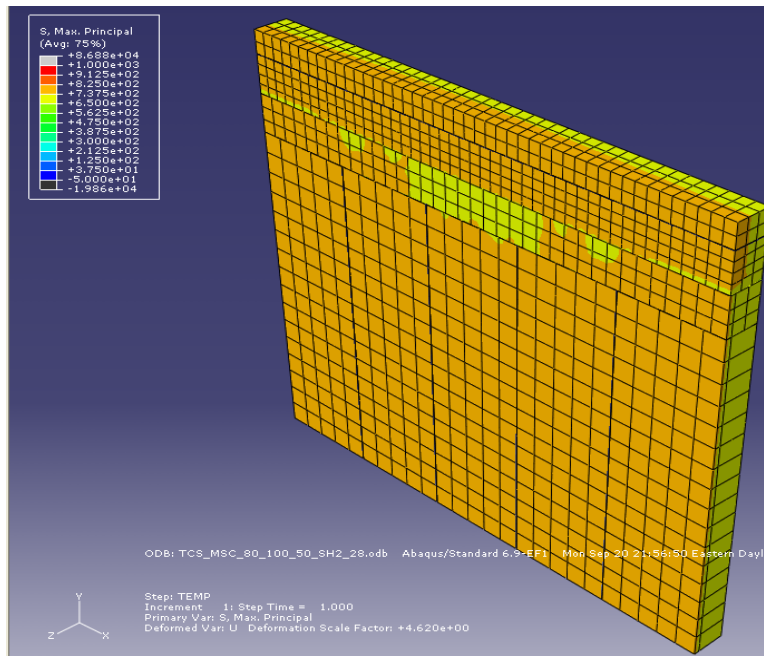


**Figure B297.** 2-ft shoulder transverse cracking model where  $T_M=80^\circ\text{F}$ ,  $T_S=100^\circ\text{F}$ , and  $T_C=50^\circ\text{F}$ , for a CTE of  $5.5 \times 10^{-6}/^\circ\text{F}$  and a stiffness of  $2.8 \times 10^6$  psi.

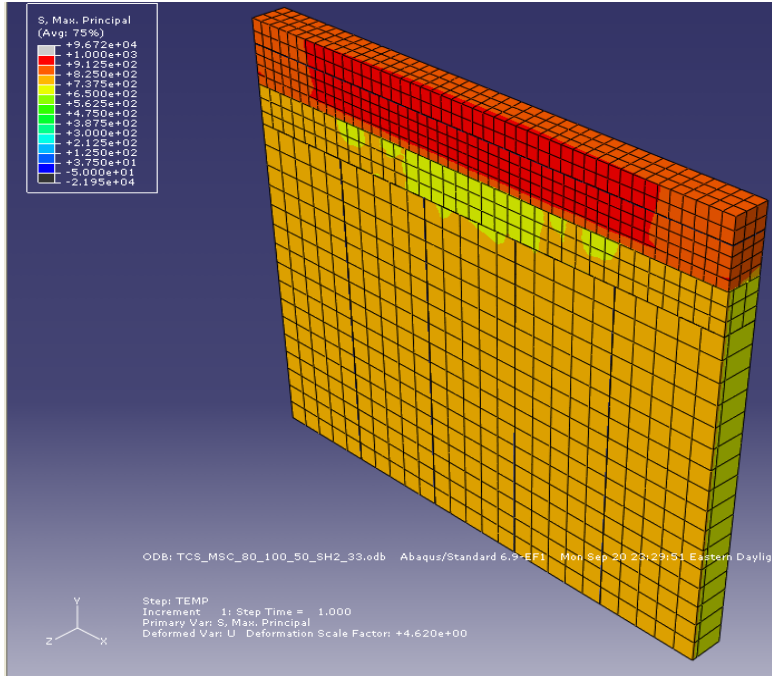


**Figure B298.** 2-ft shoulder transverse cracking model where  $T_M=80^\circ\text{F}$ ,  $T_S=100^\circ\text{F}$ , and  $T_C=50^\circ\text{F}$ , for a CTE of  $5.5 \times 10^{-6}/^\circ\text{F}$  and a stiffness of  $3.3 \times 10^6$  psi.

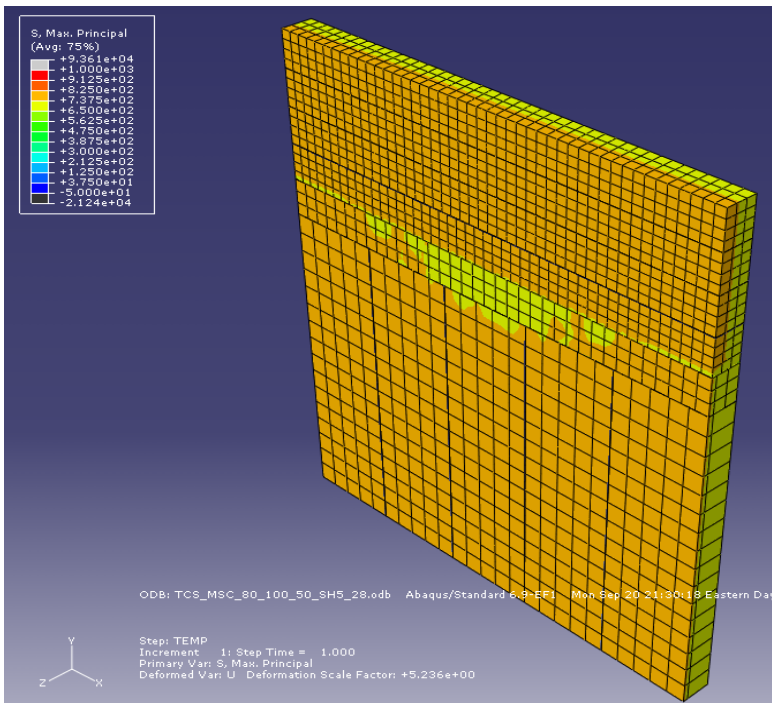


**Figure B299.** 5-ft shoulder transverse cracking model where  $T_M=80^\circ\text{F}$ ,  $T_S=100^\circ\text{F}$ , and  $T_C=50^\circ\text{F}$ , for a CTE of  $5.5 \times 10^{-6}/^\circ\text{F}$  and a stiffness of  $2.8 \times 10^6$  psi.

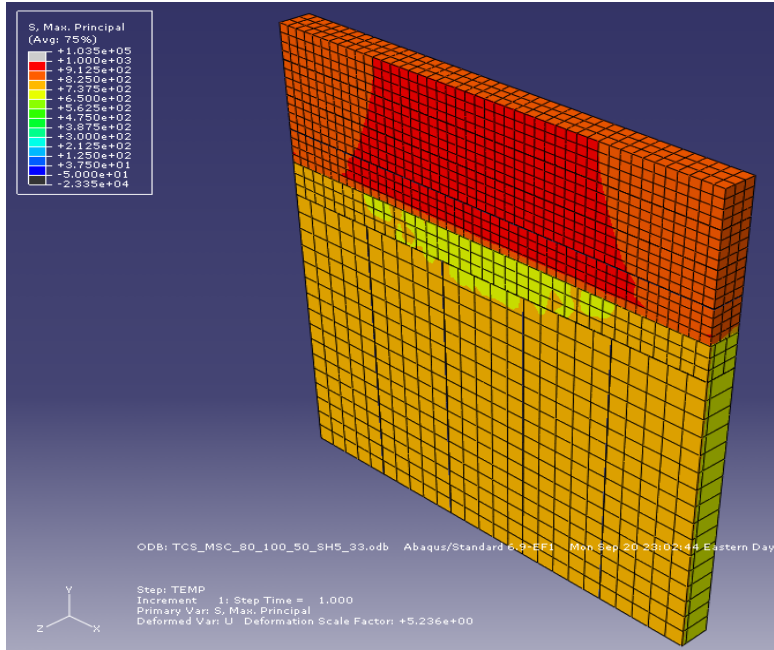


**Figure B300.** 5-ft shoulder transverse cracking model where  $T_M=80^\circ\text{F}$ ,  $T_S=100^\circ\text{F}$ , and  $T_C=50^\circ\text{F}$ , for a CTE of  $5.5 \times 10^{-6}/^\circ\text{F}$  and a stiffness of  $3.3 \times 10^6$  psi.

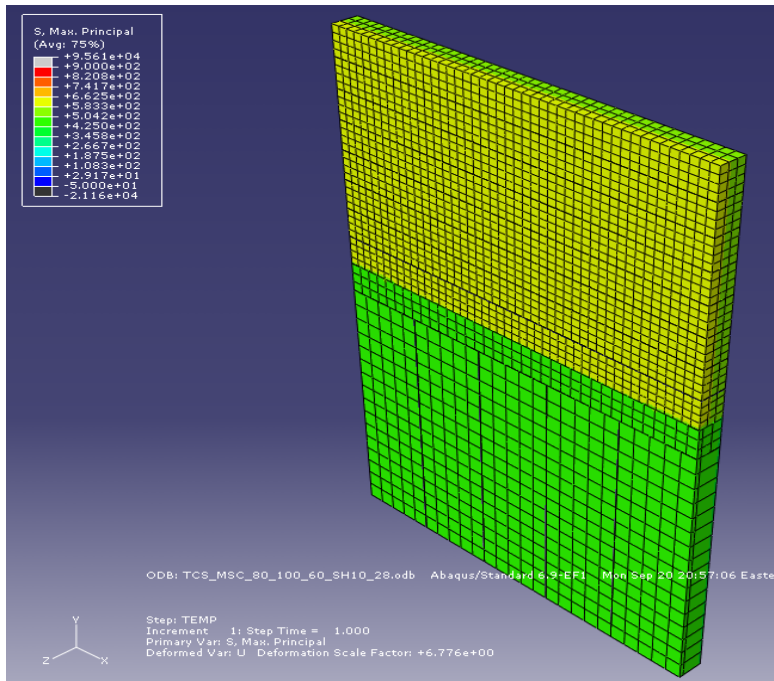


**Figure B301.** 10-ft shoulder transverse cracking model where  $T_M=80^\circ\text{F}$ ,  $T_S=100^\circ\text{F}$ , and  $T_C=60^\circ\text{F}$ , for a CTE of  $5.5 \times 10^{-6}/^\circ\text{F}$  and a stiffness of  $2.8 \times 10^6$  psi.

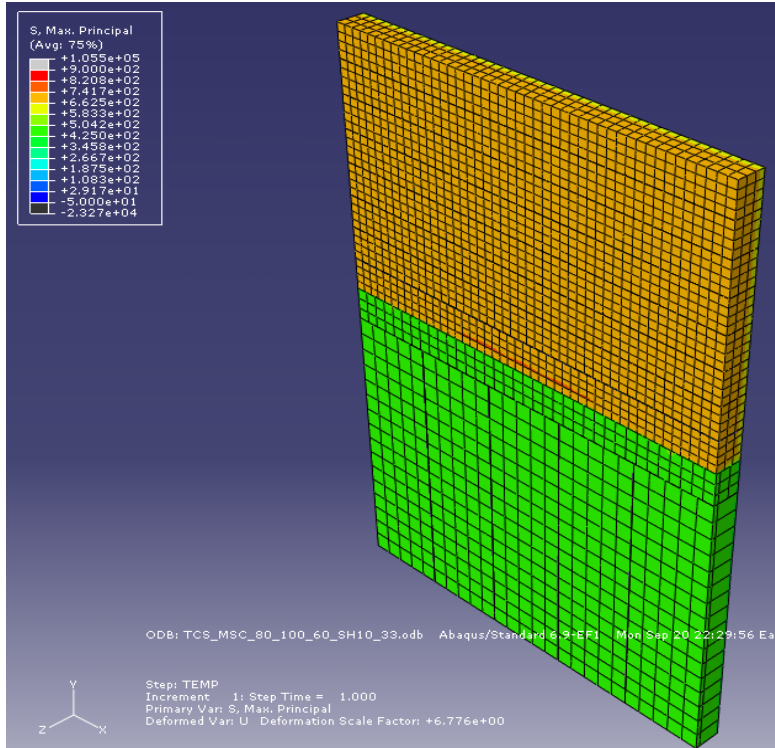


**Figure B302.** 10-ft shoulder transverse cracking model where  $T_M=80^\circ\text{F}$ ,  $T_S=100^\circ\text{F}$ , and  $T_C=60^\circ\text{F}$ , for a CTE of  $5.5 \times 10^{-6}/^\circ\text{F}$  and a stiffness of  $3.3 \times 10^6$  psi.

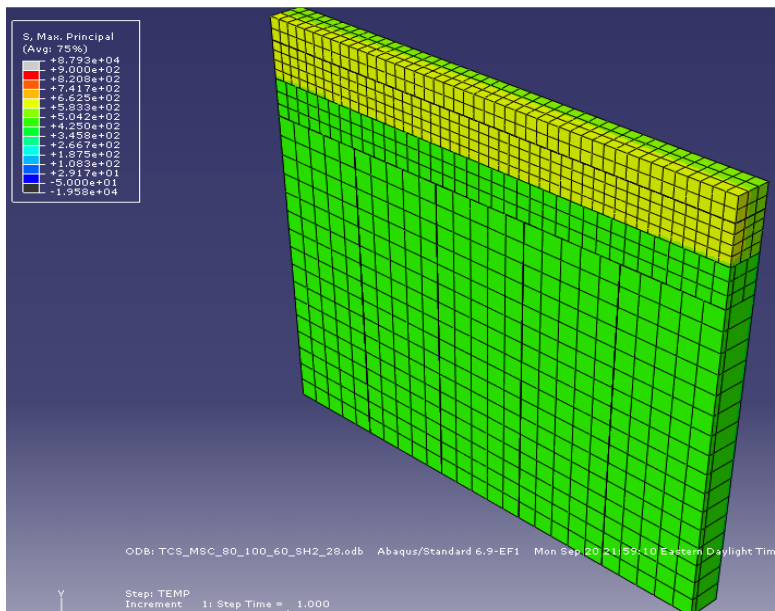


**Figure B303.** 2-ft shoulder transverse cracking model where  $T_M=80^\circ\text{F}$ ,  $T_S=100^\circ\text{F}$ , and  $T_C=60^\circ\text{F}$ , for a CTE of  $5.5 \times 10^{-6}/^\circ\text{F}$  and a stiffness of  $2.8 \times 10^6$  psi.

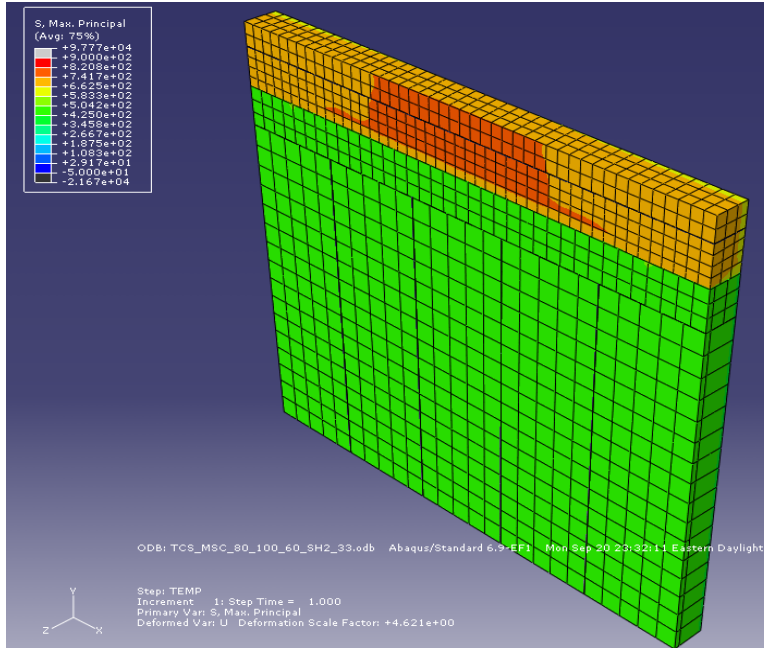


**Figure B304.** 2-ft shoulder transverse cracking model where  $T_M=80^\circ\text{F}$ ,  $T_S=100^\circ\text{F}$ , and  $T_C=60^\circ\text{F}$ , for a CTE of  $5.5 \times 10^{-6}/^\circ\text{F}$  and a stiffness of  $3.3 \times 10^6$  psi.

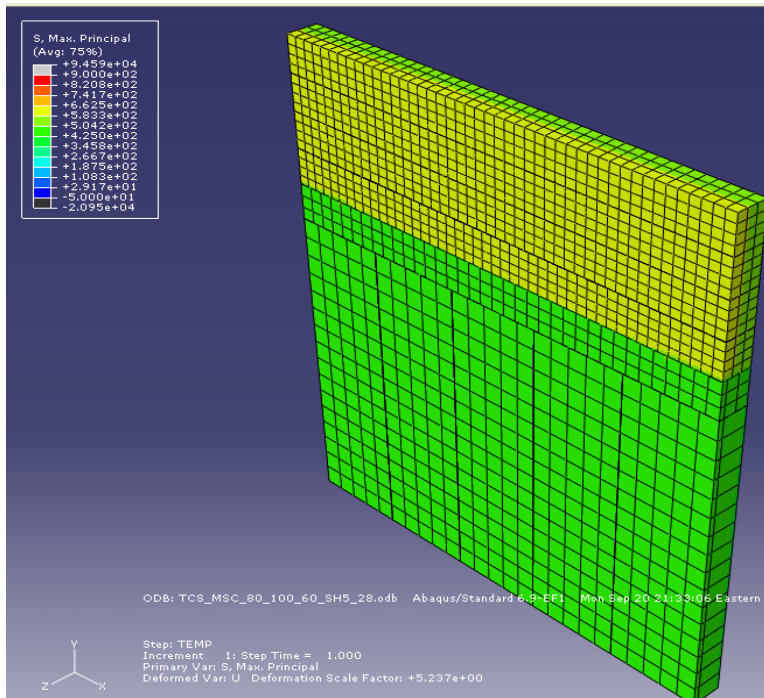


**Figure B305.** 5-ft shoulder transverse cracking model where  $T_M=80^\circ\text{F}$ ,  $T_S=100^\circ\text{F}$ , and  $T_C=60^\circ\text{F}$ , for a CTE of  $5.5 \times 10^{-6}/^\circ\text{F}$  and a stiffness of  $2.8 \times 10^6$  psi.

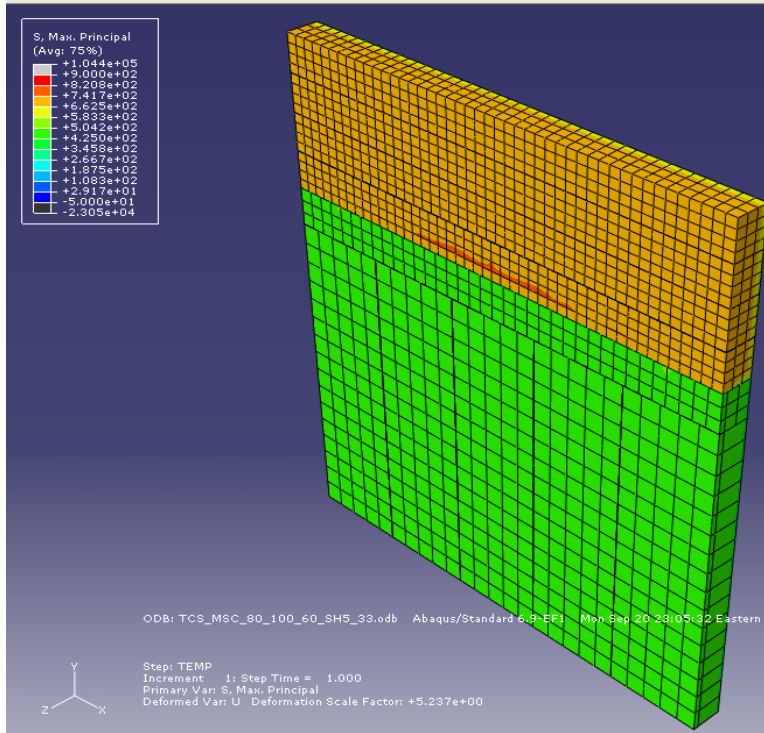


**Figure B306.** 5-ft shoulder transverse cracking model where  $T_M=80^\circ\text{F}$ ,  $T_S=100^\circ\text{F}$ , and  $T_C=60^\circ\text{F}$ , for a CTE of  $5.5 \times 10^{-6}/^\circ\text{F}$  and a stiffness of  $3.3 \times 10^6$  psi.

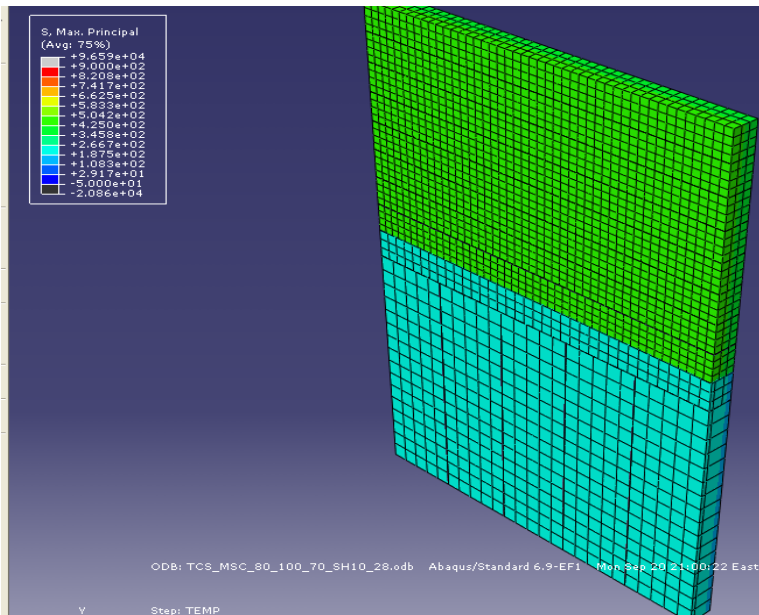


**Figure B307.** 10-ft shoulder transverse cracking model where  $T_M=80^\circ\text{F}$ ,  $T_S=100^\circ\text{F}$ , and  $T_C=70^\circ\text{F}$ , for a CTE of  $5.5 \times 10^{-6}/^\circ\text{F}$  and a stiffness of  $2.8 \times 10^6$  psi.

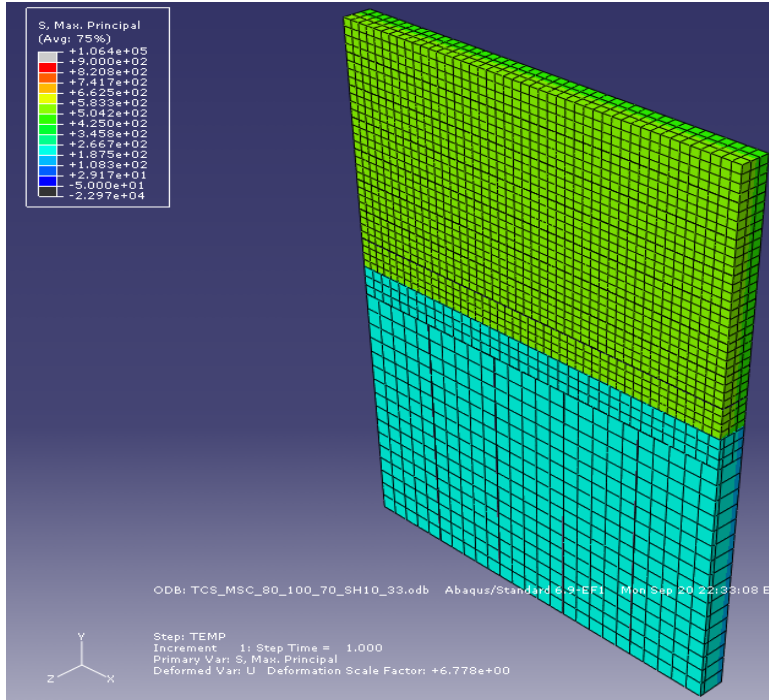


**Figure B308.** 10-ft shoulder transverse cracking model where  $T_M=80^\circ\text{F}$ ,  $T_S=100^\circ\text{F}$ , and  $T_C=70^\circ\text{F}$ , for a CTE of  $5.5 \times 10^{-6}/^\circ\text{F}$  and a stiffness of  $3.3 \times 10^6$  psi.

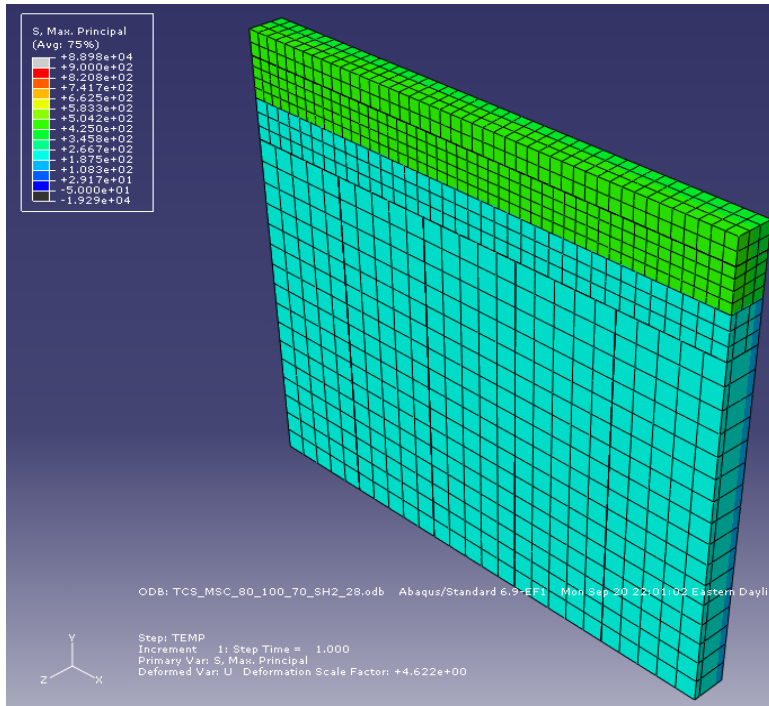


**Figure B309.** 2-ft shoulder transverse cracking model where  $T_M=80^\circ\text{F}$ ,  $T_S=100^\circ\text{F}$ , and  $T_C=70^\circ\text{F}$ , for a CTE of  $5.5 \times 10^{-6}/^\circ\text{F}$  and a stiffness of  $2.8 \times 10^6$  psi.

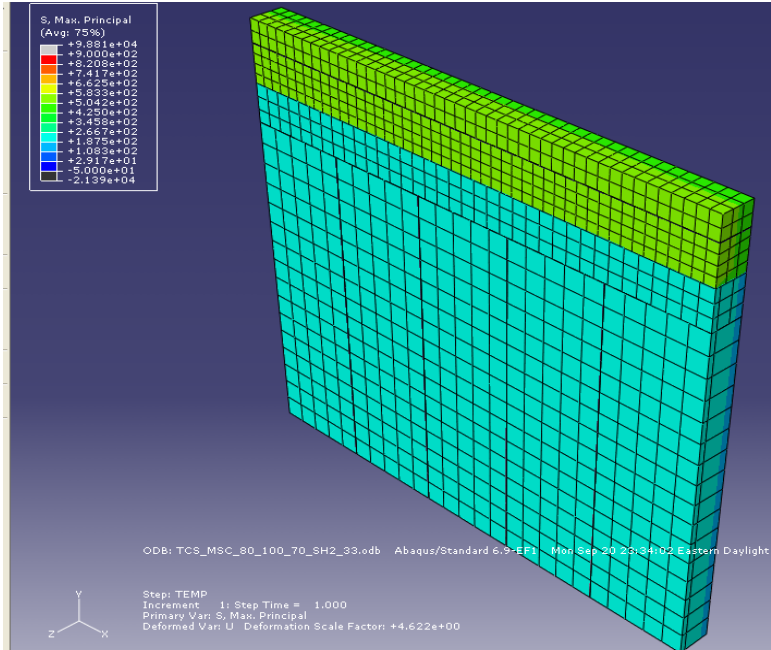


**Figure B310.** 2-ft shoulder transverse cracking model where  $T_M=80^\circ\text{F}$ ,  $T_S=100^\circ\text{F}$ , and  $T_C=70^\circ\text{F}$ , for a CTE of  $5.5 \times 10^{-6}/^\circ\text{F}$  and a stiffness of  $3.3 \times 10^6$  psi.

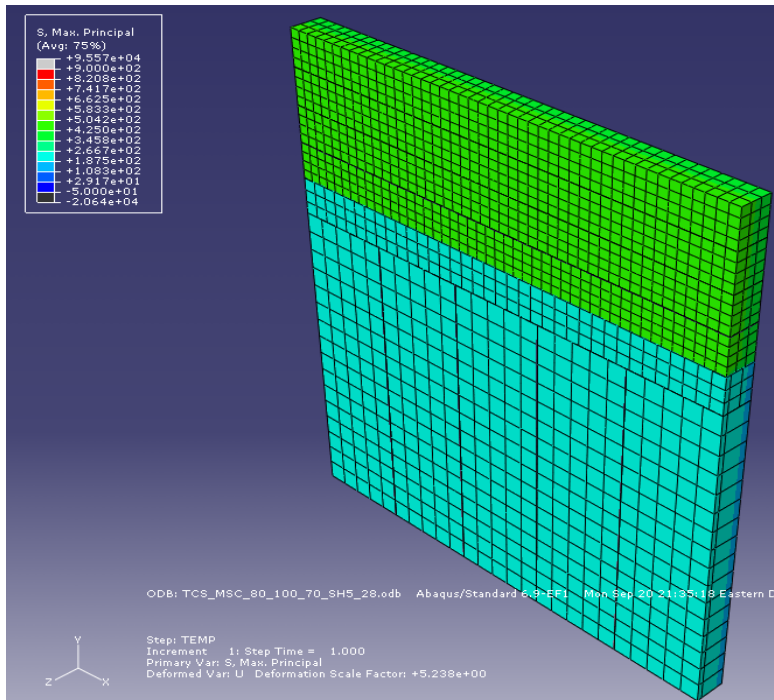


**Figure B311.** 5-ft shoulder transverse cracking model where  $T_M=80^\circ\text{F}$ ,  $T_S=100^\circ\text{F}$ , and  $T_C=70^\circ\text{F}$ , for a CTE of  $5.5 \times 10^{-6}/^\circ\text{F}$  and a stiffness of  $2.8 \times 10^6$  psi.

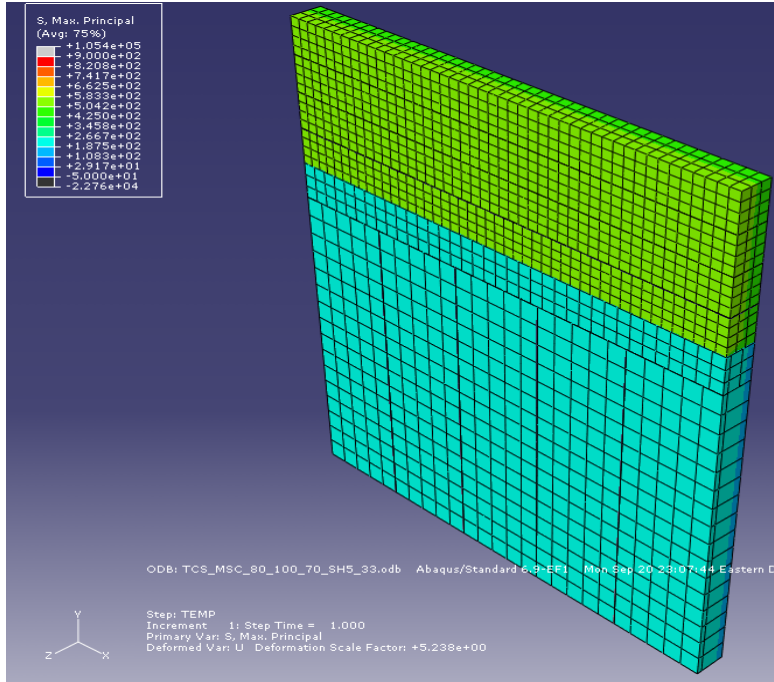


**Figure B312.** 5-ft shoulder transverse cracking model where  $T_M=80^\circ\text{F}$ ,  $T_S=100^\circ\text{F}$ , and  $T_C=70^\circ\text{F}$ , for a CTE of  $5.5 \times 10^{-6}/^\circ\text{F}$  and a stiffness of  $3.3 \times 10^6$  psi.

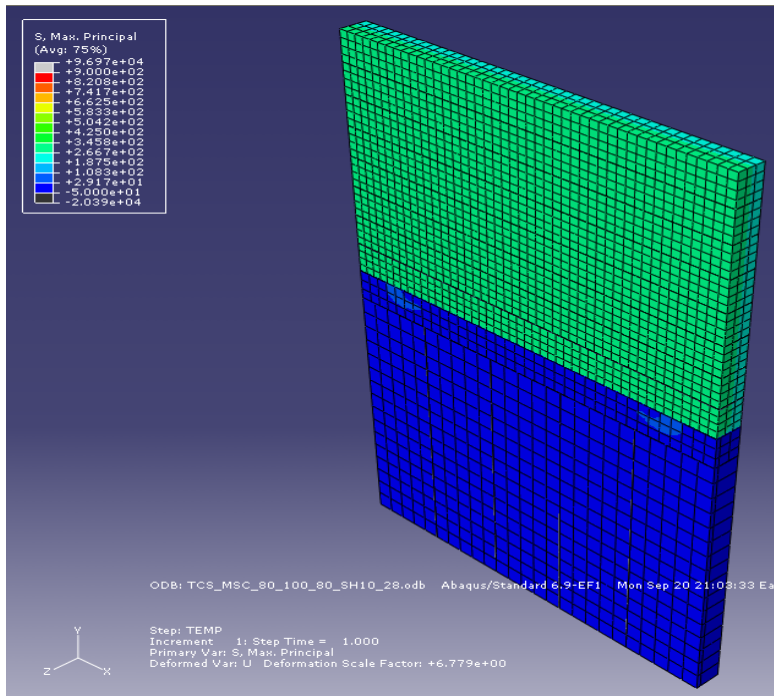


**Figure B313.** 10-ft shoulder transverse cracking model where  $T_M=80^\circ\text{F}$ ,  $T_S=100^\circ\text{F}$ , and  $T_C=80^\circ\text{F}$ , for a CTE of  $5.5 \times 10^{-6}/^\circ\text{F}$  and a stiffness of  $2.8 \times 10^6$  psi.

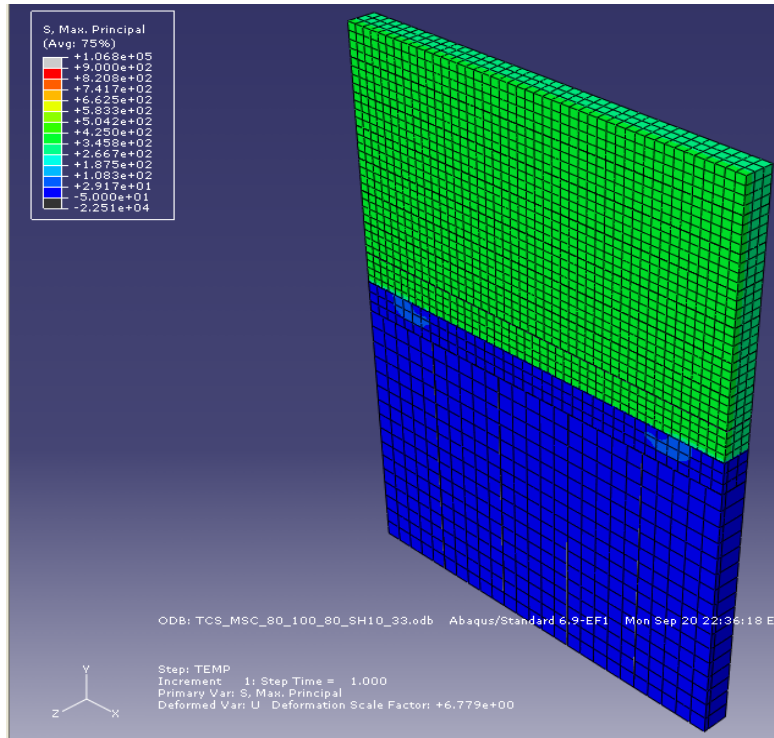


**Figure B314.** 10-ft shoulder transverse cracking model where  $T_M=80^\circ\text{F}$ ,  $T_S=100^\circ\text{F}$ , and  $T_C=80^\circ\text{F}$ , for a CTE of  $5.5 \times 10^{-6}/^\circ\text{F}$  and a stiffness of  $3.3 \times 10^6$  psi.

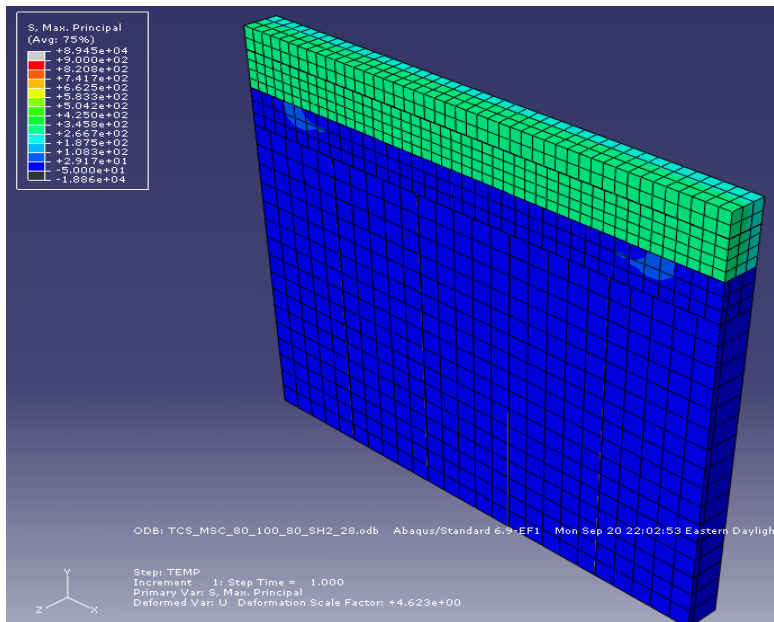


**Figure B315.** 2-ft shoulder transverse cracking model where  $T_M=80^\circ\text{F}$ ,  $T_S=100^\circ\text{F}$ , and  $T_C=80^\circ\text{F}$ , for a CTE of  $5.5 \times 10^{-6}/^\circ\text{F}$  and a stiffness of  $2.8 \times 10^6$  psi.

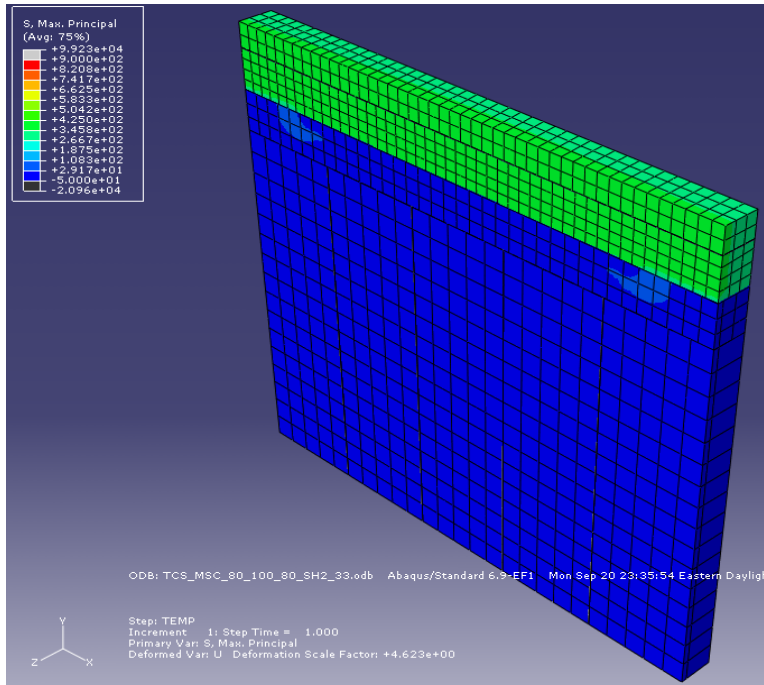


**Figure B316.** 2-ft shoulder transverse cracking model where  $T_M=80^\circ\text{F}$ ,  $T_S=100^\circ\text{F}$ , and  $T_C=80^\circ\text{F}$ , for a CTE of  $5.5 \times 10^{-6}/^\circ\text{F}$  and a stiffness of  $3.3 \times 10^6$  psi.

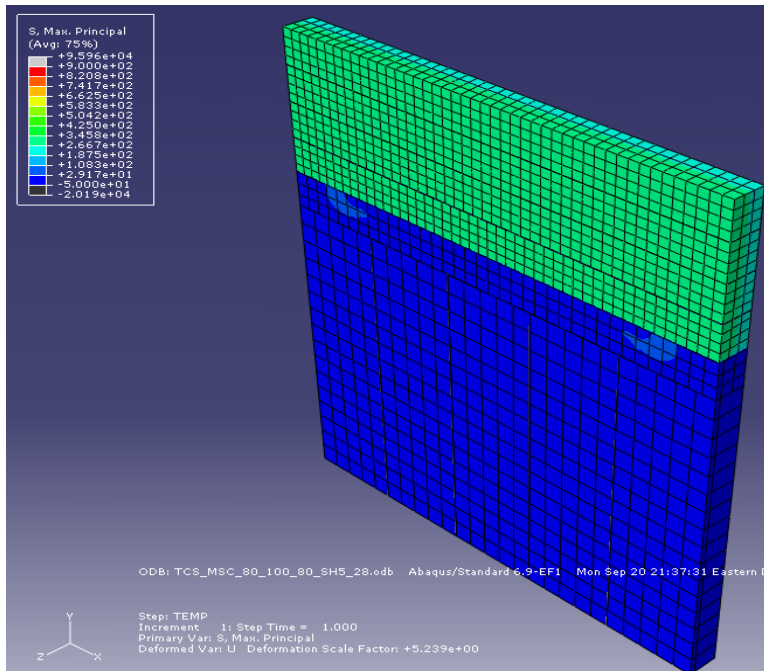


**Figure B317.** 5-ft shoulder transverse cracking model where  $T_M=80^\circ\text{F}$ ,  $T_S=100^\circ\text{F}$ , and  $T_C=80^\circ\text{F}$ , for a CTE of  $5.5 \times 10^{-6}/^\circ\text{F}$  and a stiffness of  $2.8 \times 10^6$  psi.

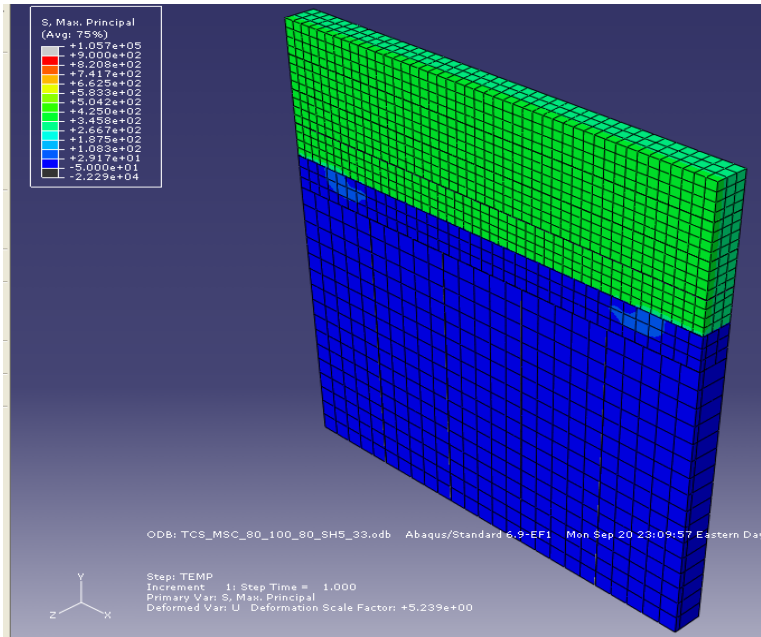


**Figure B318.** 5-ft shoulder transverse cracking model where  $T_M=80^\circ\text{F}$ ,  $T_S=100^\circ\text{F}$ , and  $T_C=80^\circ\text{F}$ , for a CTE of  $5.5 \times 10^{-6}/^\circ\text{F}$  and a stiffness of  $3.3 \times 10^6$  psi.

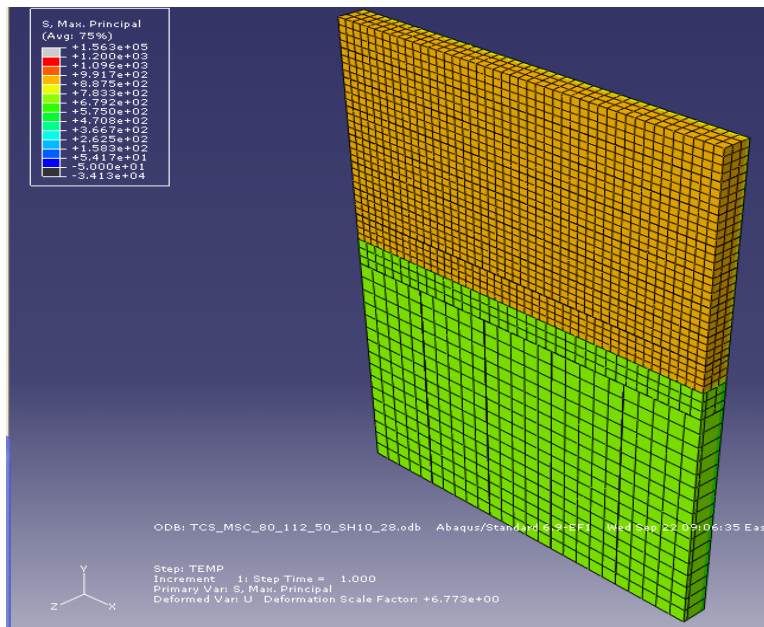


**Figure B319.** 10-ft shoulder transverse cracking model where  $T_M=80^\circ\text{F}$ ,  $T_S=110^\circ\text{F}$ , and  $T_C=50^\circ\text{F}$ , for a CTE of  $5.5 \times 10^{-6}/^\circ\text{F}$  and a stiffness of  $2.8 \times 10^6$  psi.

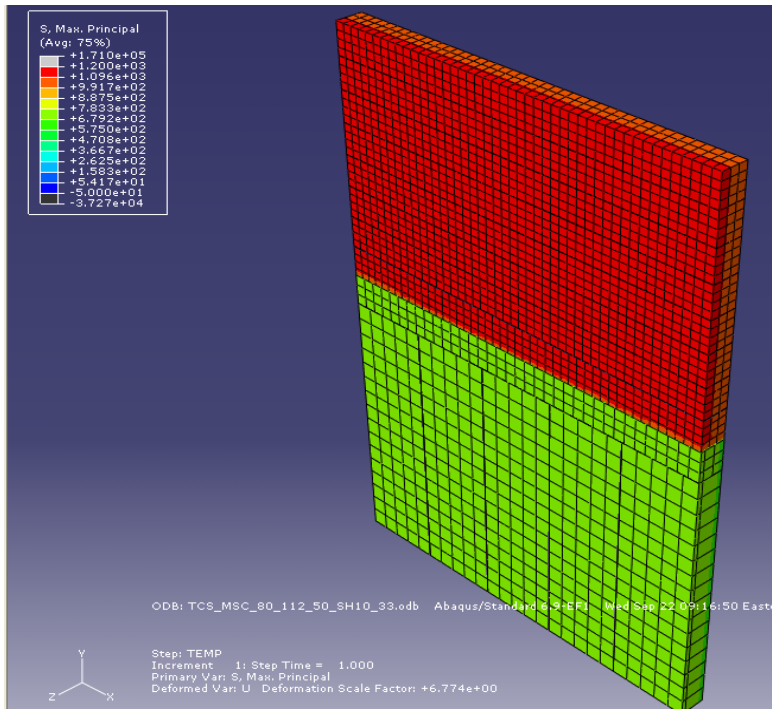


**Figure B320.** 10-ft shoulder transverse cracking model where  $T_M=80^\circ\text{F}$ ,  $T_S=110^\circ\text{F}$ , and  $T_C=50^\circ\text{F}$ , for a CTE of  $5.5 \times 10^{-6}/^\circ\text{F}$  and a stiffness of  $3.3 \times 10^6$  psi.

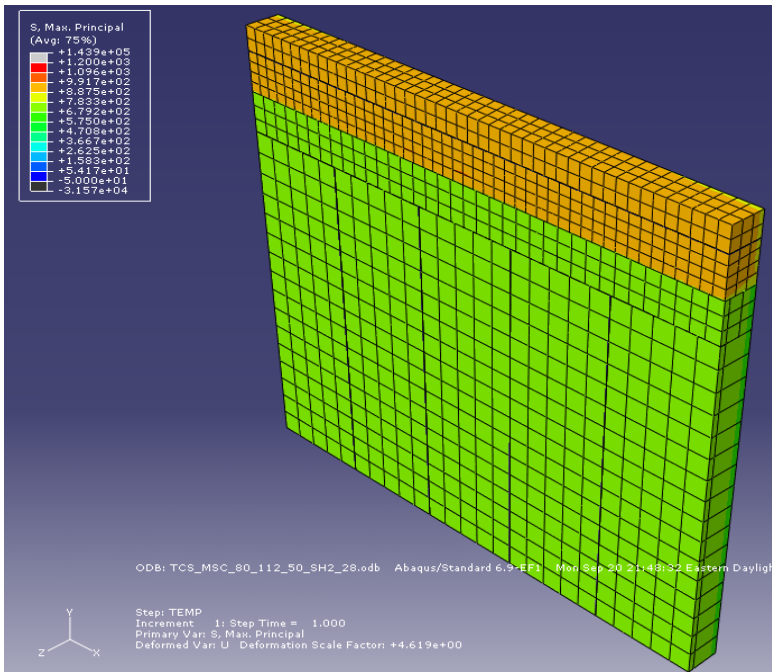


**Figure B321.** 2-ft shoulder transverse cracking model where  $T_M=80^\circ\text{F}$ ,  $T_S=110^\circ\text{F}$ , and  $T_C=50^\circ\text{F}$ , for a CTE of  $5.5 \times 10^{-6}/^\circ\text{F}$  and a stiffness of  $2.8 \times 10^6$  psi.

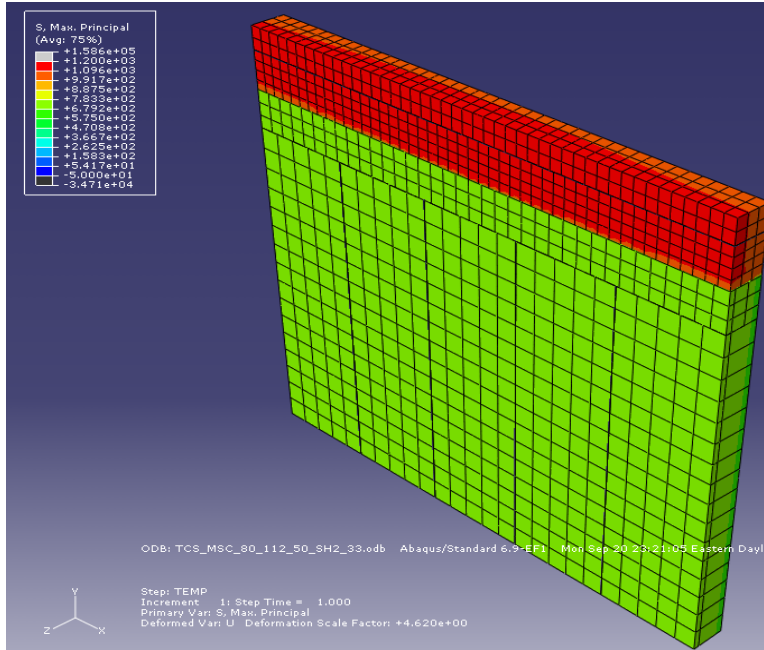


**Figure B322.** 2-ft shoulder transverse cracking model where  $T_M=80^\circ\text{F}$ ,  $T_S=110^\circ\text{F}$ , and  $T_C=50^\circ\text{F}$ , for a CTE of  $5.5 \times 10^{-6}/^\circ\text{F}$  and a stiffness of  $3.3 \times 10^6$  psi.

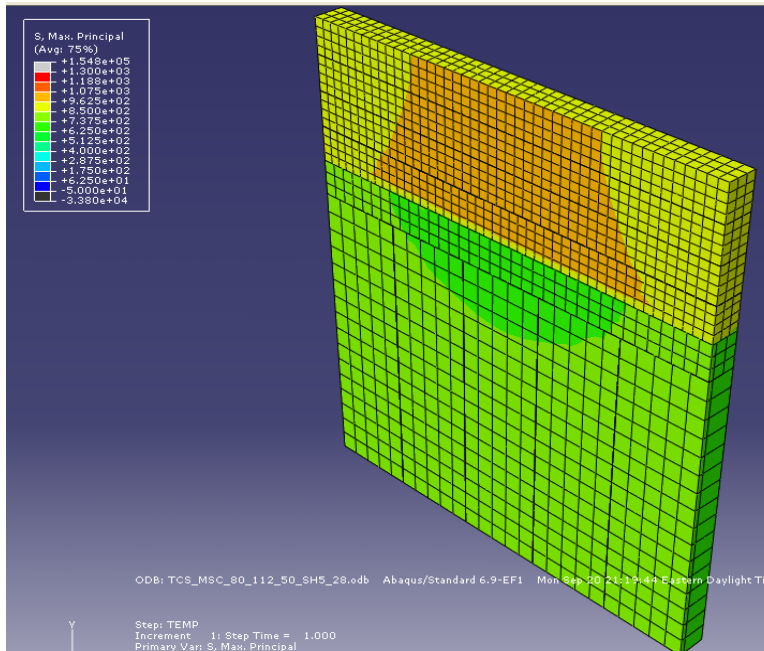


**Figure B323.** 5-ft shoulder transverse cracking model where  $T_M=80^\circ\text{F}$ ,  $T_S=110^\circ\text{F}$ , and  $T_C=50^\circ\text{F}$ , for a CTE of  $5.5 \times 10^{-6}/^\circ\text{F}$  and a stiffness of  $2.8 \times 10^6$  psi.

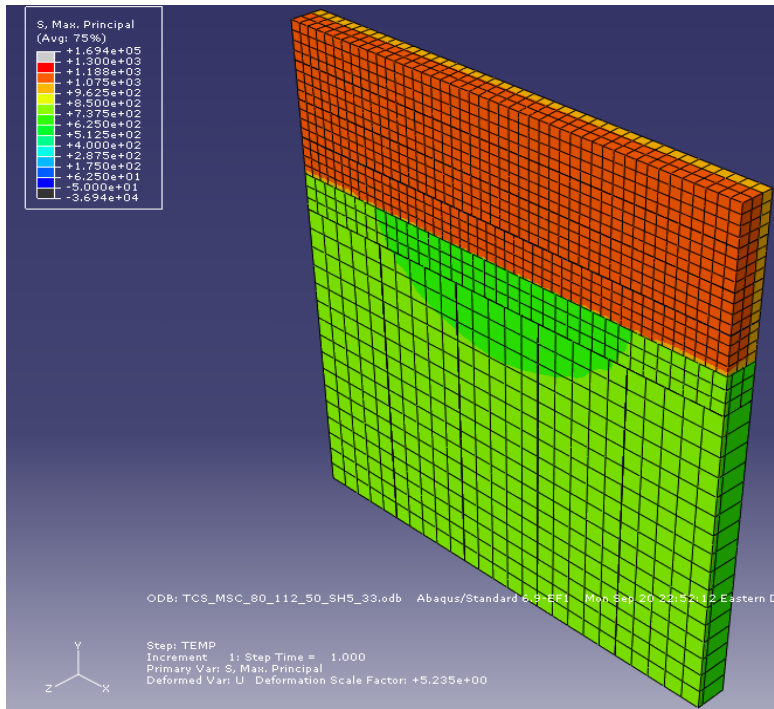


**Figure B324.** 5-ft shoulder transverse cracking model where  $T_M=80^\circ\text{F}$ ,  $T_S=110^\circ\text{F}$ , and  $T_C=50^\circ\text{F}$ , for a CTE of  $5.5 \times 10^{-6}/^\circ\text{F}$  and a stiffness of  $3.3 \times 10^6$  psi.

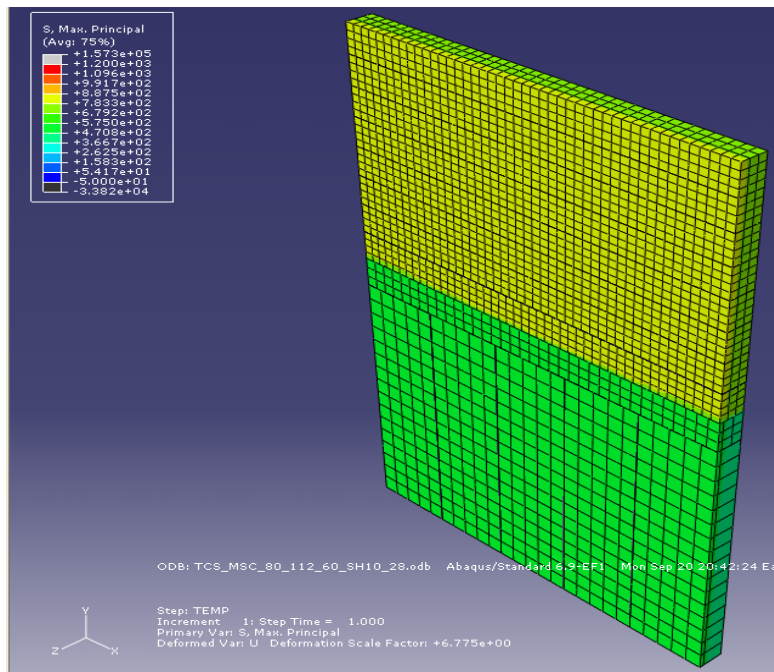


**Figure B325.** 10-ft shoulder transverse cracking model where  $T_M=80^\circ\text{F}$ ,  $T_S=110^\circ\text{F}$ , and  $T_C=60^\circ\text{F}$ , for a CTE of  $5.5 \times 10^{-6}/^\circ\text{F}$  and a stiffness of  $2.8 \times 10^6$  psi.

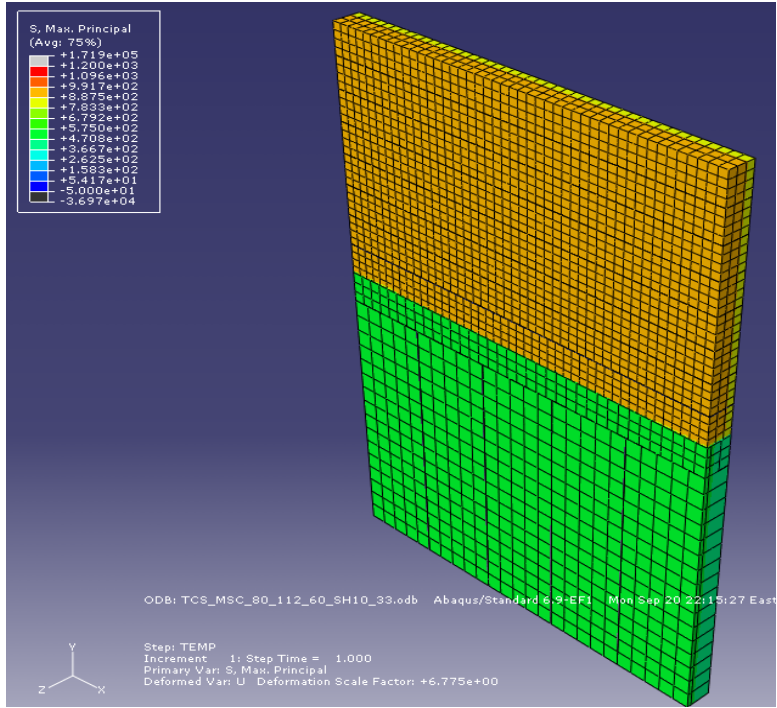


**Figure B326.** 10-ft shoulder transverse cracking model where  $T_M=80^\circ\text{F}$ ,  $T_S=110^\circ\text{F}$ , and  $T_C=60^\circ\text{F}$ , for a CTE of  $5.5 \times 10^{-6}/^\circ\text{F}$  and a stiffness of  $3.3 \times 10^6$  psi.

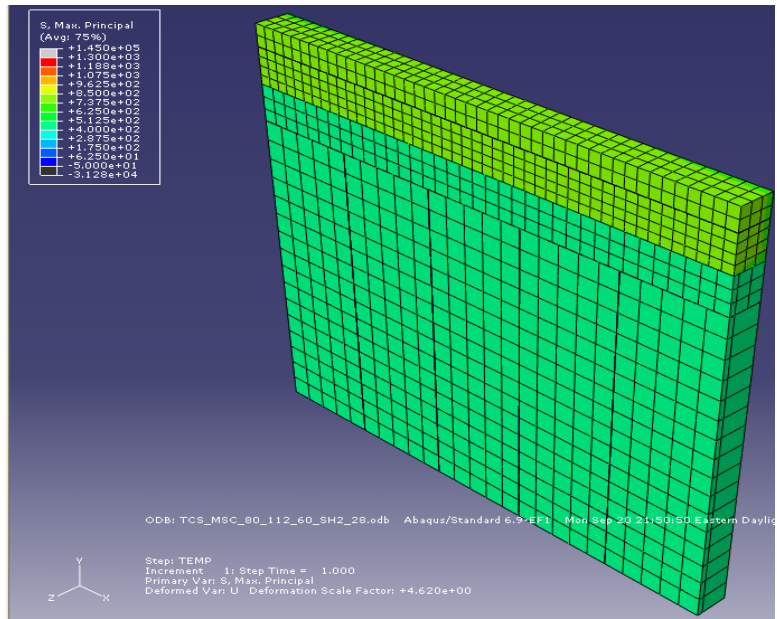


**Figure B327.** 2-ft shoulder transverse cracking model where  $T_M=80^\circ\text{F}$ ,  $T_S=110^\circ\text{F}$ , and  $T_C=60^\circ\text{F}$ , for a CTE of  $5.5 \times 10^{-6}/^\circ\text{F}$  and a stiffness of  $2.8 \times 10^6$  psi.

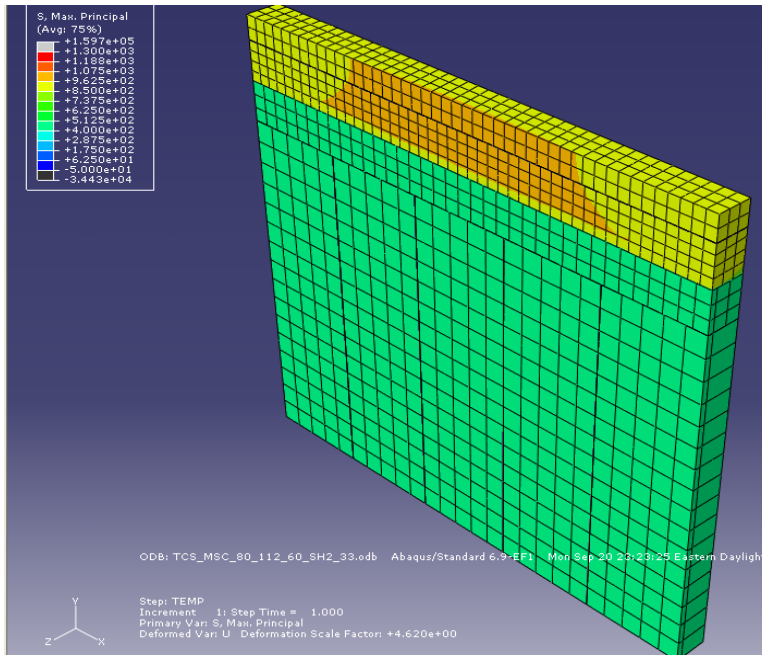


**Figure B328.** 2-ft shoulder transverse cracking model where  $T_M=80^\circ\text{F}$ ,  $T_S=110^\circ\text{F}$ , and  $T_C=60^\circ\text{F}$ , for a CTE of  $5.5 \times 10^{-6}/^\circ\text{F}$  and a stiffness of  $3.3 \times 10^6$  psi.

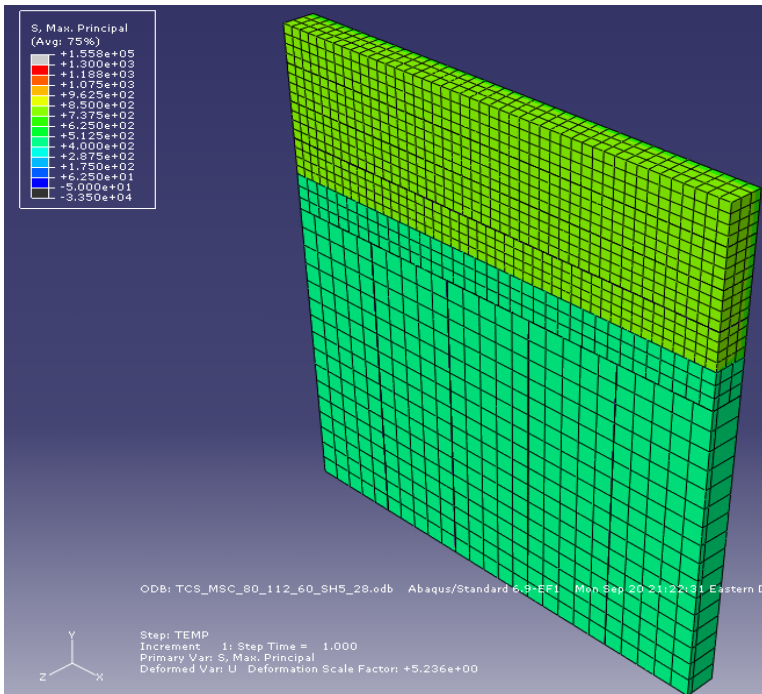


**Figure B329.** 5-ft shoulder transverse cracking model where  $T_M=80^\circ\text{F}$ ,  $T_S=110^\circ\text{F}$ , and  $T_C=60^\circ\text{F}$ , for a CTE of  $5.5 \times 10^{-6}/^\circ\text{F}$  and a stiffness of  $2.8 \times 10^6$  psi.

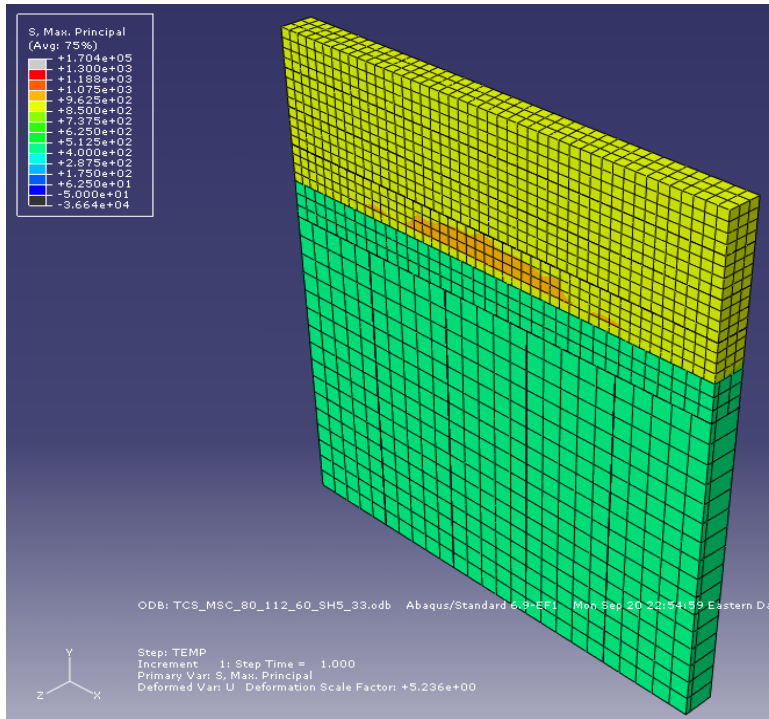


**Figure B330.** 5-ft shoulder transverse cracking model where  $T_M=80^\circ\text{F}$ ,  $T_S=110^\circ\text{F}$ , and  $T_C=60^\circ\text{F}$ , for a CTE of  $5.5 \times 10^{-6}/^\circ\text{F}$  and a stiffness of  $3.3 \times 10^6$  psi.

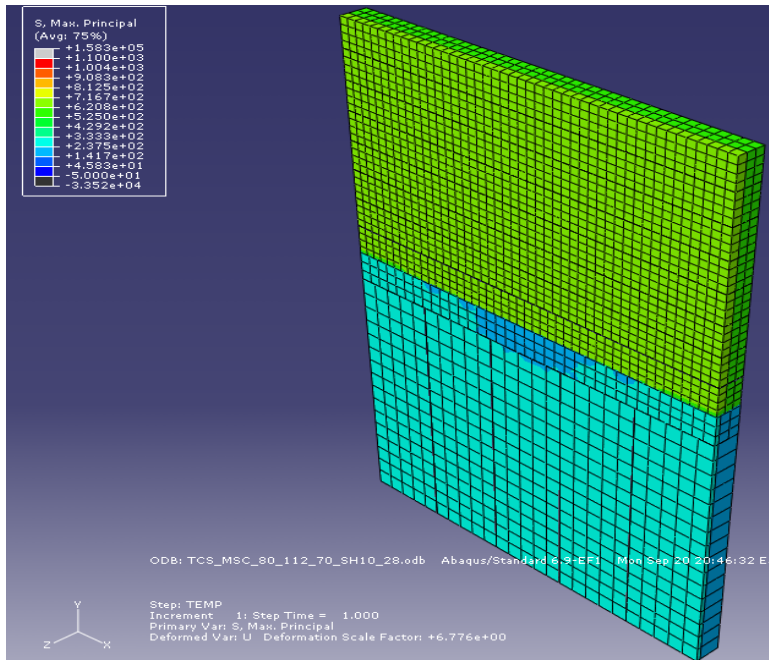


**Figure B331.** 10-ft shoulder transverse cracking model where  $T_M=80^\circ\text{F}$ ,  $T_S=110^\circ\text{F}$ , and  $T_C=70^\circ\text{F}$ , for a CTE of  $5.5 \times 10^{-6}/^\circ\text{F}$  and a stiffness of  $2.8 \times 10^6$  psi.

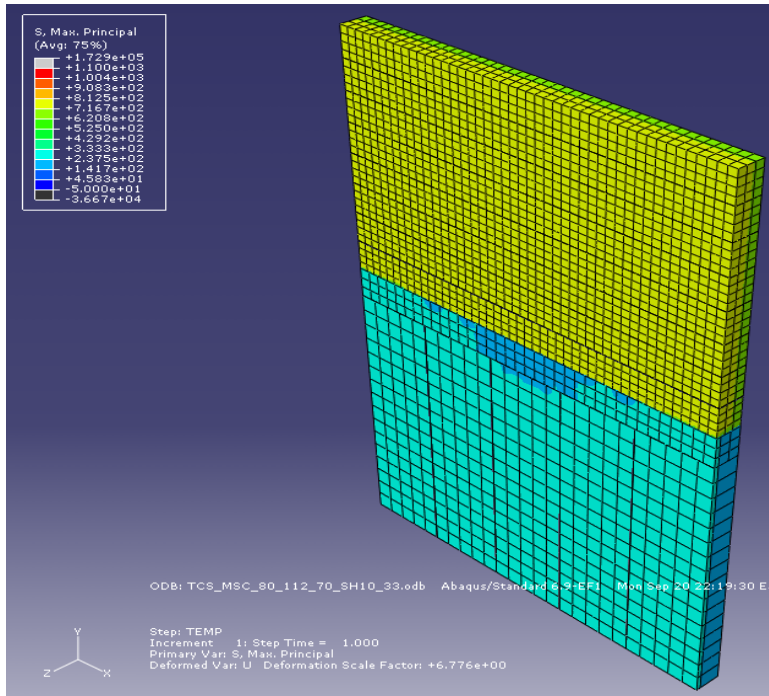


**Figure B332.** 10-ft shoulder transverse cracking model where  $T_M=80^\circ\text{F}$ ,  $T_S=110^\circ\text{F}$ , and  $T_C=70^\circ\text{F}$ , for a CTE of  $5.5 \times 10^{-6}/^\circ\text{F}$  and a stiffness of  $3.3 \times 10^6$  psi.

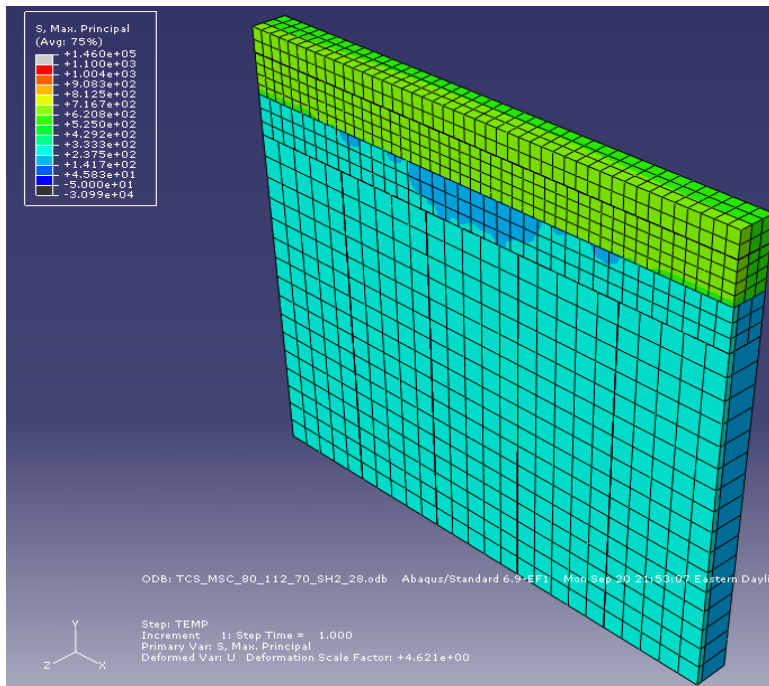


**Figure B333.** 2-ft shoulder transverse cracking model where  $T_M=80^\circ\text{F}$ ,  $T_S=110^\circ\text{F}$ , and  $T_C=70^\circ\text{F}$ , for a CTE of  $5.5 \times 10^{-6}/^\circ\text{F}$  and a stiffness of  $2.8 \times 10^6$  psi.

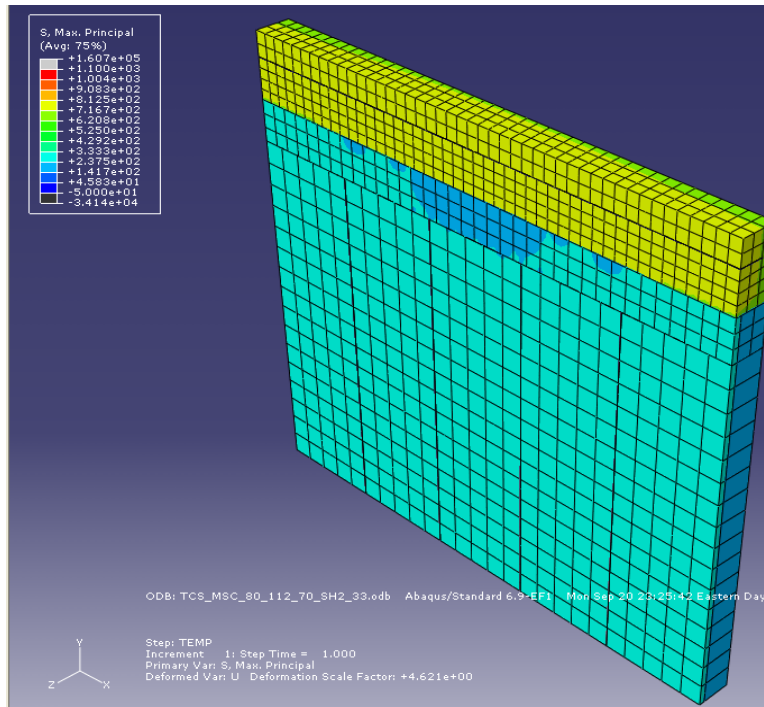


**Figure B334.** 2-ft shoulder transverse cracking model where  $T_M=80^\circ\text{F}$ ,  $T_S=110^\circ\text{F}$ , and  $T_C=70^\circ\text{F}$ , for a CTE of  $5.5 \times 10^{-6}/^\circ\text{F}$  and a stiffness of  $3.3 \times 10^6$  psi.

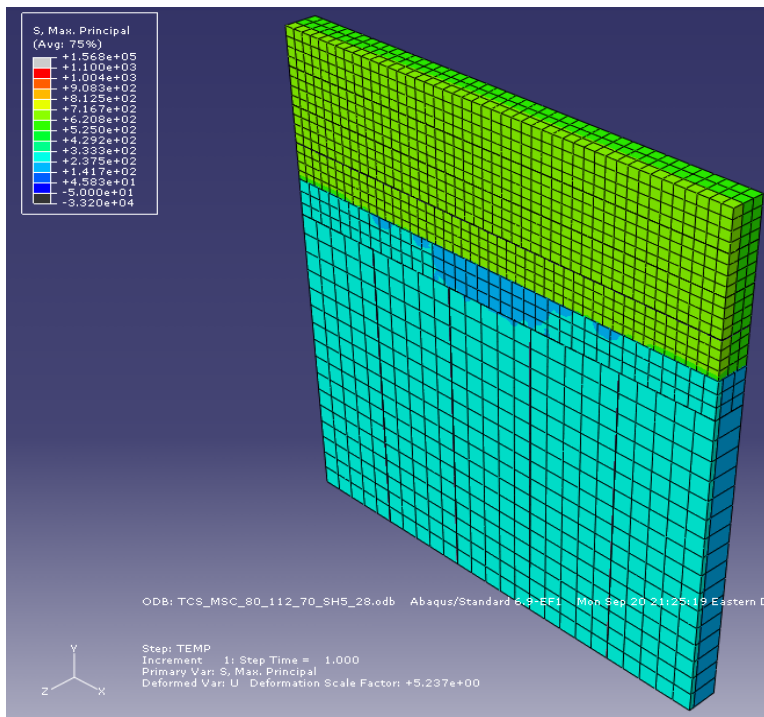


**Figure B335.** 5-ft shoulder transverse cracking model where  $T_M=80^\circ\text{F}$ ,  $T_S=110^\circ\text{F}$ , and  $T_C=70^\circ\text{F}$ , for a CTE of  $5.5 \times 10^{-6}/^\circ\text{F}$  and a stiffness of  $2.8 \times 10^6$  psi.

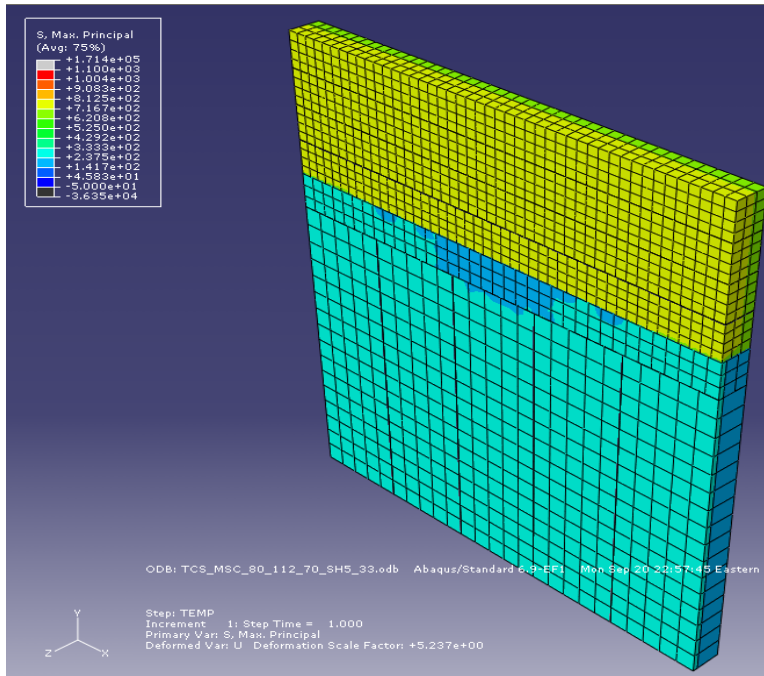


**Figure B336.** 5-ft shoulder transverse cracking model where  $T_M=80^\circ\text{F}$ ,  $T_S=110^\circ\text{F}$ , and  $T_C=70^\circ\text{F}$ , for a CTE of  $5.5 \times 10^{-6}/^\circ\text{F}$  and a stiffness of  $3.3 \times 10^6$  psi.

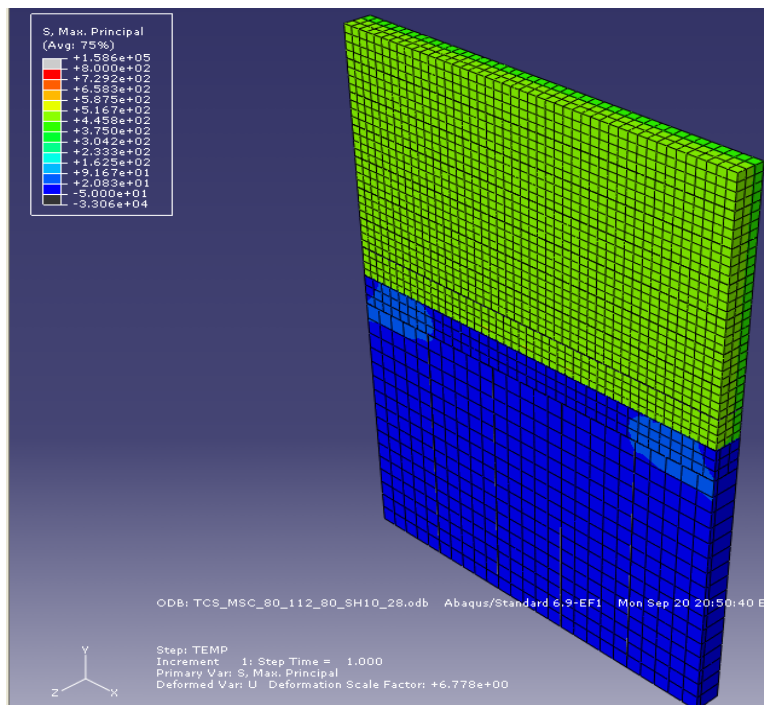


**Figure B337.** 10-ft shoulder transverse cracking model where  $T_M=80^\circ\text{F}$ ,  $T_S=110^\circ\text{F}$ , and  $T_C=80^\circ\text{F}$ , for a CTE of  $5.5 \times 10^{-6}/^\circ\text{F}$  and a stiffness of  $2.8 \times 10^6$  psi.

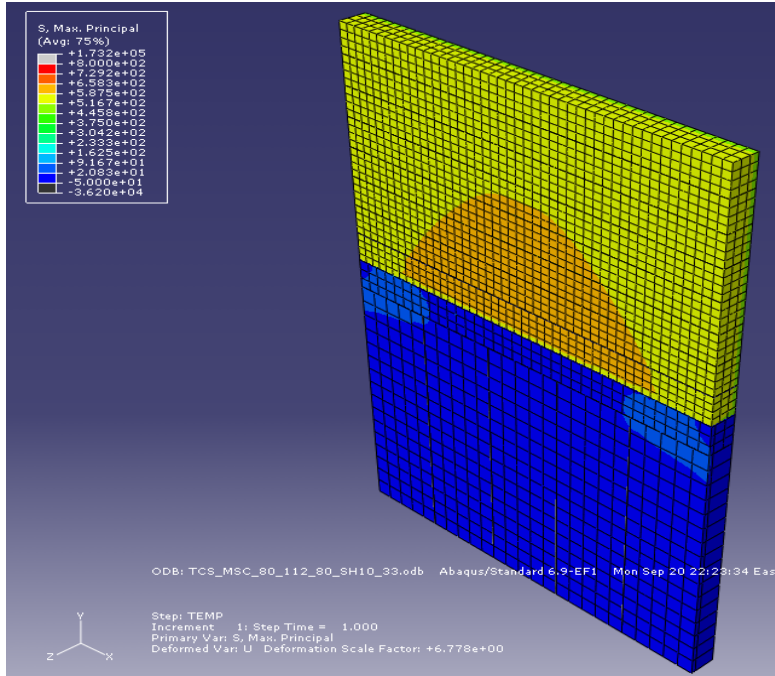


**Figure B338.** 10-ft shoulder transverse cracking model where  $T_M=80^\circ\text{F}$ ,  $T_S=110^\circ\text{F}$ , and  $T_C=80^\circ\text{F}$ , for a CTE of  $5.5 \times 10^{-6}/^\circ\text{F}$  and a stiffness of  $3.3 \times 10^6$  psi.

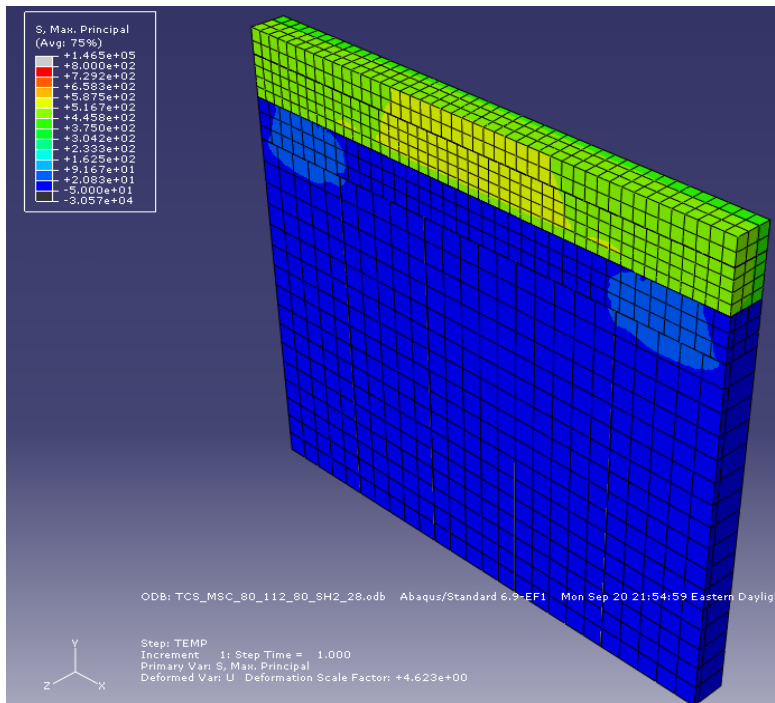


**Figure B339.** 2-ft shoulder transverse cracking model where  $T_M=80^\circ\text{F}$ ,  $T_S=110^\circ\text{F}$ , and  $T_C=80^\circ\text{F}$ , for a CTE of  $5.5 \times 10^{-6}/^\circ\text{F}$  and a stiffness of  $2.8 \times 10^6$  psi.

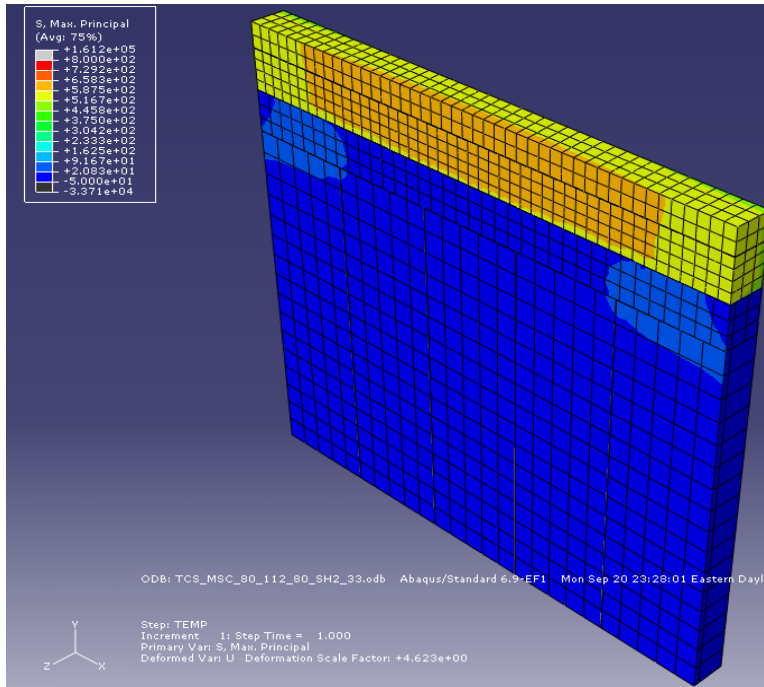


**Figure B340.** 2-ft shoulder transverse cracking model where  $T_M=80^\circ\text{F}$ ,  $T_S=110^\circ\text{F}$ , and  $T_C=80^\circ\text{F}$ , for a CTE of  $5.5 \times 10^{-6}/^\circ\text{F}$  and a stiffness of  $3.3 \times 10^6$  psi.

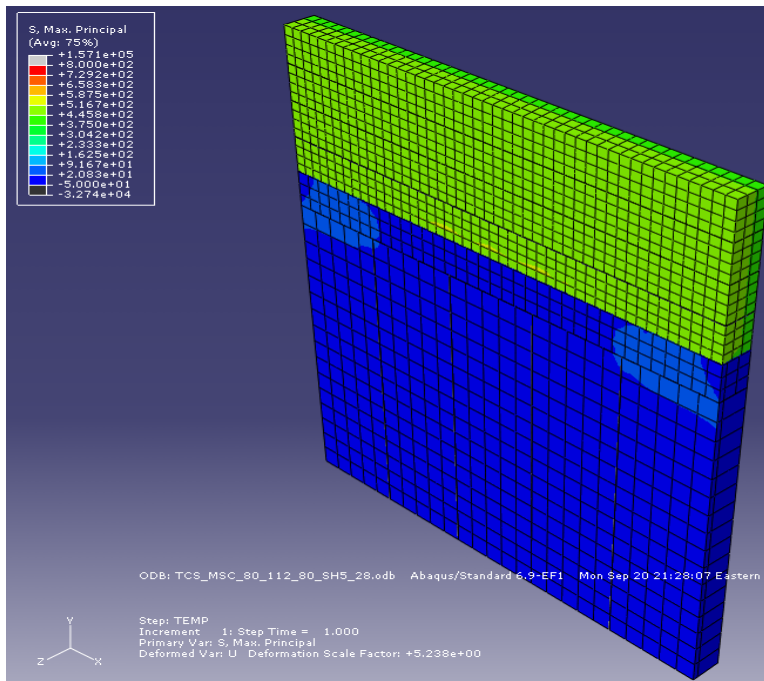


**Figure B341.** 5-ft shoulder transverse cracking model where  $T_M=80^\circ\text{F}$ ,  $T_S=110^\circ\text{F}$ , and  $T_C=80^\circ\text{F}$ , for a CTE of  $5.5 \times 10^{-6}/^\circ\text{F}$  and a stiffness of  $2.8 \times 10^6$  psi.

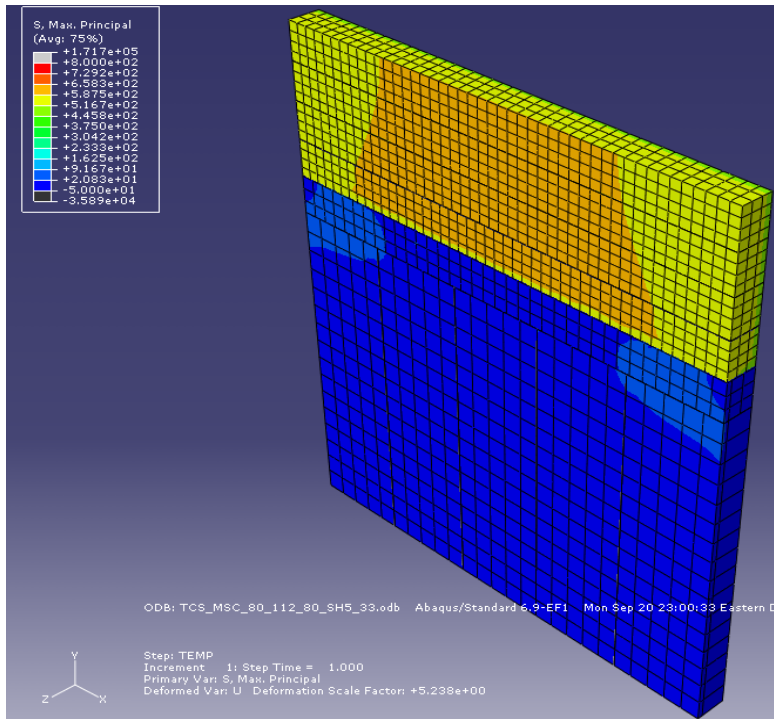


**Figure B342.** 5-ft shoulder transverse cracking model where  $T_M=80^\circ\text{F}$ ,  $T_S=110^\circ\text{F}$ , and  $T_C=80^\circ\text{F}$ , for a CTE of  $5.5 \times 10^{-6}/^\circ\text{F}$  and a stiffness of  $3.3 \times 10^6$  psi.

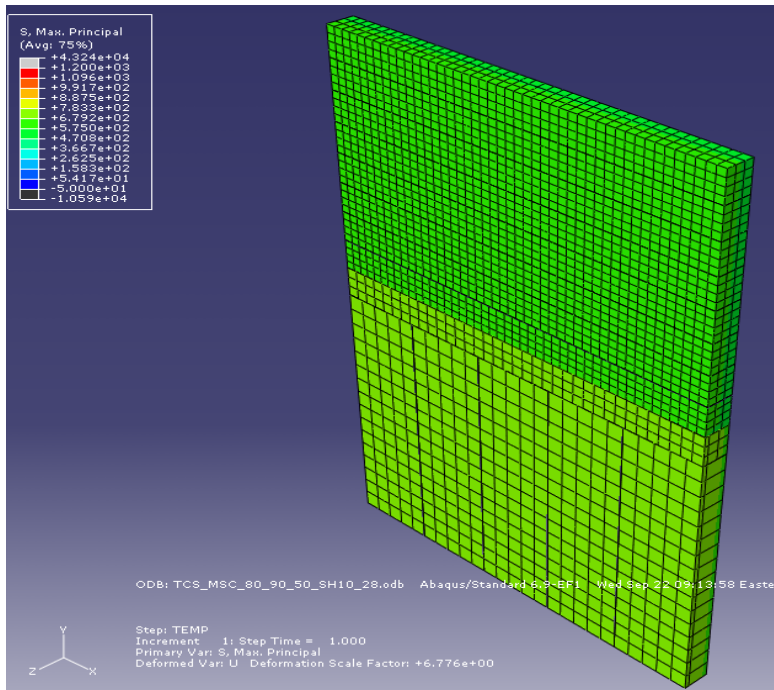


**Figure B343.** 10-ft shoulder transverse cracking model where  $T_M=80^\circ\text{F}$ ,  $T_S=90^\circ\text{F}$ , and  $T_C=50^\circ\text{F}$ , for a CTE of  $5.5 \times 10^{-6}/^\circ\text{F}$  and a stiffness of  $2.8 \times 10^6$  psi.

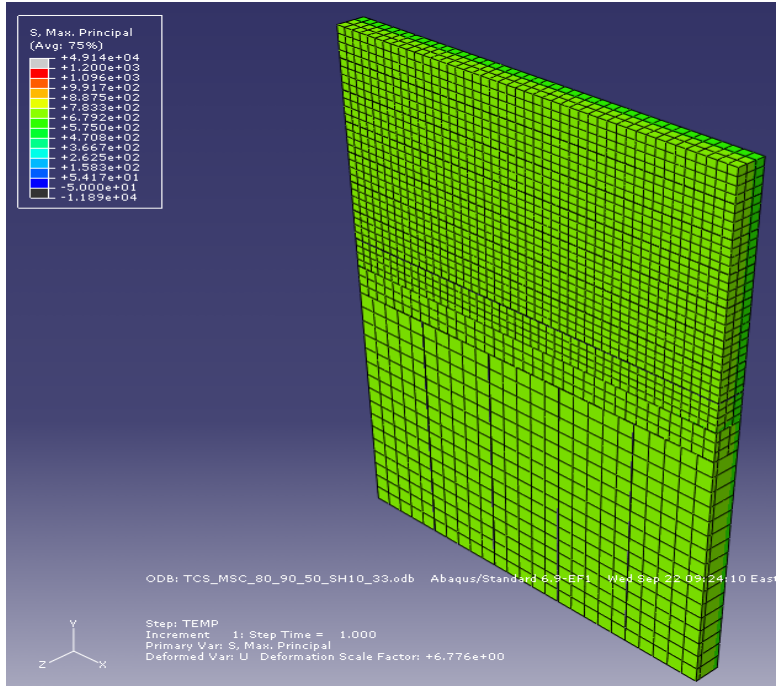


**Figure B344.** 10-ft shoulder transverse cracking model where  $T_M=80^\circ\text{F}$ ,  $T_S=90^\circ\text{F}$ , and  $T_C=50^\circ\text{F}$ , for a CTE of  $5.5 \times 10^{-6}/^\circ\text{F}$  and a stiffness of  $3.3 \times 10^6$  psi.

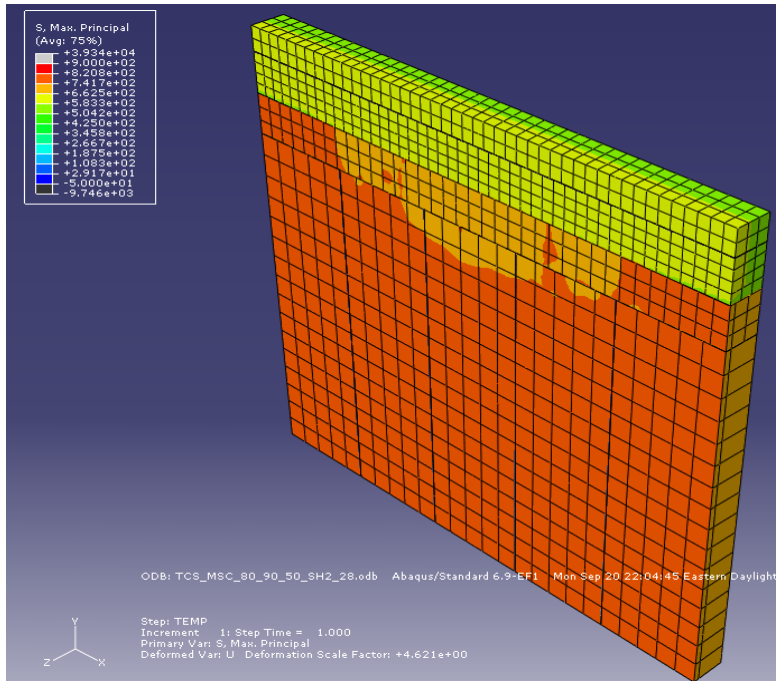


**Figure B345.** 3-ft shoulder transverse cracking model where  $T_M=80^\circ\text{F}$ ,  $T_S=90^\circ\text{F}$ , and  $T_C=50^\circ\text{F}$ , for a CTE of  $5.5 \times 10^{-6}/^\circ\text{F}$  and a stiffness of  $2.8 \times 10^6$  psi.

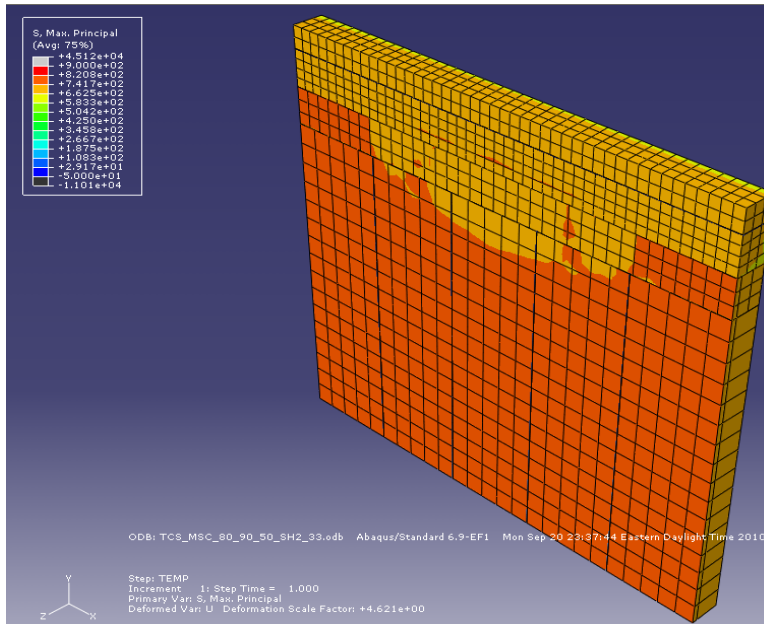


**Figure B346.** 2-ft shoulder transverse cracking model where  $T_M=80^\circ\text{F}$ ,  $T_S=90^\circ\text{F}$ , and  $T_C=50^\circ\text{F}$ , for a CTE of  $5.5 \times 10^{-6}/^\circ\text{F}$  and a stiffness of  $3.3 \times 10^6$  psi.

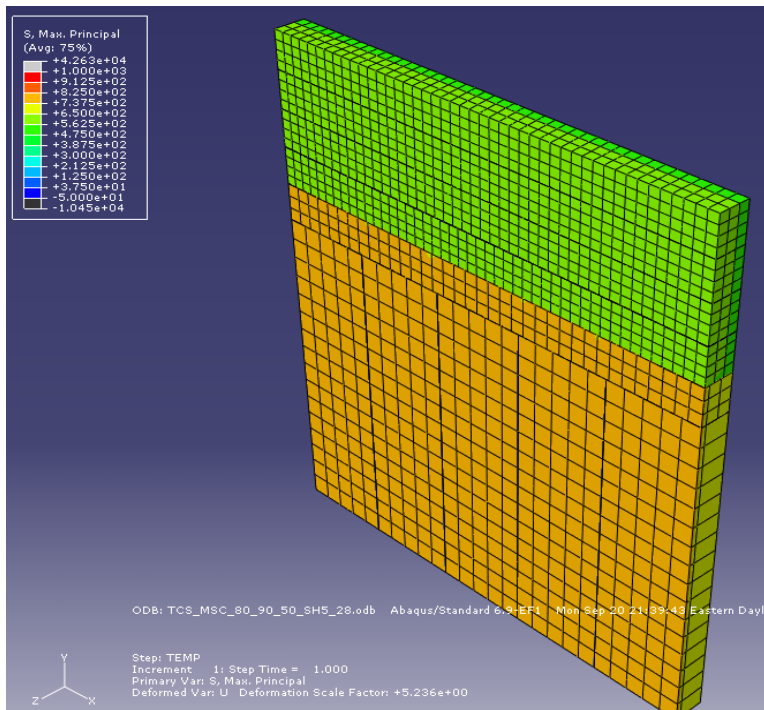


**Figure B347.** 5-ft shoulder transverse cracking model where  $T_M=80^\circ\text{F}$ ,  $T_S=90^\circ\text{F}$ , and  $T_C=50^\circ\text{F}$ , for a CTE of  $5.5 \times 10^{-6}/^\circ\text{F}$  and a stiffness of  $2.8 \times 10^6$  psi.

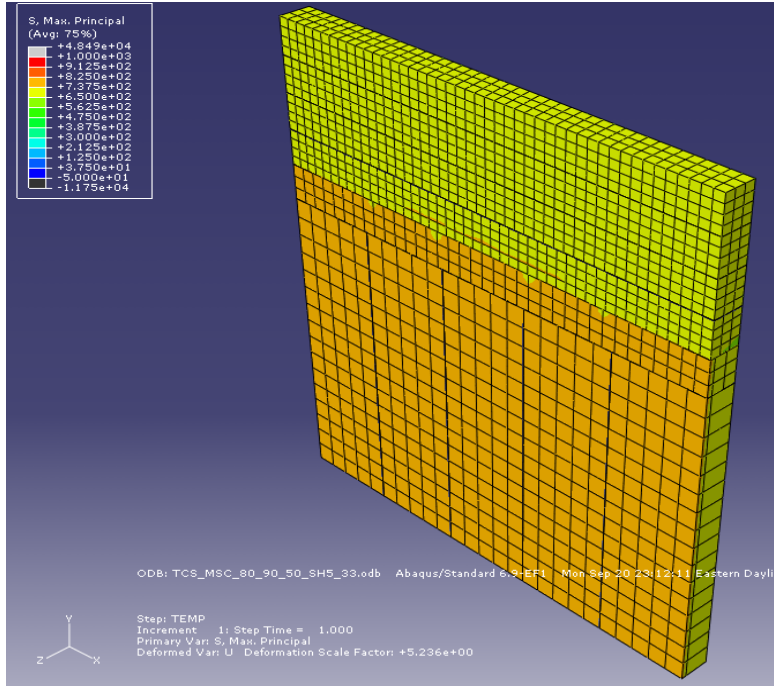


**Figure B348.** 5-ft shoulder transverse cracking model where  $T_M=80^\circ\text{F}$ ,  $T_S=90^\circ\text{F}$ , and  $T_C=50^\circ\text{F}$ , for a CTE of  $5.5 \times 10^{-6}/^\circ\text{F}$  and a stiffness of  $3.3 \times 10^6$  psi.

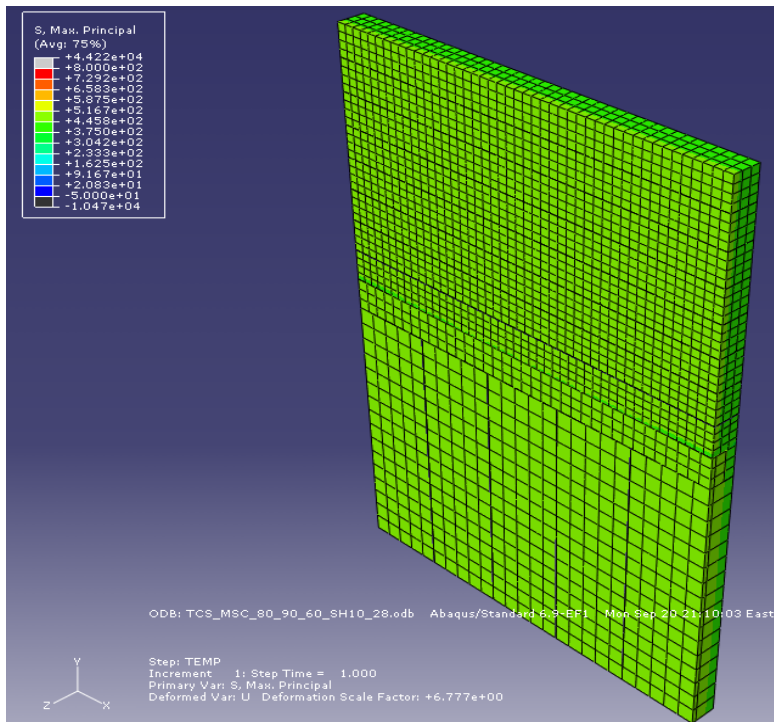


**Figure B349.** 10-ft shoulder transverse cracking model where  $T_M=80^\circ\text{F}$ ,  $T_S=90^\circ\text{F}$ , and  $T_C=60^\circ\text{F}$ , for a CTE of  $5.5 \times 10^{-6}/^\circ\text{F}$  and a stiffness of  $2.8 \times 10^6$  psi.

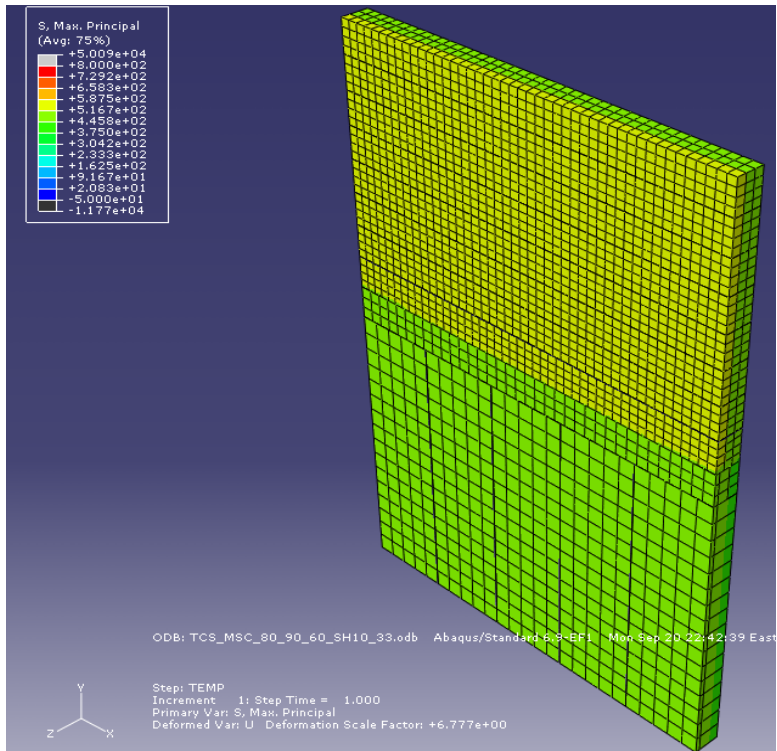


**Figure B350.** 10-ft shoulder transverse cracking model where  $T_M=80^\circ\text{F}$ ,  $T_S=90^\circ\text{F}$ , and  $T_C=60^\circ\text{F}$ , for a CTE of  $5.5 \times 10^{-6}/^\circ\text{F}$  and a stiffness of  $3.3 \times 10^6$  psi.

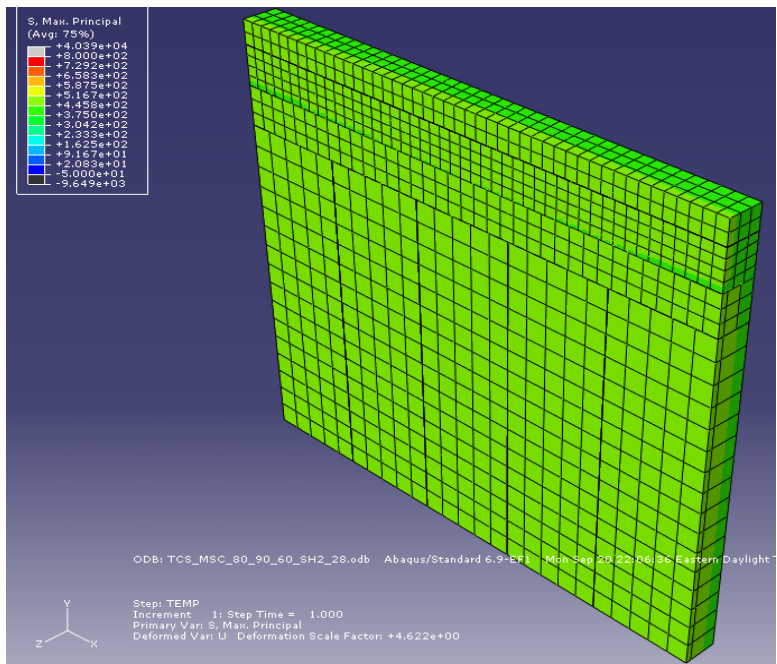


**Figure B351.** 2-ft shoulder transverse cracking model where  $T_M=80^\circ\text{F}$ ,  $T_S=90^\circ\text{F}$ , and  $T_C=60^\circ\text{F}$ , for a CTE of  $5.5 \times 10^{-6}/^\circ\text{F}$  and a stiffness of  $2.8 \times 10^6$  psi.

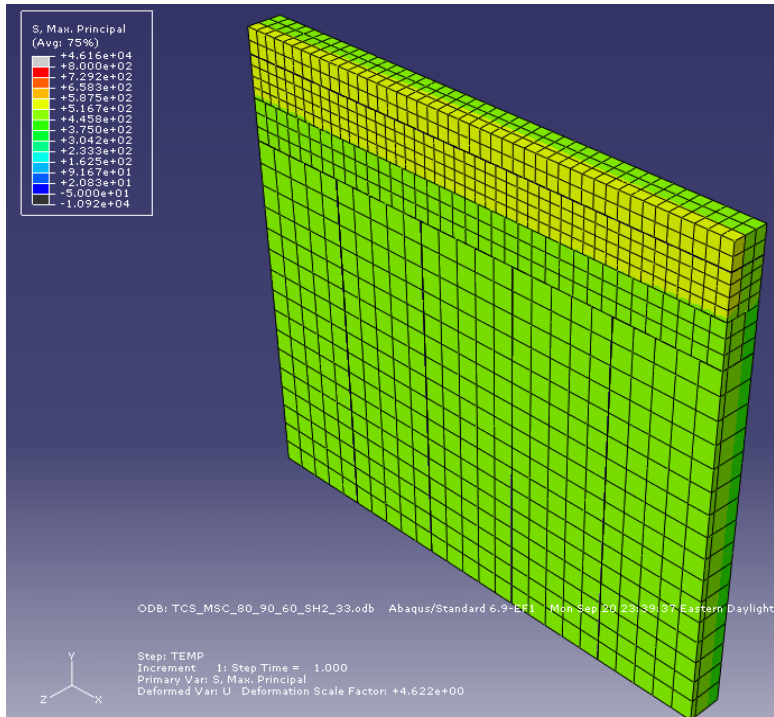


**Figure B352.** 2-ft shoulder transverse cracking model where  $T_M=80^\circ\text{F}$ ,  $T_S=90^\circ\text{F}$ , and  $T_C=60^\circ\text{F}$ , for a CTE of  $5.5 \times 10^{-6}/^\circ\text{F}$  and a stiffness of  $3.3 \times 10^6$  psi.

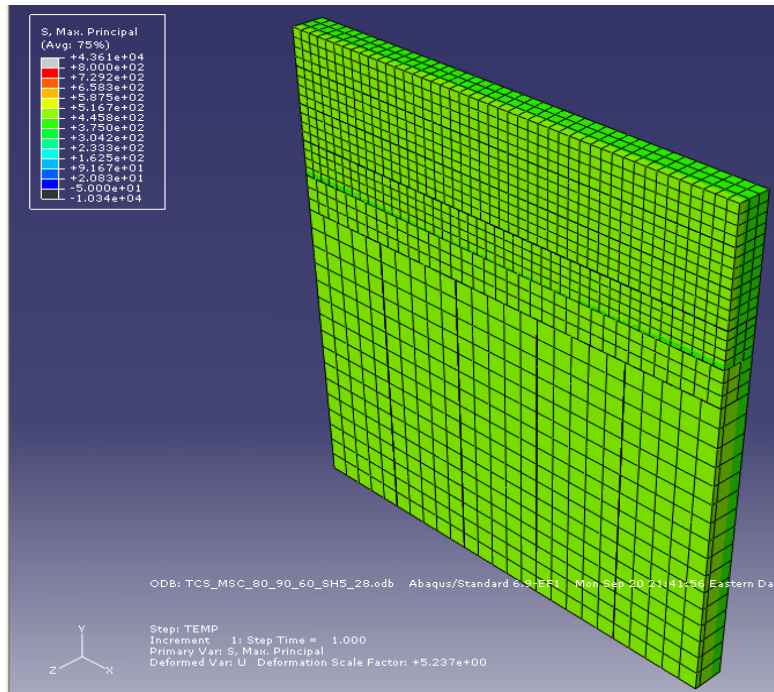


**Figure B353.** 5-ft shoulder transverse cracking model where  $T_M=80^\circ\text{F}$ ,  $T_S=90^\circ\text{F}$ , and  $T_C=60^\circ\text{F}$ , for a CTE of  $5.5 \times 10^{-6}/^\circ\text{F}$  and a stiffness of  $2.8 \times 10^6$  psi.

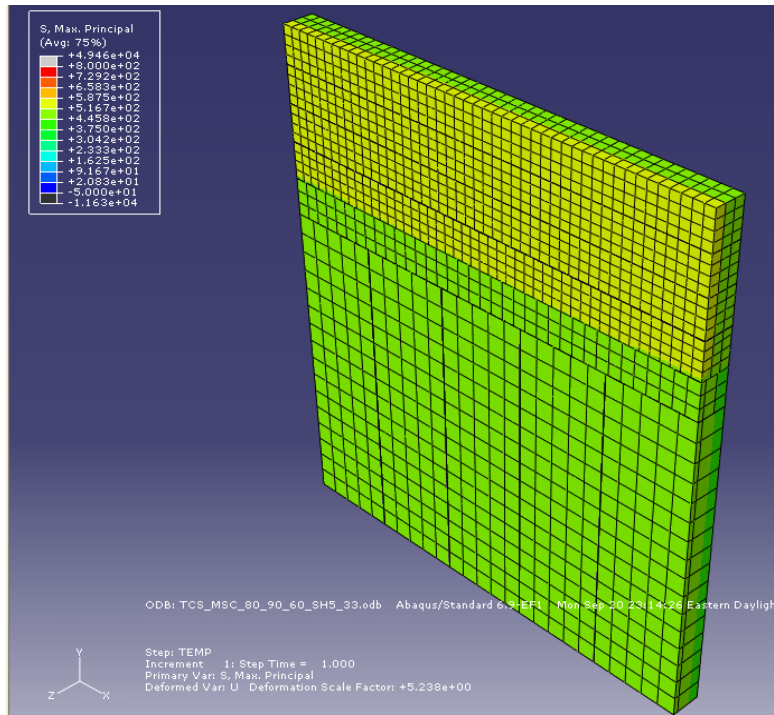


**Figure B354.** 5-ft shoulder transverse cracking model where  $T_M=80^\circ\text{F}$ ,  $T_S=90^\circ\text{F}$ , and  $T_C=60^\circ\text{F}$ , for a CTE of  $5.5 \times 10^{-6}/^\circ\text{F}$  and a stiffness of  $3.3 \times 10^6$  psi.

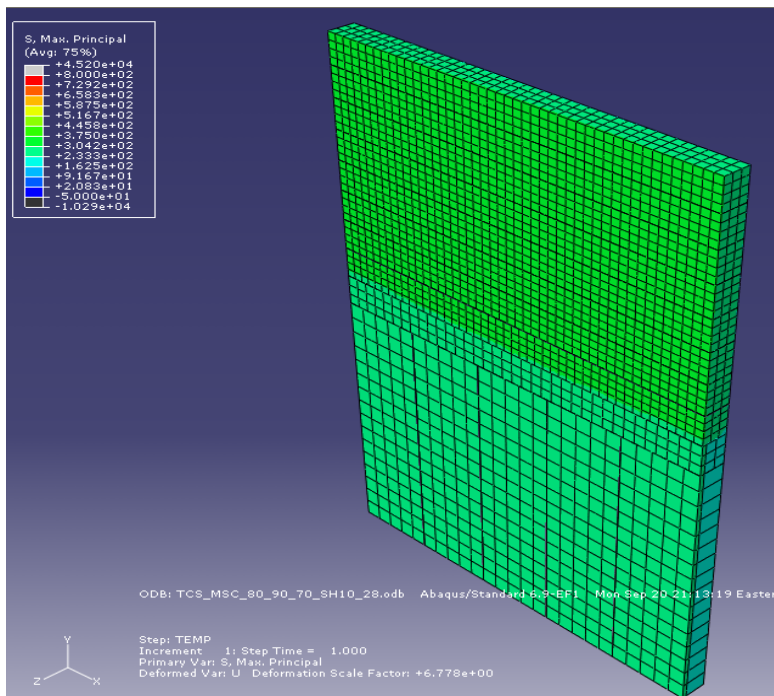


**Figure B355.** 10-ft shoulder transverse cracking model where  $T_M=80^\circ\text{F}$ ,  $T_S=90^\circ\text{F}$ , and  $T_C=70^\circ\text{F}$ , for a CTE of  $5.5 \times 10^{-6}/^\circ\text{F}$  and a stiffness of  $2.8 \times 10^6$  psi.

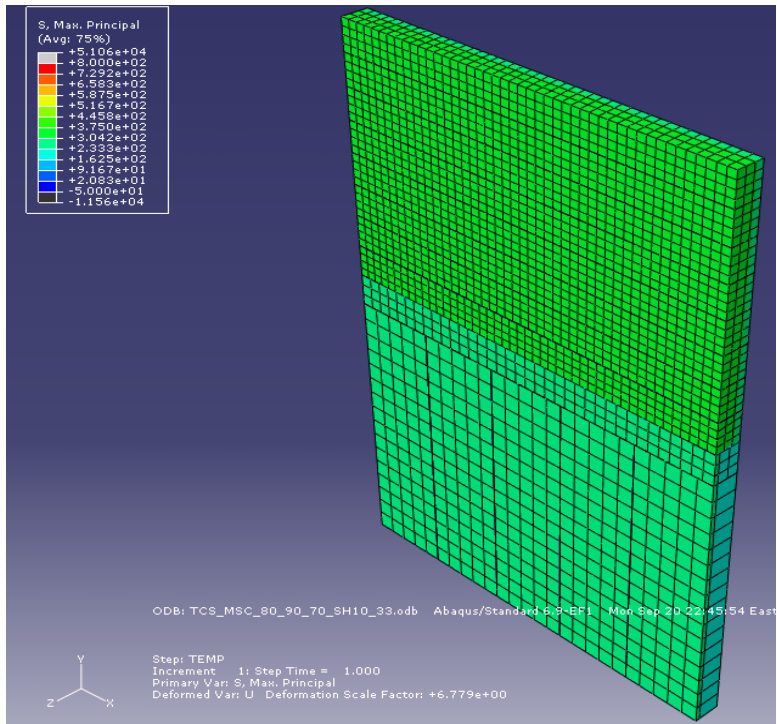


**Figure B356.** 10-ft shoulder transverse cracking model where  $T_M=80^\circ\text{F}$ ,  $T_S=90^\circ\text{F}$ , and  $T_C=70^\circ\text{F}$ , for a CTE of  $5.5 \times 10^{-6}/^\circ\text{F}$  and a stiffness of  $3.3 \times 10^6$  psi.

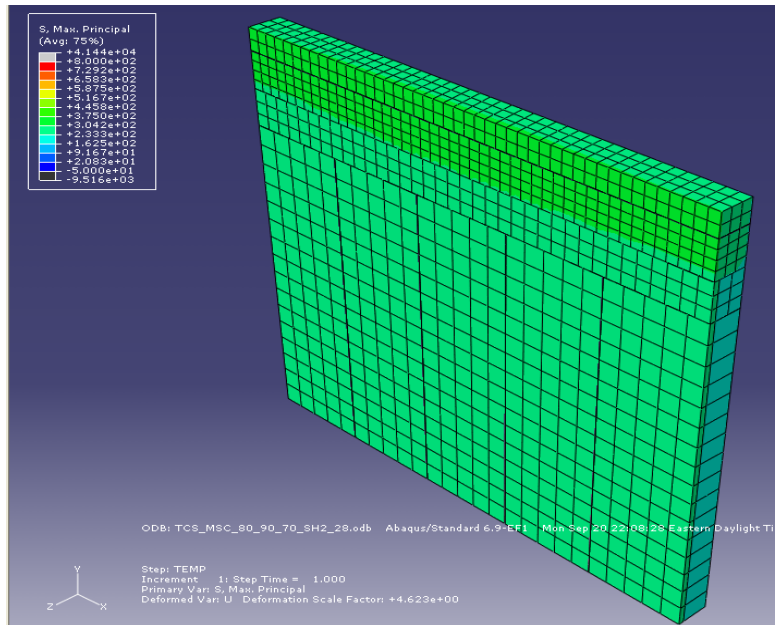


**Figure B357.** 2-ft shoulder transverse cracking model where  $T_M=80^\circ\text{F}$ ,  $T_S=90^\circ\text{F}$ , and  $T_C=70^\circ\text{F}$ , for a CTE of  $5.5 \times 10^{-6}/^\circ\text{F}$  and a stiffness of  $2.8 \times 10^6$  psi.

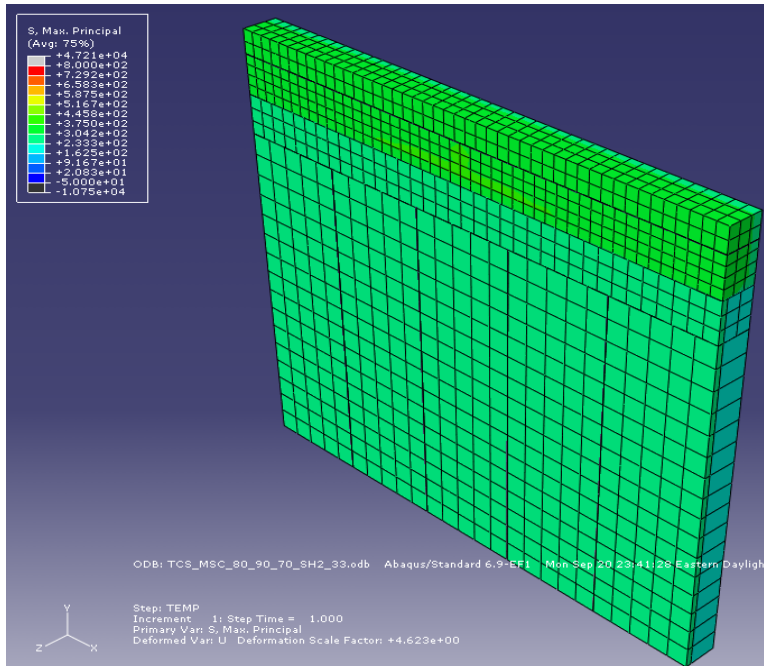


**Figure B358.** 2-ft shoulder transverse cracking model where  $T_M=80^\circ\text{F}$ ,  $T_S=90^\circ\text{F}$ , and  $T_C=70^\circ\text{F}$ , for a CTE of  $5.5 \times 10^{-6}/^\circ\text{F}$  and a stiffness of  $3.3 \times 10^6$  psi.

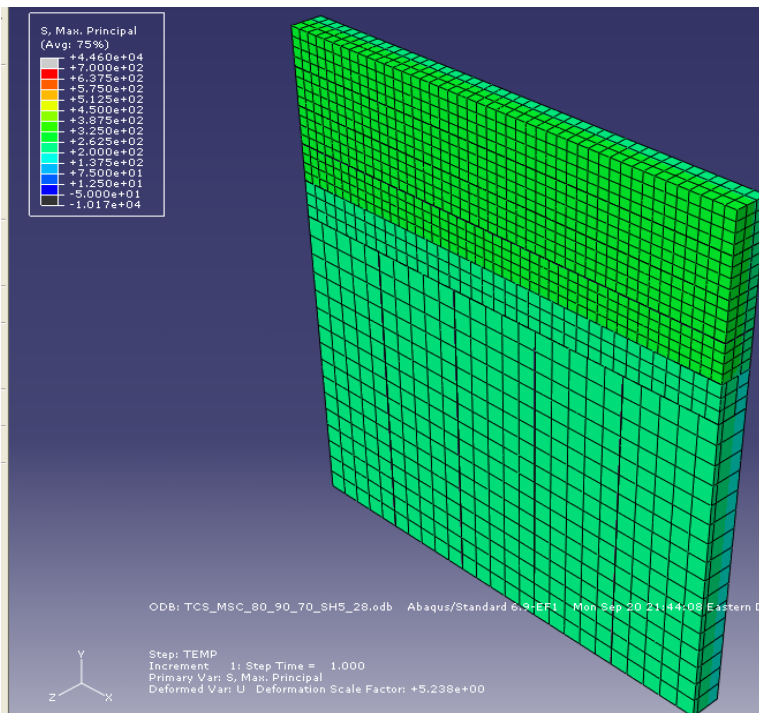


**Figure B359.** 5-ft shoulder transverse cracking model where  $T_M=80^\circ\text{F}$ ,  $T_S=90^\circ\text{F}$ , and  $T_C=70^\circ\text{F}$ , for a CTE of  $5.5 \times 10^{-6}/^\circ\text{F}$  and a stiffness of  $2.8 \times 10^6$  psi.

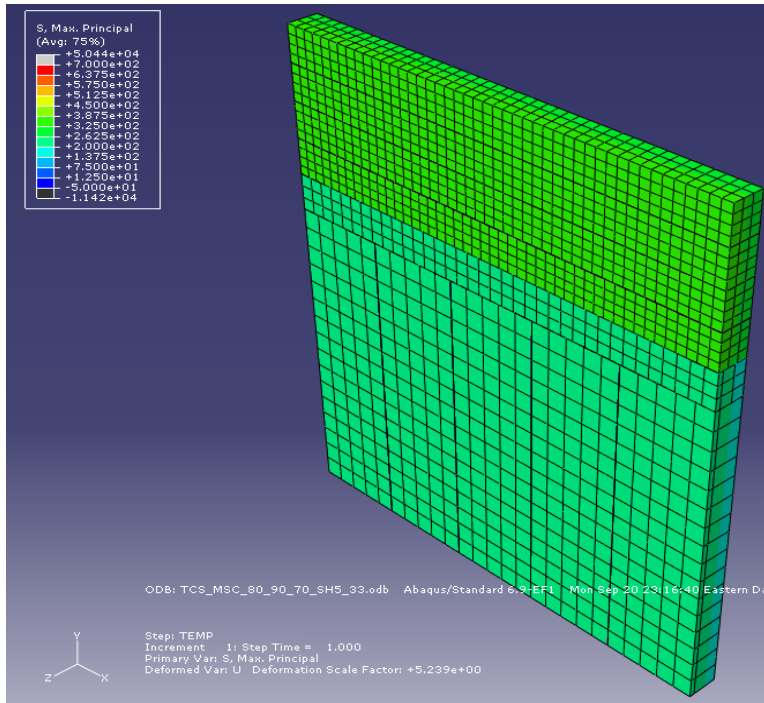


**Figure B360.** 5-ft shoulder transverse cracking model where  $T_M=80^\circ\text{F}$ ,  $T_S=90^\circ\text{F}$ , and  $T_C=70^\circ\text{F}$ , for a CTE of  $5.5 \times 10^{-6}/^\circ\text{F}$  and a stiffness of  $3.3 \times 10^6$  psi.

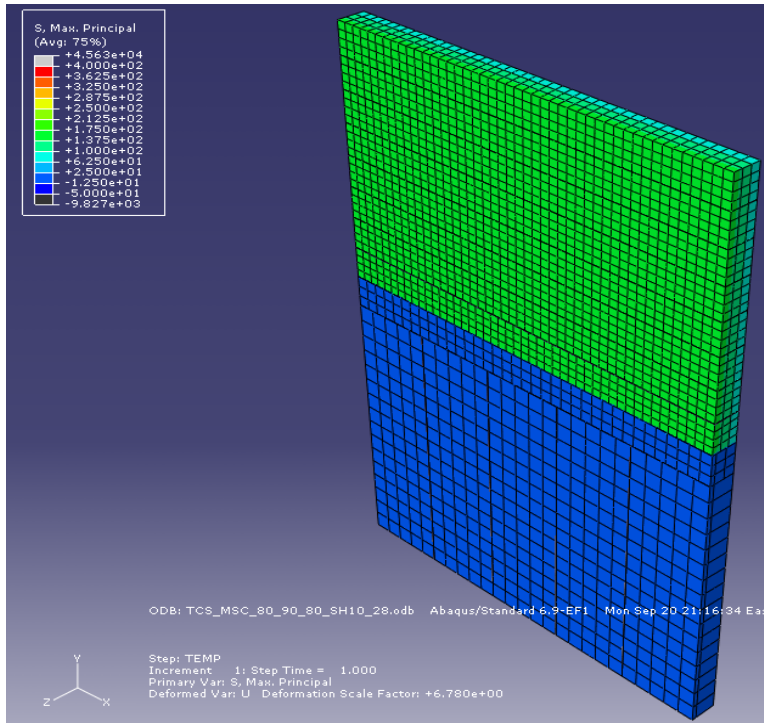


**Figure B361.** 10-ft shoulder transverse cracking model where  $T_M=80^\circ\text{F}$ ,  $T_S=90^\circ\text{F}$ , and  $T_C=80^\circ\text{F}$ , for a CTE of  $5.5 \times 10^{-6}/^\circ\text{F}$  and a stiffness of  $2.8 \times 10^6$  psi.

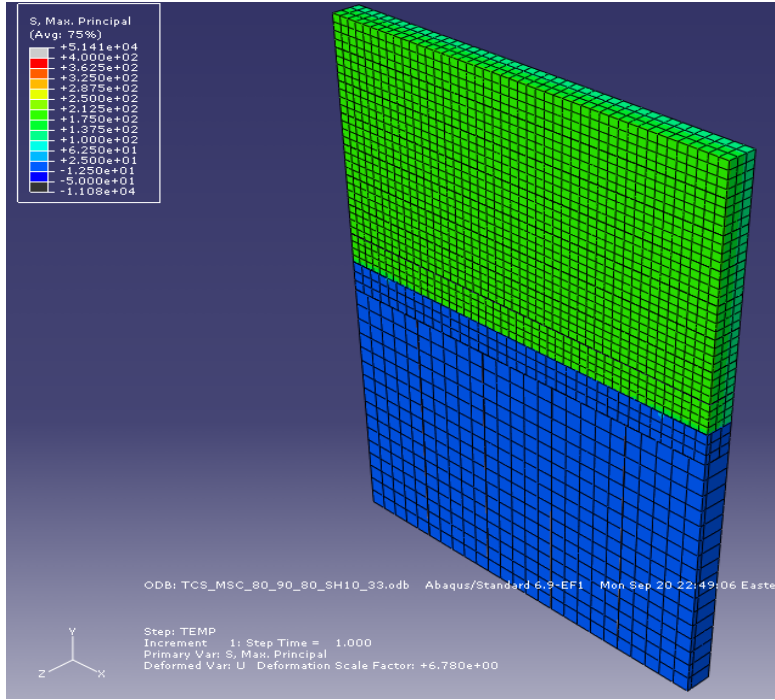


**Figure B362.** 10-ft shoulder transverse cracking model where  $T_M=80^\circ\text{F}$ ,  $T_S=90^\circ\text{F}$ , and  $T_C=90^\circ\text{F}$ , for a CTE of  $5.5 \times 10^{-6}/^\circ\text{F}$  and a stiffness of  $3.3 \times 10^6$  psi.

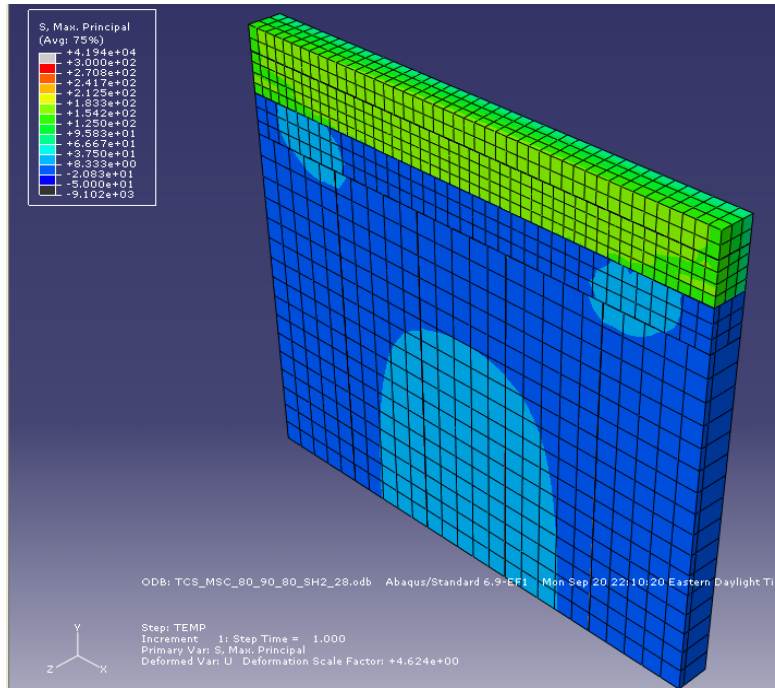


**Figure B363.** 2-ft shoulder transverse cracking model where  $T_M=80^\circ\text{F}$ ,  $T_S=90^\circ\text{F}$ , and  $T_C=80^\circ\text{F}$ , for a CTE of  $5.5 \times 10^{-6}/^\circ\text{F}$  and a stiffness of  $2.8 \times 10^6$  psi.

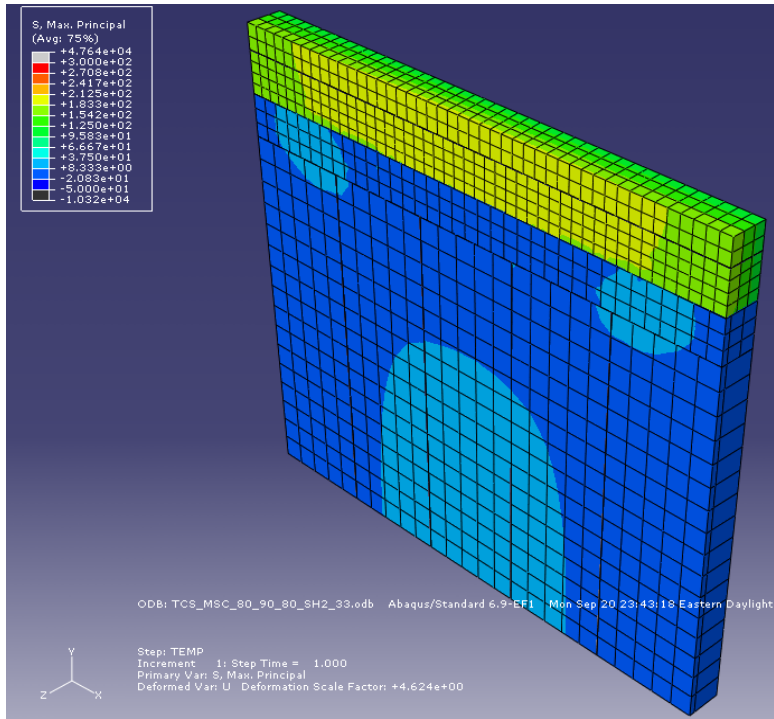


**Figure B364.** 2-ft shoulder transverse cracking model where  $T_M=80^\circ\text{F}$ ,  $T_S=90^\circ\text{F}$ , and  $T_C=80^\circ\text{F}$ , for a CTE of  $5.5 \times 10^{-6}/^\circ\text{F}$  and a stiffness of  $3.3 \times 10^6$  psi.

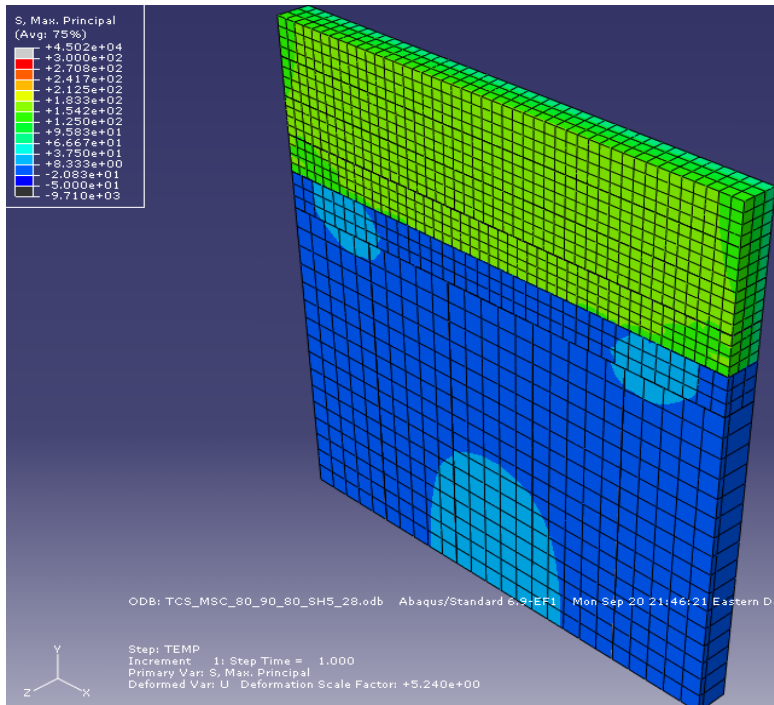


**Figure B365.** 5-ft shoulder transverse cracking model where  $T_M=80^\circ\text{F}$ ,  $T_S=90^\circ\text{F}$ , and  $T_C=80^\circ\text{F}$ , for a CTE of  $5.5 \times 10^{-6}/^\circ\text{F}$  and a stiffness of  $2.8 \times 10^6$  psi.

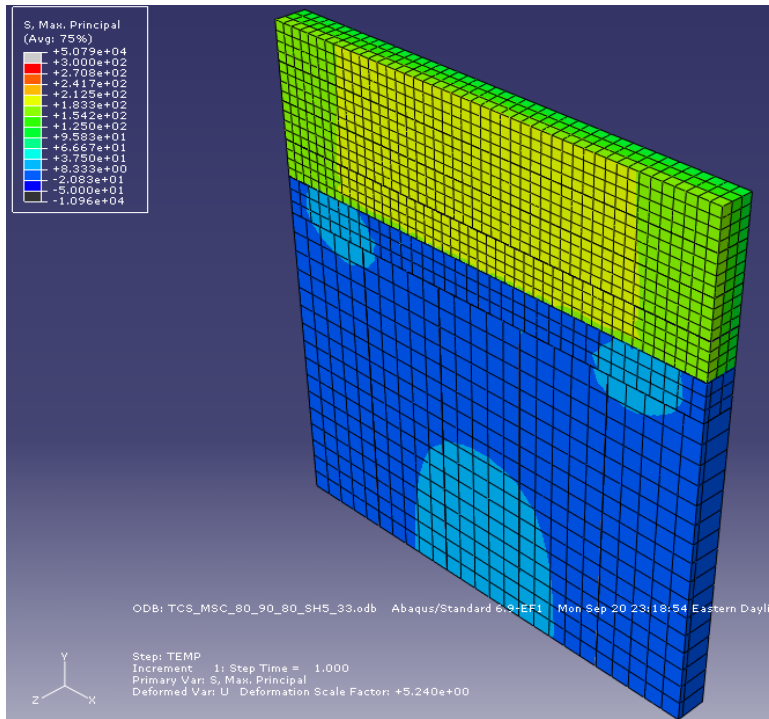


**Figure B366.** 5-ft shoulder transverse cracking model where  $T_M=80^\circ\text{F}$ ,  $T_S=90^\circ\text{F}$ , and  $T_C=80^\circ\text{F}$ , for a CTE of  $5.5 \times 10^{-6}/^\circ\text{F}$  and a stiffness of  $3.3 \times 10^6$  psi.

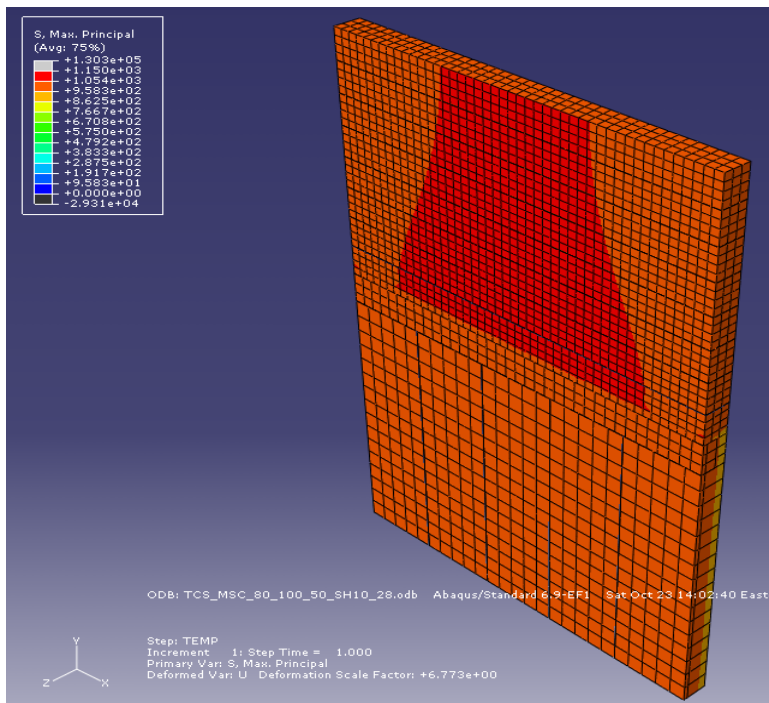


**Figure B367.** 10-ft shoulder transverse cracking model where  $T_M=80^\circ\text{F}$ ,  $T_S=100^\circ\text{F}$ , and  $T_C=50^\circ\text{F}$ , for a CTE of  $7.5 \times 10^{-6}/^\circ\text{F}$  and a stiffness of  $2.8 \times 10^6$  psi.

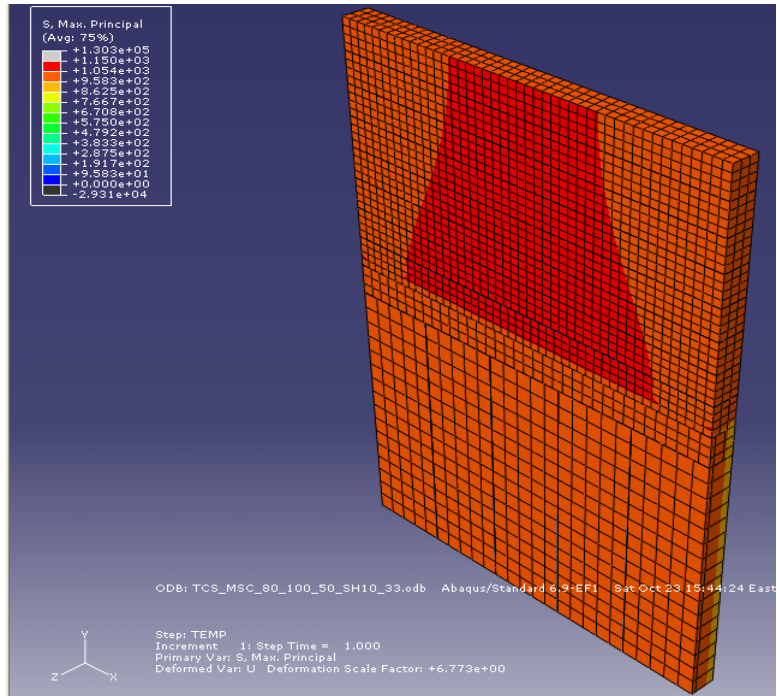


**Figure B368.** 10-ft shoulder transverse cracking model where  $T_M=80^\circ\text{F}$ ,  $T_S=100^\circ\text{F}$ , and  $T_C=50^\circ\text{F}$ , for a CTE of  $7.5 \times 10^{-6}/^\circ\text{F}$  and a stiffness of  $3.3 \times 10^6$  psi.

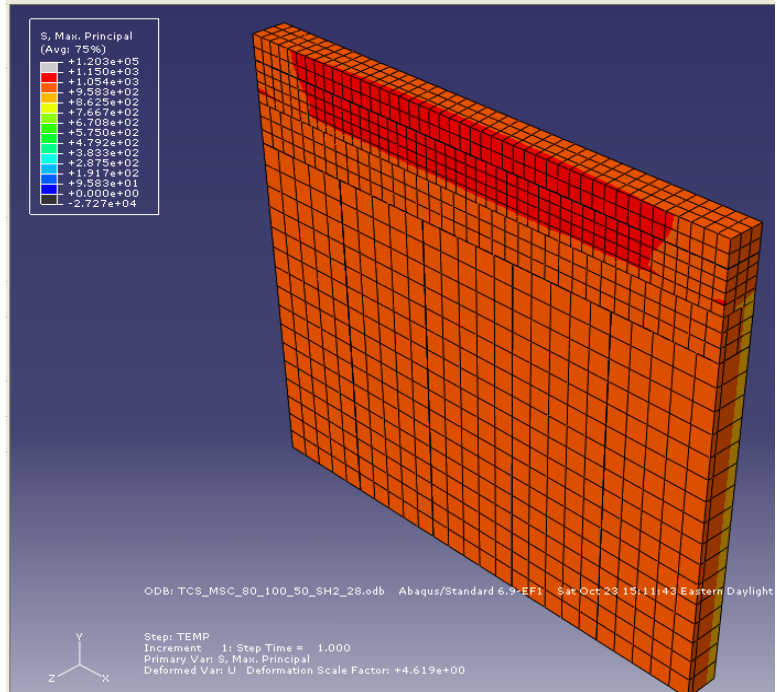


**Figure B369.** 2-ft shoulder transverse cracking model where  $T_M=80^\circ\text{F}$ ,  $T_S=100^\circ\text{F}$ , and  $T_C=50^\circ\text{F}$ , for a CTE of  $7.5 \times 10^{-6}/^\circ\text{F}$  and a stiffness of  $2.8 \times 10^6$  psi.

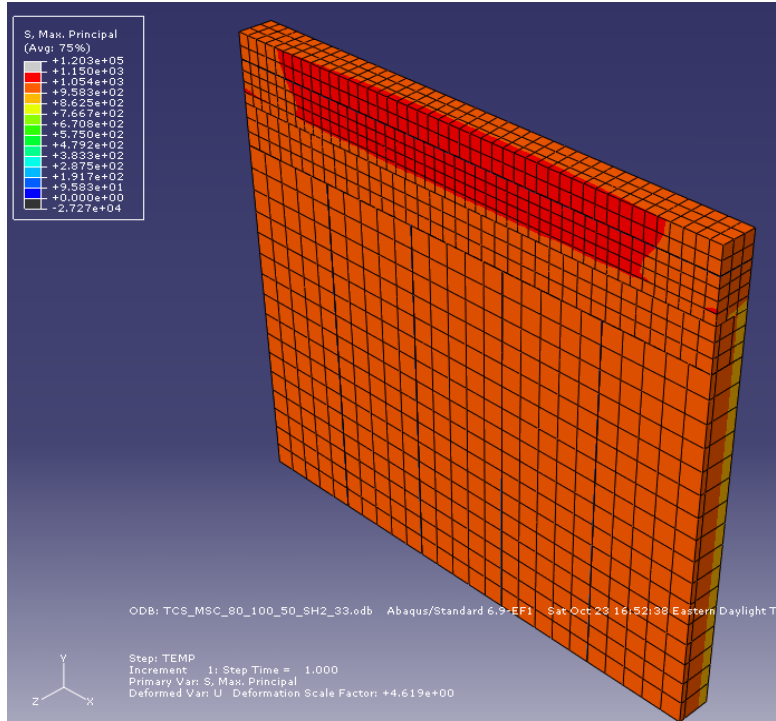


**Figure B370.** 2-ft shoulder transverse cracking model where  $T_M=80^\circ\text{F}$ ,  $T_S=100^\circ\text{F}$ , and  $T_C=50^\circ\text{F}$ , for a CTE of  $7.5 \times 10^{-6}/^\circ\text{F}$  and a stiffness of  $3.3 \times 10^6$  psi.

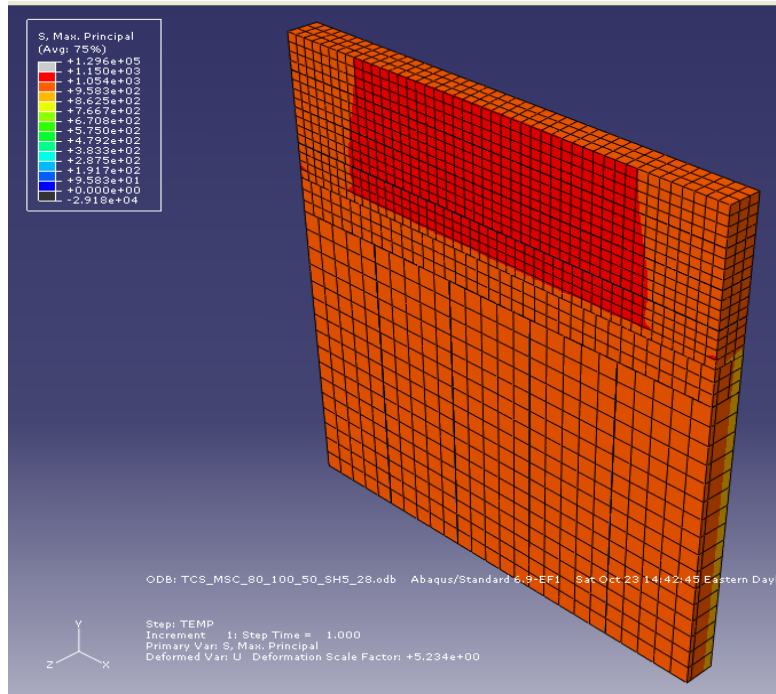


**Figure B371.** 5-ft shoulder transverse cracking model where  $T_M=80^\circ\text{F}$ ,  $T_S=100^\circ\text{F}$ , and  $T_C=50^\circ\text{F}$ , for a CTE of  $7.5 \times 10^{-6}/^\circ\text{F}$  and a stiffness of  $2.8 \times 10^6$  psi.

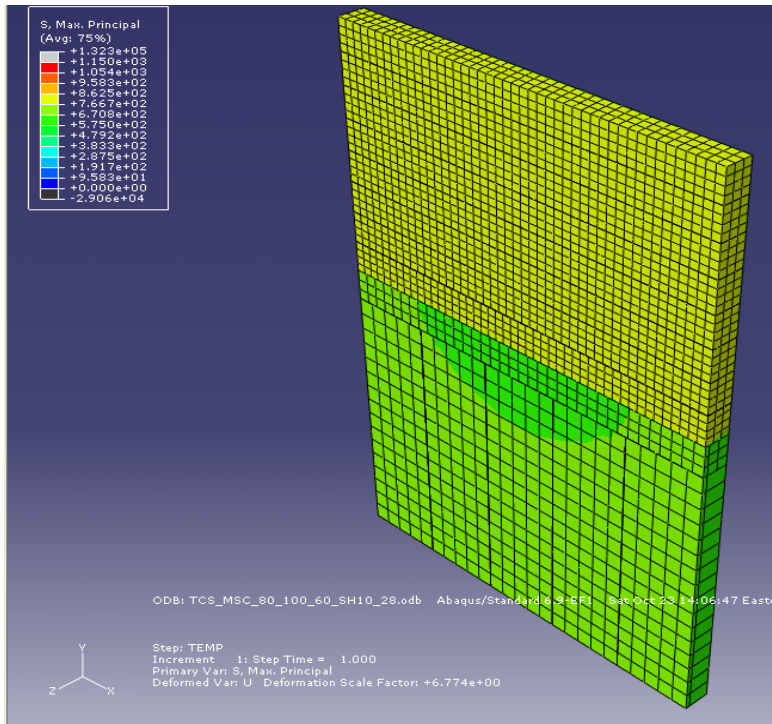


**Figure B372.** 10-ft shoulder transverse cracking model where  $T_M=80^\circ\text{F}$ ,  $T_S=100^\circ\text{F}$ , and  $T_C=60^\circ\text{F}$ , for a CTE of  $7.5 \times 10^{-6}/^\circ\text{F}$  and a stiffness of  $2.8 \times 10^6$  psi.

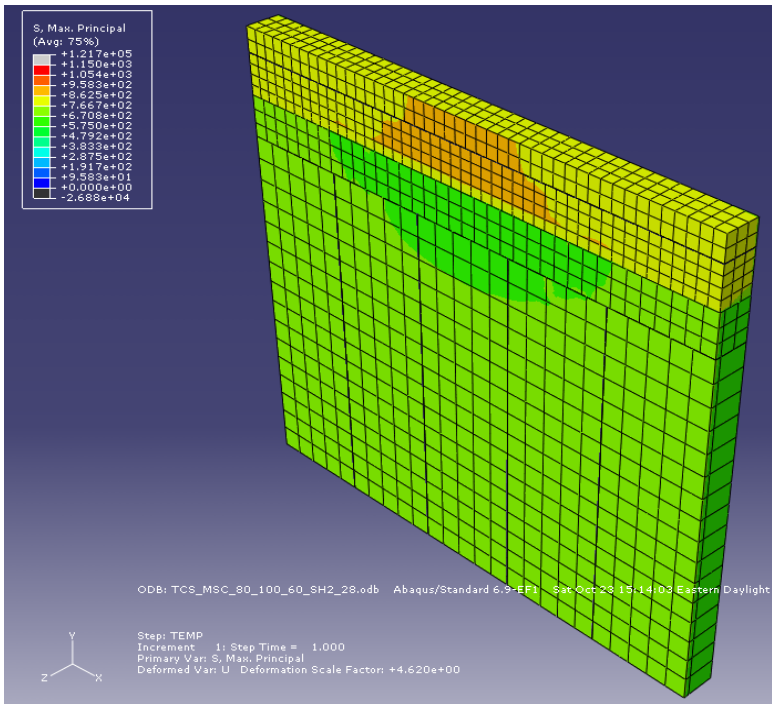


**Figure B373.** 2-ft shoulder transverse cracking model where  $T_M=80^\circ\text{F}$ ,  $T_S=100^\circ\text{F}$ , and  $T_C=60^\circ\text{F}$ , for a CTE of  $7.5 \times 10^{-6}/^\circ\text{F}$  and a stiffness of  $2.8 \times 10^6$  psi.

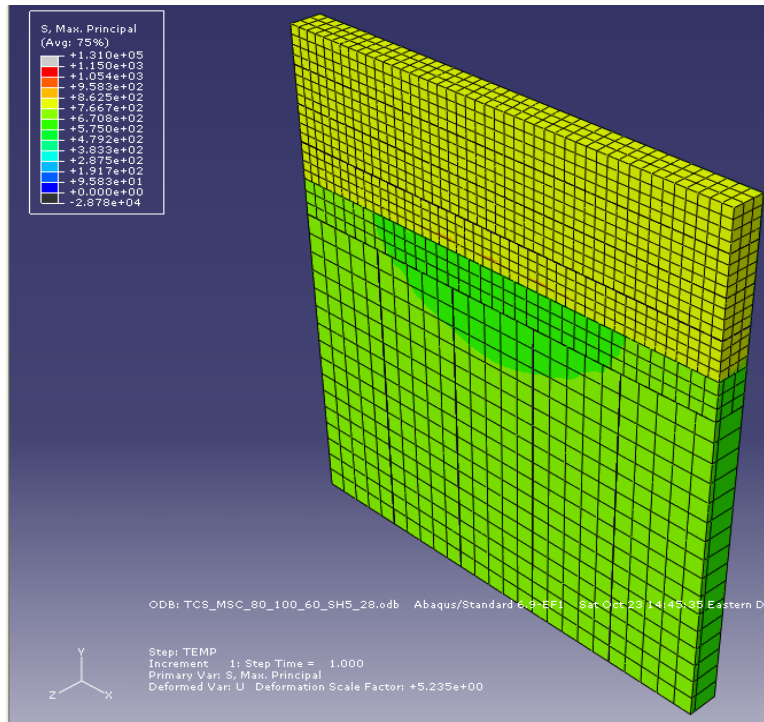


**Figure B374.** 5-ft shoulder transverse cracking model where  $T_M=80^\circ\text{F}$ ,  $T_S=100^\circ\text{F}$ , and  $T_C=60^\circ\text{F}$ , for a CTE of  $7.5 \times 10^{-6}/^\circ\text{F}$  and a stiffness of  $2.8 \times 10^6$  psi.

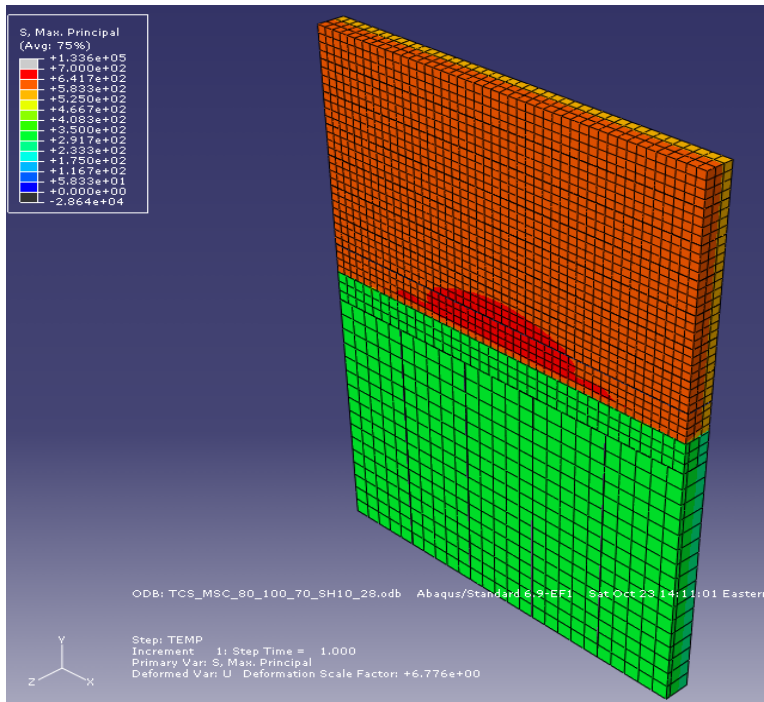


**Figure B375.** 10-ft shoulder transverse cracking model where  $T_M=80^\circ\text{F}$ ,  $T_S=100^\circ\text{F}$ , and  $T_C=70^\circ\text{F}$ , for a CTE of  $7.5 \times 10^{-6}/^\circ\text{F}$  and a stiffness of  $2.8 \times 10^6$  psi.

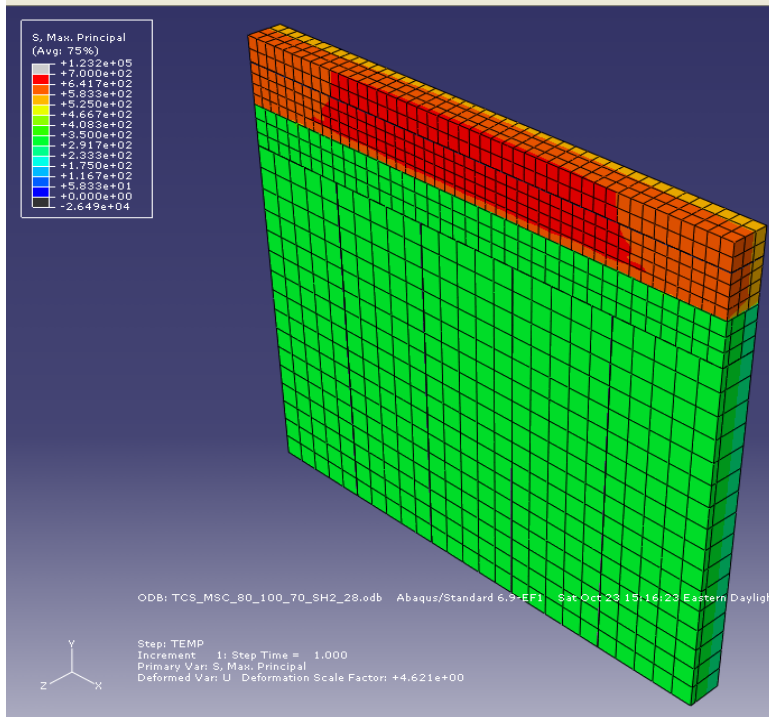


**Figure B376.** 2-ft shoulder transverse cracking model where  $T_M=80^\circ\text{F}$ ,  $T_S=100^\circ\text{F}$ , and  $T_C=70^\circ\text{F}$ , for a CTE of  $7.5 \times 10^{-6}/^\circ\text{F}$  and a stiffness of  $2.8 \times 10^6$  psi.

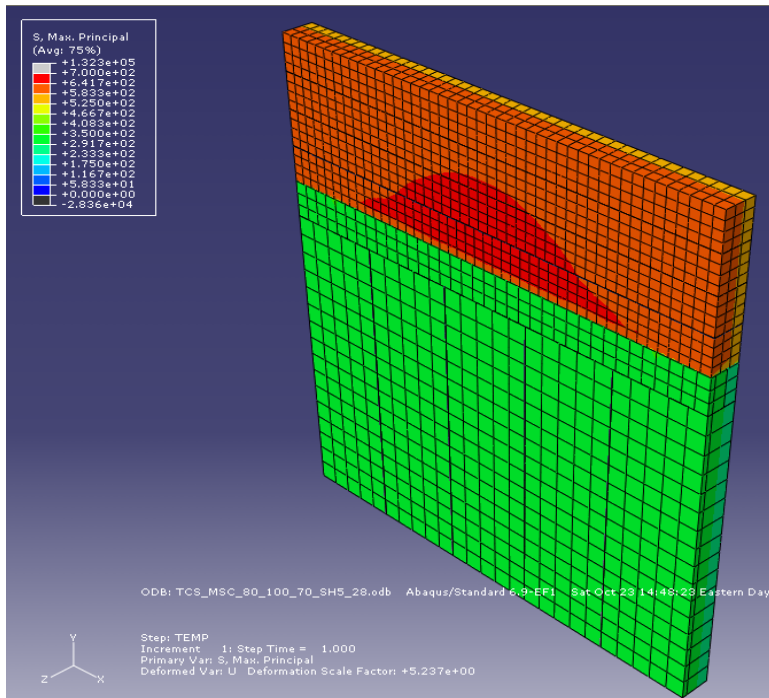


**Figure B377.** 5-ft shoulder transverse cracking model where  $T_M=80^\circ\text{F}$ ,  $T_S=100^\circ\text{F}$ , and  $T_C=70^\circ\text{F}$ , for a CTE of  $7.5 \times 10^{-6}/^\circ\text{F}$  and a stiffness of  $2.8 \times 10^6$  psi.

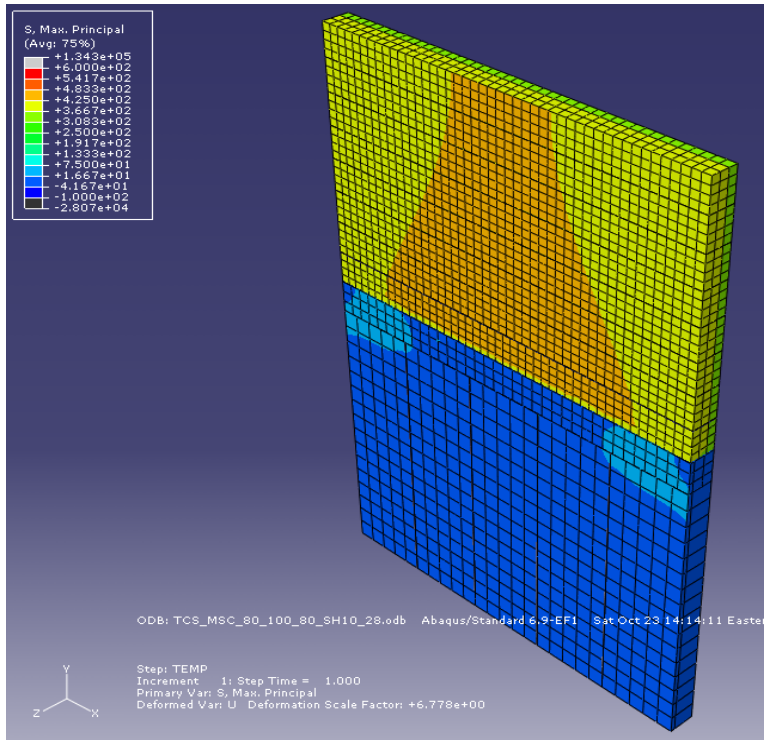


**Figure B378.** 10-ft shoulder transverse cracking model where  $T_M=80^\circ\text{F}$ ,  $T_S=100^\circ\text{F}$ , and  $T_C=80^\circ\text{F}$ , for a CTE of  $7.5 \times 10^{-6}/^\circ\text{F}$  and a stiffness of  $2.8 \times 10^6$  psi.

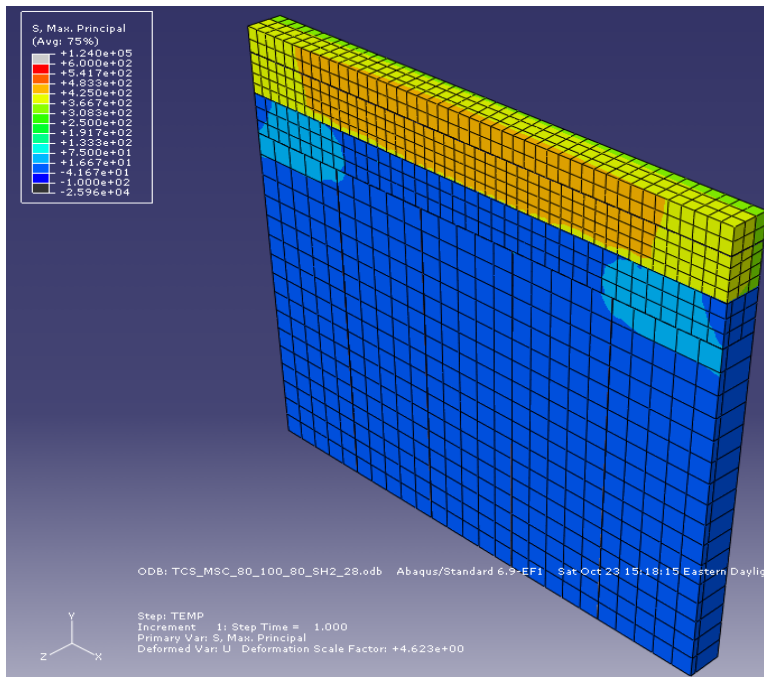


**Figure B379.** 2-ft shoulder transverse cracking model where  $T_M=80^\circ\text{F}$ ,  $T_S=100^\circ\text{F}$ , and  $T_C=80^\circ\text{F}$ , for a CTE of  $7.5 \times 10^{-6}/^\circ\text{F}$  and a stiffness of  $2.8 \times 10^6$  psi.

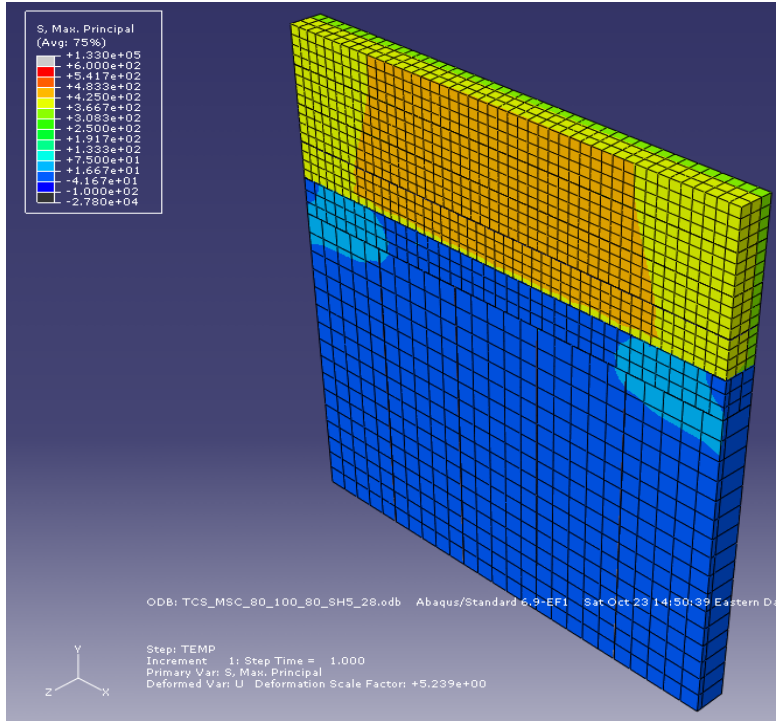


**Figure B380.** 5-ft shoulder transverse cracking model where  $T_M=80^\circ\text{F}$ ,  $T_S=100^\circ\text{F}$ , and  $T_C=80^\circ\text{F}$ , for a CTE of  $7.5 \times 10^{-6}/^\circ\text{F}$  and a stiffness of  $2.8 \times 10^6$  psi.

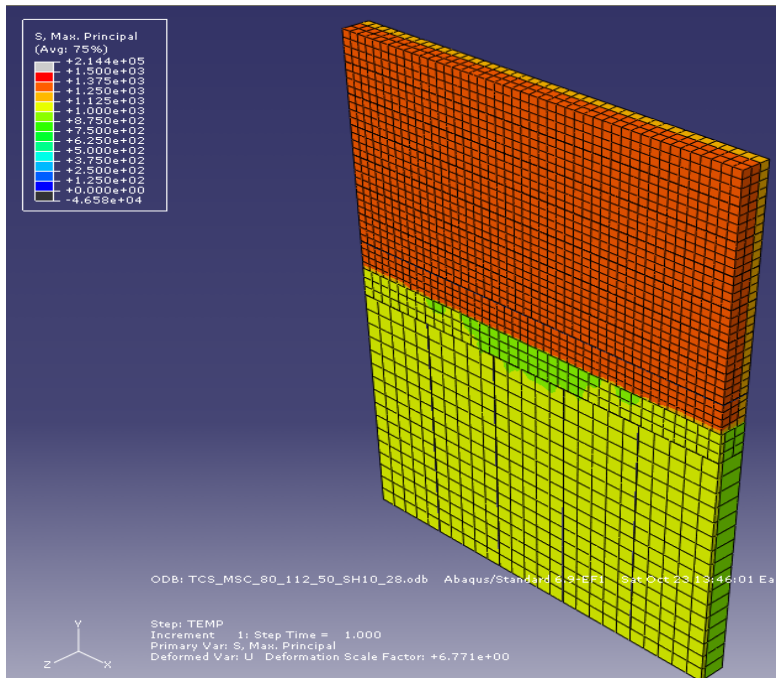


**Figure B381.** 10-ft shoulder transverse cracking model where  $T_M=80^\circ\text{F}$ ,  $T_S=110^\circ\text{F}$ , and  $T_C=50^\circ\text{F}$ , for a CTE of  $7.5 \times 10^{-6}/^\circ\text{F}$  and a stiffness of  $2.8 \times 10^6$  psi.

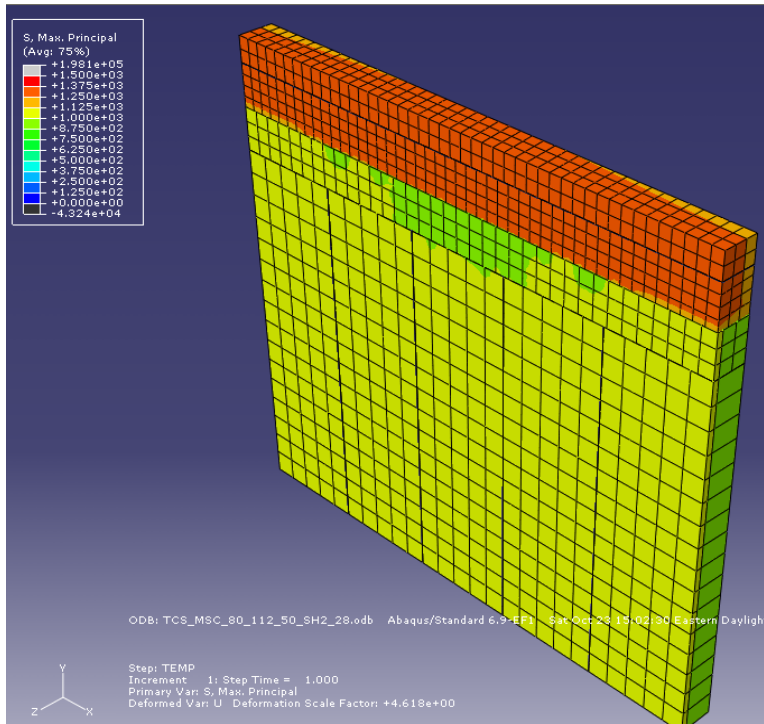


**Figure B382.** 2-ft shoulder transverse cracking model where  $T_M=80^\circ\text{F}$ ,  $T_S=110^\circ\text{F}$ , and  $T_C=50^\circ\text{F}$ , for a CTE of  $7.5 \times 10^{-6}/^\circ\text{F}$  and a stiffness of  $2.8 \times 10^6$  psi.

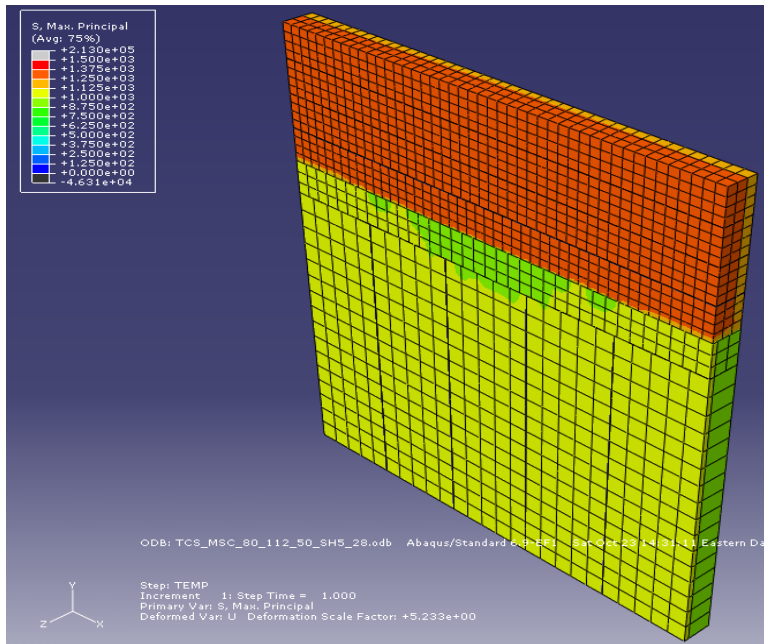


**Figure B383.** 5-ft shoulder transverse cracking model where  $T_M=80^\circ\text{F}$ ,  $T_S=110^\circ\text{F}$ , and  $T_C=50^\circ\text{F}$ , for a CTE of  $7.5 \times 10^{-6}/^\circ\text{F}$  and a stiffness of  $2.8 \times 10^6$  psi.

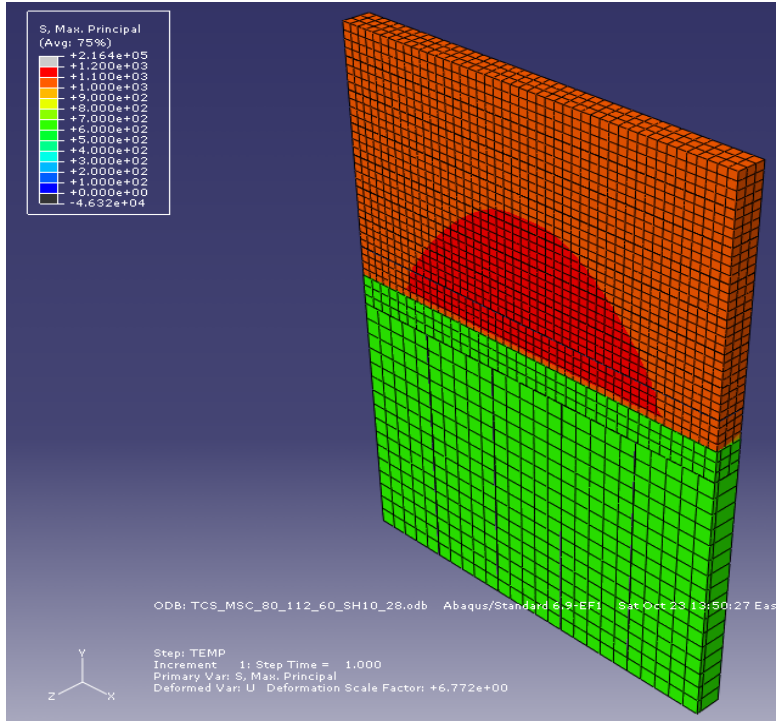


**Figure B384.** 10-ft shoulder transverse cracking model where  $T_M=80^\circ\text{F}$ ,  $T_S=110^\circ\text{F}$ , and  $T_C=60^\circ\text{F}$ , for a CTE of  $7.5 \times 10^{-6}/^\circ\text{F}$  and a stiffness of  $2.8 \times 10^6$  psi.

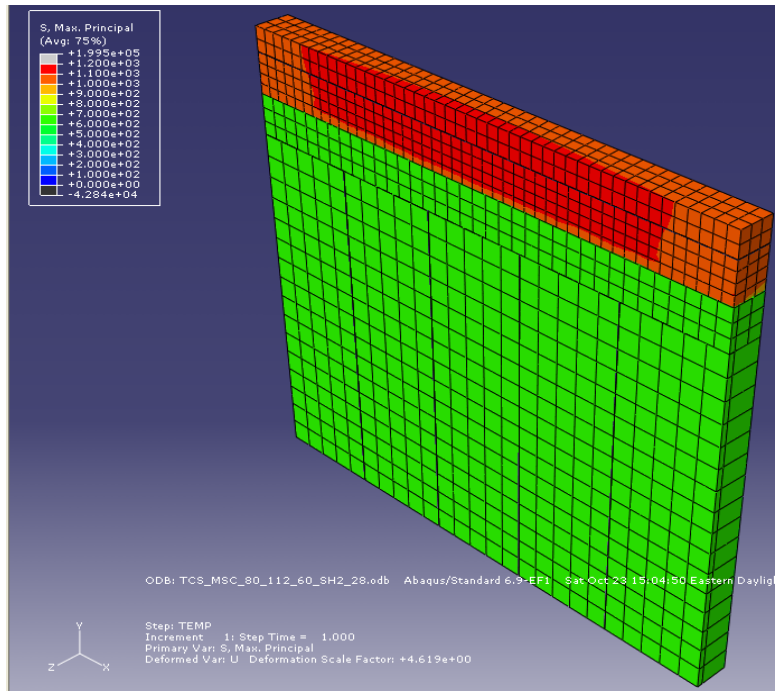


**Figure B385.** 2-ft shoulder transverse cracking model where  $T_M=80^\circ\text{F}$ ,  $T_S=110^\circ\text{F}$ , and  $T_C=60^\circ\text{F}$ , for a CTE of  $7.5 \times 10^{-6}/^\circ\text{F}$  and a stiffness of  $2.8 \times 10^6$  psi.

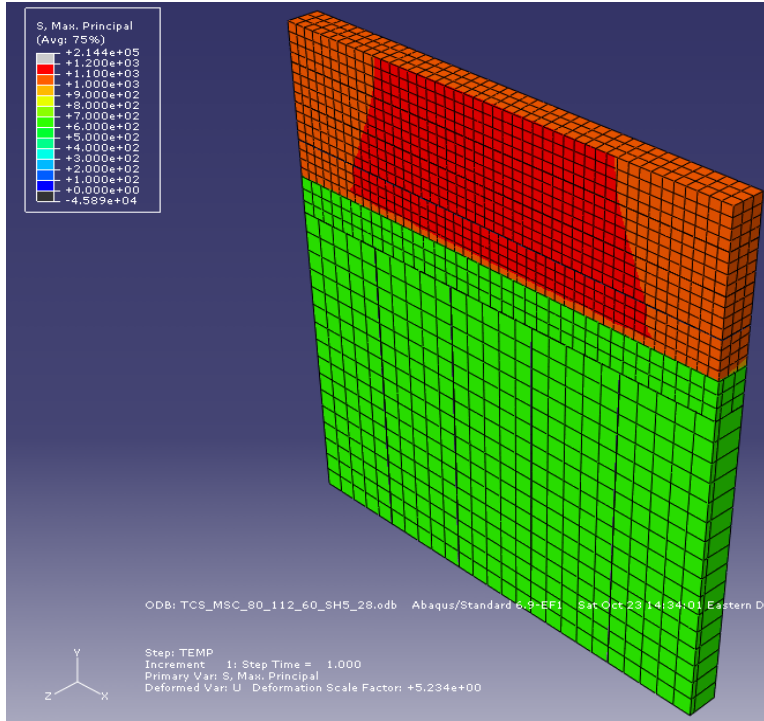


**Figure B386.** 5-ft shoulder transverse cracking model where  $T_M=80^\circ\text{F}$ ,  $T_S=110^\circ\text{F}$ , and  $T_C=60^\circ\text{F}$ , for a CTE of  $7.5 \times 10^{-6}/^\circ\text{F}$  and a stiffness of  $2.8 \times 10^6$  psi.

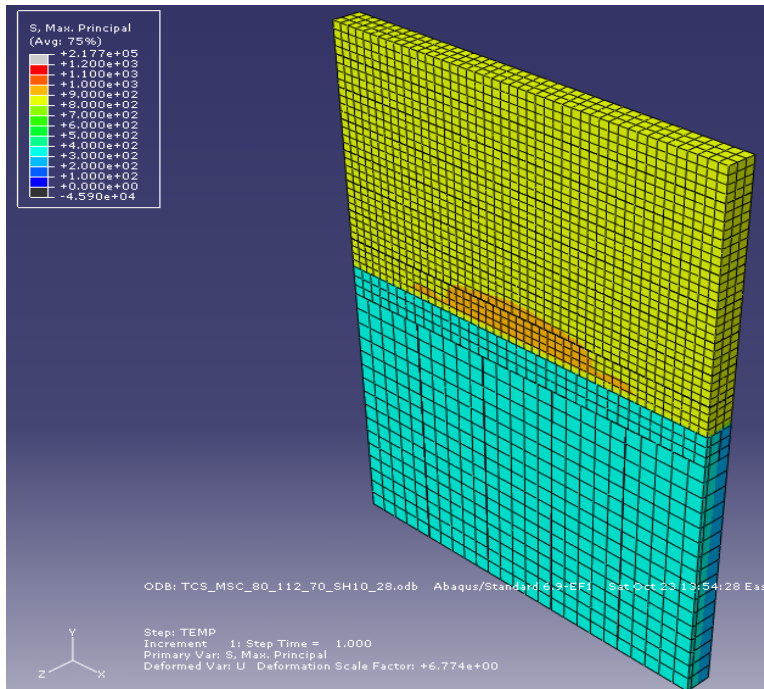


**Figure B387.** 10-ft shoulder transverse cracking model where  $T_M=80^\circ\text{F}$ ,  $T_S=110^\circ\text{F}$ , and  $T_C=70^\circ\text{F}$ , for a CTE of  $7.5 \times 10^{-6}/^\circ\text{F}$  and a stiffness of  $2.8 \times 10^6$  psi.

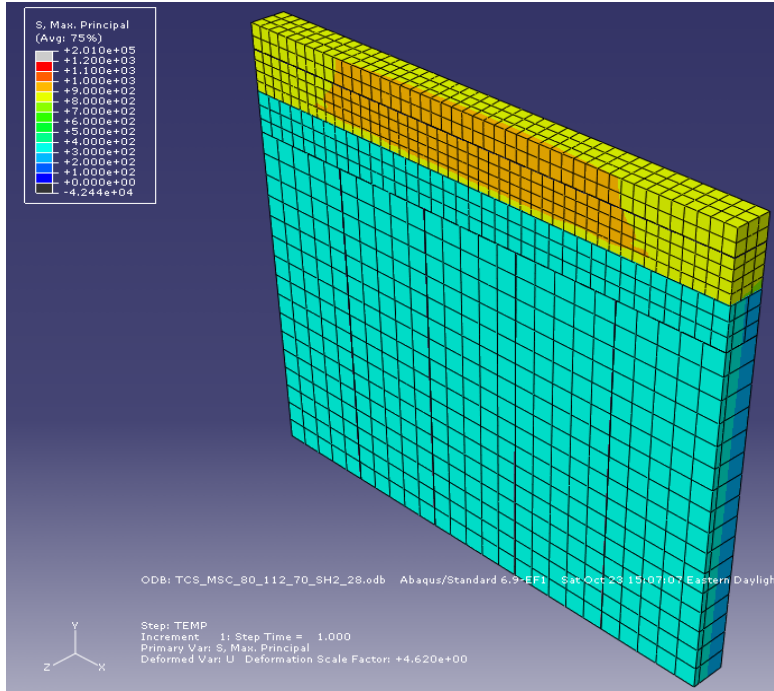


**Figure B388.** 2-ft shoulder transverse cracking model where  $T_M=80^\circ\text{F}$ ,  $T_S=110^\circ\text{F}$ , and  $T_C=70^\circ\text{F}$ , for a CTE of  $7.5 \times 10^{-6}/^\circ\text{F}$  and a stiffness of  $2.8 \times 10^6$  psi.

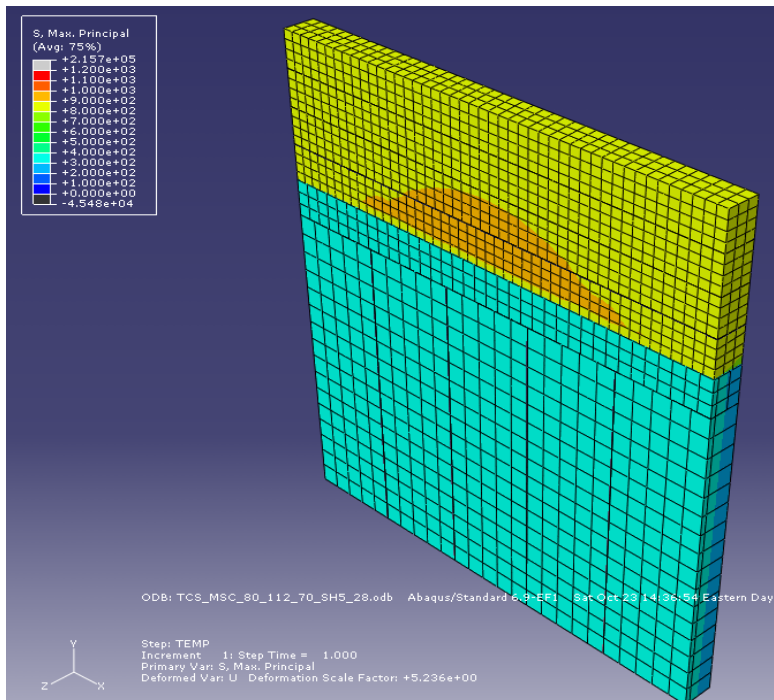


**Figure B389.** 5-ft shoulder transverse cracking model where  $T_M=80^\circ\text{F}$ ,  $T_S=110^\circ\text{F}$ , and  $T_C=70^\circ\text{F}$ , for a CTE of  $7.5 \times 10^{-6}/^\circ\text{F}$  and a stiffness of  $2.8 \times 10^6$  psi.

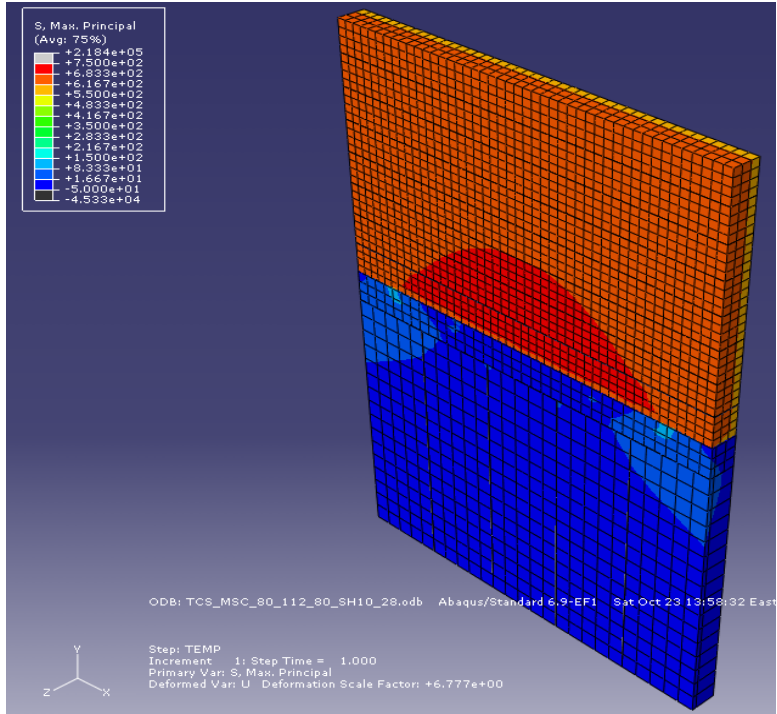


**Figure B390.** 10-ft shoulder transverse cracking model where  $T_M=80^\circ\text{F}$ ,  $T_S=110^\circ\text{F}$ , and  $T_C=80^\circ\text{F}$ , for a CTE of  $7.5 \times 10^{-6}/^\circ\text{F}$  and a stiffness of  $2.8 \times 10^6$  psi.

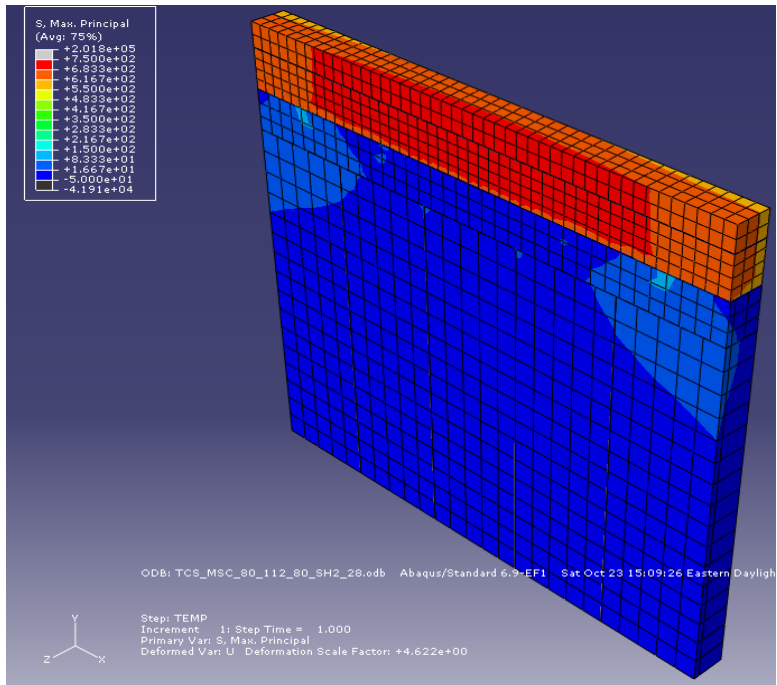


**Figure B391.** 2-ft shoulder transverse cracking model where  $T_M=80^\circ\text{F}$ ,  $T_S=110^\circ\text{F}$ , and  $T_C=80^\circ\text{F}$ , for a CTE of  $7.5 \times 10^{-6}/^\circ\text{F}$  and a stiffness of  $2.8 \times 10^6$  psi.

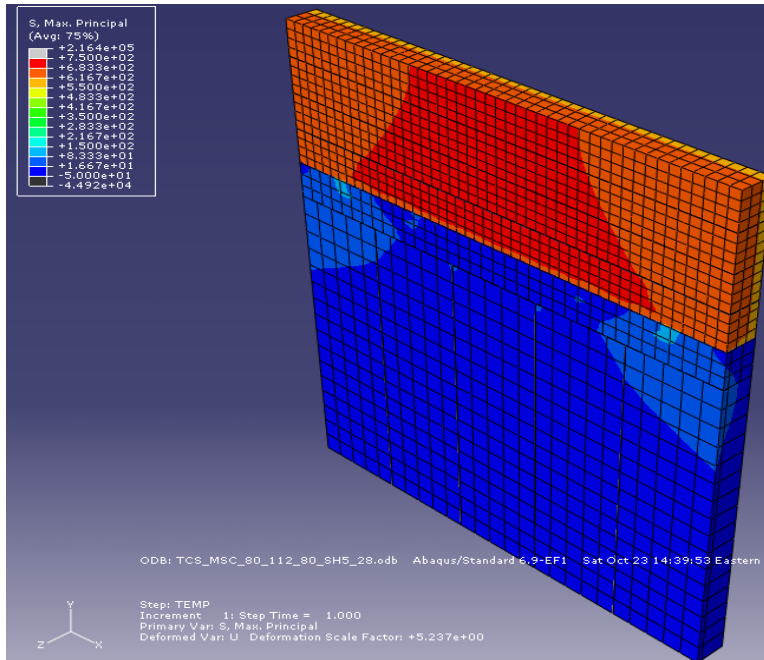


**Figure B392.** 5-ft shoulder transverse cracking model where  $T_M=80^\circ\text{F}$ ,  $T_S=110^\circ\text{F}$ , and  $T_C=80^\circ\text{F}$ , for a CTE of  $7.5 \times 10^{-6}/^\circ\text{F}$  and a stiffness of  $2.8 \times 10^6$  psi.

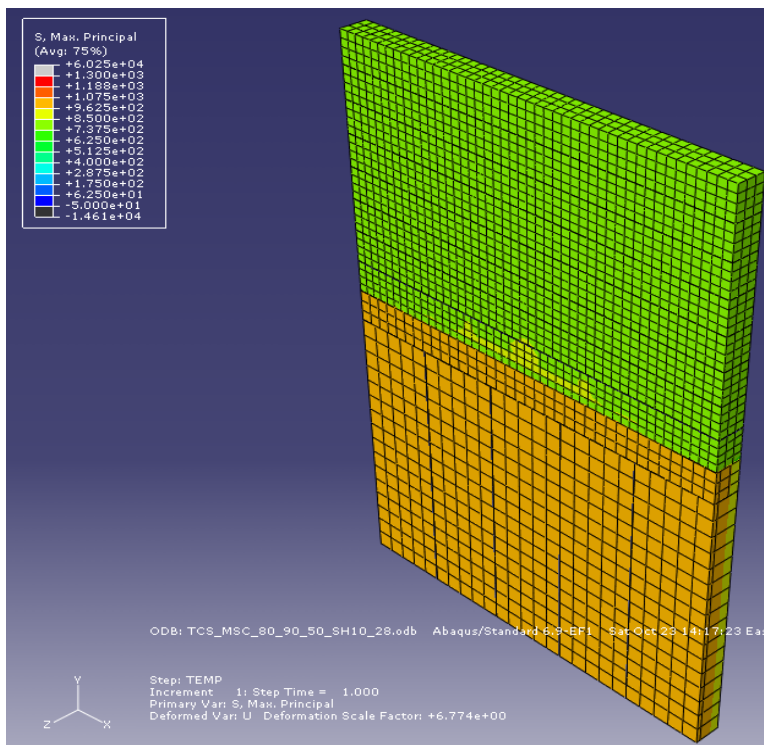


**Figure B393.** 10-ft shoulder transverse cracking model where  $T_M=80^\circ\text{F}$ ,  $T_S=90^\circ\text{F}$ , and  $T_C=50^\circ\text{F}$ , for a CTE of  $7.5 \times 10^{-6}/^\circ\text{F}$  and a stiffness of  $2.8 \times 10^6$  psi.

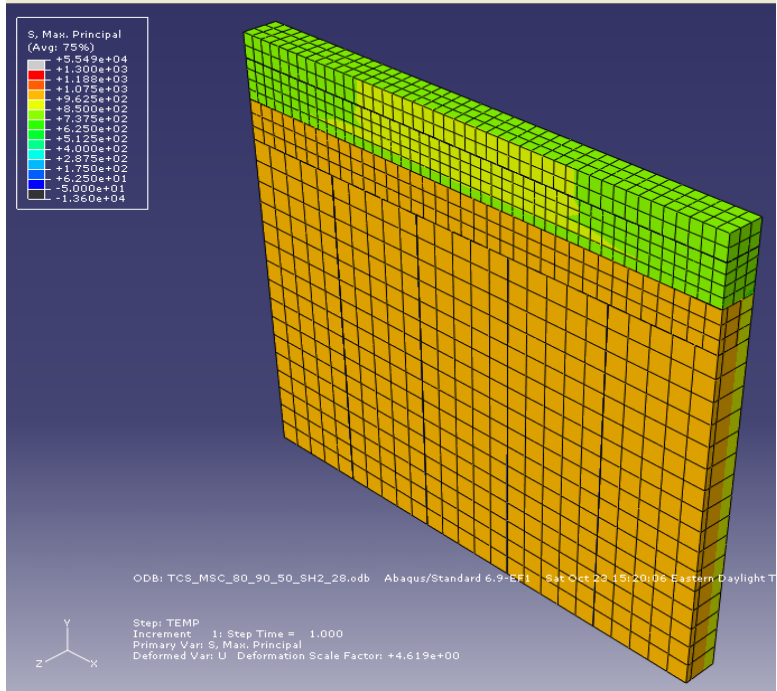


**Figure B394.** 2-ft shoulder transverse cracking model where  $T_M=80^\circ\text{F}$ ,  $T_S=90^\circ\text{F}$ , and  $T_C=50^\circ\text{F}$ , for a CTE of  $7.5 \times 10^{-6}/^\circ\text{F}$  and a stiffness of  $2.8 \times 10^6$  psi.

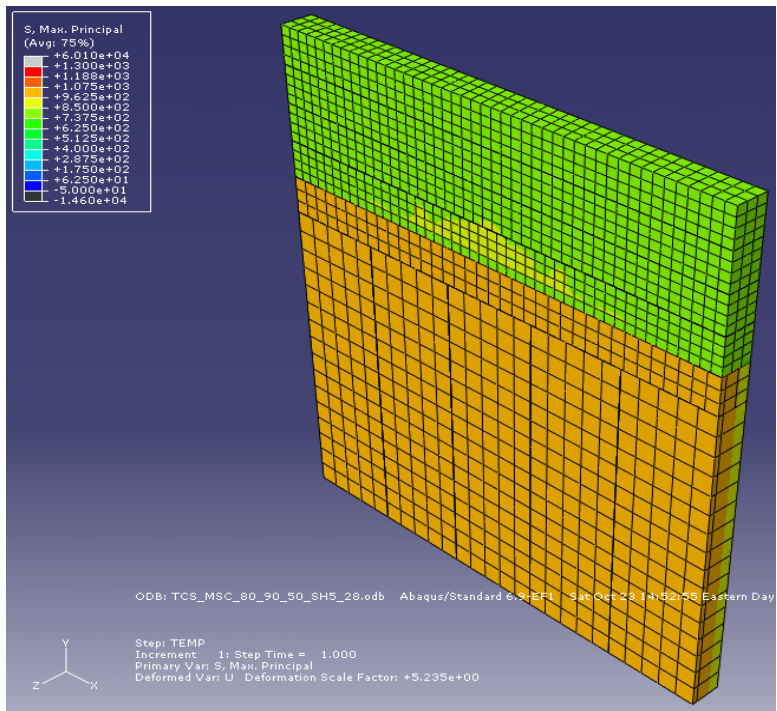


**Figure B395.** 5-ft shoulder transverse cracking model where  $T_M=80^\circ\text{F}$ ,  $T_S=90^\circ\text{F}$ , and  $T_C=50^\circ\text{F}$ , for a CTE of  $7.5 \times 10^{-6}/^\circ\text{F}$  and a stiffness of  $2.8 \times 10^6$  psi.

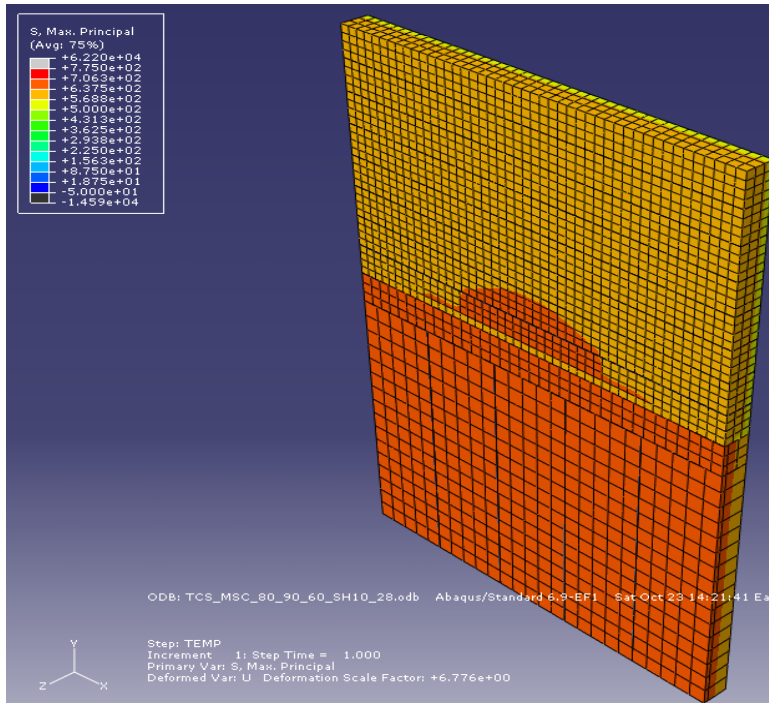


**Figure B396.** 10-ft shoulder transverse cracking model where  $T_M=80^\circ\text{F}$ ,  $T_S=90^\circ\text{F}$ , and  $T_C=60^\circ\text{F}$ , for a CTE of  $7.5 \times 10^{-6}/^\circ\text{F}$  and a stiffness of  $2.8 \times 10^6$  psi.

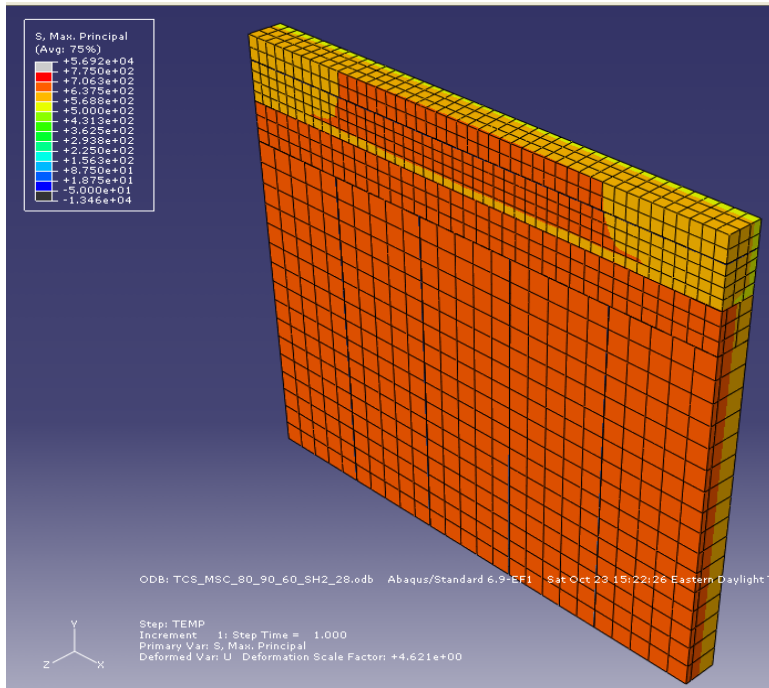


**Figure B397.** 2-ft shoulder transverse cracking model where  $T_M=80^\circ\text{F}$ ,  $T_S=90^\circ\text{F}$ , and  $T_C=60^\circ\text{F}$ , for a CTE of  $7.5 \times 10^{-6}/^\circ\text{F}$  and a stiffness of  $2.8 \times 10^6$  psi.

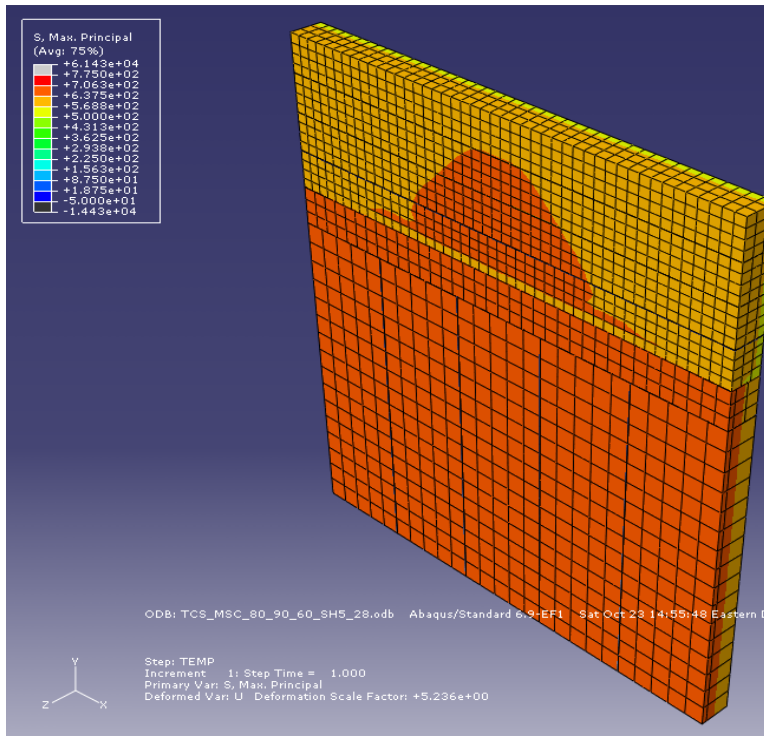


**Figure B398.** 5-ft shoulder transverse cracking model where  $T_M=80^\circ\text{F}$ ,  $T_S=90^\circ\text{F}$ , and  $T_C=60^\circ\text{F}$ , for a CTE of  $7.5 \times 10^{-6}/^\circ\text{F}$  and a stiffness of  $2.8 \times 10^6$  psi.

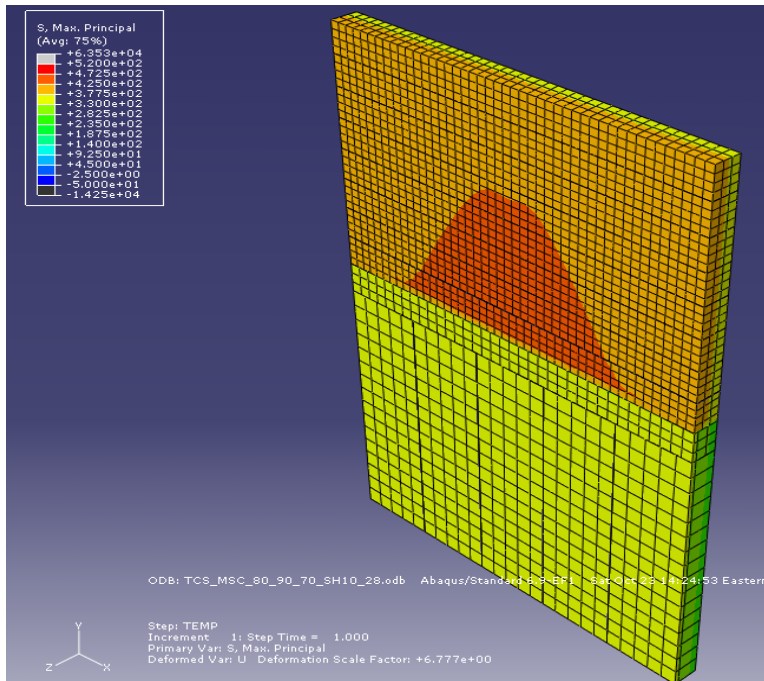


**Figure B399.** 10-ft shoulder transverse cracking model where  $T_M=80^\circ\text{F}$ ,  $T_S=90^\circ\text{F}$ , and  $T_C=70^\circ\text{F}$ , for a CTE of  $7.5 \times 10^{-6}/^\circ\text{F}$  and a stiffness of  $2.8 \times 10^6$  psi.

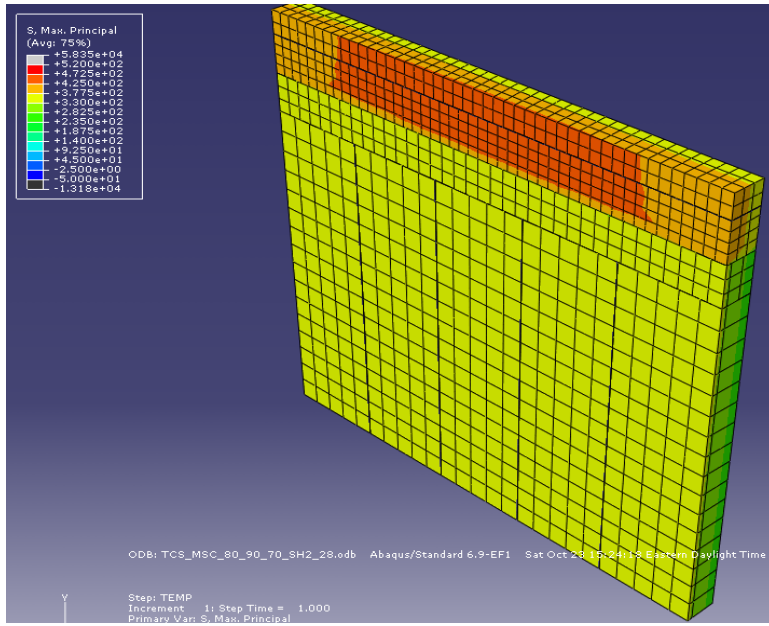


**Figure B400.** 2-ft shoulder transverse cracking model where  $T_M=80^\circ\text{F}$ ,  $T_S=90^\circ\text{F}$ , and  $T_C=70^\circ\text{F}$ , for a CTE of  $7.5 \times 10^{-6}/^\circ\text{F}$  and a stiffness of  $2.8 \times 10^6$  psi.

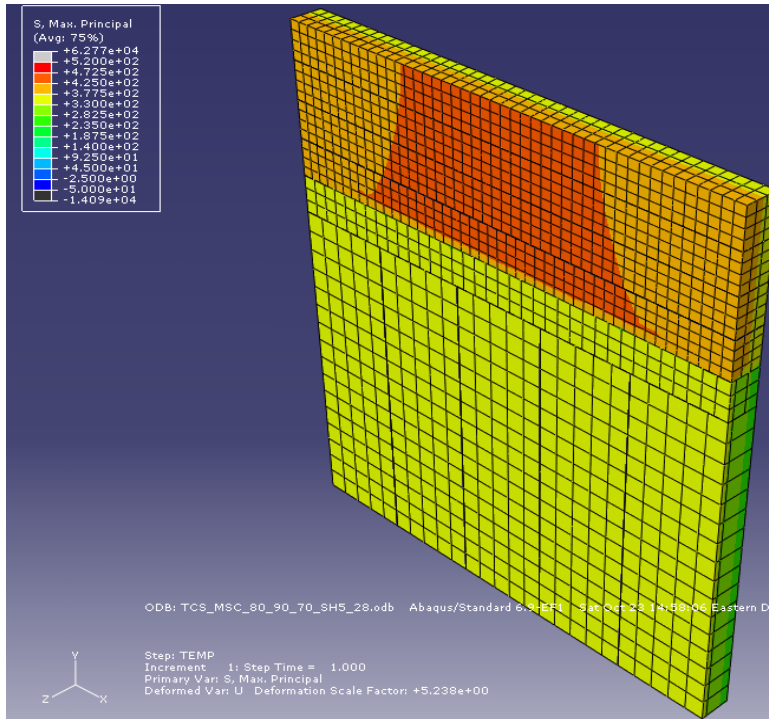


**Figure B401.** 5-ft shoulder transverse cracking model where  $T_M=80^\circ\text{F}$ ,  $T_S=90^\circ\text{F}$ , and  $T_C=70^\circ\text{F}$ , for a CTE of  $7.5 \times 10^{-6}/^\circ\text{F}$  and a stiffness of  $2.8 \times 10^6$  psi.

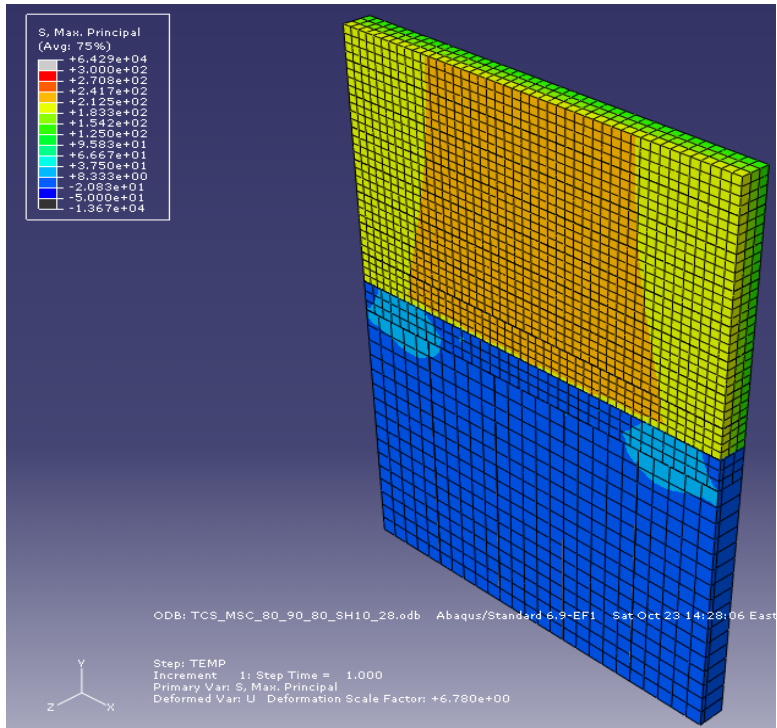


**Figure B402.** 10-ft shoulder transverse cracking model where  $T_M=80^\circ\text{F}$ ,  $T_S=90^\circ\text{F}$ , and  $T_C=80^\circ\text{F}$ , for a CTE of  $7.5 \times 10^{-6}/^\circ\text{F}$  and a stiffness of  $2.8 \times 10^6$  psi.

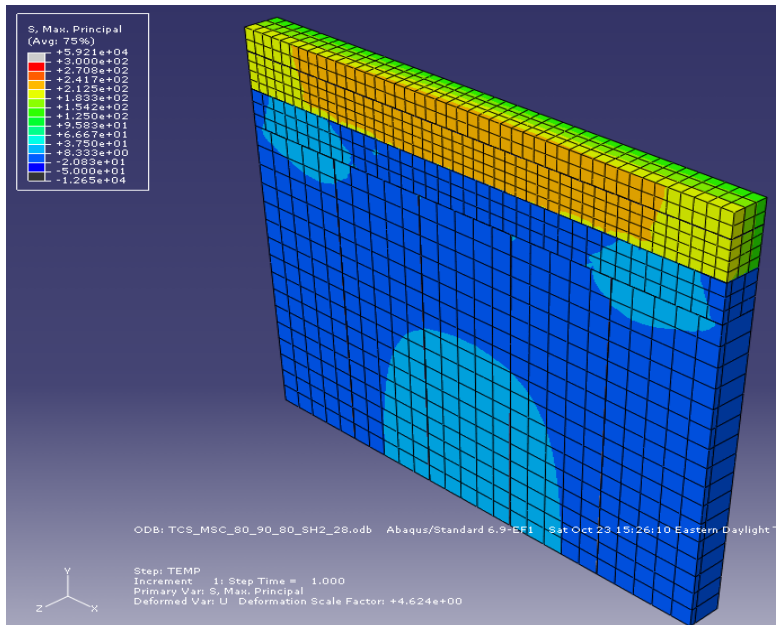


**Figure B403.** 2-ft shoulder transverse cracking model where  $T_M=80^\circ\text{F}$ ,  $T_S=90^\circ\text{F}$ , and  $T_C=80^\circ\text{F}$ , for a CTE of  $7.5 \times 10^{-6}/^\circ\text{F}$  and a stiffness of  $2.8 \times 10^6$  psi.

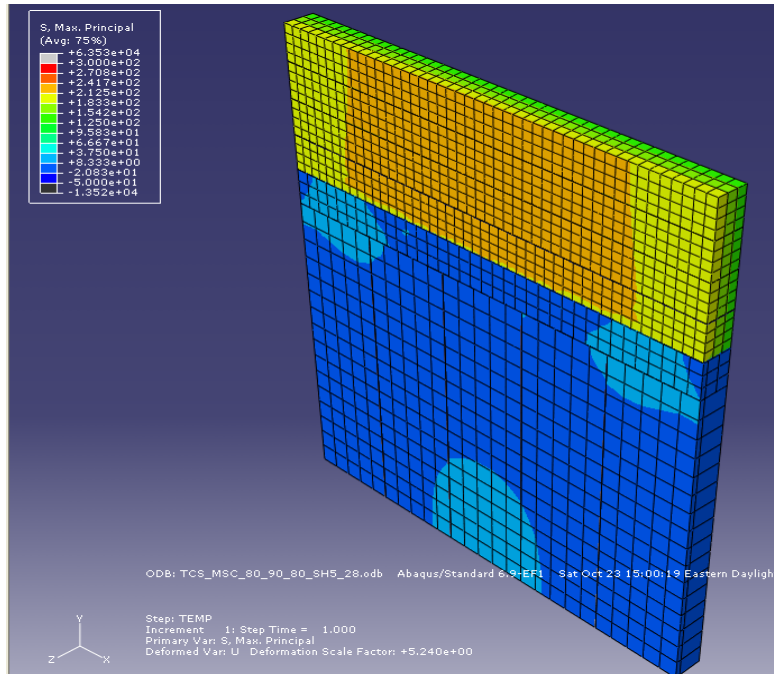


**Figure B404.** 5-ft shoulder transverse cracking model where  $T_M=80^\circ\text{F}$ ,  $T_S=90^\circ\text{F}$ , and  $T_C=80^\circ\text{F}$ , for a CTE of  $7.5 \times 10^{-6}/^\circ\text{F}$  and a stiffness of  $2.8 \times 10^6$  psi.

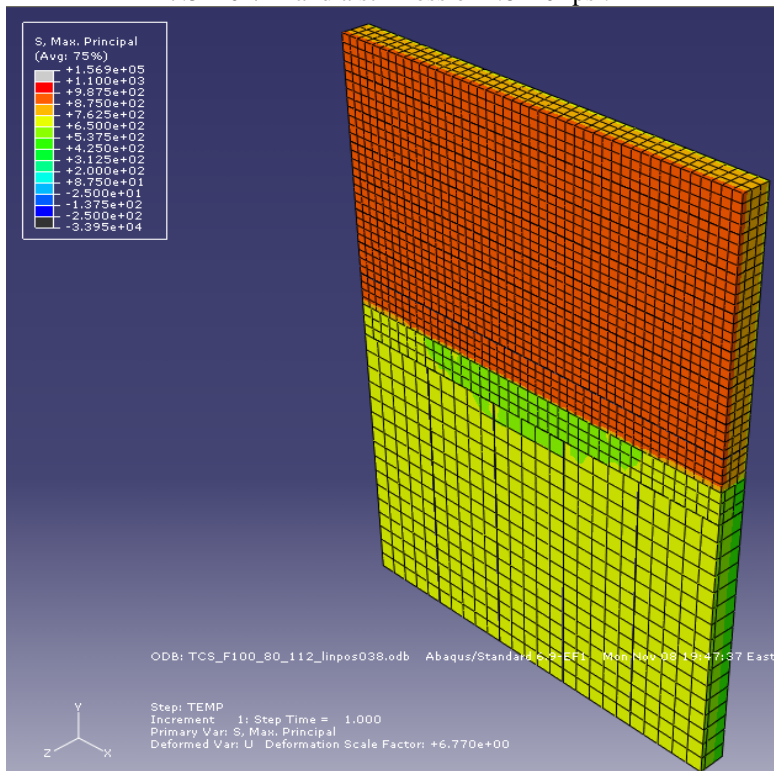


**Figure B405.** 10-ft shoulder transverse cracking model where  $T_M=80^\circ\text{F}$ ,  $T_S=110^\circ\text{F}$ , and  $T_C=-0.38$  linear gradient for a CTE of  $5.5 \times 10^{-6}/^\circ\text{F}$  and a stiffness of  $2.8 \times 10^6$  psi.

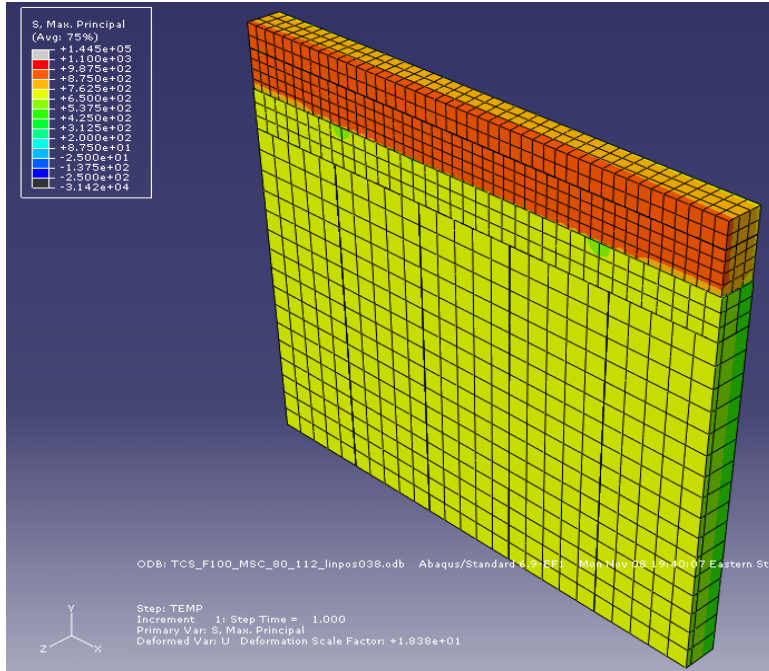


**Figure B406.** 2-ft shoulder transverse cracking model where  $T_M=80^\circ\text{F}$ ,  $T_S=110^\circ\text{F}$ , and  $T_C=-0.38$  linear gradient for a CTE of  $5.5 \times 10^{-6}/^\circ\text{F}$  and a stiffness of  $2.8 \times 10^6$  psi.

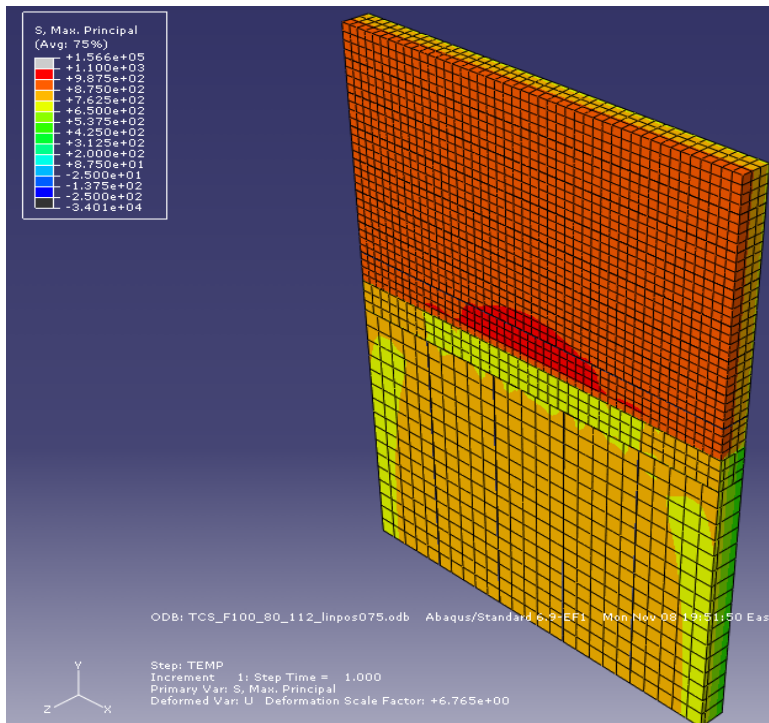


**Figure B407.** 10-ft shoulder transverse cracking model where  $T_M=80^\circ\text{F}$ ,  $T_S=110^\circ\text{F}$ , and  $T_C=-0.75$  linear gradient for a CTE of  $5.5 \times 10^{-6}/^\circ\text{F}$  and a stiffness of  $2.8 \times 10^6$  psi.

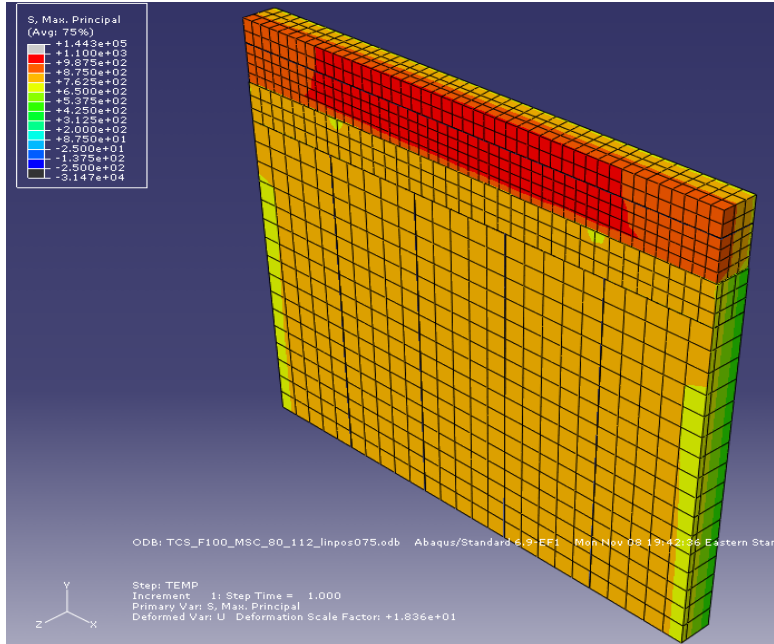


**Figure B408.** 2-ft shoulder transverse cracking model where  $T_M=80^\circ\text{F}$ ,  $T_S=110^\circ\text{F}$ , and  $T_C=-0.75$  linear gradient for a CTE of  $5.5 \times 10^{-6}/^\circ\text{F}$  and a stiffness of  $2.8 \times 10^6$  psi.

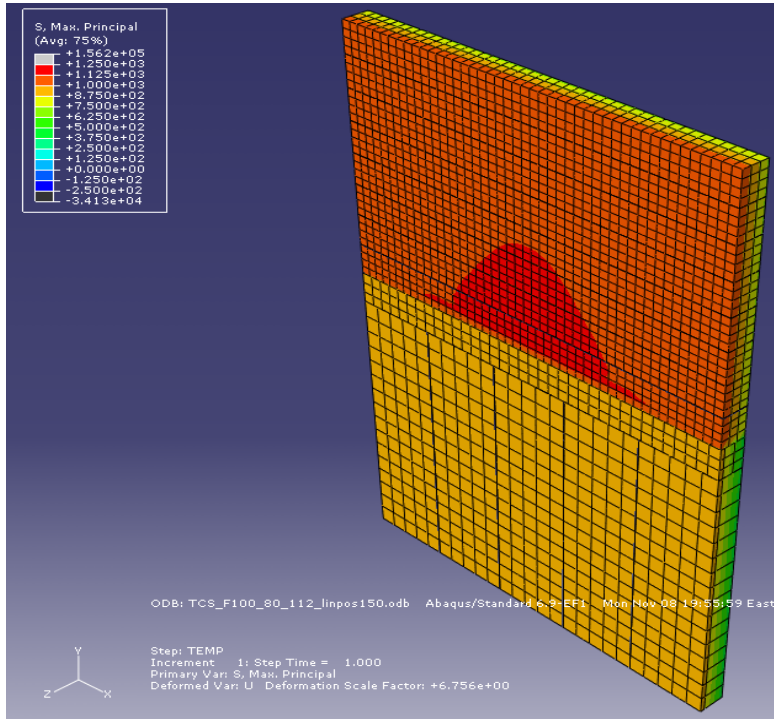


**Figure B409.** 10-ft shoulder transverse cracking model where  $T_M=80^\circ\text{F}$ ,  $T_S=110^\circ\text{F}$ , and  $T_C=-1.5$  linear gradient for a CTE of  $5.5 \times 10^{-6}/^\circ\text{F}$  and a stiffness of  $2.8 \times 10^6$  psi.

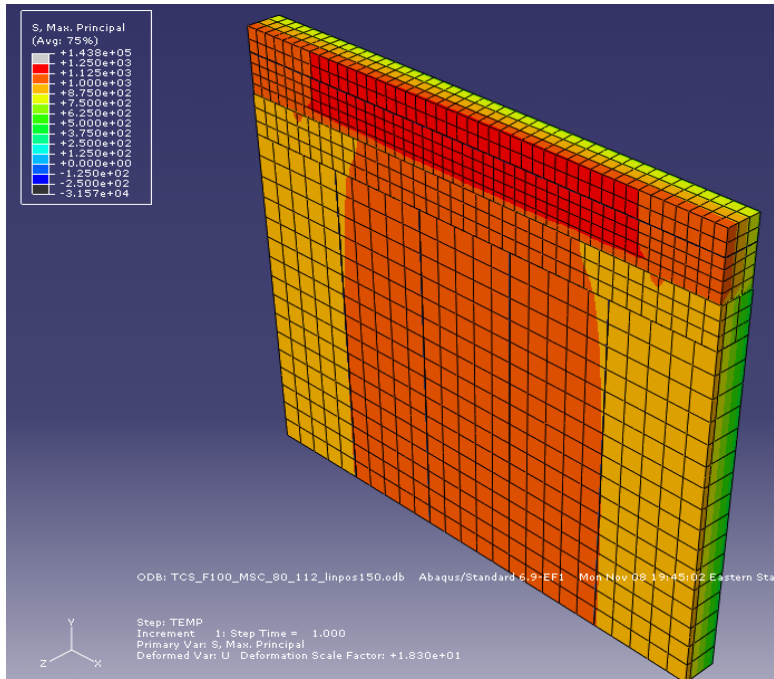


**Figure B410.** 2-ft shoulder transverse cracking model where  $T_M=80^\circ\text{F}$ ,  $T_S=110^\circ\text{F}$ , and  $T_C=-1.5$  linear gradient for a CTE of  $5.5 \times 10^{-6}/^\circ\text{F}$  and a stiffness of  $2.8 \times 10^6$  psi.

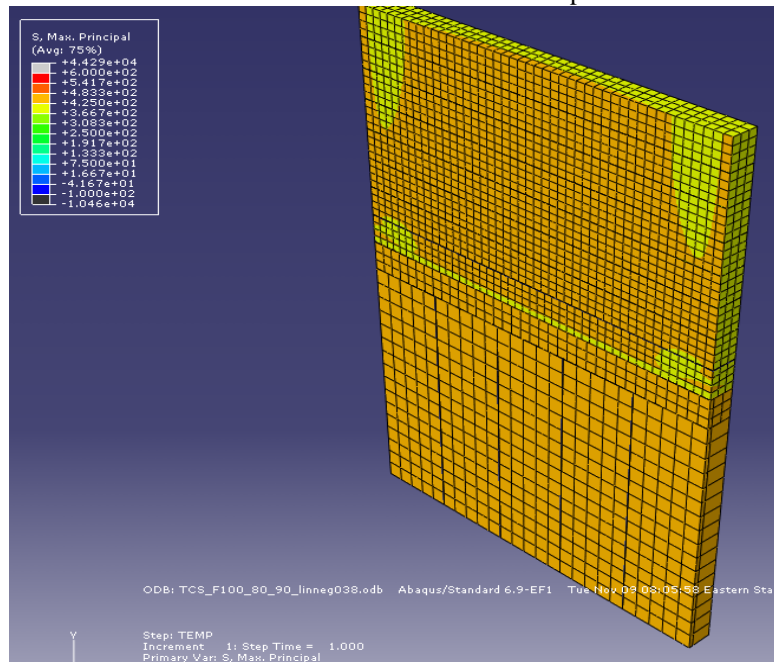


**Figure B411.** 10-ft shoulder transverse cracking model where  $T_M=80^\circ\text{F}$ ,  $T_S=90^\circ\text{F}$ , and  $T_C=+0.38$  linear gradient for a CTE of  $5.5 \times 10^{-6}/^\circ\text{F}$  and a stiffness of  $2.8 \times 10^6$  psi.

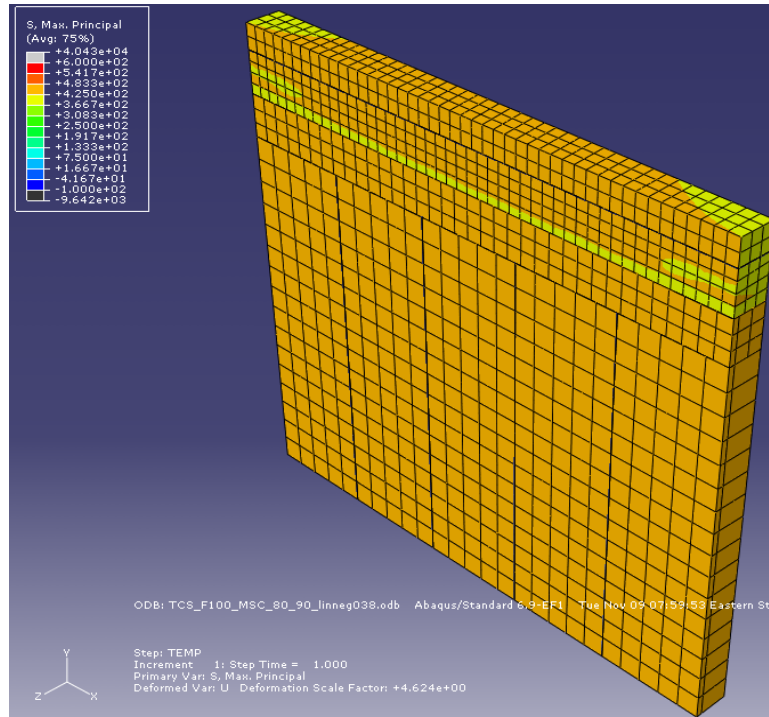


**Figure B412.** 2-ft shoulder transverse cracking model where  $T_M=80^\circ\text{F}$ ,  $T_S=90^\circ\text{F}$ , and  $T_C=+0.38$  linear gradient for a CTE of  $5.5 \times 10^{-6}/^\circ\text{F}$  and a stiffness of  $2.8 \times 10^6$  psi.

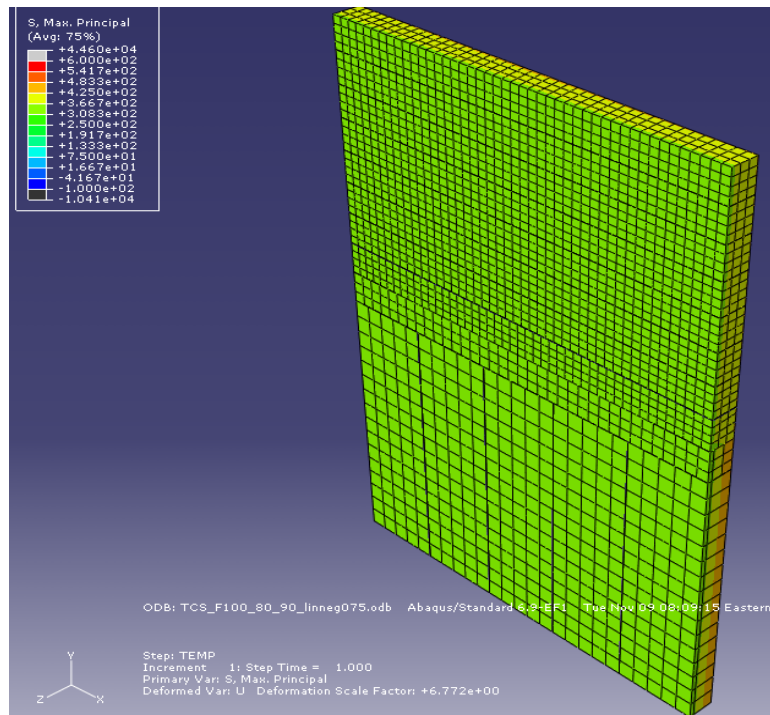


**Figure B413.** 10-ft shoulder transverse cracking model where  $T_M=80^\circ\text{F}$ ,  $T_S=90^\circ\text{F}$ , and  $T_C=+0.75$  linear gradient for a CTE of  $5.5 \times 10^{-6}/^\circ\text{F}$  and a stiffness of  $2.8 \times 10^6$  psi.

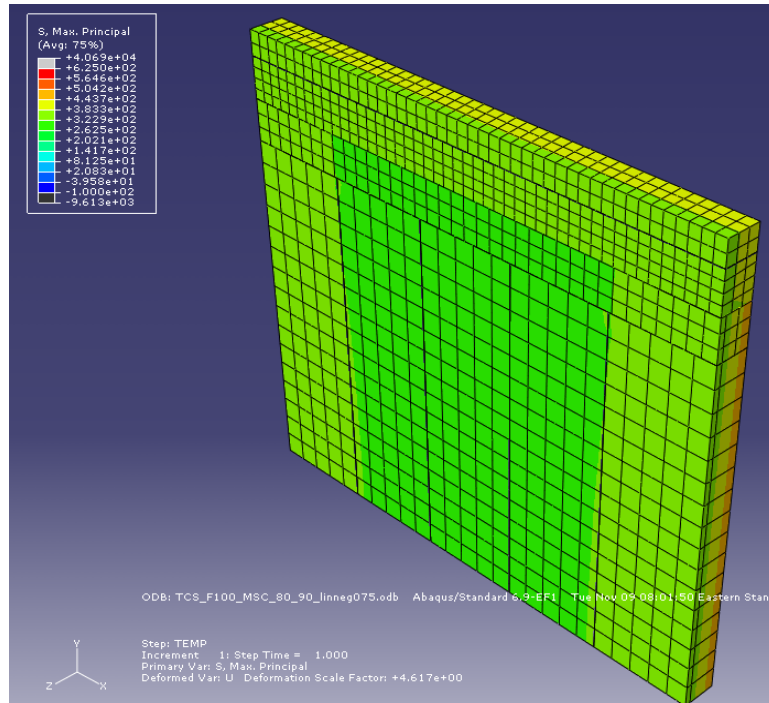


**Figure B414.** 2-ft shoulder transverse cracking model where  $T_M=80^\circ\text{F}$ ,  $T_S=90^\circ\text{F}$ , and  $T_C=+0.75$  linear gradient for a CTE of  $5.5 \times 10^{-6}/^\circ\text{F}$  and a stiffness of  $2.8 \times 10^6$  psi.

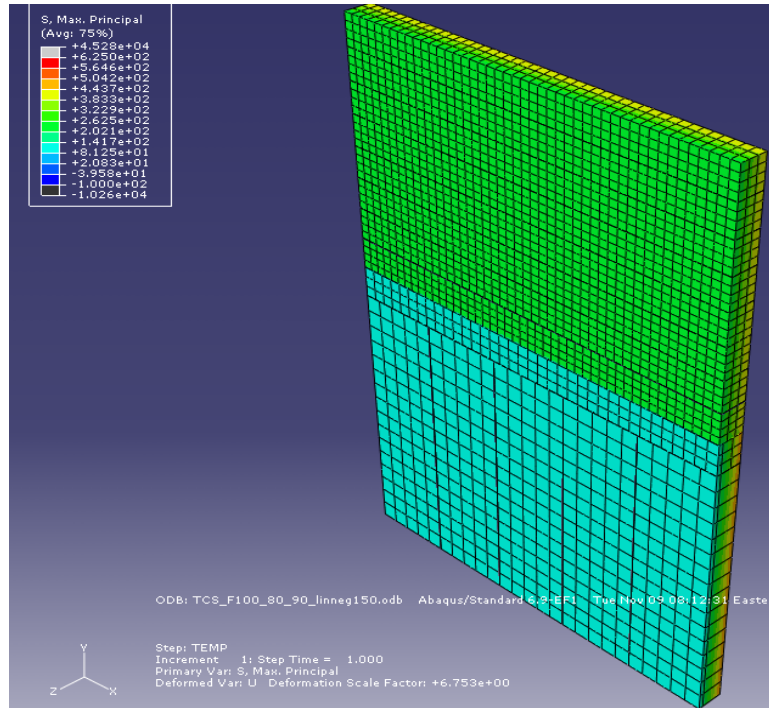


**Figure B415.** 10-ft shoulder transverse cracking model where  $T_M=80^\circ\text{F}$ ,  $T_S=90^\circ\text{F}$ , and  $T_C=+1.5$  linear gradient for a CTE of  $5.5 \times 10^{-6}/^\circ\text{F}$  and a stiffness of  $2.8 \times 10^6$  psi.

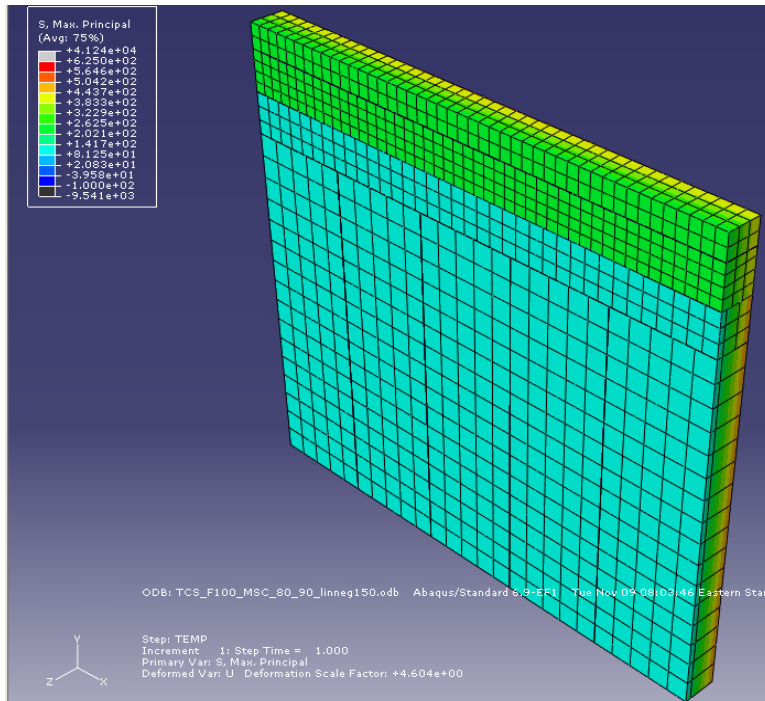


**Figure B416.** 2-ft shoulder transverse cracking model where  $T_M=80^\circ\text{F}$ ,  $T_S=90^\circ\text{F}$ , and  $T_C=+1.5$  linear gradient for a CTE of  $5.5 \times 10^{-6}/^\circ\text{F}$  and a stiffness of  $2.8 \times 10^6$  psi.

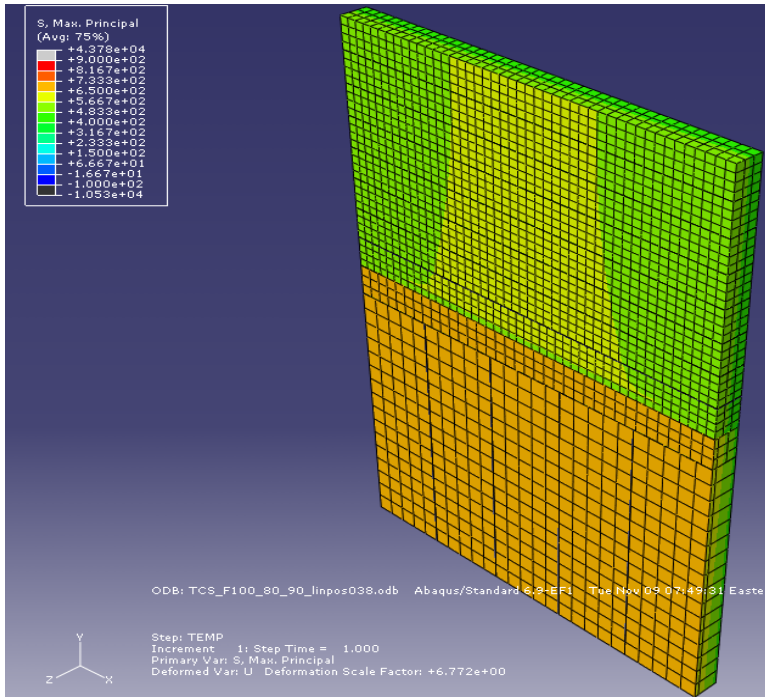


**Figure B417.** 10-ft shoulder transverse cracking model where  $T_M=80^\circ\text{F}$ ,  $T_S=90^\circ\text{F}$ , and  $T_C=-0.38$  linear gradient for a CTE of  $5.5 \times 10^{-6}/^\circ\text{F}$  and a stiffness of  $2.8 \times 10^6$  psi.

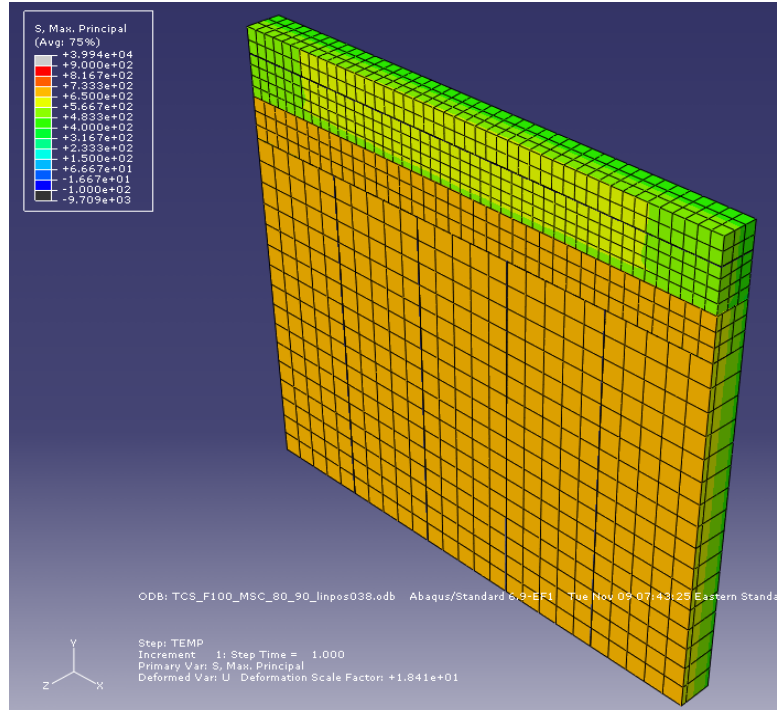


**Figure B418.** 2-ft shoulder transverse cracking model where  $T_M=80^\circ\text{F}$ ,  $T_S=90^\circ\text{F}$ , and  $T_C=-0.38$  linear gradient for a CTE of  $5.5 \times 10^{-6}/^\circ\text{F}$  and a stiffness of  $2.8 \times 10^6$  psi.

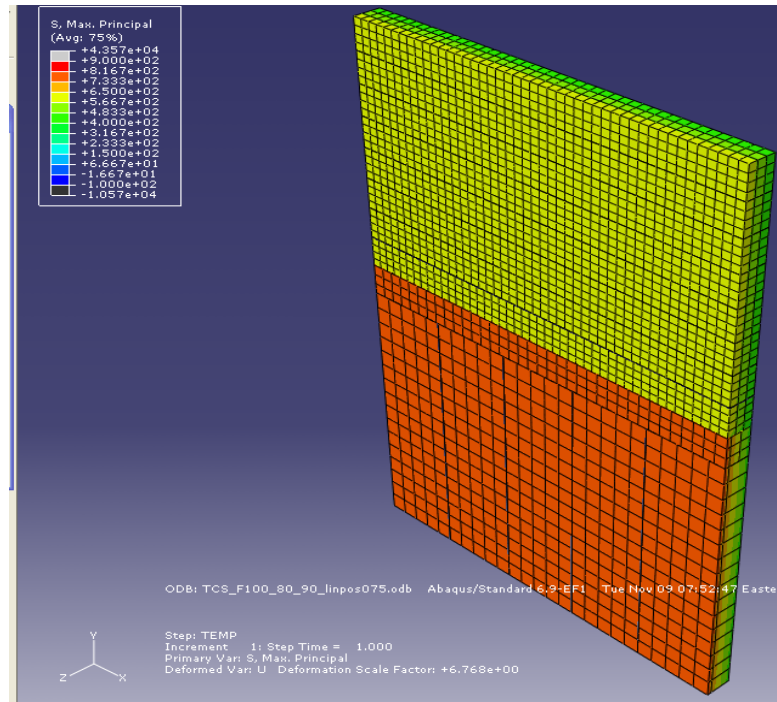


**Figure B419.** 10-ft shoulder transverse cracking model where  $T_M=80^\circ\text{F}$ ,  $T_S=90^\circ\text{F}$ , and  $T_C=-0.75$  linear gradient for a CTE of  $5.5 \times 10^{-6}/^\circ\text{F}$  and a stiffness of  $2.8 \times 10^6$  psi.

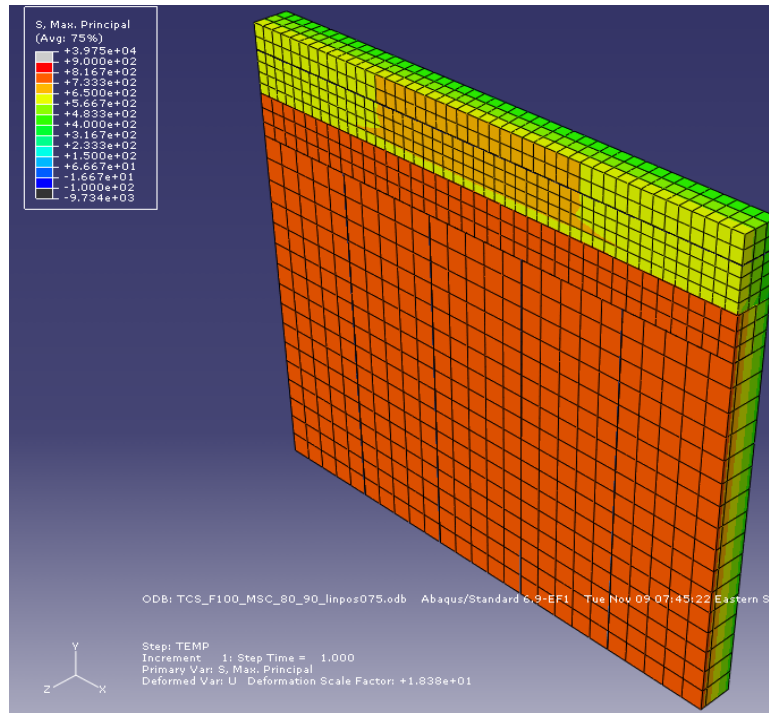


**Figure B420.** 2-ft shoulder transverse cracking model where  $T_M=80^\circ\text{F}$ ,  $T_S=90^\circ\text{F}$ , and  $T_C=-0.75$  linear gradient for a CTE of  $5.5 \times 10^{-6}/^\circ\text{F}$  and a stiffness of  $2.8 \times 10^6$  psi.

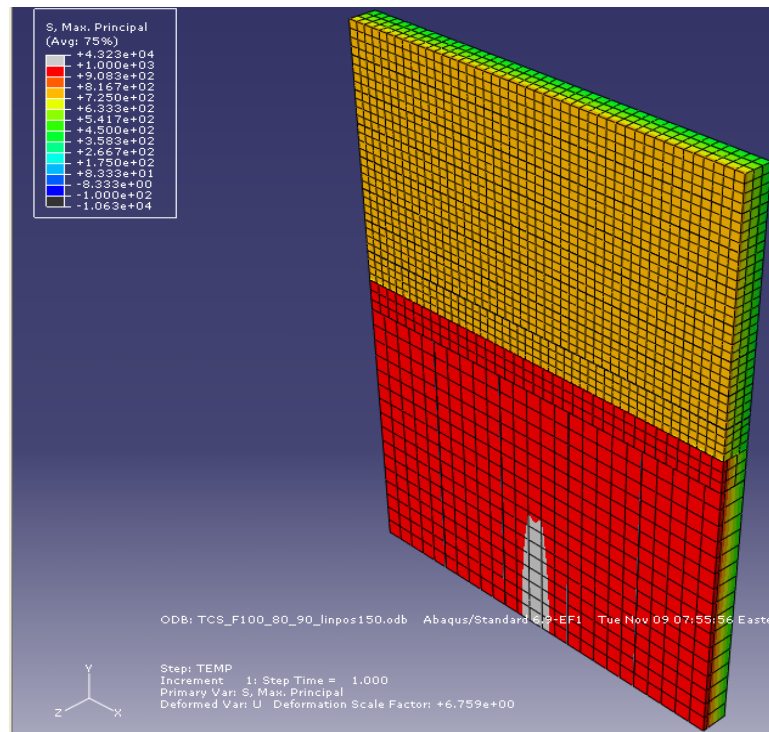


**Figure B421.** 10-ft shoulder transverse cracking model where  $T_M=80^\circ\text{F}$ ,  $T_S=90^\circ\text{F}$ , and  $T_C=-1.5$  linear gradient for a CTE of  $5.5 \times 10^{-6}/^\circ\text{F}$  and a stiffness of  $2.8 \times 10^6$  psi.

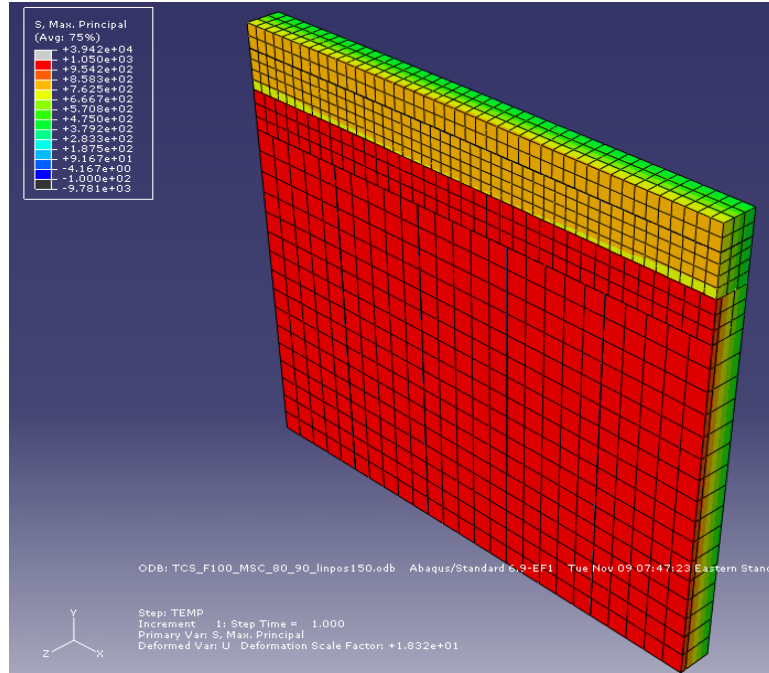


**Figure B422.** 2-ft shoulder transverse cracking model where  $T_M=80^\circ\text{F}$ ,  $T_S=90^\circ\text{F}$ , and  $T_C=-1.5$  linear gradient for a CTE of  $5.5 \times 10^{-6}/^\circ\text{F}$  and a stiffness of  $2.8 \times 10^6$  psi.

## APPENDIX C

### SAMPLE INPUT FILE FOR LONGITUDINAL SHEAR CRACKING MODEL

```
*Heading
** Job name: PRELIM_MSC_90_70_120 Model name: Model-1
** Generated by: Abaqus/CAE 6.9-EF1
**Preprint, echo=NO, model=NO, history=NO, contact=NO
**
** PARTS
**
*Part, name=DOWEL
*End Part
**
*Part, name=ISI
*End Part
**
*Part, name=ISIT
*End Part
**
*Part, name=ISO
*End Part
**
*Part, name=MI
*End Part
**
*Part, name=MIT
*End Part
**
*Part, name=MO
*End Part
**
*Part, name=MON
*End Part
```

```

**
*Part, name=OSI
*End Part
**
*Part, name=OSIT
*End Part
**
*Part, name=OSO
*End Part
**
*Part, name=TIEBAR
*End Part
**
**
** ASSEMBLY
**
*Assembly, name=Assembly
**
*Instance, name=TIEBAR-1, part=TIEBAR
    15.,    239.,    6.
    15.,    239.,    6.,    16.,    239.,    6.,    90.
*Node
    1, -0.220970869, 0.220970869,    0.
    2,  -0.3125,    0.,    0.
    3, -0.220970869, -0.220970869,    0.
    4,    0., -0.3125,    0.
    5, 0.220970869, -0.220970869,    0.
***
***
***
***
    467, -0.119588576, 0.288712353,    30.
    468,    0.,    0.3125,    29.
    469, 0.119588576, -0.288712353,    30.
    470, -0.119588576, -0.288712353,    30.
    471,    0., -0.3125,    29.
*Element, type=C3D20R
    1, 11, 10, 18, 12, 2, 1, 9, 3, 148, 147, 146, 145, 149, 150, 151,
    152, 154, 153, 155, 156
    2, 18, 16, 15, 14, 9, 7, 6, 5, 160, 159, 158, 157, 161, 162, 163,
    164, 155, 165, 166, 167
    3, 18, 10, 17, 16, 9, 1, 8, 7, 147, 169, 168, 160, 150, 170, 171,
    161, 155, 153, 172, 165
***
***
***

```

```

59, 144, 136, 143, 142, 135, 127, 134, 133, 453, 467, 466, 462, 432, 446, 445,
  441, 457, 455, 468, 463
60, 139, 138, 144, 140, 130, 129, 135, 131, 470, 452, 459, 469, 449, 431, 438,
  448, 471, 458, 457, 465
*Nset, nset=_PickedSet2, internal, generate
  1, 471, 1
*Elset, elset=_PickedSet2, internal, generate
  1, 60, 1
** Section: TIEBAR
*Solid Section, elset=_PickedSet2, material=STEEL
,
*End Instance
*Instance, name=ISIT-1, part=ISIT
  360., 200., 0.
*Node
  1, 30., 9., 12.
  2, 0., 9., 12.
  3, 0., 9., 0.
  4, 30., 9., 0.
  5, 15., 9., 5.6875
***
***
***
  347, 14.84375, 0., 6.15625
  348, 17.8660603, 0., 1.03309202
  349, 11.3564806, 0., 1.05157506
  350, 15., 0., 0.
  351, 5., 0., 12.
*Element, type=C3D20R
1, 47, 45, 19, 41, 98, 96, 68, 92, 104, 103, 102, 101, 105, 106, 107,
  108, 110, 109, 111, 112
2, 2, 47, 17, 3, 22, 98, 64, 23, 116, 115, 114, 113, 117, 118, 119,
  120, 121, 110, 122, 123
***
***
***
57, 40, 49, 18, 43, 78, 87, 36, 81, 165, 206, 175, 159, 324, 348, 330,
  321, 323, 328, 332, 309
58, 5, 21, 20, 19, 71, 74, 73, 72, 157, 198, 203, 200, 319, 344, 347,
  345, 322, 310, 340, 289
*Nset, nset=_PickedSet3, internal, generate
  1, 351, 1
*Elset, elset=_PickedSet3, internal, generate
  1, 58, 1
** Section: SH2PCC
*Solid Section, elset=_PickedSet3, material=SH2PCC

```

```

,
*End Instance
**
*Instance, name=ISI-1, part=ISI
    330.,    200.,    0.
*Node
    1,    30.,    24.,    12.
    2,    30.,    16.,    12.
    3,    30.,    8.,    12.
    4,    30.,    0.,    12.
    5,    30.,    24.,    0.
***
***
***
    93,    0.,    0.,    6.
    94,    0.,    4.,    12.
    95,    5.,    0.,    12.
    96,    5.,    0.,    0.
*Element, type=C3D20R
1, 9, 10, 14, 13, 1, 2, 6, 5, 36, 35, 34, 33, 37, 38, 39,
  40, 42, 41, 43, 44
2, 10, 11, 15, 14, 2, 3, 7, 6, 47, 46, 45, 35, 48, 49, 50,
  38, 41, 51, 52, 43
***
***
***
9, 27, 28, 32, 31, 19, 20, 24, 23, 94, 93, 92, 88, 76, 75, 74,
  70, 90, 95, 96, 91
*Nset, nset=_PickedSet2, internal, generate
  1, 96, 1
*Elset, elset=_PickedSet2, internal, generate
  1, 9, 1
** Section: SH2PCC
*Solid Section, elset=_PickedSet2, material=SH2PCC
,
*End Instance
**
*Instance, name=ISO-1, part=ISO
    -15.,    200.,    0.
*Node
    1,    15.,    24.,    12.
    2,    15.,    16.,    12.
    3,    15.,    8.,    12.
    4,    15.,    0.,    12.
    5,    15.,    24.,    0.
***

```

```

***
***
  67,    0.,    0.,    6.
  68,    0.,    4.,   12.
  69,   3.75,    0.,   12.
  70,   3.75,    0.,    0.
*Element, type=C3D20R
1, 9, 10, 14, 13, 1, 2, 6, 5, 28, 27, 26, 25, 29, 30, 31,
 32, 34, 33, 35, 36
2, 10, 11, 15, 14, 2, 3, 7, 6, 39, 38, 37, 27, 40, 41, 42,
 30, 33, 43, 44, 35
***
***
***
6, 19, 20, 24, 23, 11, 12, 16, 15, 68, 67, 66, 62, 47, 46, 45,
 38, 64, 69, 70, 65
*Nset, nset=_PickedSet2, internal, generate
 1, 70, 1
*Elset, elset=_PickedSet2, internal, generate
 1, 6, 1
** Section: SH2PCC
*Solid Section, elset=_PickedSet2, material=SH2PCC
,
*End Instance
*Instance, name=MIT-1, part=MIT
  0.,    224.,    0.
*Node
  1,    30.,    15.,    12.
  2,     0.,    15.,    12.
  3,     0.,    15.,     0.
  4,    30.,    15.,     0.
  5,    15.,    15.,   6.3125
***
***
***
 3143, 14.3086834,    187.,  5.68254471
 3144, 14.84375,    187.,  6.15625
 3145, 14.6875, 191.300003,     6.
 3146, 14.84375,    187.,  5.84375
 3147, 17.3233566,    187.,  3.34872413
*Element, type=C3D20R
1, 1, 29, 184, 183, 36, 203, 405, 404, 853, 852, 851, 850, 854, 855, 856,
 857, 859, 858, 860, 861
2, 183, 32, 4, 1, 404, 202, 37, 36, 864, 863, 862, 850, 865, 866, 867,
 857, 861, 868, 869, 859
***

```

```

***
***
***
633, 849, 848, 839, 838, 291, 290, 281, 280, 3067, 3080, 3074, 3006, 3135, 3147,
3141,
    3081, 3086, 3136, 3100, 3085
634, 831, 834, 833, 832, 273, 276, 275, 274, 3070, 3060, 3077, 3079, 3137, 3129,
3144,
    3146, 3139, 3131, 3122, 3145
*Nset, nset=_PickedSet4, internal, generate
    1, 3147, 1
*Elset, elset=_PickedSet4, internal, generate
    1, 634, 1
** Section: MLPCC
*Solid Section, elset=_PickedSet4, material=MLPCC
,
*End Instance
*Instance, name=MI-1, part=MI
    150., 224., 0.
*Node
    1, 30., 288., 12.
    2, 30., 279., 12.
    3, 30., 270., 12.
    4, 30., 261., 12.
    5, 30., 252., 12.
***
    845, 5., 9., 0.
    846, 0., 4.5, 0.
    847, 0., 0., 6.
    848, 0., 4.5, 12.
    849, 5., 0., 12.
    850, 5., 0., 0.
*Element, type=C3D20R
    1, 67, 68, 101, 100, 1, 2, 35, 34, 268, 267, 266, 265, 269, 270, 271,
    272, 274, 273, 275, 276
    2, 68, 69, 102, 101, 2, 3, 36, 35, 279, 278, 277, 267, 280, 281, 282,
    270, 273, 283, 284, 275
***
***
***
***
95, 229, 230, 263, 262, 163, 164, 197, 196, 843, 842, 841, 837, 680, 679, 678,
    674, 839, 844, 845, 840
96, 230, 231, 264, 263, 164, 165, 198, 197, 848, 847, 846, 842, 685, 684, 683,
    679, 844, 849, 850, 845
*Nset, nset=_PickedSet2, internal, generate

```

```

1, 850, 1
*Elset, elset=_PickedSet2, internal, generate
1, 96, 1
** Section: MLPCC
*Solid Section, elset=_PickedSet2, material=MLPCC
,
*End Instance
**
*Instance, name=MO-1, part=MO
-15., 224., 0.
*Node
1, 15., 288., 12.
2, 15., 279., 12.
3, 15., 270., 12.
4, 15., 261., 12.
5, 15., 252., 12.
***
***
***
617, 0., 4.5, 0.
618, 0., 0., 6.
619, 0., 4.5, 12.
620, 3.75, 0., 12.
621, 3.75, 0., 0.
*Element, type=C3D20R
1, 67, 68, 101, 100, 1, 2, 35, 34, 202, 201, 200, 199, 203, 204, 205,
206, 208, 207, 209, 210
2, 68, 69, 102, 101, 2, 3, 36, 35, 213, 212, 211, 201, 214, 215, 216,
204, 207, 217, 218, 209
***
***
***
***
63, 163, 164, 197, 196, 97, 98, 131, 130, 614, 613, 612, 608, 445, 444, 443,
436, 610, 615, 616, 611
64, 164, 165, 198, 197, 98, 99, 132, 131, 619, 618, 617, 613, 453, 452, 451,
444, 615, 620, 621, 616
*Nset, nset=_PickedSet2, internal, generate
1, 621, 1
*Elset, elset=_PickedSet2, internal, generate
1, 64, 1
** Section: MLPCC
*Solid Section, elset=_PickedSet2, material=MLPCC
,
*End Instance
**

```

```

*Instance, name=MON-1, part=MON
  510.,    224.,    0.
*Node
  1,    15., 284.503723,    0.
  2,    6., 284.503723,    0.
  3,    6.,    288.,    0.
  4,   15.,    288.,    0.
  5,    6., 284.503723,   12.
45724,    0., 282.375,    6.
45725,    0.,    282.,   6.375
45726,    1.,    282.,    6.
45727,    0., 281.625,    6.
45728,    0.,    282.,   5.625
*Element, type=C3D20R
  1,  70, 1117, 6132, 1107,  1,  41, 1099,  50, 12133, 12132, 12131, 12130, 12134,
12135, 12136,
    12137, 12139, 12138, 12140, 12141
  2, 1117, 1118, 6133, 6132,  41,  42, 1100, 1099, 12144, 12143, 12142, 12132,
12145, 12146, 12147,
    12135, 12138, 12148, 12149, 12140
***
***
***
  9471, 11147, 11146, 11145, 12129, 4553, 4552, 4551, 5535, 41823, 41821, 41828,
41824, 45723, 45721, 45728,
    45724, 45670, 45722, 45712, 45726
  9472, 11143, 11142, 11086, 12129, 4549, 4548, 4492, 5535, 41813, 41776, 41825,
41827, 45713, 45676, 45725,
    45727, 45699, 45679, 45674, 45726
*Nset, nset=_PickedSet4, internal, generate
  1, 45728,  1
*Elset, elset=_PickedSet4, internal, generate
  1, 9472,  1
** Section: MLPCC
*Solid Section, elset=_PickedSet4, material=MLPCC
,
*End Instance
**
*Instance, name=OSIT-1, part=OSIT
  0.,    632., 11.999999999999999
  0.,    632., 11.999999999999999,    1.,    632., 11.999999999999999,
180.
*Node
  1,    0.,    105.,    12.
  2,   30.,    105.,    12.
  3,   30.,    105.,    0.

```

```

    4,    0.,    105.,    0.
    5,    15.,    105.,    5.6875
***
***
***
    1440,    5.,    0.,    12.
    1441, 16.7815399,    0., 9.48902512
    1442,    15.,    0.,    12.
    1443, 10.7120934,    0., 5.54735947
    1444, 11.8120995,    0., 3.74888229
*Element, type=C3D20R
1, 17, 87, 21, 83, 109, 185, 116, 181, 394, 393, 392, 391, 395, 396, 397,
  398, 400, 399, 401, 402
2, 3, 17, 83, 2, 24, 109, 181, 25, 405, 391, 404, 403, 406, 398, 407,
  408, 409, 400, 402, 410
***
***
***
291, 389, 390, 382, 385, 133, 134, 126, 129, 1335, 1372, 1328, 1371, 1407, 1444,
1400,
    1443, 1411, 1412, 1405, 1403
292, 373, 376, 375, 374, 117, 120, 119, 118, 1366, 1356, 1355, 1349, 1438, 1428,
1427,
    1421, 1423, 1379, 1398, 1406
*Nset, nset=_PickedSet3, internal, generate
  1, 1444, 1
*Elset, elset=_PickedSet3, internal, generate
  1, 292, 1
** Section: SH10PCC
** Solid Section, elset=_PickedSet3, material=SH10PCC
,
*End Instance
**
*Instance, name=OSI-1, part=OSI
    150.,    512.,    0.
*Node
    1,    30.,    120.,    12.
    2,    30., 110.769234,    12.
    3,    30., 101.53846,    12.
    4,    30., 92.3076935,    12.
***
***
***
    352,    0., 4.61538458,    0.
    353,    0.,    0.,    6.
    354,    0., 4.61538458,    12.

```

```

355,    5.,    0.,    12.
356,    5.,    0.,    0.
*Element, type=C3D20R
1, 29, 30, 44, 43, 1, 2, 16, 15, 116, 115, 114, 113, 117, 118, 119,
120, 122, 121, 123, 124
2, 30, 31, 45, 44, 2, 3, 17, 16, 127, 126, 125, 115, 128, 129, 130,
118, 121, 131, 132, 123
***
***
***
38, 96, 97, 111, 110, 68, 69, 83, 82, 349, 348, 347, 343, 281, 280, 279,
275, 345, 350, 351, 346
39, 97, 98, 112, 111, 69, 70, 84, 83, 354, 353, 352, 348, 286, 285, 284,
280, 350, 355, 356, 351
*Nset, nset=_PickedSet2, internal, generate
1, 356, 1
*Elset, elset=_PickedSet2, internal, generate
1, 39, 1
** Section: SH10PCC
**Solid Section, elset=_PickedSet2, material=SH10PCC
,
*End Instance
*Instance, name=DOWEL-1, part=DOWEL
516., 253.996421, 5.999999999999994
516., 253.996421, 5.999999999999994, 515.422649720448, 254.573771279552,
5.4226497204479, 119.999999109416
*Node
1, -0.530330062, 0.530330062, 0.
2, -0.75, 0., 0.
3, -0.530330062, -0.530330062, 0.
4, 0., -0.75, 0.
5, 0.530330062, -0.530330062, 0.
6, 0.75, 0., 0.
***
***
***
167, 0.530330062, -0.530330062, 8.10000038
168, 0., -0.75, 8.10000038
169, -0.287012577, -0.692909658, 9.
170, -0.692909658, -0.287012577, 9.
171, -0.530330062, -0.530330062, 8.10000038
*Element, type=C3D20R
1, 18, 17, 16, 15, 9, 8, 7, 6, 58, 57, 56, 55, 59, 60, 61,
62, 64, 63, 65, 66
2, 18, 11, 10, 17, 9, 2, 1, 8, 69, 68, 67, 58, 70, 71, 72,
59, 64, 73, 74, 63

```

```

***
***
***
19, 54, 51, 50, 49, 45, 42, 41, 40, 151, 166, 165, 164, 130, 145, 144,
  143, 156, 158, 167, 168
20, 48, 47, 54, 49, 39, 38, 45, 40, 170, 161, 164, 169, 149, 140, 143,
  148, 171, 162, 156, 168
*Nset, nset=_PickedSet2, internal, generate
  1, 171,  1
*Elset, elset=_PickedSet2, internal, generate
  1, 20,  1
** Section: TIEBAR
**Solid Section, elset=_PickedSet2, material=STEEL
,
*End Instance
**
*Nset, nset=_PickedSet358, internal, instance=MIT-1, generate
  1, 3147,  1
*Nset, nset=_PickedSet358, internal, instance=MIT-1-lin-2-1, generate
  1, 3278,  1
***
***Assembly
***
*Elset, elset=__PickedSurf826_S5, internal, instance=OSIT-1-lin-4-1-lin-3-1
  1, 27, 37, 63, 73, 99, 134, 171, 208, 245, 282, 319, 356, 393, 430, 467
  504, 541, 578, 615, 652, 689, 726, 763, 800, 837, 874
*Elset, elset=__PickedSurf826_S5, internal, instance=OSIT-1-lin-2-1-lin-3-1
  1, 21, 53, 74, 95, 116, 137, 158, 179, 200, 221, 242, 263, 284
*Surface, type=ELEMENT, name=_T0_MIT-1_M, internal
  __T0_MIT-1_M_S2, S2
*Elset, elset=__T0_MIT-1_S_S2, internal, instance=MIT-1
  613, 615, 619, 620, 622, 623, 627, 628, 629, 630, 631, 633, 634
*Surface, type=ELEMENT, name=_T0_MIT-1_S, internal
  __T0_MIT-1_S_S2, S2
*Tie, name=_T0_MIT-1
  _T0_MIT-1_S, _T0_MIT-1_M
*Nset, nset=_T0_MIT-1_SN, instance=MIT-1
  3089, 3091, 3101, 3102, 3108, 3111, 3125, 3133, 3134
*Surface, type=NODE, name=_T0_MIT-1_SN, internal
  _T0_MIT-1_SN
*Tie, name=_T0_MIT-1-Nodes
  _T0_MIT-1_SN, _T0_MIT-1_M
*Elset, elset=__T0_MIT-1-lin-2-1_M_S2, internal, instance=MIT-1-lin-2-1, generate
  398, 416,  1
*Surface, type=ELEMENT, name=_T0_MIT-1-lin-2-1_M, internal
  __T0_MIT-1-lin-2-1_M_S2, S2

```

```

*Elset, elset=__T0_MIT-1-lin-2-1_S_S2, internal, instance=MIT-1-lin-2-1
648, 649, 652, 654, 655, 656, 659, 661, 663, 665, 666
*Surface, type=ELEMENT, name=_T0_MIT-1-lin-2-1_S, internal
__T0_MIT-1-lin-2-1_S_S2, S2
*Tie, name=_T0_MIT-1-lin-2-1
_T0_MIT-1-lin-2-1_S, _T0_MIT-1-lin-2-1_M
*Nset, nset=_T0_MIT-1-lin-2-1_SN, instance=MIT-1-lin-2-1
3215, 3218, 3223, 3224, 3246, 3247, 3252, 3260, 3268, 3273
*Surface, type=NODE, name=_T0_MIT-1-lin-2-1_SN, internal
_T0_MIT-1-lin-2-1_SN
*Tie, name=_T0_MIT-1-lin-2-1-Nodes
_T0_MIT-1-lin-2-1_SN, _T0_MIT-1-lin-2-1_M
*Elset, elset=__T0_MIT-1-lin-3-1_M_S2, internal, instance=MIT-1-lin-3-1, generate
398, 416, 1
*Surface, type=ELEMENT, name=_T0_MIT-1-lin-3-1_M, internal
__T0_MIT-1-lin-3-1_M_S2, S2
*Elset, elset=__T0_MIT-1-lin-3-1_S_S2, internal, instance=MIT-1-lin-3-1
657, 659, 663, 664, 666, 667, 671, 672, 673, 674, 675, 677, 678
*Surface, type=ELEMENT, name=_T0_MIT-1-lin-3-1_S, internal
__T0_MIT-1-lin-3-1_S_S2, S2
*Tie, name=_T0_MIT-1-lin-3-1
_T0_MIT-1-lin-3-1_S, _T0_MIT-1-lin-3-1_M
*Nset, nset=_T0_MIT-1-lin-3-1_SN, instance=MIT-1-lin-3-1
3271, 3273, 3283, 3284, 3290, 3293, 3307, 3315, 3316
*Surface, type=NODE, name=_T0_MIT-1-lin-3-1_SN, internal
_T0_MIT-1-lin-3-1_SN
*Tie, name=_T0_MIT-1-lin-3-1-Nodes
_T0_MIT-1-lin-3-1_SN, _T0_MIT-1-lin-3-1_M
*Elset, elset=__T0_MIT-1-lin-4-1_M_S2, internal, instance=MIT-1-lin-4-1, generate
398, 416, 1
*Surface, type=ELEMENT, name=_T0_MIT-1-lin-4-1_M, internal
__T0_MIT-1-lin-4-1_M_S2, S2
*Elset, elset=__T0_MIT-1-lin-4-1_S_S2, internal, instance=MIT-1-lin-4-1
657, 659, 663, 664, 666, 667, 671, 672, 673, 674, 675, 677, 678
*Surface, type=ELEMENT, name=_T0_MIT-1-lin-4-1_S, internal
__T0_MIT-1-lin-4-1_S_S2, S2
*Tie, name=_T0_MIT-1-lin-4-1
_T0_MIT-1-lin-4-1_S, _T0_MIT-1-lin-4-1_M
*Nset, nset=_T0_MIT-1-lin-4-1_SN, instance=MIT-1-lin-4-1
3271, 3273, 3283, 3284, 3290, 3293, 3307, 3315, 3316
*Surface, type=NODE, name=_T0_MIT-1-lin-4-1_SN, internal
_T0_MIT-1-lin-4-1_SN
*Tie, name=_T0_MIT-1-lin-4-1-Nodes
_T0_MIT-1-lin-4-1_SN, _T0_MIT-1-lin-4-1_M
*Elset, elset=__T0_MIT-1-lin-5-1_M_S2, internal, instance=MIT-1-lin-5-1, generate
398, 416, 1

```

```

*Surface, type=ELEMENT, name=_T0_MIT-1-lin-5-1_M, internal
__T0_MIT-1-lin-5-1_M_S2, S2
*Elset, elset=__T0_MIT-1-lin-5-1_S_S2, internal, instance=MIT-1-lin-5-1
648, 649, 652, 654, 655, 656, 659, 661, 663, 665, 666
*Surface, type=ELEMENT, name=_T0_MIT-1-lin-5-1_S, internal
__T0_MIT-1-lin-5-1_S_S2, S2
*Tie, name=_T0_MIT-1-lin-5-1
__T0_MIT-1-lin-5-1_S, __T0_MIT-1-lin-5-1_M
*Nset, nset=_T0_MIT-1-lin-5-1_SN, instance=MIT-1-lin-5-1
3215, 3218, 3223, 3224, 3246, 3247, 3252, 3260, 3268, 3273
*Surface, type=NODE, name=_T0_MIT-1-lin-5-1_SN, internal
__T0_MIT-1-lin-5-1_SN
*Tie, name=_T0_MIT-1-lin-5-1-Nodes
__T0_MIT-1-lin-5-1_SN, __T0_MIT-1-lin-5-1_M
*Elset, elset=__T0_MIT-1-lin-2-1-1_M_S2, internal, instance=MIT-1-lin-2-1-1, generate
398, 416, 1
*Surface, type=ELEMENT, name=_T0_MIT-1-lin-2-1-1_M, internal
__T0_MIT-1-lin-2-1-1_M_S2, S2
*Elset, elset=__T0_MIT-1-lin-2-1-1_S_S2, internal, instance=MIT-1-lin-2-1-1
657, 659, 663, 664, 666, 667, 671, 672, 673, 674, 675, 677, 678
*Surface, type=ELEMENT, name=_T0_MIT-1-lin-2-1-1_S, internal
__T0_MIT-1-lin-2-1-1_S_S2, S2
*Tie, name=_T0_MIT-1-lin-2-1-1
__T0_MIT-1-lin-2-1-1_S, __T0_MIT-1-lin-2-1-1_M
*Nset, nset=_T0_MIT-1-lin-2-1-1_SN, instance=MIT-1-lin-2-1-1
3271, 3273, 3283, 3284, 3290, 3293, 3307, 3315, 3316
*Surface, type=NODE, name=_T0_MIT-1-lin-2-1-1_SN, internal
__T0_MIT-1-lin-2-1-1_SN
*Tie, name=_T0_MIT-1-lin-2-1-1-Nodes
__T0_MIT-1-lin-2-1-1_SN, __T0_MIT-1-lin-2-1-1_M
*Elset, elset=__T0_MIT-1-lin-3-1-1_M_S2, internal, instance=MIT-1-lin-3-1-1, generate
398, 416, 1
*Surface, type=ELEMENT, name=_T0_MIT-1-lin-3-1-1_M, internal
__T0_MIT-1-lin-3-1-1_M_S2, S2
*Elset, elset=__T0_MIT-1-lin-3-1-1_S_S2, internal, instance=MIT-1-lin-3-1-1
657, 659, 663, 664, 666, 667, 671, 672, 673, 674, 675, 677, 678
*Surface, type=ELEMENT, name=_T0_MIT-1-lin-3-1-1_S, internal
__T0_MIT-1-lin-3-1-1_S_S2, S2
*Tie, name=_T0_MIT-1-lin-3-1-1
__T0_MIT-1-lin-3-1-1_S, __T0_MIT-1-lin-3-1-1_M
*Nset, nset=_T0_MIT-1-lin-3-1-1_SN, instance=MIT-1-lin-3-1-1
3271, 3273, 3283, 3284, 3290, 3293, 3307, 3315, 3316
*Surface, type=NODE, name=_T0_MIT-1-lin-3-1-1_SN, internal
__T0_MIT-1-lin-3-1-1_SN
*Tie, name=_T0_MIT-1-lin-3-1-1-Nodes
__T0_MIT-1-lin-3-1-1_SN, __T0_MIT-1-lin-3-1-1_M

```

```

*Elset, elset=__T0_MIT-1-lin-2-1-lin-2-1_M_S2, internal, instance=MIT-1-lin-2-1-lin-2-
1, generate
  398, 416, 1
*Surface, type=ELEMENT, name=_T0_MIT-1-lin-2-1-lin-2-1_M, internal
__T0_MIT-1-lin-2-1-lin-2-1_M_S2, S2
*Elset, elset=__T0_MIT-1-lin-2-1-lin-2-1_S_S2, internal, instance=MIT-1-lin-2-1-lin-2-
1
  648, 649, 652, 654, 655, 656, 659, 661, 663, 665, 666
*Surface, type=ELEMENT, name=_T0_MIT-1-lin-2-1-lin-2-1_S, internal
__T0_MIT-1-lin-2-1-lin-2-1_S_S2, S2
*Tie, name=_T0_MIT-1-lin-2-1-lin-2-1
_T0_MIT-1-lin-2-1-lin-2-1_S, _T0_MIT-1-lin-2-1-lin-2-1_M
*Nset, nset=_T0_MIT-1-lin-2-1-lin-2-1_SN, instance=MIT-1-lin-2-1-lin-2-1
3215, 3218, 3223, 3224, 3246, 3247, 3252, 3260, 3268, 3273
*Surface, type=NODE, name=_T0_MIT-1-lin-2-1-lin-2-1_SN, internal
__T0_MIT-1-lin-2-1-lin-2-1_SN
*Tie, name=_T0_MIT-1-lin-2-1-lin-2-1-Nodes
__T0_MIT-1-lin-2-1-lin-2-1_SN, _T0_MIT-1-lin-2-1-lin-2-1_M
*Elset, elset=__T0_MIT-1-lin-2-1-lin-3-1_M_S2, internal, instance=MIT-1-lin-2-1-lin-3-
1, generate
  398, 416, 1
*Surface, type=ELEMENT, name=_T0_MIT-1-lin-2-1-lin-3-1_M, internal
__T0_MIT-1-lin-2-1-lin-3-1_M_S2, S2
*Elset, elset=__T0_MIT-1-lin-2-1-lin-3-1_S_S2, internal, instance=MIT-1-lin-2-1-lin-3-
1
  648, 649, 652, 654, 655, 656, 659, 661, 663, 665, 666
*Surface, type=ELEMENT, name=_T0_MIT-1-lin-2-1-lin-3-1_S, internal
__T0_MIT-1-lin-2-1-lin-3-1_S_S2, S2
*Tie, name=_T0_MIT-1-lin-2-1-lin-3-1
__T0_MIT-1-lin-2-1-lin-3-1_S, _T0_MIT-1-lin-2-1-lin-3-1_M
*Nset, nset=_T0_MIT-1-lin-2-1-lin-3-1_SN, instance=MIT-1-lin-2-1-lin-3-1
3215, 3218, 3223, 3224, 3246, 3247, 3252, 3260, 3268, 3273
*Surface, type=NODE, name=_T0_MIT-1-lin-2-1-lin-3-1_SN, internal
__T0_MIT-1-lin-2-1-lin-3-1_SN
*Tie, name=_T0_MIT-1-lin-2-1-lin-3-1-Nodes
__T0_MIT-1-lin-2-1-lin-3-1_SN, _T0_MIT-1-lin-2-1-lin-3-1_M
*Elset, elset=__T0_MIT-1-lin-3-1-lin-2-1_M_S2, internal, instance=MIT-1-lin-3-1-lin-2-
1, generate
  506, 526, 1
*Surface, type=ELEMENT, name=_T0_MIT-1-lin-3-1-lin-2-1_M, internal
__T0_MIT-1-lin-3-1-lin-2-1_M_S2, S2
*Elset, elset=__T0_MIT-1-lin-3-1-lin-2-1_S_S2, internal, instance=MIT-1-lin-3-1-lin-2-
1
  833, 834, 835, 837, 838, 839, 845, 846, 847, 848, 849, 850, 851, 852, 853, 855
  856, 857, 859, 860, 861, 863, 864
*Surface, type=ELEMENT, name=_T0_MIT-1-lin-3-1-lin-2-1_S, internal

```

```

__T0_MIT-1-lin-3-1-lin-2-1_S_S2, S2
*Tie, name=__T0_MIT-1-lin-3-1-lin-2-1
__T0_MIT-1-lin-3-1-lin-2-1_S, __T0_MIT-1-lin-3-1-lin-2-1_M
*Nset, nset=__T0_MIT-1-lin-3-1-lin-2-1_SN, instance=MIT-1-lin-3-1-lin-2-1
4141, 4143, 4167, 4170, 4171, 4176, 4180, 4181, 4214, 4216, 4224
*Surface, type=NODE, name=__T0_MIT-1-lin-3-1-lin-2-1_SN, internal
__T0_MIT-1-lin-3-1-lin-2-1_SN
*Tie, name=__T0_MIT-1-lin-3-1-lin-2-1-Nodes
__T0_MIT-1-lin-3-1-lin-2-1_SN, __T0_MIT-1-lin-3-1-lin-2-1_M
*Elset, elset=__T0_MIT-1-lin-3-1-lin-3-1_M_S2, internal, instance=MIT-1-lin-3-1-lin-3-
1, generate
362, 380, 1
*Surface, type=ELEMENT, name=__T0_MIT-1-lin-3-1-lin-3-1_M, internal
__T0_MIT-1-lin-3-1-lin-3-1_M_S2, S2
*Elset, elset=__T0_MIT-1-lin-3-1-lin-3-1_S_S2, internal, instance=MIT-1-lin-3-1-lin-3-
1
657, 658, 660, 664, 665, 667, 668, 672, 673, 674, 675, 676, 678
*Surface, type=ELEMENT, name=__T0_MIT-1-lin-3-1-lin-3-1_S, internal
__T0_MIT-1-lin-3-1-lin-3-1_S_S2, S2
*Tie, name=__T0_MIT-1-lin-3-1-lin-3-1
__T0_MIT-1-lin-3-1-lin-3-1_S, __T0_MIT-1-lin-3-1-lin-3-1_M
*Nset, nset=__T0_MIT-1-lin-3-1-lin-3-1_SN, instance=MIT-1-lin-3-1-lin-3-1
3279, 3281, 3291, 3292, 3298, 3301, 3314, 3320, 3321
*Surface, type=NODE, name=__T0_MIT-1-lin-3-1-lin-3-1_SN, internal
__T0_MIT-1-lin-3-1-lin-3-1_SN
*Tie, name=__T0_MIT-1-lin-3-1-lin-3-1-Nodes
__T0_MIT-1-lin-3-1-lin-3-1_SN, __T0_MIT-1-lin-3-1-lin-3-1_M
*Elset, elset=__T0_MIT-1-lin-4-1-lin-2-1_M_S2, internal, instance=MIT-1-lin-4-1-lin-2-
1, generate
712, 732, 1
*Surface, type=ELEMENT, name=__T0_MIT-1-lin-4-1-lin-2-1_M, internal
__T0_MIT-1-lin-4-1-lin-2-1_M_S2, S2
*Elset, elset=__T0_MIT-1-lin-4-1-lin-2-1_S_S2, internal, instance=MIT-1-lin-4-1-lin-2-
1
503, 504, 505, 508, 509, 514, 515, 516, 517, 518, 519, 520, 522
*Surface, type=ELEMENT, name=__T0_MIT-1-lin-4-1-lin-2-1_S, internal
__T0_MIT-1-lin-4-1-lin-2-1_S_S2, S2
*Tie, name=__T0_MIT-1-lin-4-1-lin-2-1
__T0_MIT-1-lin-4-1-lin-2-1_S, __T0_MIT-1-lin-4-1-lin-2-1_M
*Nset, nset=__T0_MIT-1-lin-4-1-lin-2-1_SN, instance=MIT-1-lin-4-1-lin-2-1
2766, 2768, 2774, 2776, 2801, 2804, 2818, 2820, 2825
*Surface, type=NODE, name=__T0_MIT-1-lin-4-1-lin-2-1_SN, internal
__T0_MIT-1-lin-4-1-lin-2-1_SN
*Tie, name=__T0_MIT-1-lin-4-1-lin-2-1-Nodes
__T0_MIT-1-lin-4-1-lin-2-1_SN, __T0_MIT-1-lin-4-1-lin-2-1_M

```

```

*Elset, elset=__T0_MIT-1-lin-4-1-lin-3-1_M_S2, internal, instance=MIT-1-lin-4-1-lin-3-
1, generate
  2880, 2914, 1
*Surface, type=ELEMENT, name=_T0_MIT-1-lin-4-1-lin-3-1_M, internal
__T0_MIT-1-lin-4-1-lin-3-1_M_S2, S2
*Elset, elset=__T0_MIT-1-lin-4-1-lin-3-1_S_S2, internal, instance=MIT-1-lin-4-1-lin-3-
1
  2162, 2166, 2168, 2169, 2170, 2172, 2174, 2175, 2177, 2180, 2181, 2182, 2183, 2184,
2185, 2186
  2187, 2188, 2189, 2190, 2191, 2192, 2193, 2194, 2195, 2196, 2197, 2198, 2199, 2201,
2202, 2203
  2204, 2205, 2206, 2207, 2208, 2209, 2210, 2211, 2212, 2213, 2215, 2216, 2217
*Surface, type=ELEMENT, name=_T0_MIT-1-lin-4-1-lin-3-1_S, internal
__T0_MIT-1-lin-4-1-lin-3-1_S_S2, S2
*Tie, name=_T0_MIT-1-lin-4-1-lin-3-1
_T0_MIT-1-lin-4-1-lin-3-1_S, _T0_MIT-1-lin-4-1-lin-3-1_M
*Nset, nset=_T0_MIT-1-lin-4-1-lin-3-1_SN, instance=MIT-1-lin-4-1-lin-3-1
  10751, 10753, 10759, 10766, 10767, 10774, 10786, 10792, 10795, 10797, 10812, 10813,
10839, 10841, 10876
*Surface, type=NODE, name=_T0_MIT-1-lin-4-1-lin-3-1_SN, internal
__T0_MIT-1-lin-4-1-lin-3-1_SN
*Tie, name=_T0_MIT-1-lin-4-1-lin-3-1-Nodes
__T0_MIT-1-lin-4-1-lin-3-1_SN, _T0_MIT-1-lin-4-1-lin-3-1_M
*Elset, elset=__T0_MIT-1-lin-5-1-lin-2-1_M_S2, internal, instance=MIT-1-lin-5-1-lin-2-
1, generate
  436, 454, 1
*Surface, type=ELEMENT, name=_T0_MIT-1-lin-5-1-lin-2-1_M, internal
__T0_MIT-1-lin-5-1-lin-2-1_M_S2, S2
*Elset, elset=__T0_MIT-1-lin-5-1-lin-2-1_S_S2, internal, instance=MIT-1-lin-5-1-lin-2-
1
  635, 638, 640, 641, 644, 645, 646, 647, 648, 651, 654
*Surface, type=ELEMENT, name=_T0_MIT-1-lin-5-1-lin-2-1_S, internal
__T0_MIT-1-lin-5-1-lin-2-1_S_S2, S2
*Tie, name=_T0_MIT-1-lin-5-1-lin-2-1
_T0_MIT-1-lin-5-1-lin-2-1_S, _T0_MIT-1-lin-5-1-lin-2-1_M
*Nset, nset=_T0_MIT-1-lin-5-1-lin-2-1_SN, instance=MIT-1-lin-5-1-lin-2-1
  3175, 3176, 3180, 3182, 3194, 3195, 3209, 3226, 3227
*Surface, type=NODE, name=_T0_MIT-1-lin-5-1-lin-2-1_SN, internal
__T0_MIT-1-lin-5-1-lin-2-1_SN
*Tie, name=_T0_MIT-1-lin-5-1-lin-2-1-Nodes
__T0_MIT-1-lin-5-1-lin-2-1_SN, _T0_MIT-1-lin-5-1-lin-2-1_M
*Elset, elset=__T0_MIT-1-lin-5-1-lin-3-1_M_S2, internal, instance=MIT-1-lin-5-1-lin-3-
1, generate
  1474, 1514, 1
*Surface, type=ELEMENT, name=_T0_MIT-1-lin-5-1-lin-3-1_M, internal
__T0_MIT-1-lin-5-1-lin-3-1_M_S2, S2

```

\*Elset, elset=\_\_T0\_MIT-1-lin-5-1-lin-3-1\_S\_S2, internal, instance=MIT-1-lin-5-1-lin-3-  
 1  
 2310, 2313, 2316, 2317, 2318, 2320, 2321, 2324, 2325, 2329, 2331, 2333, 2335, 2337,  
 2338, 2340  
 2341, 2342, 2343, 2344, 2345, 2346, 2347, 2348, 2349, 2350, 2351  
 \*Surface, type=ELEMENT, name=\_\_T0\_MIT-1-lin-5-1-lin-3-1\_S, internal  
 \_\_T0\_MIT-1-lin-5-1-lin-3-1\_S\_S2, S2  
 \*Tie, name=\_\_T0\_MIT-1-lin-5-1-lin-3-1  
 \_\_T0\_MIT-1-lin-5-1-lin-3-1\_S, \_\_T0\_MIT-1-lin-5-1-lin-3-1\_M  
 \*Nset, nset=\_\_T0\_MIT-1-lin-5-1-lin-3-1\_SN, instance=MIT-1-lin-5-1-lin-3-1  
 680, 11044, 11045, 11048, 11049, 11064, 11065, 11070, 11072, 11094, 11095, 11107,  
 11110, 11122, 11125, 11126  
 11143,  
 \*Surface, type=NODE, name=\_\_T0\_MIT-1-lin-5-1-lin-3-1\_SN, internal  
 \_\_T0\_MIT-1-lin-5-1-lin-3-1\_SN  
 \*Tie, name=\_\_T0\_MIT-1-lin-5-1-lin-3-1-Nodes  
 \_\_T0\_MIT-1-lin-5-1-lin-3-1\_SN, \_\_T0\_MIT-1-lin-5-1-lin-3-1\_M  
 \*\* Constraint: D1  
 \*Tie, name=D1, adjust=yes  
 \_\_PickedSurf742, \_\_PickedSurf741  
 \*\* Constraint: D2  
 \*Tie, name=D2, adjust=yes  
 \_\_PickedSurf744, \_\_PickedSurf743  
 \*\* Constraint: D3  
 \*Tie, name=D3, adjust=yes  
 \_\_PickedSurf746, \_\_PickedSurf745  
 \*\* Constraint: D4  
 \*Tie, name=D4, adjust=yes  
 \_\_PickedSurf748, \_\_PickedSurf747  
 \*\* Constraint: D5  
 \*Tie, name=D5, adjust=yes  
 \_\_PickedSurf750, \_\_PickedSurf749  
 \*\* Constraint: D6  
 \*Tie, name=D6, adjust=yes  
 \_\_PickedSurf752, \_\_PickedSurf751  
 \*\* Constraint: IS1  
 \*Tie, name=IS1, adjust=yes  
 \_\_PickedSurf313, \_\_PickedSurf312  
 \*\* Constraint: IS2  
 \*Tie, name=IS2, adjust=yes  
 \_\_PickedSurf315, \_\_PickedSurf314  
 \*\* Constraint: IS3  
 \*Tie, name=IS3, adjust=yes  
 \_\_PickedSurf317, \_\_PickedSurf316  
 \*\* Constraint: IS4  
 \*Tie, name=IS4, adjust=yes

\_PickedSurf319, \_PickedSurf318  
\*\* Constraint: IS5  
\*Tie, name=IS5, adjust=yes  
\_PickedSurf321, \_PickedSurf320  
\*\* Constraint: IS6  
\*Tie, name=IS6, adjust=yes  
\_PickedSurf323, \_PickedSurf322  
\*\* Constraint: IS7  
\*Tie, name=IS7, adjust=yes  
\_PickedSurf325, \_PickedSurf324  
\*\* Constraint: IS8  
\*Tie, name=IS8, adjust=yes  
\_PickedSurf327, \_PickedSurf326  
\*\* Constraint: IS9  
\*Tie, name=IS9, adjust=yes  
\_PickedSurf329, \_PickedSurf328  
\*\* Constraint: IS10  
\*Tie, name=IS10, adjust=yes  
\_PickedSurf331, \_PickedSurf330  
\*\* Constraint: IS11  
\*Tie, name=IS11, adjust=yes  
\_PickedSurf333, \_PickedSurf332  
\*\* Constraint: IS12  
\*Tie, name=IS12, adjust=yes  
\_PickedSurf335, \_PickedSurf334  
\*\* Constraint: IS13  
\*Tie, name=IS13, adjust=yes  
\_PickedSurf337, \_PickedSurf336  
\*\* Constraint: IS14  
\*Tie, name=IS14, adjust=yes  
\_PickedSurf339, \_PickedSurf338  
\*\* Constraint: IS15  
\*Tie, name=IS15, adjust=yes  
\_PickedSurf341, \_PickedSurf340  
\*\* Constraint: IS16  
\*Tie, name=IS16, adjust=yes  
\_PickedSurf343, \_PickedSurf342  
\*\* Constraint: IS17  
\*Tie, name=IS17, adjust=yes  
\_PickedSurf345, \_PickedSurf344  
\*\* Constraint: IS18  
\*Tie, name=IS18, adjust=yes  
\_PickedSurf347, \_PickedSurf346  
\*\* Constraint: M1  
\*Tie, name=M1, adjust=yes  
\_PickedSurf277, \_PickedSurf276

\*\* Constraint: M2  
\*Tie, name=M2, adjust=yes  
\_PickedSurf279, \_PickedSurf278  
\*\* Constraint: M3  
\*Tie, name=M3, adjust=yes  
\_PickedSurf281, \_PickedSurf280  
\*\* Constraint: M4  
\*Tie, name=M4, adjust=yes  
\_PickedSurf283, \_PickedSurf282  
\*\* Constraint: M5  
\*Tie, name=M5, adjust=yes  
\_PickedSurf285, \_PickedSurf284  
\*\* Constraint: M6  
\*Tie, name=M6, adjust=yes  
\_PickedSurf287, \_PickedSurf286  
\*\* Constraint: M7  
\*Tie, name=M7, adjust=yes  
\_PickedSurf289, \_PickedSurf288  
\*\* Constraint: M8  
\*Tie, name=M8, adjust=yes  
\_PickedSurf291, \_PickedSurf290  
\*\* Constraint: M9  
\*Tie, name=M9, adjust=yes  
\_PickedSurf293, \_PickedSurf292  
\*\* Constraint: M10  
\*Tie, name=M10, adjust=yes  
\_PickedSurf295, \_PickedSurf294  
\*\* Constraint: M11  
\*Tie, name=M11, adjust=yes  
\_PickedSurf297, \_PickedSurf296  
\*\* Constraint: M12  
\*Tie, name=M12, adjust=yes  
\_PickedSurf299, \_PickedSurf298  
\*\* Constraint: M13  
\*Tie, name=M13, adjust=yes  
\_PickedSurf301, \_PickedSurf300  
\*\* Constraint: M14  
\*Tie, name=M14, adjust=yes  
\_PickedSurf303, \_PickedSurf302  
\*\* Constraint: M15  
\*Tie, name=M15, adjust=yes  
\_PickedSurf305, \_PickedSurf304  
\*\* Constraint: M16  
\*Tie, name=M16, adjust=yes  
\_PickedSurf307, \_PickedSurf306  
\*\* Constraint: M17

\*Tie, name=M17, adjust=yes  
 \_PickedSurf309, \_PickedSurf308  
 \*\* Constraint: M18  
 \*Tie, name=M18, adjust=yes  
 \_PickedSurf311, \_PickedSurf310  
 \*\* Constraint: OS1  
 \*Tie, name=OS1, adjust=yes  
 \_PickedSurf241, \_PickedSurf240  
 \*\* Constraint: OS2  
 \*Tie, name=OS2, adjust=yes  
 \_PickedSurf243, \_PickedSurf242  
 \*\* Constraint: OS3  
 \*Tie, name=OS3, adjust=yes  
 \_PickedSurf245, \_PickedSurf244  
 \*\* Constraint: OS4  
 \*Tie, name=OS4, adjust=yes  
 \_PickedSurf247, \_PickedSurf246  
 \*\* Constraint: OS5  
 \*Tie, name=OS5, adjust=yes  
 \_PickedSurf249, \_PickedSurf248  
 \*\* Constraint: OS6  
 \*Tie, name=OS6, adjust=yes  
 \_PickedSurf251, \_PickedSurf250  
 \*\* Constraint: OS7  
 \*Tie, name=OS7, adjust=yes  
 \_PickedSurf253, \_PickedSurf252  
 \*\* Constraint: OS8  
 \*Tie, name=OS8, adjust=yes  
 \_PickedSurf255, \_PickedSurf254  
 \*\* Constraint: OS9  
 \*Tie, name=OS9, adjust=yes  
 \_PickedSurf257, \_PickedSurf256  
 \*\* Constraint: OS10  
 \*Tie, name=OS10, adjust=yes  
 \_PickedSurf259, \_PickedSurf258  
 \*\* Constraint: OS11  
 \*Tie, name=OS11, adjust=yes  
 \_PickedSurf261, \_PickedSurf260  
 \*\* Constraint: OS12  
 \*Tie, name=OS12, adjust=yes  
 \_PickedSurf263, \_PickedSurf262  
 \*\* Constraint: OS13  
 \*Tie, name=OS13, adjust=yes  
 \_PickedSurf265, \_PickedSurf264  
 \*\* Constraint: OS14  
 \*Tie, name=OS14, adjust=yes

\_PickedSurf267, \_PickedSurf266  
\*\* Constraint: OS15  
\*Tie, name=OS15, adjust=yes  
\_PickedSurf269, \_PickedSurf268  
\*\* Constraint: OS16  
\*Tie, name=OS16, adjust=yes  
\_PickedSurf271, \_PickedSurf270  
\*\* Constraint: OS17  
\*Tie, name=OS17, adjust=yes  
\_PickedSurf273, \_PickedSurf272  
\*\* Constraint: OS18  
\*Tie, name=OS18, adjust=yes  
\_PickedSurf275, \_PickedSurf274  
\*\* Constraint: TB1  
\*Tie, name=TB1, adjust=yes  
\_PickedSurf181, \_PickedSurf180  
\*\* Constraint: TB2  
\*Tie, name=TB2, adjust=yes  
\_PickedSurf183, \_PickedSurf182  
\*\* Constraint: TB3  
\*Tie, name=TB3, adjust=yes  
\_PickedSurf185, \_PickedSurf184  
\*\* Constraint: TB4  
\*Tie, name=TB4, adjust=yes  
\_PickedSurf187, \_PickedSurf186  
\*\* Constraint: TB5  
\*Tie, name=TB5, adjust=yes  
\_PickedSurf189, \_PickedSurf188  
\*\* Constraint: TB6  
\*Tie, name=TB6, adjust=yes  
\_PickedSurf191, \_PickedSurf190  
\*\* Constraint: TB7  
\*Tie, name=TB7, adjust=yes  
\_PickedSurf193, \_PickedSurf192  
\*\* Constraint: TB8  
\*Tie, name=TB8, adjust=yes  
\_PickedSurf195, \_PickedSurf194  
\*\* Constraint: TB9  
\*Tie, name=TB9, adjust=yes  
\_PickedSurf197, \_PickedSurf196  
\*\* Constraint: TB10  
\*Tie, name=TB10, adjust=yes  
\_PickedSurf199, \_PickedSurf198  
\*\* Constraint: TB11  
\*Tie, name=TB11, adjust=yes  
\_PickedSurf201, \_PickedSurf200

\*\* Constraint: TB12  
\*Tie, name=TB12, adjust=yes  
\_PickedSurf203, \_PickedSurf202  
\*\* Constraint: TB13  
\*Tie, name=TB13, adjust=yes  
\_PickedSurf205, \_PickedSurf204  
\*\* Constraint: TB14  
\*Tie, name=TB14, adjust=yes  
\_PickedSurf207, \_PickedSurf206  
\*\* Constraint: TB15  
\*Tie, name=TB15, adjust=yes  
\_PickedSurf209, \_PickedSurf208  
\*\* Constraint: TB16  
\*Tie, name=TB16, adjust=yes  
\_PickedSurf211, \_PickedSurf210  
\*\* Constraint: TB17  
\*Tie, name=TB17, adjust=yes  
\_PickedSurf213, \_PickedSurf212  
\*\* Constraint: TB18  
\*Tie, name=TB18, adjust=yes  
\_PickedSurf215, \_PickedSurf214  
\*\* Constraint: TB19  
\*Tie, name=TB19, adjust=yes  
\_PickedSurf217, \_PickedSurf216  
\*\* Constraint: TB20  
\*Tie, name=TB20, adjust=yes  
\_PickedSurf219, \_PickedSurf218  
\*\* Constraint: TB21  
\*Tie, name=TB21, adjust=yes  
\_PickedSurf221, \_PickedSurf220  
\*\* Constraint: TB22  
\*Tie, name=TB22, adjust=yes  
\_PickedSurf223, \_PickedSurf222  
\*\* Constraint: TB23  
\*Tie, name=TB23, adjust=yes  
\_PickedSurf225, \_PickedSurf224  
\*\* Constraint: TB24  
\*Tie, name=TB24, adjust=yes  
\_PickedSurf227, \_PickedSurf226  
\*\* Constraint: TB25  
\*Tie, name=TB25, adjust=yes  
\_PickedSurf229, \_PickedSurf228  
\*\* Constraint: TB26  
\*Tie, name=TB26, adjust=yes  
\_PickedSurf231, \_PickedSurf230  
\*\* Constraint: TB27

```

*Tie, name=TB27, adjust=yes
_PickedSurf233, _PickedSurf232
** Constraint: TB28
*Tie, name=TB28, adjust=yes
_PickedSurf235, _PickedSurf234
** Constraint: TB29
*Tie, name=TB29, adjust=yes
_PickedSurf237, _PickedSurf236
** Constraint: TB30
*Tie, name=TB30, adjust=yes
_PickedSurf239, _PickedSurf238
*End Assembly
**
**
** MATERIALS
**
*Material, name=MLPCC
*Density
0.0839,
*Elastic
4.5e+06, 0.17
*Expansion
4.0e-06,
*Material, name=SH2PCC
*Density
0.0839,
*Elastic
4.5e+06, 0.17
*Expansion
4.0e-06,
*Material, name=SH10PCC
*Density
0.0839,
*Elastic
4.5e+06, 0.17
*Expansion
4.0e-06,
*Material, name=STEEL
*Density
0.28,
*Elastic
2.9e+07, 0.3
**
**
** INTERACTION PROPERTIES
**

```

```

*Surface Interaction, name=PCConPCC
1.,
*Friction
0.,
*Surface Behavior, no separation, pressure-overclosure=HARD
**
** BOUNDARY CONDITIONS
**
** Name: ISL Type: Displacement/Rotation
*Boundary
_PickedSet823, 1, 1
_PickedSet823, 2, 2
** Name: ISMORTAR Type: Displacement/Rotation
*Boundary
_PickedSet832, 1, 1
_PickedSet832, 2, 2
** Name: ISR Type: Displacement/Rotation
*Boundary
_PickedSet820, 1, 1
_PickedSet820, 2, 2
** Name: OSL Type: Displacement/Rotation
*Boundary
_PickedSet824, 1, 1
_PickedSet824, 2, 2
** Name: OSMORTAR Type: Displacement/Rotation
*Boundary
_PickedSet833, 1, 1
_PickedSet833, 2, 2
** Name: OSR Type: Displacement/Rotation
*Boundary
_PickedSet819, 1, 1
_PickedSet819, 2, 2
**
** PREDEFINED FIELDS
**
** Name: ISini Type: Temperature
*Initial Conditions, type=TEMPERATURE
_PickedSet359, 70.
** Name: MLini Type: Temperature
*Initial Conditions, type=TEMPERATURE
_PickedSet358, 80.
** Name: OSini Type: Temperature
*Initial Conditions, type=TEMPERATURE
_PickedSet360, 70.
**
** INTERACTIONS

```

```

**
** Interaction: FOUNDATION
*Foundation
__PickedSurf352_S3, F3, 100.
__PickedSurf352_S4, F4, 100.
__PickedSurf352_S6, F6, 100.
__PickedSurf352_S5, F5, 100.
__PickedSurf352_S1, F1, 100.
** Interaction: ISML
*Contact Pair, interaction=PCConPCC, type=SURFACE TO SURFACE
__PickedSurf349, __PickedSurf348
** Interaction: OSML
*Contact Pair, interaction=PCConPCC, type=SURFACE TO SURFACE
__PickedSurf351, __PickedSurf350
** -----
**
** STEP: GRAVITY
**
*Step, name=GRAVITY
*Static
1., 1., 1e-05, 1.
**
** LOADS
**
** Name: GRAVITY   Type: Gravity
*Dload
__PickedSet810, GRAV, 386.4, 0., 0., 1.
**
** OUTPUT REQUESTS
**
*Restart, write, frequency=0
**
** FIELD OUTPUT: F-Output-1
**
*Output, field
*Node Output
CF, NT, RF, U
*Element Output, directions=YES
LE, PE, PEEQ, PEMAG, S
*Contact Output
CDISP, CSTRESS
**
** HISTORY OUTPUT: H-Output-1
**
*Output, history, variable=PRESELECT
*End Step

```

```

** -----
**
** STEP: TEMP
**
*Step, name=TEMP
*Static
1., 1., 1e-05, 1.
**
** LOADS
**
** Name: BASETRACTIONLEFT  Type: Surface traction
*Dload
_PickedSurf814, TRSHR, 0.8, 1., 0., 0.
** Name: BASETRACTIONRIGHT  Type: Surface traction
*Dload
_PickedSurf815, TRSHR, 0.8, -1., 0., 0.
**
** PREDEFINED FIELDS
**
** Name: ENTIRE MODEL  Type: Temperature
*Temperature
_PickedSet827, 90.
**
** OUTPUT REQUESTS
**
*Restart, write, frequency=0
**
** FIELD OUTPUT: F-Output-1
**
*Output, field
*Node Output
CF, NT, RF, U
*Element Output, directions=YES
LE, PE, PEEQ, PEMAG, S
*Contact Output
CDISP, CSTRESS
**
** HISTORY OUTPUT: H-Output-1
**
*Output, history, variable=PRESELECT
*End Step

```

## APPENDIX D

### SAMPLE INPUT FILE FOR SHOULDER TRANSVERSE CRACKING MODEL

```
*Heading
** Job name: TCS_MSC_80_112_50_SH2_28 Model name: Model-1
** Generated by: Abaqus/CAE 6.9-EF1
**Preprint, echo=NO, model=NO, history=NO, contact=NO
**
** PARTS
**
*Part, name=M
*End Part
**
*Part, name=SO
*End Part
**
*Part, name=TIEBAR
*End Part
**
*Part, name=TM
*End Part
**
*Part, name=TS
*End Part
**
**
** ASSEMBLY
**
*Assembly, name=Assembly
**
*Instance, name=TIEBAR-1, part=TIEBAR
    36.,    165.,    10.
    36.,    165.,    10.,    37.,    165.,    10.,    90.
```

\*Node

1,	-0.220970869,	0.220970869,	0.
2,	-0.3125,	0.,	0.
3,	-0.220970869,	-0.220970869,	0.
4,	0.,	-0.3125,	0.
5,	0.220970869,	-0.220970869,	0.
6,	0.3125,	0.,	0.
7,	0.220970869,	0.220970869,	0.

\*\*\*

\*\*\*

\*\*\*

\*\*\*

465,	0.220970869,	-0.220970869,	29.
466,	0.119588576,	0.288712353,	30.
467,	-0.119588576,	0.288712353,	30.
468,	0.,	0.3125,	29.
469,	0.119588576,	-0.288712353,	30.
470,	-0.119588576,	-0.288712353,	30.
471,	0.,	-0.3125,	29.

\*Element, type=C3D20R

1,	11,	10,	18,	12,	2,	1,	9,	3,	148,	147,	146,	145,	149,	150,	151,	152,	154,	153,	155,	156
2,	18,	16,	15,	14,	9,	7,	6,	5,	160,	159,	158,	157,	161,	162,	163,	164,	155,	165,	166,	167
3,	18,	10,	17,	16,	9,	1,	8,	7,	147,	169,	168,	160,	150,	170,	171,	161,	155,	153,	172,	165
4,	13,	12,	18,	14,	4,	3,	9,	5,	174,	146,	157,	173,	175,	151,	164,	176,	177,	156,	155,	167
5,	20,	19,	27,	21,	11,	10,	18,	12,	181,	180,	179,	178,	148,	147,	146,	145,	183,	182,	184,	185

\*\*\*

\*\*\*

\*\*\*

\*\*\*

56,	130,	129,	135,	131,	121,	120,	126,	122,	449,	431,	438,	448,	428,	410,	417,	427,	450,	437,	436,	444
57,	137,	136,	144,	138,	128,	127,	135,	129,	454,	453,	452,	451,	433,	432,	431,	430,	456,	455,	457,	458
58,	144,	142,	141,	140,	135,	133,	132,	131,	462,	461,	460,	459,	441,	440,	439,	438,	457,	463,	464,	465
59,	144,	136,	143,	142,	135,	127,	134,	133,	453,	467,	466,	462,	432,	446,	445,	441,	457,	455,	468,	463
60,	139,	138,	144,	140,	130,	129,	135,	131,	470,	452,	459,	469,	449,	431,	438,	448,	471,	458,	457,	465

\*Nset, nset=\_PickedSet2, internal, generate

1,	471,	1
----	------	---

```

*Elset, elset=_PickedSet2, internal, generate
  1, 60, 1
** Section: STEEL
*Solid Section, elset=_PickedSet2, material=STEEL
,
*End Instance
**
*Instance, name=M-1, part=M
  150.,      6.,      4.
*Node
  1,      36.,      129.,      10.
  2,      36.,      0.,      10.
  3,      36.,      72.,      0.
  4,      36.,      0.,      0.
  5,      36.,      129.,      0.
  6,      0.,      0.,      10.
  7,      0.,      0.,      0.
***
***
***
***
  1046,      0.,      112.875,      11.
  1047,      3.5999999,      112.875,      12.
  1048,      0.,      116.90625,      12.
  1049,      0.,      120.9375,      11.
  1050,      3.5999999,      120.9375,      12.
  1051,      0.,      124.96875,      12.
  1052,      0.,      129.,      11.
  1053,      3.5999999,      129.,      12.
*Element, type=C3D20R
  1, 80, 131, 191, 73, 1, 15, 35, 5, 310, 309, 308, 307, 311, 312, 313,
    314, 316, 315, 317, 318
  2, 131, 132, 192, 191, 15, 16, 34, 35, 321, 320, 319, 309, 322, 323, 324,
    312, 315, 325, 326, 317
  3, 132, 133, 193, 192, 16, 17, 33, 34, 329, 328, 327, 320, 330, 331, 332,
    323, 325, 333, 334, 326
  4, 133, 134, 194, 193, 17, 18, 32, 33, 337, 336, 335, 328, 338, 339, 340,
    331, 333, 341, 342, 334
***
***
***
***
  157, 55, 56, 120, 119, 179, 178, 304, 303, 708, 1043, 1042, 1040, 625, 993, 992,
    990, 709, 704, 1044, 1041
  158, 56, 57, 121, 120, 178, 177, 305, 304, 703, 1046, 1045, 1043, 620, 996, 995,
    993, 704, 699, 1047, 1044

```

```

159, 57, 58, 122, 121, 177, 176, 306, 305, 698, 1049, 1048, 1046, 615, 999, 998,
  996, 699, 692, 1050, 1047
160, 58, 10, 13, 122, 176, 77, 127, 306, 691, 1052, 1051, 1049, 608, 1002, 1001,
  999, 692, 693, 1053, 1050
*Nset, nset=_PickedSet2, internal, generate
  1, 1053, 1
*Elset, elset=_PickedSet2, internal, generate
  1, 160, 1
** Section: MAINLINE
*Solid Section, elset=_PickedSet2, material=MAINLINE
,
*End Instance
**
*Instance, name=TM-1, part=TM
  6., 135., 4.
*Node
  1, 180., 0., 10.
  2, 180., 15., 10.
  3, 180., 15., 12.
  4, 180., 0., 12.
  5, 0., 15., 10.
  6, 0., 15., 12.
  7, 0., 0., 12.
***
***
***
***
  3340, 88.5255203, 15., 4.08893633
  3341, 119.77903, 15., 5.77902889
  3342, 118.832169, 15., 4.8640027
  3343, 118.195236, 15., 4.22469521
  3344, 149.34053, 15., 7.8931303
  3345, 118.848541, 15., 3.26672173
  3346, 151.748962, 15., 4.22053671
*Element, type=C3D20R
  1, 102, 281, 351, 33, 1, 25, 28, 4, 940, 939, 938, 937, 941, 942, 943,
    944, 946, 945, 947, 948
  2, 281, 282, 352, 351, 25, 26, 27, 28, 951, 950, 949, 939, 952, 953, 954,
    942, 945, 955, 956, 947
  3, 282, 138, 137, 352, 26, 2, 3, 27, 959, 958, 957, 950, 960, 961, 962,
    953, 955, 963, 964, 956
  4, 101, 283, 353, 34, 102, 281, 351, 33, 968, 967, 966, 965, 940, 939, 938,
    937, 970, 969, 971, 972
  5, 283, 284, 354, 353, 281, 282, 352, 351, 975, 974, 973, 967, 951, 950, 949,
    939, 969, 976, 977, 971
***

```

```

***
***
***
562, 294, 292, 886, 924, 144, 143, 572, 610, 1066, 2790, 2866, 2857, 1071, 3268, 3344,
  3335, 1070, 1052, 3269, 3266
563, 925, 932, 915, 888, 611, 618, 601, 574, 2867, 2840, 2859, 2523, 3345, 3318, 3337,
  3001, 3005, 3320, 3015, 3003
564, 932, 925, 927, 881, 618, 611, 613, 567, 2867, 2848, 2865, 2838, 3345, 3326, 3343,
  3316, 3320, 3005, 2949, 3319
565, 903, 879, 892, 910, 589, 565, 578, 596, 2834, 2498, 2627, 2868, 3312, 2976, 3105,
  3346, 3313, 2979, 2978, 2973
566, 876, 935, 907, 936, 562, 621, 593, 622, 2809, 2849, 2686, 2862, 3287, 3327, 3164,
  3340, 3289, 3103, 3116, 3166
567, 713, 899, 903, 910, 236, 585, 589, 596, 2550, 2836, 2868, 2851, 3028, 3314, 3346,
  3329, 3032, 3033, 3313, 2973
*Nset, nset=_PickedSet3, internal, generate
  1, 3346, 1
*Elset, elset=_PickedSet3, internal, generate
  1, 567, 1
** Section: MAINLINE
** Solid Section, elset=_PickedSet3, material=MAINLINE
,
*End Instance
**
**
*Instance, name=TS-1, part=TS
  6., 150., 4.
*Node
  1, 119.72937, 0., 5.84375
  2, 119.72937, 0., 6.15625
  3, 120., 0., 6.3125
  4, 120.27063, 0., 6.15625
  5, 120.27063, 0., 5.84375
  6, 120., 0., 5.6875
  7, 59.7293663, 0., 5.84375
***
***
***
***
  7485, 65.6640015, 15., 3.9525404
  7486, 61.9066353, 15., 9.73663521
  7487, 60.6521759, 15., 12.
  7488, 63.6868362, 15., 6.61477709
  7489, 64.9302979, 15., 7.30597878
  7490, 65.3901291, 15., 6.01650715
  7491, 146.057343, 15., 4.64199352
*Element, type=C3D20R

```

```

1, 397, 305, 387, 292, 806, 714, 796, 701, 2049, 2048, 2047, 2046, 2050, 2051, 2052,
2053, 2055, 2054, 2056, 2057
2, 281, 6, 5, 144, 690, 415, 414, 553, 2061, 2060, 2059, 2058, 2062, 2063, 2064,
2065, 2067, 2066, 2068, 2069
3, 84, 145, 242, 247, 493, 554, 651, 656, 2073, 2072, 2071, 2070, 2074, 2075, 2076,
2077, 2079, 2078, 2080, 2081
4, 241, 137, 69, 145, 650, 546, 478, 554, 2085, 2084, 2083, 2082, 2086, 2087, 2088,
2089, 2091, 2090, 2092, 2078
5, 194, 241, 145, 84, 603, 650, 554, 493, 2094, 2082, 2073, 2093, 2095, 2089, 2074,
2096, 2097, 2091, 2078, 2079
***
***
***
***
1392, 1633, 1545, 1446, 1634, 2042, 1954, 1855, 2043, 6282, 5849, 6213, 6318, 7453, 7020,
7384,
7489, 7457, 7022, 6892, 7386
1393, 1634, 1503, 1425, 1308, 2043, 1912, 1834, 1717, 6214, 5703, 6314, 6319, 7385, 6874,
7485,
7490, 7386, 6879, 6878, 7481
1394, 1380, 1475, 1635, 1636, 1789, 1884, 2044, 2045, 5958, 6312, 6320, 6297, 7129, 7483,
7491,
7468, 6412, 6369, 7333, 6719
1395, 1636, 1635, 1631, 1539, 2045, 2044, 2040, 1948, 6320, 6160, 6198, 5543, 7491, 7331,
7369,
6714, 6719, 7333, 7335, 6718
1396, 1573, 1580, 1633, 1632, 1982, 1989, 2042, 2041, 6295, 6283, 6317, 6273, 7466, 7454,
7488,
7444, 6532, 7458, 7457, 7446
*Nset, nset=_PickedSet3, internal, generate
1, 7491, 1
*Elset, elset=_PickedSet3, internal, generate
1, 1396, 1
** Section: SHOULDER
** Solid Section, elset=_PickedSet3, material=SHOULDER
,
*End Instance
**
*Instance, name=SO-1, part=SO
5.99999999999989, 165., 4.
*Node
1, 0., 0., 0.
2, 0., 4.5, 0.
3, 0., 9., 0.
4, 3.9130435, 0., 0.
5, 3.9130435, 4.5, 0.

```

```

    6, 3.9130435,    9.,    0.
    7, 7.826087,    0.,    0.
***
***
***
***
    1868,    180.,    2.25,    12.
    1869,    178.,    4.5,    12.
    1870,    180.,    4.5,    10.
    1871,    180.,    0.,    10.
    1872,    180.,    6.75,    12.
    1873,    178.,    9.,    12.
    1874,    180.,    9.,    10.
*Element, type=C3D20R
  1, 139, 140, 143, 142, 1, 2, 5, 4, 556, 555, 554, 553, 557, 558, 559,
    560, 562, 561, 563, 564
  2, 140, 141, 144, 143, 2, 3, 6, 5, 567, 566, 565, 555, 568, 569, 570,
    558, 561, 571, 572, 563
  3, 142, 143, 146, 145, 4, 5, 8, 7, 554, 575, 574, 573, 559, 576, 577,
    578, 564, 563, 579, 580
  4, 143, 144, 147, 146, 5, 6, 9, 8, 565, 582, 581, 575, 570, 583, 584,
    576, 563, 572, 585, 579
  5, 145, 146, 149, 148, 7, 8, 11, 10, 574, 588, 587, 586, 577, 589, 590,
    591, 580, 579, 592, 593
***
***
***
***
265, 541, 542, 545, 544, 403, 404, 407, 406, 1844, 1853, 1852, 1851, 1479, 1488, 1487,
    1486, 1847, 1846, 1854, 1855
266, 542, 543, 546, 545, 404, 405, 408, 407, 1848, 1857, 1856, 1853, 1483, 1492, 1491,
    1488, 1846, 1850, 1858, 1854
267, 544, 545, 548, 547, 406, 407, 410, 409, 1852, 1861, 1860, 1859, 1487, 1496, 1495,
    1494, 1855, 1854, 1862, 1863
268, 545, 546, 549, 548, 407, 408, 411, 410, 1856, 1865, 1864, 1861, 1491, 1500, 1499,
    1496, 1854, 1858, 1866, 1862
269, 547, 548, 551, 550, 409, 410, 413, 412, 1860, 1869, 1868, 1867, 1495, 1504, 1503,
    1502, 1863, 1862, 1870, 1871
270, 548, 549, 552, 551, 410, 411, 414, 413, 1864, 1873, 1872, 1869, 1499, 1508, 1507,
    1504, 1862, 1866, 1874, 1870
*Nset, nset=_PickedSet2, internal, generate
  1, 1874, 1
*Elset, elset=_PickedSet2, internal, generate
  1, 270, 1
** Section: SHOULDER
**Solid Section, elset=_PickedSet2, material=SHOULDER

```

```

,
*End Instance
**
*Instance, name=TIEBAR-1-lin-2-1, part=TIEBAR
    66.,    165.,    10.
    66.,    165.,    10.,    67.,    165.,    10.,    90.
*Node
    1, -0.220970869, 0.220970869,    0.
    2,  -0.3125,    0.,    0.
    3, -0.220970869, -0.220970869,    0.
    4,    0., -0.3125,    0.
    5, 0.220970869, -0.220970869,    0.
    6,  0.3125,    0.,    0.
    7, 0.220970869, 0.220970869,    0.
***
***
***
***
    462, 0.110485435, 0.110485435,    30.
    463, 0.220970869, 0.220970869,    29.
    464,  0.3125,    0.,    29.
    465, 0.220970869, -0.220970869,    29.
    466, 0.119588576, 0.288712353,    30.
    467, -0.119588576, 0.288712353,    30.
    468,    0.,  0.3125,    29.
    469, 0.119588576, -0.288712353,    30.
    470, -0.119588576, -0.288712353,    30.
    471,    0., -0.3125,    29.
*Element, type=C3D20R
    1, 11, 10, 18, 12, 2, 1, 9, 3, 148, 147, 146, 145, 149, 150, 151,
    152, 154, 153, 155, 156
    2, 18, 16, 15, 14, 9, 7, 6, 5, 160, 159, 158, 157, 161, 162, 163,
    164, 155, 165, 166, 167
    3, 18, 10, 17, 16, 9, 1, 8, 7, 147, 169, 168, 160, 150, 170, 171,
    161, 155, 153, 172, 165
    4, 13, 12, 18, 14, 4, 3, 9, 5, 174, 146, 157, 173, 175, 151, 164,
    176, 177, 156, 155, 167
    5, 20, 19, 27, 21, 11, 10, 18, 12, 181, 180, 179, 178, 148, 147, 146,
    145, 183, 182, 184, 185
***
***
***
***
    55, 135, 127, 134, 133, 126, 118, 125, 124, 432, 446, 445, 441, 411, 425, 424,
    420, 436, 434, 447, 442
    56, 130, 129, 135, 131, 121, 120, 126, 122, 449, 431, 438, 448, 428, 410, 417,

```

427, 450, 437, 436, 444  
 57, 137, 136, 144, 138, 128, 127, 135, 129, 454, 453, 452, 451, 433, 432, 431,  
 430, 456, 455, 457, 458  
 58, 144, 142, 141, 140, 135, 133, 132, 131, 462, 461, 460, 459, 441, 440, 439,  
 438, 457, 463, 464, 465  
 59, 144, 136, 143, 142, 135, 127, 134, 133, 453, 467, 466, 462, 432, 446, 445,  
 441, 457, 455, 468, 463  
 60, 139, 138, 144, 140, 130, 129, 135, 131, 470, 452, 459, 469, 449, 431, 438,  
 448, 471, 458, 457, 465  
 \*Nset, nset=\_PickedSet2, internal, generate  
 1, 471, 1  
 \*Elset, elset=\_PickedSet2, internal, generate  
 1, 60, 1  
 \*\* Section: STEEL  
 \*Solid Section, elset=\_PickedSet2, material=STEEL  
 ,  
 \*End Instance  
 \*\*  
 \*Nset, nset=\_PickedSet65, internal, instance=TM-1  
 5, 6, 7, 8, 9, 19, 29, 30, 31, 32, 173, 224, 225, 265, 655, 656  
 1577, 1578, 1579, 1580, 1585, 1586, 1587, 1590, 1591, 1592, 2050, 2051, 2055, 2056, 2058,  
 2059  
 2677, 2681, 2682, 2684, 3155, 3159, 3160, 3162  
 \*Nset, nset=\_PickedSet65, internal, instance=M-1-lin-5-1  
 6, 7, 8, 9, 10, 13, 14, 44, 45, 46, 47, 48, 49, 50, 51, 52  
 53, 54, 55, 56, 57, 58, 59, 60, 61, 62, 63, 64, 65, 66, 67, 68  
 69, 70, 71, 72, 108, 109, 110, 111, 112, 113, 114, 115, 116, 117, 118, 119  
 120, 121, 122, 688, 689, 690, 691, 696, 697, 698, 701, 702, 703, 706, 707, 708  
 711, 712, 713, 716, 717, 718, 721, 722, 723, 726, 727, 728, 731, 732, 733, 736  
 737, 738, 741, 742, 743, 746, 747, 748, 751, 752, 753, 756, 757, 758, 761, 762  
 763, 766, 767, 768, 1004, 1005, 1006, 1009, 1010, 1012, 1013, 1015, 1016, 1018, 1019, 1021  
 1022, 1024, 1025, 1027, 1028, 1030, 1031, 1033, 1034, 1036, 1037, 1039, 1040, 1042, 1043,  
 1045  
 1046, 1048, 1049, 1051, 1052  
 \*Elset, elset=\_PickedSet65, internal, instance=TM-1  
 106, 107, 108, 159, 160, 312, 313, 465, 466  
 \*Elset, elset=\_PickedSet65, internal, instance=M-1-lin-5-1  
 65, 66, 67, 68, 69, 70, 71, 72, 73, 74, 75, 76, 77, 78, 79, 80  
 145, 146, 147, 148, 149, 150, 151, 152, 153, 154, 155, 156, 157, 158, 159, 160  
 \*\*\*  
 \*\*\*  
 \*\*\*  
 \*Surface, type=ELEMENT, name=\_PickedSurf150, internal  
 \_\_PickedSurf150\_S4, S4  
 \_\_PickedSurf150\_S3, S3  
 \_\_PickedSurf150\_S6, S6

```

__PickedSurf150_S5, S5
** Constraint: M1
*Tie, name=M1, adjust=yes
_PickedSurf41, _PickedSurf40
** Constraint: M2
*Tie, name=M2, adjust=yes
_PickedSurf43, _PickedSurf42
** Constraint: M3
*Tie, name=M3, adjust=yes
_PickedSurf45, _PickedSurf44
** Constraint: M4
*Tie, name=M4, adjust=yes
_PickedSurf47, _PickedSurf46
** Constraint: M5
*Tie, name=M5, adjust=yes
_PickedSurf145, _PickedSurf144
** Constraint: S1
*Tie, name=S1, adjust=yes
_PickedSurf48, _PickedSurf49
** Constraint: T1
*Tie, name=T1, adjust=yes
_PickedSurf90, _PickedSurf89
** Constraint: T2
*Tie, name=T2, adjust=yes
_PickedSurf92, _PickedSurf91
** Constraint: T3
*Tie, name=T3, adjust=yes
_PickedSurf55, _PickedSurf54
** Constraint: T4
*Tie, name=T4, adjust=yes
_PickedSurf57, _PickedSurf56
** Constraint: T5
*Tie, name=T5, adjust=yes
_PickedSurf59, _PickedSurf58
*End Assembly
**
** MATERIALS
**
*Material, name=MAINLINE
*Density
0.0839,
*Elastic
4.5e+06, 0.2
*Expansion
5.5e-06,
*Material, name=SHOULDER

```

```

*Density
0.0839,
*Elastic
3.3e+06, 0.2
*Expansion
5.5e-06,
*Material, name=STEEL
*Elastic
2.9e+07, 0.3
**
** INTERACTION PROPERTIES
**
*Surface Interaction, name=PCCPCC
1.,
*Friction
0.,
*Surface Behavior, no separation, pressure-overclosure=HARD
**
** BOUNDARY CONDITIONS
**
** Name: Body Type: Symmetry/Antisymmetry/Encastre
*Boundary
_PickedSet131, YSYMM
** Name: MLB Type: Displacement/Rotation
*Boundary
_PickedSet67, 2, 2
**
** PREDEFINED FIELDS
**
** Name: MLBOTini Type: Temperature
*Initial Conditions, type=TEMPERATURE
_PickedSet136, 80.
** Name: MLTOPini Type: Temperature
*Initial Conditions, type=TEMPERATURE
_PickedSet137, 80.
** Name: SHini Type: Temperature
*Initial Conditions, type=TEMPERATURE
_PickedSet70, 90.
**
** INTERACTIONS
**
** Interaction: FOUNDATION
*Foundation
__PickedSurf118_S5, F5, 100.
__PickedSurf118_S4, F4, 100.
__PickedSurf118_S6, F6, 100.

```

```

__PickedSurf118_S2, F2, 100.
__PickedSurf118_S3, F3, 100.
** Interaction: MLSH
*Contact Pair, interaction=PCCPCC, type=SURFACE TO SURFACE
__PickedSurf95, __PickedSurf94
** -----
**
** STEP: GRAVITY
**
*Step, name=GRAVITY
*Static
1., 1., 1e-05, 1.
**
** LOADS
**
** Name: GRAVITY  Type: Gravity
*Dload
__PickedSet117, GRAV, 386.4, 0., 0., -1.
**
** OUTPUT REQUESTS
**
*Restart, write, frequency=0
**
** FIELD OUTPUT: F-Output-1
**
*Output, field, variable=PRESELECT
**
** HISTORY OUTPUT: H-Output-1
**
*Output, history, variable=PRESELECT
*End Step
** -----
**
** STEP: TEMP
**
*Step, name=TEMP
*Static
1., 1., 1e-05, 1.
**
** LOADS
**
** Name: MLTRACBOT  Type: Surface traction
*Dload
__PickedSurf141, TRSHR, 0.8, 0., -1., 0.
** Name: MLTRACLEFT  Type: Surface traction
*Dload

```

\_PickedSurf138, TRSHR, 0.8, 1., 0., 0.  
 \*\* Name: MLTRACRIGHT Type: Surface traction  
 \*Dsload  
 \_PickedSurf139, TRSHR, 0.8, -1., 0., 0.  
 \*\* Name: MLTRACTOP Type: Surface traction  
 \*Dsload  
 \_PickedSurf140, TRSHR, 0.8, 0., 1., 0.  
 \*\* Name: SHTRACBOT Type: Surface traction  
 \*Dsload  
 \_PickedSurf150, TRSHR, 0.8, 0., -1., 0.  
 \*\* Name: SHTRACLEFT Type: Surface traction  
 \*Dsload  
 \_PickedSurf143, TRSHR, 0.8, 1., 0., 0.  
 \*\* Name: SHTRACRIGHT Type: Surface traction  
 \*Dsload  
 \_PickedSurf142, TRSHR, 0.8, -1., 0., 0.  
 \*\* Name: SHTRACTOP Type: Surface traction  
 \*Dsload  
 \_PickedSurf149, TRSHR, 0.8, 0., 1., 0.  
 \*\*  
 \*\* PREDEFINED FIELDS  
 \*\*  
 \*\* Name: ML Type: Temperature  
 \*Temperature  
 \_PickedSet71, 50.  
 \*\* Name: SH Type: Temperature  
 \*Temperature  
 \_PickedSet72, 50.  
 \*\*  
 \*\* OUTPUT REQUESTS  
 \*\*  
 \*Restart, write, frequency=0  
 \*\*  
 \*\* FIELD OUTPUT: F-Output-1  
 \*\*  
 \*Output, field, variable=PRESELECT  
 \*\*  
 \*\* HISTORY OUTPUT: H-Output-1  
 \*\*  
 \*Output, history, variable=PRESELECT  
 \*End Step

## BIBLIOGRAPHY

- ABAQUS/CAE. (2007). *Version 6.7*. Providence, Rhode Island: Dassault Systems.
- American Concrete Pavement Association. *Cause, Prevention, and Repair of Longitudinal Shear Cracking*. R&T Update, American Concrete Pavement Association, Skoike, IL.
- ARA Inc., ERES Consultants Division. (2004). *Guide for Mechanistic-Empirical Design of New and Rehabilitated Pavement Structures*. Design Guide, National Cooperative Highway Research Program.
- Asbahan, R. (2009). *EFFECTS OF THE BUILT-IN CONSTRUCTION GRADIENT AND ENVIRONMENTAL CONDITIONS ON JOINTED PLAIN CONCRETE PAVEMENTS*. Phd Thesis, University of Pittsburgh, Pittsburgh, PA.
- Federal Highway Administration. (1988). *Longitudinal Cracking at Transverse Joints of New JPCP with PCC Shoulders*. Washington D.C.
- Federal Highway Administration. (1990). *Paved Shoulders*. Technical Advisory T 5040.29.
- Huang, Y. H. (2004). *Pavement Analysis and Design, Second Edition*. Upper Saddle Ridge, NJ: Pearson Prentice Hall.
- Kuo, C.-M. (1994). *Three-Dimensional Finite Element Analysis of Concrete Pavement*. University of Illinois at Urbana-Champaign, Department of Civil Engineering. Urbana, Illinois: UMI Dissertation Services.
- Kupfer, H., Hilsdorf, H. K., & Rusch, H. (1969). Biaxial Strength of Concrete. *Journal of the American Concrete Institute* , 66 (8), 656-666.
- Lee, Y.-H., Wu, H.-T., & Yen, S.-T. (2004). Parameter studies and verifications on three-dimensional finite element analysis of rigid pavements. *Canadian Journal of Civil Engineering* , 31 (5), 782-796.
- Maitra, S. R., Reddy, K. S., & Ramachandra, L. S. (2009). Experimental Evaluation of Interface Friction and Study of Its Influence on Concrete Pavement Response. *Journal of Transportation Engineering* , 135 (8), 563-571.

- Ruiz, J. M., Rasmussen, R. O., Chang, G. K., Dick, J. C., & Nelson, K. P. (2005). *Computer-Based Guidelines For Concrete Pavements Volume II—Design and Construction Guidelines and HIPERPAV II User's Manual*. The Transtec Group. McLean, VA: FHWA.
- Tayabji, S., & Lotfi, H. (2003). *Pennsylvania I-81 (Franklin County) Pavement Cracking*. Construction Technology Laboratories, Columbia, MD.
- Wells, S. A. (2005). *Early Age Response of Jointed Plain Concrete Pavements to Environmental Loads*. Masters Thesis, University of Pittsburgh, Civil and Environmental Engineering, Pittsburgh.
- Westergaard, H. M. (1927). Analysis of Stresses in Concrete Pavements Due to Variations of Temperature. *Proceedings from the 6th Annual Meeting Highway Research Board* , 201-215.
- Zapata, C. E., & Houston, W. N. (2008). *NCHRP Report 602 Calibration and Validation of the Enhanced Integrated Climatic Model for Pavement Design*. Washington D.C.: Transportation Research Board.